Trinity College Dublin
Coláiste na Tríonóide, Baile Átha Cliath
The University of Dublin

Examining the Radiation-induced Bystander Effect (RIBE) and its Effect on Metabolism and Inflammation in Gastrointestinal Cancers

Aisling Heeran

Student No. 15313815

Ph.D. Thesis

Submitted to Trinity College Dublin for the degree of Doctor of Philosophy

May 2021

Trinity St. James's Cancer Institute, Trinity Translational Medicine Institute, Department of Surgery, Trinity College Dublin and St. James's Hospital.

Thesis Supervisors: Prof. Jacintha O'Sullivan (Primary Supervisor), Dr Niamh Lynam-Lennon (Secondary Supervisor)

Declaration

I declare that this thesis has not been submitted as an exercise for a degree at this or any other university and it is entirely my own work.

I agree to deposit this thesis in the University's open access institutional repository or allow the library to do so on my behalf, subject to Irish Copyright Legislation and Trinity College Library conditions of use and acknowledgement.

I consent to the examiner retaining a copy of the thesis beyond the examining period, should they so wish (EU GDPR May 2018).

_____ _____

Aisling Heeran Date

Thesis abstract

Radiation therapy is a mainstay of treatment for cancer. However, resistance to therapy remains a major clinical problem in rectal and oesophageal cancer, with at best only 27-30% of patients achieving a complete pathological response which is associated with enhanced patient outcomes. The mechanisms underlying treatment resistance are poorly understood. The radiation-induced bystander effect (RIBE) describes the plethora of biological events occurring in unirradiated cells adjacent to irradiated cells. RIBE has been linked experimentally to numerous hallmarks of cancer however, the examination of RIBE induction using human *ex vivo* models remains largely unknown in the literature.

We investigated the effect of *in vitro* RIBE induction on mitochondrial metabolism and function and radiosensitivity in an *in vitro* model of colorectal cancer (CRC) and oesophageal adenocarcinoma (OAC), using a radiosensitive and a radioresistant cell line of both models. *In vitro* we did not observe any significant alterations in any of the parameters measured following RIBE induction using a single fraction of a clinically relevant dose of 1.8 Gy radiation in CRC cell lines. However, following RIBE induction using repeated fractions of 1.8 Gy radiation we identified a differential response in the radioresistant and radiosensitive OAC cell lines. Moreover, following RIBE induction using repeated fractions of 1.8 Gy radiation, we observed alterations in mitochondrial metabolism and function in both the radiosensitive and radioresistant cell line, as well as alterations in DNA repair in the radioresistant cell line.

Since *in vitro* RIBE induction in the CRC model did not produce robust RIBE responses, we then investigated the effect of RIBE induction using a human *ex vivo* explant model of normal rectal tissue and rectal cancer tissue. RIBE induction *ex vivo* produced alterations in bystander cellular metabolism, with reductions in oxidative phosphorylation (OXPHOS) in bystander cells that were exposed to conditioned media (CM) from both irradiated normal and cancer tissue. Glycolysis was significantly reduced in bystander cells exposed to CM from irradiated rectal cancer tissue. RIBE induction did not alter mitochondrial function, however, elevated levels of reactive oxygen species (ROS) were observed in bystander cells treated with CM from rectal cancer tissue compared to normal rectal tissue. To gain a further understanding of the metabolites that may be driving these alterations, we examined the metabolomic landscape of normal rectal tissue and rectal cancer tissue pre- and post-radiation using ^{1}HNMR. Leucine levels

were significantly reduced in the CM of irradiated rectal cancer tissue compared to irradiated normal rectal tissue. Since obese rectal cancer patients have been reported to have poorer clinical outcomes, we correlated our biological end-point results with parameters of body composition and found significant correlations between visceral fat area (VFA) and leucine and ethanol in the rectal cancer secretome and levels of glycolysis and ATP production in bystander cells treated with the CM from the irradiated rectal cancer tissue.

Since metabolism and inflammation are highly dependent and interconnecting processes, we next investigated the inflammatory landscape of *ex vivo* normal rectal tissue and rectal cancer tissue both pre- and post-radiation. We have shown that the rectal cancer microenvironment is more inflammatory than the normal rectal microenvironment, with elevated levels of 19 inflammatory proteins in the rectal cancer microenvironment; Flt-1, P1GF, CCL20, IFN-γ, IL-10, IL-6, GM-CSF, IL-12/IL-23p40, IL-17A, IL-1α, IL-17A/F, IL-1RA, TSLP, CCL26, CXCL10, CCL22, CCL3, CCL4 and CCL17. Following radiation, IL-15 and CCL22 were elevated in the microenvironment of normal rectal tissue while no factor was significantly altered in the rectal cancer microenvironment. The irradiated rectal cancer microenvironment was the most potent inducer of dendritic cell maturation, suggesting that radiation does not negatively impact the ability of the rectal cancer microenvironment to mount an anti-tumour immune response. We also found significant correlations between body composition parameters and secreted factors, including correlations between VFA and CCL20 and inverse correlations between skeletal muscle and angiogenic markers including Flt-1 and VEGF-D.

Having observed correlations between measures of obesity and response of bystander cells to radiation, levels of metabolites in the tumour microenvironment (TME) and altered levels of inflammatory proteins in the TME of obese individuals we profiled for the first time the metabolic signatures of *ex vivo* adipose tissue using Seahorse technology. We demonstrated that it was possible to determine the metabolic profiles of *ex vivo* adipose tissue depots using Seahorse technology and that OXPHOS predominates in visceral adipose tissue while there is a trend towards higher utilisation of glycolysis in subcutaneous adipose tissue. We then profiled the inflammatory protein secretions from both adipose tissue depots and found that there were significantly higher levels of angiogenic, vascular injury and proinflammatory secretions in the visceral compared to

subcutaneous adipose tissue. There were also early indications in this preliminary study that obesity may alter the metabolic profile and inflammatory secretome of adipose tissue.

Overall, the findings of this thesis have identified the interesting interplay of secreted factors and cell types within the TME as possible important determinants in regulating bystander cellular metabolism and innate immune responses in rectal cancer. We have also identified alterations in cellular behaviour, the metabolomic landscape and inflammatory protein secretions in obese patients compared to their non-obese counterparts. We have shown that Seahorse technology is a useful tool for profiling the metabolic signature of adipose tissue for future functional studies to more closely examine the interplay between obesity and RIBE and treatment responses in GI patients.

Acknowledgements

Firstly, I would like to thank my supervisor Prof. Jacintha O'Sullivan for your continuous support and guidance over the course of my Ph.D. Thank you for being so generous with your time and your infinite well of knowledge. Your wisdom and patience never ceased to amaze me! Thank you for always encouraging me, pushing me outside my comfort zone and reminding me to believe in myself. It has been an absolute pleasure working with you and I couldn't have asked for a better supervisor.

I would also like to thank my co-supervisor Dr Niamh Lynam-Lennon for your support and willingness to help and share your knowledge throughout my project. Your eagle-eye was invaluable to this write up! Thank you for always being so approachable and pleasant, it was great working with you.

Thank you to Dr Margaret Dunne and Dr Mia Morrissey for your help with the immune work and answering my endless questions! Thank you to Prof. Lorraine Brennan, Dr Heleena Moni Bottu and Orla Prendiville in UCD for your help with the metabolomics work. Thank you to Croí Buckley, Rebecca O'Brien, Dr Noel Donlon, Dr Timothy Nugent, Niamh Clarke and Anshul Bhardwaj for your tremendous work with the lower and upper GI biobanks.

I would like to express my utmost gratitude to the patients who so kindly donated their samples to this research, without your generosity, none of this would have been possible. Thank you to Dr Cara Dunne, Mr. John Larkin, Mr. Paul McCormick and Mr. Brian Mehigan for your work recruiting patients to this study. Thank you to the Irish Research Council for funding this Ph.D. project.

A huge thanks to the amazing team of PIs, post-docs, Ph.D. students and biobank managers in the Department of Surgery for creating and maintaining a most pleasant work environment. Stephen, Joanne, Melissa, Margaret, Mia, Martin, Sarah and Simone, thank you for your encouragement and passing on your knowledge and skills over the last few years. Anshul, Emma, Niamh, Andrew, Croí, Rebecca, Jason, Noel, Maria, Fiona, Klaudia, Cliona, Jim, Tim, Eimear and Laura, thank you for everything over the last few years, it has been a pleasure to work with you. You're a great bunch of scientists and a most wonderful group of people. Thanks for making my time in the department so much fun. Aoife, thank you for always sending me on protocols, answering my never-ending

questions and always being so positive and encouraging. Special thanks to Amy for helping me with literally everything and being so generous with your time and thanks to Susan for always being such a calming influence and reminding me that it would all be ok!

Jill and Suzie, my incredibly intelligent cousins, thank you for answering all of my stats/radiation therapy questions over the last while!

Thanks to Janet for being so flexible and understanding and to Pamela, Muireann, Blathnaid, Chloe, Leah, Kelsey, Mag, Caoimhe, Niamh, Gabrielle and Ciara for always being so helpful and trying to keep my stress levels to a minimum!

Thanks to the Killiney swims crew and the WattsUp crew for the laughs and providing an escape from the writing, especially over the last few months!

Thanks to Joanne for always being willing to go on holidays, reminding me that life gets better after a Ph.D. and introducing me to The 2 Johnnies! Sinéad, thanks for listening to me rant and going running/on general adventures with me to escape the thesis! Ciara, you were a wonderful housemate and thanks for all the laughs over the last 3 years. Sarah and Eimear, thanks for always reminding me to believe in myself and reminding me why I was doing this! Emer, Theresa, Vicky and the extended Flannery cycling gang, thanks for all the adventures (no matter how ridiculous they were getting!) and picnics, providing much needed breaks all along the way.

To my wonderful parents Pat and Geraldine, thank you for always encouraging me and supporting me in everything I do. Thank you for always believing in me. You have afforded me every opportunity and I couldn't have done this without you. I'm so lucky to have you both. Thanks to my sister Aoife for helping with graphics and general tech issues.

Ph.D. Outputs

Publications

Aisling B. Heeran, Helen P. Berrigan and Jacintha O'Sullivan. The Radiation Induced Bystander Effect (RIBE) and its Connections with the Hallmarks of Cancer. *Radiat Res*, 2019 Dec;192(6):668-679.

Aisling B. Heeran, Helen P. Berrigan, Croí E. Buckley, Heelena Moni Bottu, Orla Prendiville, Amy M. Buckley, Niamh Clarke, Noel E. Donlon, Timothy Nugent, Michael Durand, Cara Dunne, John O. Larkin, Brian Mehigan, Paul McCormick, Lorraine Brennan, Niamh Lynam-Lennon, Jacintha O'Sullivan. Radiation Induced Bystander Effect (RIBE) alters mitochondrial metabolism using a human rectal cancer ex vivo explant model. Transl Oncol. 2021 Jan;14(1):100882.

Aisling B. Heeran, Margaret R. Dunne, Maria Morrissey, Croí E. Buckley, Niamh Clarke, Aoife Cannon, Noel E. Donlon, Timothy Nugent, Michael Durand, Cara Dunne, John O. Larkin, Brian Mehigan, Paul McCormick, Niamh Lynam-Lennon, Jacintha O'Sullivan. The Protein Secretome is Altered in Rectal Cancer Tissue Compared to Normal Rectal Tissue, and Alterations in the Secretome Induce Enhanced Innate Immune Responses. Cancers (Basel). 2021 Feb 2;13(3):571.

Gillian Barber, Akanksha Anand, Katarzyna Oficjalska, James J. Phelan, **Aisling B. Heeran**, Ewelina Flis, Niamh E. Clarke, Jenny A. Watson, Julia Strangmann, Brian Flood, Hazel O'Neill, Dermot O'Toole, Finbar MacCarthy, Narayanasamy Ravi, John V. Reynolds, Elaine W. Kay, Michael Quante, Jacintha O'Sullivan, Emma M. Creagh. Characterising Caspase-1 Involvement During Esophageal Disease Development. Cancer Immunol Immunother. 2020 Dec;69(12):2635-2649.

Kayleigh Slater, **Aisling B. Heeran**, Rebeca Sanz-Pamplona, Helen Kalirai, Arman Rahman, Mays Helmi, Sandra Garcia-Mulero, Fiona O'Connell, Rosa Bosch, Anna Portela, Alberto Villanueva, Josep Maria Piulats, William M. Gallagher, Lasse D. Jensen, Sarah E. Coupland, Jacintha O'Sullivan and Breandán N. Kennedy. High Cysteinyl Leukotriene Receptor 1 Expression Correlates with Poor Survival of Uveal Melanoma Patients and Cognate Antagonist Drugs Modulate the Growth, Cancer Secretome, and Metabolism of Uveal Melanoma Cells. Cancers (Basel). 2020 Oct 13;12(10):2950

Under review:

Aisling B. Heeran, Jessica McCready, Margaret R. Dunne, Noel E. Donlon, Anshul Bhardwaj, Kathleen A. J. Mitchelson, Amy M. Buckley, Narayanasamy Ravi, Helen M. Roche, John V. Reynolds, Niamh Lynam-Lennon and Jacintha O'Sullivan. Opposing immune-metabolic signature in visceral versus subcutaneous adipose tissue in patients with adenocarcinoma of the oesophagus and the oesophagogastric junction

Oral Presentations (Presenting Author)

Young Cancer Researchers Networking 2018, Cork 21st-22nd June 2018;

Title: Profiling the tissue secretome in normal rectal and rectal cancer tissue. **Authors: Aisling Heeran**, Croí Buckley, Margaret Dunne, Amy Buckley, Niamh Clarke, Susan Kennedy, Aoife Cannon, Cara Dunne, John Larkin, Niamh Lynam-Lennon, Jacintha O'Sullivan.

Irish Association of Pharmacologists Annual Meeting 2018, Belfast 30th November 2018;

Title: Investigating the effect of radiation on the *ex vivo* normal rectal and rectal cancer secretome and the effect of this secretome on cellular metabolism. **Authors: Aisling Heeran**, Margaret Dunne, Maria Morrissey, Helen Berrigan, Croí Buckley, Amy Buckley, Niamh Clarke, Aoife Cannon, Cara Dunne, John Larkin, Niamh Lynam-Lennon, Jacintha O'Sullivan.

The 11th International Cancer Conference 2019, Dublin 24th-25th September 2019;

Title: Radiation Induced Bystander Effect (RIBE) induction using human *ex vivo* explants induces significant changes in the tissue secretome, immune cell function and bystander cellular metabolism. **Authors: Aisling Heeran**, Margaret Dunne, Maria Morrissey, Helen Berrigan, Croí Buckley, Amy Buckley, Niamh Clarke, Aoife Cannon, Cara Dunne, John Larkin, Niamh Lynam-Lennon, Jacintha O'Sullivan.

The 45th Annual Meeting of the European Radiation Research Society (ERRS 2020), Lund, Sweden (Virtual Conference) 13th-17th September 2020;

Title: Examining the effect of radiation on the secretome of normal and rectal cancer tissue and how this secretome interacts with the innate immune system. **Authors: Aisling Heeran**, Margaret Dunne, Maria Morrissey, Croí Buckley, Niamh Clarke, Aoife Cannon, Noel Donlon, Timothy Nugent, Michael Durand, Cara Dunne, John Larkin, Brian Mehigan, Paul McCormick, Niamh Lynam-Lennon, Jacintha O'Sullivan.

The 45th Annual Meeting of the European Radiation Research Society (ERRS 2020), Lund, Sweden (Virtual Conference) 13th-17th September 2020;

Title: RIBE induction using human ex vivo explants causes alterations in mitochondrial metabolism in bystander cells. **Authors: Aisling Heeran**, Helen P. Berrigan, Croí E. Buckley, Heelena Bottu, Amy M. Buckley, Niamh Clarke, Noel E. Donlon, Timothy Nugent, Michael Durand, Cara Dunne, John Larkin, Brian Mehigan, Paul McCormick, Lorraine Brennan, Niamh Lynam-Lennon, Jacintha O'Sullivan.

Poster Presentations (Presenting Author)

Irish Association of Cancer Research Meeting 2018, Dublin 21st-23rd February 2018;

Title: Influence of metabolic dysfunction on the mammary adipose tissue secretome; potential implications for breast tumorigenesis. **Authors: Aisling Heeran**, Paul A. Carroll, Laura A. Healy, Terence Boyle, M John Kennedy, Elizabeth M. Connolly, Sarah A. McGarrigle.

Irish Society of Immunology Meeting 2018, Dublin 30th-31st August 2018;

Title: Profiling inflammatory protein secretions from the *ex vivo* rectal cancer microenvironment compared to normal rectal tissue. **Authors: Aisling Heeran**, Margaret Dunne, Croí Buckley, Amy Buckley, Niamh Clarke, Aoife Cannon, Cara Dunne, John Larkin, Niamh Lynam-Lennon, Jacintha O'Sullivan.

Irish Association of Cancer Research Meeting 2019, Belfast 20th-22nd February 2019;

Title: RIBE-induction using human *ex vivo* explants induces significant changes in the tissue secretome, immune cell function and bystander cellular metabolism. **Authors: Aisling Heeran**, Margaret Dunne, Maria Morrissey, Helen Berrigan, Croí Buckley,

Susan Kennedy, Amy Buckley, Niamh Clarke, Aoife Cannon, Cara Dunne, John Larkin, Niamh Lynam-Lennon, Jacintha O'Sullivan.

International Congress of Radiation Research 2019, Manchester 25th-29th August 2019;

Title: RIBE-induction using human *ex vivo* explants induces significant changes in the tissue secretome, immune cell function and bystander cellular metabolism. **Authors: Aisling Heeran,** Margaret Dunne, Maria Morrissey, Helen Berrigan, Croí Buckley, Amy Buckley, Niamh Clarke, Aoife Cannon, Cara Dunne, John Larkin, Niamh Lynam-Lennon, Jacintha O'Sullivan.

The 11th International Cancer Conference 2019, Dublin 24th-25th September 2019;

Title: Characterising the immune-metabolic signature in visceral and subcutaneous adipose tissue in oesophageal adenocarcinoma patients. **Authors: Aisling Heeran**, Jessica McCready, Margaret Dunne, Anshul Bhardwaj, Amy Buckley, Narayanasamy Ravi, John Reynolds, Jacintha O'Sullivan.

Irish Association of Cancer Research Meeting 2020, Galway 26th-28th February 2020;

Title: Radiation induced bystander effect (RIBE) induction using human ex vivo explants induces significant changes in the tissue secretome, immune cell function and bystander cellular metabolism. **Authors:** Aisling Heeran, Margaret Dunne, Maria Morrissey, Helen Berrigan, Croí Buckley, Amy Buckley, Niamh Clarke, Aoife Cannon, Cara Dunne, John Larkin, Lorraine Brennan, Niamh Lynam-Lennon, Jacintha O'Sullivan.

Irish Association of Cancer Research Meeting 2020, Galway 26th-28th February 2020;

Title: Opposing immune-metabolic signatures in visceral versus subcutaneous adipose tissue in patients with adenocarcinoma of the oesophagus and oesophagogastric junction. **Authors:** Aisling B. Heeran, Jessica McCready, Margaret R. Dunne, Anshul Bhardwaj, Amy M. Buckley, Narayanasamy Ravi, John V. Reynolds, Jacintha O'Sullivan.

Awards:

Jane Grimson Medal of Excellence awarded for being the highest ranked postgraduate scholar in the STEM domain under the Irish Research Council 2017 Awards call.

Best oral presentation at Young Cancer Researchers Networking 2018 held in Cork 21st-22nd June 2018.

Best oral presentation at Irish Association of Pharmacologists Annual Meeting 2018 held in Belfast 30th November 2018.

Travel bursary to attend the Eurolife Winter School 'Structure and Function of Genomes in Homeostasis and Disease' 16th-21st December 2018, Obergurgl, Austria.

Allergan Innovation Award 2019 to investigate bystander events in rectal cancer patients.

Scholar-in-Training Award from the Irish Radiation Research Society to attend the International Congress of Radiation Research in Manchester, UK, August 2019.

IACR AOIFA Conference Award to attend the European Radiation Research Society Annual Meeting in Lund, Sweden, September 2020.

Courses:

Postgraduate certificate in Innovation and Entrepreneurship – Opportunity Generation and Recognition – October 2017 – 5 ECTS.

Planning and Managing your Research and Career – January – April 2018 – 5 ECTS.

Postgraduate certificate in Innovation and Entrepreneurship – Intellectual Property – March 2019 – 5 ECTS.

Fire Safety Workshop – 24th October 2017, Trinity College Dublin.

Good Clinical Practice – 10th November 2017, Clinical Research Facility, St. James's Hospital.

Cryogenics Safety Workshop – 16th November 2017, Trinity College Dublin.

Case Studies in Drug Discovery and Development – January – March 2018.

Chemical Safety Workshop – 26th April 2018, Trinity College Dublin.

Biological Safety Workshop – 24th October 2018, Trinity College Dublin.

Irish Cancer Society Mental Well-being Workshop – 8th November 2018.

Epigeum Research Integrity Training – December 2018.

Outreach activities:

Transition Year Programme PCR Practical – 27th February 2018

TTMI TAP Day – Acids and Bases Station – 11th April 2018

Lay talk to Dutch Students from Nijmegen on TTMI field trip – 4th May 2018

Gout and Crystal Arthropathy Clinic MMUH – engaging pharmacists for a study quantifying opinion on colchicine use – January 2019

Lay talk to Belgian Students on TTMI field trip – 12th February 2019

Input on educational seminar for pharmacists on immunology – November 2019.

BT Young Scientist Exhibition – assisting with a project 'Teenage fixation with supplemented protein due to social media' - November 2020.

Teaching:

Problem-based learning tutorials in medical ethics – 1st Year Medical Students, September 2018 – October 2020.

Contents

List of Tables

List of Figures

Abbreviations

^{1}HNMR	Nuclear magnetic resonance
3-DCRT	3-dimensional conformal radiotherapy
53BP1	p53 binding protein 1
5-FU	5-fluorouracil
ACM	Adipose conditioned media
AKT	Protein kinase B
AMPK	AMP activated protein kinase
ANOVA	Analysis of variance
AP endonuclease	Apurinic/Apyrimidinic endonuclease
AP-1	Activator protein 1
APC	Allophycocyanin
ASCO	American Society of Clinical Oncology
ATCC	American Type Culture Collection
ATP	Adenosine triphosphate
Bax	Bcl-2 associated X protein
BCA	Bicinchoninic acid
Bcl-2	B cell lymphoma 2
bFGF	Fibroblast growth factor (basic)
BMI	Body mass index
BrdU	Bromodeoxyuridine
BSA	Bovine serum albumin
CAF	Cancer-associated fibroblast
cAMP	Cyclic adenosine monophosphate
CCL	Chemokine ligand
CCR	Chemokine receptor
CD	Cluster of differentiation
CDC2	Cyclin dependent kinase
CDKN1A	Cyclin dependent kinase inhibitor 1 A
cDNA	Complementary deoxyribonucleic acid

CEA	Carcinoembryonic antigen
cfDNAox	Cell free oxidised DNA
CM	Conditioned media
CNS	Central nervous system
COX-2	Cyclooxygenase-2
CPMG	Carr-Purcell-Meiboom-Gill
CRC	Colorectal cancer
CRM	Circumferential resected margin
CRP	C-reactive protein
CRT	Chemoradiation
CSF	Colony stimulating factor
CT	Computed tomography
Ct	Threshold cycle
D_2O	Deuterium oxide
DC	Dendritic cell
DCF	Dichlorofluorescein
DMEM	Dulbecco's Modified Eagle Medium
DMSO	Dimethyl sulfoxide
DRE	Digital rectal examination
DSB	Double strand break
EC	Endothelial cell
ECAR	Extracellular acidification rate
EDTA	Ethylenediaminetetraacetic acid
EGFR	Epidermal growth factor receptor
ELISA	Enzyme-linked immunosorbent assay
EMM	Extramural vascular invasion
ERK	Extracellular signal regulated kinase
ERUS	Endoscopic rectal ultrasound
EUA	Examination under anaesthetic
EUS	Endoscopic ultrasound

EVs	Extracellular vesicles
FBS	Foetal bovine serum
FCCP	Carbonyl cyanide-p-trifluoromethoxyphenylhydrazone
FDG-PET	Fluorodeoxyglucose positron emission tomography
Flt-1	Fms related receptor tyrosine kinase 1
GDF-15	Growth/differentiation factor 15
GEJ	Gastroesophageal junction
GERD	Gastroesophageal reflux disease
GI	Gastrointestinal
GJIC	Gap junctional intercellular communication
GM-CSF	Granulocyte-macrophage colony-stimulating factor
Gy	Gray
H+ Leak	Proton leak
H2AX	H2A histone family member 2 X
HA	High abundance
HIF	Hypoxia inducible factor
HLA-DR	Human leukocyte antigen – DR isotype
HUVEC	Human umbilical vein endothelial cells
IBD	Inflammatory bowel disease
ICAM	Intercellular adhesion molecule
ICCM	Irradiated cell conditioned media
IFN	Interferon
IL	Interleukin
IMRT	Intensity modulated radiotherapy
IP-10	Interferon gamma induced protein 10
JAK	Janus kinase
LARC	Locally-advanced rectal cancer
LC-3	Microtubule-associated protein 1 light chain 3
LDR	Low dose response
LET	Linear energy transfer

LPS	Lipopolysaccharide
MCP	Monocyte chemoattractant protein
MDC	Macrophage derived chemokine
MDSC	Myeloid-derived suppressor cell
MDT	Multidisciplinary team
MEF	Mouse embryonic fibroblast
MEK	Mitogen activated protein kinase
MFI	Mean fluorescent intensity
MIP	Macrophage inflammatory protein
MLH1	MutL Homolog 1
MMP	Matrix metalloproteinase
MMS19	MMS19 Homolog, Cytosolic Iron-Sulfur Assembly Component
MN	Micronuclei
MRI	Magnetic resonance imaging
MS-CT	Multi-slice computed tomography
mtDNA	Mitochondrial DNA
mtMP	Mitochondrial membrane potential
NADH	Nicotinamide adenine dinucleotide + hydrogen
NCM	Normal conditioned media
Neo-CRT	Neoadjuvant chemoradiation
NF-κB	Nuclear factor kappa B
NK cells	Natural killer cells
NKT cells	Natural killer T cells
NO	Nitric oxide
NTT	Normal tissue tolerance
OAC	Oesophageal adenocarcinoma
OCR	Oxygen consumption rate
OGJ	Oesophagogastric junction
OPLS-DA	Orthogonal partial least squares discriminate analysis
OS	Overall survival

OXPHOS	Oxidative phosphorylation
P1GF	Placental growth factor
PARP1	Poly [ADP-Ribose] polymerase 1
PBS	Phosphate buffered saline
PCA	Principle component analysis
PCNA	Proliferating cell nuclear antigen
pCR	Complete pathological response
PCR	Polymerase chain reaction
PD-1	Programmed cell death protein 1
PDGF	Platelet derived growth factor
PD-L1	Programmed death-ligand 1
PE	Plating efficiency
PET	Positron emission tomography
PET-CT	Positron emission tomography computed tomography
PLS-DA	Partial least squares discriminate analysis
PPM	Parts per million
RIBE	Radiation-induced bystander effect
RIRE	Radiation-induced rescue effect
ROS	Reactive oxygen species
RPM	Revolutions per minute
RPMI 1640	Roswell Park Memorial Institute 1640
RR	Relative risk
SAA	Serum amyloid A
SASP	Senescence associated secretory phenotype
SAT	Subcutaneous adipose tissue
SCC	Squamous cell carcinoma
SCE	Sister chromatid exchanges
SCPRT	Short course pre-operative radiotherapy
SEM	Standard error of the mean
SMUG1	Single strand selective monofunctional uracil-DNA glycosylase 1

STAT-3	Signal transducer and activator or transcription 3
SVF	Stromal vascular fraction
T reg	Regulatory T cell
TAE	Tris acetate EDTA
TAM	Tumour associated macrophage
TARC	Thymus and activation regulated chemokine
TCA	Tricarboxylic acid
TCM	Tumour conditioned media
TEM	Transanal endoscopic microsurgery
TGF-β	Transforming growth factor beta
TLD	Tumour lethal dose
TLR	Toll like receptor
TME	Tumour microenvironment
TNF	Tumour necrosis factor
TP53	Tumour protein 53
TRG	Tumour regression grade
TRS	Tumour regression score
TSLP	Thymic stromal lymphopoietin
TSP	Sodium trimethyl [2,2,3,3-$^{2}H_{4}$] propionate
US	Ultrasound
VAT	Visceral adipose tissue
VCAM	Vascular cell adhesion molecule
VEGF	Vascular epidermal growth factor
VFA	Visceral fat area

Chapter 1 General Introduction

This chapter has been published in part in **Heeran AB**, Berrigan HP, O'Sullivan J. The Radiation-Induced Bystander Effect (RIBE) and its Connections with the Hallmarks of Cancer. Radiat Res. 2019 Oct;192(6):668–79

1.1 Rectal cancer

1.1.1 Epidemiology and incidence of rectal cancer

Colorectal cancer (CRC) is the 3rd most commonly diagnosed cancer globally, accounting for 10.2% of all new cancer diagnoses, and the 2nd leading cause of cancer death, accounting for 9.2% of cancer deaths (1). Over 1.8 million cases of CRC are diagnosed each year and the annual death toll from the disease stands at approximately 881,000 (1). Almost 3,000 cases of CRC are diagnosed in Ireland each year and nearly 1,000 people die annually from the disease. In Ireland, CRC is the 2nd most common cancer in males and the 3rd most common cancer in females. CRC is the 2nd leading cause of cancer death in both men and women in Ireland accounting for 12% and 10% of cancer deaths, respectively (2). In Ireland, 57% of CRCs present at late stage (stage II/III) with 25% of those presenting at metastatic stage (stage IV) (2).

Rectal cancer is usually adenocarcinoma, occurring in the distal 15 cm of the gastrointestinal (GI) tract as measured from the anal verge (3, 4). Approximately 700,000 cases of rectal cancer are diagnosed globally each year and the annual death toll owing to the disease is approximately 310,000. This equates to 3.9% of all cancer incidence and 3.2% of all cancer deaths (1). Rectal cancer accounts for 35% of all CRC cases within the European Union with 125,000 cases per year (4). There are ~700 cases of rectal cancer diagnosed in Ireland annually. Rectal cancer is more common in males than females in Ireland with approximately two-thirds of all cases presenting in males (2). The incidence of rectal cancer in Ireland is projected to almost double in both genders between 2020-2045 (5). Furthermore, the mortality rate from rectal cancer in Ireland is predicted to increase by almost 25% by 2035 (6). In Ireland, 5-year survival for patients with cancer of the rectum and anus is 63% (2).

Given the anatomical relationship between the colon and the rectum, colon and rectal cancers are often considered the same disease. However, the main difference between the two is the higher rate of local recurrence with rectal cancer (7, 8). This influences treatment, with rectal cancer patients presenting with locally-advanced disease receiving neoadjuvant chemoradiotherapy (neo-CRT) prior to surgery followed by adjuvant chemotherapy, while patients with locally-advanced colon cancers receive surgery followed by chemotherapy if there is nodal involvement or high-risk features (9). Among the reasons cited for increased local recurrence rates in rectal cancer are anatomical

influences. The rectum is located in the posterior pelvis and presents a more technically demanding surgical technique in comparison to surgery for colon cancer. The abdomen has ample room for obtaining wide negative margins, however, the pelvic inlet is narrow thus presenting more difficulty in obtaining the same negative margins for rectal cancer (9).

A further difference between colon and rectal cancers is the greater propensity of rectal cancers to metastasise to the lung, while colon cancer tends to metastasise to the liver (10, 11). Anatomy has been cited as a reason behind this with the inferior rectal vein draining into the inferior vena cava and subsequently into the lungs while the colon drains into the portal vein making the liver the first organ encountered by circulating tumour cells (9). However, there is a lack of data supporting this hypothesis and it is unknown if biological characteristics of the tumour subtypes may also determine metastatic site.

1.1.2 Risk factors for rectal cancer

Historically the risk factors for both colon and rectal cancer have been categorised together. However, the aetiology of colon and rectal cancers differ (12) as do the treatment modalities for both cancers. Regular use of non-steroidal anti-inflammatory drugs are considered protective against rectal cancer (13) and higher circulating vitamin D levels are inversely correlated with rectal cancer risk (14).

There is conflicting evidence in the literature regarding the impact of body mass index (BMI) on rectal cancer risk. A Canadian study reported an increased risk of rectal cancer in both genders for those in the highest quartile of total caloric intake. In the same study, obesity (BMI>30 kg/m^2) was found to be associated with increased risk of rectal cancer in women while a BMI>25 kg/m^2 in men was associated with increased risk of rectal cancer. Given the close association between physical activity, caloric intake and BMI, analysis of the interaction between these factors and their effect on rectal cancer risk found that those in the highest categories of BMI and caloric intake and the lowest categories of physical activity levels were at the highest risk of developing rectal cancer (15). Wei *et al.* also report differential effects of BMI on rectal cancer risk between males and females with females in the highest category of BMI having significantly increased risk of rectal cancer (12). Larsson and Wolk report differential effects of BMI on rectal cancer risk in women when compared to men, with BMI being positively associated with rectal cancer risk in men but not women (16).

Family history of CRC is a confirmed risk factor for the development of CRC with approximately 30% of patients with CRC harbouring a familial component (17). The number of first-degree relatives with CRC and the age at diagnosis, with those with a first degree relative diagnosed before 50 years of age being at increased risk of developing the disease (18). However, it has been reported that the effect of family history on rectal cancer risk is lower than that for colon cancer (19).

1.1.3 Diagnosis and staging of rectal cancer

The diagnosis of rectal cancer involves a digital rectal exam (DRE), full blood count, liver and renal function tests, carcinoembryonic antigen (CEA) and a computed tomography (CT) exam of the abdomen and thorax to establish presence of metastasis (4). Rigid rectoscopy and pre-operative colonoscopy to the caecal pole are required. For early-stage tumours, endoscopic rectal ultrasound (ERUS) may identify early tumours suitable for transanal endoscopic microsurgery (TEM). ERUS is of limited utility for patients with locally-advanced rectal cancer (LARC) (4).

Pelvic magnetic resonance imaging (MRI) is the best test to determine locoregional clinical staging. MRI should be conducted on patients to allow for pre-surgical management of patients as well as determining the extent of surgery (4). **Figure 1.1** summarises the approach to diagnosing rectal cancer. **Table 1-1** depicts the diagnostic workup for primary rectal cancer. **Table 1-2** outlines the staging for rectal cancer.

1.1.4 Treatment for rectal cancer

The treatment for rectal cancer depends on the stage of the cancer. Patients with cT1N0 rectal cancer may be suitable for TEM. Radical total mesorectal excision is appropriate for more advanced rectal cancers including cT2c/T3a/T3b as the risk of recurrence and mesorectal lymph node involvement is high. This involves removal of mesorectal fat and lymph nodes (4).

For intermediate tumours, that is cT3a/3b and cN1-2, the use of neoadjuvant radiotherapy or neoadjuvant chemoradiation (neo-CRT) is controversial as the risk of local recurrence is low provided the surgeon conducts good-quality total mesorectal excision and removes the mesorectal nodes *en bloc* (4). For LARC, (>cT3b) and those with extramural vascular invasion (EMM) patients usually receive neo-CRT.

Two radiotherapy regimes exist for the treatment of rectal cancer; short course preoperative radiotherapy (SCPRT) and long course preoperative radiotherapy (CRT). SCPRT consists of 25 Gy of x-ray irradiation administered over one week followed by immediate surgery within 10 days of completion of SCPRT. CRT is recommended between 45-50.4 Gy x-ray irradiation over 25-28 fractions. In cases where the circumferential resected margin (CRM) is predicted to be positive, a further boost of 5.4 Gy x-ray irradiation in 3 fractions can be given (4). Pre-operative chemotherapy is often combined with neoadjuvant radiation therapy in LARC. Neo-CRT consists of either oral capecitabine or a continuous IV infusion of 5-FU. Where neoadjuvant chemotherapy alone is used the combination is a fluoropyrimidine and oxaliplatin (4). Treatment modalities for rectal cancer are summarised in **Figure 1.2**.

1.1.5 Response rates in rectal cancer

Response to neo-CRT in rectal cancer is classified according to tumour regression grade (TRG)/tumour regression score (TRS), a system that quantifies the presence of residual tumour cells and the extent of fibrosis. In St. James's Hospital, TRS is quantified according to the American Joint Committee on Cancer (20) four-point scale as outlined in **Table 1-3** below. Beddy *et al.* proposed a modified three-point TRG system for classification of rectal cancer patients post-neo-CRT that was significantly associated with outcome in rectal cancer patients (21). Treatment resistance is a considerable problem in rectal cancer tumours with only ~22% of patients achieving a complete pathological response (pCR) to neo-CRT (22), which is the best predictor of long-term outcome for patients (23). In their recent meta-analysis, Kong *et al.* reported that TRG was of prognostic value in predicting long-term outcomes in rectal cancer patients (24). Multiple clinical trials demonstrated a favourable benefit for neo-CRT compared to post-operative chemoradiation for patients with LARC but there was no difference in overall survival observed between the groups (25-28). Patients in the neo-CRT group had reduced toxicities and reduced rates of local recurrence (25-28). Therefore, improving response to neo-CRT in rectal cancer patients will improve long-term patient outcomes.

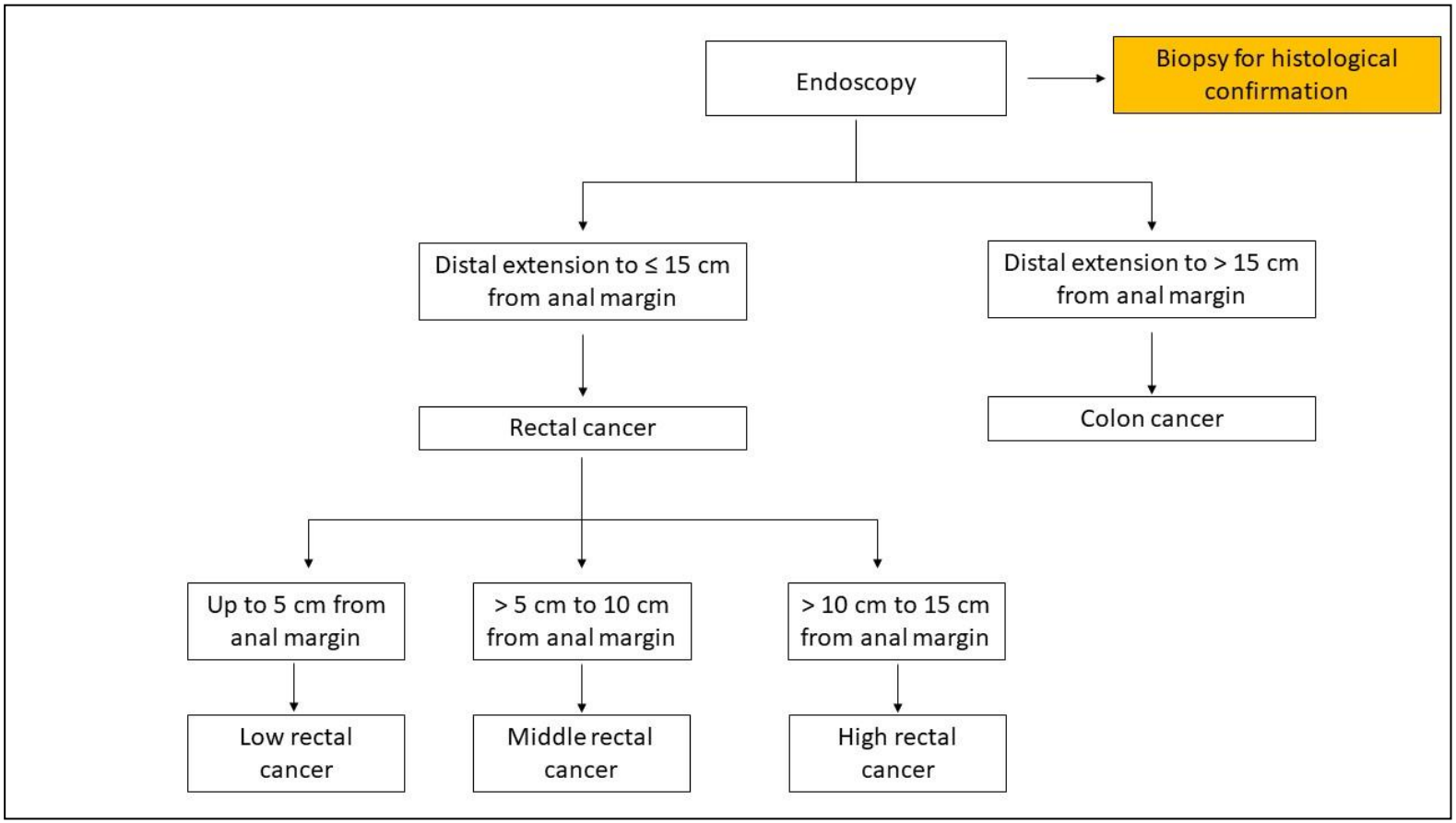

Figure 1.1 Schematic of rectal cancer diagnosis pathway

Schematic illustration of rectal cancer diagnosis pathway. Biopsies are taken at diagnostic endoscopy for histological confirmation. Tumours located > 15 cm from anal margin are colon cancers and those ≤ 15 cm from the anal margin are rectal cancers. Rectal cancers are further classified into low, middle and high based on their distance from the anal margin. Adapted from (4).

Table 1-1 Diagnostic work up in primary rectal cancer. Adapted from (4).

Parameter	**Method of choice**
Location (distance from anal verge)	DRE/palpitation Rigid sigmoidoscopy (Flexible endoscopy)
Morphological verification	Biopsy
cT stage	
Early	ERUS MRI
Intermediate/advanced	MRI (ERUS)
Sphincter infiltration	MRI (ERUS, palpitation, EUA)
cN stage	MRI (CT, ERUS)
M stage	CT, MRI (or US) of the liver/abdomen CT of the thorax PET-CT if extensive EMM for other sites
Evaluation for all patients	MDT discussion

Methods in brackets are less optimal. Abbreviations: CT, computed tomography; DRE, digital rectal examination; EMM, extramural vascular invasion; ERUS, endorectal ultrasound; EUA, examination under anaesthetic; MDT, multidisciplinary team; MRI; magnetic resonance imaging; PET, positron emission tomography; US, ultrasound.

Table 1-2 UICC TNM Classification for colon and rectal cancer. Adapted from (29).

T- Primary tumour	
Tx	Primary tumour cannot be assessed
T0	No evidence of primary tumour
Tis	Carcinoma *in situ*: invasion of lamina propria
T1	Tumour invades submucosa
T2	Tumour invades muscularis propria
T3	Tumour invades subserosa or into non-peritonealised pericolic or perirectal tissues
T4	Tumour directly invades other organs or structures and/or perforates visceral peritoneum
T4a	Tumour perforates visceral peritoneum
T4b	Tumour directly invades other organs or structures
N – Regional lymph nodes	
Nx	Regional lymph nodes cannot be assessed
N0	No regional lymph node metastasis
N1	Metastasis in 1 – 3 regional lymph nodes
N1a	Metastasis in 1 regional lymph node
N1b	Metastasis in 2 – 3 regional lymph nodes
N1c	Tumour deposits in the subserosa, or in non-peritonealised pericolic or perirectal soft tissue without regional lymph node involvement
N2	Metastasis in 4 or more regional lymph nodes
N2a	Metastasis in 4-6 regional lymph nodes
N2b	Metastasis in 7 or more regional lymph nodes
M – Distant metastasis	
M0	No distant metastasis
M1	Distant metastasis
M1a	Metastasis confined to one organ (liver, lung, ovary, non-regional lymph nodes), without peritoneal metastasis
M1b	Metastasis in more than one organ
M1c	Metastasis to the peritoneum with or without other organ involvement

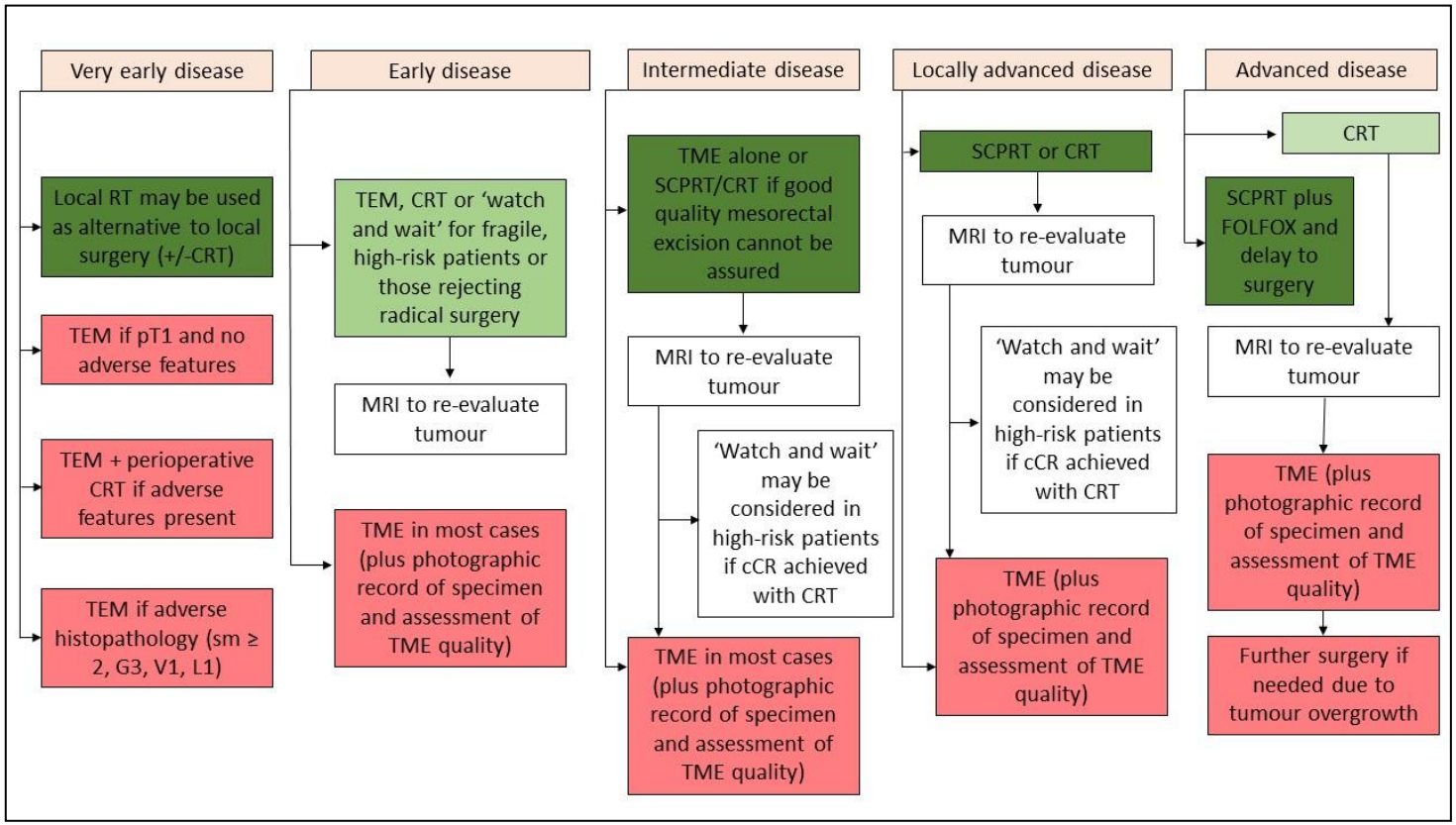

Figure 1.2 Schematic of rectal cancer treatment

Schematic illustration of rectal cancer treatment according to disease stage. Abbreviations: cCR, complete clinical response; CRT, chemoradiotherapy; FOLFOX, leucovorin/fluorouracil/oxaliplatin; RT, radiotherapy; SCPRT, short course pre-operative radiotherapy; TEM, transanal endoscopic microsurgery; TME, total mesorectal excision. Adapted from (4).

Table 1-3 Tumour regression score used in St. James's Hospital, Dublin

Score	Definition
TRS 0	No viable cancer cells
TRS 1	Single cells or small rare groups of cancer cells
TRS 2	Residual cancer with evident tumour regression
TRS 3	No evident tumour regression

1.1.6 Biomarkers of response in rectal cancer

Biomarkers represent a useful tool in the management of cancer in terms of predicting and monitoring treatment response. Numerous biomarkers have been associated with response to neo-CRT in LARC, however none are clinically approved to stratify patients into treatment groups. Clinical biomarkers such as tumour size, clinical T and N stage, distance from the anal verge and time interval between completion of neo-CRT and surgery have been associated with response to neo-CRT in rectal cancer (30). A lower mean distance from the anal verge was observed in patients achieving a pCR (30).

A meta-analysis failed to find predictive value for KRAS mutation status on pCR, tumour downstaging following treatment or cancer related death (31). Mucinous rectal adenocarcinomas also represent a biomarker of poor response to neo-CRT (32). Wild-type p53 has been associated with a good response to pCR (33).

CEA has been extensively studied as a marker of response to neo-CRT in LARC, with higher CEA levels associated with decreased likelihood of achieving pCR. Probst *et al.* conducted a large study of 18,113 rectal cancer patients and found that elevated CEA, classified according to the reference ranges for testing laboratories in each facility, was independently associated with pCR (34). Numerous studies have investigated the connection between elevated CEA and pCR in rectal cancer patients (summarised in (35)). Approximately half of all studies use a cut-off of 5 ng/mL however there has not been a validated cut-off that is predictive of improved response to neo-CRT (35).

Multiple other biomarkers have been investigated. DNA methylation signatures have been associated with disease-free survival (36). Global gene expression profiles have identified gene signatures capable of differentiating responders from non-responders to neo-CRT (37, 38). Expression of numerous other proteins including EGFR, VEGF, p21, Bax, BCL-2, ki67, COX-2, HIF-1α, thymidylate synthase, MMP-9, MMP-2 and E-

cadherin have also been investigated as biomarkers of response to treatment in rectal cancer, however none have been clinically approved (35).

1.1.7 Impact of obesity on treatment response in rectal cancer

The global obesity pandemic presents a huge problem given the association between excess body fatness and risk of certain cancers (39). However, the impact of obesity on cancer does not stop at risk of cancer development, it also plays a role in patient outcome. There are varying reports in the literature on the effect of obesity on treatment outcome in rectal cancer patients. Sun *et al.* have reported that obesity, as measured by BMI, was associated with poorer T downstaging and a higher likelihood of a poorer response to neo-CRT (40). Furthermore, obesity was associated with intraoperative technical difficulties. Patients in the highest BMI category had a longer operative time, were more likely to undergo an open procedure and had higher rates of positive CRM (40). Rates of local recurrence were significantly higher in the most obese group of patients (40).

Visceral obesity as measured by the ratio of visceral adipose tissue (VAT) to subcutaneous adipose tissue (SAT) calculated from CT scans, has been associated with reduced disease-free survival and increased risk of local recurrence (41). Meyerhardt *et al.* reported that obesity was associated with increased risk of local recurrence in male patients but not female patients (42). Seishima *et al*. report favourable outcomes in patients with elevated BMI, including enhanced disease-free survival and reduced risk of distant metastasis in a Japanese cohort of rectal cancer patients (43).

There are several reasons why obese patients may have poorer oncological outcomes. Firstly, dosing of chemotherapeutic drugs may be based on ideal body weight or body surface area for obese patients, although the American Society of Clinical Oncology (ASCO) recommends use of actual body weight for dosing, a systematic review found that dose reductions occurred in 40% of obese patients (44). Secondly, positioning of obese patients for radiotherapy has been cited by Irish radiographers as a difficulty experienced when conducting treatment planning for obese patients. Excess adipose tissue was quoted as causing difficulty in achieving reproducibility (45).

1.2 Oesophageal cancer

1.2.1 Epidemiology and incidence of oesophageal cancer

Oesophageal cancer is the 7th most common cancer worldwide and the 6th leading cause of cancer death (1). Globally there are over 572,000 cases of oesophageal cancer diagnosed per annum, accounting for 3.2% of all cancer diagnoses. The annual death toll from oesophageal cancer stands at 508,000, accounting for 5.3% of all cancer deaths (1).

The annual incidence of oesophageal cancer in Ireland stands at about 475 cases and similar to rectal cancer, is more common in males, with the male to female ratio being almost 2:1. The death toll from oesophageal cancer in Ireland is approximately 400 deaths per annum, making it the 5th most common cause of cancer death in Ireland (2). By 2045, it is estimated that the number of oesophageal cancers diagnosed will increase by over 100% in men and 60% in women (5).

The two main histological subtypes of oesophageal cancer are squamous cell carcinoma (SCC) and oesophageal adenocarcinoma (OAC) and they differ by histology, risk factors and geographical patterns (46). Oesophageal SCC is the predominant subtype, accounting for 88% of all oesophageal cancer cases in 2012, with OAC accounting for only 12% of cases (47). Oesophageal SCC predominates in Eastern and Central Asia, parts of Africa and South America. The disease is typically more common in men than women (69% vs 31%), especially in lower risk countries, however, in countries with increased prevalence of the disease, the ratio of men: women with oesophageal SCC is closer to 1:1 (47). Risk factors for the development of oesophageal SCC include tobacco smoking, alcohol consumption, chewing betel quid and consumption of hot foods and pickled vegetables (reviewed in (47)).

The epidemiology of OAC has changed over the last 30 years. There has been a rapid increase in the rates of OAC in Western countries (47). As with SCC, OAC occurs more commonly in males than in females (47). OAC is an exemplar model of an obesity-associated cancer and this rapid increase in OAC coincides with the rising obesity epidemic (48). Risk factors for the development of OAC include gastroesophageal reflux disease (GERD), obesity and smoking tobacco (49). OAC is a dismal disease with a 5-year survival rate of ~20% (50). Forty percent of OAC patients are diagnosed at a late stage and 5-year survival in these patients is below 3% (51). In Ireland, the 5-year survival

rate for oesophageal cancer is 22%, making it one of the six cancers with the lowest survival rate (2).

1.2.2 Link between OAC and obesity

Obesity is a known risk factor for OAC with a strong positive linear dose response (52). The overall relative risk (RR) of OAC is 1.71 for a BMI falling within the overweight category (25-30 kg/m^2) and the overall RR is 2.34 for BMI ≥30 kg/m^2 (52). It has been estimated that 41% of cases of OAC in males are attributable to overweight and obesity and 4% of OAC cases in females (53).

There are several proposed mechanisms linking obesity and OAC. Firstly, it is postulated that it may be a mechanical mechanism whereby excess abdominal adiposity may be contributing to GERD through increasing intra-gastric pressure and disrupting the gastroesophageal junction and lower oesophageal sphincter (54). This increase in GERD predisposes to development of Barrett's oesophagus, a condition whereby the stratified squamous epithelium of the oesophagus is replaced by a metaplastic columnar epithelium (55), and subsequent OAC. Barrett's oesophagus affects ~2% of the population in Western societies (56), however, only 0.12-0.14% of patients with Barrett's oesophagus go on to develop OAC and this sequence has not empirically shown to be causal (57). OAC development in obese patients has also been shown to be independent of symptomatic reflux, therefore other mechanisms are likely at play (54).

The mechanisms underlying obesity-associated cancers are poorly understood in humans. Most studies have been performed *in vitro* or in animal models (reviewed in (58)). Obesity is a state of chronic inflammation and inflammation is one of the enabling characteristics of cancer (59). Excess adiposity leads to enhanced adipokines and pro-inflammatory cytokines disrupting the balance of pro- and anti-inflammatory signals (reviewed in (58)). Obesity and systemic inflammation have been tightly associated with the development of insulin resistance. The pro-mitogenic and carcinogenic effects of insulin have been extensively studied but are still somewhat unclear (60). Insulin is implicated in pro-tumorigenic signalling in obese individuals (61). Obesity also alters the immune microenvironment (62). We have shown that VAT secretes a plethora of inflammatory cytokines at significantly higher levels than SAT (chapter 6). Also, in patients with increased number and size of adipocytes, areas of hypoxia within the adipose tissue may occur. This in turn leads to upregulation of angiogenesis (63).

Adipokines are altered in obese individuals, most notably, there is a reduction in adiponectin and increased levels of leptin. Adiponectin possesses anti-tumour properties in that it is pro-apoptotic (64), anti-proliferative and inhibits angiogenesis and inflammation (65). Leptin exhibits the direct opposite properties (66). There is a consistent inverse relationship between adiponectin levels (66) and cancer risk, although the epidemiological evidence for leptin is less consistent (67).

1.2.3 Diagnosis and staging of oesophageal cancer

Diagnosis of OAC involves an upper gastrointestinal endoscopy and biopsies taken from suspect areas (68). For poorly differentiated tumours, it is recommended that immunohistochemical staining is performed to determine whether they are SCC or OAC (68). Clinical staging determines the initial treatment of oesophageal cancer and a CT scan of the neck, chest and abdomen should be completed. Endoscopic ultrasound (EUS) should be conducted in patients that are candidates for surgery to determine T and N stages. Positron emission tomography-computed tomography (PET-CT) should be performed in patients prior to oesophagectomy to identify distant metastasis to avoid surgery in these patients (68).

1.2.4 Treatment of oesophageal adenocarcinoma

The treatment for OAC is based primarily on the tumour stage, location, histology, patient performance status and comorbidities (68). The standard of care for locally-advanced OAC is neoadjuvant chemotherapy or neo-CRT with a combination of a platinum and a fluoropyrimidine for 8-9 weeks pre-operatively with or without radiation at a dose of 41.4-50.5 Gy (68). The Neo-AEGIS trial is a phase III multicentre open-labelled, randomised control trial sponsored by Cancer Trials Ireland. Patients with cT2-3, N0-3, M0 adenocarcinoma of the oesophagus or gastroesophageal junction are randomised 1:1 to either the modified MAGIC regimen consisting of epirubicin, cisplatin and 5-FU or epirubicin, cisplatin and capecitabine, or to the CROSS arm consisting of paclitaxel and carboplatin and 41.4 Gy of radiation in 23 fractions (1.8 Gy per fraction) (69). Since the commencement of the Neo-AEGIS trial, the FLOT protocol, consisting of docetaxel, leucovorin, oxaliplatin and 5-FU, has shown superiority to MAGIC in terms of tumour regression in patients with gastric or gastroesophageal adenocarcinoma (70). Therefore, the investigating clinician may decide between FLOT or MAGIC as arm A of the trial. Surgery is performed within 3-10 weeks of completion of neoadjuvant therapy (69). The

modified MAGIC arm of the trial consists of three pre- and three post-operative cycles of chemotherapy, each cycle lasting three weeks. The CROSS arm consists of four and a half weeks of radiation with five weekly cycles of chemotherapy (69). As of October 2020, a total of 371 patients have been recruited to the Neo-AEGIS trial, with 125 patients recruited from St. James's Hospital. Treatment for oesophageal cancer is summarised in **Figure 1.3** and the schematic for the Neo-AEGIS trial is summarised in **Figure 1.4**.

1.2.5 Response rates in OAC

The pathological assessment of resected tumours is conducted according to the Mandard grading system which is a five-point scale as indicated in **Table 1-4** below (71).

The rate of pCR in OAC is low, at best 30% (72). Achievement of pCR is associated with better outcomes in patients, including increased overall survival and disease-free survival (73). Reynolds *et al.* (74) and Donlon *et al.* (75) found that achievement of a node-negative status was more predictive of overall survival than TRG. Powell *et al.* found an association between high neutrophil to lymphocyte ratio and poor response to neo-CRT and overall survival in OAC patients (76).

Table 1-4 Mandard grading system for OAC specimens

Score	Definition
TRG 1	Complete pathological response
TRG 2	Rare residual cancer cells scattered throughout fibrosis
TRG 3	Increase in number of residual cancer cells but fibrosis still predominates
TRG 4	Residual cancer cells outgrowing fibrosis
TRG 5	Complete absence of regression change

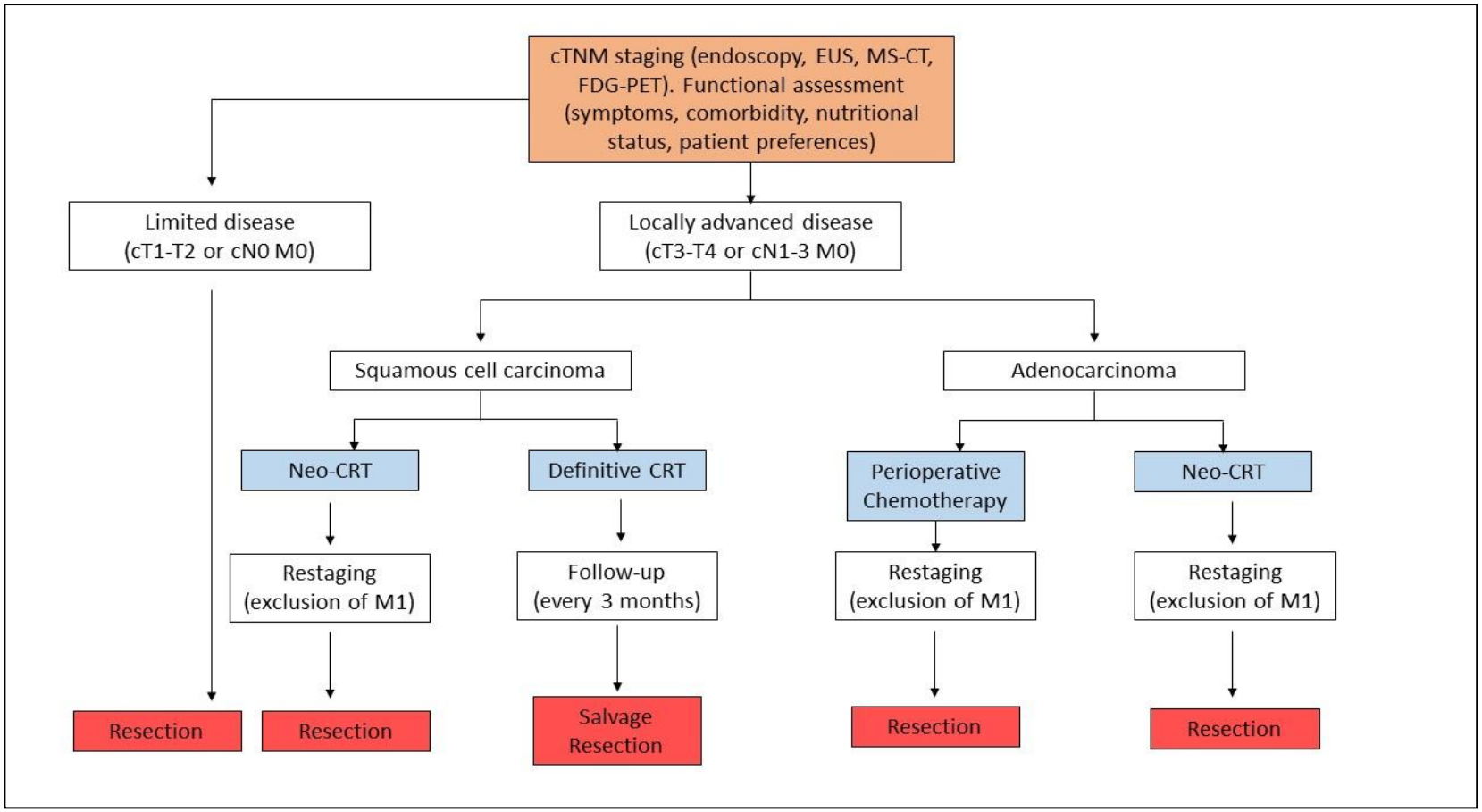

Figure 1.3 Algorithm for treatment of local/locoregional resectable thoracic oesophageal cancer

Schematic illustration of algorithm for treatment of resectable oesophageal cancer. Limited disease is treated by resection. Locally-advanced disease is classified as either a SCC or adenocarcinoma. SCC is treated with neo-CRT or definitive CRT followed by restaging and follow-up, respectively. Adenocarcinoma is treated with perioperative chemotherapy or neo-CRT followed by resection. Abbreviations: CRT, chemoradiotherapy; EUS, endoscopic ultrasound; FDG-PET, fluorodeoxyglucose positron emission tomography; MS-CT, multi-slice computed tomography. Adapted from (68).

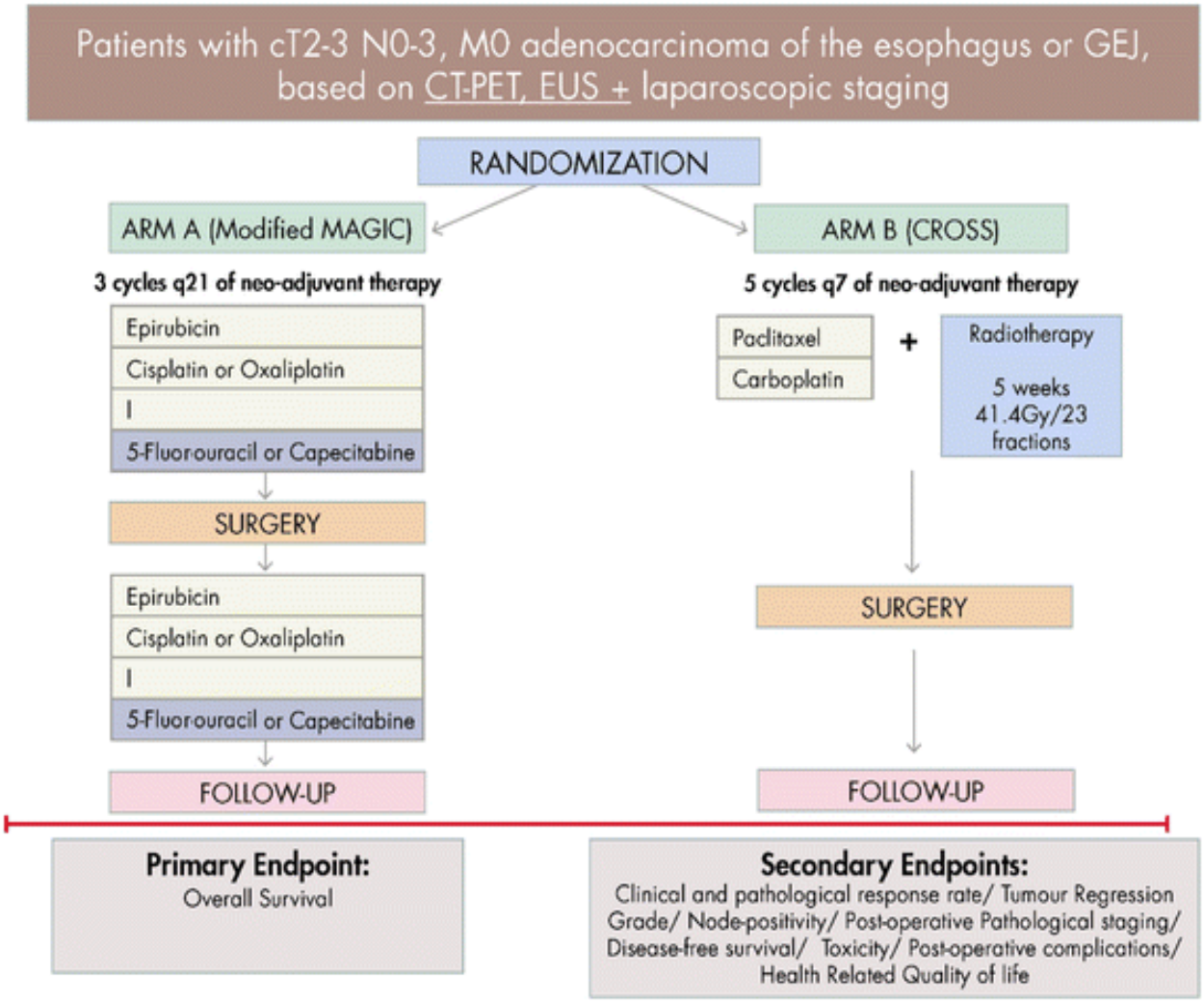

Figure 1.4 Neo-AEGIS trial schematic

Schematic illustration of the Neo-AEGIS trial comprising two arms; the modified MAGIC arm and the CROSS arm. Primary and secondary end-points are also outlined. Abbreviations: CT-PET, computed tomography positron emission tomography; EUS, endoscopic ultrasound; GEJ, gastroesophageal junction. Taken from (69).

1.2.6 Biomarkers of response in OAC

There are no clinically approved biomarkers to predict treatment response in OAC patients. However, a systematic review and meta-analysis of 56 reported biomarkers of response to neoadjuvant treatment in oesophageal cancer reported that low expression of ERCC1, miR-200c, thymidylate synthase and COX-2 and high expression of CDC25B and p16 were associated with predicting response to treatment. VEGF, EGFR, cyclin D1, Bcl-2 and Bax were not associated with predicting treatment response (77). A limitation of this study was the failure to separate oesophageal SCC from OAC, which are different diseases and demonstrate differing responses to cytotoxic therapy (78).

1.2.7 Influence of obesity on treatment response

While the influence of obesity on disease risk in OAC is well-documented, the effect of obesity status on treatment response to chemotherapy and radiation therapy is poorly understood. A study by Mongan *et al.* suggested that overweight or obese OAC patients were more likely to have a better response to neo-CRT compared to patients of a healthy weight (79). This *in vitro* study reported that the addition of adipose conditioned media (ACM) from VAT resulted in an improved radioresponse in a radioresistant OAC cell line, irrespective of the obesity status of the patient or whether or not the patient had cancer (79). Only ACM generated from VAT from patients that received neo-CRT induced radiosensitisation in a radiosensitive OAC cell line (79). These results suggest that radiosensitive and radioresistant tumours may have a differential response to factors secreted from VAT. It appears that in a radioresistant model, the radiosensitising effects are owing to factors secreted from VAT as opposed to cancer effects or bystander effects following cancer treatment (79). The mechanistic basis of this enhanced response is unclear. However, it was possible to discriminate between ACM from non-cancer patients and ACM from a cohort of OAC patients receiving surgery only or a cohort receiving neo-CRT. Higher levels of threonine, lysine and valine and lower levels of glucose were observed in the ACM of OAC patients receiving surgery as their only treatment modality compared to their cancer-free counterparts. When compared to a cohort of OAC patients receiving neo-CRT, the ACM from the non-cancer controls had elevated levels of glucose and reduced levels of threonine, lysine, valine, isoleucine and glycine (79). Given the role of these metabolites in energy metabolism, it suggests that mitochondrial metabolism is altered in the adipose tissue of OAC patients and that neo-

CRT can cause further alterations in this metabolic profile. To date, our understanding of adipose tissue metabolism and its connection to inflammation is scant. However, alterations in metabolism, angiogenesis and inflammatory mediators have previously been shown to be implicated in treatment response in OAC (80). Furthermore, it is known that alterations in factors secreted from adipose tissue from obese OAC patients result in altered cellular metabolism and mitochondrial function (81). Specifically, ACM generated from obese patients had significantly higher levels of lactate and reduced levels of alanine, ethanol, isoleucine, leucine and valine compared to ACM from a non-obese cohort of OAC patients (81). There is a highly dynamic inter-relationship between inflammation and metabolism, wherein cellular metabolites can drive the nature of the inflammatory response, but equally inflammatory signals can disrupt metabolism. Cellular metabolism defines immune cell functionality, wherein anaerobic glycolysis versus oxidative phosphorylation (OXPHOS) promotes a pro-inflammatory milieu (82). Conversely, interrupting immune metabolism inhibits the capability to mount a pro-inflammatory macrophage response (83, 84). Elucidating the metabolic and inflammatory signatures of VAT and SAT may help reveal the mechanisms underlying the observed enhanced response to neo-CRT in overweight and obese patients.

1.3 Radiation therapy as a treatment modality for cancer

Approximately half of all patients receive radiation therapy as part of their cancer treatment and it is estimated that radiation therapy contributes about 40% to curative treatment (85). In addition to being an effective treatment for cancer, radiation therapy is also very cost effective. It has previously been reported as making up approximately 5% of the total cost of cancer care (86). Radiation induces DNA double strand breaks (DNA-DSBs) resulting in the loss of the reproductive integrity of a cell. This damage can occur directly or indirectly through the formation of free radicals via radiolysis of water within the cell. These free radicals in turn induce DNA damage (87).

The successful eradication of tumours by radiation depends on the radiosensitivity of the tumour and the normal tissue tolerance (NTT) of surrounding normal tissue. The tumour lethal dose (TLD) is the dose required to completely eradicate the tumour. This leads to the calculation of the therapeutic index, that is the ratio of NTT/TLD (88). **Figure 1.5** illustrates the tumour control probability and normal tissue complication probability curves, representing TLD and NTT respectively. Doses of radiation for cancer are typically delivered in fractions and this is based on the four R's of radiation therapy; repair, repopulation, redistribution and reoxygenation. Repair allows normal tissue to recover between fractions thus limiting toxicity (89). Repopulation is considered one of the main reasons for treatment failure. Regrowth of tumour cells may occur during fractionation as with the repair of normal tissue comes the repair and regrowth of tumour tissue (90). Redistribution refers to the fact that cells display differential radiosensitivities at different stages of the cell cycle. Cells are most sensitive to radiation in mitosis and most resistant to radiation in S-phase (91). Fractionation allows redistribution of cells in S-phase to more sensitive phases of the cell cycle (92). Reoxygenation of tumours is important as cells in the centre of the tumour are hypoxic and more radioresistant, fractionation of radiotherapy regimens allows these cells to be reoxygenated (89).

There are numerous ways of delivering radiation therapy, but the most common method is external beam radiation therapy. Three-Dimensional Conformal Radiotherapy (3-DCRT) is where the radiation field is conformed to the shape of the area requiring treatment and is particularly useful where the treatment site is near important organs such as in oesophageal cancer, where the target is located close to the heart. Simulation sessions acquire images that are then used to target the tumour and avoid sensitive organs.

This may be achieved through multileaf collimators, which can be moved using the computer to the desired position (88). Intensity-modulated radiotherapy (IMRT) is another mechanism of delivering radiation. This allows customisation of the shape and intensity of radiation delivered to the target treatment area. This results in several intensity modulated radiation fields resulting in a tailored dose of radiation to maximise tumour kill and minimise normal tissue damage (93). Brachytherapy is a method of delivering radiation therapy that involves insertion of a radioactive material inside or directly adjacent to the tumour. This may be used for cancers such as cervical or prostate cancer where a device may be inserted adjacent to the tumour to provide radiation therapy (88).

Radiotherapy is often accompanied by toxicities which can be classified as early or late. Early toxicities are those which occur in rapidly dividing tissues and include skin erythema, diarrhoea and mild odynophagia (94). Late effects can occur months and even years after radiotherapy and damage to the microvasculature and depletion of stem cells are responsible for these effects (95). Such effects include fibrosis, complete dryness of the mouth unresponsive to salivary stimulation and pneumonitis (94).

Another late effect of radiotherapy is the occurrence of secondary cancers. About 19% of adult cancer patients experience a secondary cancer (96) and among those associated with treatment, radiation therapy is estimated to account for only 8% of these secondary cancers (97). An increased occurrence of secondary cancers has been observed in rectal cancer patients that have received radiation therapy. Of note, the most common secondary cancers occurred within the irradiated volume (i.e. the pelvis) and included carcinogenesis of the urinary bladder, prostate and colon (98). This observation is not exclusive to rectal cancer patients. Similar results have been observed in patients treated for carcinoma of the prostate (99, 100), CNS (101), uterus (102) and breast (103), with secondary malignancies occurring within the irradiated field.

Sigurdson and Jones conducted an extensive review of the literature and concluded that mechanisms for radiation-induced cancers in humans remains speculative (104). Also, despite the technological advancements in radiation therapy and the ability to focus radiation therapy to target tissues, the albeit reduced occurrence of secondary cancers within the irradiated volume (102, 105) still remains a problem.

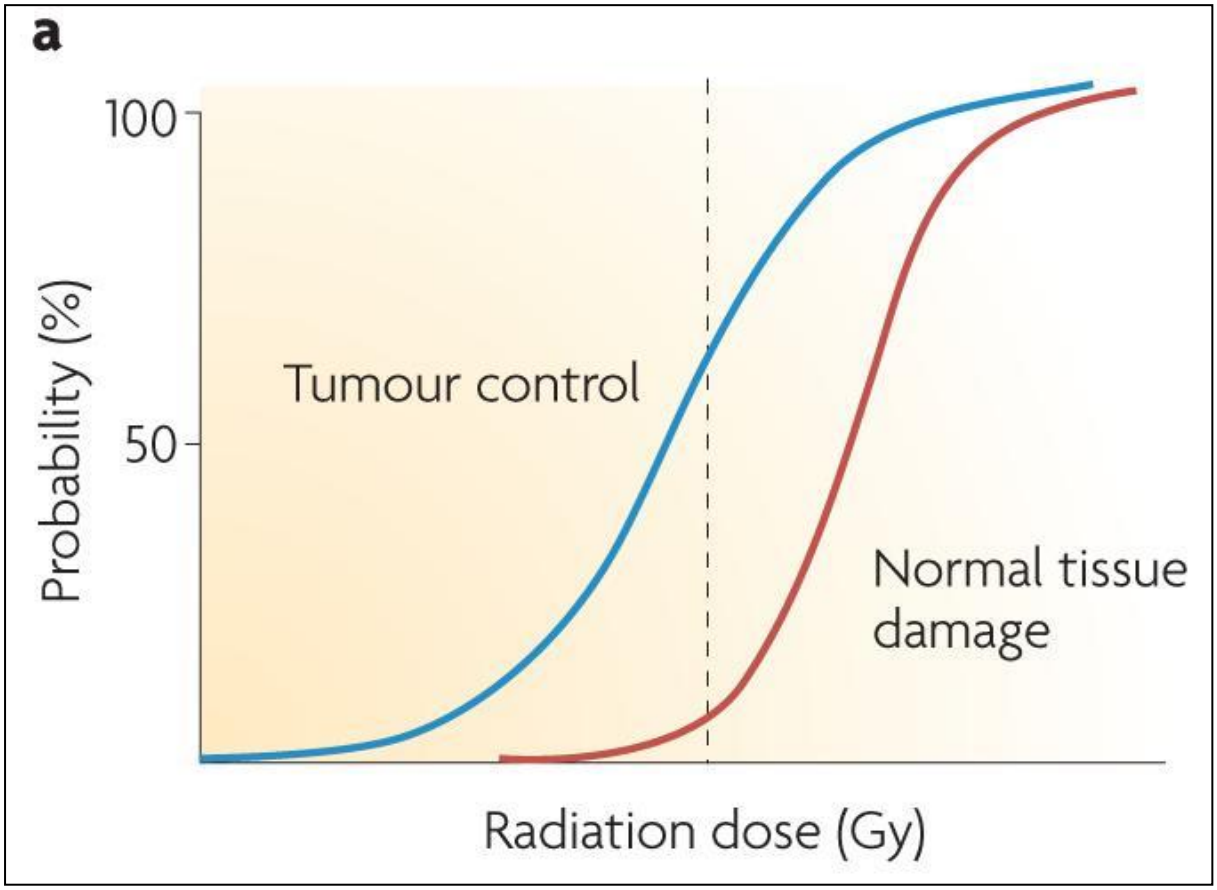

Figure 1.5 Dose response curve for radiotherapy

Tumour control probability is indicated in blue and normal tissue damage is indicated in red. With increasing dose of radiation, the probability of tumour control increases. However, there will be some normal tissue unavoidably included in the treatment volume. The probability of normal tissue damage also increases with increasing dose of radiation. Radiotherapy regimens have been developed to maximise tumour control and minimise normal tissue damage. The dotted line represents the dose associated with ~60% tumour control and ~5% severe late toxicity. Taken from (106).

1.4 The tumour microenvironment

Cancers are not simply a mass of a single cell type but are more like pseudo-organs. The tumour microenvironment (TME) describes the milieu of malignant and non-malignant cells and their interactions. Non-transformed cells, or stromal cells, are recruited to the TME and often possess tumour-promoting functions (107). Communication between cell types within the TME is facilitated, at least partially, by soluble mediators such as inflammatory cytokines, chemokines, growth factors and matrix remodelling enzymes. The TME consists of multiple cell types including T cells, cancer-associated fibroblasts (CAFs), pericytes, B cells, NK cells, tumour-associated macrophages (TAMs), dendritic cells (DCs), myeloid-derived suppressor cells (MDSC) and vascular endothelial cells (108). Hanahan and Coussens have described in their review the evidence linking cells within the TME to the hallmarks of cancer (108). In this review they describe the contribution of infiltrating immune cells, CAFs and angiogenic vascular cells to deregulation of cellular bioenergetics and avoiding immune destruction. The perturbed angiogenic network within tumours can result in hypoxia, altering tumour metabolism. Activated macrophages within tumours have been associated with altered tumour metabolism. CAFs are heavily implicated in dysregulated tumour metabolism, whereby they undergo a metabolic switch to aerobic glycolysis and secrete macromolecular precursors to support cancer cell proliferation (reviewed in (108)). Similarly, infiltrating cells contribute to the immune and inflammatory landscape of tumours. Infiltrating immune cells may exert an immunosuppressive phenotype via regulatory T cells (T regs), MDSCs, TAMs and secretion of immunosuppressive cytokines (reviewed in (108)). Given the involvement of the TME in conferring the hallmarks of cancer upon the tumour, it is unsurprising that the TME is also implicated in treatment response. Cytotoxic therapy may drive stromal cells into senescence and these cells can then continue to secrete factors that confer an advantage upon the cancer cells (109). Alterations in the TME following cytotoxic therapy may exert changes in the milieu of secreted factors. This in turn may favour therapeutic resistance or cancer recurrence (109). A graphical illustration of the TME is presented in **Figure 1.6**.

The evidence presented above highlights the importance of choosing the correct models to study the effects of treatment on tumour response. Due consideration must be given to the tumour as almost a pseudo-organ. Therefore, *ex vivo* models represent a useful tool

for studying cancer biology since they maintain the 3-D architecture of tumours as well as encompassing the entire TME.

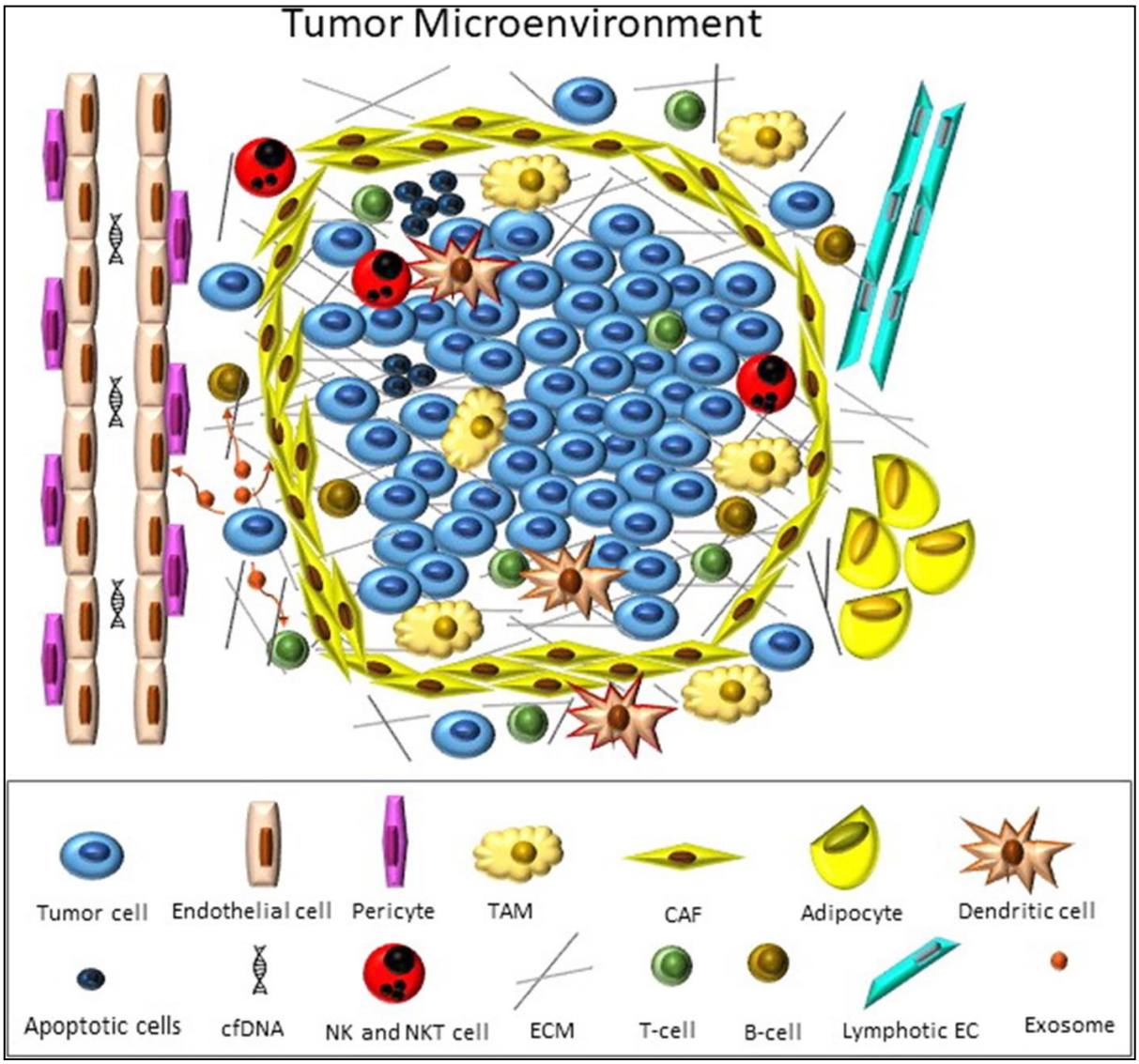

Figure 1.6 The tumour microenvironment

The TME consists of various cell types including endothelial cells, pericytes, tumour associated macrophages (TAMs), cancer-associated fibroblasts (CAFs), adipocytes, dendritic cells, apoptotic cells, cell-free DNA (cfDNA), natural killer (NK) and natural killer T (NKT) cells, extracellular matrix (ECM), T cells, B cells, lymphotic endothelial cells (EC) and exosomes. Taken from (110).

1.5 Metabolism and cancer

Metabolism can be defined as a series of biochemical reactions whereby energy is provided to biological systems. Dysregulated metabolism is a recognised hallmark of cancer (59) and the role of altered metabolism in treatment response has been the topic of much investigation in recent years. Previous work in our group has shown that enhanced OXPHOS is associated with treatment resistance (111), while our group, and others, have demonstrated that a reduction in OXPHOS is associated with an enhanced radioresponse (80, 112-114).

There are several metabolic pathways utilised by cells, but this study focuses on OXPHOS and glycolysis. Under aerobic conditions, non-malignant non-proliferating cells mainly metabolise glucose to carbon dioxide via oxidation of pyruvate in the TCA cycle. NADH is a product of this reaction, which subsequently fuels OXPHOS. This process is efficient in terms of ATP production, yielding 36 molecules of ATP per molecule of glucose, with minimal lactate production. In normal non-transformed tissue under anaerobic conditions, large amounts of lactate are produced through the metabolism of glucose to pyruvate to lactate. This is a less efficient mechanism of ATP production, resulting in 2 molecules of ATP per molecule of glucose and is termed anaerobic glycolysis (115) (**Figure. 1.7**).

Otto Warburg was the first to describe metabolic reprogramming in malignant cells, whereby even in the presence of oxygen, cancer cells exhibited lactic fermentation, a term known as aerobic glycolysis or the Warburg effect (116). In malignant tissue, even in the presence of sufficient oxygen, large amounts of lactate are produced through a process termed aerobic glycolysis. Aerobic glycolysis is an inefficient mechanism of energy production yielding four molecules of ATP per molecule of glucose (115). The metabolism of proliferating non-malignant tissue is analogous to that of cancer cells, utilising the less energy efficient process of aerobic glycolysis. One possible explanation is that inefficient ATP production is only problematic when energy sources are scarce, which is not the case for proliferating normal cells (115). The second reason for the use of inefficient energy production pathways is that proliferating cells require macromolecular precursors for cell division, with glucose and glutamine providing most of the carbon, nitrogen, free energy and intermediate products required. Therefore, converting all of the glucose to carbon dioxide and producing 36 molecules of ATP per

molecule of glucose overruns the energy requirements of proliferating cells but fails to meet the macromolecular requirements (115). Hence, aerobic glycolysis provides sufficient energy in terms of ATP for proliferating cells but also provides macromolecular precursors for biosynthesis in proliferating malignant cells.

The historic view that malignant cells fulfil their bioenergetic requirements solely by anaerobic metabolism has fallen out of favour in recent decades (117). Tumours possess great metabolic plasticity, which may be utilised to produce metabolites to drive oncogenesis (118) or adapt mitochondrial circuitries to function in anabolic or bioenergetic purposes (119). Recent research has shown that ATP derived from glycolysis is highly dependent on cancer cell type and can range from less than 1% to greater than 60%, with the remaining ATP being derived from OXPHOS (120). Interestingly, it has been shown *in vitro* that cell lines cultured in conditions of low glucose exhibit higher rates of OXPHOS and little aerobic glycolysis (121).

1.5.1 Metabolism and treatment response in cancer

Evidence from our group has indicated that higher levels of OXPHOS in OAC is associated with a radioresistant phenotype. In an *in vitro* isogenic model of radioresistance, oxygen consumption rate (OCR), a measure of OXPHOS, was higher in radioresistant cells. This finding was translatable to human tumour samples, with ATP5B, a marker of OXPHOS, being expressed at higher levels in pre-treatment tumour tissue from OAC patients identified as having a poor response to neo-CRT (111). In line with this observation, Buckley *et al.* have demonstrated that a small molecule inhibitor, Pyrazinib, capable of reducing OXPHOS levels in OAC cells enhances radiosensitivity (80). Therapeutic strategies involving the pharmacological targeting of OXPHOS have produced promising results in terms of radiosensitisation (80, 112, 113).

The biguanide metformin, used in the treatment of type 2 diabetes mellitus and has been the subject of much investigation in the field of radiosensitisation in recent years. Metformin inhibits complex I of the mitochondria and therefore reduces OXPHOS (122, 123). Rao *et al.* in their systematic review and meta-analysis concluded that patients with diabetes mellitus and taking metformin had a higher likelihood of achieving a pCR to neoadjuvant treatment and higher 2-year and 5-year overall survival rates compared to patients with or without diabetes not taking metformin (124).

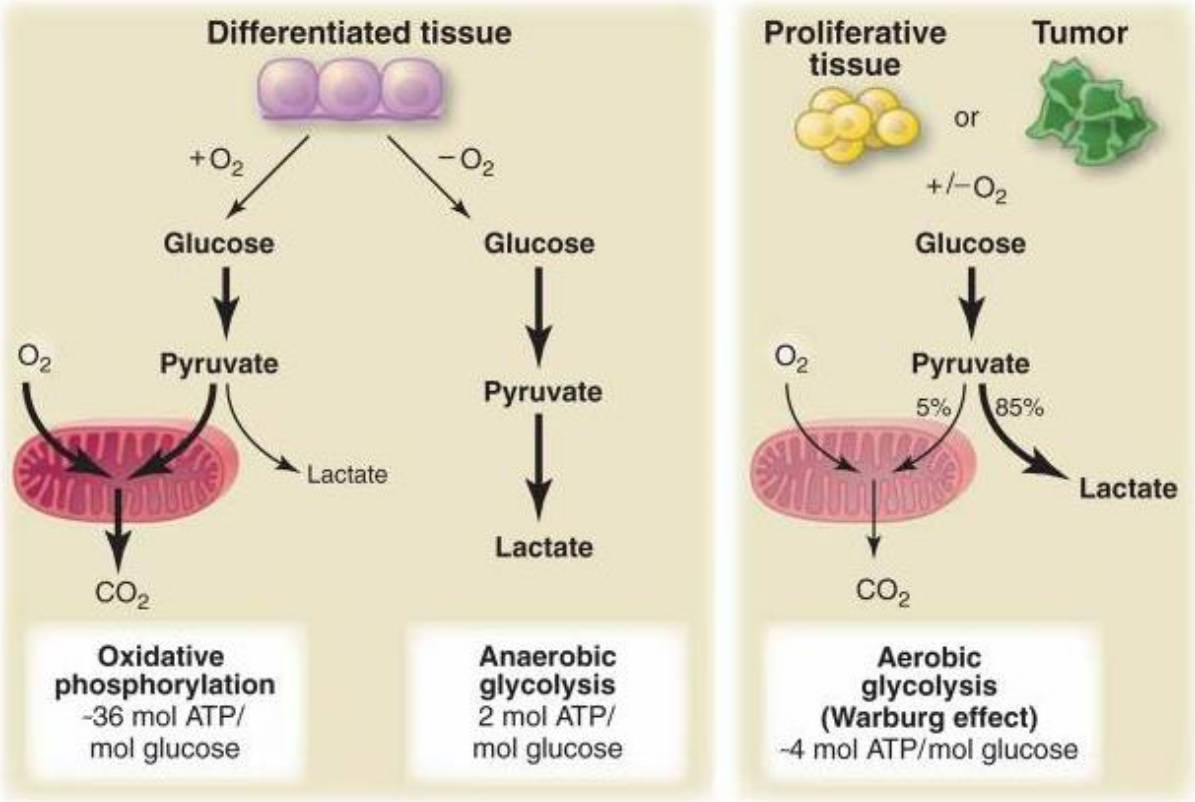

Figure 1.7 Schematic representation of oxidative phosphorylation, anaerobic glycolysis and aerobic glycolysis

Schematic illustration of the differences between OXPHOS, anaerobic glycolysis and aerobic glycolysis (Warburg effect). In differentiated tissue in the presence of oxygen, glucose is metabolised to pyruvate which is then oxidised to CO_2 in the mitochondria in the process of OXPHOS generating ~36 molecules ATP/molecule glucose. In the absence of oxygen, glucose is metabolised to pyruvate, which in turn generates lactate during anaerobic glycolysis, generating 2 molecules ATP/molecule glucose. Proliferating tissue and tumour tissue utilise aerobic glycolysis in the presence of oxygen whereby glucose is converted to pyruvate. The majority of the pyruvate is converted to lactate and a small amount of the pyruvate is oxidised to CO_2 in the mitochondria, generating ~4 molecules ATP/molecule glucose. Taken from (115).

1.6 Inflammation and cancer

Chronic inflammation is associated with cancer, and multiple environmental and lifestyle factors linked to cancer development have an association with chronic inflammation, including chronic infections, obesity, smoking and inhalation of pollutants (125).

Not only is inflammation capable of causing cancer development, but it is also involved in cancer progression, metastasis and treatment response (126). It has long been noticed that immune cells infiltrate tumours at varying densities and recapitulate inflammation observed in normal tissues. Historically this was viewed as an attempt by the immune system to eradicate the tumour, however, in the last two decades it has become increasingly evident that this landscape may be pro-tumorigenic. Such an inflammatory landscape is capable of providing growth factors, DNA damaging agents such as reactive oxygen species (ROS) and survival advantages to neoplastic cells and so inflammation has been termed an enabling characteristic of cancer (59).

Cancer treatment such as radiotherapy and chemotherapy induce cell death in the form of apoptosis but also necrosis, which leads to an inflammatory response. The net result of this inflammatory response is controversial as it may enhance the anti-tumour immune response through cross-presentation of tumour antigens, but it may also lead to a pro-tumorigenic inflammatory response (reviewed in (126)).

The TME consists of multiple immune cells with differing functions including TAMs, which are generally considered pro-tumorigenic, and T cells which depending on their effector function may exert pro- or anti-tumour effects (reviewed in (126)). However, the cytokine and chemokine landscape of the TME may be more relevant than immune cell contents, as these soluble mediators may promote or inhibit tumorigenesis irrespective of their source (127). Cytokines within the TME may activate pro-tumorigenic transcription factors such as NF-κB, STAT-3 and AP-1 and promote angiogenesis (128, 129).

1.7 RIBE and its connections with the hallmarks of cancer

Given the importance of radiation as a treatment modality in both rectal and oesophageal cancer but the very limited pCR rate in both diseases, it is important to understand the effect of radiation on the microenvironment in both of these cancers. Furthermore, gaining an understanding of the effect of radiation and the signals this releases into the microenvironment may yield a greater understanding of radioresistance mechanisms.

The central paradigm surrounding radiation-induced damage was that radiation traversed DNA molecules and deposited energy that induced damage in the irradiated cell leading to mutation, transformation or cell death. (130). However, accumulating evidence has indicated that damage occurs in more cells than are 'hit' directly with radiation. This phenomenon is termed RIBE. RIBE refers to the plethora of biological phenomena occurring in non-irradiated cells as a result of signal transmission from an irradiated cell (131). The cell consequently acts as if it has been irradiated and cell behaviour mimics that of cells that have been directly irradiated, exhibiting signs of increased genomic damage, altered frequency of apoptosis, increased mutagenesis, DNA damage, reduced clonogenic efficiency and oncogenic transformation (132). RIBE signalling occurs via two main mechanisms; gap junctional intercellular communication (GJIC) and release of soluble factors into the extracellular space as illustrated in **Figure 1.8**. The phenomenon was first described as far back as the 1950's (133, 134) but it has been a focus of extensive research since the 1990s in an attempt to elucidate the underlying mechanisms controlling these biological effects. Early reports of RIBE involve the observation of clastogenic factors in the blood of animals and patients that received low-linear energy transfer (LET) irradiation (reviewed in (135)). The investigation of the effect of high-LET radiation at low fluences began in 1992 when Nagasawa and Little observed more sister chromatid exchanges (SCEs) in cells than were directly hit by low fluences of α-particles (136). This effect was reproduced by others (137) and Azzam *et al.* reported that this effect was mediated through GJIC (138).

RIBE events have been poorly defined in the literature with the broad definition being 'bystander effects describe any effect induced in a cell as a result of another cell(s) being exposed to radiation' (139). Experimental studies have reported bystander effects in adjacent cells, a different organ or a different animal model to the irradiated cell

(reviewed in (139)). This led to Blyth and Sykes defining bystander effects as either bystander effects, abscopal effects or cohort effects according to **Table 1-5** below (139).

Experimental methods for studying bystander events consist of cell culture medium transfer experiments, co-culture experiments, partial shielding experiments and use of microbeams (140). Cell culture media transfer experiments involve the irradiation of cells in culture followed by harvesting the media and transfer of this media onto unirradiated bystander cells. Similar to the co-culture experimental technique, RIBE events are owing to soluble factors within the cell culture media. Co-culture experimental techniques are related to media transfer experiments and allow the separation of irradiated and non-irradiated cells in culture to share the same medium (140). Partial shielding experiments involve shielding cells in a proportion of the dish and irradiating the exposed cells (140). This allows comparison of the effects of radiation on the unirradiated (shielded) cells and the directly irradiated cells in the dish. This means that any effects observed in unirradiated cells are owing to a soluble factor within the media, since the cells are not in direct contact to facilitate GJIC. Microbeams allow the precise delivery of a specified dose of radiation to a specified location and can be used to investigate RIBE events (141). Experimental end-points for RIBE have largely looked at genomic instability events (136, 142-144), cell survival assays (145), ROS formation (146) with more recent focus shifting to mitochondrial assays and their involvement in RIBE (147, 148). To date, RIBE has been demonstrated experimentally both *in vitro* and *in vivo* in various cell types (136, 149, 150), tissue explants (151), 3D tissue models (152, 153), fish (154, 155) and rodent (156) models. While experimental data has shown that RIBE induces a range of effects in unirradiated bystander cells, many of which are recognised hallmarks of cancer, the clinical significance of RIBE in cancer patients remains largely elusive.

RIBE appears to be saturated at very low doses and does not appear to follow a linear dose-response relationship as has been repeatedly demonstrated experimentally (157-159), indicating an obvious difference between direct and indirect (RIBE) radiation responses. The models surrounding radiation protection assume a linear no-threshold model (LNT) whereby the dose of radiation is related to the biological effect. The LNT model is used to estimate health risks from low dose radiation (LDR) exposures. The LNT model extrapolates risks from high dose radiation exposures to LDR exposures. The underlying assumption is that the primary cause of radiation-induced cancer is DNA damage, with DNA mutation increasing linearly with increasing dose of radiation.

Therefore, the model assumes that with increasing dose of radiation there is an increased risk of cancer. The model also assumes that ionising radiation always produces adverse health effects and that each ionising event increases health risk proportionally. The response curve was developed using the 'hit theory', whereby only the cells directly traversed by radiation responded to the exposure (reviewed in (160)).

However, there are a number of emerging phenomena at LDR exposures including bystander responses, adaptive responses and genomic instability (161). As defined earlier, bystander responses describe the plethora of biological consequences in unirradiated cells as a result of signal transmission from irradiated cells. An adaptive response occurs where a small priming dose reduces the effect of a subsequent small but larger dose of radiation. Genomic instability occurs where damage to DNA alters it and may cause additional genetic changes in subsequent cell divisions. The significance of these phenomena on cancer risk remains largely elusive (161).

There is also ample evidence to support the anti-tumour effects of radiation occurring via non-targeted radiation effects known as the abscopal effect in animal models, though the phenomenon is a rarer event in patients. The abscopal effect describes an event whereby local irradiation can reduce tumour growth outside the field of radiation (162). Abscopal events differ from bystander events in that abscopal events are observed in areas outside the irradiated volume while RIBE events typically refer to unirradiated cells within an irradiated volume (139). Increasing evidence links RIBE to the hallmarks of cancer and the potential role of RIBE in the therapeutic response. **Figure 1.9** summarises the evidence linking RIBE with the hallmarks of cancer.

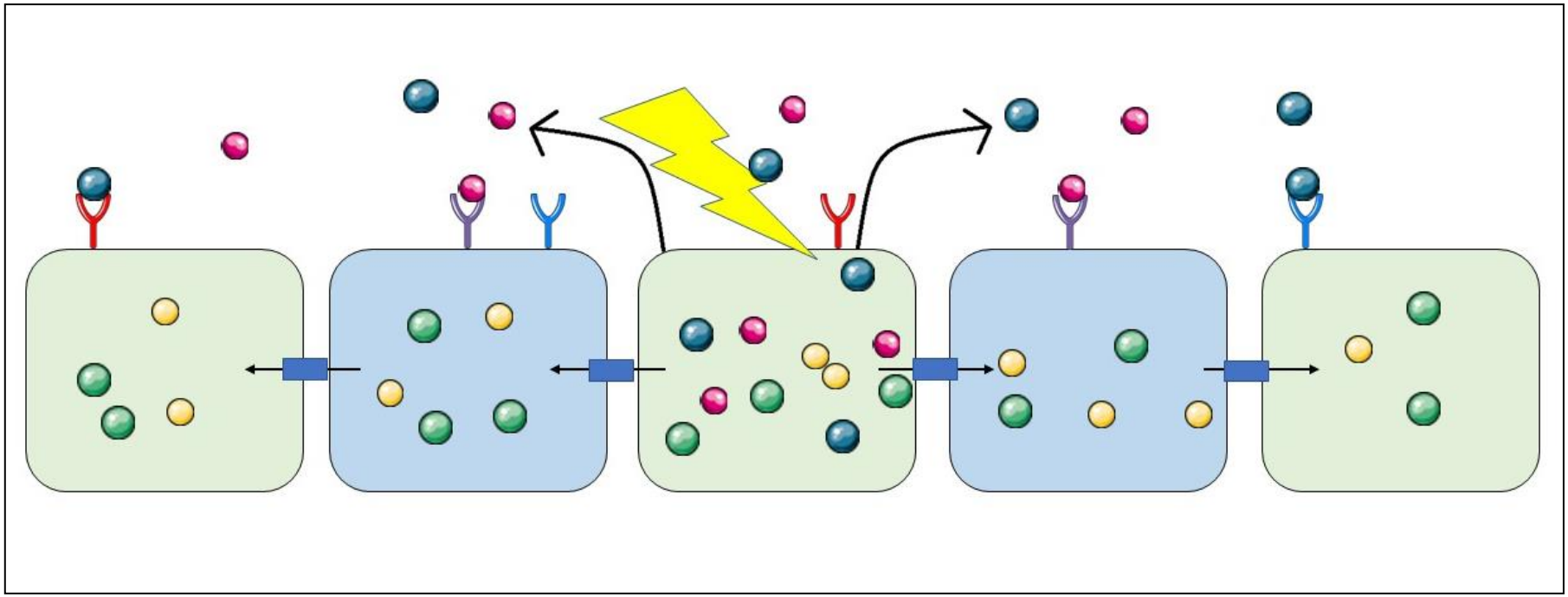

Figure 1.8 Schematic illustration of RIBE signalling mechanisms

RIBE signalling mechanisms occur by gap junctional intercellular communication (GJIC) indicated by black arrows with blue boxes and release of soluble mediators into the extracellular space as indicated by curved arrows and blue and pink circles. GJIC involves the passage of small molecules from one cell to another via transmembrane channels (163). Soluble mediators may be released from cells into the extracellular space and signal to neighbouring cells to exert RIBE effects.

Table 1-5 Radiation-induced signalling effects classified by human exposure scenarios. Taken from (139).

Effect class	Working definition	Exposure type	Dose constraints	Example exposure scenarios
Bystander effects	Radiation-induced, signal mediated effects in unirradiated cells within an irradiated volume	Whole or partial-body exposures	Radiation dose low enough to spare some cells within an irradiated volume from direct energy deposition	-Daily natural background -Inhalation of radon progeny -Security X-ray screening -High altitude flights
Abscopal effects	Radiation-induced effects in unirradiated tissues outside of an irradiated volume	Partial-body exposures	Radiation dose unlimited, but confined to an irradiated volume, sparing tissues outside the volume from direct energy deposition	-Radiotherapy to localized tumour -Physical contact with small radioactive source -Bio-concentration of radionuclide e.g. radioiodine
Cohort effects	Radiation-induced, signal mediated effects between irradiated cells within an irradiated volume	Whole or partial-body exposures	Radiation doses producing multiple irradiated cells within an irradiated volume	-CT scanning -Radiotherapy -Radiation accidents/incidents

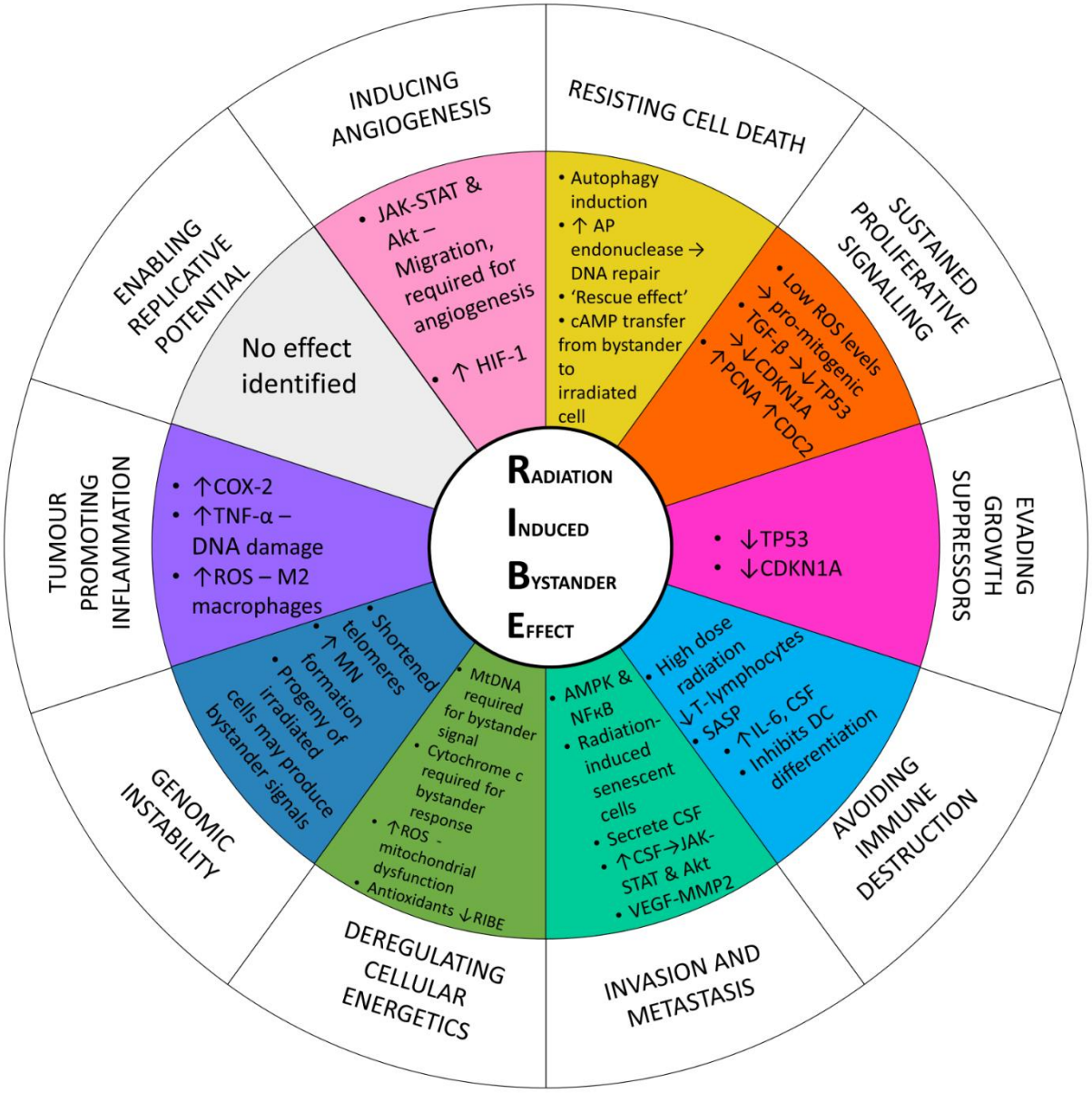

Figure 1.9 RIBE and its connections with the hallmarks of cancer

Schematic illustrating the connection between RIBE and the hallmarks of cancer. RIBE has been linked experimentally to a number of hallmarks of cancer. RIBE has been implicated in **resisting cell death** through induction of autophagy, enhanced DNA repair mechanisms, derivation of a 'rescue effect' from non-irradiated cells through transfer of cAMP and increased expression of anti-apoptotic miRNA. **Sustained proliferative signalling** has been observed in bystander cells and has been associated with low levels of ROS exerting a pro-mitogenic effect and increased PCNA and CDC2. Decreased levels of TP53 and CDKN1A has been linked to **evasion of growth suppressors** in bystander cells. RIBE has been linked to tumour cell immune destruction at low doses of radiation through increased numbers of T lymphocytes but **tumour immune evasion** at high doses of radiation through decreased T lymphocytes. RIBE-induced senescence has been linked to the senescence-associated secretory phenotype (SASP) which may increase GM-CSF and IL-6 leading to immunosuppression. RIBE may play a role in **invasion and**

metastasis through induction of AMPK and NF-κB. SASP may cause secretion of GM-CSF which may in turn activate JAK-STAT-Akt pathway. RIBE has also been associated with increased VEGF and MMP-2. **Deregulation of cellular energetics** may be induced by RIBE as mitochondrial DNA is required for a bystander signal and cytochrome c is required for a bystander response. ROS have also been heavily implicated in RIBE and may induce mitochondrial dysfunction, while antioxidants have been shown to abrogate RIBE. RIBE may play a role in **genomic instability** through shortening of telomeres and thus inducing chromatin-bridge formation. RIBE has been associated with increased micronuclei formation and the progeny of irradiated cells may also be capable of inducing bystander effects. Inflammatory mediators have been shown to be upregulated during RIBE induction including COX-2 and TNF-α linking RIBE to **tumour-promoting inflammation**. Furthermore, ROS may induce M2 macrophages. RIBE may **induce angiogenesis** in tumours owing to activation of JAK-STAT-Akt therefore inducing migration and also through upregulation of HIF-1α. Taken from (164).

1.7.1 Resisting cell death

To enable development of carcinogenesis, tumour cells must evade cell death and tumour suppressor signalling. Cancer cells have multiple mechanisms for resisting cell death including evasion of apoptotic signalling pathways and autophagy. Autophagy is the process whereby a cell self-degrades to eliminate damaged cell components or re-establish homeostatic energy balance during times of physiological stress and this can be both a protective mechanism, promoting tumour cell death but on the other hand it may facilitate tumour growth (165).

Induction of autophagy under certain conditions of stress allows resulting catabolites to be utilised for biosynthesis and growth and thus promote carcinogenesis. Under conditions of severe stress, such as during chemotherapy and radiotherapy, cells have been shown to induce autophagy, which enables tumour cell survival rather than enhancing killing (166). Furthermore, induction of autophagy may cause tumour cells to enter a reversible dormant state (167) which may represent a problem for tumour regrowth at a later stage (59).

Recent studies have implicated autophagy in RIBE. Interestingly, increased levels of autophagy proteins microtubule-associated protein 1 light chain 3 (LC-3) and Beclin-1 have been observed in hepatoma bystander cells eliciting an autophagy response (168). Wang *et al.* have demonstrated that inhibition of LC-3 and Beclin-1 with siRNA resulted in an increase in micronuclei (MN) formation in the hepatoma bystander cells (168). Therefore, it may be possible that autophagy elicits a protective response in bystander cells by minimising the induction of genomic instability. However, given that autophagy may act as a double-edged sword in cancer development and progression, autophagy in this setting may allow damaged cells to enter dormancy and recommence cycling at a later stage. Preliminary studies have demonstrated that using chloroquine derivatives in combination with standard anti-cancer therapy results in more favourable survival outcomes in patients with glioblastoma multiforme (169, 170). Preclinical studies have implicated autophagy in modulating treatment resistance in glioma cells (171, 172).

Enhanced DNA repair presents another mechanism by which RIBE may promote cell death evasion. Iyer and Lehnert observed an increase in radioresistance in human fibroblast cells previously exposed to conditioned media from irradiated fibroblasts. This observed effect was found to occur in conjunction with increases in AP-endonuclease, a

DNA base excision repair enzyme (173). Therefore, RIBE may induce DNA repair mechanisms in irradiated cells thus facilitating cell death evasion.

In 2011 Chen *et al.* discovered another phenomenon closely related to RIBE, known as the radiation-induced rescue effect (RIRE) (174). This occurrence involves the derivation of benefits by the irradiated cells or organism from signals released from bystander cells (174, 175). Chen *et al.* observed a reduction in 53BP1 loci, a reduction in MN formation and an increase in survival in irradiated fibroblasts when they were co-cultured with unirradiated bystander cells. Similarly, co-culture of irradiated HeLa cells with unirradiated fibroblasts resulted in reduced MN formation in HeLa cells (174) therefore suggesting that normal bystander cells can rescue irradiated tumour cells, an observation which may provide an insight into radioresistance mechanisms. He *et al.* recently presented further evidence for this reciprocal bystander effect. Co-culture of irradiated macrophages with unirradiated hepatocytes yielded a reduction in MN formation in the irradiated macrophages. The observed effect was found to arise as a result of cyclic adenosine monophosphate (cAMP) transfer from bystander cells to the irradiated cells (176). Lam *et al.* also speculated that NF-κB may also play a role in the observed effect (177). Further evidence for this rescue effect has been documented in Drosophila whereby activation of the anti-apoptotic microRNA *bantam* protected neighbouring cells from radiation-induced cell death (178). These findings are novel, as previous studies have investigated the effect of directly irradiated cells to confer changes on the bystander cells without consideration to the bi-directional nature of bystander signals. Further evidence of the rescue effect was demonstrated *in vivo* in zebrafish embryos where irradiated zebrafish embryos sharing media with unirradiated zebrafish exhibited a reduced number of γH2AX foci compared to irradiated zebrafish embryos that did not share media with unirradiated zebrafish embryos (179).

Mancuso *et al.* reported a dose-dependent increase in apoptotic cells in the cerebellum of mice that received partial body irradiation. An increase in brain tumorigenesis was also observed in mice exposed to partial body irradiation (180). This study demonstrates the double-edge nature of non-targeted effects of radiation whereby local radiation may induce abscopal anti-tumour effects at distal sites due to increased apoptotic cells. However, local irradiation may also induce tumorigenesis at distal sites.

1.7.2 Sustained proliferative signalling

Fundamental to the development of oncogenesis is the ability of cancer cells to sustain chronic proliferation. Experimental evidence indicates that RIBE is capable of causing enhanced cell proliferation (181). The mechanisms by which this observed phenomenon occurs are unclear, however it appears that contact with irradiated cells may be required in order for bystander cells to exhibit an enhanced proliferative effect (181, 182). This data suggests that, in contrast to other bystander-mediated effects (183, 184), the mechanisms underlying enhanced bystander cell proliferation are not mediated via GJIC or long-range extracellular communication. Observation of enhanced proliferation in rat liver epithelial cells incapable of GJIC provides additional evidence supporting the notion that GJIC does not mediate the observed effect (182).

TGF-β1 appears to be implicated in the observed pro-mitogenic effects of RIBE in normal human diploid lung fibroblasts (185). Iyer and Lehnert have demonstrated that low levels of TGF-β1 co-occur with reduced expression of TP53 and CDKN1A and upregulation of PCNA and CDC2 which in combination appear to drive cellular proliferation in normal human diploid lung fibroblasts (185). Co-culture of SCC cells in the presence of irradiated fibroblasts has also resulted in an increase in SCC cellular proliferation (186).

1.7.3 Evading growth suppressors

In addition to its ability to induce pro-mitogenic responses in cells, RIBE appears to also downregulate tumour suppressors. TP53 is the archetypal tumour suppressor and has exhibited reduced protein expression in cells exposed to media from irradiated cells (185). Moreover, Iyer and Lehnert, in the same experiment demonstrated reduced CDKN1A expression in conjunction with reduced TP53 (185). Human diploid lung fibroblasts exposed to autologous conditioned media from cells irradiated with low dose γ-irradiation exhibited an enhanced clonogenic survival coupled with a reduction in TP53 levels and enhanced AP-endonuclease levels. However, cells treated directly with low dose γ-irradiation demonstrated an increase in TP53 levels and unchanged AP-endonuclease levels thus indicating a differential response to direct and indirect radiation (187). An *in vivo* mouse model involving cranial irradiation and shielding of the body resulted in increased levels of p53 in the spleen of the mouse, in line with increased apoptosis (188). The aforementioned reciprocal effect described by He *et al.* appears to occur in a p53-dependent mechanism whereby cAMP negatively regulates p53 (176).

A study investigating the effect of p53 status in HCT116 colorectal cancer cells on bystander response demonstrated that both wild-type and p53-null cells were capable of responding to autologous bystander signals, exhibiting decreased viability. p53-null cells showed increased apoptosis and MN formation in comparison to their wild-type counterparts, while senescence could only be induced in wild-type bystander cells exposed to autologous bystander signals (189). However, it appears that p53 wild-type cells produce stronger senescence-inducing signals than p53-null cells (189). Therefore, while it appears that wild-type p53 exerts its tumour suppressor function through induction of senescence, senescent cells may subsequently promote tumour growth as will be discussed under the heading 'Avoiding immune destruction'.

The irradiation chimera model provides further evidence for the role of p53 in RIBE events. This model involves the surgical clearance of the mammary epithelium in BALB/c mice followed by whole body irradiation and subsequent transplantation of syngeneic mammary fragments. In contrast to wild-type p53 transplants, p53-null transplants developed palpable tumours in both the irradiated and mock-irradiated groups. Whole body irradiation of mice was found to accelerate tumour growth (190). This study importantly demonstrates the effect of radiation on the microenvironment and its influence on tumour development and aggressiveness. It also demonstrates the role of p53 in modulating tumour development in response to bystander signals.

Camphausen *et al.* demonstrated a dose-dependent abscopal effect in murine models of Lewis lung carcinoma and fibrosarcoma. Hind leg irradiation induced tumour growth delay in tumours at the midline dorsum. This observed effect was found to be dependent on p53 with the abscopal effect only observed in p53 wild-type mice and pharmacological inhibition of p53 also abrogating the abscopal effect (191).

Thus, it is apparent that RIBE may confer an ability to evade growth suppressors and avoid cell cycle arrest upon bystander cells in some model systems. However, there is evidence to suggest that p53 upregulation plays a role in RIBE-induced cell death (188). Therefore, it is possible that RIBE may be a double-edged sword in treatment response and elucidating the mechanisms favouring a shift in p53 status towards a tumour suppressor function may have clinical implications for cancer patients, particularly in terms of development of secondary malignancies and resistance to treatment.

1.7.4 Activating invasion and metastasis

RIBE has been linked to the promotion of invasion in breast cancer cell lines. The phenomenon is thought to occur via activation of AMPK and NF-κB signalling pathways, with inhibition of these pathways, attenuating the invasive potential of the breast cancer cells (192).

PTTG1 is an oncogene associated with tumour invasion and poor prognosis (193, 194). Cells devoid of or that express low levels of PTTG1 enter senescence, an irreversible state of dormancy, after irradiation (195, 196). It has been demonstrated that activation of autophagy activates radiation-induced senescence in cells devoid of PTTG1, with inhibition of autophagy resulting in higher levels of apoptosis in directly irradiated breast cancer cells (197). Senescent cells have been shown to induce RIBE through secretion of CSF2/GM-CSF which promotes invasion and migration with inhibition of senescence blocking CSF-induced bystander effect in breast cancer cells (197). Interestingly, CSF may promote tumour migration as it has been shown to promote migration in *in vitro* lung cancer models (198), while blocking CSF with an antibody impedes migration in bystander cells (197).

Promotion of migration, invasion and tumour survival via phosphorylation of the JAK-STAT and AKT pathways are major signalling pathways in oncogenesis. Conditioned media from irradiated breast cancer cells has been shown to phosphorylate JAK-STAT and AKT via the presence of CSF2 with inhibition of phosphorylation of JAK-STAT and AKT resulting in the loss of the invasive phenotype (197).

In response to radiation, hepatocellular carcinoma cells have been shown to adopt a more invasive phenotype, which also appears to increase invasive potential of neighbouring bystander cells. The bystander effect mediating enhanced invasiveness appears to be controlled through a paracrine mechanism mediated by the VEGF-MMP-2 pathway (199).

Kamochi *et al.* have demonstrated enhanced invasiveness in SCC cells co-cultured with irradiated fibroblasts (186). This more invasive phenotype was accompanied by an increase in expression of several molecules associated with enhanced motility, invasion and proliferation including MMP-1, MMP-9, laminin 5, filamin-A, Raf-1, MEK-1 and ERK1/2 (186). However, it may be possible that this enhanced invasiveness may be cell

type specific because the same invasive phenotype was not observed when HEp-2 cells were investigated in this model system (186).

1.7.5 Inducing angiogenesis

To date, little is understood about the effect of RIBE on promoting angiogenesis. A recent study by Huang *et al.* indicates that conditioned media from irradiated breast cancer cells is capable of inducing angiogenesis in the chorioallantoic membrane assay. Furthermore, phosphorylation of JAK-STAT and AKT in conditioned media-treated HUVECs along with inhibition of endogenous autophagy resulted in increased migration and invasion which is required for angiogenesis. Of note, activation of autophagy inhibited these observed effects (197).

In contrast, tumours arising from irradiated tumour cells co-cultured with non-irradiated cells prior to implantation into a murine model exhibited reduced vascularisation and hampered angiogenesis thus potentially slowing tumour growth. In the same study, cytokine profiling and proteomic analysis revealed a panel of cytotoxic, pro-inflammatory and pro-apoptotic chemokines, cytokines and growth factors in the supernatant of the irradiated cells (200). Among the elevated cytokines were IL-2, VEGF, GM-CSF and PDGF (200), which suggests a pro-angiogenic response but also an anti-tumour immune response. Fontanella *et al.* have also demonstrated an upregulation of HIF-1 in the bystander field (201), which is heavily involved in angiogenesis. The effect of RIBE on angiogenesis is largely not well understood. Perhaps failure to employ appropriate experimental models to investigate *in vitro* and *in vivo* angiogenic effects of RIBE may account for this gap in knowledge. Also, experimental end-points largely focus on genomic instability events or cell death mechanisms.

1.8 RIBE and emerging hallmarks of cancer

1.8.1 Deregulating cellular energetics

Oxidative stress and ROS are well-documented players in the manifestation of RIBE (146, 202-204). ROS can result from endogenous sources such as cell metabolism or exogenous sources causing cellular stress such as chemotherapeutic drugs and radiation therapy. Two important observations prompted interest in the role of the mitochondria in the RIBE response. Firstly, the mitochondria are an important source of ROS within the cell and secondly, the observation that direct DNA damage was not required to elicit RIBE (205) led to an increased interest in other cellular components such as the mitochondria in RIBE.

Experimental evidence has confirmed the involvement of mitochondria in RIBE (147, 148). Interestingly, mitochondria appear to have a dual role in RIBE, firstly they appear to function in producing a bystander signal and secondly, they are involved in the cellular response to the RIBE signal (204, 206). Tartier *et al.* demonstrated that HeLa cells deficient in mitochondrial DNA (mtDNA) are incapable of producing a bystander signal (204). There is conflicting *in vitro* evidence around the role of mtDNA in responding to RIBE signals (204, 206), however, the possibility that the role of the mitochondria in RIBE is cell line specific has not been excluded. Inhibition of mitochondrial function has also been shown to inhibit RIBE signalling and response in human lymphoblastoid cells (206). Thus, it appears that the role of the mitochondria in RIBE is complex and multi-factorial. It appears that the mitochondria may have a dual role in RIBE – generation of a RIBE signal and response to that signal.

Gorman *et al.* have demonstrated that a bystander effect in a novel *ex vivo* model of CRC is capable of inducing increased mtDNA mutations in bystander cells (207). Based on the inverse correlation between ROS levels and random mitochondrial genome mutations, the authors hypothesised that the increased mutation burden was owing, at least partly, to events other than increased ROS levels (207). Interestingly, high levels of ROS have been shown to exert DNA damage, cell cycle arrest and apoptosis, however, low levels of ROS may have pro-mitogenic effects (208). Transmission of RIBE signals via oxidised cell-free DNA (cfDNAox) released from dying cells is an emerging concept (209). cfDNAox increases in cell culture media following irradiation in conjunction with radiation-induced cell death (209). cfDNAox appears to increase intracellular ROS levels rapidly

after exposure which appears to be owing to increased *NOX4* expression (209). This in turn was observed to cause an increase in oxidised nuclear DNA. Antioxidants have been repeatedly shown to attenuate a RIBE response though not completely abrogate it (149, 168, 210). These results are in line with the commonly proposed model that ROS plays an important role in RIBE, but that other signalling pathways and molecules are involved. Also, ROS signalling appears to be short-lived with levels returning to baseline within 24 h of exposure to conditioned media (168), therefore, underscoring the likely participation of other pathways and molecules in these complex RIBE events.

Emerit *et al.* investigated the effect of antioxidants on RIBE in humans. Addition of plasma from workers involved in the Chernobyl disaster to cell cultures of whole blood obtained from healthy donors induced increased levels of chromosomal aberrations compared to plasma from healthy controls (211). Treatment of cases with Gingko Biloba extract, an herbal medicinal product with known antioxidant properties, obliterated clastogenic factors from plasma and eradicated the ability of the plasma to induce chromosomal aberrations on cell cultures when subjects were treated with 3 x 40 mg doses per day for two months (211). While these results are interesting, study numbers were small, and cases were not followed up over time to investigate if the observed eradication of clastogenic factors had any clinical significance. Furthermore, while ROS undoubtedly play a role in RIBE, it is becoming increasingly evident that RIBE is a multifactorial process, therefore further investigation into the utility of antioxidants in mitigating the RIBE response is required.

Extracellular vesicles (EVs) represent another mechanism of RIBE signalling capable of inducing increases in cellular ROS. Unirradiated cells treated with EVs from irradiated cell conditioned media (ICCM) exhibit increased ROS production (212) and enhanced MN formation and 53BP1 loci (213). Rastogi *et al.* have shown that EVs secreted from irradiated Mouse Embryonic Fibroblast (MEF) cells inhibit colony formation in unirradiated bystander MEFs. This effect was diminished upon removal of EVs from the ICCM. This effect is thought to be ROS-dependent as ICCM from irradiated MEFs containing EVs was found to elevate cellular ROS levels in bystander MEFs and treatment with N-acetylcysteine, an antioxidant, restored colony formation ability and reduced cellular ROS levels in the MEFs treated with ICCM from irradiated MEFs (212).

Calcium signalling has been widely reported to play a crucial role in RIBE signalling and response. Increases in intracellular calcium levels appears to be an early response in RIBE events. There appears to be a bidirectional cross-talk between oxidative stress and calcium signalling pathways with inhibition of ROS generating pathways blocking calcium flux (146).

The longevity of RIBE signals cannot be explained by ROS solely. ROS are short-lived and highly reactive molecules. Cytochrome c, a component of the mitochondria essential for ATP synthesis through OXPHOS, also appears to be implicated in RIBE responses. *In vitro* evidence suggests that cytochrome c is not required to produce a bystander signal but MEF cells deficient in cytochrome c do not produce a bystander response (214), which links in with experimental results from Tartier *et al.* (204). An attenuated level of ROS was also observed in cytochrome c deficient MEF bystander cells (214), thus further highlighting the potential involvement of cytochrome c in RIBE. Mitochondrial dysfunction appears to occur in tandem with increased ROS levels, with alterations in mitochondrial membrane potential (mtMP) observed in conjunction with increased ROS levels in human hepatoma cells (168). As discussed previously, RIBE is known to induce autophagy in bystander cells and this is thought to be in response to elevated ROS levels (168).

He *et al.* have demonstrated an increase in cytochrome c in hepatoma cell lines capable of inducing a bystander effect. Inhibition of cytochrome c release with ciclosporin treatment abrogated RIBE events in bystander cells, while administration of exogenous cytochrome c induced bystander events similar to those induced by the irradiated hepatoma cell lines (215).

A recent publication has identified radiation-induced biophoton signalling as a modulator of cellular metabolism (216). HCT116 colorectal cancer cells exposed to biophoton bystander signals had diminished mitochondrial complex I and complex V activity which culminates in the reduction in ATP production thus representing mitochondrial dysfunction (216).

The vast evidence presented thus far makes it impossible to deny the role of ROS in RIBE responses, however, it is apparent that other signalling pathways are involved. Manipulation of ROS levels through use of antioxidants may be of benefit in ameliorating RIBE events but the exact timing or dosage of antioxidants required would be difficult to

decipher. Also, it is important to remember that radiation therapy exerts its cytotoxic effects through DNA damage, which is heavily dependent on the presence of ROS, therefore the implications of antioxidant use would require careful consideration. **Figure 1.10** summarises the involvement of the mitochondria and ROS in bystander events.

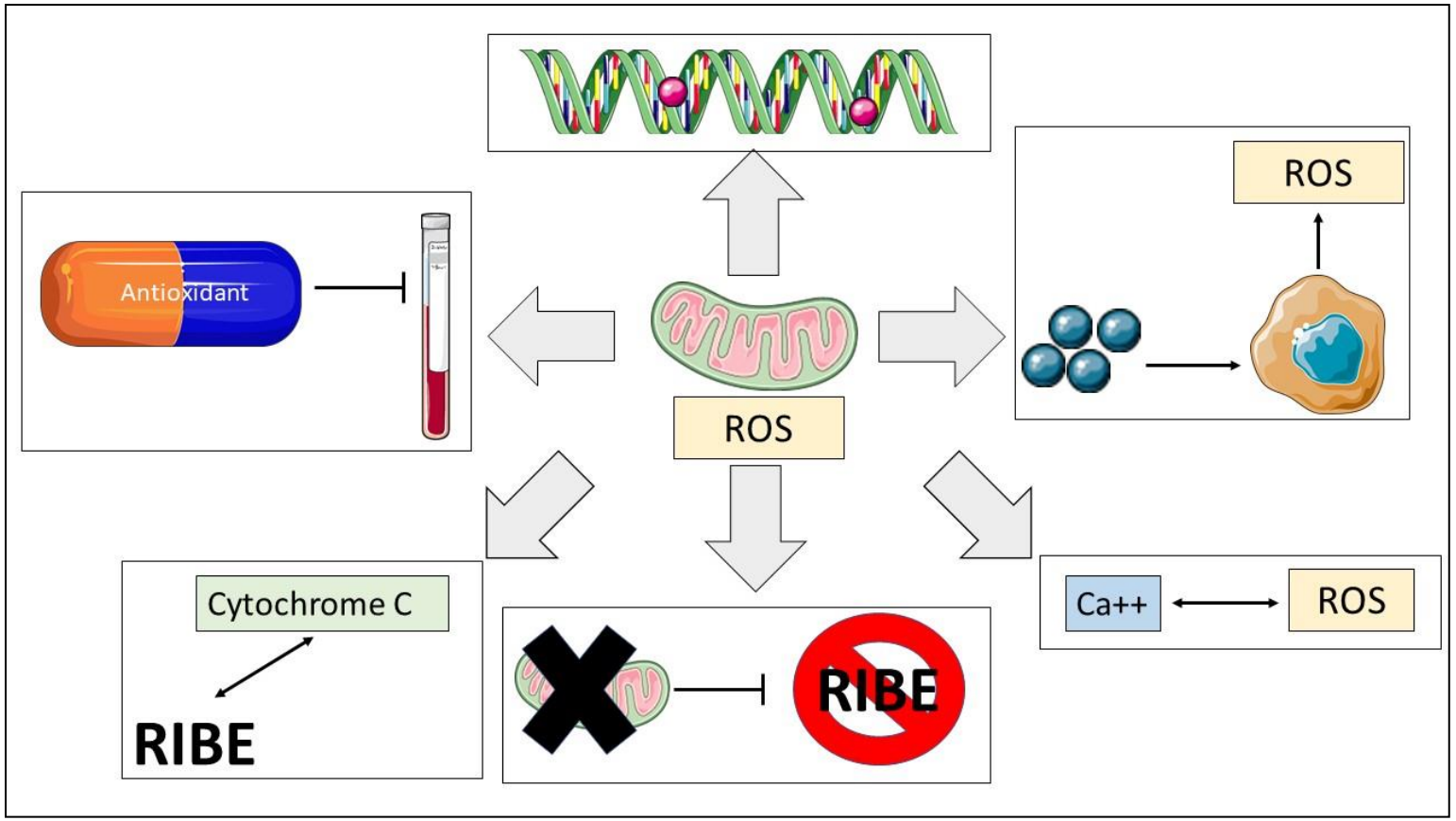

Figure 1.10 Schematic of the involvement of the mitochondria and ROS in RIBE

ROS and the mitochondria are integral to RIBE. The mitochondria are a significant source of ROS. ROS has been implicated in RIBE-induced DNA damage. EVs have been implicated in the RIBE-induced increase in cellular ROS. Calcium fluxes and ROS have an intricate cross-talk in RIBE events. Inhibition of mitochondrial function inhibits RIBE. Cytochrome c plays an important role in RIBE. Treatment with antioxidants reduces clastogenic factors in the blood of radiation-exposed workers.

1.8.2 Avoiding immune destruction

The importance of the immune system in protection against carcinogenesis has been the focus of extensive research in recent years. Evidence for the involvement of the immune system in RIBE in a rat model is presented by Calveley *et al.* where irradiation of the lung resulted in increased inflammatory cytokines both within and outside the radiation field (217).

Liu *et al.* have shown that the ability of irradiated murine macrophages to stimulate murine T lymphocytes through bystander signalling mechanisms depends on the dose of radiation used. Low doses of 0.075 Gy of x-irradiation induce a stimulatory effect on T lymphocytes whereas suppression was observed when the macrophages were irradiated with a higher, more clinically relevant dose of 2 Gy x-irradiation (218).

Another mechanism facilitating RIBE-induced tumour immune evasion is radiation-induced cellular senescence. Cellular senescence is an irreversible state of cell cycle arrest and is considered a tumour suppressive mechanism, whereby damaged cells enter quiescence to suppress tumour growth (219). However, while cellular senescence is considered an anti-tumour mechanism, despite being dormant, these cells remain metabolically active and may undergo alterations in protein expression and cytokine secretion, a phenomenon known as the senescence-associated secretory phenotype (SASP) (219). SASP allows tumours to utilise the secreted proteins as catabolic products to drive tumour growth (220). This SASP phenotype may contribute to RIBE-induced evasion of immune destruction through the secretion of IL-6 and GM-CSF (192). DNA damaged cells entering senescence have been shown to increase secretion of IL-6 (221). The secretion of GM-CSF and IL-6 may represent a mechanism of tumour cell immune evasion due to inhibition of dendritic cell (DC) differentiation (222).

The interplay between RIBE and DCs has not been extensively investigated. Direct irradiation does not alter surface expression of DC maturation markers or DC cytokine secretion in either mature or immature DCs (223). Furthermore, DC-induced T cell proliferation is not altered when the DCs have been directly irradiated. However, when DCs and T cells are co-cultured and directly irradiated, the proliferative capacity of T cells is reduced (223). There is also *in vitro* evidence to suggest that factors secreted from directly irradiated tumour cells may enhance DC function. Kulzer *et al.* have shown that the supernatants of SW480 CRC cells treated with a norm- or hypo-fractionation regimen

of radiotherapy resulted in significant enhancement of DC maturation markers compared to supernatants from mock-irradiated SW480 cells (224). Similarly, increases in DC-secreted inflammatory cytokines including IL-12p70, IL-8, IL-6 and TNF-α were observed in the DCs treated with supernatants from the irradiated SW480 cells (224).

In vivo investigation of the effect of RIBE on splenic lymphocyte populations revealed a RIBE-induced reduction in the number of CD4+ and CD8+ T lymphocytes in recipient mice injected with EVs from directly irradiated mice, while the number of toll-like receptor (TLR) 4 expressing DCs were significantly reduced. In contrast, in directly irradiated mice, the number of TLR4 expressing DCs were significantly increased (225). Given the role of CD4+ and CD8+ T lymphocytes and DCs in anti-tumour immunity, these results may suggest a differential mechanism of immune activation in directly irradiated and bystander systems and may suggest that RIBE impairs anti-tumour immunity.

Anti-tumour immunity has been implicated in radiation abscopal effects (226). There have been several case studies reporting spontaneous and complete resolution of tumours distal from the irradiated volume, i.e. abscopal effects (227-229). Demaria *et al*. have demonstrated that abscopal effects are immune-mediated using a growth factor, Flt3-Ligand in order to enhance the number of DCs and consequently T cell activation in mice with a mammary carcinoma, concluding that T cells are required for distant tumour inhibition induced by radiation (230). Recent advances in immunotherapy have led to the combination of immunotherapy with radiation therapy to enhance this abscopal effect. Pre-clinical models combining anti-PD-1 and anti-PD-L1 immunotherapy with radiation have demonstrated enhanced abscopal effects (reviewed in (231)). Therefore, non-targeted effects of radiation may play a dual role in anti-tumour immunity.

1.9 RIBE and enabling characteristics of cancer

1.9.1 Tumour-promoting inflammation

Cyclooxygenase-2 (COX-2) is involved in the inflammatory process and appears to be upregulated in bystander cells *in vitro* with COX-2 inhibition appearing to abrogate RIBE in normal human lung fibroblast cells (232). However, *in vivo* models failed to demonstrate an effect of COX-2 inhibition on bystander responses in a *Patched-1* heterozygous mouse model (233). Hei *et al.* have proposed a unifying model of bystander signalling involving increased levels of COX-2 culminating in elevated nitric oxide (NO) (234).

Macrophages are thought to be key players in RIBE. One hypothesis is that the response of macrophages is not a result of direct irradiation but owing to phagocytosis of apoptotic cells (235). This may trigger release of TNF-α from macrophages which is capable of inducing DNA damage (236). Lorimore *et al.* have identified a role for macrophages in the RIBE response. Cells exposed to irradiated macrophage conditioned media exhibited cytogenetic aberrations that did not differ from cells exposed to irradiated conditioned media from whole bone marrow (237). It is also possible that macrophages may at least partially contribute to the oxidative stress observed in bystander cells as antioxidant treatment of the irradiated macrophage conditioned media abrogated the observed bystander effects (237). TNF-α may play a role in the observed effect of macrophages on DNA damage (237). TNF-α is a radio-inducible cytokine and has been shown to be involved in the clonogenic survival of bystander lung cancer cells *in vitro*, however, it is possible that this is cell line specific (238). Another mechanism linking macrophages and inflammation to RIBE may be through ROS signalling. ROS is known to induce a shift in macrophage phenotype towards M2, which is closely associated with TAMs (239).

While the clinical impact of the observed contribution of COX-2 to RIBE has not yet been investigated, this observation is interesting from a clinical perspective as pharmacological manipulation maybe possible.

1.9.2 Genome instability and mutation

The phenomenon of chromosomal instability and mutagenesis and its contribution to the development of cancer is well-documented (59, 240). Studies investigating RIBE largely use genomic instability events as experimental end-points, therefore underscoring the

close association between RIBE and genomic instability. Experimental evidence implicating genomic instability in the RIBE process was described as far back as 1992, with the observation of increased number of SCEs in non-irradiated cells neighbouring the irradiated cells (136). Since then, numerous experiments investigating the RIBE effect produced high levels of genomic instability and it was clear that this instability was not a direct consequence of cells being traversed directly by radiation (142-144).

Telomeres are multiple repeat sequences at the end of chromosomes protecting DNA ends from fusion. Over time telomeres become shortened and lose their ability to protect the ends of DNA and this threatens the viability of a cell. Critically shortened telomeres are a feature of many tumours (241), which may lead to chromosomal instability through telomeric fusions, thus contributing to the chromosomal alterations in daughter cells (242). This may in turn trigger the breakage-fusion-bridge cycle, which is thought to be an important player in the development of carcinogenesis (243). Gorman *et al.* have shown that telomere shortening and elevated levels of chromatin bridge formation occur in bystander cells exposed to irradiated tumour conditioned media using a novel *ex vivo* model system of colorectal cancer (159). Overexpression of the mitochondrial antioxidant manganese superoxide dismutase in bystander cells rescued these genomic instability events (159). Interestingly, coinciding with an increase in intracellular ROS induced by increased cfDNAox, was an increase in DNA damage repair pathways (209). Therefore, it appears that cfDNAox may cause short term cell cycle arrest to allow DNA repair mechanisms and antioxidant systems to be activated, but on the other hand, it may also drive genomic instability events. Nuclear Abl was also found to be implicated in RIBE. Irradiation of wild-type MEFs increased nuclear levels of Abl, an effect not observed in MEFs mutated for the nuclear-localisation signals. The EVs produced from mutated MEFs were not capable of inducing ROS production in bystander cells, thus suggesting a role for Abl in RIBE-induced ROS in bystander cells. Rescue of nuclear Abl restored ROS-inducing capacity of EVs (212). Szatmari *et al.* have demonstrated a role for EVs in RIBE induction *in vivo* (225). EVs were isolated from directly irradiated mice and transferred to unirradiated recipient mice and an increase in γH2AX foci was observed in the spleens of the recipient mice and an increase in chromosomal aberrations in the recipient mice (225). These observations underscore the connectivity between oxidative stress and genomic instability. Given the role of telomere shortening and breakage-fusion-bridge cycles in the induction of genomic instability and subsequent

development of carcinogenesis, it may be possible that the induction of genomic instability in bystander cells may contribute to the development of secondary cancers within the irradiated volume.

Genomic instability events induced by RIBE activity appear to be at least partly due to calcium signalling. Lyng *et al.* and Shao *et al.* have demonstrated rapid fluxes of calcium following exposure to ICCM (244, 245) with inhibition of calcium fluxes through use of calcium channel blockers leading to inhibition of RIBE events (244). Interestingly, NO, another molecule with well-documented roles in RIBE signalling, appears to work synergistically with calcium in manifesting RIBE, with inhibition of nitric oxide synthase (NOS) blocking calcium signalling (146). Shao *et al.* have demonstrated that use of an NO scavenger abrogated the increased MN formation observed in bystander cells (205). Similarly, increased cell proliferation, MN formation and DNA-DSBs, mimicking RIBE responses, were observed in bystander cells upon addition of an NO-donor (246). Matsumoto *et al.* have also implicated NO in RIBE-induced radioresistance (247).

The nature of observed genomic instability events differ between cells that have been directly irradiated and bystander cells. Increased frequency of point mutations predominate in bystander cells, whereas partial and whole gene deletions appear more common in irradiated cells (248). Similarly, the progeny of surviving irradiated cells exhibit increased frequency of point mutations (249). Progeny of directly irradiated cells transplanted into animal models are capable of causing neoplastic changes *in vivo* (250). This finding may be of interest in elucidating the causative mechanisms for the development of secondary malignancies following irradiation given the similar pattern of genomic instability between bystander cells and progeny of directly irradiated cells.

The issue of RIBE is further complicated by the fact that the bystander effect appears to be transgenerational. Lyng *et al.* have shown that progeny of irradiated human keratinocytes are capable of producing a bystander signal that elicits a response in bystander cells that does not differ from the response to the original irradiated cell (157). Therefore, it is highly likely that RIBE-induced genomic instability events propagate in the progeny of both the surviving irradiated cells and bystander cells.

As mentioned earlier, secondary cancers pose a risk to patients receiving radiation therapy for a primary cancer. Taken together with the evidence linking RIBE to genomic

instability, these results make it tempting to speculate that bystander cells harbouring point mutations may also be capable of neoplastic transformation *in vivo.*

Adding to the complexity of RIBE, is the observation that genetic differences and environmental factors appear to influence individual response to RIBE. Mothersill *et al.* have previously shown that RIBE responses differ between patients, with some individuals being more sensitive to RIBE than others (251). Interestingly, smokers appear to be less sensitive to RIBE-induced cell death in bystander cells (252). Perhaps RIBE-induced cell death may represent a protective mechanism by which cells with excessive genomic instability or damage are removed. Insensitivity to RIBE-induced apoptosis in smokers may allow damaged cells to propagate and it is tempting to speculate that this may contribute to an increased risk of secondary cancers in these individuals.

Sigurdson and Jones conducted an extensive review of the literature and concluded that mechanisms for radiation-induced cancers in humans remains speculative (104). While, to date, the clinical significance of RIBE is unknown, given the extensive range of genomic instability induced by RIBE, it would not be unreasonable to hypothesise that RIBE may be a contributing factor to the increased risk of secondary cancers adjacent to the irradiated field. Also, despite the technological advancements in radiation therapy and the ability to focus radiation therapy to target tissues, the albeit reduced occurrence of secondary cancers within the irradiated volume (102, 105) still remains a problem.

1.10 Conclusion

This review highlights the potential role for RIBE in carcinogenesis and treatment resistance. RIBE has been strongly linked to multiple hallmarks of cancer including genomic instability, altered cellular energetics, enhanced proliferation and resisting cell death. However, the majority of evidence stems from *in vitro* investigations. While undoubtedly this is essential in elucidating the underlying molecular basis of RIBE in a simple model prior to investigation in a more advanced system, there are shortcomings associated with *in vitro* experimentation. Knockdown of genes may cause deficiencies in other cell signalling pathways, drug treatments used to inhibit pathways can have non-specific side-effects and *in vitro* conditions fail to truly recapitulate physiological conditions. Also, it may be possible that RIBE events are spatially, temporally and genetically orchestrated events.

To date, the clinical significance of RIBE in cancer patients remains largely unknown. Unravelling the molecular basis of RIBE *in vivo* using appropriate models will yield a greater understanding of the clinical implications of RIBE for cancer patients and potentially enable manipulation of the TME to reduce the potentially negative implications associated with RIBE and boost response to radiation treatment *in vivo*. **Table 1-6** summarises the experimental evidence linking RIBE with the hallmarks of cancer.

Table 1-6 Experimental evidence linking RIBE with the hallmarks of cancer

Hallmark of cancer	Experimental evidence	Ref
Resisting cell death	Induction of autophagy	(168)
	Enhanced DNA repair	(173)
	Radiation-induced rescue effect (RIRE)	(174)
	Anti-apoptotic microRNA	(178)
Sustained proliferative signalling	Alterations in TGF-β levels driving mitogenic effects	(185)
Evading growth suppressors	Reduced TP53 levels	(185)
	Enhanced AP-endonuclease levels	(187)
Activating invasion and metastasis	Activation of AMPK and NF-κB	(192)
	SASP phenotype secreting CSF-2	(197)
	Phosphorylation of JAK-STAT and AKT	(197)
	Enhanced invasiveness through VEGF-MMP2 pathway	(199)
	Enhanced expression of MMP-1, MMP-9, laminin 5, filamin-A, Raf-1, MEK-1 and ERK1/2	(186)
Inducing angiogenesis	Phosphorylation of JAK-STAT and AKT	(197)
	Elevation of IL-2, VEGF, GM-CSF and PDGF	(200)
	Upregulation of HIF-1	(201)
Enabling replicative potential	No effect identified	
Deregulating cellular energetics	Cells deficient in mtDNA do not produce bystander response	(204)
	Induction of mtDNA mutations	(207)
	Transmission of RIBE signals via cfDNAox	(209)
	Antioxidants abrogate clastogenic factors in workers involved in Chernobyl disaster	(211)
	EVs from irradiated cells increase ROS in bystander cells	(212)
	Cells deficient in cytochrome c do not respond to bystander signals	(214)
Avoiding immune destruction	Increased IL-6 and GM-CSF may inhibit DC differentiation	(192)
	Reduced CD4+ and CD8+ T lymphocytes in mice following RIBE	(225)
	Off-target effects may have positive effects via the abscopal effect	(227) (228) (229)
Tumour promoting inflammation	Upregulation of COX-2	(232) (234)
	Secretion of TNF-α from macrophages	(236)
Genomic instability and mutation	Increased SCEs	(136)
	Telomere shortening and increased chromatin bridge formation	(159)
	EVs induce enhanced levels of γH2AX in bystander cells	(225)
	NO-induced MN formation	(205)

1.11 Aims and objectives

1.11.1 Overall hypothesis

We hypothesise that RIBE induction will cause alterations in cellular mitochondrial metabolism and mitochondrial function in bystander cells. Moreover, we hypothesise that the normal rectal tissue and rectal cancer tissue inflammatory secretomes and metabolomes will differ, and they will interact differentially with the innate immune system. We hypothesise that radiation will further alter these secretomes. Finally, we hypothesise that visceral and subcutaneous adipose tissue depots will have opposing immune-metabolic signatures with visceral adipose tissue secreting higher levels of inflammatory mediators when compared with subcutaneous adipose tissue.

1.11.2 Overall aim

Investigate the effect of *in vitro* and *ex vivo* RIBE induction on bystander mitochondrial metabolism and mitochondrial function. Examine the effect of radiation in both normal rectal tissue and rectal cancer tissue on the metabolomic and inflammatory landscape of their respective microenvironments and correlate these results with patient clinical characteristics. Profile the immune-metabolic signature of visceral and subcutaneous adipose tissue in OAC patients.

1.11.3 Specific aims of thesis

1. Investigate the effect of *in vitro* RIBE induction using a radioresistant and radiosensitive model of CRC on bystander mitochondrial metabolism, mitochondrial function, radiosensitivity and DNA repair.
2. Investigate the effect of *in vitro* RIBE induction using a radioresistant and radiosensitive model of OAC on bystander mitochondrial metabolism, mitochondrial function, radiosensitivity and DNA repair.
3. Examine the effect of *ex vivo* RIBE induction using a novel human *ex vivo* model of normal rectal tissue and rectal cancer tissue on bystander cellular metabolism and mitochondrial function in rectal cancer cells. Profile the metabolomic landscape of *ex vivo* normal rectal and rectal cancer tissue pre- and post-radiation. Correlate biological end-points examined with patient clinical characteristics.

4. Profile the inflammatory secretome of normal rectal and rectal cancer tissue pre- and post-radiation and examine the interaction between this secretome and the innate immune system. Correlate levels of secreted proteins and DC maturation markers with patient clinical characteristics.
5. Determine the immune-metabolic signatures of visceral and subcutaneous adipose tissue depots using Seahorse technology and the MSD multiplex ELISA platform. Correlate immune secretions with metabolic readouts to generate an immune-metabolic signature. Correlate immune-metabolic readouts with patient clinical characteristics.

Chapter 2 Effect of *in vitro* RIBE induction on bystander cellular mitochondrial metabolism, mitochondrial function and radiosensitivity in a radiosensitive and radioresistant model of colorectal cancer

2.1 Introduction

Radiation therapy is one of the pillars of cancer treatment and involves the delivery of radiation doses to the tumour to induce DNA double strand breaks (DNA-DSBs) and consequently cell death (85). However, it is known that the effects of radiation are not limited to the cells that have been directly 'hit' with radiation. This phenomenon known as the radiation-induced bystander effect (RIBE), is extensively discussed in chapter 1, and describes the altered behaviour in unirradiated cells that are adjacent to irradiated cells (130). This signal transmission may occur via gap junctional intercellular communication (GJIC) or via release of soluble mediators into the extracellular environment (253).

A large proportion of rectal cancer patients receive radiation therapy as part of their treatment (4) however, the complete pathological response (pCR) rate is relatively low with only ~22% of patients achieving a pCR (22). As discussed in chapter 1, the mechanisms underlying this treatment resistance are poorly understood. It is unknown if some off-target effects of radiation may contribute to a radioresistant phenotype.

RIBE end-points have largely focussed on DNA damage and cell death, but it is well-documented that the mitochondria and reactive oxygen species (ROS) play an important role in both RIBE induction and RIBE response (146, 202-204). Not only are the mitochondria important in RIBE, mitochondria are integral to all aspects of carcinogenesis from tumour initiation through to progression, resistance to therapy and regulating cancer stem cell biology (254). Mitochondrial DNA (mtDNA) mutations accumulate in a large number of malignancies (255). Such mtDNA mutations may alter mitochondrial metabolism and promote tumour growth (256) as well as promoting a highly metastatic phenotype (257). Furthermore, the mitochondria have been identified as important players in also regulating treatment response (258, 259).

A phenomenon closely related to RIBE is the radiation-induced rescue effect (RIRE) whereby irradiated cells derive benefits from their unirradiated neighbouring cells (174). This occurrence has been reported in *in vitro* and *in vivo* models including Drosophila (178) and zebrafish (179). The association between this phenomenon and radiation resistance in the clinic has not previously been investigated. One mechanism by which RIRE occurs is as a result of cAMP transfer from the unirradiated to the irradiated cells (176), once again highlighting the importance of the mitochondria in inducing off-target

radiation effects and changes in cell behaviour in response to radiation. Mitochondrial depolarisation and depletion of intracellular cAMP in the bystander cells coincided with restoration of cAMP and reduced micronuclei (MN) formation, indicative of radiation-induced DNA damage, in the irradiated cells (176). The therapeutic importance of RIRE has not yet been elucidated, however, the aforementioned *in vitro* data suggest that it may play a role in radioresistance.

It is apparent that the mitochondria are central and targetable players in the carcinogenic process. To date, the effect of clinically relevant doses of radiation on bystander cellular function has not been elucidated in rectal cancer and it is unknown if RIBE responses differ between radioresistant and radiosensitive cells. Furthermore, the effect of repeated fractions of clinically relevant doses of radiation on bystander cellular activity, and whether this differs from the effect of a single fraction remains elusive. This chapter examined the effect of RIBE induction on bystander cellular metabolism, mitochondrial function, radiosensitivity and cellular proliferation following a single fraction of a clinically relevant dose of radiation and following repeated fractions of a clinically relevant dose of 1.8 Gray (Gy) x-ray radiation. This study was conducted in a model of inherent radioresistance, the SW837 rectal cancer cell line and in an inherent model of radiosensitivity, the HCT116 colon cancer cell line.

2.2 Overall objective and specific aims of chapter 2

The aim of this chapter was to investigate the effect of *in vitro* RIBE induction on bystander cellular metabolism, mitochondrial function and radiosensitivity in a radioresistant and a radiosensitive model of colorectal cancer (CRC).

The specific aims for chapter 2 are;

1. Elucidate the effect of *in vitro* RIBE induction following a single fraction and repeated fractions of 1.8 Gy x-irradiation on bystander cellular metabolism in the inherently radioresistant SW837 rectal cancer cell line and the radiosensitive colon cancer HCT116 cell line.
2. Examine the effect of *in vitro* RIBE induction following a single fraction and repeated fractions of 1.8 Gy x-irradiation on bystander cellular mitochondrial function in SW837 and HCT116 cell lines.
3. Determine the effect of *in vitro* RIBE induction following a single fraction of 1.8 Gy x-irradiation on bystander cellular radiosensitivity in SW837 and HCT116 cell lines.
4. Investigate the effect of *in vitro* RIBE induction following repeated fractions of 1.8 Gy x-irradiation on bystander cellular proliferation in SW837 and HCT116 cell lines.
5. Investigate the effect of *in vitro* RIBE induction following repeated fractions of 1.8 Gy x-irradiation on expression of DNA repair genes in bystander HCT116 cells.

2.3 Materials and methods

2.3.1 Cell culture maintenance

SW837 cells, a rectal adenocarcinoma cell line [American Type Culture Collection (ATCC), VA, USA] were maintained in Leibovitz's L15 Media [Lonza Group Ltd., Switzerland] supplemented with 10% foetal bovine serum (FBS), 1% L-glutamine, 1% penicillin and 1% streptomycin. SW837 cells were maintained in closed-capped 'non-vented' 75 cm^2 Nunc™ EasYFlasks™ at 37°C.

HCT116, a colon carcinoma cell line [ATCC, VA, USA] were maintained in Roswell Park Memorial Institute 1640 (RPMI 1640) [Lonza Group Ltd., Switzerland] supplemented with 10% FBS, 1% penicillin and 1% streptomycin. HCT116 cells were maintained in vented 75 cm^2 Nunc™ EasYFlasks™ at 37°C and 5% CO_2/95% air.

2.3.2 Cell sub-culture

SW837 cells and HCT116 cells were passaged twice weekly upon reaching 70-80% confluence, as estimated by a light microscope. Media, phosphate buffer saline (PBS) and trypsin protease Ethylene Diamine Tetra Acetic Acid (Trypsin-EDTA) [Lonza Group, Switzerland] were heated to 37°C in a water bath. All reagents and utensils were sterilised using ethanol (70% v/v) [Lennox, Ireland] prior to introduction to a grade II sterile laminar hood. Media was discarded from flask and cells were rinsed with 5 mL PBS. Trypsin-EDTA was added to flask to displace adherent cells (1 mL for 25 cm^2 flask and 2.5 mL for 75 cm^2 flask) and incubated at 37°C for 5 min. Cells were hand-detached from flask. An equal volume of complete media was added to flask to neutralise Trypsin-EDTA and a 10 mL sterile pipette [Starstedt, Germany] was used to rinse cells adhering to the base of the flask. SW837 cells were passaged at a 1:3 or 1:4 ratio and HCT116 cells were passaged at a 1:8 or 1:10 ratio depending on experimental requirements.

2.3.3 Cell counting

Cells were trypsinised as previously described. Cell counting was performed using a Bright Line haemocytometer [Hausser Scientific, PA, USA]. Cells were centrifuged at 1300 RPM for 3 min and the supernatant was discarded. The cell pellet was resuspended in 1 mL of complete RPMI 1640. A 20 µL volume of cell suspension was added to 180 µL of trypan blue and mixed by pipetting, and 20 µL of this solution was added to the

haemocytometer. Viable unstained cells were counted in the four corner squares of the haemocytometer. The number of cells/mL was calculated as follows;

Average no. of cells x 10^4 x dilution factor (10)

2.3.4 Cryopreservation of cells

Cells were trypsinised as previously described and the cell suspension was transferred to a sterile 15 mL tube. Cells were centrifuged at 1300 RPM for 3 min and the supernatant was discarded. The cell pellet was resuspended in 3 mL of FBS supplemented with 10% dimethyl sulfoxide (DMSO), a cryoprotectant, and transferred to sterile 2 mL cryotubes, each containing 1 mL of the suspension. Cells were stored in a Mr. Frosty freezing container overnight to gradually lower the temperature of the cells by 1°C per minute to -80°C. Cells were then stored in liquid nitrogen until needed.

2.3.5 Mycoplasma testing

Cell culture supernatant (1 mL) was isolated from a confluent 75 cm^2 flask. The tube was centrifuged at 2000 RPM for 1 min to collect any cell debris.

A polymerase chain reaction (PCR) was set up in 0.2 mL tubes, to contain per reaction:

- 25 µL of Green GoTaq (polymerase enzyme)
- 1 µL of sense primer (10 µM) (5′- GGGAGCAAACAGGATTAGATACCCT-3′)
- 1 µL of anti-sense primer (10 µM) (5′-TGCACCATCTGTCACTCTGTTAACCTC-3′)
- 22 µL of molecular biology sterile grade water
- 1 µL of cell culture supernatant

A mycoplasma PCR negative (molecular biology sterile grade water) and a mycoplasma PCR positive (cell culture supernatant from a mycoplasma contaminated cell line) were included. The PCR reaction was set up as an initialisation set at 95°C for 5 min followed by 40 cycles of a denaturing step at 94°C for 30 s, an annealing step at 55°C for 30 s and an elongation/extension step at 72°C for 1 min followed by a final extension step at 72°C for 10 min.

A 2% agarose gel was made by dissolving 2 g of agarose in 100 mL of Tris acetate EDTA (TAE) buffer and heating in a microwave until the agarose dissolved. SYBR Safe DNA gel stain (10 µL) was added to the agarose mix and the gel was poured into the gel

preparation tank and a 15-well comb was inserted into the mixture. The gel was allowed to set for 30 min at room temperature. Once the gel had set, the gel was placed in the electrophoresis tank and the comb was removed from the gel. TAE buffer was added to cover the gel. PCR-amplified products (18 µL) were added to the wells and the gel was run at 100 V for 1 h. Gel was then imaged on a Fusion Fx imaging system.

2.3.6 Irradiation

Radiation was delivered using an XStrahl RS225 x-irradiator at a dose rate of 1.73 Gy/min (195kV, 15mA) [XSTRAHL, Surrey, UK].

2.3.7 Generation of irradiated cell conditioned media (ICCM)

SW837 and HCT116 cells were seeded in RPMI 1640 complete cell culture media in 6-well plates at a density of $7x10^5$ cells/well and $2x10^5$ cells/well, respectively, and allowed to adhere for 24 h at 37°C and 5% CO_2/95% air. Following 24 h incubation, cells were either mock-irradiated or irradiated with a clinically relevant dose of 1.8 Gy of radiation. Cells were incubated for 24 h following irradiation and ICCM was harvested and stored at -80°C until required.

For ICCM generated from cumulative fractions of radiation, SW837 cells and HCT116 cells were seeded at $2x10^5$ cells/well and $5x10^4$ cells/well in 2 mL of complete RPMI 1640 in a 12-well plate. Cells were allowed to adhere overnight at 37°C and 5% CO_2/95% air. Immediately prior to radiation, media was removed and replaced with 2 mL fresh complete RPMI 1640. Cells were irradiated with 1.8 Gy radiation at 24 h intervals. Cells were incubated for 24 h after mock-irradiation or irradiation and media was harvested and stored at -80°C.

Due to the large volume of ICCM required for clonogenic assays, 75 cm^2 flasks were used to generate ICCM. SW837 cells were seeded in a 75 cm^2 flask at a density of $5x10^6$ cells/flask in complete RPMI 1640. Cells were incubated for 48 h at 37°C and 5% CO_2/95% air. Following 48 h incubation, immediately prior to irradiation, media was discarded from flask and replaced with 13 mL of fresh complete RPMI 1640. Flasks were either mock-irradiated or irradiated with 1.8 Gy radiation and allowed to incubate for 24 h at 37°C and 5% CO_2/95% air. Following 24 h incubation the media was harvested and stored at -80°C until required.

HCT116 cells were seeded in a 75 cm^2 flask at a density of $3x10^6$ cells/flask in complete RPMI 1640. Cells were incubated for 24 h at 37°C and 5% CO_2/95% air. Following 24 h incubation, immediately prior to irradiation, media was discarded from flask and replaced with 13 mL of fresh complete RPMI 1640. Flasks were either mock-irradiated or irradiated with 1.8 Gy radiation and allowed to incubate for 24 h. Following 24 h incubation the media was harvested and stored at -80°C until required.

2.3.8 Crystal violet assay

SW837 cells were fixed in 1% glutaraldehyde in PBS for 15 min at room temperature and HCT116 cells were fixed with 4% paraformaldehyde in PBS at room temperature for 10 min. Fixative was removed and cells were washed twice with PBS and stained with 0.1% crystal violet solution for 30 min at room temperature. Stain was removed and cells were washed twice with H_2O and allowed to air-dry overnight. Cells were incubated with 1% Triton X-100 in PBS on plate shaker for 1 h. Absorbance was read at 595 nm on a VersaMax microplate reader [Molecular Devices, CA, USA].

2.3.9 Seahorse analysis in SW837 and HCT116 cells

SW837 cells were seeded in triplicate at a density of $3x10^4$ cells/well and HCT116 cells were seeded at a density of $1.3x10^4$ cells/well in 24-well XFe24 cell culture microplates [Agilent Technologies, Santa Clara, CA, USA] in a volume of 100 µL and allowed to adhere at 37°C and 5% CO_2/95% air. Following 3 h incubation, an additional 150 µL per well of complete RPMI 1640 cell culture media was added. Twenty-four hours after initial seeding, cells were treated with ICCM and allowed to incubate for 24 h at 37°C and 5% CO_2/95% air. Following 24 h incubation 37°C and 5% CO_2/95% air, ICCM was removed and cells were washed with unbuffered Dulbecco's Modified Eagles Medium (DMEM) supplemented with 10 mM glucose, 10 mM sodium pyruvate and 2% L-glutamine (pH 7.4) and incubated for 1 h at 37°C in a CO_2-free incubator. Oxygen consumption rate (OCR) and extracellular acidification rate (ECAR) were measured using a Seahorse Biosciences XFe24 Extracellular Flux Analyser [Agilent Technologies, Santa Clara, CA, USA]. Three basal measurements of OCR and ECAR were taken over 24 min consisting of three repeats of mix (3 min)/wait (2 min)/measure (3 min) to determine basal respiration and glycolysis. Following the injection of 3 mitochondrial inhibitors oligomycin (2 µg/mL), FCCP (5 µM) and antimycin A (2 µM), 3 additional measures were obtained. All measurements were normalised to cell number using the

crystal violet assay as described in *section 2.3.8*, transferring the eluted stain to a 96-well plate before reading. Metabolic parameters were calculated according to **Table 2-1** below.

Table 2-1 Metabolic parameter calculations

Metabolic parameter	**Calculation**
Basal respiration	OCR at baseline – OCR post-antimycin A
ATP production	OCR at baseline – OCR post-oligomycin
Maximal respiration	OCR post-FCCP – OCR post-antimycin A
Proton leak	OCR post-oligomycin – OCR post-antimycin A
Non-mitochondrial respiration	OCR post antimycin A

2.3.10 Mitochondrial membrane potential measurement

Mitochondrial membrane potential (mtMP) was assessed using the fluorescent probe Rhodamine 123. SW837 cells were seeded at a density of $3x10^4$ cells/well and HCT116 cells were seeded at a density of $1x10^4$ cells/well in a 96-well plate and incubated at 37°C and 5% CO_2/95% air for 24 h. Following 24 h incubation, cells were treated with 100 µL of autologous ICCM for 24 h. Following 24 h incubation ICCM was removed and mtMP was assessed by adding 50 µL of Rhodamine 123 (5 µM) in PBS-Mg and incubated at 37°C for 30 min protected from light. Following 30 min incubation, Rhodamine 123 solution was removed and 100 µL of PBS was added to read the plate. Fluorescence was read on an FLx800 fluorescence microplate reader [Mason Technology Dublin, Ireland] at excitation 485/20 and emission 528/20. All measurements were normalised to cell number using the crystal violet assay, as described in *section 2.3.8*.

2.3.11 Mitochondrial mass measurement

Mitochondrial mass was assessed using the fluorescent probe MitoTracker Green. SW837 cells were seeded at a density of $3x10^4$ cells/well and HCT116 cells were seeded at a density of $1x10^4$ cells/well in a 96-well plate and incubated at 37°C and 5% CO_2/95% air for 24 h. Following 24 h incubation, cells were treated with 100 µL of autologous ICCM for 24 h. Following 24 h incubation, ICCM was removed and mitochondrial mass was assessed by adding 50 µL of MitoTracker Green (0.3 µM) in PBS-Mg and incubated at 37°C and 5% CO_2/95% air protected from light for 30 min. Following 30 min incubation, MitoTracker Green solution was removed and 100 µL of PBS was added to

read the plate. Fluorescence was read on an FLx800 fluorescence microplate reader [Mason Technology Dublin, Ireland] at excitation 485/20 and emission 528/20. All measurements were normalised to cell number using the crystal violet assay, as described in *section 2.3.8*.

2.3.12 Reactive oxygen species measurement

Reactive oxygen species (ROS) was assessed using the fluorescent probe 2'-7'-dichlorofluorescien (2'-7'-DCF). SW837 cells were seeded at a density of $3x10^4$ cells/well and HCT116 cells were seeded at a density of $1x10^4$ cells/well in a 96-well plate at 37°C and 5% CO_2/95% air for 24 h. Following 24 h incubation, cells were treated with 100 µL of autologous ICCM for 24 h. Following 24 h incubation ICCM was removed and ROS was assessed by adding 2'-7'-DCF (5 µM) in PBS-Mg and incubated for 30 min at 37°C and 5% CO_2/95% air protected from light. Following 30 min incubation, 2'-7'-DCF solution was removed and 100 µL of PBS was added to read the plate. Fluorescence was read on an FLx800 fluorescence microplate reader [Mason Technology Dublin, Ireland] at excitation 485/20 and emission 528/20. All measurements were normalised to cell number using the crystal violet assay, as described in section *2.3.8*.

2.3.13 Bromodeoxyuridine (BrdU) proliferation assay

BrdU proliferation assay was used as a surrogate marker of radiosensitivity to examine the effect of RIBE induction following repeated fractions of radiation in bystander cells. SW837 cells were seeded at a density of $2x10^4$ cells/well and HCT116 cells were seeded at a density of $5x10^3$ cells/well in 100 µL complete RPMI 1640 in a 96-well plate and were incubated at 37°C and 5% CO_2/95% air for 24 h. Cells were treated with ICCM for 24 h. Following 24 h incubation in ICCM, cells were either mock-irradiated or irradiated with 1.8 Gy radiation and allowed to incubate for 24 h at 37°C and 5% CO_2/95% air. Cell proliferation was analysed using BrdU proliferation ELISA assay [Roche, Germany] according to the manufacturer's instructions. BrdU labelling reagent was diluted 1/100 in RPMI 1640 and 10 µL was added to each well. The plate was placed on plate shaker for 5 min at 200 RPM to mix contents prior to incubation for 24 h at 37°C. Media was then removed, and the plate was incubated for 10 min at 37°C to dry. Cells were fixed by adding 200 µL of FixDenat per well and incubated for 30 min at room temperature. FixDenat solution was then removed and 100 µL of a 1/100 dilution of anti-BrdU

antibody (diluted in Antibody Dilution Buffer) was added to each well and incubated at room temperature for 90 min. Wells were washed 3 times with 200 µL of 1/10 dilution of washing buffer in deionised water. Substrate (100 µL) was added to each well and incubated at room temperature for 30 min until the colour developed. A 25 µL volume of H_2SO_4 (1 M) was added to each well to stop the reaction. The plate was read within 5 min of adding H_2SO_4 at 450 nm with correction at 690 nm using a VersaMax microplate reader [Molecular Devices, CA, USA]. All ICCM proliferation readings were expressed as a percentage of RPMI 1640 control with RPMI proliferation levels set to 100%.

The initial attempt at performing a clonogenic assay with ICCM resulted in complete obliteration of the cells and colonies did not grow. To assess if this was a true RIBE effect a BrdU assay was used to assess the effect of RIBE induction following a single fraction of radiation on cellular proliferation in SW837 cells also. For this BrdU assay SW837 cells were seeded at $3x10^4$ cells/well. RIBE did not inhibit cellular proliferation in this assay, prompting us to alter the clonogenic protocol and the seeding densities of cells used to generate the ICCM.

2.3.14 Clonogenic assay

SW837 cells were seeded in triplicate in a 6-well plate in complete RPMI 1640 at densities ranging from $3x10^3$ cells/well to $1x10^4$ cells/well depending on the radiation dose delivered (**Table 2-2**). Cells were incubated for 24 h at 37°C and 5% CO_2/95% air. Following 24 h incubation, cells were treated with ICCM from either mock-irradiated or irradiated SW837 cells. Control wells were treated with fresh complete RPMI 1640. Cells were incubated for 24 h at 37°C and 5% CO_2/95% air. Following 24 h incubation, cells were irradiated at the doses ranging from 0 Gy to 6 Gy. Following irradiation, cells were incubated for 9 d. Following 9 d incubation cells were fixed and stained with 25% methanol and 0.05% crystal violet for 30 min at room temperature.

Table 2-2 Seeding densities for SW837 clonogenic assay

Radiation Dose Administered	Cell Number Seeded
0 Gy	3,000
2 Gy	6,000
4 Gy	8,000
6 Gy	10,000

HCT116 cells were seeded in triplicate in a 6-well plate in complete RPMI 1640 at the densities described in **Table 2-3** below. Cells were incubated for 24 h at 37°C and 5% CO_2/95% air. Following 24 h incubation cells were treated with ICCM from either mock-irradiated or HCT116 cells irradiated with 1.8 Gy radiation. Control wells were treated with fresh complete RPMI 1640. Cells were incubated for 24 h at 37°C and 5% CO_2/95% air. Following 24 h incubation, cells were irradiated at the doses outlined below. Following irradiation, cells were incubated for 8 d. Following 8 d incubation cells were fixed with 4% paraformaldehyde for 10 min at room temperature and stained with 0.1% crystal violet for 30 min at room temperature.

Table 2-3 Seeding densities for HCT116 clonogenic assay

Radiation Dose Administered	Cell Number Seeded
0 Gy	500
2 Gy	1,000
4 Gy	2,000
6 Gy	4,000

Colonies consisting of 50 cells or more were counted using the GelCount colony counter. Plating efficiency (PE) was calculated using the following formula:

(No. of colonies formed/No. of cells seeded) x 100

Surviving fraction was calculated using the following formula:

(No. of colonies counted)/(No. of cells seeded x PE)

2.3.15 RNA isolation

HCT116 cells were seeded at a density of $3x10^5$ cells/well in complete RPMI 1640 in 6-well plates and allowed to adhere overnight. Following 24 h treatment with 1.5 mL ICCM per well, cells were collected by trypsinisation and stored at -80°C until required. RNA was isolated from cell lines using the TRI Reagent® method. Cell pellets were retrieved from -80°C and allowed to return to room temperature for 30 min. Samples were resuspended in 0.5 mL TRI Reagent® by repeatedly pipetting solution to ensure complete lysis of cells. Samples were incubated at room temperature for 5 min. Bromochloropropane (50 µL) was added to each sample and the sample vortexed for 10 s. Samples were then centrifuged at 13,400 x g for 15 min at 4°C. The upper aqueous

phase was transferred to a new 1.5 mL Eppendorf tube and 250 µL of isopropanol was added to each tube. Samples were vortexed and incubated at room temperature for 5 min. Samples were then centrifuged at 13,400 x g for 8 mins at 4°C and the supernatant was discarded. RNA pellet was washed in 70% ethanol and centrifuged at 7,500 x g for 5 min at 4°C. The supernatant was discarded, and the pellet was air dried for 5 min. The RNA pellet was resuspended in 30 µL RNase free molecular grade water and stored at -80°C.

2.3.16 RNA quantification

RNA quantification was determined spectrophotometrically using a Nanodrop 1000 spectrophotometer (version 3.1.0, Nanodrop technologies, DE, USA). A 1 µL volume of RNase-free molecular grade water was used to blank the instrument prior to RNA quantification. One microlitre of each sample of isolated RNA was loaded onto the instrument and concentration was measured in ng/µL. 260:280 and 260:230 ratios were recorded to analyse RNA quality.

2.3.17 cDNA synthesis

RNA samples were thawed on ice for 10 min. Total RNA (1 µg) was reverse transcribed to cDNA using the following protocol. Random hexamer primers (1 µL) were added to each total RNA sample and the volume adjusted to 11 µL with RNase free water and centrifuged briefly to pool the contents. Samples were heated to 70°C for 10 min and immediately chilled for 1 min at 4°C. A master mix of reverse transcriptase components was prepared according to **Table 2-4**. Master mix (8 µL) was added to each sample and briefly vortexed. Samples were centrifuged to pool samples and placed in a thermocycler and incubated at 37°C for 1 h then 10 min at 70°C and held at 4°C. Resulting cDNA was stored at -20°C.

Table 2-4 Master mix components for cDNA synthesis

Component	**Volume per sample**
5x reaction buffer	4 µL
dNTP mix (1:1:1:1)	1 µL
RNase out	0.5 µL
Reverse Transcriptase enzyme	0.5 µL
Molecular grade water	2 µL

2.3.18 Quantitative real-time PCR

cDNA reverse transcribed from RNA as described in *section 2.3.17* was used as a template for quantitative real-time PCR. A master mix of PCR components was made up to contain (per PCR reaction): 10 µL of Taqman Master Mix [2X, Applied Biosystems, CA, USA], 8 µL of nuclease-free water, cDNA (1 µL) and 1 µL of Taqman Gene Expression Assay (FAM) probes for *MLH1*, *MMS19*, *PARP1*, *SMUG1* and *18S* were added in duplicate to a 96-well MicroAmp Optical reaction plate. A non-template control using 1 µL of nuclease free water instead of cDNA was included. The plate was sealed using an optical adhesive cover and the plate was centrifuged briefly to pool the contents of each well and eliminate air bubbles. Quantitative real-time PCR was performed using an ABI Quant Studio 5 real-time thermal cycler. The plate was heated to 50°C for 2 min, then 95°C for 10 min followed by 40 cycles of 15 s at 95°C and 1 min at 60°C.

2.3.19 Quantitative real-time PCR data analysis

Data analysis was performed using the $2^{-\Delta\Delta Ct}$ relative quantification method (260). The threshold cycle (Ct) was calculated for each well and the expression levels of target genes were normalised to the expression of the endogenous control (*18S*). Gene expression levels were only reported if the transcript amplified before 35 cycles.

2.3.20 Statistical analysis

Statistical analysis was performed using GraphPad Prism 5 Software [GraphPad Software, CA, USA]. All data is expressed as mean ± SEM. Statistical tests used are indicated in the relevant figure legend. Statistical significance was considered at $p<0.05$.

The methodology employed in this chapter is summarised in **Figure 2.1**.

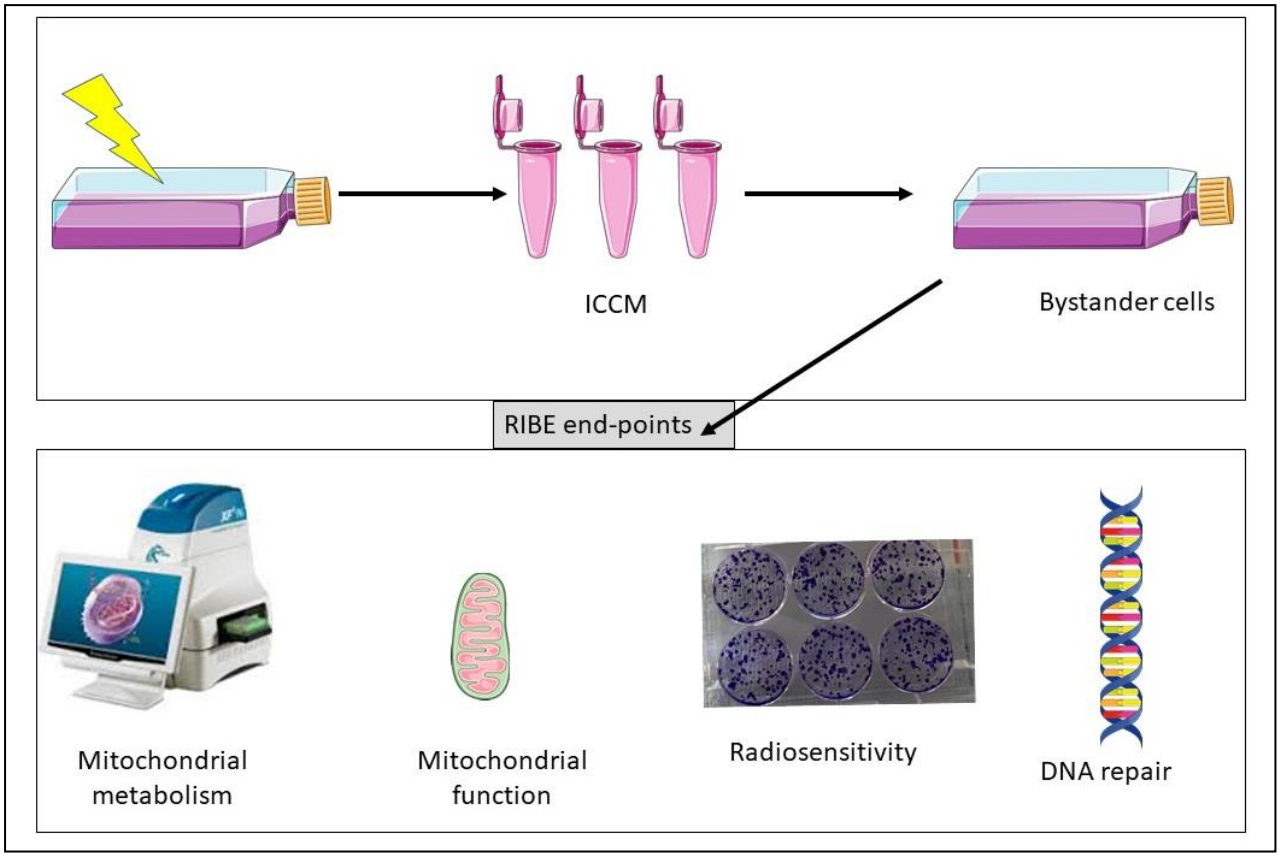

Figure 2.1 Schematic illustration of methodology employed in chapter 2

SW837 and HCT116 cells were either mock-irradiated or irradiated with 1.8 Gy radiation and incubated for 24 h. Following 24 h incubation ICCM was harvested. SW837 and HCT116 bystander cells were treated with ICCM for 24 h and RIBE end-points including mitochondrial metabolism, mitochondrial function, radiosensitivity and expression of DNA repair genes were assessed.

2.4 Results

Investigate the effect of *in vitro* RIBE induction on bystander cellular mitochondrial metabolism, mitochondrial function and radiosensitivity in a radioresistant model, the SW837 rectal cancer cells and a radiosensitive model, the HCT116 colorectal cancer cell line.

The mitochondria and ROS have been extensively linked to RIBE (146, 202-204). Therefore, we investigated the effect of RIBE induction *in vitro* on bystander cellular metabolism in both a radioresistant and a radiosensitive model. The Seahorse technology allows measurement of various components of cellular metabolism in real-time, allowing us to assess the levels of oxidative phosphorylation (OXPHOS) and glycolysis in both cell lines. Cells may also be treated with various mitochondrial complex inhibitors to assess the capacity of the cells to produce ATP, their level of maximal respiration and the extent of non-mitochondrial respiration occurring in cells.

Investigating the effect of RIBE induction *in vitro* on bystander cellular mitochondrial metabolism, mitochondrial function and radiosensitivity in a radioresistant rectal cancer cell line

2.4.1 RIBE induction *in vitro* does not alter OCR, ECAR or OCR:ECAR ratio in bystander SW837 cells

Oxygen consumption rate (OCR), a measure of OXPHOS was not significantly different in bystander SW837 cells exposed to ICCM from irradiated or mock-irradiated SW837 cells (p=0.31). As we did not see alterations in the OXPHOS pathway, we examined the effect of RIBE induction on glycolysis as measured by ECAR. ECAR did not differ significantly between SW837 cells treated with ICCM from irradiated or mock-irradiated SW837 cells (p=0.10). OCR:ECAR ratio remained unchanged between SW837 bystander cells treated with ICCM from either irradiated or mock-irradiated SW837 cells (p=0.77) (**Figure 2.2**).

2.4.2 RIBE induction *in vitro* does not alter basal respiration, ATP production, maximal respiration, proton leak or non-mitochondrial respiration in bystander SW837 cells

Basal respiration levels remained unchanged in SW837 cells treated for 24 h with ICCM from either irradiated or mock-irradiated SW837 cells (p=0.23). Similarly, OCR-linked ATP production was not significantly different in bystander SW837 cells treated with ICCM from irradiated SW837 cells compared to ICCM from mock-irradiated SW837

cells (p=0.17). Maximal respiration did not differ significantly in bystander SW837 cells treated with ICCM from either irradiated or mock-irradiated SW837 cells (p=0.46). The difference in proton leak between SW837 bystander cells treated with ICCM from either irradiated or mock-irradiated SW837 cells did not reach statistical significance (p=0.78). Non-mitochondrial respiration was not significantly different in SW837 cells exposed to ICCM from irradiated or mock-irradiated SW837 cells (p=0.32) (**Figure 2.3**).

2.4.3 RIBE induction *in vitro* does not alter mitochondrial membrane potential, reactive oxygen species or mitochondrial mass in SW837 bystander cells

Whilst no statistically significant alterations in bystander cellular metabolism were demonstrated in bystander SW837 cells, we wanted to investigate potential alterations to mitochondrial function through assessment of surrogate markers of mitochondrial function; mtMP, ROS and mitochondrial mass in SW837 cells. There was no significant difference in mtMP (p=0.44), ROS (p=0.11) or mitochondrial mass (p=0.24) in SW837 cells exposed to ICCM from irradiated or mock-irradiated SW837 cells (**Figure 2.4**).

2.4.4 RIBE induction *in vitro* does not alter radiosensitivity in SW837 bystander cells

The effect of *in vitro* RIBE induction on the radiosensitivity of SW837 bystander cells at 2 Gy, 4 Gy and 6 Gy was investigated using the gold standard clonogenic assay. No significant difference was observed in surviving fraction of SW837 cells exposed to ICCM from either irradiated or mock-irradiated SW837 cells at any of the doses assessed (p>0.05) (**Figure 2.5A**).

2.4.5 RIBE induction *in vitro* induces an increase in bystander SW837 cellular proliferation

Our initial attempts at clonogenic experiments used a higher seeding density for the generation of ICCM and the clonogenic assays failed to grow and form colonies in the SW837 cells exposed to ICCM. In order to investigate if this was a true bystander effect or a result of nutrient exhaustion in cell culture media, a BrdU proliferation assay was performed. Exposure of bystander SW837 cells to ICCM from irradiated SW837 cells resulted in a small but statistically significant increase in proliferation when compared to SW837 cells exposed to ICCM from mock- irradiated SW837 cells (p=0.006). However, given the modest increase in cellular proliferation coupled with the absence of an effect in the other RIBE end-point assays, we will not be extrapolating a bystander effect from this assay. (**Figure 2.5B**).

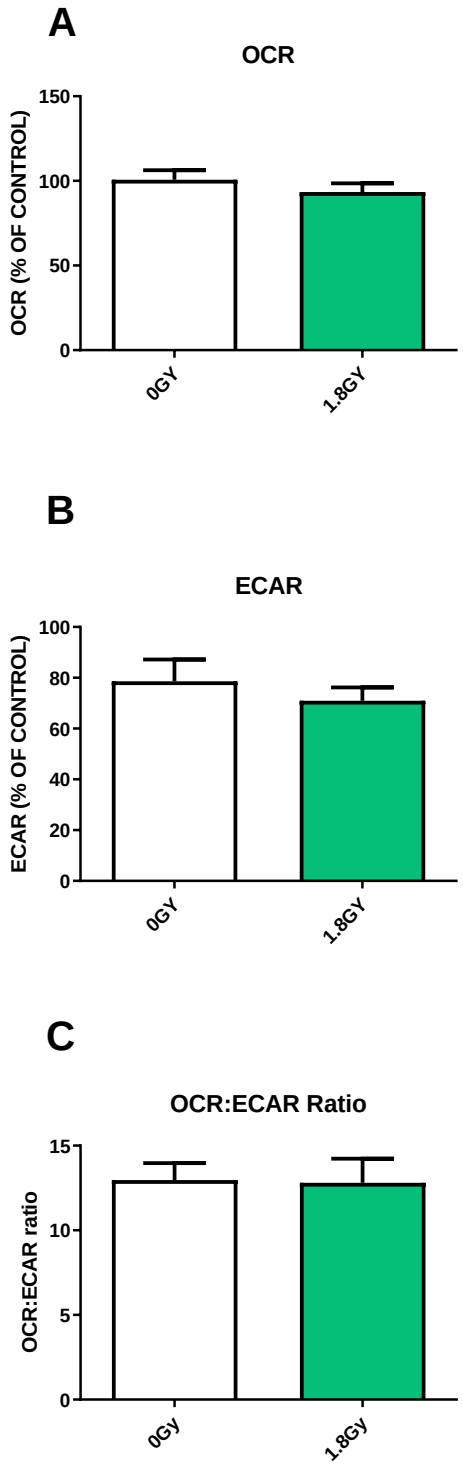

Figure 2.2 Effect of in vitro RIBE induction on OCR, ECAR and OCR:ECAR ratio in bystander SW837 cells

There was no significant difference in (**A**) OCR, (**B**) ECAR or (**C**) OCR:ECAR ratio in SW837 bystander cells exposed to ICCM from either irradiated or mock-irradiated SW837 cells. All data expressed as mean ± SEM. Statistical analysis was performed using a paired *t*-test. *n*=4.

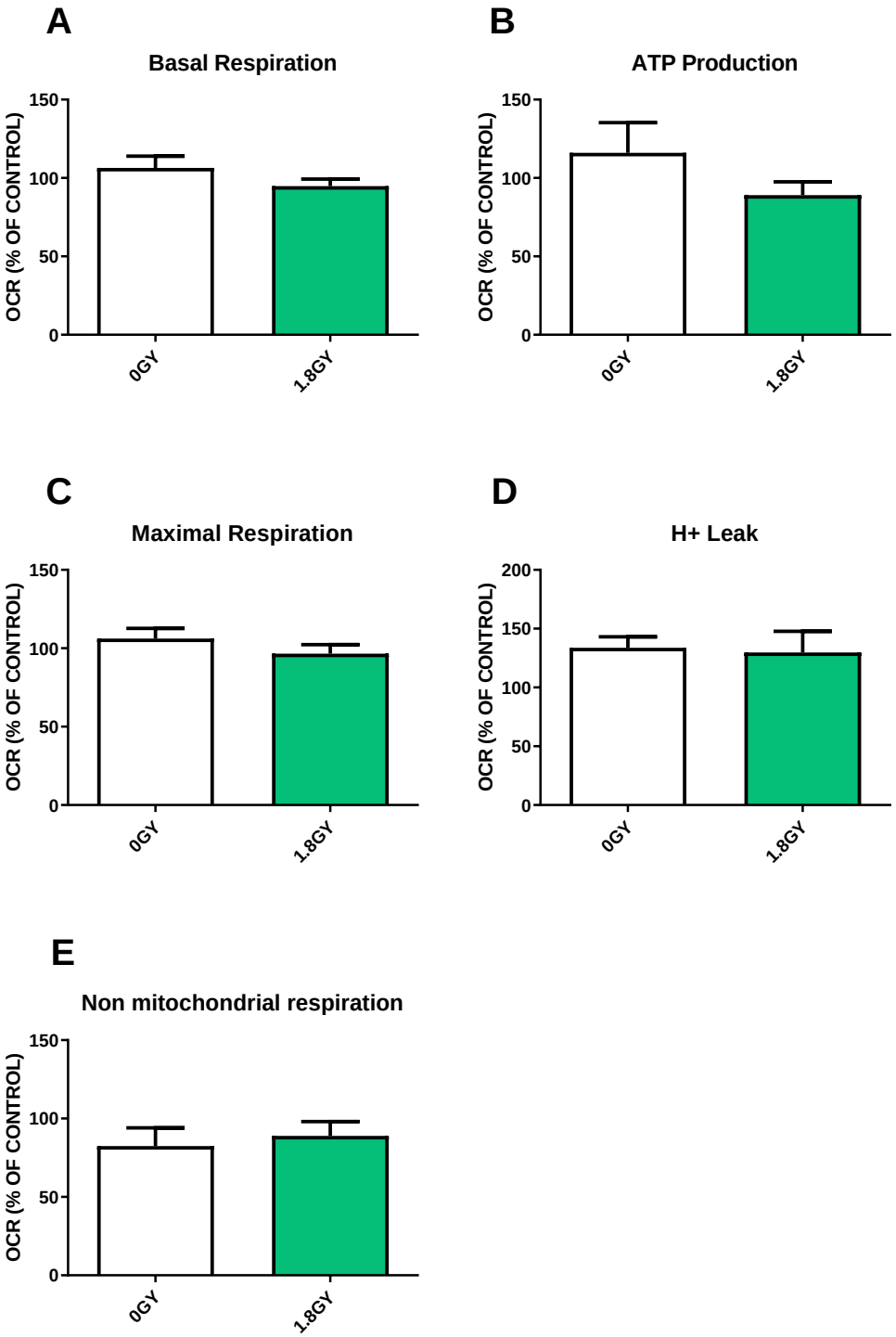

Figure 2.3 Effect of in vitro RIBE induction on basal respiration, ATP production, maximal respiration, proton leak and non-mitochondrial respiration in bystander SW837 cells

There was no significant difference in (**A**) basal respiration, (**B**) OCR-linked ATP production, (**C**) maximal respiration, (**D**) proton leak or (**E**) non-mitochondrial respiration in SW837 bystander cells exposed to ICCM from either irradiated or mock-irradiated SW837 cells. All data expressed as mean ± SEM. Statistical analysis was performed using a paired *t*-test. *n*=4.

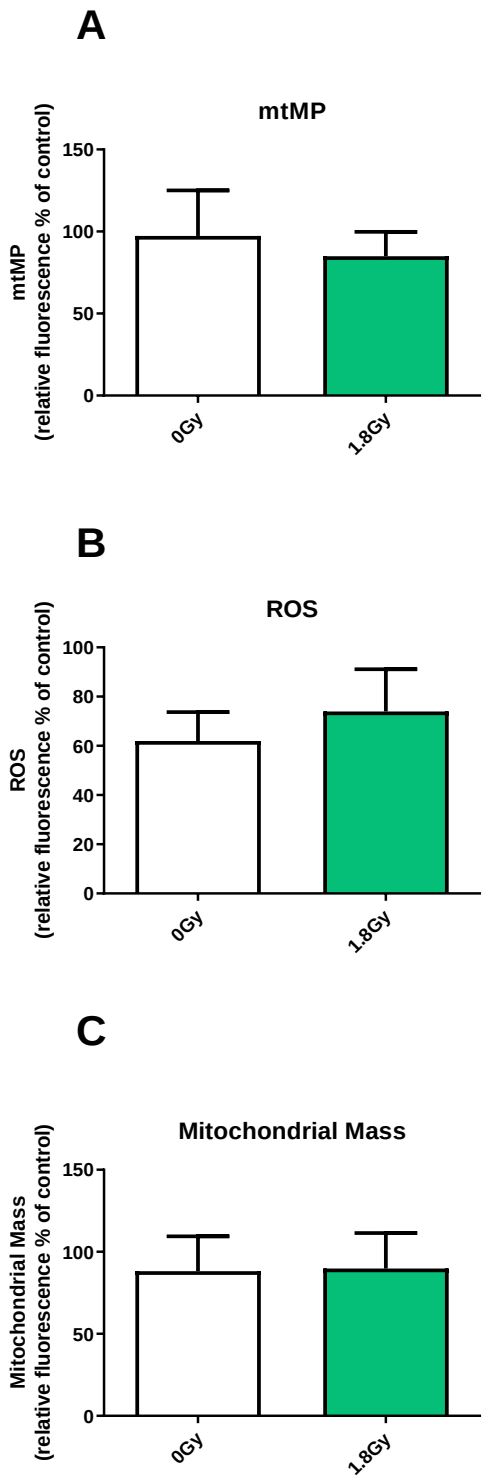

Figure 2.4 Effect of in vitro RIBE induction on mitochondrial function in bystander SW837 cells

No significant difference in (**A**) mtMP, (**B**) ROS or (**C**) mitochondrial mass was observed in bystander SW837 cells treated with ICCM from SW837 cells. All data expressed as mean ± SEM. Statistical analysis by paired *t*-test. *n*=5.

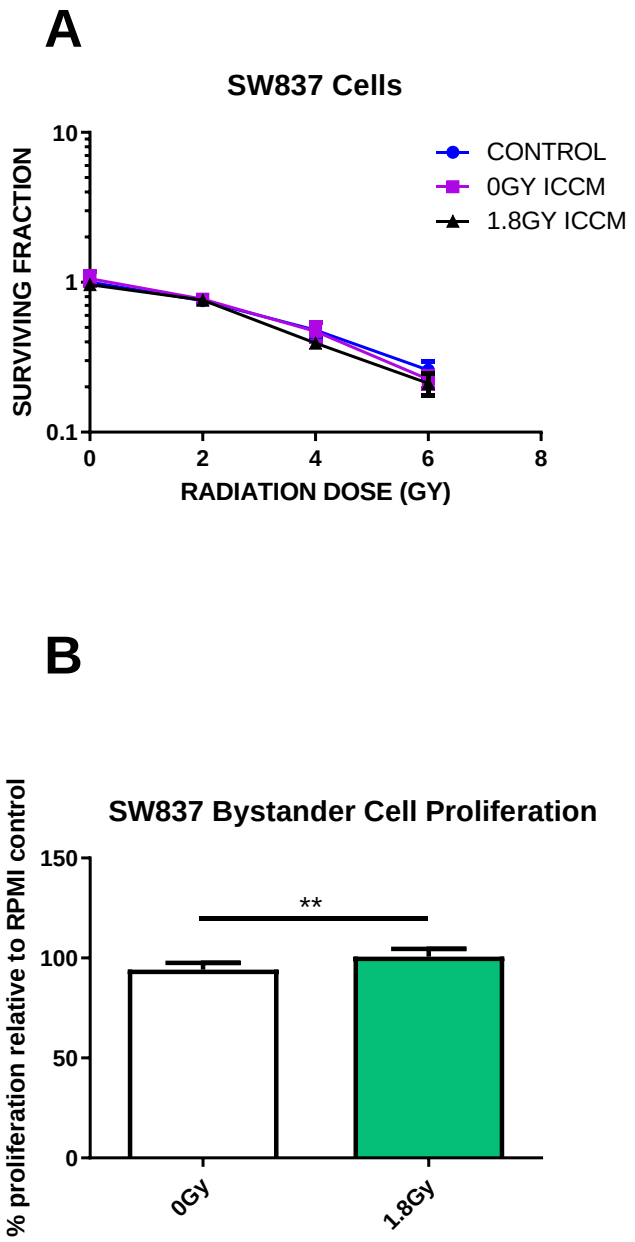

Figure 2.5 Effect of in vitro RIBE induction on bystander SW837 clonogenic survival and cellular proliferation

(**A**) There was no significant difference in clonogenic survival in SW837 cells treated with ICCM from irradiated SW837 cells compared to those treated with ICCM from mock-irradiated SW837 cells at 0 Gy, 2 Gy, 4 Gy or 6 Gy doses of radiation. (**B**) There was a statistically significant increase in bystander SW837 cellular proliferation when SW837 cells were exposed to ICCM from irradiated SW837 cells compared to those exposed to ICCM from mock-irradiated SW837 cells. All data is expressed as mean ± SEM. Statistical analysis was performed by (**A**) one-way ANOVA or (**B**) paired *t*-test. $^{**}p<0.01$. $n=3$.

Investigating the effect of RIBE induction *in vitro* on bystander cellular mitochondrial metabolism, mitochondrial function and radiosensitivity in a radiosensitive colorectal cancer cell line

2.4.6 RIBE induction *in vitro* does not alter OCR, ECAR or OCR:ECAR ratio in bystander HCT116 cells

There was no significant difference in OCR (p=0.16), ECAR (p=0.86) or OCR:ECAR ratio (p=0.66) in bystander HCT116 cells exposed to ICCM from mock-irradiated HCT116 cells compared to irradiated HCT116 cells (**Figure 2.6**).

2.4.7 RIBE induction *in vitro* does not alter basal respiration, ATP production, maximal respiration, proton leak or non-mitochondrial respiration in bystander HCT116 cells

Basal respiration levels remained unchanged in HCT116 cells treated for 24 h with ICCM from either irradiated or mock-irradiated HCT116 cells (p=0.16). Similarly, OCR-linked ATP production was not significantly different in bystander HCT116 cells treated with ICCM from irradiated HCT116 cells, when compared to ICCM from mock-irradiated HCT116 cells (p=0.81). Maximal respiration did not differ significantly in bystander HCT116 cells treated with ICCM from either irradiated or mock-irradiated HCT116 cells (p=0.31). The difference in proton leak between HCT116 bystander cells treated with ICCM from either irradiated or mock-irradiated HCT116 cells did not reach statistical significance (p=0.057). Non-mitochondrial respiration was not significantly different in HCT116 cells exposed to ICCM from irradiated or mock-irradiated HCT116 cells (p=0.42) (**Figure 2.7**).

2.4.8 RIBE induction *in vitro* does not alter mitochondrial membrane potential, reactive oxygen species or mitochondrial mass in HCT116 bystander cells

No significant differences in mtMP (p=0.51), ROS (p=0.88) or mitochondrial mass (p=0.88) were observed in HCT116 cells exposed to ICCM from either mock-irradiated or irradiated HCT116 cells (**Figure 2.8**).

2.4.9 RIBE induction *in vitro* does not alter radiosensitivity of HCT116 bystander cells

The effect of *in vitro* RIBE induction on the radiosensitivity of HCT116 bystander cells at 2 Gy, 4 Gy and 6 Gy was investigated using the gold standard clonogenic assay. No significant difference was observed in surviving fraction of HCT116 cells exposed to

ICCM from either irradiated or mock-irradiated HCT116 cells at any of the doses assessed (p>0.05) (**Figure 2.9**).

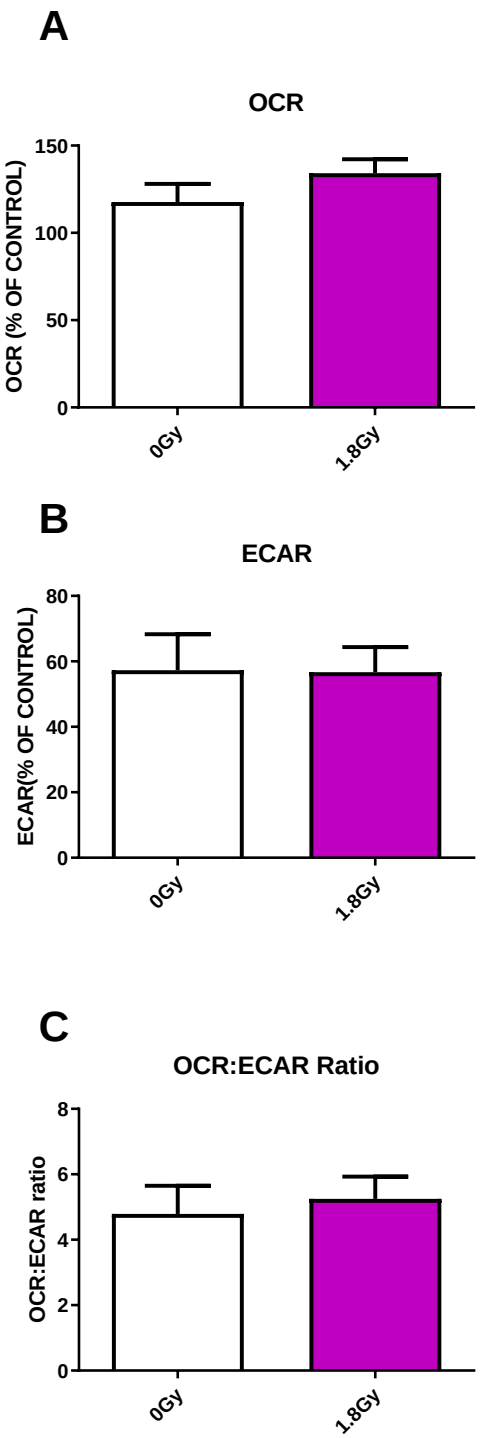

Figure 2.6 Effect of in vitro RIBE induction on cellular OCR, ECAR and OCR:ECAR ratio in bystander HCT116 cells

There was no significant difference in (**A**) OCR, (**B**) ECAR or (**C**) OCR:ECAR ratio in HCT116 cells exposed to ICCM from irradiated HCT116 cells compared to ICCM from mock-irradiated HCT116 cells. All data expressed as mean ± SEM. Statistical analysis was performed using a paired *t*-test. *n*=4.

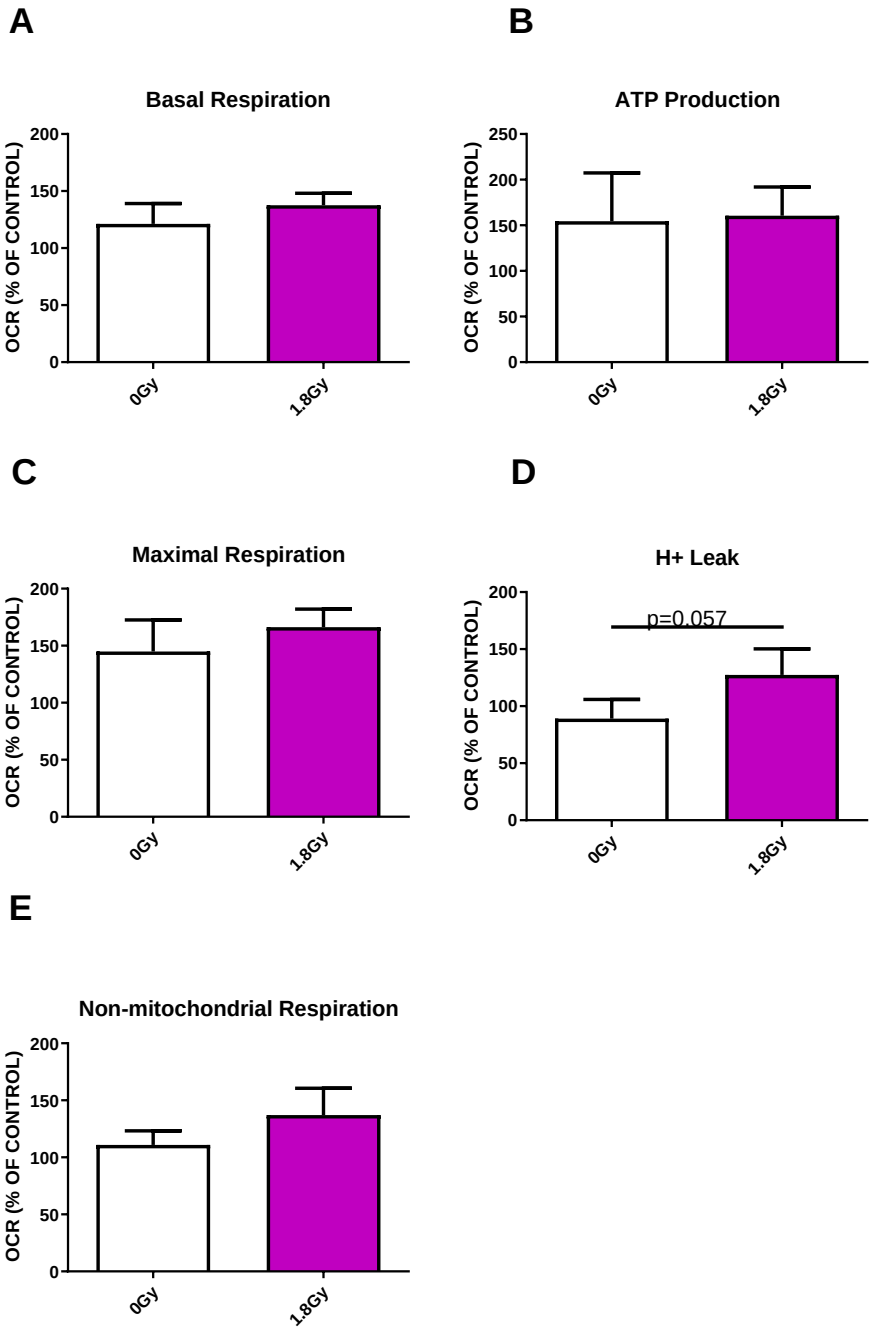

Figure 2.7 Effect of in vitro RIBE induction on HCT116 bystander cellular metabolism

(**A**) Basal respiration, (**B**) OCR-linked ATP production, (**C**) maximal respiration, (**D**) proton leak or (**E**) non-mitochondrial respiration were not significantly different in HCT116 bystander cells exposed to ICCM from irradiated HCT116 cells, when compared to ICCM from mock-irradiated HCT116 cells. All data expressed as mean ± SEM. Statistical analysis was performed using a paired *t*-test. *n*=4.

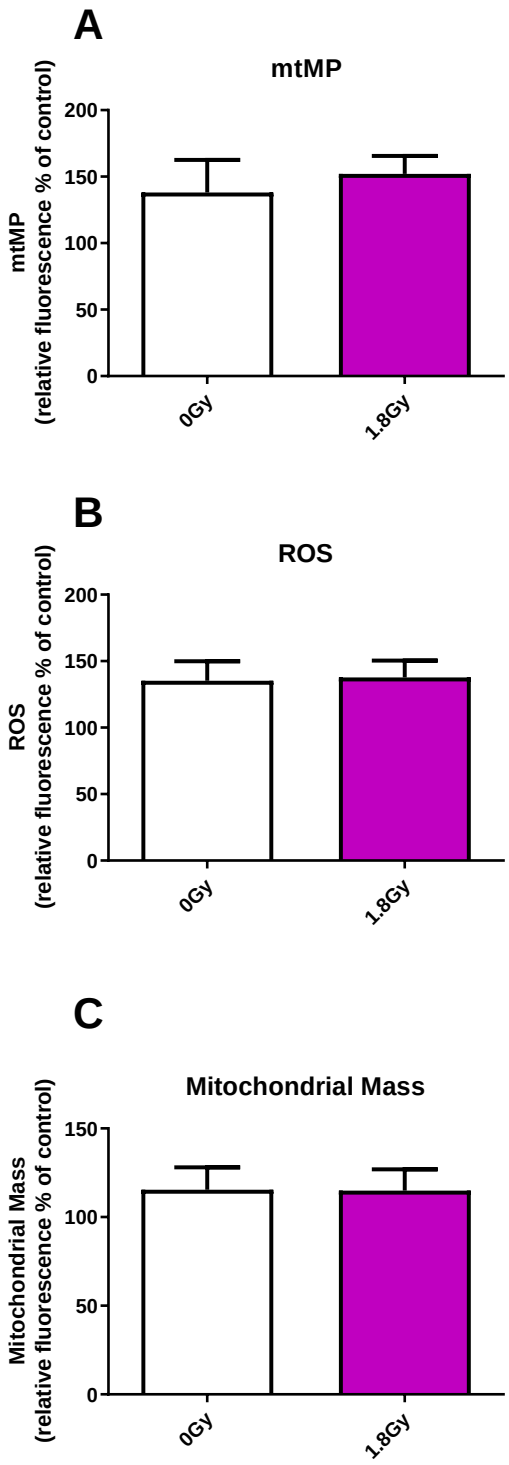

Figure 2.8 Effect of in vitro RIBE induction on mitochondrial function in bystander HCT116 cells

No significant difference in (**A**) mtMP, (**B**) ROS or (**C**) mitochondrial mass was observed in bystander HCT116 cells treated with ICCM from mock-irradiated or irradiated HCT116 cells. All data expressed as mean ± SEM. Statistical analysis was performed using a paired *t*-test. *n*=4.

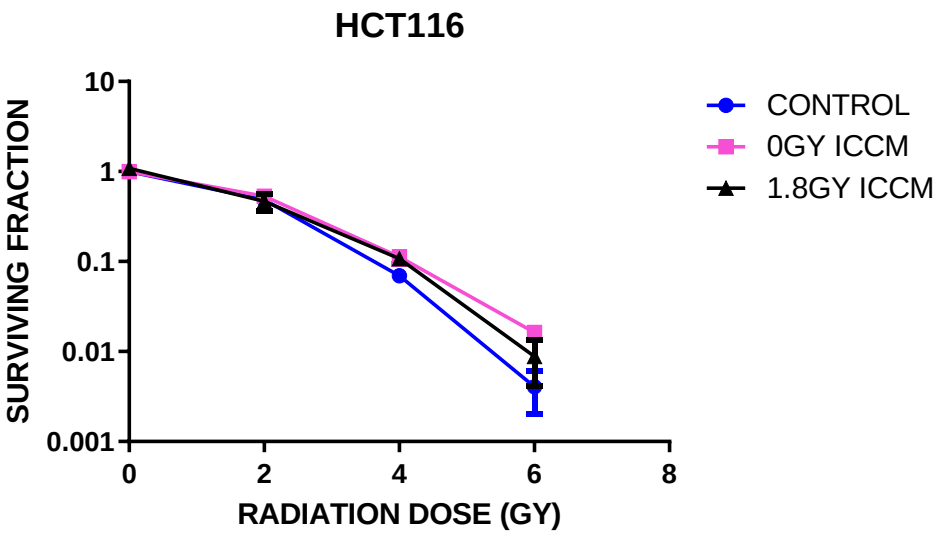

Figure 2.9 Effect of in vitro RIBE induction on bystander HCT116 clonogenic survival

There was no significant difference in clonogenic survival in HCT116 cells treated with ICCM from irradiated HCT116 cells compared to those treated with ICCM from mock-irradiated HCT116 cells at 0 Gy, 2 Gy, 4 Gy or 6 Gy doses of radiation. All data is expressed as mean ± SEM. Statistical analysis by one-way ANOVA. *n*=3.

Investigating the effect of RIBE induction *in vitro* on bystander cellular mitochondrial metabolism, mitochondrial function and cellular proliferation in a radioresistant rectal cancer cell line following repeated fractions of clinically relevant doses of radiation

As no significant alterations in bystander cellular mitochondrial metabolism, mitochondrial function or radiosensitivity were demonstrated in SW837 cells following exposure to ICCM from SW837 cells treated with a single fraction of a clinically relevant dose of radiation, we investigated the effect of repeated fractions of 1.8 Gy on bystander events in these cells. Repeated fractions of radiation more accurately reflect the clinical scenario where patients attend for a daily fraction of 1.8 Gy radiation for a total of 25-28 fractions.

2.4.10 RIBE induction *in vitro* following one to three repeated fractions of radiation does not alter OCR, ECAR or OCR:ECAR ratio in bystander SW837 cells

OCR, ECAR or OCR:ECAR ratio was not significantly different in bystander SW837 cells following pre-incubation with ICCM from SW837 cells treated with between one and three fractions of radiation (p>0.05 for all fractions) (**Figure 2.10**).

2.4.11 RIBE induction *in vitro* following one to three repeated fractions of radiation does not alter basal respiration, ATP production, maximal respiration, proton leak or non-mitochondrial respiration in bystander SW837 cells

Levels of basal respiration, OCR-linked ATP production, maximal respiration, proton leak and non-mitochondrial respiration remained unchanged in SW837 cells treated for 24 h with ICCM from SW837 cells that received between one and three fractions of 1.8 Gy radiation (p>0.05 for all fractions) (**Figure 2.11**).

2.4.12 RIBE induction *in vitro* induces increases in ROS levels following two fractions of 1.8 Gy radiation but does not cause any alterations in mitochondrial membrane potential or mitochondrial mass in bystander SW837 cells

ROS levels were significantly increased in bystander SW837 cells following exposure to ICCM from cells that received 2 x 1.8 Gy fractions of radiation (p=0.03). There was no significant difference in mtMP or mitochondrial mass in bystander SW837 cells following pre-incubation for 24 h with ICCM from SW837 cells treated with between one and three fractions of 1.8 Gy (p>0.05 for all fractions) (**Figure 2.12**).

2.4.13 RIBE induction *in vitro* does not alter bystander cellular proliferation in mock-irradiated or irradiated SW837 cells

We were unable to perform a clonogenic assay on bystander cells incubated with ICCM generated from cells treated with repeated fractions of radiation as this experimental set up consisted of cells growing in this media for 4 d. Therefore, it was not possible for this media to support the growth of cells in a clonogenic assay. Instead, we utilised a BrdU assay to assess the effect of RIBE induction following repeated fractions of radiation on cellular proliferation in mock-irradiated and irradiated cells as a surrogate marker of radiosensitivity. We did not see any significant alterations in bystander cellular proliferation following exposure of SW837 cells to autologous ICCM from cells irradiated with between one and three fractions of 1.8 Gy radiation (p>0.05 for all fractions) (**Figure 2.13**).

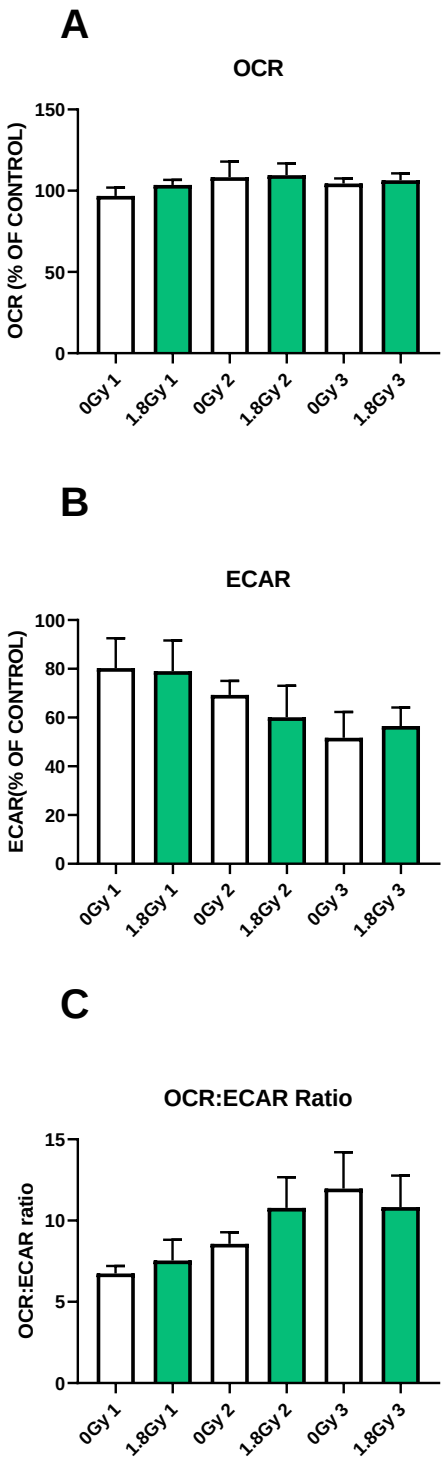

Figure 2.10 Effect of in vitro RIBE induction following repeated fractions of radiation on OCR, ECAR and OCR:ECAR ratio in bystander SW837 cells

There was no significant difference in (**A**) OCR, (**B**) ECAR or (**C**) OCR:ECAR ratio in bystander SW837 cells following exposure to ICCM from SW837 cells treated with between one and three fractions of 1.8 Gy radiation. All data expressed as mean ± SEM. Statistical analysis was performed using a paired *t*-test. *n*=3.

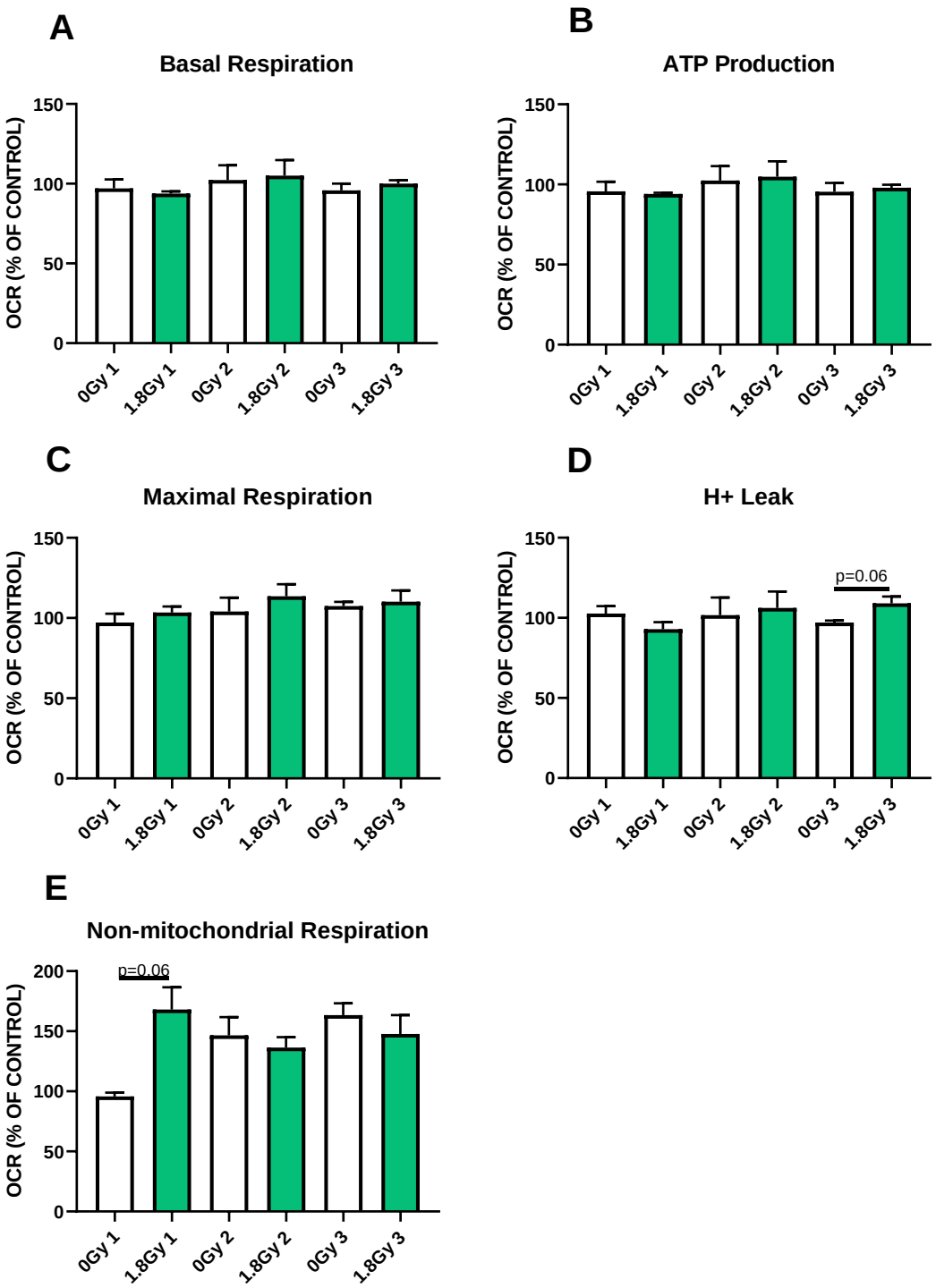

Figure 2.11 Effect of in vitro RIBE induction following between one and three fractions of radiation on basal respiration, ATP production, maximal respiration, proton leak and non-mitochondrial respiration in bystander SW837 cells

There was no significant difference in (**A**) basal respiration, (**B**) OCR-linked ATP production, (**C**) maximal respiration, (**D**) proton leak or (**E**) non-mitochondrial respiration in bystander SW837 cells treated with ICCM from SW837 cells that received between one and three fractions of 1.8 Gy radiation. All data expressed as mean ± SEM. Statistical analysis was performed using a paired *t*-test. *n*=3.

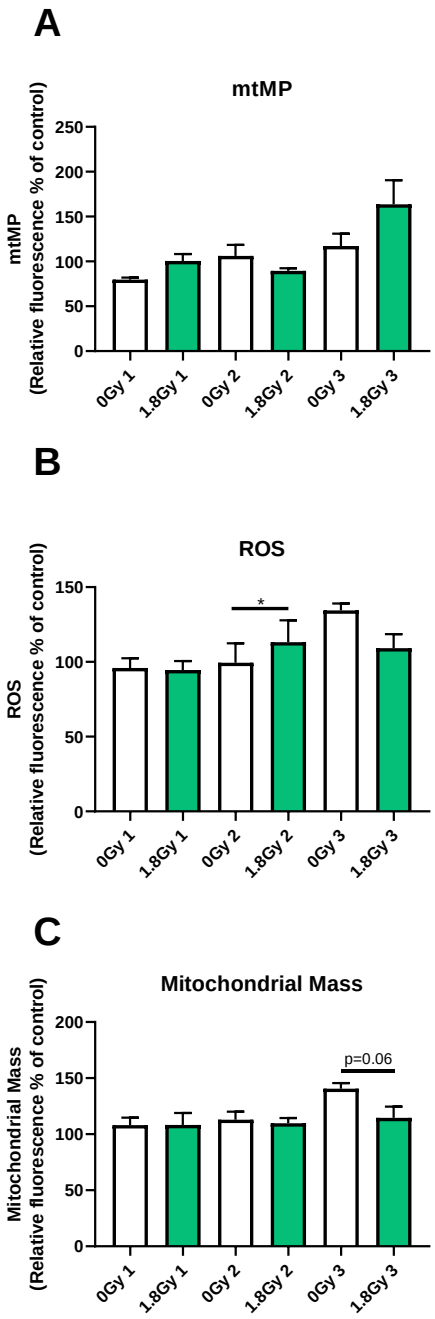

Figure 2.12 Effect of in vitro RIBE induction following between one and three fractions of radiation on mitochondrial function in bystander SW837 cells

There was no significant difference in (**A**) mtMP in bystander SW837 cells treated with ICCM from SW837 cells treated with between one and three fractions of radiation. (**B**) ROS levels were significantly elevated in bystander SW837 cells treated with ICCM from SW837 cells that received 2 x 1.8 Gy fractions of radiation. (**C**) There was no significant difference in mitochondrial mass in bystander SW837 cells following RIBE induction after repeated fractions of 1.8 Gy radiation. All data expressed as mean ± SEM. Statistical analysis was performed using a paired *t*-test. $n=3$. $*p<0.05$.

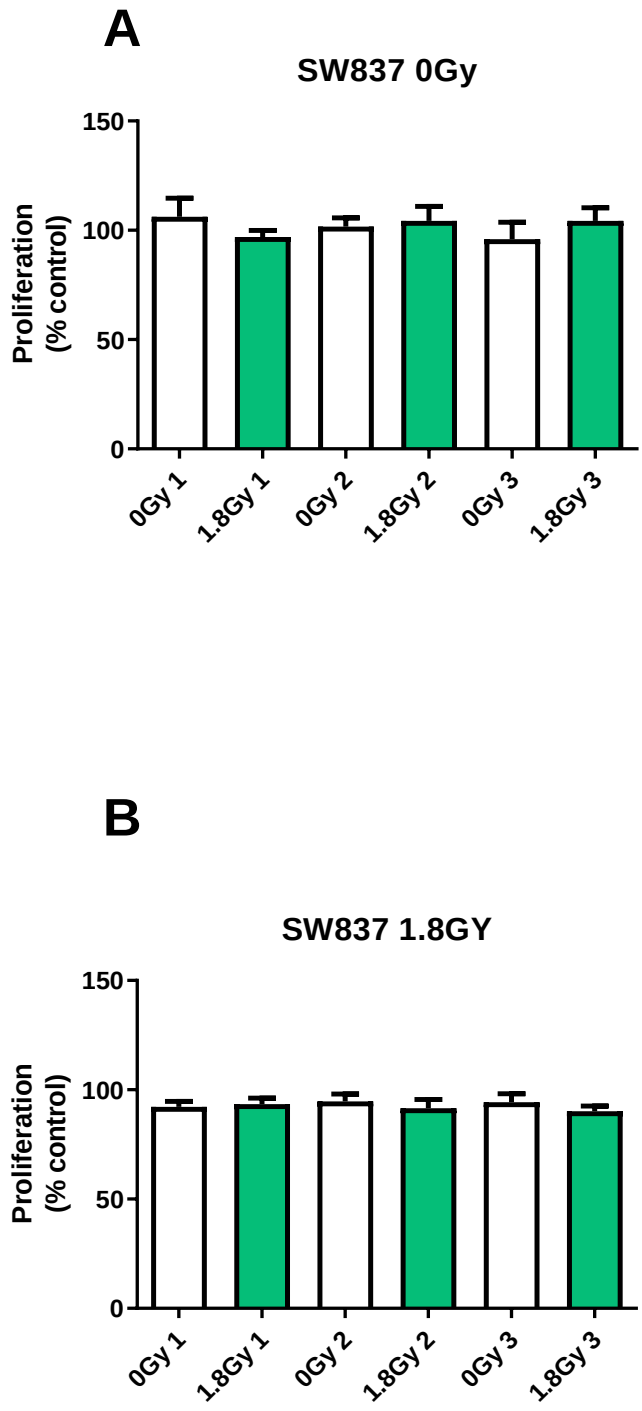

Figure 2.13 Effect of in vitro RIBE induction following repeated fractions of radiation on cellular proliferation in bystander mock-irradiated and irradiated SW837 cells

There was no significant difference in cellular proliferation in (**A**) mock-irradiated or (**B**) irradiated bystander SW837 cells treated with ICCM from SW837 cells that received between one and three fractions of radiation. All data expressed as mean ± SEM. Statistical analysis was performed using a paired *t*-test. *n*=3.

Investigating the effect of RIBE induction *in vitro* on bystander cellular mitochondrial metabolism, mitochondrial function and cellular proliferation in a radiosensitive colon cancer cell line following repeated fractions of clinically relevant doses of radiation

As no significant alterations in cellular metabolism, mitochondrial function or radiosensitivity were demonstrated in HCT116 cells following exposure to ICCM from HCT116 cells treated with a single fraction of a clinically relevant dose of 1.8 Gy x-irradiation, we investigated the effect of repeated fractions of 1.8 Gy radiation on bystander events.

2.4.14 RIBE induction *in vitro* following one to three repeated fractions of radiation does not alter OCR, but alters ECAR and OCR:ECAR ratio in bystander HCT116 cells

OCR was not significantly different in bystander HCT116 cells following pre-incubation with ICCM from HCT116 cells treated with between one and three fractions of radiation ($p>0.05$ for all fractions). ECAR was significantly increased in bystander HCT116 cells following treatment with ICCM from HCT116 cells exposed to a single fraction of 1.8 Gy radiation. There was no difference in ECAR in bystander HCT116 cells following treatment with ICCM from HCT116 cells treated with either two or three fractions of 1.8 Gy radiation ($p>0.05$). OCR:ECAR ratio was significantly reduced in bystander HCT116 cells following treatment with ICCM from HCT116 cells treated with a single fraction of 1.8 Gy radiation. There was no difference in OCR:ECAR ratio in HCT116 cells treated with ICCM from HCT116 cells exposed to two or three fractions of 1.8 Gy radiation ($p>0.05$) (**Figure 2.14**).

2.4.15 RIBE induction *in vitro* following one to three repeated fractions of radiation does not alter basal respiration, ATP production, maximal respiration, proton leak or non-mitochondrial respiration

Basal respiration levels remained unchanged in HCT116 cells treated for 24 h with ICCM from between one and three fractions of 1.8 Gy radiation ($p>0.05$ for all fractions). Similarly, OCR-linked ATP production was not significantly different in bystander HCT116 cells treated with ICCM from HCT116 cells treated with between one and three fractions of 1.8 Gy radiation ($p>0.05$ for all fractions). Maximal respiration did not differ significantly in bystander HCT116 cells treated with ICCM from HCT116 cells treated with between one and three fractions of 1.8 Gy radiation ($p>0.05$ for all fractions). There was no effect of ICCM from HCT116 cells irradiated with all other fractionation

regimens (p>0.05 for all fractions) on proton leak. Non-mitochondrial respiration was not significantly different in HCT116 cells exposed to ICCM from HCT116 cells treated with between one and three fractions of 1.8 Gy radiation (p>0.05 for all fractions) (**Figure 2.15**).

2.4.16 RIBE induction *in vitro* does not cause any alterations in mitochondrial function, specifically reactive oxygen species, mitochondrial membrane potential and mitochondrial mass

There was no significant difference in ROS, mtMP or mitochondrial mass in bystander HCT116 cells following pre-incubation for 24 h with ICCM from HCT116 cells treated with between one and three fractions of 1.8 Gy (p>0.05 for all fractions) (**Figure 2.16**).

2.4.17 RIBE induction *in vitro* following three fractions of 1.8 Gy radiation alters bystander cellular proliferation in irradiated HCT116 cells

We observed a significant increase in cellular proliferation in irradiated bystander HCT116 cells treated with ICCM from HCT116 cells that received 3 x 1.8 Gy fractions of radiation (p=0.01). There were no significant alterations in mock-irradiated bystander HCT116 cells treated with ICCM from HCT116 cells that received between one and three fractions of radiation. Similarly, there were no significant differences in proliferation in irradiated HCT116 cells treated with ICCM from HCT116 cells that received one or two fractions of 1.8 Gy (p>0.05) (**Figure 2.17**).

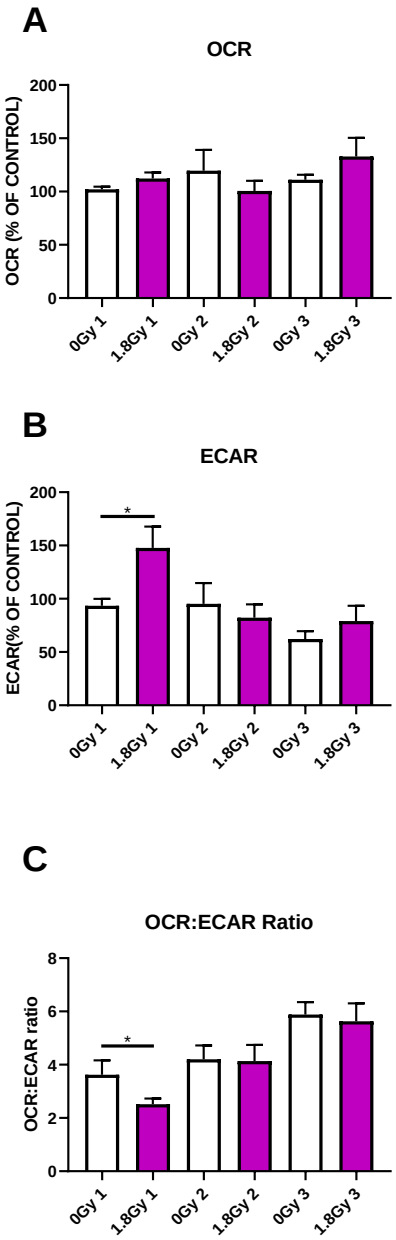

Figure 2.14 Effect of RIBE induction following repeated fractions of 1.8 Gy radiation on OCR, ECAR and OCR:ECAR ratio in bystander HCT116 cells

(**A**) There were no significant differences in OCR in HCT116 bystander cells exposed to ICCM from HCT116 cells exposed to between one and three fractions of 1.8 Gy radiation. (**B**) ECAR was significantly increased in HCT116 cells treated with ICCM from HCT116 cells exposed to a single fraction of 1.8 Gy radiation. ECAR was not significantly different in HCT116 cells treated with ICCM from HCT116 cells exposed to either two and three fractions of 1.8 Gy radiation. (**C**) OCR:ECAR ratio was significantly reduced in HCT116 cells treated with ICCM from HCT116 cells exposed to a single fraction of 1.8 Gy radiation. OCR:ECAR ratio did not differ significantly between HCT116 cells treated with ICCM from HCT116 cells exposed to either two or three fractions of 1.8 Gy radiation. All data expressed as mean ± SEM. Statistical analysis was performed using a paired *t*-test. *$p<0.05$. $n=4$.

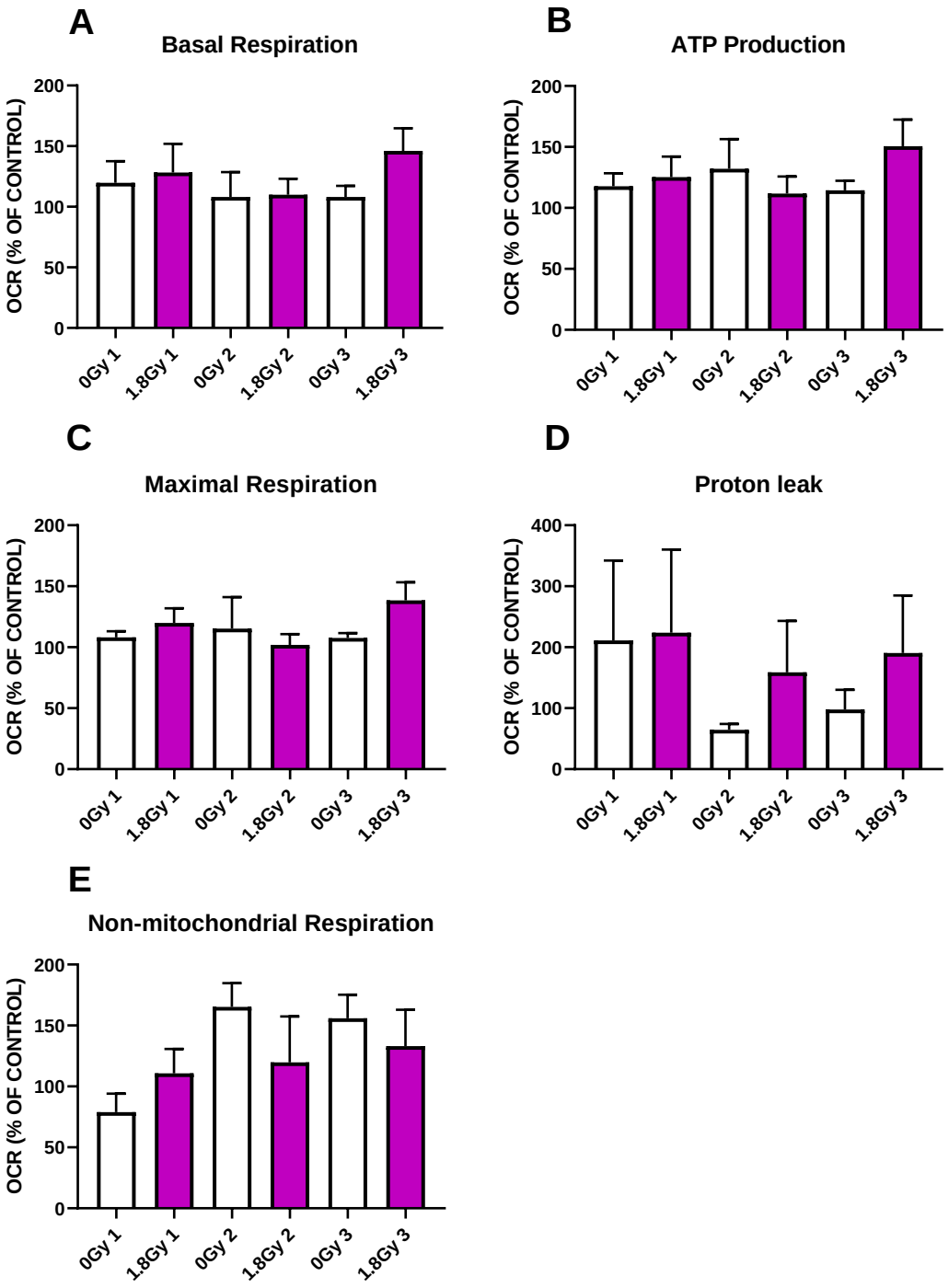

Figure 2.15 Effect of RIBE induction following repeated fractions of 1.8 Gy radiation on basal respiration, ATP production, maximal respiration, proton leak and non-mitochondrial in bystander HCT116 cells

There were no significant differences in (**A**) basal respiration, (**B**) OCR-linked ATP production, (**C**) maximal respiration, (**D**) proton leak or (**E**) non-mitochondrial respiration between bystander HCT116 cells treated with ICCM from HCT116 cells exposed to between one and three fractions of 1.8 Gy radiation. All data expressed as mean ± SEM. Statistical analysis was performed using a paired *t*-test. *n*=4.

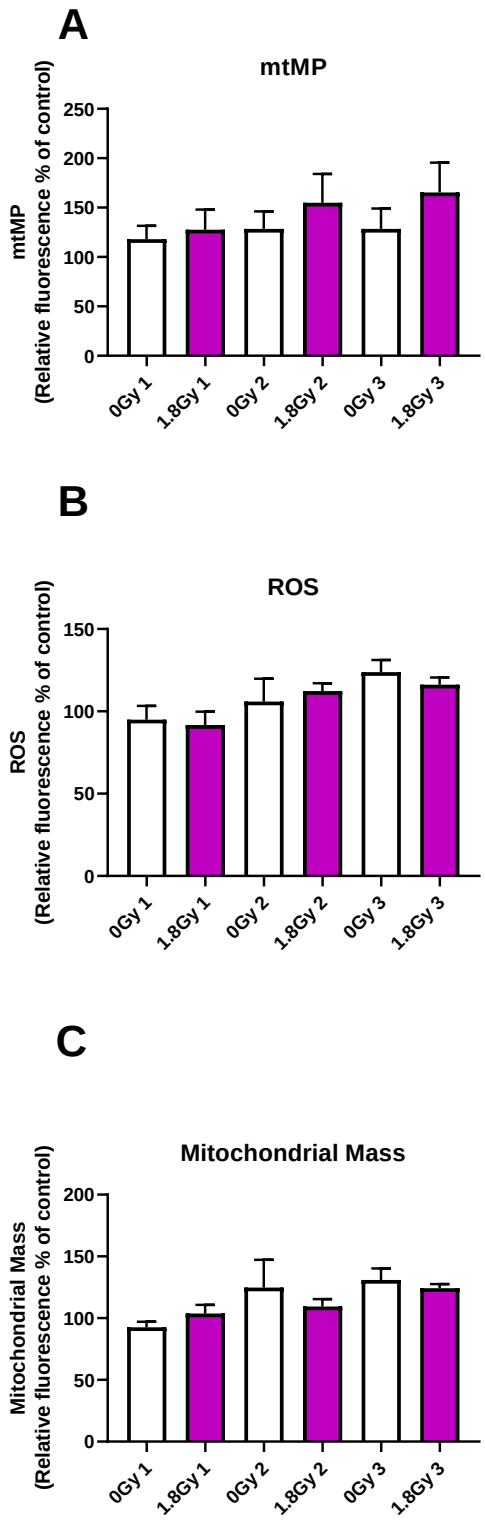

Figure 2.16 Effect of in vitro RIBE induction following repeated fractions of radiation on mitochondrial function in bystander HCT116 cells

There were no significant differences in (**A**) mtMP, (**B**) ROS or (**C**) mitochondrial mass in bystander HCT116 cells treated with ICCM from HCT116 cells exposed to between one and three fractions of 1.8 Gy radiation. All data expressed as mean ± SEM. Statistical analysis was performed using a paired *t*-test. *n*=4.

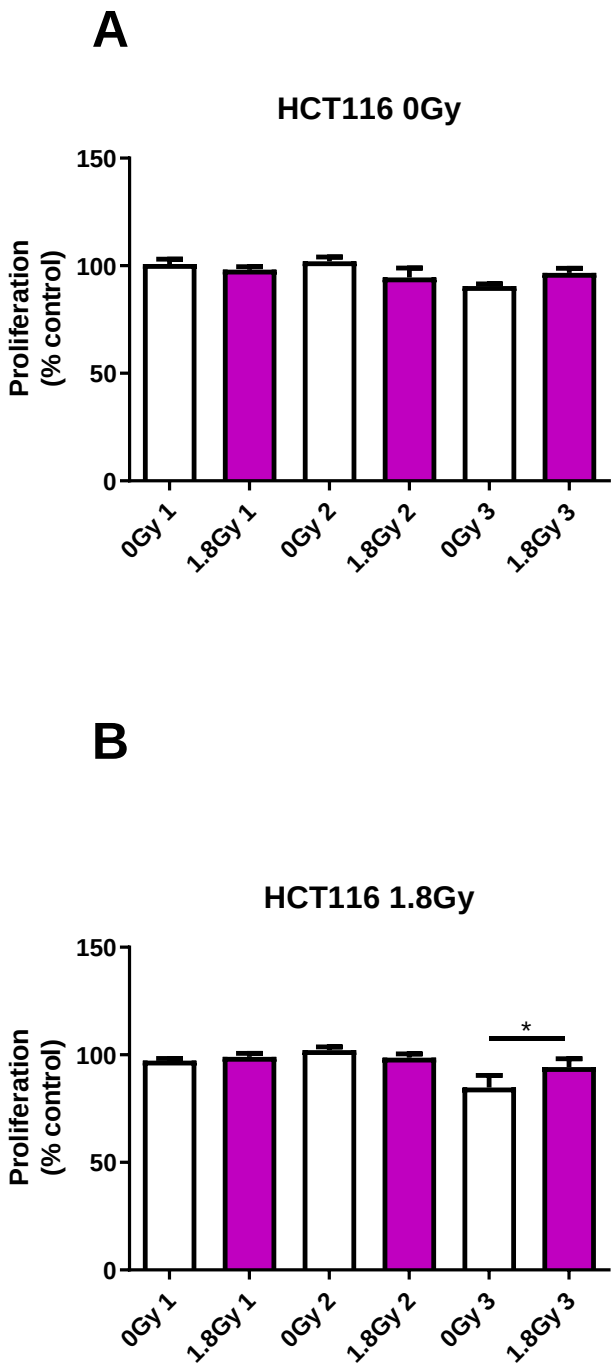

Figure 2.17 Effect of RIBE induction following repeated fractions of 1.8 Gy radiation on cellular proliferation in mock-irradiated and irradiated HCT116 cells

(**A**) There were no significant differences in cellular proliferation in mock-irradiated HCT116 cells treated with ICCM from HCT116 cells treated with between one and three fractions of 1.8 Gy radiation. (**B**) There was a significant increase in cellular proliferation in irradiated HCT116 cells treated with ICCM from HCT116 cells treated with 3 x 1.8 Gy fractions of radiation. Cellular proliferation was not altered by ICCM from HCT116 cells that received either one or two fractions of 1.8 Gy radiation. Data expressed as mean ± SEM. Statistical analysis was performed using a paired *t*-test. **p*<0.05. *n*=3.

2.4.18 RIBE induction *in vitro* following up to three fractions of 1.8 Gy radiation does not alter expression of the DNA repair genes *PARP1, SMUG1, MMS19* or *MLH1* in bystander HCT116 cells

Having observed alterations in bystander cellular metabolism, specifically alterations in glycolysis and OCR:ECAR ratio in bystander HCT116 cells exposed to ICCM generated following repeated fractions of radiation, we examined the expression of four DNA repair genes; *PARP1, SMUG1, MMS19* and *MLH1*. Glycolysis upregulation has been associated with a radioresistant phenotype through the induction of DNA repair (261), therefore we hypothesised that the increased glycolysis observed in HCT116 cells may be associated with enhanced expression of DNA repair genes. Previous work in our group has demonstrated that alterations in the expression levels of *PARP1*, *SMUG1*, *MMS19* and *MLH1* in patient tumours are associated with treatment response (262).

No significant alterations in the expression of *PARP1*, *SMUG1*, *MMS19* or *MLH1* in HCT116 cells were demonstrated following exposure of the cells to autologous ICCM from HCT116 cells that received between one and three fractions of 1.8 Gy radiation ($p>0.05$ for all fractions) (**Figure 2.18**).

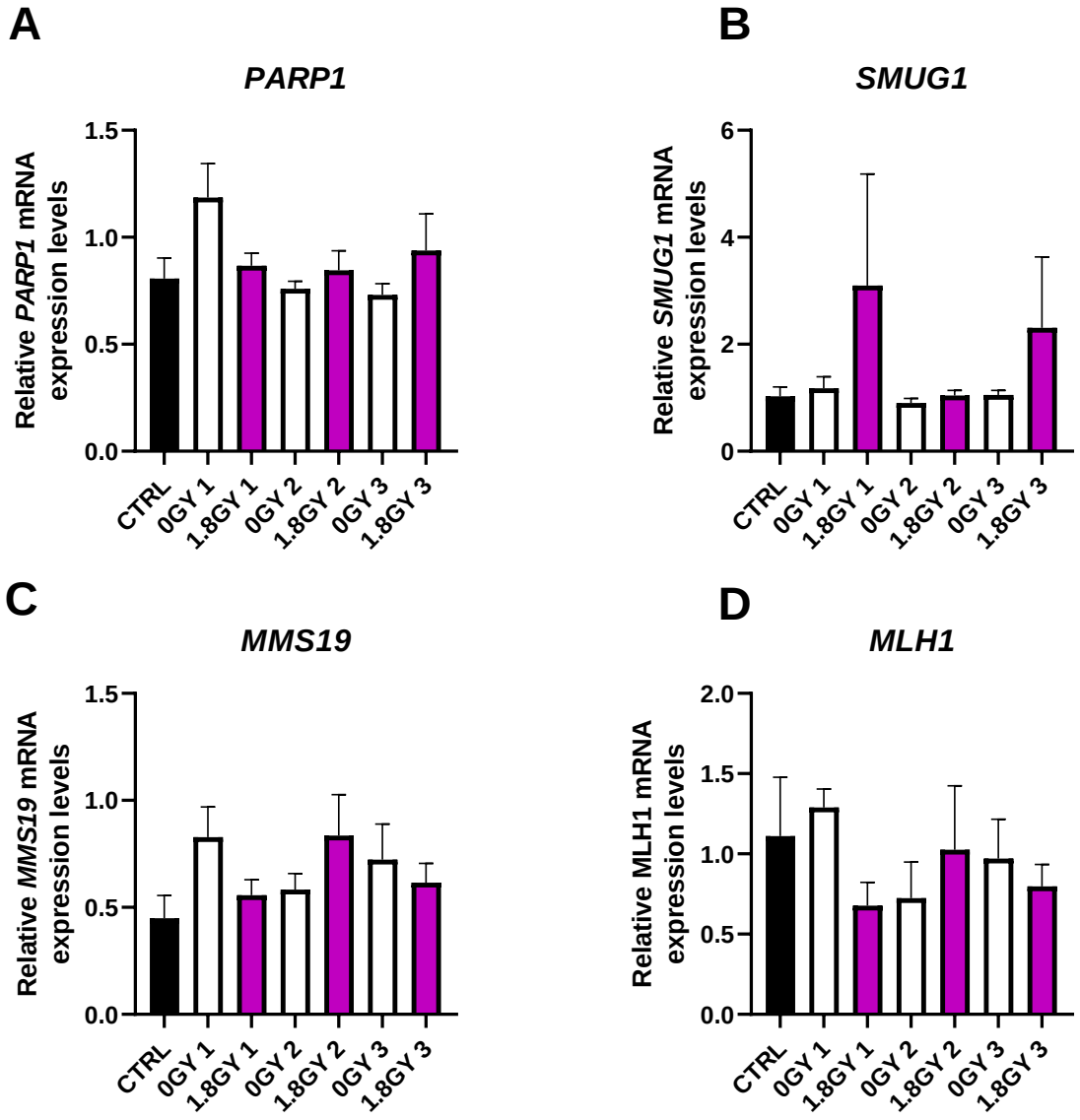

Figure 2.18 Effect of in vitro RIBE induction following repeated fractions of 1.8 Gy on the expression of DNA repair genes PARP1, SMUG1, MMS19 and MLH1 in bystander HCT116 cells

There were no significant differences in the levels of (**A**) *PARP1*, (**B**) *SMUG1*, (**C**) *MMS19* or (**D**) *MLH1* in HCT116 cells treated with ICCM from HCT116 cells receiving between one and three fractions of 1.8 Gy radiation. Data expressed as mean ± SEM. Statistical analysis was performed using a paired *t*-test. *n*=3.

2.5 Summary of findings from chapter 2

- *In vitro* RIBE induction did not induce any changes in OXPHOS, glycolysis or mitochondrial function, specifically mtMP, ROS and mitochondrial mass in a radioresistant model of rectal cancer following a single fraction of 1.8 Gy radiation.
- *In vitro* RIBE induction caused significant increases in ROS levels following 2 x 1.8 Gy fractions of radiation in a radioresistant model of rectal cancer.
- *In vitro* RIBE induction altered glycolysis and OCR:ECAR ratio in HCT116 cells following a single fraction of radiation in the experimental set-up examining repeated fractions of radiation.
- *In vitro* RIBE induction did not induce any changes in radiosensitivity in a radioresistant model of rectal cancer or a radiosensitive model of colon cancer following a single fraction of 1.8 Gy radiation.
- *In vitro* RIBE induction did not induce alterations in expression of DNA repair genes, specifically *PARP1*, *SMUG1*, *MMS19* or *MLH1* in a radiosensitive model of colon cancer following multiple fractions of radiation.

2.6 Discussion

The overall aim of this chapter was to investigate the effect of *in vitro* RIBE induction in CRC in an inherently radioresistant and an inherently radiosensitive cell line. Specifically, we examined the effect of *in vitro* RIBE induction on mitochondrial energy metabolism, mitochondrial function, specifically mtMP, ROS and mitochondrial mass, radiosensitivity and expression of DNA repair genes.

No significant bystander response was demonstrated in either inherently radioresistant cells, the SW837 rectal cancer cell line, or in inherently radiosensitive cells, the HCT116 colon cancer cell line following a single fraction of a clinically relevant dose of 1.8 Gy x-irradiation. These results were unexpected as the role of ROS and the mitochondria in RIBE events have been heavily reported (146, 202-204). One limitation of the experimental model employed in these studies is that it only considers secretion of soluble mediators into the extracellular space as a mechanism of RIBE induction and no consideration is given to another important mechanism of RIBE signalling via cell-to-cell contact or gap junctional intercellular communication (GJIC).

This study adopted a novel approach to studying RIBE events, in that clinically relevant doses of radiation were used. Rectal cancer patients typically receive 1.8 Gy of x-radiation per fraction (4). The majority of RIBE studies use very low doses of radiation, which typically range from 0.05 Gy to 1 Gy, much lower than would be used in neoadjuvant radiotherapy regimens. RIBE events, in particular bystander cell killing, have previously been reported to occur at this dose range and it has been hypothesised that this is a mechanism of removing damaged cells (263). However, since these doses of radiation are largely irrelevant to cancer therapy and may instead be more important in calculating risks from low dose environmental radiation exposure, we utilised clinically relevant doses of radiation. Another novel approach of this study is the use of x-radiation, which is the most clinically relevant as it is the type of radiation received by rectal cancer patients. The majority of RIBE studies use γ-radiation and α-particle radiation.

Evidence exists to suggest that p53 status has a role to play in the response to RIBE. For this reason, we chose a p53 wild-type cell line, the HCT116 colon cancer cell line and a p53 mutant cell line, the SW837 rectal cancer cell line. Since p53 mutations are found in between 10% to 100% of cancers (264) we believed it was important to include a p53 mutant cell line in our study. Mothersill *et al*. have shown that p53 null and mutant

HCT116 cells are capable of producing a bystander signal but the p53 null cells are incapable of responding to RIBE signals (145). It is therefore surprising that we did not see any bystander effect in the HCT116 cells. This may be due to the radiation dose used, with RIBE events typically becoming saturated at lower doses of radiation. It may also be due to the RIBE end-points investigated in our study, we examined the effect on the mitochondrial function and metabolism, while Mothersill *et al.* investigated clonogenic survival (145). We did not observe any changes in clonogenic survival however, the experimental protocol utilised was different, with Mothersill *et al.* harvesting the ICCM at 1 h post-irradiation. While p53 status may be a possible reason for not observing a bystander effect in SW837 cells, in chapter 4 we demonstrated a bystander response in this cell line in response to *ex vivo* RIBE induction. Furthermore, p53 mutations are diverse and it is unknown if wild-type p53 is necessary for a bystander response to be seen or if specific p53 mutations allow a cell to experience a bystander effect.

Since we did not observe a RIBE response following a single fraction of a clinically relevant dose of radiation, we investigated the effect of repeated fractions of radiation on RIBE events, since this reflects the clinical scenario whereby patients receive daily fractions of radiation. Few groups have investigated this topic. Mothersill and Seymour conducted experiments in human keratinocytes in 2002 with repeated fractions of radiation delivered at 2 h intervals and the media harvested 1 h after the final fraction of radiation. They concluded that exposure to ICCM from fractionated regimens gave lower survival of cells, when compared to ICCM from single dose radiation exposures (265). More recently, Widel investigated the effect of fractionation on melanoma cells in a transwell co-culture system and concluded that fractionation induced higher levels of micronuclei (MN) formation and apoptosis in both directly hit and bystander cells (266). Additionally, investigation of the effect of a fractionated regimen on QU-DB lung cancer cells revealed higher levels of MN formation with increasing number of fractions of 2 Gy γ-radiation (267).

Interestingly, and surprisingly, in the experiments involving the utilisation of cumulative fractions of radiation to induce RIBE, we observed alterations in mitochondrial metabolism, specifically increases in ECAR and a reduction on OCR:ECAR ratio in HCT116 cells after a single fraction of 1.8 Gy radiation. This was unexpected since we did not observe a difference in our initial experiments involving a single fraction of 1.8 Gy. Cell seeding densities were lower in our protocol for repeated radiation exposures

since the cells were growing for 5 d instead of 3 d as in our initial experiments. This suggests that cell seeding density may indeed have significant implications for bystander signal production. It has been previously demonstrated that higher cell densities produce more robust bystander responses (268) therefore, our results differ from the literature. Further study of the effect of various seeding densities on bystander events may offer more insight into this observation. This may be of clinical relevance with shrinking tumour volumes as treatment progresses since the density of tumour cells within the irradiated volume would be reducing.

Having observed an increase in glycolysis in HCT116 cells following exposure to a single fraction of radiation in the fractionation experiments, we examined the effect of RIBE induction following repeated fractions of 1.8 Gy on cellular proliferation and expression of DNA repair genes to determine if this increase in glycolysis was associated with enhanced DNA repair and a more radioresistant phenotype as has been reported in the literature (261). Previous work in our group has shown that alterations in the expression of *PARP1*, *SMUG1*, *MMS19* and *MLH1* is associated with treatment response in OAC patient tumours, with patients exhibiting sensitivity to neo-CRT having reduced levels of the aforementioned DNA repair genes (262). We did not however observe any differences in expression of these DNA repair genes following RIBE induction in HCT116 cells.

We did not observe any alterations in mitochondrial metabolism following RIBE induction utilising repeated fractions of 1.8 Gy radiation in SW837 cells. We observed an increase in ROS levels following exposure to ICCM from SW837 cells that received 2 x 1.8 Gy of radiation. This suggests that repeated fractions of radiation may induce oxidative stress in bystander cells however, this appears to be transient as this effect was not observed following 3 x 1.8 Gy fractions. It may be possible that the cells have adapted and upregulated their antioxidant systems to scavenge the increased ROS levels. Furthermore, ROS are short lived molecules and therefore may be degraded after a further 24 h. These results corroborate the literature that ROS are important players in RIBE events (146, 202-204). However, given the absence of any other observed changes in end-points investigated, it is unclear what significance this result has in terms of treatment response.

A BrdU assay was used to assess cell proliferation as a surrogate marker of radiosensitivity. It was not possible to evaluate the effect of repeated fractions of radiation

on bystander cellular radiosensitivity by clonogenic assay since the cells had been in culture for 5 d and the nutritional content of the media was insufficient to support the growth of single cell colonies. We observed an increase in cellular proliferation in bystander HCT116 cells following RIBE induction using 3 x 1.8 Gy fractions of x-radiation in irradiated HCT116 cells. We believe this result should be interpreted with caution given the absence of any mitochondrial, metabolic or DNA repair gene alterations. One potential reason for this observation is that the irradiated HCT116 cells did not reach the same level of confluence as the mock-irradiated HCT116 cells following 3 x 1.8 Gy fractions of radiation owing to the intrinsic radiosensitivity of these cells. It was evident that the media was not as depleted of nutrients as the 3 x 0 Gy fraction wells. Therefore, it may be possible that better nutrient availability in the media may have contributed to this observed effect. While statistical significance was not observed in the mock-irradiated HCT116 cells treated with ICCM from 3 x 1.8 Gy irradiated HCT116 cells, a similar trend was observed (p=0.08). There was no effect on cellular proliferation in SW837 cells following exposure to ICCM from the fractionated regimen. However, we observed a small but significant increase in cellular proliferation in SW837 cells in our initial experiments using a single fraction of radiation. Once again, cell seeding densities differed between the experiments, suggesting that cell density may influence bystander responses. The purpose of this BrdU experiment in SW837 cells was to determine if the cell obliteration by the ICCM for clonogenic experiments was a true effect or as a result of the media being too exhausted to support colony formation.

While this study used a novel and clinically relevant approach to investigate *in vitro* RIBE events in rectal cancer, there are limitations. One such limitation was the lack of availability of a radiosensitive rectal cancer cell line and thus a model of colon cancer, the HCT116 cell line, was used as the model of inherent radiosensitivity in this study. Previous unpublished work in our group has characterised the radiosensitivities of a panel of rectal cancer cells lines, SW837, HRA-19 and SW1463 cell lines. All cell lines are inherently radioresistant (Croí Buckley, Rebecca O'Brien, unpublished data). Another limitation of the study is the use of *in vitro* models as they fail to recapitulate the tumour microenvironment (TME) of cancer tissue. *In vitro* models consist of a single cell type growing in a monolayer and fail to mimic the 3-D structure observed in tumours. Also, tumours consist of various cell types such as immune cells, stromal cells, secreted factors and various biological processes such as angiogenesis and hypoxic areas that are not seen

in *in vitro* models. For this reason, we next investigated the effect of RIBE induction in an *ex vivo* model of rectal cancer in chapter 4.

Chapter 3 Effect of *in vitro* RIBE induction on bystander cellular metabolism, mitochondrial function and radiosensitivity in an oesophageal adenocarcinoma isogenic model of radioresistance

3.1 Introduction

In chapter 2, we investigated the effect of *in vitro* radiation-induced bystander effect (RIBE) responses in inherently radiosensitive and radioresistant models of colorectal cancer (CRC). In this chapter, we examined the same RIBE biological end-points in an *in vitro* model of acquired radioresistance in oesophageal adenocarcinoma (OAC). As mentioned in the introduction, OAC is an aggressive disease with a 5-year survival rate of approximately 20% (50). Furthermore, 40% of patients are diagnosed at late stage and have a 5-year survival rate of less than 3% (51). One of the main reasons proposed for the poor survival in OAC is the inherent difficulty in boosting response to treatment in this cancer type. The standard of care for locally-advanced OAC is neoadjuvant chemotherapy or chemoradiation followed by surgery (68). However, the complete pathological response (pCR) rate remains low, at less than 30% (72). Achievement of pCR is associated with enhanced patient outcomes, including increased overall and disease-free survival (269). The mechanisms of radioresistance in OAC have not been fully elucidated but several mechanisms have been proposed. Lynam-Lennon *et al.* have shown that alterations in DNA repair efficiency may be involved in radioresistance in OAC cells (270), Buckley *et al.* have shown that levels of Leukaemia Inhibitory Factor are significantly higher in radioresistant OAC cells and in the serum of patients with radioresistant OAC tumours (271). Alterations in cellular metabolism and mitochondrial function have also been implicated in radioresistance mechanisms in OAC (80, 111).

As previously discussed, the mitochondria are integral to RIBE while reactive oxygen species (ROS) and oxidative stress have well-documented roles in RIBE. Given the problem of radioresistance in OAC tumours, understanding the effect of RIBE induction on the mitochondria explores the possible relevance that off-target effects of radiation may have on treatment response. Understanding these effects may yield potential therapeutic targets as identifying the effects of RIBE induction on mitochondrial metabolism and function may reveal specific mitochondrial vulnerabilities that may be actionable targets.

Targeting enhanced oxidative phosphorylation (OXPHOS) has been an approach used to sensitise resistant cancer cells to radiation. Pyrazinib (80), atovaquone (112), papaverine (113) and metformin (114) have all been used as therapeutic agents to sensitise cancer cells to radiation therapy. The ability to reduce oxygen consumption rate (OCR), a

measure of OXPHOS, is a common property of these four drugs (80, 112-114). It is well-documented that a large proportion of tumours have hypoxic regions (272). As discussed in chapter 1, reoxygenation of tumours is crucial to the success of radiation therapy (89). Oxygen is an electrophile and fixes radiation-induced damage, increasing the toxicity of radiation therapy by 2.5-fold (273). Multiple approaches to increase oxygen delivery or oxygenation of tumours have been trialled to enhance the efficacy of radiation therapy. However, it has been suggested that reducing the tumour demand for oxygen by inhibiting mitochondrial respiration may yield enhanced tumour oxygenation. Mathematical modelling predicts that reducing OCR will more effectively reduce hypoxia compared to attempts to enhance oxygen delivery to tumours (274).

This notion of 'metabolic radiosensitisation' prompted us to investigate the effect of *in vitro* RIBE induction on OCR and other parameters of mitochondrial metabolism to gain a greater understanding of any potential implications of secreted factors from irradiated cells on tumour cell metabolism. Given the poor response to radiation of OAC tumours, we investigated the role of off-target effects of radiation on bystander cellular metabolism, mitochondrial function and radioresistance following a single fraction of a clinically relevant dose of radiation in addition to repeated fractions of a clinically relevant dose of radiation. To the best of our knowledge, this is the first study to investigate RIBE using clinically relevant doses of radiation on known parameters of radioresistance in a model of OAC.

3.2 Overall objective and specific aims of chapter 3

The aim of this chapter was to elucidate the effect of *in vitro* RIBE induction on bystander cellular metabolism, mitochondrial function and radiosensitivity in an isogenic model of acquired radioresistance in OAC.

The specific aims of chapter 3;

1. Elucidate the effect of *in vitro* RIBE induction on bystander cellular mitochondrial metabolism in an isogenic model of radioresistance; OE33P (radiosensitive) and OE33R (radioresistant) cell lines.
2. Examine the effect of *in vitro* RIBE induction on bystander cellular mitochondrial function in OE33P and OE33R cell lines.
3. Determine the effect of *in vitro* RIBE induction on bystander cellular radiosensitivity in OE33P and OE33R cell lines.
4. Investigate the effect of *in vitro* RIBE induction on bystander cellular proliferation in OE33P and OE33R cell lines.
5. Investigate the effect of RIBE induction on expression of DNA repair genes in OE33P and OE33R cell lines.

3.3 Materials and methods

3.3.1 Cell Culture

The human OE33 oesophageal adenocarcinoma cell line was obtained from the European Collection of Authenticated Cell Cultures (ECACC). The isogenic model of radioresistance OAC; OE33P (radiosensitive) and OE33R (radioresistant) was generated as previously described (270).

3.3.2 Cell sub-culture

OE33P and OE33R cells, were maintained in Roswell Park Memorial Institute 1640 (RPMI 1640) [Lonza Group Ltd., Switzerland] supplemented with 10% foetal bovine serum (FBS), 1% penicillin and 1% streptomycin. OE33P and OE33R cells were maintained in vented 75 cm^2 Nunc^{TM} EasYFlasks^{TM} at 37°C and 5% CO_2/95% air. Cells were passaged upon reaching 70-80% confluence as estimated by a light microscope as described in *section 2.3.2*. OE33P cells were passaged at a 1:8 or 1:10 ratio and OE33R cells were passaged at a 1:6 or 1:8 ratio depending on experimental requirements.

3.3.3 Irradiation

Radiation was delivered using an XStrahl RS225 x-irradiator at a dose rate of 1.73 Gray (Gy)/min (195kV, 15mA) [XSTRAHL, Surrey, UK].

3.3.4 Generation of irradiated cell conditioned media (ICCM)

To generate ICCM for a single fraction of 1.8 Gy radiation, OE33P and OE33R cells were seeded in a 12-well plate at a density of $1x10^5$ cells/well in 2 mL complete RPMI 1640. Cells were incubated for 24 h at 37°C and 5% CO_2/95% air. Following 24 h incubation, cells were either mock-irradiated or irradiated with 1.8 Gy radiation and incubated for a further 24 h at 37°C and 5% CO_2/95% air. Following 24 h incubation, the supernatant was harvested and stored at -80°C until required.

To generate ICCM for repeated fractions of 1.8 Gy radiation, OE33P and OE33R cells were seeded in a 12-well plate at a density of $5x10^4$ cells/well in 2 mL complete RPMI 1640. Cells were incubated for 24 h at 37°C and 5% CO_2/95% air. Following 24 h incubation, immediately prior to irradiation, media was removed from the wells and replaced with 2 mL of complete RPMI 1640. Cells were either mock-irradiated or irradiated with 1.8 Gy radiation and incubated for a further 24 h at 37°C and 5% CO_2/95%

air. Following 24 h incubation, the supernatant was harvested from the single fraction dose of cells and stored at -80°C until required. A second fraction of 1.8 Gy radiation was delivered to the remaining cells and they were incubated for 24 h at 37°C and 5% CO_2/95% air. Following 24 h incubation, the supernatant was harvested from cells receiving 2 x 1.8 Gy fractions of radiation and stored at -80°C until required. A third fraction of 1.8 Gy radiation was delivered to the remaining cells, after which they were incubated for 24 h. Following 24 h incubation the supernatant was harvested and stored at -80°C until required.

ICCM for clonogenic experiments was generated using 75 cm^2 flasks. OE33P cells were seeded in a 75 cm^2 flask at a density of $7.5x10^5$ cells/flask in complete RPMI 1640. OE33R cells were seeded in a 75 cm^2 flask at a density of $1x10^6$ cells/flask in complete RPMI 1640. Cells were incubated for 24 h at 37°C and 5% CO_2/95% air. Following 24 h incubation, immediately prior to irradiation, media was discarded from flask and replaced with 13 mL of complete fresh media. Cells were either mock-irradiated or irradiated with 1.8 Gy radiation and incubated for 24 h. Following 24 h incubation, media was harvested and stored at -80°C until further processed.

3.3.5 Crystal violet assay

OE33P and OE33R cells were fixed in 1% glutaraldehyde and crystal violet assay was performed as described in *section 2.3.8.*

3.3.6 Seahorse analysis in OE33P and OE33R cells

OE33P cells were seeded in triplicate at a density of $1.1x10^3$ cells/well and OE33R cells were seeded at a density of $1.3x10^3$ cells/well in 24-well XFe24 cell culture microplates [Agilent Technologies, Santa Clara, CA, USA] and seahorse analysis was conducted as described in *section 2.3.9.* All measurements were normalised to cell number using the crystal violet assay as described in *section 3.3.5,* transferring the eluted stain to a 96-well plate before reading.

3.3.7 Mitochondrial membrane potential measurement

OE33P and OE33R cells were seeded at $8x10^3$ and $1x10^4$ cells/well respectively in a 96-well plate and mitochondrial membrane potential (mtMP) was assessed using the fluorescent probe Rhodamine 123 as described in *section 2.3.10.* All measurements were normalised to cell number using the crystal violet assay, as described in *section 3.3.5.*

3.3.8 Mitochondrial mass measurement

OE33P and OE33R cells were seeded at $8x10^3$ and $1x10^4$ cells/well respectively in a 96-well plate and mitochondrial mass was assessed as previously described in *section 2.3.11*. All measurements were normalised to cell number using the crystal violet assay, as described in *section 3.3.5*.

3.3.9 Reactive oxygen species measurement

OE33P and OE33R cells were seeded at $8x10^3$ and $1x10^4$ cells/well respectively in a 96-well plate and ROS was assessed as previously described in *section 2.3.12*. All measurements were normalised to cell number using the crystal violet assay, as described in section *3.3.5*.

3.3.10 Clonogenic assay

OE33P and OE33R cells were seeded in triplicate in a 6-well plate in complete RPMI 1640 at the densities indicated in **Table 3-1** and **3-2**. Cells were incubated for 24 h at 37°C and 5% CO_2/95% air. Following 24 h incubation cells were treated with ICCM from either mock-irradiated or irradiated SW837 cells. Control wells were treated with fresh complete RPMI 1640. Cells were incubated for 24 h at 37°C and 5% CO_2/95% air. Following 24 h incubation, cells were irradiated at the doses ranging from 0 Gy to 6 Gy. Following irradiation, cells were incubated for 7-10 d. Following 7-10 d incubation cells were fixed and stained with 25% methanol and 0.05% crystal violet for 30 min at room temperature.

Colonies consisting of 50 cells or more were counted using the GelCount colony counter. Plating efficiency (PE) was calculated using the following formula:

(No. of colonies formed/No. of cells seeded) x 100

Surviving fraction was calculated using the following formula:

(No. of colonies counted)/(No. of cells seeded x PE)

Table 3-1 Seeding densities for OE33P clonogenic assay

Radiation Dose Administered	Cell Number Seeded
0 Gy	1000
2 Gy	1500
4 Gy	3000
6 Gy	6000

Table 3-2 Seeding densities for OE33R clonogenic assay

Radiation Dose Administered	Cell Number Seeded
0 Gy	1500
2 Gy	1500
4 Gy	3000
6 Gy	6000

3.3.11 Bromodeoxyuridine (BrdU) proliferation assay

OE33P and OE33R cells were seeded at $5x10^3$ cells/well in 100 µL complete RPMI 1640 in a 96-well plate and were incubated for 24 h at 37°C/5% CO_2/95% air. Cell proliferation was analysed using BrdU proliferation ELISA assay [Roche, Germany] according to the manufacturer's instructions and as described in *section 2.3.13*. All ICCM proliferation readings were expressed as a percentage of RPMI control with RPMI proliferation levels set to 100%.

3.3.12 RNA isolation

OE33P and OE33R cells were seeded at a density of $3x10^5$ cells/well in complete RPMI 1640 in 6-well plates and allowed to adhere overnight. Following 24 h treatment with 1.5 mL ICCM per well, RNA was isolated from cell lines using the TRI Reagent® method as described in *section 2.3.15*.

3.3.13 RNA quantification

RNA quantification was determined spectrophotometrically using a Nanodrop 1000 spectrophotometer (version 3.1.0, Nanodrop technologies, DE, USA) as described in *section 2.3.16*.

3.3.14 cDNA synthesis

RNA samples were thawed on ice for 10 min. For each sample 1 µg total RNA was reverse transcribed to cDNA as described in *section 2.3.17*.

3.3.15 Quantitative real-time PCR

Quantitative real-time PCR was performed as described in *section 2.3.18.*

3.3.16 Quantitative real-time PCR data analysis

Data analysis was performed using the $2^{-\Delta\Delta Ct}$ relative quantification method (260). The threshold cycle (Ct) was calculated for each well and the expression levels of target genes were normalised to the expression of the endogenous control (*18S*). Gene expression levels were only reported if the transcript amplified before 35 cycles.

3.3.17 Statistical analysis

Statistical analysis was performed using GraphPad Prism 5 Software [GraphPad Software, CA, USA]. All data is expressed as mean ± SEM. Statistical test used is indicated in relevant figure legend. Statistical significance was considered at $p<0.05$.

The methodology employed in this chapter is summarised in **Figure 3.1**.

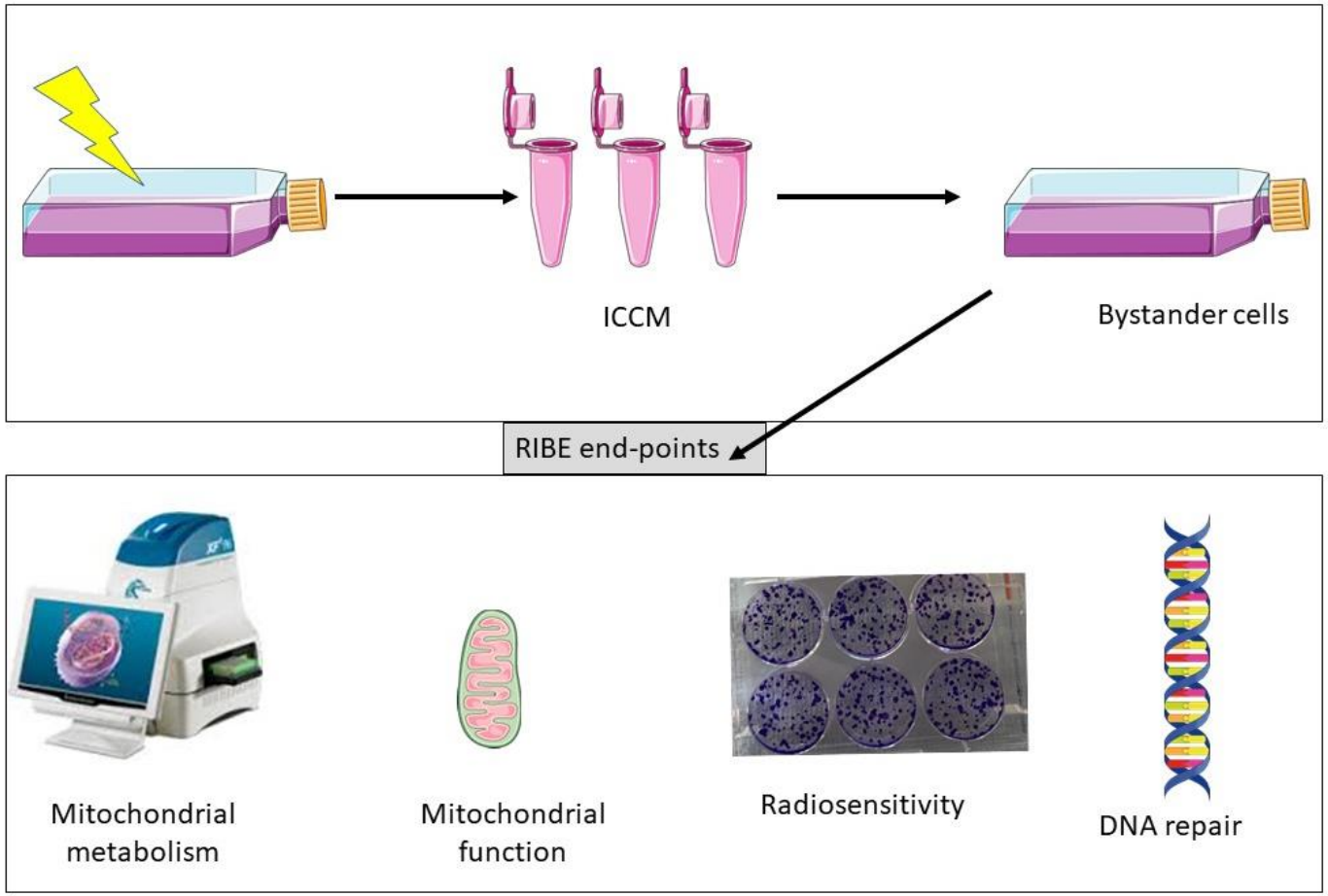

Figure 3.1 Schematic illustration of methodology employed in chapter 3

OE33P and OE33R cells were either mock-irradiated or irradiated with 1.8 Gy radiation and incubated for 24 h. Following 24 h incubation ICCM was harvested. OE33P and OE33R bystander cells were treated with ICCM for 24 h and RIBE end-points including mitochondrial metabolism, mitochondrial function, radiosensitivity and expression of DNA repair genes were assessed.

3.4 Results

Investigate the effect of *in vitro* RIBE induction in an isogenic model of radioresistance in OAC

We investigated the effect of *in vitro* RIBE induction on mitochondrial energy metabolism, mitochondrial function and radiosensitivity in an isogenic model of radioresistance in OAC. This novel model of radioresistance was generated by chronic irradiation of OE33 cells with clinically relevant doses of x-ray radiation as described above in the methods. This resulted in the generation of a radioresistant cell line; OE33R that is significantly more radioresistant than its age and passage matched control OE33P cell line (270).

3.4.1 RIBE induction *in vitro* did not have any significant effect on OCR, ECAR or OCR:ECAR ratio in OE33P cells

In vitro RIBE induction did not demonstrate any effect on OCR in the radiosensitive OE33P cells (p=0.42). Extracellular acidification rate (ECAR) was unchanged between OE33P cells treated with ICCM from either mock-irradiated or irradiated OE33P cells (p=0.91). OCR:ECAR ratio was not significantly altered in OE33P cells treated with ICCM from mock-irradiated or irradiated OE33P cells (p=0.27) (**Figure 3.2**).

3.4.2 RIBE induction *in vitro* causes significant reductions in proton leak in OE33P cells but has no effect on basal respiration, ATP production, maximal respiration or non-mitochondrial respiration

Basal respiration is unchanged between OE33P cells treated with ICCM from mock-irradiated or irradiated OE33P cells (p=0.18). Similarly, OCR-linked ATP production was unaffected by *in vitro* RIBE induction in OE33P cells (p=0.47). There was no significant difference in maximal respiration between OE33P cells treated with ICCM from mock-irradiated or irradiated OE33P cells (p=0.37). There was a significant reduction in proton leak in OE33P cells treated with ICCM from irradiated OE33P cells, when compared to those treated with ICCM from mock-irradiated OE33P cells (p=0.02). Non-mitochondrial respiration remained unchanged between OE33P cells treated with ICCM from mock-irradiated or irradiated OE33P cells (p=0.97) (**Figure 3.3**).

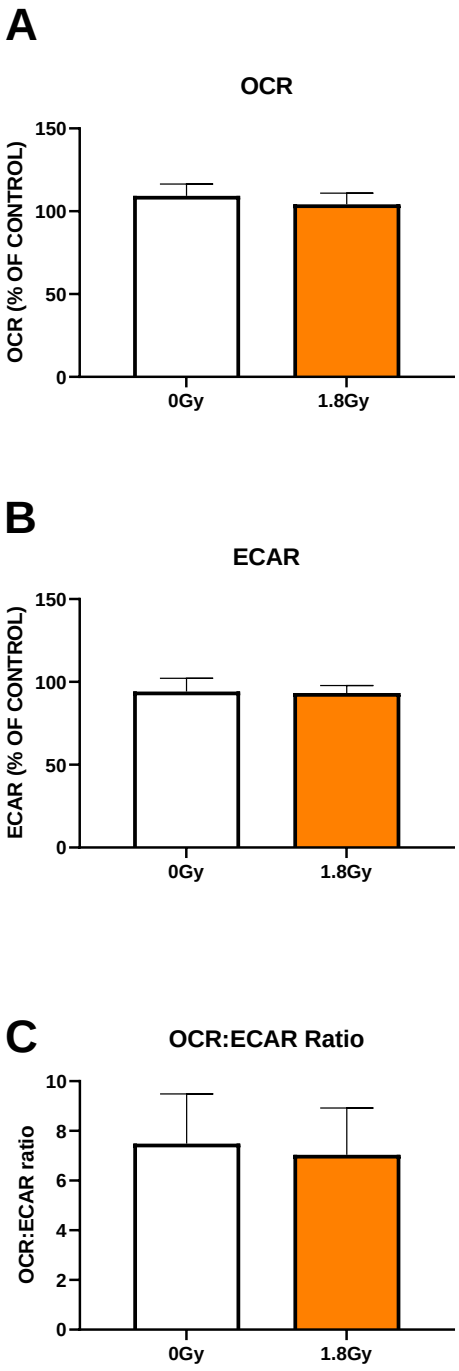

Figure 3.2 Effect of in vitro RIBE induction on OCR, ECAR and OCR:ECAR ratio in OE33P cells

There was no significant difference in (**A**) OCR, (**B**) ECAR or (**C**) OCR:ECAR ratio in OE33P cells treated with ICCM from mock-irradiated or irradiated OE33P cells. All data expressed as mean ± SEM. Statistical analysis was performed using a paired *t*-test. *n*=4.

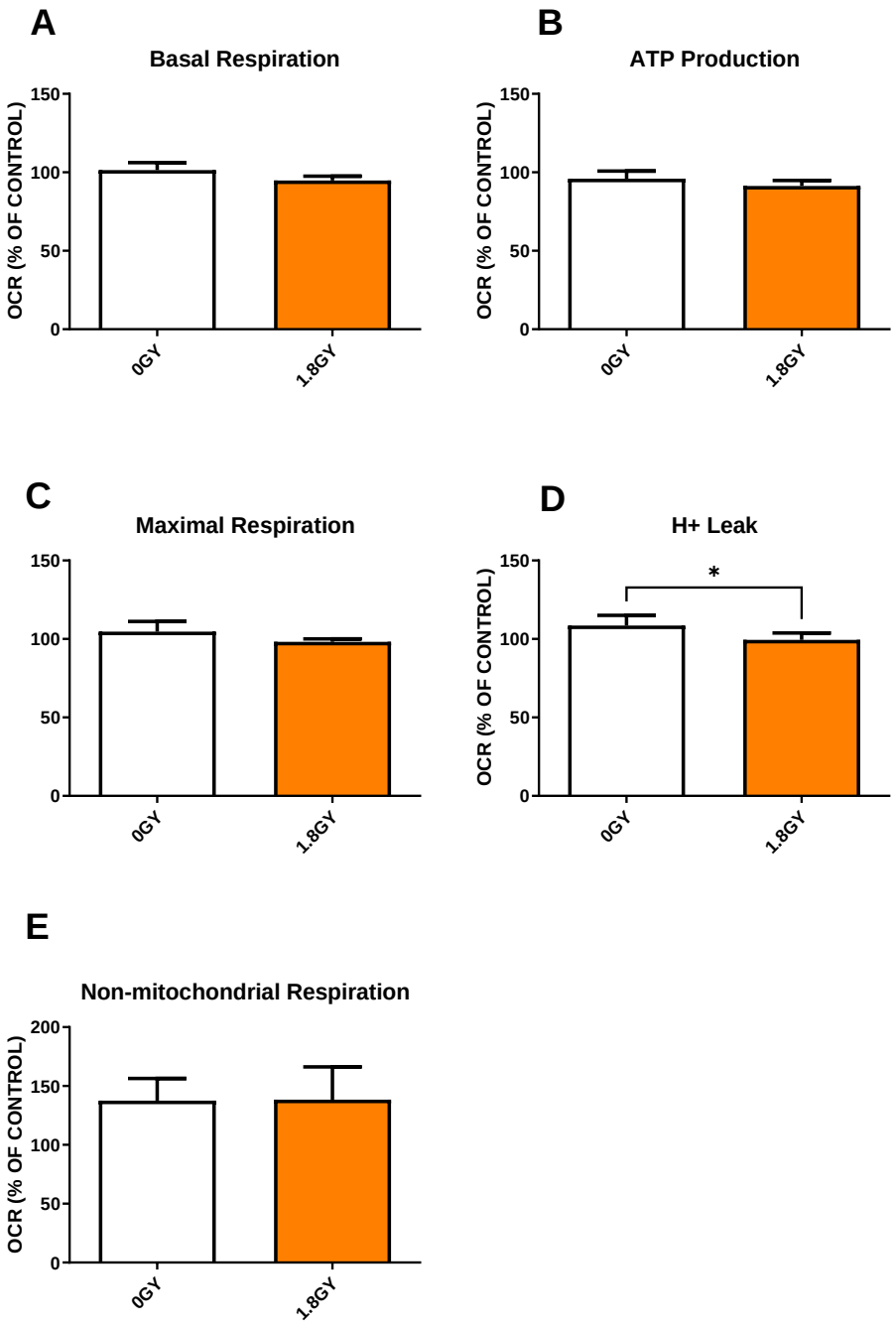

Figure 3.3 Effect of in vitro RIBE induction on basal respiration, ATP production, maximal respiration, proton leak and non-mitochondrial respiration in OE33P cells

There was no significant difference in (**A**) basal respiration (**B**) OCR-linked ATP production or (**C**) maximal respiration between OE33P cells treated with ICCM from mock-irradiated or irradiated OE33P cells. (**D**) Proton leak was significantly lower in OE33P cells treated with ICCM from irradiated OE33P cells compared to ICCM from mock-irradiated OE33P cells. (**E**) There was no significant difference in non-mitochondrial respiration between OE33P cells treated with ICCM from mock-irradiated or irradiated OE33P cells. All data expressed as mean ± SEM. Statistical analysis performed using a paired *t*-test. *$p<0.05$. $n=4$.

3.4.3 RIBE induction *in vitro* does not alter mitochondrial membrane potential, reactive oxygen species or mitochondrial mass in OE33P bystander cells

Since no statistically significant alterations were observed in bystander cellular metabolism in OE33P cells exposed to ICCM from irradiated compared to mock-irradiated OE33P cells, with the exception of proton leak, we investigated potential alterations to mitochondrial function through assessment of mtMP, ROS and mitochondrial mass in OE33P cells.

mtMP was measured using the Rhodamine 123 assay. There was no significant difference in mtMP in OE33P cells exposed to ICCM from irradiated compared to mock-irradiated OE33P cells (p=0.44). ROS levels were not significantly different in OE33P cells treated with ICCM from irradiated compared to mock-irradiated OE33P cells (p=0.90). No significant difference in mitochondrial mass was observed between bystander OE33P cells treated with ICCM from irradiated compared to mock-irradiated OE33P cells (p=0.44) (**Figure 3.4**).

3.4.4 RIBE induction *in vitro* does not alter radiosensitivity in OE33P bystander cells

The effect of *in vitro* RIBE induction on the radiosensitivity of OE33P bystander cells was investigated at 2 Gy, 4 Gy and 6 Gy using the gold standard clonogenic assay. No significant difference was observed in surviving fraction of OE33P cells exposed to ICCM from either irradiated or mock-irradiated OE33P cells at any of the radiation doses assessed (p>0.05) (**Figure 3.5**).

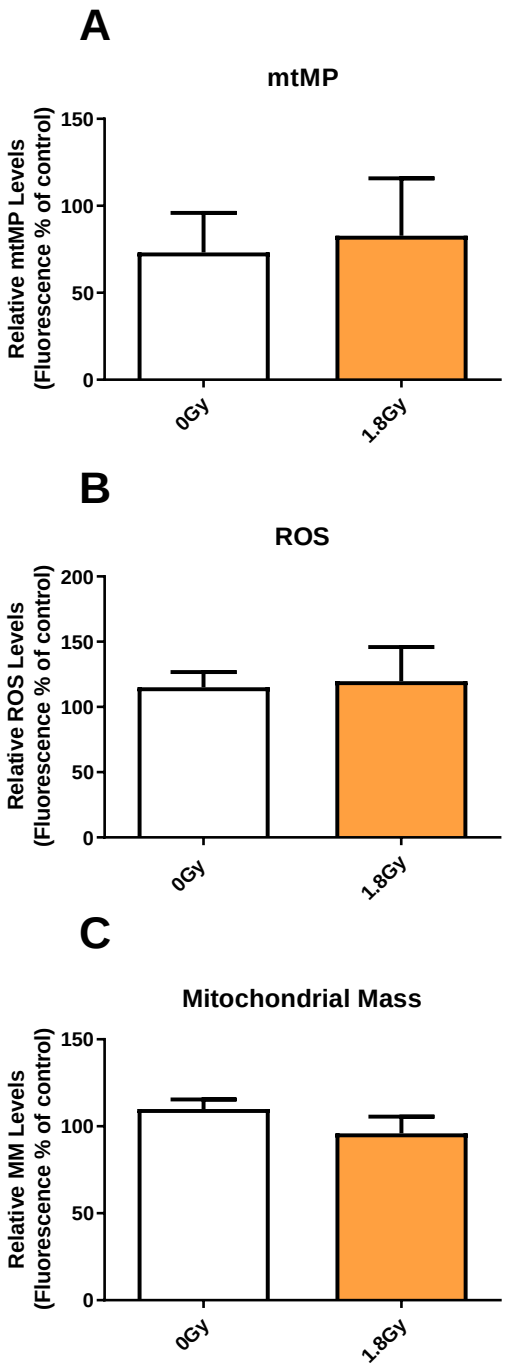

Figure 3.4 Effect of in vitro RIBE induction on mitochondrial function in bystander OE33P cells

No significant difference in (**A**) mtMP (**B**) ROS or (**C**) mitochondrial mass was observed in bystander OE33P cells treated with ICCM from irradiated compared to mock-irradiated OE33P cells. All data expressed as mean ± SEM. Statistical analysis was performed by paired *t*-test. *n*=3.

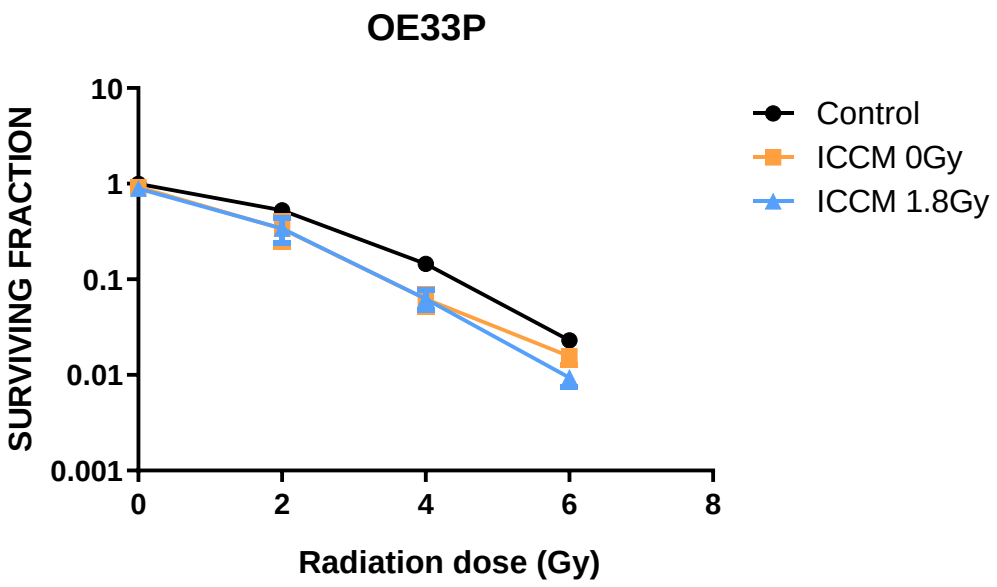

Figure 3.5 Effect of in vitro RIBE induction on radiosensitivity in OE33P cells

There was no significant difference in cellular radiosensitivity in OE33P cells following exposure to autologous ICCM from irradiated or mock-irradiated cells. All data expressed as mean ± SEM. Statistical analysis was performed using a one-way ANOVA. *n*=4.

3.4.5 RIBE induction *in vitro* did not have any significant effect on OCR, ECAR or OCR:ECAR ratio in OE33R cells

In vitro RIBE induction did not demonstrate any effect on OCR in the radioresistant OE33R cells (p=0.54). ECAR was unchanged between OE33R cells treated with ICCM from either mock-irradiated or irradiated OE33R cells (p=0.71). OCR:ECAR ratio was not significantly altered in OE33R cells treated with ICCM from irradiated compared to mock-irradiated OE33R cells (p=0.26) (**Figure 3.6**).

3.4.6 RIBE induction *in vitro* has no effect on basal respiration, ATP production, maximal respiration, proton leak or non-mitochondrial respiration in OE33R cells

Basal respiration was unchanged between OE33R cells treated with ICCM from mock-irradiated, when compared to irradiated OE33R cells (p=0.40). Similarly, OCR-linked ATP production was unchanged by *in vitro* RIBE induction in OE33R cells (p=0.51). There was no significant difference in maximal respiration between OE33R cells treated with ICCM from mock-irradiated compared to irradiated OE33R cells (p=0.88). There was no significant difference in proton leak in OE33R cells treated with ICCM from irradiated OE33R cells compared to those treated with ICCM from mock-irradiated OE33R cells (p=0.41). Non-mitochondrial respiration remained unchanged between OE33R cells treated with ICCM from mock-irradiated compared to irradiated OE33R cells (p=0.91) (**Figure 3.7**).

3.4.7 RIBE induction *in vitro* causes significant increases in mitochondrial membrane potential and reactive oxygen species but not mitochondrial mass in OE33R bystander cells

Similar to OE33P cells, no statistically significant alterations were detected in bystander cellular metabolism in OE33R cells exposed to ICCM from irradiated and mock-irradiated OE33R cells. However, we wanted to investigate potential alterations to mitochondrial function through assessment of mtMP, ROS and mitochondrial mass in OE33R cells.

There was a significant increase in mtMP in OE33R bystander cells treated with ICCM from irradiated OE33R cells, when compared to mock-irradiated OE33R cells (p=0.04). ROS levels were significantly higher in OE33R cells treated with ICCM from irradiated compared to mock-irradiated OE33R cells (p=0.01). No significant difference in

mitochondrial mass was observed between bystander OE33R cells treated with ICCM from irradiated compared to mock-irradiated OE33R cells (p=0.12) (**Figure 3.8**)

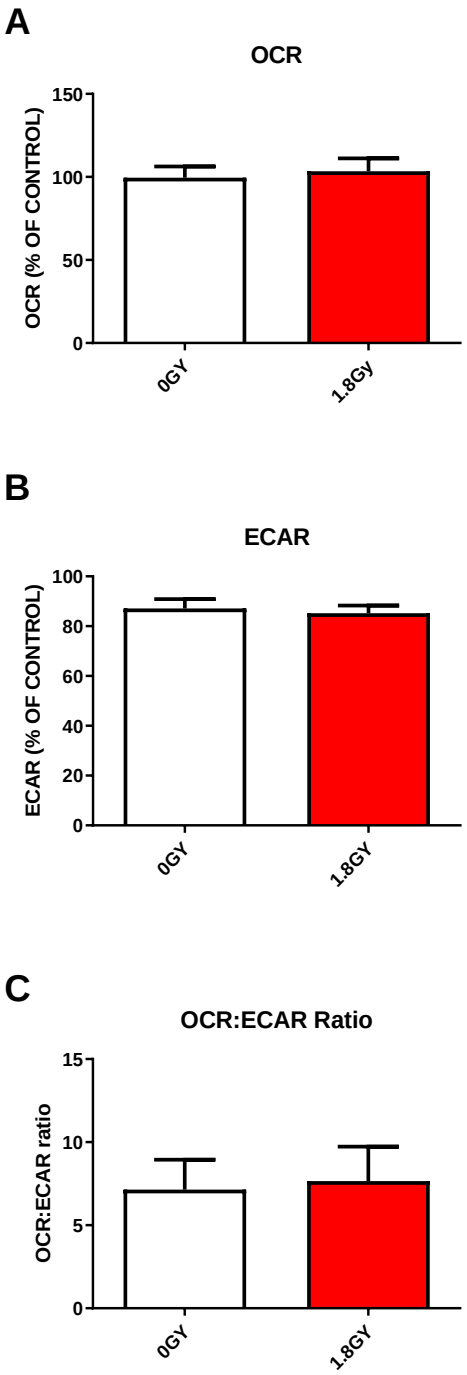

Figure 3.6 Effect of in vitro RIBE induction on OCR, ECAR and OCR:ECAR ratio in OE33R cells

(**A**) There was no significant difference in OCR in OE33R cells treated with ICCM from mock-irradiated compared to irradiated OE33R cells. (**B**) ECAR was not significantly different in OE33R cells treated with ICCM from mock-irradiated versus irradiated OE33R cells. (**C**) OCR:ECAR ratio remained unchanged in OE33R cells treated with ICCM from mock-irradiated compared to irradiated OE33R cells. All data expressed as mean ± SEM. Statistical analysis was performed using a paired *t*-test. *n*=4.

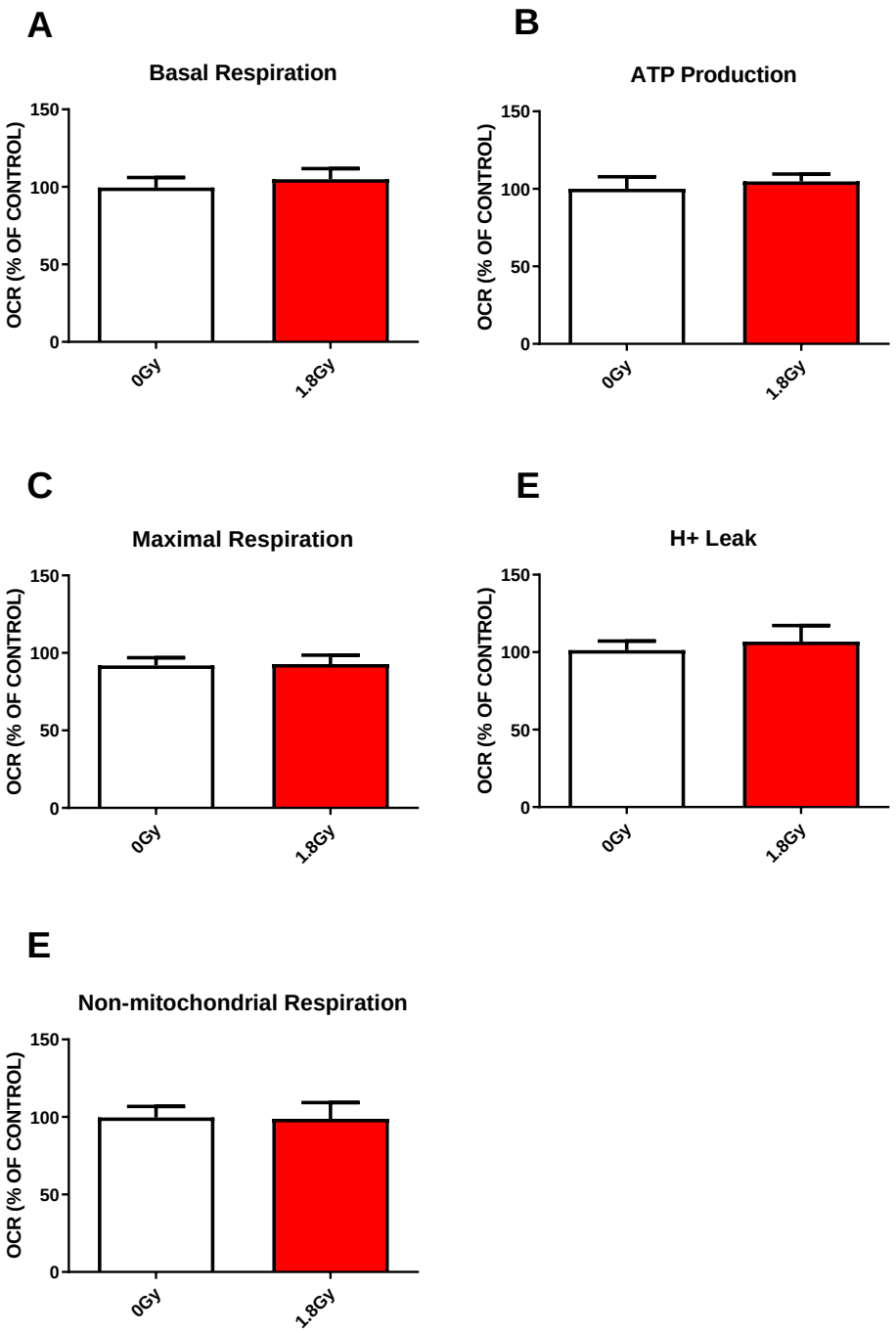

Figure 3.7 Effect of in vitro RIBE induction on basal respiration, ATP production, maximal respiration, proton leak and non-mitochondrial respiration in OE33R cells

There was no significant difference in (**A**) basal respiration (**B**) OCR-linked ATP production, (**C**) maximal respiration (**D**) proton leak or (**E**) non-mitochondrial respiration between OE33R cells treated with ICCM from mock-irradiated compared to irradiated OE33R cells. All data expressed as mean ± SEM. Statistical analysis was performed using a paired *t*-test. *n*=4.

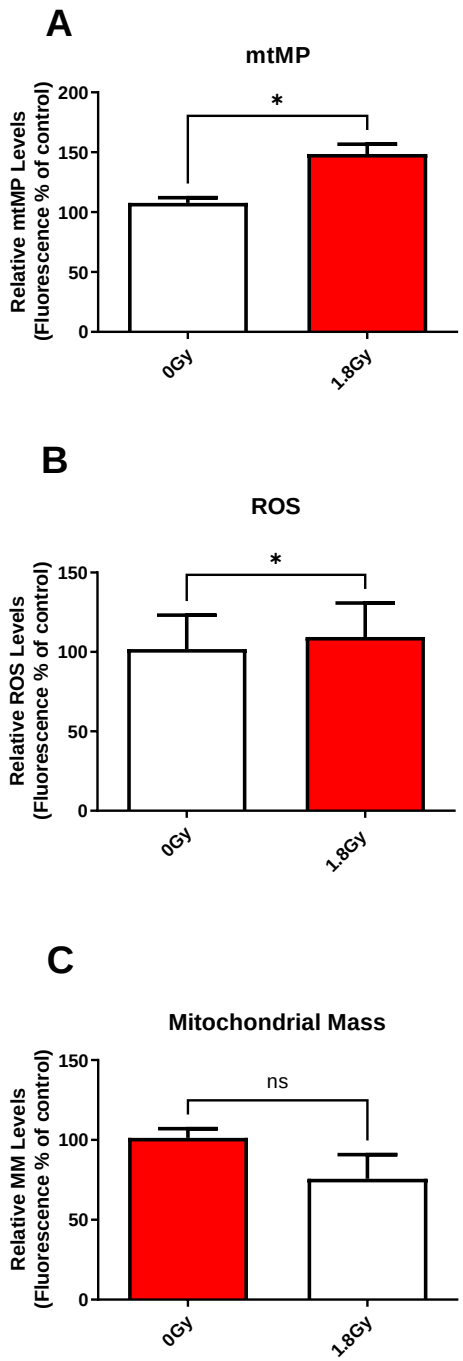

Figure 3.8 Effect of in vitro RIBE induction on mitochondrial function in bystander OE33R cells

(**A**) mtMP was significantly increased in bystander OE33R cells treated with ICCM from irradiated OE33R cells compared to mock-irradiated OE33R cells. (**B**) There was a significant increase in ROS levels in OE33R cells treated with ICCM from irradiated OE33R cells compared to mock-irradiated OE33R cells. (**C**) No significant difference in mitochondrial mass was observed in bystander OE33R cells treated with ICCM from irradiated OE33R cells compared to mock-irradiated OE33R cells. All data expressed as mean ± SEM. Statistical analysis by paired *t*-test. *p<0.05, ns = non-significant. *n*=3.

3.4.8 RIBE induction *in vitro* does not alter radiosensitivity in OE33R bystander cells

The effect of *in vitro* RIBE induction on the radiosensitivity of OE33R bystander cells was investigated at 2 Gy, 4 Gy and 6 Gy using the clonogenic assay. No significant difference was observed in surviving fraction of OE33R cells exposed to ICCM from either irradiated or mock-irradiated OE33R cells at any of the radiation doses assessed (p>0.05) (**Figure 3.9**).

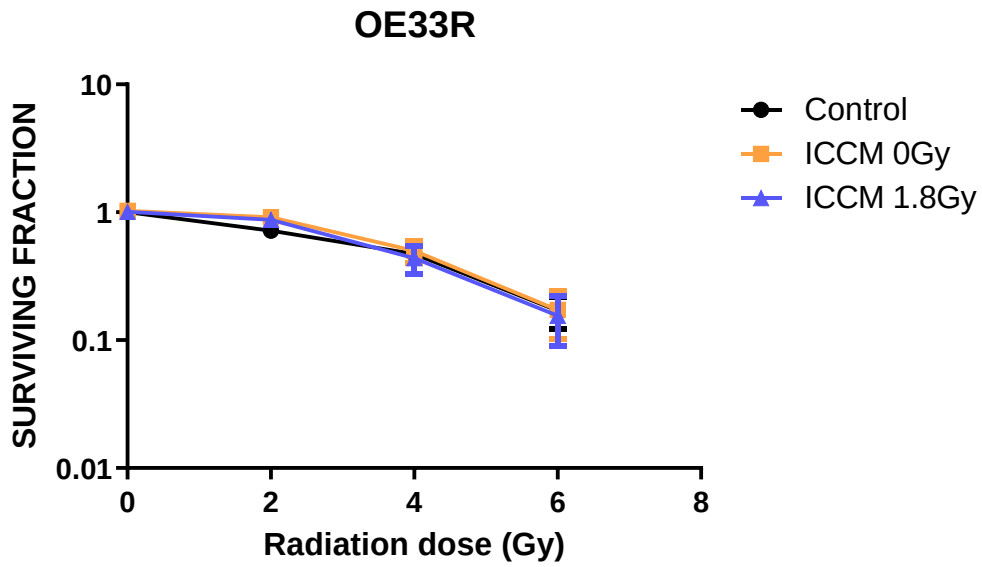

Figure 3.9 Effect of in vitro RIBE induction on radiosensitivity in OE33R cells

There was no significant difference in cellular radiosensitivity in OE33R cells following exposure to autologous ICCM. All data expressed as mean ± SEM. Statistical analysis was performed using a one-way ANOVA. *n*=4.

Investigating the effect of RIBE induction *in vitro* on bystander cellular mitochondrial metabolism, mitochondrial function and cellular proliferation in an isogenic model of radioresistant OAC following repeated fractions of clinically relevant doses of radiation

Having observed changes in OE33R cellular mitochondrial function following RIBE induction after a single fraction of a clinically relevant dose of radiation but no changes in mitochondrial metabolism, we investigated the effects of repeated fractions of a clinically relevant dose of radiation on mitochondrial metabolism and mitochondrial function in an isogenic model of radioresistance in OAC. The reason for choosing repeated fractions of 1.8 Gy radiation at 24 h intervals is to accurately reflect the clinical scenario whereby patients receive a daily fraction of 1.8 Gy, up to a total of 41.4 Gy, in the clinic.

3.4.9 RIBE induction *in vitro* following repeated fractions of radiation induces alterations in OCR, ECAR and OCR:ECAR ratio in bystander OE33P cells

OCR was significantly increased in bystander OE33P cells following treatment with ICCM from OE33P cells that received two fractions of 1.8 Gy radiation (p=0.04). There were no significant changes in OCR in OE33P cells treated with ICCM from OE33P cells receiving one or three fractions of 1.8 Gy radiation (p>0.05). Similarly, following treatment with ICCM from OE33P cells receiving two fractions of 1.8 Gy radiation, there was a significant increase in ECAR (p=0.003). A significant increase in ECAR was demonstrated in cells treated with ICCM from cells receiving three fractions of 1.8 Gy radiation (p=0.04). No change in ECAR was observed in bystander cells following treatment with ICCM from OE33P cells that received a single fraction of 1.8 Gy radiation (p>0.05). OCR:ECAR ratio was significantly reduced (p=0.04) in bystander OE33P cells treated with ICCM from OE33P cells that received two fractions of radiation (**Figure 3.10**).

3.4.10 RIBE induction following repeated fractions of radiation *in vitro* induces significant alterations in maximal respiration and non-mitochondrial respiration but not basal respiration, ATP production or proton leak in OE33P bystander cells

Basal respiration levels and OCR-linked ATP production remained unchanged in OE33P cells treated with ICCM from OE33P cells receiving between one and three fractions of 1.8 Gy radiation (p>0.05 for all fractions). Maximal respiration was significantly increased in OE33P bystander cells treated with ICCM from OE33P cells receiving two fractions of 1.8 Gy radiation (p=0.01). There was no difference in maximal respiration in

OE33P cells treated with ICCM from OE33P cells that received either one or three fractions of 1.8 Gy radiation (p>0.05). Proton leak was unaffected in bystander OE33P cells following exposure to ICCM from OE33P cells that received between one and three fractions of 1.8 Gy radiation (p>0.05). There was a significant increase in non-mitochondrial respiration in OE33P cells treated with ICCM from OE33P cells that received two fractions of 1.8 Gy radiation (p=0.02). Non-mitochondrial respiration was not significantly different in OE33P cells exposed to ICCM from OE33P cells exposed to between one or three fractions of 1.8 Gy radiation (p>0.05) (**Figure 3.11**).

3.4.11 RIBE induction *in vitro* induces alterations in mitochondrial membrane potential but not reactive oxygen species or mitochondrial mass in OE33P bystander cells

mtMP was significantly higher in bystander OE33P cells exposed to ICCM from OE33P cells that received a single fraction of 1.8 Gy radiation (p=0.03). There was no significant difference in mtMP in OE33P cells exposed to ICCM from OE33P cells that received either two or three fractions of 1.8 Gy radiation (p>0.05 for all fractions). ROS levels were not significantly different in OE33P cells treated with ICCM from OE33P cells exposed to either one or two fractions of 1.8 Gy radiation (p>0.05 for all fractions). It was not possible to obtain ROS readings for 3 x 1.8 Gy fractions of radiation as the cells persistently detached in the assay. No significant difference in mitochondrial mass was observed between bystander OE33P cells treated with ICCM from OE33P cells exposed to between one and three fractions of 1.8 Gy radiation (p>0.05 for all fractions) (**Figure 3.12**)

3.4.12 RIBE induction *in vitro* does not alter bystander cellular proliferation in mock-irradiated or irradiated OE33P cells

We were unable to perform a clonogenic assay on bystander cells following repeated fractions of radiation because the media was unable to support the growth of single cell colonies. Therefore, we utilised a BrdU assay to assess the effect of RIBE induction following repeated fractions of radiation on cellular proliferation in mock-irradiated and irradiated cells as a surrogate marker of radiosensitivity. We did not see any significant alterations in bystander cellular proliferation following exposure of OE33P cells to autologous ICCM from cells irradiated with between one and three fractions of 1.8 Gy radiation (p>0.05 for all fractions) (**Figure 3.13**).

3.4.13 RIBE induction *in vitro* does not cause alterations in the expression of DNA repair genes in OE33P cells

There were no significant differences in the expression of the DNA repair genes *PARP1*, *SMUG1*, *MMS19* or *MLH1* in OE33P cells treated with ICCM from OE33P cells that received between one and three fractions of radiation ($p>0.05$ for all fractions) (**Figure 3.14**).

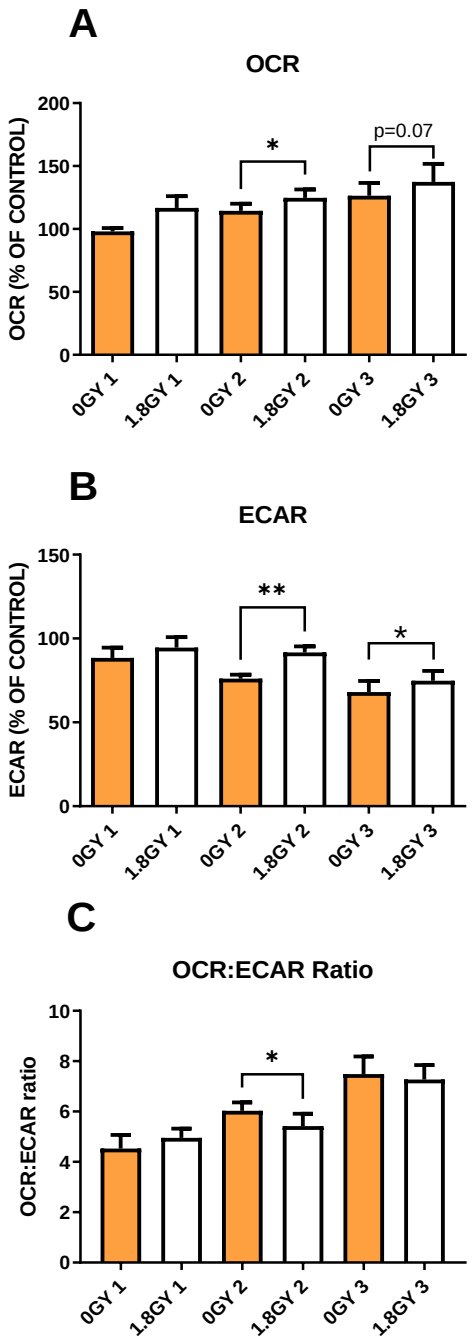

Figure 3.10 Effect of RIBE induction following repeated fractions of 1.8 Gy radiation on OCR, ECAR and OCR:ECAR ratio in bystander OE33P cells

(**A**) There was a significant increase in OCR in bystander OE33P cells treated with ICCM from OE33P cells exposed to 2 x 1.8 Gy radiation. There was no significant difference in OCR following treatment with ICCM from OE33P cells exposed to one or three fractions of 1.8 Gy. (**B**) ECAR was significantly increased in OE33P bystander cells following treatment with ICCM from OE33P cells that received two and three fractions of 1.8 Gy radiation. (**C**) OCR:ECAR ratio was significantly reduced in OE33P cells treated with ICCM from cells that received two fractions of radiation. All data expressed as mean ± SEM. Statistical analysis was performed using a paired *t*-test. *$p<0.05$, **$p<0.01$. $n=4$.

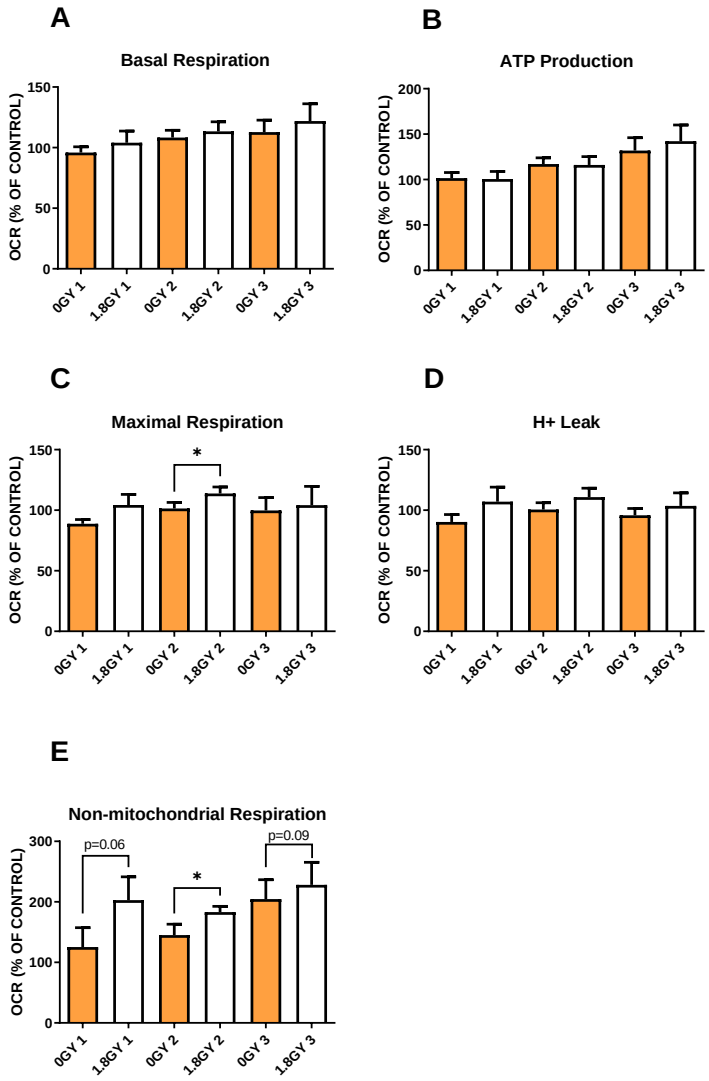

Figure 3.11 Effect of RIBE induction following repeated fractions of 1.8 Gy radiation on basal respiration, ATP production, maximal respiration, proton leak and non-mitochondrial respiration in bystander OE33P cells

There was no significant difference in (**A**) basal respiration or (**B**) OCR-linked ATP production between OE33P cells treated with ICCM from OE33P cells that received between one and three fractions of 1.8 Gy radiation. (**C**) There was a significant increase in maximal respiration in OE33P bystander cells treated with ICCM from OE33P cells that received 2 x 1.8 Gy fractions of radiation. There was no difference in maximal respiration in OE33P cells treated with ICCM from OE33P cells that received between one and three fractions of 1.8 Gy radiation. (**D**) Proton leak did not differ significantly between OE33P cells that received between one and three fractions of 1.8 Gy radiation (**E**) There was a significant increase in non-mitochondrial respiration in OE33P bystander cells treated with ICCM from OE33P cells that received 2 x 1.8 Gy fractions of radiation. There was no difference in non-mitochondrial respiration in OE33P cells treated with ICCM from OE33P cells following between one and three fractions of 1.8 Gy radiation. All data expressed as mean ± SEM. Statistical analysis was performed using a paired *t*-test. **p*<0.05. n=4.

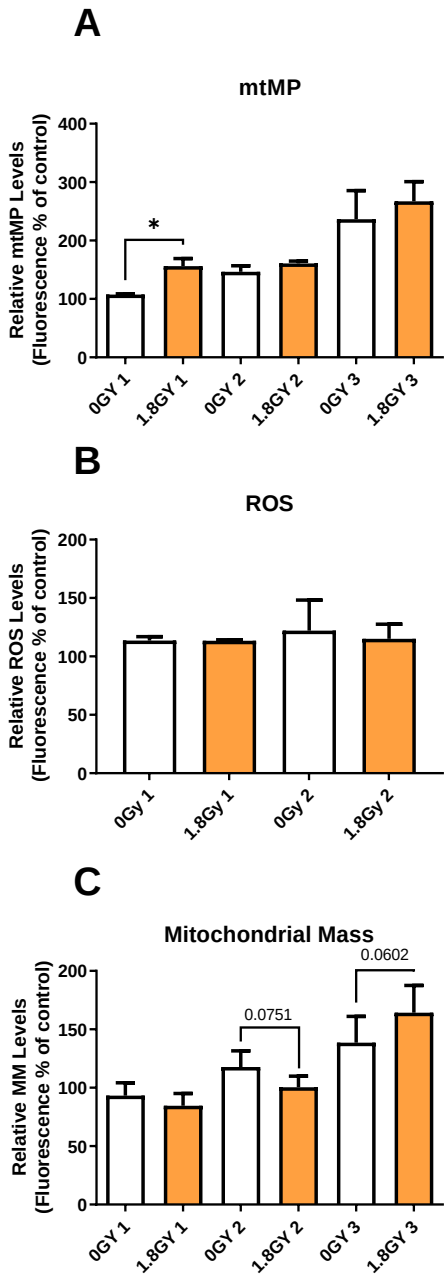

Figure 3.12 Effect of in vitro RIBE induction following repeated fractions of radiation on mitochondrial function in bystander OE33P cells

(**A**) mtMP was significantly increased in OE33P cells treated with ICCM from OE33P cells that received a single fraction of 1.8 Gy radiation. There were no significant differences in mtMP in bystander OE33P cells treated with ICCM from OE33P cells exposed to two and three fractions of 1.8 Gy radiation. (**B**) There was no significant difference in ROS in bystander OE33P cells treated with ICCM from OE33P cells exposed to either one or two fractions of 1.8 Gy radiation. (**C**) There was no significant difference in mitochondrial mass in bystander OE33P cells treated with ICCM from OE33P cells exposed to between one and three fractions of 1.8 Gy radiation. All data expressed as mean ± SEM. Statistical analysis by paired *t*-test. *$p<0.05$. $n=4$ for mtMP and mitochondrial mass, $n=3$ for ROS.

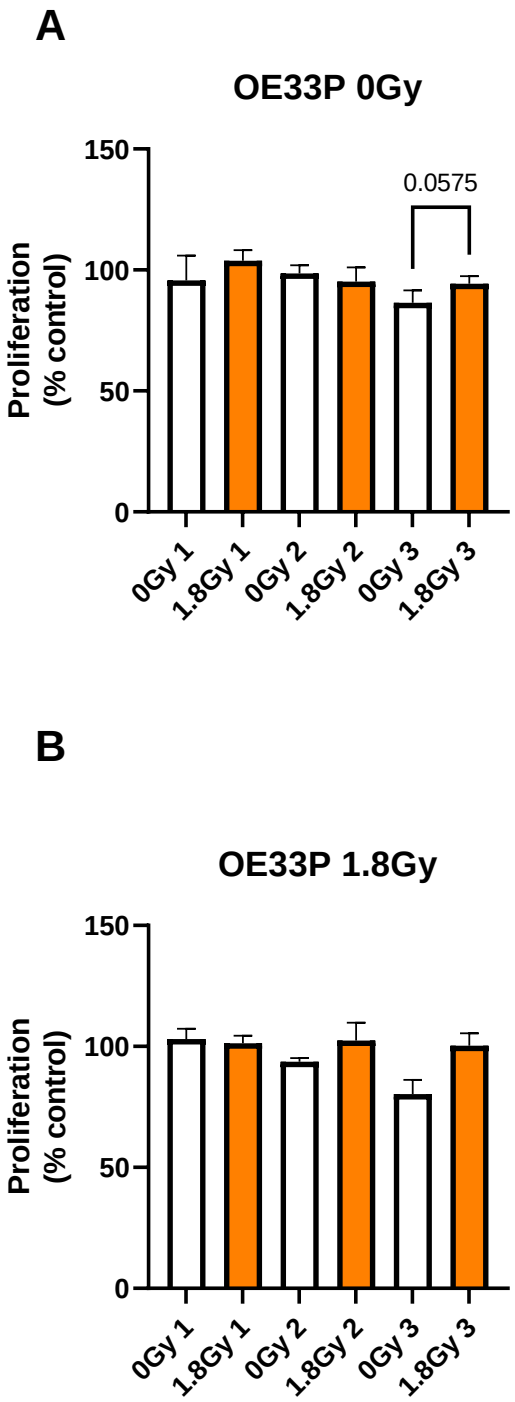

Figure 3.13 Effect of in vitro RIBE induction following repeated fractions of radiation on cellular proliferation in bystander mock-irradiated and irradiated OE33P cells

There was no significant difference in cellular proliferation in (**A**) mock-irradiated or (**B**) irradiated bystander OE33P cells treated with ICCM from OE33P cells. All data expressed as mean ± SEM. Statistical analysis by paired *t*-test. *n*=3.

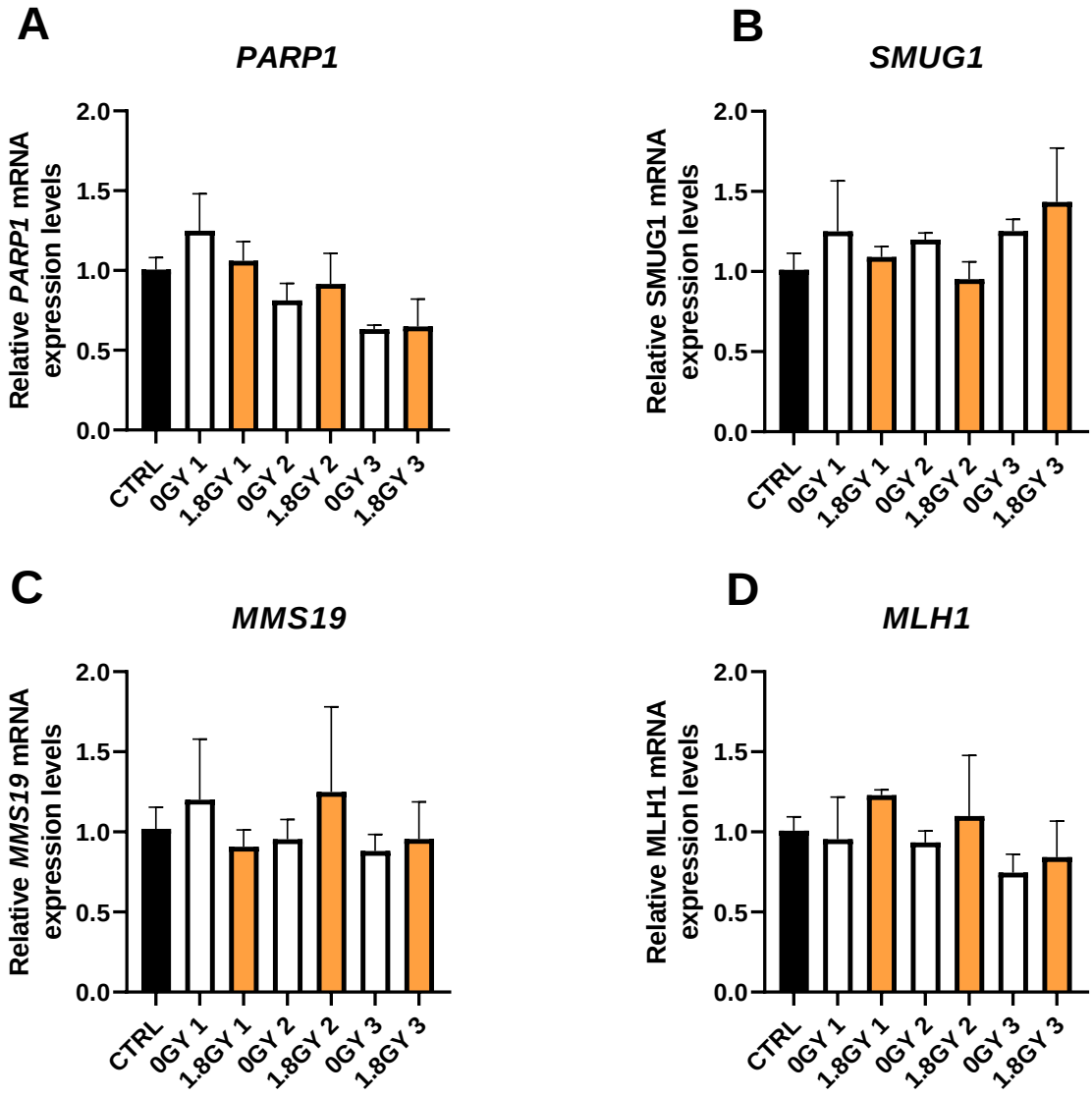

Figure 3.14 Effect of in vitro RIBE induction following repeated fractions of radiation on expression of DNA repair genes in bystander OE33P cells

There was no significant difference in the expression of (**A**) *PARP1*, (**B**) *SMUG1*, (**C**) *MMS19* or (**D**) *MLH1* in OE33P cells treated with ICCM from OE33P cells that received between one and three fractions of 1.8 Gy radiation. All data expressed as mean ± SEM. Statistical analysis by paired *t*-test. *n*=3.

3.4.14 RIBE induction *in vitro* following repeated fractions of radiation induces alterations in OCR and ECAR but not OCR:ECAR ratio in bystander OE33R cells

OCR was significantly decreased in bystander OE33R cells following treatment with ICCM from OE33R cells that received three fractions of 1.8 Gy radiation (p=0.01). There were no significant changes in OCR in OE33R cells treated with ICCM from OE33R cells receiving one or two fractions of 1.8 Gy radiation (p>0.05). Following treatment with ICCM from OE33R cells receiving two fractions of 1.8 Gy radiation, there was a significant increase in ECAR (p=0.006). No change in ECAR was observed in bystander OE33R cells following treatment with ICCM from OE33R cells that received a single fraction or three fractions of 1.8 Gy radiation (p>0.05). OCR:ECAR ratio was significantly reduced in OE33R cells treated with ICCM from OE33R cells that received 2 x 1.8 Gy fractions of radiation (p=0.01). No alterations in OCR:ECAR ratio were observed in OE33R cells treated with ICCM from OE33R cells that received either one or three fractions of 1.8 Gy radiation (**Figure 3.15**).

3.4.15 RIBE induction following repeated fractions of radiation *in vitro* induces significant alterations in proton leak but not basal respiration, ATP production, maximal respiration or non-mitochondrial respiration in OE33R bystander cells

Basal respiration levels remained unchanged in OE33R cells treated with ICCM from OE33R cells receiving between one and three fractions of 1.8 Gy radiation (p>0.05 for all fractions). Similarly, OCR-linked ATP production was not significantly altered in bystander OE33R cells treated with ICCM from OE33R cells receiving between one and three fractions of 1.8 Gy radiation (p>0.05 for all fractions). There were no differences in maximal respiration in OE33R cells treated with ICCM from OE33R cells that received between one and three fractions of 1.8 Gy radiation (p>0.05). Proton leak was unaffected in bystander OE33R cells following exposure to ICCM from OE33R cells that received either a single or two fractions of 1.8 Gy radiation (p>0.05). There was a significant reduction in proton leak in OE33R bystander cells following treatment with ICCM from OE33R cells that were exposed to three fractions of 1.8 Gy radiation (p=0.02). Non-mitochondrial respiration was not significantly altered in OE33R cells exposed to ICCM from OE33R cells exposed to between one and three fractions of 1.8 Gy radiation (p>0.05) (**Figure 3.16**).

3.4.16 RIBE induction *in vitro* induces alterations in mitochondrial membrane potential but not reactive oxygen species or mitochondrial mass in OE33R bystander cells

mtMP was significantly reduced in bystander OE33R cells exposed to ICCM from OE33R cells that received two fractions of 1.8 Gy radiation (p=0.03). There was no significant difference in mtMP in OE33R cells exposed to ICCM from OE33R cells treated with either one or three fractions of 1.8 Gy radiation (p>0.05 for all fractions). ROS levels are not significantly different in OE33R cells treated with ICCM from OE33R cells exposed to either one or two fractions of 1.8 Gy radiation (p>0.05 for all fractions). It was not possible to obtain ROS readings for 3 x 1.8 Gy fractions of radiation as the cells persistently detached in the assay. No significant differences in mitochondrial mass were observed between bystander OE33R cells treated with ICCM from OE33R cells exposed to between one and three fractions of 1.8 Gy radiation (p>0.05 for all fractions) (**Figure 3.17**).

3.4.17 RIBE induction *in vitro* following a single fraction of radiation induces significant reductions in cellular proliferation in both mock-irradiated and irradiated OE33R cells

Using cellular proliferation as a surrogate of radiosensitivity, we observed a significant reduction in bystander cellular proliferation in OE33R cells exposed to ICCM from OE33R cells that received a single fraction of 1.8 Gy radiation. This observation occurred in both mock-irradiated and irradiated OE33R cells (p<0.05). There were no differences in cellular proliferation in bystander OE33R cells treated with ICCM from OE33R cells that received either two or three fractions of 1.8 Gy radiation (**Figure 3.18**).

3.4.18 RIBE induction *in vitro* following three fractions of radiation causes alterations in the expression of *PARP1* and *MLH1* in OE33R cells

RIBE induction following 3 x 1.8 Gy fractions of radiation caused significant elevations in the expression of *PARP1* and *MLH1* in OE33R cells (p<0.05). Expression levels of *MMS19* showed a trend towards increased levels following RIBE induction with 3 x 1.8 Gy fractions but this did not reach statistical significance (p=0.051). *SMUG1* levels were not altered by RIBE induction. *PARP1*, *MMS19* and *MLH1* levels were not altered by RIBE induction after a single or two fractions of 1.8 Gy radiation (p>0.05 for all fractions) (**Figure 3.19**).

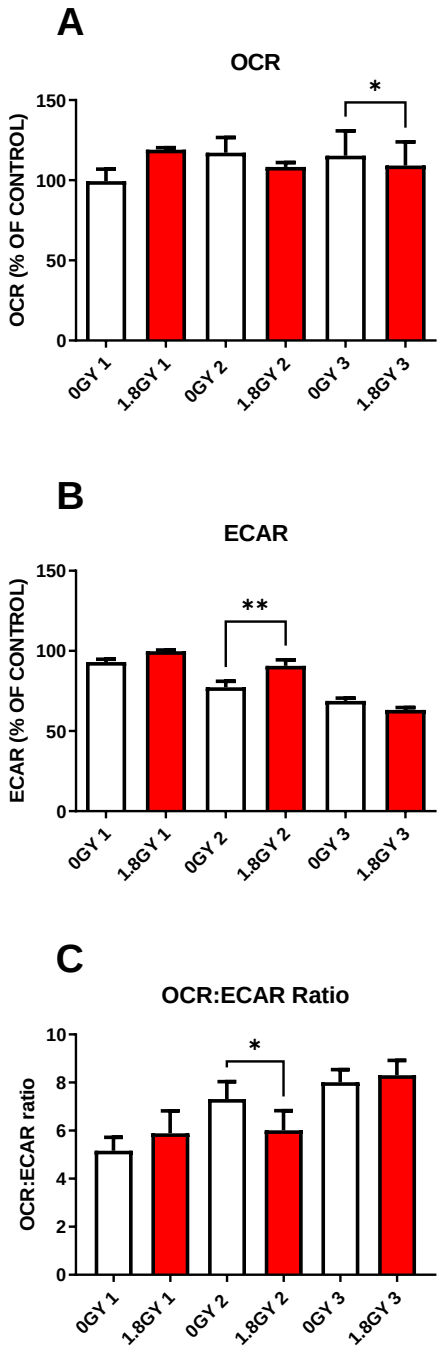

Figure 3.15 Effect of RIBE induction following repeated fractions of 1.8 Gy radiation on OCR, ECAR and OCR:ECAR ratio in bystander OE33R cells

(**A**) There was a significant decrease in OCR in bystander OE33R cells treated with ICCM from OE33R cells exposed to 3 x 1.8 Gy fractions of radiation. There were no significant differences in OCR following treatment with ICCM from OE33R cells exposed to one or two fractions of 1.8 Gy. (**B**) ECAR was significantly increased in OE33R bystander cells following treatment with ICCM from OE33R cells that received two fractions of 1.8 Gy radiation. (**C**) OCR:ECAR ratio did not differ significantly in bystander OE33R cells treated with ICCM from OE33R cells exposed to between one and three fractions of 1.8 Gy radiation. All data expressed as mean ± SEM. Statistical analysis was performed using a paired *t*-test. *$p<0.05$. $n=3$

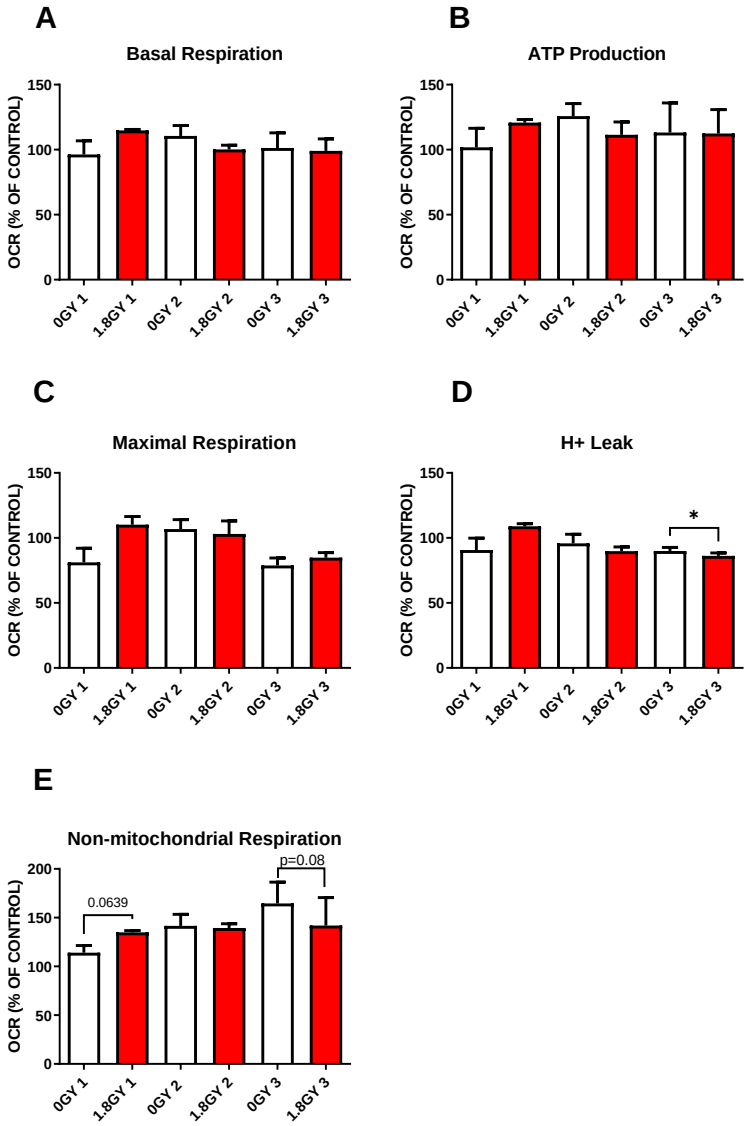

Figure 3.16 Effect of RIBE induction following repeated fractions of 1.8 Gy radiation on basal respiration, ATP production, maximal respiration, proton leak and non-mitochondrial in bystander OE33R cells

There was no significant difference in (**A**) basal respiration, (**B**) OCR-linked ATP production or (**C**) maximal respiration in OE33R cells treated with ICCM from OE33R cells following between one and three fractions of 1.8 Gy radiation. (**D**) Proton leak did not differ significantly between OE33R cells treated with ICCM from OE33R cells following between one and two fractions of 1.8 Gy radiation. There was a significant reduction in proton leak in bystander OE33R cells following treatment with OE33R cells that received three fractions of 1.8 Gy radiation. (**E**) There was no difference in non-mitochondrial respiration in OE33R cells treated with ICCM from OE33R cells following between one and three fractions of 1.8 Gy radiation. All data expressed as mean ± SEM. Statistical analysis by paired *t*-test. *$p<0.05$. $n=3$.

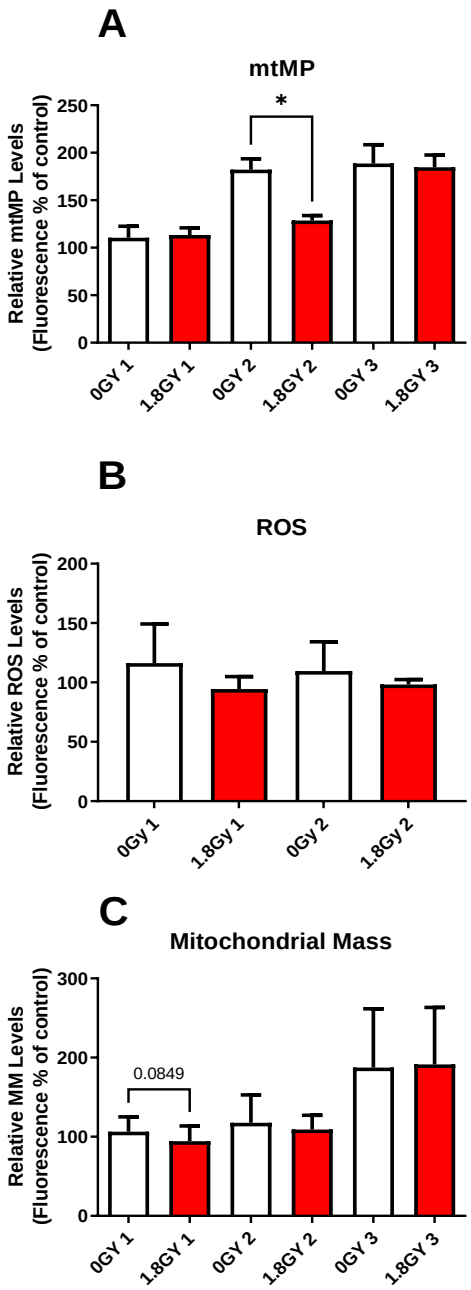

Figure 3.17 Effect of in vitro RIBE induction following repeated fractions of radiation on mitochondrial function in bystander OE33R cells

(**A**) mtMP was significantly decreased in OE33R cells treated with ICCM from OE33R cells that received two fractions of 1.8 Gy radiation. There were no significant differences in mtMP in bystander OE33R cells treated with ICCM from OE33R cells exposed to either one or three fractions of 1.8 Gy radiation. (**B**) There were no significant differences in ROS in bystander OE33R cells treated with ICCM from OE33R cells exposed to either one or two fractions of 1.8 Gy radiation. (**C**) There were no significant differences in mitochondrial mass in bystander OE33R cells treated with ICCM from OE33R cells exposed to between one and three fractions of 1.8 Gy radiation. All data expressed as mean ± SEM. Statistical analysis by paired *t*-test. *$p<0.05$. $n=4$ for mtMP and mitochondrial mass, $n=3$ for ROS.

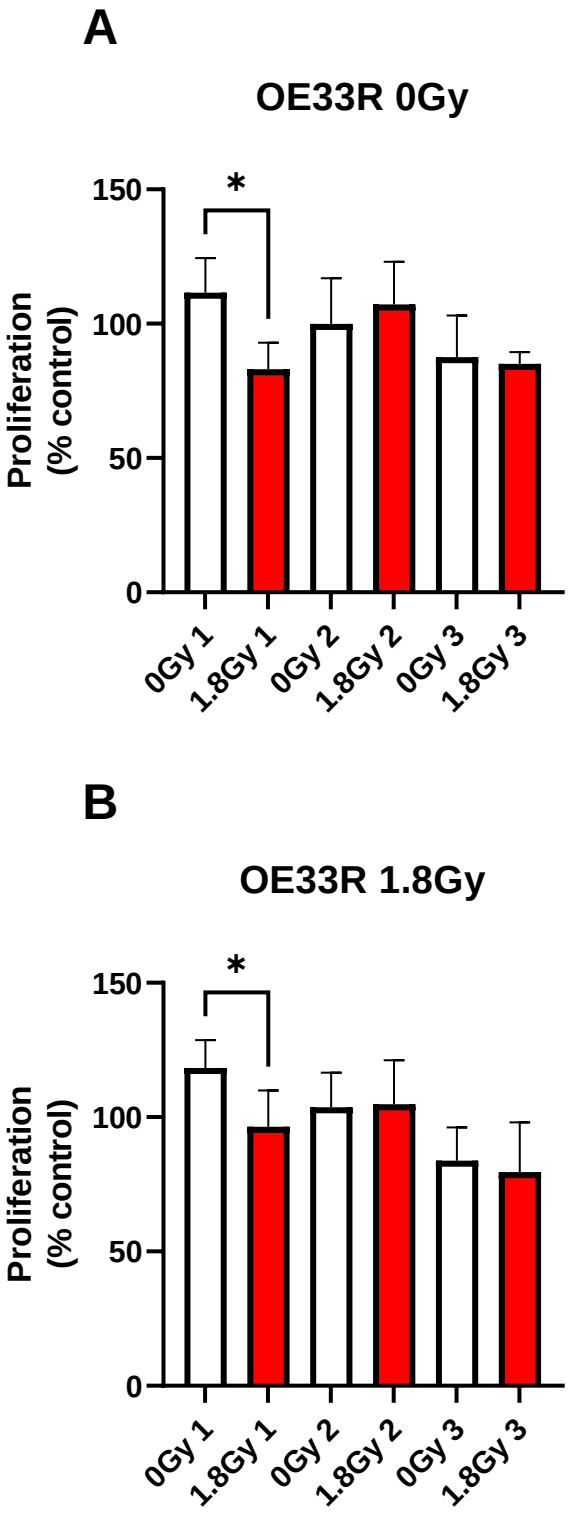

Figure 3.18 Effect of in vitro RIBE induction following repeated fractions of radiation on cellular proliferation in bystander mock-irradiated and irradiated OE33R cells

There was a significant reduction in cellular proliferation in (**A**) mock-irradiated and (**B**) irradiated bystander OE33R cells treated with ICCM from OE33R cells following a single fraction of 1.8 Gy radiation. All data expressed as mean ± SEM. Statistical analysis by paired *t*-test. *$p<0.05$. $n=3$.

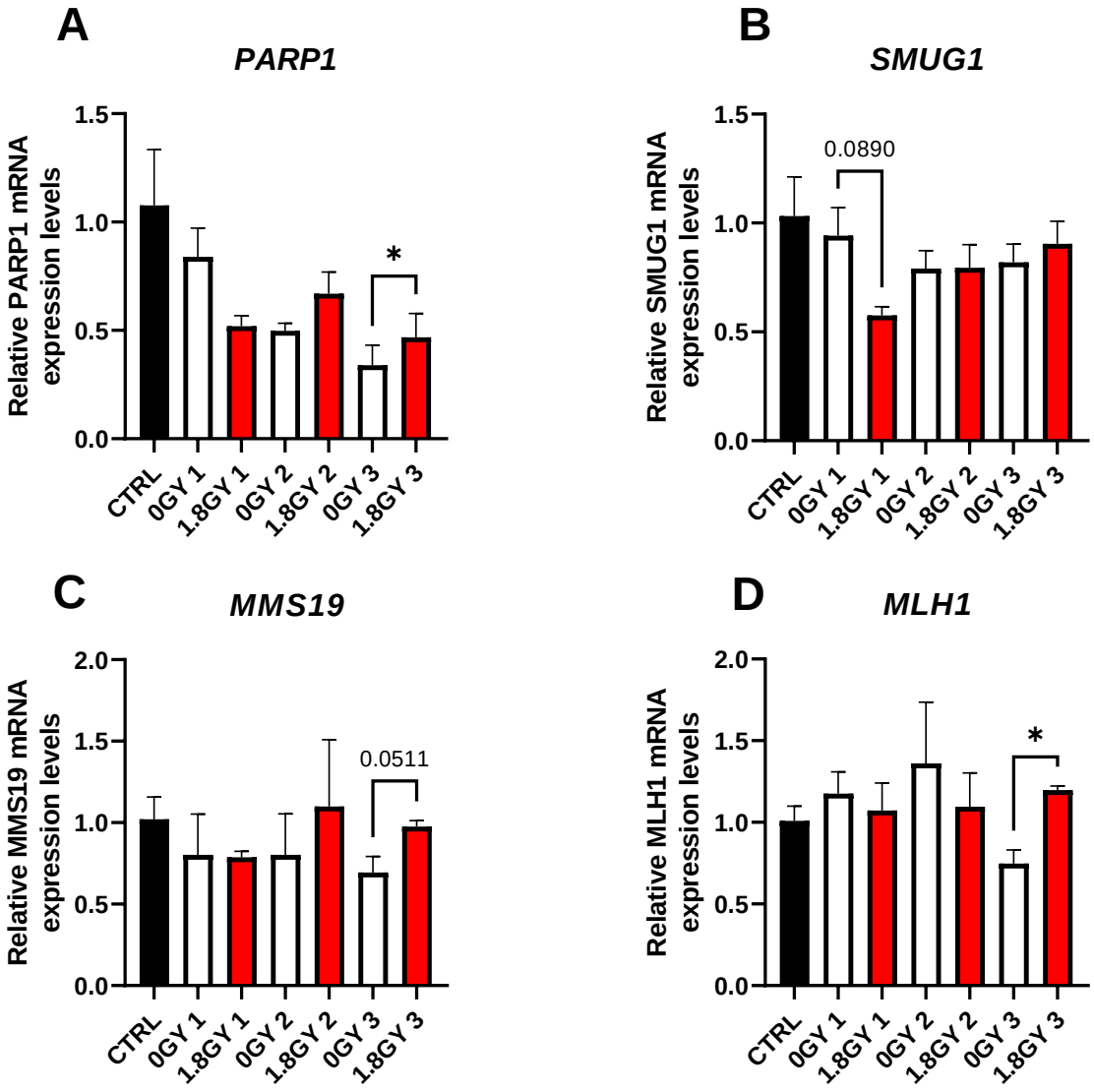

Figure 3.19 Effect of in vitro RIBE induction following repeated fractions of radiation on expression of DNA repair genes in bystander OE33R cells

(**A**) *PARP1* was significantly elevated in OE33R cells treated with ICCM from OE33R cells that received 3 x 1.8 Gy fractions of radiation. (**B**) There were no significant differences in the expression of *SMUG1* in OE33R cells following RIBE induction with between one and three fractions of radiation. (**C**) Expression of *MMS19* was not significantly altered in OE33R cells treated with ICCM from OE33R cells that received one or two fractions of 1.8 Gy radiation. *MMS19* levels in OE33R cells treated with ICCM from OE33R cells that received three fractions of 1.8 Gy radiation showed a trend towards higher levels, however this did not reach statistical significance. (**D**) *MLH1* expression levels were significantly elevated in OE33R cells following exposure to ICCM from OE33R cells that received 3 x 1.8 Gy fractions of radiation. All data expressed as mean ± SEM. Statistical analysis by paired *t*-test. *$p<0.05$. $n=3$.

3.5 Summary of findings from chapter 3

- RIBE induction *in vitro* following a single fraction of 1.8 Gy x-irradiation did not alter mitochondrial metabolism or radiosensitivity in the radiosensitive OE33P cells. mtMP was elevated in OE33P cells treated with ICCM from OE33P cells that received a single fraction of 1.8 Gy radiation in the repeated fractionation experimental set up.
- RIBE induction *in vitro* following a single fraction of 1.8 Gy x-irradiation did not alter mitochondrial metabolism or radiosensitivity in the radioresistant OE33R cell line. It did induce alterations in mitochondrial function, specifically increases in mtMP and ROS levels.
- *In vitro* RIBE induction following repeated fractions of 1.8 Gy x-irradiation caused increases in OCR, ECAR, maximal respiration and non-mitochondrial respiration in OE33P cells. It did not affect cellular proliferation or the expression of the DNA repair genes *PARP1*, *SMUG1*, *MMS19* or *MLH1*.
- In OE33R cells, *in vitro* RIBE induction following repeated fractions of 1.8 Gy x-irradiation caused alterations in OCR, ECAR, mtMP, cellular proliferation and expression of the DNA repair genes *PARP1* and *MLH1*.

3.6 Discussion

Similar to the results obtained in chapter 2 investigating the effects of RIBE induction following a single fraction of 1.8 Gy radiation on bystander cellular metabolism, we did not see any significant differences in bystander cellular metabolism in the radiosensitive OE33P cell line, with the exception of proton leak. In the radioresistant OE33R cell line, there were no significant alterations in bystander cellular metabolism following *in vitro* RIBE induction using a single fraction of 1.8 Gy radiation. We see a differential response in mitochondrial function between OE33P and OE33R cells following RIBE induction after a single fraction of a clinically relevant dose of ionising radiation. OE33R cells demonstrate a significant increase in mtMP and ROS in response to RIBE induction while mtMP and ROS remain unchanged in OE33P cells. ROS are well recognised players in RIBE events; therefore, it is surprising that there was no increase in OE33P cells following RIBE induction. However, similar results were obtained in chapter 2, whereby no increase in ROS was observed following *in vitro* RIBE induction in CRC. It is unusual that mtMP increased with a concomitant increase in ROS. Increases in ROS may cause depolarisation of mtMP and trigger mitophagy, a process whereby defective mitochondria are degraded to maintain a healthy population of mitochondria (275).

Interestingly, while no significant alterations in bystander energy metabolism were observed following RIBE induction after a single fraction of 1.8 Gy, repeated fractions of 1.8 Gy induced significant alterations in bystander metabolism in both OE33P and OE33R cells. RIBE induction following two fractions of 1.8 Gy radiation induced significant increases in OXPHOS and glycolysis in OE33P cells. The enhancement of glycolysis persisted following RIBE induction after three fractions of 1.8 Gy radiation. In line with increases in OXPHOS levels, an increase in maximal respiration was observed following RIBE induction after two fractions of 1.8 Gy radiation. The response of OE33R cells to RIBE induction following repeated fractions of radiation was different to that of OE33P cells. OE33R cells demonstrated a reduction in OXPHOS when exposed to ICCM from OE33R cells that received 3 x 1.8 Gy fractions of radiation. Similar to the OE33P cells, there was also an enhancement of glycolysis in the OE33R cells treated with ICCM from OE33R cells that received 2 x 1.8 Gy fractions of radiation. However, this appears to be transient and did not persist following three fractions of radiation.

Enhanced OXPHOS has been repeatedly shown to be associated with a radioresistant phenotype. Lynam-Lennon *et al.* have reported higher levels of OXPHOS in an isogenic model of OAC radioresistance (111). In head and neck squamous cell carcinoma, the isogenic model of radioresistance exhibited higher levels of OXPHOS compared to the radiosensitive parental cell line (276). While extensive evidence links enhanced OXPHOS to radioresistance, likely through potentiation of hypoxia, this is unlikely to be the case in 2-D cell culture models which are well oxygenated. It has also been reported that enhanced OXPHOS leads to enhanced production of ROS which in turn triggers a homeostatic upregulation of antioxidant systems to remove excess ROS (277). This can inhibit ROS-induced DNA damage and promote radioresistance (278). Glycolysis upregulation has also been linked to radioresistance. In the radiosensitive OE33P cells, glycolysis was upregulated following RIBE induction after two and three fractions of 1.8 Gy radiation. Similarly, in the OE33R cells, glycolysis was upregulated following RIBE induction after two fractions of 1.8 Gy radiation. Bhatt *et al.* have shown that a transient increase in glycolysis confers a radioresistant phenotype owing to increased DNA repair in glioma, oral carcinoma and human embryonic kidney cell lines (261). Moreover, lactic acid accumulation is a result of upregulated glycolysis and accumulation of lactic acid in a mouse model of HNSCC has been shown to be associated with radioresistance (279). Metabolic plasticity is also a likely mechanism conferring radioresistance. The role of metabolic reprogramming and its function in facilitating proliferation of cancer cells was discussed in *section 1.5*, however, emerging evidence highlights a role for same in radioresistance (280). The ability of cancer cells to adapt to the nutrient availability within the TME by shifting its metabolic programming, confers a survival advantage (281).

mtMP was elevated in OE33R cells following RIBE induction after a single fraction of 1.8 Gy radiation. mtMP was reduced in OE33R cells following RIBE induction after two fractions of radiation. It has been shown that radioresistance may be conferred by elevated mtMP or a failure to decrease mtMP. Li *et al.* reported a radioresistant phenotype in head and neck cancer cells overexpressing Growth/Differentiation factor 15 (GDF15). They found that the mechanism of radioresistance induced by GDF15 was as a result of elevated mtMP and reduced ROS production in these cells (282). Similarly, Shonai *et al.* demonstrated that a failure to depolarise mtMP in Jurkat cells inhibited radiation-induced cell death. MEK/ERK-mediated signals were found to be responsible for the maintenance

of mtMP (283). Moreover, Dong *et al.* were able to radiosensitise an acquired model of radioresistance in oesophageal SCC through HDAC inhibition which resulted in the loss of mtMP (284).

In order to further probe the potential importance of the observed alterations in mitochondrial metabolism and mitochondrial function we investigated the effect of RIBE induction *in vitro* on expression of DNA repair genes. Specifically, we investigated levels of *PARP1*, *SMUG1*, *MMS19* and *MLH1* as these have been previously shown to be associated with patient treatment response in OAC (262). Interestingly, we observed increases in the expression of *PARP1* and *MLH1* in our radioresistant model of disease, the OE33R cells, following RIBE induction using 3 x 1.8 Gy fractions of radiation. Expression levels of *MMS19* showed a trend towards elevated levels also, though this did not reach statistical significance. This may indicate that RIBE induction following repeated fractions of radiation may confer benefits on bystander cells. As we were unable to conduct a clonogenic assay on bystander cells following repeated fractions of radiation for the reasons outlined in chapter 2, we utilised a BrdU cell proliferation assay as a surrogate of radiosensitivity. While no alterations in cellular proliferation were observed in the radiosensitive OE33P cells following RIBE induction using repeated fractions of radiation, we did observe a significant reduction in cellular proliferation in OE33R cells following RIBE induction using a single fraction of 1.8 Gy. This suggests that RIBE induction may have an inhibitory effect on cellular proliferation in a model of acquired radioresistance. This phenomenon was observed in both mock-irradiated and irradiated OE33R cells. This reduction in cellular proliferation coincided with a near significant reduction in expression levels of *SMUG1* so it may be possible that RIBE induction following a single fraction of radiation may reduce DNA repair and inhibit cellular proliferation. It is also possible that cell-cycle may be affected. Parlanti *et al.* have previously demonstrated that a multiprotein complex consisting of components involved in DNA base-excision repair, cell cycle regulation and DNA replication (285). A concurrent reduction in OXPHOS was observed with enhanced DNA repair and enhanced cellular proliferation in this study. It has previously been shown that inhibition of *PARP1* in human keratinocytes caused an enhancement of UVB-induced OXPHOS (286). In the same study, *PARP1* inhibition reduced cell proliferation (286).

The clonogenic assay is the gold standard for assessing radiosensitivity *in vitro*. Surprisingly, we did not see any differences in radiosensitivity in either the radiosensitive

OE33P cells or the radioresistant OE33R cells following RIBE induction after a single fraction of 1.8 Gy radiation. The phenomenon of the radiation-induced rescue effect (RIRE), as discussed in chapter 1 has also been documented in the literature. This involves the derivation of benefits by the irradiated cells or organism from signals released from bystander cells (174, 175). Fibroblasts exposed to autologous ICCM exhibited enhanced radioresistance owing to upregulation of DNA repair (173). Evidence for RIRE has been discussed extensively in chapter 1 but briefly, co-culture experiments of irradiated cells and unirradiated bystander cells induced reductions in DNA damage in the irradiated cells (174-177). RIBE induction following a single fraction of a clinically relevant dose of radiation did not appear to induce any alterations in bystander cell survival. The majority of evidence discussing RIRE has utilised co-culture experiments, therefore it is unlikely that secreted factors may play a role in this response. The likely factors involved in RIRE have been outlined in chapter 1 and include NF-κB (177) and cAMP (176) in *in vitro* models and anti-apoptotic miRNA in *in vivo* models (178).

RIBE-induced cell death is a well-documented occurrence in *in vitro* models. McMahon *et al.* developed a Monte Carlo model of cellular radiation response. This model predicted that the bystander response contributes significantly to cell killing even in cell populations that have been uniformly irradiated. At lower doses of radiation, bystander killing contributes to 80% of radiation-induced cell kill and this falls to between 25% and 50% at higher doses of 4 Gy in a normal fibroblast cell line and a prostate cancer cell line, respectively (287).

One potential reason for the failure to observe any alterations in clonogenic survival may be the mutated p53 status of OE33 cells. Hanu *et al*. have previously shown that OE33 cells are capable of producing a bystander signal but are incapable of responding to that signal (288). p53 status has been shown to play a role in certain bystander events. The HCT116 colon cancer cell line is p53 wild-type and we did not observe a bystander effect in terms of clonogenic survival following RIBE induction after a single fraction of 1.8 Gy radiation in chapter 2. However, it is well known that over 50% of human tumours have a mutated p53 status. Furthermore, a recent systematic review and meta-analysis identified that 57% of OAC tumours harboured p53 mutations and this was associated with poorer patient outcomes (289). Therefore, the OE33P and OE33R cells are a clinically relevant model to investigate RIBE events as they have a mutated p53 status, thus representing a large proportion of OAC tumours. Cheng *et al.* have shown that p53

wild-type lung cancer cells are more radiosensitive than their counterparts with mutated p53 (290). Since OAC is an inherently radioresistant malignancy with more than half of all tumours being p53 mutated, we felt this model was representative. Furthermore, this model has previously been shown to be representative of patient tumours with alterations in mitochondrial metabolism and cytokine levels *in vitro* also demonstrated in patient tumours (111, 271).

In summary, RIBE resulting from repeated fractions of radiation induced alterations in mitochondrial metabolism, mitochondrial function, cellular proliferation and expression of DNA repair genes in the radioresistant model of OAC. The results were however mixed in terms of the effects seen after exposure to between one and three fractions. Thus, it remains unclear the exact effects that RIBE has on the end-points we investigated, with radiosensitivity being our main end-point of interest since this has the greatest impact on patient care. Investigation of the effects of RIBE induction in this model on γH2AX kinetics may offer a greater insight into the temporal effects of RIBE on radiosensitivity. H2AX is a key protein involved in DNA repair. In the presence of DNA damage it is phosphorylated on the 139th serine residue and in this phosphorylated form it is termed γH2AX (reviewed in (291)). Therefore, studying the kinetics of γH2AX may offer a greater understanding into the level of DNA damage induced by RIBE and the level of DNA repair occurring. While enhanced expression of DNA repair genes and upregulation of glycolysis suggest a negative impact of RIBE on cancer cell growth and survival, we also observed reductions in mtMP and cellular proliferation. Therefore, investigation of RIBE events in *ex vivo* explant model systems with potential to further examine the phenomenon in animal models may further elucidate the clinical importance of RIBE in OAC patients.

Chapter 4 Radiation-induced Bystander Effect (RIBE) alters mitochondrial metabolism using a human rectal cancer *ex vivo* explant model

This chapter has been published in part in **Heeran AB**, Berrigan HP, Buckley CE, Bottu HM, Prendiville O, Buckley AM, Clarke N, Donlon NE, Nugent TS, Durand M, Dunne C, Larkin JO, Mehigan B, McCormick P, Brennan L, Lynam-Lennon N, O'Sullivan J. Radiation-induced Bystander Effect (RIBE) alters mitochondrial metabolism using a human rectal cancer ex vivo explant model. Transl Oncol. 2021 Jan;14(1):100882.

4.1 Introduction

In chapter 2, we did not observe any significant alterations in bystander cellular metabolism, mitochondrial function or radiosensitivity using *in vitro* models of colorectal cancer (CRC) following a single fraction of 1.8 Gy x-ray radiation. While *in vitro* 2-D models undoubtedly present a useful model for studying molecular events in cancer cells, their limitations must also be considered. Such models comprise of a single cell type i.e. the cancer cells, and do not represent the complexity or architecture of the tumour microenvironment (TME). Tumours can be considered pseudo-organs, in that they consist of various cell types and extracellular matrix constituents that interact and signal with each other (292). It is known that the various cell types, secreted factors and structural components of the TME influence cancer development, progression and treatment response (292). Therefore, for this study, we utilised a novel *ex vivo* explant model system of both normal non-malignant rectal tissue and rectal cancer tissue to recapitulate the 3-D structure and microenvironment of both tissue types and assess radiation bystander effects.

RIBE induction has been linked experimentally to numerous hallmarks of cancer (164) and the mitochondria have been centrally implicated in RIBE (204, 206). Gorman *et al.* have previously reported more pronounced effects in the mitochondria of bystander cells in response to RIBE induction from an *ex vivo* model of CRC compared to normal adjacent tissue in CRC patients (207). The authors in this study reported increased random mitochondrial mutations and decreased mtMP in bystander CRC cells in response to *ex vivo* RIBE induction, however, it is unknown whether this directly affects mitochondrial metabolism. As alluded to previously, mitochondrial metabolism is a key player in treatment response in gastrointestinal malignancies, in particular the response to radiation therapy (80, 111). Therapeutic targeting of OXPHOS by pharmacological inhibition has been shown to enhance radiosensitivity (80, 112, 113). Therefore, gaining an understanding of the metabolic consequences of exposure to the irradiated TME in rectal cancer cells may pave the way for identifying targets for enhancing treatment response. Moreover, we investigated if RIBE induction in normal rectal tissue exerted differential metabolic consequences, when compared to malignant rectal tissue. In addition, we profiled the metabolomic landscape in both tissue types pre- and post-radiation to identify any associations with altered metabolic responses in bystander cells.

The evidence linking obesity with oesophageal adenocarcinoma (OAC) and rectal cancer is discussed extensively in chapter 1, however, it is emerging that obesity also plays a role in the treatment outcome in these malignancies (40, 79, 293, 294). Overweight and obese OAC patients have been shown to have an enhanced response to neo-CRT (79), while poorer outcomes have been reported in overweight and obese rectal cancer patients (40, 293, 294). The exact mechanisms underpinning these observations remain largely elusive, however, elements such as a more technically demanding surgery in obese patients with rectal cancer (40) and suboptimal dosing of chemotherapeutic agents using ideal body weight, though it is recommended that actual body weight is used for drug dosing (44) have been cited as potential mechanisms.

Adipose conditioned media (ACM) from obese OAC patients has previously been demonstrated to induce a metabolic shift towards glycolysis in OAC cells. Metabolomic profiling revealed an altered glycolysis and amino acid-related signature in the ACM from obese patients. These results translated to patient samples where higher expression of *PKM2*, a glycolytic marker was associated with obesity (81). This data may suggest that modulation of metabolic pathways in obese patients gives rise to altered tumour metabolic and radiation responses. Circulating metabolites in the sera of obese CRC patients have been shown to be different to lean CRC patients and healthy controls (295). Given the evidence linking altered metabolism and metabolic landscapes in tumours of obese patients, we also investigated if the metabolomic signature in the TME of rectal cancer patients was associated with obesity status.

To the best of our knowledge, this is the first study to investigate RIBE induction in an *ex vivo* model of rectal cancer. We investigated the effect of *ex vivo* RIBE induction using rectal cancer and normal rectal tissue on bystander cellular metabolism, mitochondrial function and metabolomic profiling of the normal and cancer tissue microenvironments to determine if the bystander effects differed between normal and malignant rectal tissue. We hypothesised that *ex vivo* RIBE induction would induce metabolic alterations and alter mitochondrial function and these would differ between normal compared to malignant tissue. We also hypothesised that obesity status would be associated with metabolic perturbations in these bystander cells.

4.2 Overall objective and specific aims of chapter 4

The overall objective of chapter 4 was to assess the effect of *ex vivo* RIBE induction in a novel explant model system of normal rectal and rectal cancer tissue on rectal cancer bystander cells. We investigated if the response to RIBE signals differs between normal rectal tissue and rectal cancer tissue.

The specific aims of this chapter were:

1. Examine the effect of *ex vivo* RIBE induction in an explant model of both normal rectal tissue and malignant rectal tissue on mitochondrial metabolism in bystander SW837 rectal cancer cells.
2. Evaluate the effect of *ex vivo* RIBE induction in the aforementioned explant models on mitochondrial function, specifically ROS and mitochondrial membrane potential in bystander SW837 rectal cancer cells.
3. Profile the metabolome of normal rectal tissue and rectal cancer tissue both pre- and 24 h post-radiation using ^{1}HNMR technology.
4. Correlate patient anthropometric measures with metabolic parameters and metabolite levels from the normal rectal and rectal cancer microenvironments.

4.3 Materials and methods

4.3.1 Patient recruitment

Patients undergoing diagnostic endoscopy for rectal cancer and lower gastrointestinal investigations were prospectively recruited to this study between January 2018 and November 2018. Informed written patient consent was obtained for the use of patient tissue and data in this study. Ethical approval was granted by the St. James's Hospital/ AMNCH Research Ethics Committee. Patient data was pseudo-anonymised prior to sample access and all samples were coded with a unique biobank number assigned by the biobank manager. Biopsies were obtained from treatment-naïve patients at diagnostic endoscopy. A total of 12 patients with histologically confirmed rectal cancer were recruited to the study and 8 patients that did not have cancer (normal, non-cancer controls). All clinical and pathological data was obtained following written informed consent. Clinical data was obtained from patient records. Histological confirmation of tumour tissue and non-malignant tissue in patient diagnostic biopsies was performed by a pathologist using routine haematoxylin and eosin staining. Tumour regression score (TRS) was assigned by a pathologist following surgery in all patients receiving neoadjuvant treatment. Visceral fat area (VFA), subcutaneous fat area, intermuscular fat and skeletal muscle were calculated from a pre-operative diagnostic computed tomography (CT) scan by an experienced radiologist. Patients with a VFA greater than 163.8 cm^2 (males) and 80.1 cm^2 (females) were classified as obese (296). Patient characteristics for both normal (non-cancer) controls and rectal cancer patients are outlined in **Table 4-1**.

4.3.2 Generation of tumour conditioned media and normal conditioned media

Tumour conditioned media (TCM) and normal conditioned media (NCM) were generated by gently washing the biopsy four times in PBS supplemented with 1% penicillin-streptomycin, 1% Fungizone® (amphotericin B) and 0.1% gentamicin. The biopsy was then placed in 1 ml of M199 media supplemented with 10% FBS, 1% penicillin-streptomycin, 1% Fungizone, 0.1% gentamicin and 1 μg/ml insulin. Biopsies were incubated for 80 min at 37°C and 5% CO_2/95% air. Following 80 min incubation, biopsies were either mock-irradiated (0 Gy) or irradiated with 1.8 Gy x-ray radiation using an XStrahl RS225 x-irradiator at a dose rate of 1.73 Gy/min (195kV, 15mA) [XSTRAHL, Surrey, UK]. Biopsies were then incubated for 24 h at 37°C and 5% CO_2.

Following 24 h incubation the media was harvested and stored in 2 ml cryotubes at -80°C until required for analysis. The matched cultured biopsies were snap-frozen in liquid nitrogen and stored at -80°C. SW837 rectal cancer cells were used as bystander cells for all experiments. For all experiments a 1:1 dilution of TCM/NCM in M199 was used for all assays. This dilution was chosen based on optimisation experiments using TCM/NCM on SW837 cells with no differences being observed between the neat use of TCM/NCM and a 1:1 dilution of TCM/NCM with M199.

4.3.3 Assessment of bystander metabolic profiles using Seahorse technology

SW837 cells were seeded in duplicate at a density of 30,000 cells/well in a 24-well XFe24 cell culture microplate [Agilent Technologies, Santa Clara, CA, USA] in a volume of 100 µl per well and allowed to adhere at 37°C and 5% CO_2/95% air. Following 3 h incubation, an additional 150 µl per well of complete media was added to each well. Twenty-four hours after initial seeding, cells were treated with NCM or TCM from the human normal or rectal cancer *ex vivo* explants for 24 h. Metabolic analysis of cellular mitochondrial metabolism was performed using Seahorse technology as described in *section 2.3.9.* All metabolic measurements were normalised to cell number using the crystal violet assay, transferring the eluted stain to a 96-well plate before reading as described in *section 2.3.8*.

4.3.4 Assessment of reactive oxygen species levels in bystander cells

Reactive oxygen species (ROS) was assessed using the fluorescent probe 2'-7'-dichlorofluorescien (2'-7'-DCF). SW837 cells were seeded at 30,000 cells/well in a 96-well plate for 24 h. Following 24 h incubation, cells were treated with 100 µl of TCM or NCM for 24 h. NCM/TCM was removed following 24 h incubation and ROS was assessed as described in *section 2.3.12*. All measurements were normalised to cell number using the crystal violet assay as described in *section 2.3.8*.

4.3.5 Assessment of mitochondrial membrane potential in bystander cells

Mitochondrial membrane potential (mtMP) was assessed using the fluorescent probe Rhodamine 123. SW837 cells were seeded at 30,000 cells/ well in a 96-well plate for 24 h. Following 24 h incubation, cells were treated with 100 µl of TCM or NCM for 24 h. Following 24 h incubation, TCM/NCM was removed and mtMP was assessed as described in *section 2.3.10.* All measurements were normalised to cell number using the crystal violet assay as described in *section 2.3.8*.

4.3.6 Evaluation of changes in the metabolome of normal and rectal cancer ex vivo explants in response to radiation using metabolomics

A total of 250 µl deuterium oxide (D_2O) and 10 µl sodium trimethyl [2,2,3,3-$^2H_4$] propionate (TSP) (0.005 g/ml) were added to each 300 µl TCM, NCM and control sample. Spectra were acquired on a 600-MHz Varian nuclear magnetic resonance (^{1}HNMR) spectrometer (Varian Limited, Oxford, United Kingdom) by using the Carr-Purcell-Meiboom-Gill (CPMG) pulse sequence at 25°C. Spectra were acquired with 16384 data points and 256 scans. Water suppression was achieved during the relaxation delay (3.0 s). ^{1}HNMR spectra were referenced to TSP and were processed manually with Chenomx NMR Suite [Version 8.3; Chenomx Edmonton, Canada] by using a line broadening of 0.2 Hz, and all spectra were phase and baseline corrected. Using 0.005 ppm bins, spectra were converted into 1360 spectral regions. The water region (4.0 to 6.0 ppm) was excluded, and data normalised to the total area of the spectral integral. Identification of discriminating metabolites was also performed using Chenomx NMR Suite. Metabolites were profiled in the Chenomx NMR Suite.

4.3.7 Statistical analysis

GraphPad Prism 5 software was used to perform statistical analysis. All data is expressed as mean ± SEM. Data was analysed by paired and unpaired *t*-test, as stated in each figure legend. Correlation analysis was performed using Pearson's correlation coefficient.

Multivariate statistical analysis was performed for the metabolomics data analyses with Simca- P+ software [Version 13.0.3; Umetrics, Umea°, Sweden]. Unsupervised principal component analysis (PCA) was applied to the metabolomics data to explore any trends in the data for the various comparison groups, followed by partial least square discriminant analysis (PLS-DA) and orthogonal partial least squares discriminant analysis (OPLS-DA). The goodness-of-fit parameter (R^2) and the predictive ability parameter (Q^2) was used to describe the quality of all models. Discriminating metabolites were determined based on analysis of an S-line plot. An independent t-test was performed on discriminating metabolite areas between comparison groups using IBM SPSS Statistics version 24. Statistical significance was considered if $p \leq 0.05$.

Figure 4.1 illustrates the methodology utilised in this chapter.

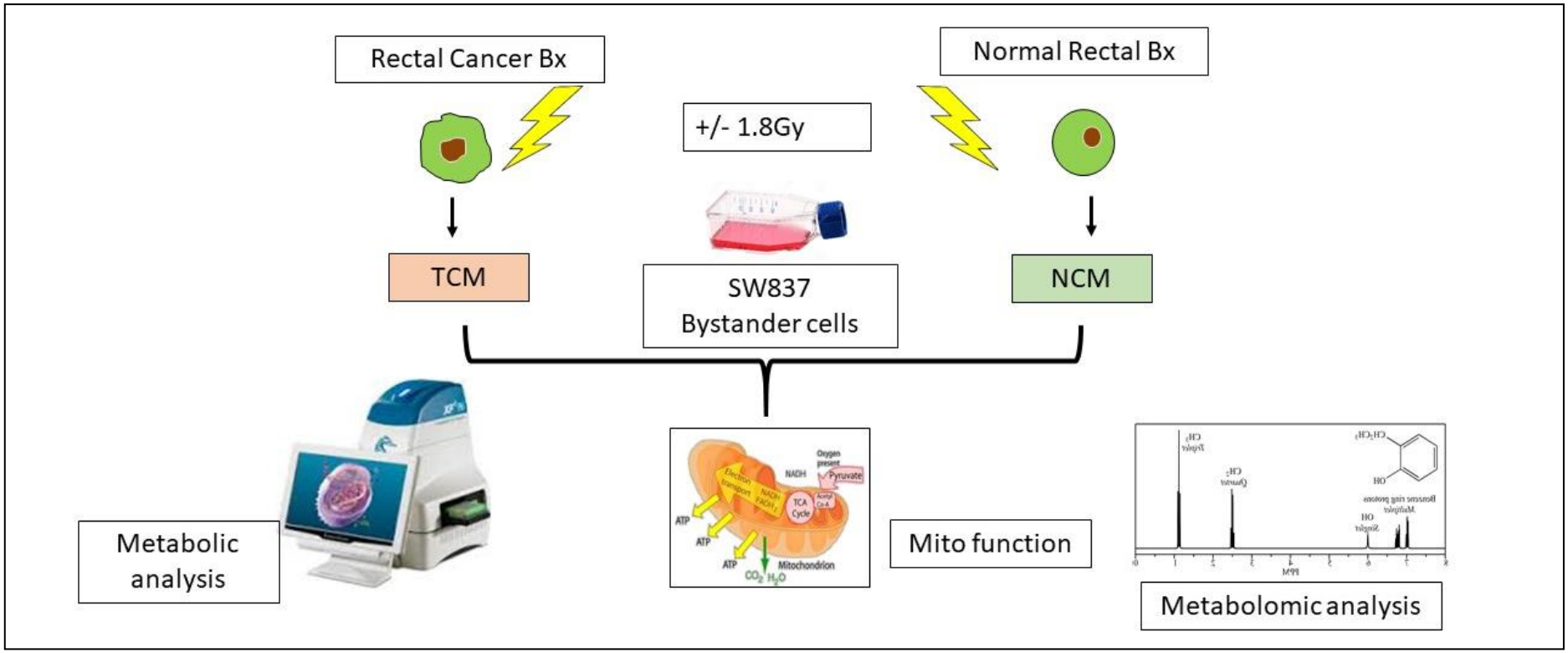

Figure 4.1 Schematic illustration of methodology used in chapter 4

Normal rectal and rectal cancer biopsies were either mock-irradiated or irradiated with 1.8 Gy radiation and cultured for 24 h. The resultant NCM and TCM was used to treat bystander SW837 cells. The metabolic profiling and examination of the mitochondrial function of the bystander cells was conducted. Metabolomic analysis was performed on the NCM and TCM from mock-irradiated and irradiated biopsies.

4.4 Results

4.4.1 Patient characteristics

Treatment naïve endoscopic specimens were taken from 20 patients undergoing endoscopic assessment at St. James's Hospital, Dublin between January 2018 and November 2018. Endoscopic specimens were taken from patients with rectal cancer (n=12) and patients that did not have rectal cancer i.e. histologically normal (n=8). All clinical data on these patient samples is shown in **Table 4-1**.

Table 4-1 Patient characteristics

			Percent (%)
Age (rectal cancer patients)	Mean ± SD	65.16 ± 9.71	
	Range	55-89	
Age (control patients)	Mean ± SD	58.75 ± 11.42	
	Range	44-76	
Gender (rectal cancer patients)	Male (n)	8	66.67
	Female (n)	4	33.33
Gender (control patients)	Male (n)	3	37.5
	Female (n)	5	62.5
Obesity status (visceral fat area)	Obese	8	66.67
	Non obese	4	33.33
Histology	Adenocarcinoma (n)	12	100
Stage of differentiation	Moderate (n)	12	100
T stage	T1 (n)	1	8.33
	T2 (n)	2	16.67
	T3 (n)	8	66.67
	T4 (n)	1	8.33
N stage	N0 (n)	6	50
	N1 (n)	5	41.67
	N2 (n)	1	8.33
M stage	M0 (n)	11	91.67
	M1 (n)	1	8.33
Neoadjuvant CRT	Received neo-CRT (n)	6	50
Neoadjuvant CT	Received neo-CT only (n)	1	8.33
Neoadjuvant RT	Received neo-RT only (n)	1	8.33
Surgery [a]	Received surgery (n)	11	91.67
TRS [b]	0 (n)	2	28.57
	1 (n)	3	42.85
	2 (n)	1	14.28
	3 (n)	1	14.28

Abbreviations; CRT; chemoradiotherapy, CT; chemotherapy, RT; radiotherapy, TRS; tumour regression score. [a] One patient did not receive surgery, [b] TRS available for 7 patients as 4 went straight to surgery and 1 did not receive surgery

4.4.2 RIBE induction ex vivo induces significant changes in oxidative phosphorylation and glycolysis in bystander rectal cancer cells

Following 24 h treatment with either TCM or NCM, OCR, a measure of OXPHOS, and ECAR, a measure of glycolysis, were assessed. Significant reductions in OCR were observed in bystander cells exposed to NCM from irradiated normal rectal tissue, when compared to those exposed to the NCM from the mock-irradiated normal rectal tissue (p=0.01). Similarly, there was a significant reduction in OCR in SW837 bystander cells exposed to TCM from irradiated rectal cancer tissue compared to those exposed to TCM from mock-irradiated rectal cancer tissue (p=0.03) (**Figure 4.2A)**. Bystander SW837 rectal cancer cells treated for 24 h with TCM from irradiated rectal cancer biopsies, demonstrated a significant reduction in ECAR, when compared to SW837 cells treated with TCM from mock-irradiated biopsies (p=0.014) (**Figure 4.2B**).

OCR:ECAR ratio was not significantly different in SW837 cells treated with NCM from mock-irradiated or irradiated normal rectal tissue (p=0.25), or cancer tissue (p=0.38). No difference was observed in OCR:ECAR ratio between SW837 cells treated with NCM or TCM (p=0.21) (**Figure 4.2C**).

This data has demonstrated for the first time in real-time, significant metabolic alterations in bystander cells following exposure to TCM and NCM from human rectal biopsies. Moreover, we have demonstrated a differential response in bystander cells exposed to TCM from malignant rectal tissue and NCM from normal rectal tissue, with alterations in glycolysis only observed in bystander cells exposed to TCM from malignant tissue.

4.4.3 RIBE induction ex vivo in both normal rectal tissue and rectal cancer tissue causes significant reductions in basal respiration, ATP production and maximal respiration in bystander SW837 cells

Basal respiration was significantly lower in SW837 cells exposed to NCM from irradiated normal rectal tissue, when compared to SW837 cells exposed to NCM from mock-irradiated normal rectal tissue (p=0.009). Similarly, basal respiration was significantly lower in SW837 cells treated with TCM from irradiated rectal cancer tissue, when compared to mock irradiated rectal cancer tissue (p=0.029) (**Figure 4.3A**).

A significant reduction in OCR-linked ATP production was observed in SW837 bystander cells treated with NCM from irradiated biopsies, when compared to SW837 cells exposed to NCM from mock-irradiated biopsies (p=0.039). OCR-linked ATP

production was significantly lower in SW837 cells treated with TCM from irradiated rectal cancer biopsies, when compared to mock-irradiated rectal cancer biopsies (p=0.043). Significantly lower levels of OCR-linked ATP production were observed in SW837 cells treated with TCM from mock-irradiated biopsies, when compared to those treated with NCM from mock-irradiated biopsies (p=0.011) (**Figure 4.3B**).

Maximal respiration was significantly reduced in SW837 cells treated with NCM from irradiated normal rectal tissue, when compared to those treated with NCM from mock-irradiated tissue (p=0.009). SW837 cells exposed to TCM from irradiated rectal cancer tissue demonstrated a significant reduction in maximal respiration, when compared to SW837 cells treated with TCM from mock-irradiated rectal cancer tissue (p=0.017) (**Figure 4.3C**).

Proton leak was significantly reduced in SW837 cells treated with TCM from irradiated rectal cancer tissue compared to mock-irradiated rectal cancer tissue (p=0.02). The difference in proton leak between SW837 cells treated with NCM from mock-irradiated or irradiated normal rectal tissue did not reach statistical significance (p=0.076) (**Figure 4.3D**).

There was no significant difference in non-mitochondrial respiration between SW837 cells treated with NCM from either mock-irradiated or irradiated normal rectal tissue (p=0.59) or cancer tissue (p=0.60) (**Figure 4.3E**).

To date, most of the bystander research has utilised *in vitro* models, however, our work now recapitulates the complexity of the tumour and normal microenvironment encompassing the 3D architecture and multiple cell types. This is the first study to profile real-time metabolic changes in cells following exposure to culture media from human rectal cancer and normal rectal biopsies.

4.4.4 Rectal cancer secretome induces a significant increase in reactive oxygen species levels compared to the normal rectal secretome in bystander SW837 cells

Given the observed RIBE-induced alterations in mitochondrial metabolism and the well-documented role of the mitochondria in RIBE, we investigated the effect of *ex vivo* RIBE induction on mitochondrial function, specifically ROS and mtMP. ROS levels were significantly higher in SW837 cells following TCM treatment from mock-irradiated rectal cancer tissue, when compared to NCM from mock-irradiated normal rectal tissue

(p=0.04). The difference in ROS levels in SW837 cells treated with TCM from irradiated rectal cancer tissue, when compared to SW837 cells treated with NCM from irradiated normal rectal tissue was not significant (p=0.08) nor did ROS levels change between SW837 cells treated with NCM from either irradiated or mock-irradiated normal rectal tissue (p=0.21), or between bystander cells treated with TCM from irradiated or mock-irradiated rectal cancer tissue (p=0.54) (**Figure 4.4A**). No changes in mtMP were detected in bystander cells exposed to all *ex vivo* conditions (**Figure 4.4B**).

These results suggest that the rectal cancer microenvironment induces higher levels of oxidative stress compared to the normal rectal microenvironment, but that RIBE *per se* does not alter mitochondrial function following 24 h exposure to TCM or NCM in bystander cells.

4.4.5 Metabolomic profiling of NCM and TCM from mock-irradiated and irradiated normal rectal and rectal cancer tissue

To better understand what metabolites may be driving these observed mitochondrial and metabolic bystander events, metabolomic screening was performed on the TCM and NCM pre- and post-radiation. A weak PLS-DA model was obtained for TCM from irradiated rectal cancer tissue vs NCM from irradiated normal rectal tissue (R^2x=0.591, Q2=0.153), indicating no major changes in the global metabolomic profile (**Figure 4.5A-B**). No other changes in the global metabolomic profiles were observed when comparing the mock-irradiated and irradiated samples. However, profiling of specific metabolites revealed that the amino acid leucine was significantly different between NCM from irradiated normal rectal tissue, when compared to TCM from irradiated rectal cancer tissue (p=0.041) (**Figure 4.6A**). Leucine levels were reduced in the TCM from irradiated rectal cancer tissue compared to NCM from irradiated normal rectal tissue (**Table 4-2**). There were no significant changes in levels of acetate, alanine, ethanol, isoleucine, lactate, methionine, N-acetyl-L-alanine, phenylalanine or valine (**Figure 4.6B-J**) (**Table 4-2**).

No significant differences were observed in levels of any metabolite studied between the mock-irradiated normal rectal tissue and the mock-irradiated rectal cancer tissue (**Figure 4.7A-J**) (**Table 4-3**).

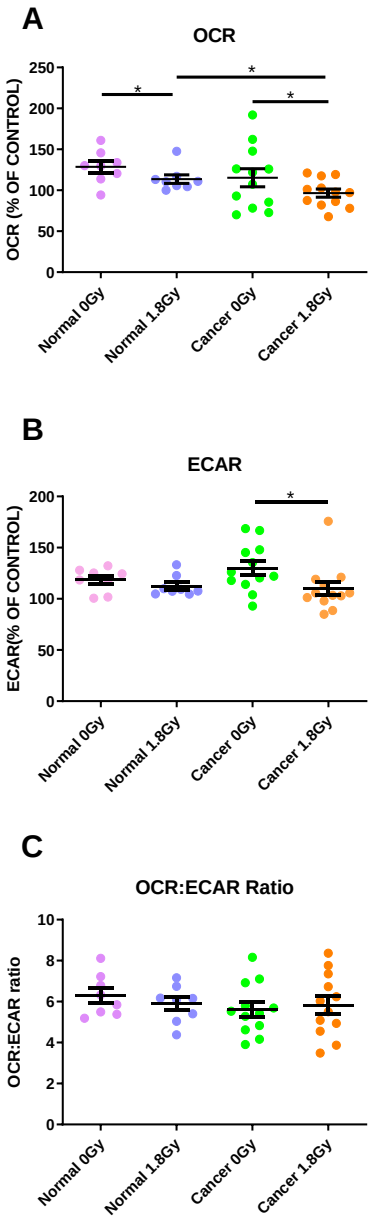

Figure 4.2 Effect of ex vivo RIBE induction in normal rectal tissue and rectal cancer tissue on OCR, ECAR and OCR:ECAR ratio in bystander SW837 cells

(**A**) *Ex vivo* RIBE induction in both normal rectal and rectal cancer tissue causes significant reductions in OCR in bystander SW837 cells, when compared to cells exposed to the unirradiated tissue secretome. (**B**) ECAR is significantly reduced in bystander SW837 cells treated with TCM from irradiated rectal cancer tissue compared to mock-irradiated rectal cancer tissue. (**C**) OCR:ECAR ratio is not significantly different in bystander SW837 cells treated with NCM or TCM from irradiated *ex vivo* explants compared to their unirradiated controls. All data expressed as mean ± SEM. Statistical analysis was performed by paired *t*-test for 0 Gy vs 1.8 Gy when comparing the same tissue and unpaired *t*-test when comparing different tissue. *$p<0.05$, $n=8$ normal, $n=12$ cancer.

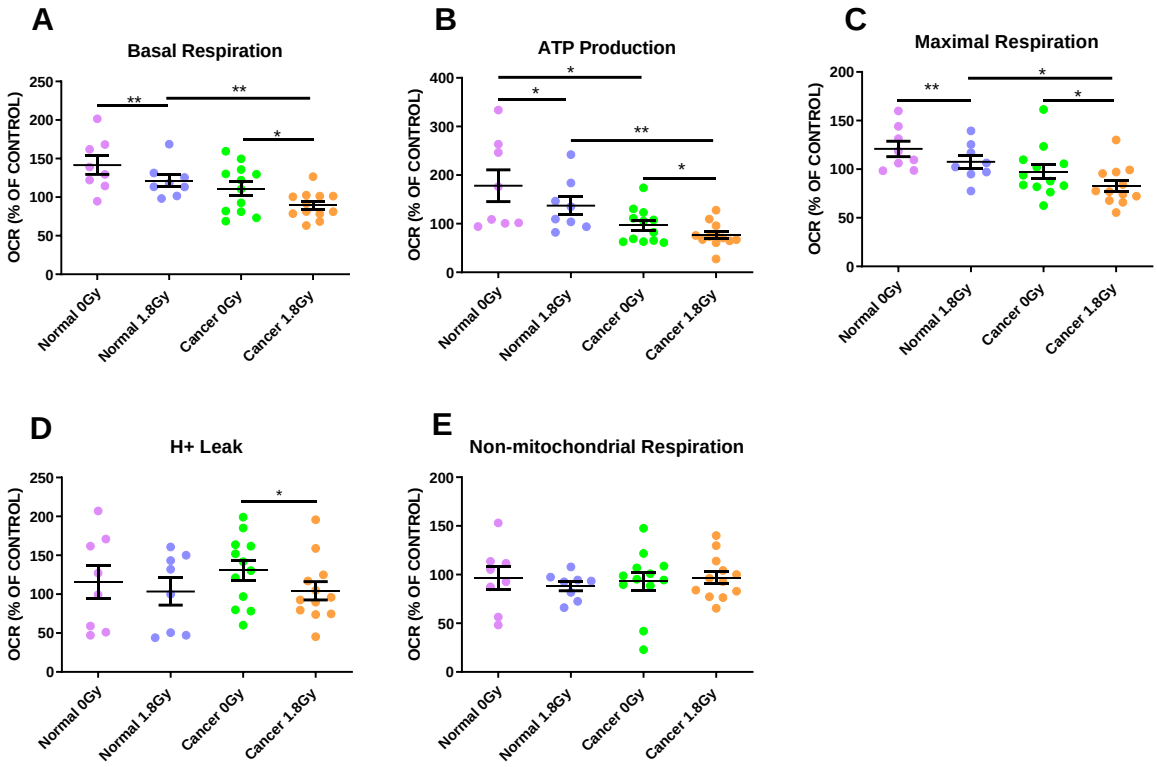

Figure 4.3 Effect of ex vivo RIBE induction on SW837 bystander basal respiration, ATP production, maximal respiration, proton leak and non-mitochondrial respiration

(**A**) RIBE induction in *ex vivo* normal rectal and rectal cancer tissue induces significant reductions in basal respiration in bystander SW837 cells, when compared to cells exposed to the unirradiated tissue secretome. (**B**) OCR-linked ATP production is significantly reduced in bystander SW837 cells treated with NCM and TCM from irradiated normal and rectal cancer tissue, respectively. OCR-linked ATP production is significantly reduced in bystander cells treated with TCM from the cancer secretome compared to NCM from the normal rectal secretome. (**C**) *Ex vivo* RIBE induction in both normal rectal and rectal cancer tissue significantly reduces maximal respiration in bystander SW837 rectal cancer cells. (**D**) Proton leak was significantly reduced in bystander SW837 cells treated with TCM from irradiated compared to mock-irradiated rectal cancer tissue. (**E**) Non-mitochondrial respiration was not significantly different in SW837 cells treated with NCM or TCM from irradiated normal rectal and rectal cancer biopsies compared to mock-irradiated biopsies. All data expressed as mean ± SEM. Statistical analysis was performed using a paired *t*-test for 0 Gy vs 1.8 Gy when comparing the same tissue and unpaired *t*-test when comparing different tissue. $**p<0.01$, $*p<0.05$, $n=8$ normal, $n=12$ cancer.

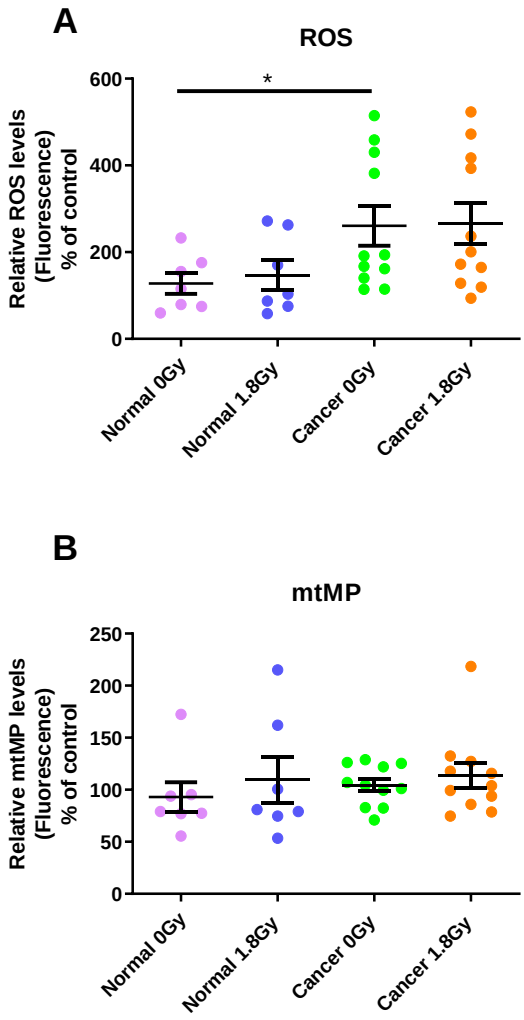

Figure 4.4 The cancer secretome increases ROS levels but not mtMP in bystander SW837 rectal cancer cells

(**A**) ROS levels are significantly higher in bystander SW837 cells treated with TCM from rectal cancer tissue compared to cells treated with NCM from normal rectal tissue. (**B**) mtMP levels are not significantly different in bystander SW837 cells exposed to TCM from rectal cancer tissue compared to NCM from normal rectal tissue. All data expressed as mean ± SEM. Statistical analysis was performed using a paired *t*-test for 0 Gy vs 1.8 Gy when comparing the same tissue and unpaired *t*-test when comparing different tissue. *$p<0.05$, $n=7$ normal, $n=11$ cancer.

A.

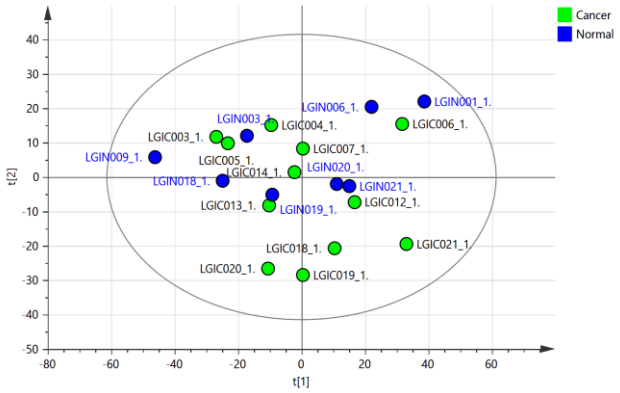

B.

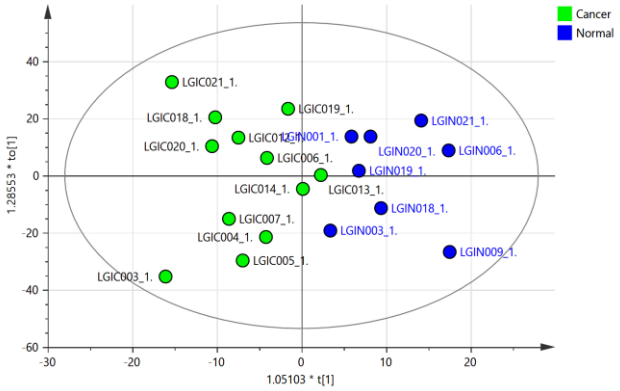

Figure 4.5 The metabolite profile differs between irradiated normal rectal tissue and irradiated rectal cancer tissue

(**A**) Score plot model generated on NMR spectra revealing the cellular metabolite differences between Cancer 1.8 Gy versus Normal 1.8 Gy by principal component analysis (PCA -UV) model of all samples; based on NMR spectra with model parameters R^2X, R^2Y, Q^2; Separation between metabolites obtained from the groups were shown as Normal 1.8 Gy (blue) and Cancer 1.8 Gy (green). (**B**) Score plot model generated on NMR spectra revealing the cellular metabolite differences between Cancer showing separation between Cancer 1.8 Gy versus Normal 1.8 Gy with model parameters R^2X, R^2Y, Q^2; Separation between metabolites obtained from the groups were shown as Normal 1.8 Gy (blue) and Cancer 1.8 Gy (green). (OPLS-DA). *n*=8 for normal, *n*=12 for cancer.

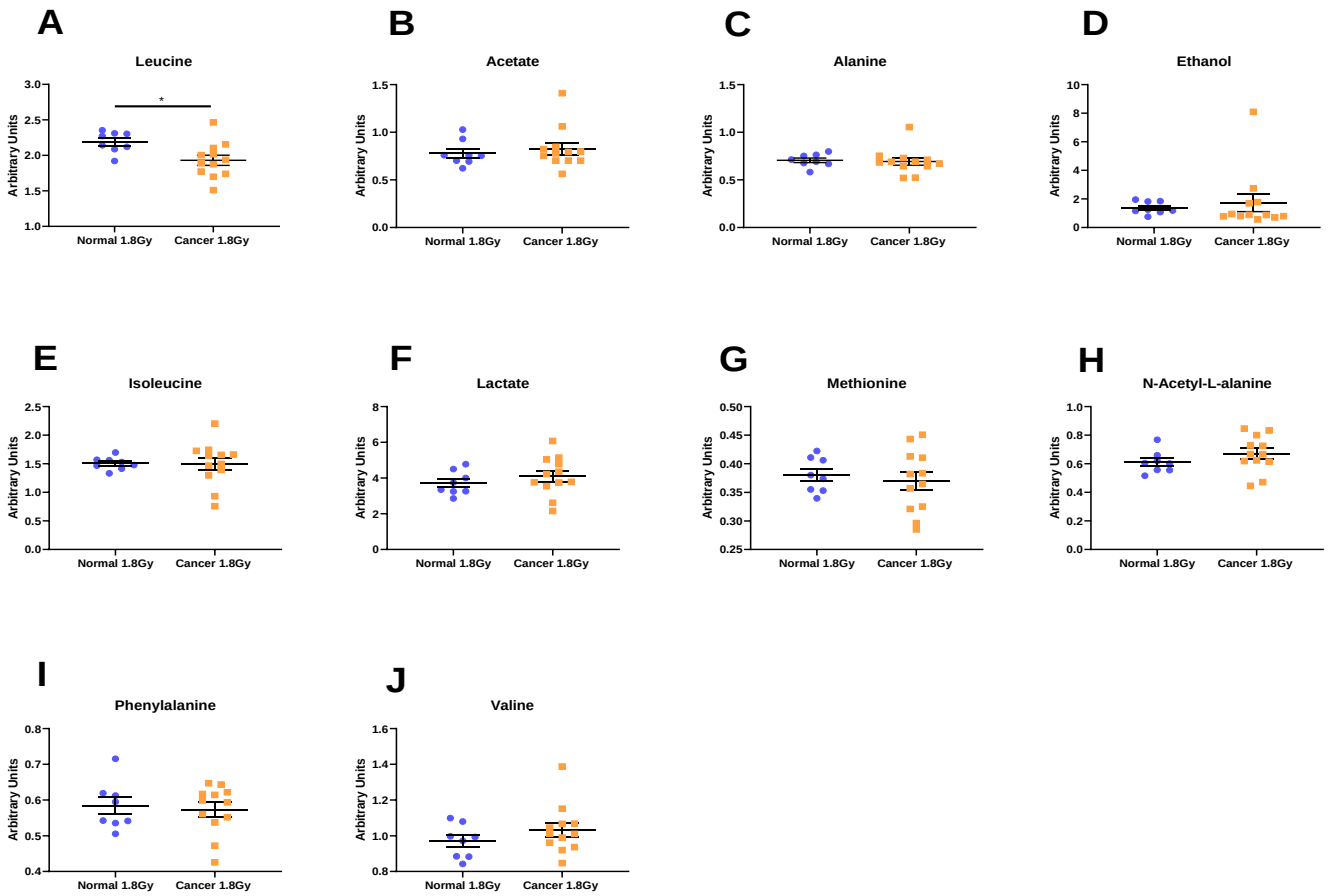

Figure 4.6 Leucine levels are reduced in the secretome of irradiated rectal cancer tissue compared to irradiated normal rectal tissue

(**A**) Leucine levels are significantly reduced in the secretome of irradiated rectal cancer tissue compared to irradiated normal rectal tissue. There was no significant difference in (**B**) acetate. (**C**) alanine (**D**) ethanol (**E**) isoleucine (**F**) lactate (**G**) methionine (**H**) N-acetyl-L-alanine (**I**) phenylalanine or (**J**) valine levels between the irradiated rectal cancer secretome and the irradiated normal rectal secretome. All data expressed as mean ± SEM. Statistical analysis was performed using an unpaired *t*-test. **p*<0.05, *n*=8 normal, *n*=12 cancer.

Table 4-2 Table of metabolites discriminating NCM from irradiated normal rectal tissue compared to TCM from irradiated rectal cancer tissue

Metabolite	**NCM 1.8 Gy**		**TCM 1.8 Gy**		***p*-value***
	Mean	SD	Mean	SD	
Acetate	0.7827	0.1249	0.8306	0.2283	0.662
Alanine	0.7030	0.0635	0.6938	0.1411	0.708
Ethanol	1.3171	0.4497	1.8056	2.1846	0.987
Isoleucine	1.5234	0.1155	1.4831	0.3967	0.542
Lactate	3.7899	0.6603	4.0801	1.1393	0.676
Leucine	***2.1545***	***0.1728***	***1.9359***	***0.2590***	***0.041***
Methionine	0.3837	0.0305	0.3653	0.0556	0.328
N-Acetyl-L-Alanine	0.6235	0.0824	0.6648	0.1322	0.522
Phenylalanine	0.5868	0.0636	0.5700	0.0704	0.567
Valine	0.9712	0.0876	1.0369	0.1432	0.250
***Statistical Analysis performed on log transformed variables**					

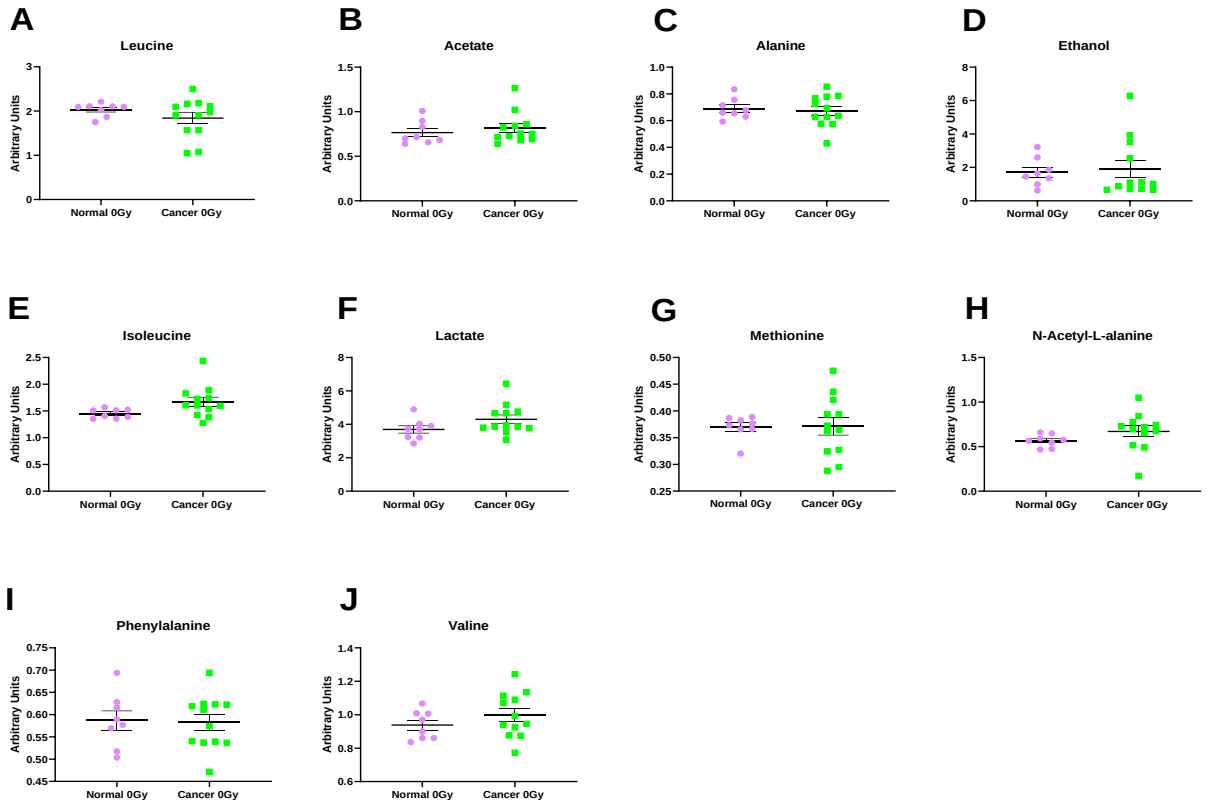

Figure 4.7 Metabolite levels do not differ between the mock-irradiated normal rectal secretome and the mock-irradiated rectal cancer secretome

There was no significant difference in (**A**) leucine (**B**) acetate (**C**) alanine (**D**) ethanol (**E**) isoleucine (**F**) lactate (**G**) methionine (**H**) N-acetyl-L-alanine (**I**) phenylalanine or (**J**) valine levels between the irradiated rectal cancer secretome and the irradiated normal rectal secretome. All data expressed as mean ± SEM. Statistical analysis was performed by unpaired *t*-test. *n*=8 normal, *n*=12 cancer

Table 4-3 Table of metabolites comparing NCM from mock-irradiated normal rectal tissue compared to TCM from mock-irradiated rectal cancer tissue

Metabolite	**NCM 0Gy**		**TCM 0Gy**		***p*-value***
	Mean	SD	Mean	SD	
Acetate	0.7662	0.1321	0.8143	0.1748	0.517
Alanine	0.6899	0.0769	0.6733	0.1180	0.730
Ethanol	1.7167	0.8482	1.9263	1.7919	0.763
Isoleucine	1.4527	0.0848	1.6706	0.3008	0.063
Lactate	3.6969	0.6265	4.3033	0.8963	0.115
Leucine	2.0320	0.1496	1.8410	0.4458	0.191
Methionine	0.3700	0.0219	0.3710	0.0568	0.954
N-Acetyl-L-Alanine	0.5666	0.0705	0.6712	0.2136	0.201
Phenylalanine	0.5868	0.0612	0.5828	0.0601	0.887
Valine	0.9384	0.0854	0.9982	0.1341	0.250
***Statistical Analysis performed on log transformed variables**					

4.4.6 Linking mitochondrial function to energy metabolism

In order to determine if there was any relationship between altered energy metabolism and mitochondrial function in bystander cells, we correlated ROS and mtMP levels with metabolic readouts obtained from the Seahorse. In the bystander cells treated with NCM from the mock-irradiated normal rectal secretome, there was a significant inverse correlation between ROS and OCR (R=-0.8105, p=0.02), basal respiration (R=-0.8194, p=0.02), OCR-linked ATP production (R=-0.7718, p=0.04) and maximal respiration (R=-0.8101, p=0.02). In the bystander SW837 cells treated with NCM from the irradiated normal rectal secretome, non-mitochondrial respiration correlated with ROS (R=0.8315, p=0.02) and there was an inverse correlation between ROS and maximal respiration (R=-0.7648, p=0.04) and proton leak (R=-0.7554, p=0.04) (**Table 4-4**).

In SW837 cells treated with the mock-irradiated rectal cancer secretome, there were significant inverse correlations between ROS and OCR (R=-0.8101, p=0.002), basal respiration (R=-0.8745, p=0.0004), proton leak (R=-0.7988, p=0.003), maximal respiration (R=-0.6696, p=0.02) and mtMP (R=-0.7229, p=0.01) and there was a significant positive correlation between ROS and OCR:ECAR ratio (R=0.8136, p=0.002). In bystander cells treated with the irradiated rectal cancer secretome, there was an inverse correlation between ROS and OCR (R=-0.7223, p=0.01) and a positive correlation between ROS and OCR:ECAR ratio (R=0.9064, p=0.0001) (**Table 4-5**).

mtMP correlated with OCR (R=0.7038, p=0.01), basal respiration (R=0.8013, p=0.003), H+ leak (R=0.7147, p=0.01) and maximal respiration (R=0.6305, p=0.03) in bystander cells treated with TCM from mock-irradiated rectal cancer tissue. Similarly, there was a positive correlation between mtMP and OCR (R=0.6343, p=0.03) and maximal respiration (R=0.6817, p=0.02) in bystander cells treated with TCM from irradiated rectal cancer tissue (**Table 4-6**).

All metabolic and mitochondrial function data was analysed according to T stage and N stage and no significant differences were detected between any metabolic readout or mitochondrial function parameter in either the unirradiated or irradiated malignant tissue.

Table 4-4 Correlation between ROS levels and metabolic parameters in normal tissue

NORMAL 0 GY				NORMAL 1.8 GY			
FACTOR	**R value**	**p-value**	**n**	**FACTOR**	**R value**	**p-value**	**n**
OCR	-0.8105	0.02	7	Non-mitochondrial respiration	0.8315	0.02	7
Basal respiration	-0.8194	0.02	7	Maximal respiration	-0.7648	0.04	7
ATP production	-0.7718	0.04	7	H+ leak	-0.7554	0.04	7
Maximal respiration	-0.8101	0.02	7				

Table 4-5 Correlation between ROS levels and metabolic parameters in cancer tissue

CANCER 0 GY				CANCER 1.8 GY			
FACTOR	**R value**	**p-value**	**n**	**FACTOR**	**R value**	**p-value**	**n**
OCR	-0.8101	0.002	11	OCR	-0.7223	0.01	11
Basal Respiration	-0.8745	0.0004	11	OCR:ECAR Ratio	0.9064	0.0001	11
H+ leak	-0.7988	0.003	11				
Maximal respiration	-0.6696	0.02	11				
OCR:ECAR Ratio	0.8136	0.002	11				
mtMP	-0.7229	0.01	11				

Table 4-6 Correlation between mtMP levels and metabolic parameters

CANCER 0 GY				CANCER 1.8 GY			
FACTOR	**R value**	**p-value**	**n**	**FACTOR**	**R value**	**p-value**	**n**
OCR	0.7038	0.01	11	OCR	0.6343	0.03	11
Basal respiration	0.8013	0.003	11	Maximal respiration	0.6817	0.02	11
H+ leak	0.7147	0.01	11				
Maximal respiration	0.6305	0.03	11				

4.4.7 Linking bystander cell metabolism to metabolite levels in the secretome of normal and cancer tissue

To determine if there was any relationship between metabolite levels in the secretome of normal rectal tissue and rectal cancer tissue both pre- and post-radiation and bystander cellular metabolism, we conducted correlation analysis to identify any relationship between these factors. We found a significant correlation between OCR in bystander cells and methionine levels in the secretome of mock-irradiated normal rectal tissue (R=0.7139, p=0.04). We also demonstrated correlations between non-mitochondrial respiration and alanine (R=0.7452, p=0.03) and phenylalanine (R=0.8073, p=0.01) levels in the secretome of mock-irradiated normal rectal tissue. There was an inverse correlation between proton leak and phenylalanine (R=-0.7501, p=0.03). OCR:ECAR ratio in bystander cells correlated with levels of isoleucine (R=0.7657, p=0.02), N-acetyl-l-alanine (R=0.8154, p=0.01), phenylalanine (R=0.7542, p=0.03), valine (R=0.8357, p=0.009) and alanine (R=0.7874, p=0.02) in mock-irradiated normal rectal tissue. In bystander cells exposed to NCM from irradiated normal rectal tissue, OCR:ECAR ratio correlated inversely with both acetate (R=-0.7736, p=0.02) and lactate (-0.7161, p=0.04) (**Table 4-7**).

In bystander cells treated with TCM from mock-irradiated rectal cancer tissue, non-mitochondrial respiration correlated inversely with ethanol levels in the secretome of mock-irradiated rectal cancer tissue (R=-0.7399, p=0.005). In bystander cells treated with TCM from irradiated rectal cancer tissue, OCR correlated with methionine levels in the secretome of this TCM (R=0.5812, p=0.04). Basal respiration in bystander cells treated with TCM from irradiated rectal cancer tissue correlated with methionine (R=0.6561, p=0.02) and N-acetyl-L-alanine (R=0.5760, p=0.05). Proton leak correlated with methionine (R=0.8092, p=0.008) and N-acetyl-L-alanine (R=0.7029, p=0.03) while maximal respiration also correlated with methionine (R=0.7315, p=0.006). Interestingly, OCR:ECAR ratio in bystander cells treated with TCM from irradiated rectal cancer tissue correlated inversely with methionine (R=-0.7017, p=0.01), N-acetyl-L-alanine (R=-0.7165, p=0.008) and alanine (R=-0.7045, p=0.01). This is a differential response to the cells treated with NCM from irradiated normal rectal tissue (**Table 4-8**).

This highlights the differential relationship between altered metabolites and metabolic parameters in bystander cells treated with NCM and TCM, which was dependant on whether the tissues received radiation.

Table 4-7 Correlation between metabolic parameters in bystander cells and metabolites in the secretome of normal rectal tissue

NORMAL 0GY					NORMAL 1.8GY				
FACTOR	**Metabolite**	**R value**	**p-value**	**n**	**FACTOR**	**Metabolite**	**R value**	**p-value**	**n**
OCR	Methionine	0.7139	0.04	8	OCR:ECAR Ratio	Acetate	-0.7736	0.02	8
Non mitochondrial respiration	Alanine	0.7452	0.03	8	OCR:ECAR Ratio	Lactate	-0.7161	0.04	8
Non mitochondrial respiration	Phenylalanine	0.8073	0.01	8					
H+ leak	Phenylalanine	-0.7501	0.03	8					
OCR:ECAR Ratio	Isoleucine	0.7657	0.02	8					
OCR:ECAR Ratio	N-acetyl L-alanine	0.8154	0.01	8					
OCR:ECAR Ratio	Phenylalanine	0.7542	0.03	8					
OCR:ECAR Ratio	Valine	0.8357	0.009	8					
OCR:ECAR Ratio	Alanine	0.7874	0.02	8					

Table 4-8 Correlation between metabolic parameters in bystander cells and metabolites in the secretome of rectal cancer tissue

CANCER 0GY					CANCER 1.8GY				
FACTOR	**Metabolite**	**R value**	**p-value**	**n**	**FACTOR**	**Metabolite**	**R value**	**p-value**	**n**
Non-mitochondrial respiration	Ethanol	-0.7399	0.005	12	OCR	Methionine	0.5812	0.04	12
					Basal Respiration	Methionine	0.6561	0.02	12
					Basal Respiration	N-Acetyl-L-alanine	0.5760	0.05	12
					H+ leak	Methionine	0.8092	0.008	9
					H+ leak	N-Acetyl-L-alanine	0.7029	0.03	9
					Maximal Respiration	Methionine	0.7315	0.006	12
					OCR:ECAR Ratio	Methionine	-0.7017	0.01	12
					OCR:ECAR Ratio	N-Acetyl-L-alanine	-0.7165	0.008	12
					OCR:ECAR Ratio	Alanine	-0.7045	0.01	12

4.4.8 Linking body composition analysis to metabolism and mitochondrial function in bystander cells and metabolite levels in the secretome of rectal cancer tissue

It has been reported that overweight or obese rectal cancer patients have a poorer response to neoadjuvant treatment compared to their counterparts of a normal weight (40) (293), in addition to worse local control following neoadjuvant treatment and surgery (294). We examined the relationship between body composition and bystander cellular response to TCM from both irradiated and mock-irradiated rectal cancer biopsies.

We found a significant correlation between ECAR in bystander SW837 cells treated with TCM from irradiated rectal cancer biopsies and VFA (R=0.6446, p=0.02) and skeletal muscle mass (R=0.8034, p=0.001). There was also a significant correlation between OCR-linked ATP production in bystander SW837 cells treated with TCM from irradiated rectal cancer biopsies and VFA (R=0.6204, p=0.03) (**Table 4-9**). Of note, these observations only occurred in the bystander cells treated with TCM from irradiated rectal cancer biopsies, perhaps suggesting that obesity status may influence the behaviour of bystander cells following radiation. It is well-documented that upregulation of glycolysis is associated with a radioresistant phenotype (279) (297) (298) (299) and induces DNA repair pathways (261). Therefore, it may be possible that factors secreted from the TME of obese individuals may alter the metabolism of tumour cells and which may facilitate a more radioresistant phenotype resulting in poorer patient outcomes.

We found significant correlations between VFA and leucine (R=0.6395, p=0.02) and ethanol (R=0.5972, p=0.04) and intermuscular fat and ethanol (R=0.6483, p=0.02) levels in the TCM from mock-irradiated rectal cancer tissue (**Table 4-10**). This data suggest that obesity status may influence the local milieu of rectal cancer tissue by altering specific metabolite levels in the TME.

Table 4-9 Correlation between metabolic parameters and body composition analysis in bystander cells treated with TCM from irradiated rectal cancer biopsies i.e. Cancer 1.8 Gy

Body composition parameter	**FACTOR**	**R value**	**p-value**	**n**
VFA	ECAR	0.6446	0.02	12
VFA	ATP production	0.6204	0.03	12
Skeletal muscle	ECAR	0.8034	0.001	12

Abbreviations: VF, visceral fat area; ECAR, extracellular acidification rate (glycolysis)

Table 4-10 Correlation between body composition parameters and metabolites in the secretome of unirradiated rectal cancer tissue i.e. Cancer 0 Gy

Body composition parameter	**Metabolite**	**R value**	**p-value**	**n**
VFA	Leucine	0.6395	0.02	12
VFA	Ethanol	0.5972	0.04	12
Intermuscular fat	Ethanol	0.6483	0.02	12

Abbreviations: VFA, visceral fat area

4.5 Summary of findings from chapter 4

- *Ex vivo* RIBE induction in an explant model system of both normal rectal tissue and rectal cancer tissue induces metabolic alterations in bystander SW837 cells, specifically reductions in OXPHOS.
- *Ex vivo* RIBE induction in an explant model system of rectal cancer induces alterations in glycolysis in bystander SW837 cells, a phenomenon only observed following RIBE induction in malignant rectal tissue.
- The rectal cancer secretome induces higher levels of ROS in SW837 bystander cells, when compared to the normal rectal secretome.
- Leucine levels are significantly higher in the secretome of irradiated normal rectal tissue compared to irradiated rectal cancer tissue.
- Visceral fat area correlated with ECAR and OCR-linked ATP production in bystander cells treated with TCM from irradiated rectal cancer tissue.
- Visceral fat area correlated with levels of leucine and ethanol in the mock-irradiated rectal cancer TME.

4.6 Discussion

Using a novel human *ex vivo* explant model of rectal cancer and normal rectal tissue, we have shown for the first time that RIBE induction *ex vivo* causes significant alterations in cellular energy metabolism in bystander cells. We have demonstrated that metabolite profiles, specifically leucine concentrations, differed in the secretome between irradiated rectal cancer tissue and irradiated normal rectal tissue, with leucine levels being reduced in the irradiated cancer secretome compared to the irradiated normal secretome. We have demonstrated significant differences in ROS in bystander cells exposed to the rectal cancer, when compared to the normal rectal secretome. We demonstrated significant correlations between VFA and ECAR and OCR-linked ATP production in bystander cells treated with TCM from irradiated rectal cancer biopsies, while ECAR also correlated with skeletal muscle mass in these bystander cells.

The majority of bystander work to date has employed *in vitro* models and 3D tissue models (153), with others employing *in vivo* models such as fish (154, 155) and rodents (156). Our work in this study explores the complexity of the TME in rectal cancer and in the normal rectal tissue microenvironment, using human *ex vivo* explants. Importantly, these whole biopsy explants recapitulate the microenvironment of both normal and malignant rectal tissue. This allows us to capture the effect of radiation on all cell types within these microenvironments and elucidate if the response of bystander cancer cells to RIBE signals differs between normal and malignant tissue. Failure to observe RIBE events in our *in vitro* models used in chapter 2 underpins the importance of recapitulating the TME and 3-D architecture of tumours to gain a greater understanding into responses of malignant and normal rectal tissue to radiation.

We have shown that *ex vivo* RIBE induction in both normal rectal tissue and rectal cancer tissue causes significant reductions in OXPHOS in bystander SW837 rectal cancer cells. Le *et al.* have previously shown reduced complex I activity in the mitochondria of bystander HCT116 CRC cells exposed to RIBE-induced biophoton signalling (216). In our study, OCR-linked ATP production and maximal respiration were also significantly reduced following RIBE in bystander cells, which is in line with reduced OCR in these cells. Interestingly, a reduction in glycolysis was only observed following RIBE induction in malignant tissue. A more pronounced effect on glycolysis was expected in bystander cells exposed to TCM since malignant tissue is known to have a greater

tendency to employ aerobic glycolysis compared to normal tissue (300). To date, this is the first study to investigate the effect of RIBE induction on real-time cellular metabolism using Seahorse technology in real-time.

ROS are well-recognised participants in RIBE events (202, 204, 245). Mitochondria are an important source of endogenous ROS and also, traversal of the nucleus with radiation was not required to exert RIBE effects (205) and antioxidants can abrogate RIBE (211). Given the observed changes in mitochondrial metabolism observed in our study combined with the well-recognised role for the mitochondria in RIBE, we examined the effect of *ex vivo* RIBE induction on bystander rectal cancer cellular mitochondrial function, specifically ROS production and mtMP.

RIBE-induction *ex vivo* did not alter the mtMP or ROS levels in bystander SW837 rectal cancer cells. Similar results were obtained by Gorman *et al.* in bystander SW480 cells. However, the authors did report significantly reduced levels of mtMP in bystander cells exposed to TCM and NCM from irradiated CRC tissue and irradiated normal adjacent tissue compared to their unirradiated controls (207). ROS are known to be short-lived molecules and studies have shown changes in ROS and mtMP levels as early as 4 h and 12 h, following exposure to conditioned media but levels of both ROS and mtMP returned to normal at 24 h (168). It may be possible in our study that ROS and mtMP returned to baseline levels following 24 h treatment with TCM and NCM from irradiated tissue.

The rectal cancer secretome caused significant elevations in ROS levels in bystander SW837 cells, when compared to bystander cells exposed to the normal rectal secretome. It is well-documented that cancer cells have significantly higher levels of ROS compared to normal cells, owing to oncogenic transformation, including altered cellular metabolism, genetic mutation and a pro-tumorigenic microenvironment (301). Elevated ROS promotes oncogenic DNA mutations and may activate oncogenic signalling pathways (117). ROS may also be capable of initiating oncogenic signalling pathways such as EGFR (302) and MAPK (303) signalling pathways. Therefore, it is unsurprising that ROS levels were higher in bystander cells exposed to the rectal cancer microenvironment, when compared to the normal rectal microenvironment.

To better understand what metabolites may be driving these mitochondrial and metabolic bystander events, metabolomic screening was performed. PCA analysis of ^{1}HNMR spectra obtained from screening the TCM and NCM from both irradiated and mock-

irradiated rectal cancer and normal rectal tissue allowed separation of the irradiated normal and the irradiated cancer tissue secretome. Further analysis of the metabolite profile of the TCM and NCM indicated reduced levels of leucine in the secretome of the irradiated rectal cancer tissue compared to the irradiated normal rectal tissue. The literature strongly supports this observation. Arenas *et al.* have shown that serum leucine levels are significantly lower in breast cancer patients compared to control patients and following radiation therapy, leucine levels return to levels observed in control patients (304). He *et al.* report higher levels of leucine within the pancreas of mice bearing pancreatic tumours compared to the pancreas of control mice (305). Ching *et al.* found significantly lower levels of leucine in the plasma of cancer patients receiving chemotherapy (306). The authors postulated that these observations were owing to enhanced uptake of leucine by cancer cells (304-306). Since the metabolites in our study were not labelled, it was not possible to determine whether alterations in these metabolites were owing to altered secretion of metabolites by the tissue or altered uptake by cancer tissue. However, we believe it is likely owing to enhanced uptake of leucine by cancer cells, as reported in the literature. Following a full course of radiation therapy, Arenas *et al.* observed that leucine levels returned to levels observed in control patients after a full course of radiation therapy. It is important to note that the changes in serum leucine concentrations post-radiotherapy were observed following a full treatment course of radiation therapy (304). It may be possible that a single fraction of a clinically relevant dose of radiation, as used in our study may be insufficient to restore metabolite levels in the TME to that observed in non-cancerous tissue. Overall, limited numbers of studies have investigated the difference in metabolites between normal and cancer tissue as well as the effect of radiation on metabolite levels. A limitation of our study is the number of participants, with 8 controls and 12 cancer patients, it may be possible that no difference in leucine levels was observed between the unirradiated control samples and the unirradiated tumour samples as a result of low power.

There was a significant inverse correlation between ROS and mtMP in bystander SW837 cells treated with TCM from mock-irradiated rectal cancer tissue. This result was expected since increases in ROS are known to cause depolarisation of mtMP, which in turn triggers mitophagy (275). We found significant inverse correlations between OCR and ROS levels in bystander SW837 rectal cancer cells treated with both NCM and TCM. This result however, was unexpected since previous work in our group has shown that

ROS levels were higher in OAC cells with higher OCR (111). However, since ROS are short-lived molecules it may be possible that higher ROS levels would be observed at earlier time-points, between 0-6 h.

Interestingly, we observed a significant correlation between ECAR and OCR-linked ATP production in bystander SW837 cells treated with TCM from irradiated rectal cancer biopsies and the patient's VFA. Of note, this observation only occurred in the bystander cells treated with TCM from irradiated rectal cancer biopsies, perhaps suggesting that obesity status may influence the behaviour of bystander cells following radiation. This is an interesting and clinically relevant result as it has been reported that overweight and obese patients have poorer responses to neoadjuvant treatment and worse outcomes in rectal cancer (40, 293, 294). Moreover, when we correlated levels of metabolites in the secretome of mock-irradiated rectal cancer tissue we found significant correlations between VFA and leucine and ethanol. Also, intermuscular fat correlated with ethanol levels. This is an interesting observation and may suggest that obesity status alters the TME by influencing the levels of secreted metabolites, which may be functionally important. Correlations were also demonstrated between metabolites in the microenvironment of both tumour and normal tissue pre- and post-radiation and bystander cellular metabolic parameters, suggesting that altered metabolite levels cause cellular metabolism changes and obesity status impacts the levels of metabolites.

It is well-documented that upregulation of glycolysis is associated with a radioresistant phenotype (279, 297-299) and induces DNA repair pathways (261). Moreover, Lynam-Lennon *et al.* have demonstrated an enhancement of glycolysis when OAC cells were exposed to adipose conditioned media from obese patients (81). Similarly, elevated ATP levels are associated with enhanced radioresistance (111), while reduction of ATP levels have been associated with increased radiosensitivity (80, 307). While further elucidation of the mechanisms linking obesity with poorer response rates in rectal cancer is needed, this data offers insight into the effect of bystander signals from rectal cancer biopsies and how obesity modulates the bystander response.

To the best of our knowledge, this is the first study to investigate *ex vivo* RIBE induction in normal rectal tissue from healthy controls compared to rectal cancer tissue and its effect on bystander cellular metabolism and mitochondrial function. While the role of the mitochondria and ROS are well established in RIBE events *in vitro*, this novel study

extends the understanding of the role of the mitochondria to RIBE events using a human *ex vivo* model of disease. Radiation is used in both the neoadjuvant and adjuvant setting in rectal cancer patients but a complete pathological response (pCR) is only observed in a small subset of patients in the neoadjuvant setting. Further understanding of the biological effects of radiation on unirradiated cells near the irradiated volume and how this relates to treatment response may reveal potential therapeutic targets to enhance radiosensitivity in the neoadjuvant setting.

Chapter 5 The protein secretome is altered in rectal cancer tissue compared to normal rectal tissue and alterations in the secretome induce enhanced innate immune responses

This chapter has been published in part in **Heeran AB**, Dunne MR, Morrissey M, Buckley CE, Clarke N, Cannon A, Donlon NE, Nugent TS, Durand M, Dunne C, Larkin JO, Mehigan B, McCormick P, Lynam-Lennon N, O'Sullivan J. The Protein Secretome is Altered in Rectal Cancer Tissue Compared to Normal Rectal Tissue, and Alterations in the Secretome Induce Enhanced Innate Immune Responses. Cancers (Basel). 2021 Feb 2;13(3):571.

5.1 Introduction

Virchow observed in the 19th century that tumours often develop in a background of chronic inflammation (308) and accumulating evidence over the last number of decades has led to inflammation emerging as a hallmark of cancer (59). In chapter 4 we demonstrated alterations in the tumour microenvironment (TME) in response to radiation and the effects of these alterations on bystander cellular metabolism. Specifically, we investigated mitochondrial alterations including reactive oxygen species (ROS) production and altered metabolites in the TME. ROS and the mitochondria are tightly linked to inflammation with some data indicating that ROS derived from the mitochondria may act as endogenous carcinogens that are capable of inducing pro-oncogenic pathways in inflammation-associated cancers (303). Colorectal cancer (CRC) is one such cancer that has a strong link between chronic inflammation and cancer development. Inflammatory bowel disease (IBD) is a risk factor for the development of CRC with increasing risk of CRC development with longer disease duration (309). Furthermore, the use of anti-inflammatory drugs is associated with a reduced incidence of CRC, thus underscoring the importance of inflammation in the development of CRC (310, 311). In this chapter, we profiled the inflammatory milieu of rectal cancer and identified differentially secreted factors in the rectal cancer TME compared to the normal rectal microenvironment. We also examined the effect of direct radiation on the levels of these factors secreted from the TME. Finally, we examined the effect of the normal and malignant rectal cancer microenvironments both pre- and post-radiation on the innate immune system, specifically on dendritic cell (DC) maturation.

The TME describes the milieu of cancer cells, infiltrating immune cells, secreted factors and the extracellular matrix. The interaction between the tumour cells and the surrounding microenvironment profoundly affects tumour progression and treatment response (312). Much work to date has investigated the CRC TME, and while the colon and rectum are anatomically related, treatment regimens and response rates differ between the cancer types (313, 314). The interplay between the TME, secreted inflammatory mediators and immune cell function and how it may be altered by radiation is poorly understood in the context of rectal cancer. Furthermore, to fully understand the alterations occurring in the rectal cancer microenvironment and its interaction with the immune system, it is important to also gain an understanding of the microenvironment in a non-cancerous rectal tissue (normal) model for comparison.

Secreted factors from the TME may both positively and negatively impact on cancer development. Radiation is known to induce alterations in secreted factors from skin tissue (315), however, the differential effects of clinically relevant doses of radiation on the normal rectal tissue secretome compared to the rectal cancer tissue secretome is unknown. To date, a comprehensive profiling of the rectal cancer protein secretome and the normal rectal secretome has not been conducted. For this study we utilised an *ex vivo* explant model system which maintains the 3-D architecture of tumour and normal tissue and faithfully recapitulates their microenvironments.

The importance of the immune system and its role in carcinogenesis is pivotal (316) and evidence supports the role of the immune system in the radiation response (226). DCs are professional antigen presenting cells that reside in blood and tissues in an immature state. Their main function is to recognise pathogens, capture, process and present antigens to T cells to elicit an antigen-specific immune response (317). DCs are essential for anti-tumour immunity and it has been reported that DCs in patients with cancer are incapable of launching a sufficient anti-tumour response (317). It is becoming increasingly evident that radiation may alter the immune system and inflammatory pathways (318). Historically, radiation was considered immunosuppressive with the radiosensitivity of lymphocytes being the dominant explanation for this, however in recent years radiation is considered immunomodulatory (319). It is thought that radiation induces innate receptor signalling and subsequent maturation of DCs through tumour cell death and release of endogenous TLR agonists (319). Furthermore, injection of immature DCs into an irradiated tumour site induced strong tumour-specific cytotoxic T lymphocyte activity in a poorly immunogenic mouse tumour model (320).

In this study, we have profiled for the first time the protein secretome of both normal (non-cancer) rectal tissue and rectal cancer tissue pre- and post-radiation and examined how these different secretomes affect the innate immune system, specifically DC maturation.

5.2 Overall hypothesis and specific aims of chapter 5

We hypothesise that the protein secretome will differ between the normal rectal and rectal cancer tissue microenvironments and radiation will alter these secretomes. We also hypothesise that the normal and malignant protein secretome will interact differently with the innate immune system, inducing differential levels of DC maturation markers.

Specific aims:

1. Profile the inflammatory secretome of normal rectal tissue and rectal cancer tissue both pre- and post-radiation.
2. Examine the interaction between the normal and rectal cancer secretome with DCs both pre- and post-radiation.
3. Correlate inflammatory secretions from DCs incubated with TCM and NCM with DC maturation markers.
4. Examine the relationship between the levels of secreted proteins and DC maturation markers with patient clinical characteristics including T stage, N stage and parameters of body composition.

5.3 Materials and methods

5.3.1 Patient recruitment

Patients undergoing diagnostic endoscopy for rectal cancer and lower gastrointestinal investigations were prospectively recruited to this study between January 2018 and November 2018. Informed written patient consent was obtained for the use of patient tissue and data in this study. Ethical approval was granted by the St. James's Hospital/ AMNCH Research Ethics Committee. Patient data was pseudo-anonymised prior to sample access. Biopsies were obtained from treatment-naïve patients at diagnostic endoscopy. A total of 12 patients with histologically confirmed rectal cancer were recruited to the study and 8 patients that did not have cancer (normal, non-cancer controls). All clinical and pathological data was obtained following written informed consent. Clinical data was obtained from patient records. Histological confirmation of tumour tissue and non-malignant tissue in patient diagnostic biopsies was performed by a pathologist using routine haematoxylin and eosin staining. Tumour regression score (TRS) was assigned by a pathologist following surgery in all patients receiving neoadjuvant treatment. Visceral fat area (VFA), subcutaneous fat area, intermuscular fat and skeletal muscle were calculated from a pre-operative diagnostic computed tomography (CT) scan by an experienced radiologist. Patients with a VFA greater than 163.8 cm^2 (males) and 80.1 cm^2 (females) were classified as obese (296). Patient characteristics are outlined in **Table 5-1**.

5.3.2 Generation of tumour conditioned media and normal conditioned media

Tumour conditioned media (TCM) and normal conditioned media (NCM) were generated as described in *section 4.3.2*. TCM and NCM was diluted 1:1 with M199 prior to use in experiments below. Any dilutions below refer to the dilution of this 1:1 media.

5.3.3 Mesoscale Discovery 54-plex ELISA

To assess angiogenic, vascular injury, inflammatory, cytokine and chemokine secretions, a 54-plex ELISA kit spread across 7 plates was used [Meso Scale Diagnostics, USA]. The 54-multiplex kit was used to quantify the secretions of CRP, CCL11 (Eotaxin), CCL26 (Eotaxin-3), FGF(basic), Flt-1, GM-CSF, ICAM-1, IFN-γ, IL-10, IL-12/IL-23p40, IL-12p70, IL-13, IL-15, IL-16, IL-17A, IL-17A/F, IL-17B, IL-17C, IL-17D, IL-

1RA, IL-1α, IL-1β, IL-2, IL-21, IL-22, IL-23, IL-27, IL-3, IL-31, IL-4, IL-5, IL-6, IL-7, IL-8, IL-8 (HA), IL-9, CXCL10 (IP-10), CCL2 (MCP-1), CCL13 (MCP-4), CCL22 (MDC), CCL3 (MIP-1α), CCL4 (MIP-1β), CCL20 (MIP-3α), PlGF, SAA, CCL17 (TARC), Tie-2, TNF-α, TNF-β, TSLP, VCAM-1, VEGF-A, VEGF-C and VEGF-D from NCM and TCM. Secretion data for all factors was normalised appropriately to rectal tissue protein content using the BCA assay (Pierce). All assays were run as per manufacturer's recommendations, with an alternative protocol overnight supernatant incubation being used for all assays except vascular injury and angiogenesis.

5.3.4 Dendritic cell isolation and culture

Human monocyte-derived immature DCs were generated from peripheral blood mononuclear cells obtained from buffy coat preparations (National Blood Centre, St. James's Hospital, Dublin) by density gradient centrifugation (Lymphoprep) as described (321, 322). Briefly, monocytes were isolated by positive selection using anti-CD14 magnetic microbeads as described by the manufacturer [Miltenyi Biotec, Germany] and seeded at a density of $1x10^6$ cells/mL in 6-well plates in 3 mL of RPMI-1640 medium containing 10% defined low-endotoxin HyClone FBS [Thermo Fischer Scientific, MA, USA], 1% penicillin/streptomycin, 1% Fungizone, human granulocyte macrophage colony-stimulating factor (50 ng/mL) [Immunotools, Germany], and human IL-4 (70 ng/mL) [Immunotools, Germany] in a humidified atmosphere with 5% CO_2 at 37°C. Cells were fed at day 3 by replacing half the medium made up with fresh cytokines. At day 6, $CD11c^+$ cells exhibited an immature DC phenotype capable of upregulating maturation markers following LPS activation.

5.3.5 Stimulation of monocyte-derived dendritic cells

Freshly generated DCs were plated in 96-well plates at $2x10^5$ cells in 200 µL RPMI 1640 media supplemented with 10% defined HyClone FBS [Thermo Fisher Scientific, MA, USA] and stimulated with a 1:2 dilution of TCM or NCM, or matched background media controls, for 4-5 h before exposure to 10 µg/mL of ultrapure TLR4 agonist *Escherichia coli* lipopolysaccharide [LPS-EB; Invivogen] overnight. Supernatants were harvested and frozen, and cells were assessed for expression of surface markers as described below.

5.3.6 Flow cytometry

DCs were stained with the following antibody panel: phycoerythrin (PE)- anti-CD80 (2D10), PerCP-Cy5.5- anti-CD86 (IT2.2), Pe-Cy7- anti-CD83 (HB15), Brilliant Violet 421- anti-PD-L1 (29E.2A3), Brilliant Violet 510- anti-CD11c (3.9), allophycocyanin (APC)- anti-CD54 (HA58), and APC-Cy7- anti-HLA-DR (L243) [Biolegend, CA, USA]. Samples were acquired on a DAKO CyAn ADP flow cytometer [Beckman Coulter, CA, USA] with compensation performed with positive and negative compensation beads [BD Biosciences, CA, USA]. Gating on and analysis of $CD11c^+$ cells was performed using FlowJo software [Tree Star Inc., OR, USA].

5.3.7 Protein isolation and quantification from rectal tissue

Rectal tissue samples were placed on ice and 200 μL of RIPA buffer supplemented with one PhosSTOP phosphatase inhibitor and one Complete Mini protease inhibitor tablet per 10 mL was added to each sample. Samples were ruptured using a metal bead and the Qiagen tissue lyser at 25 Hz for 2 min. Samples were transferred to an Eppendorf tube and centrifuged at 13,000 x g for 20 min at 4°C. Isolated protein was quantified using BCA assay as per manufacturer's instructions.

5.3.8 Statistical analysis

GraphPad Prism 9 software was used to perform statistical analysis. All data is expressed as mean ± SEM. Statistical test used is indicated in the relevant figure legend. Correlation analysis was performed using Spearman's correlation coefficient. Statistical significance considered at $p<0.05$.

Figure 5.1 illustrates the methodology employed in this study.

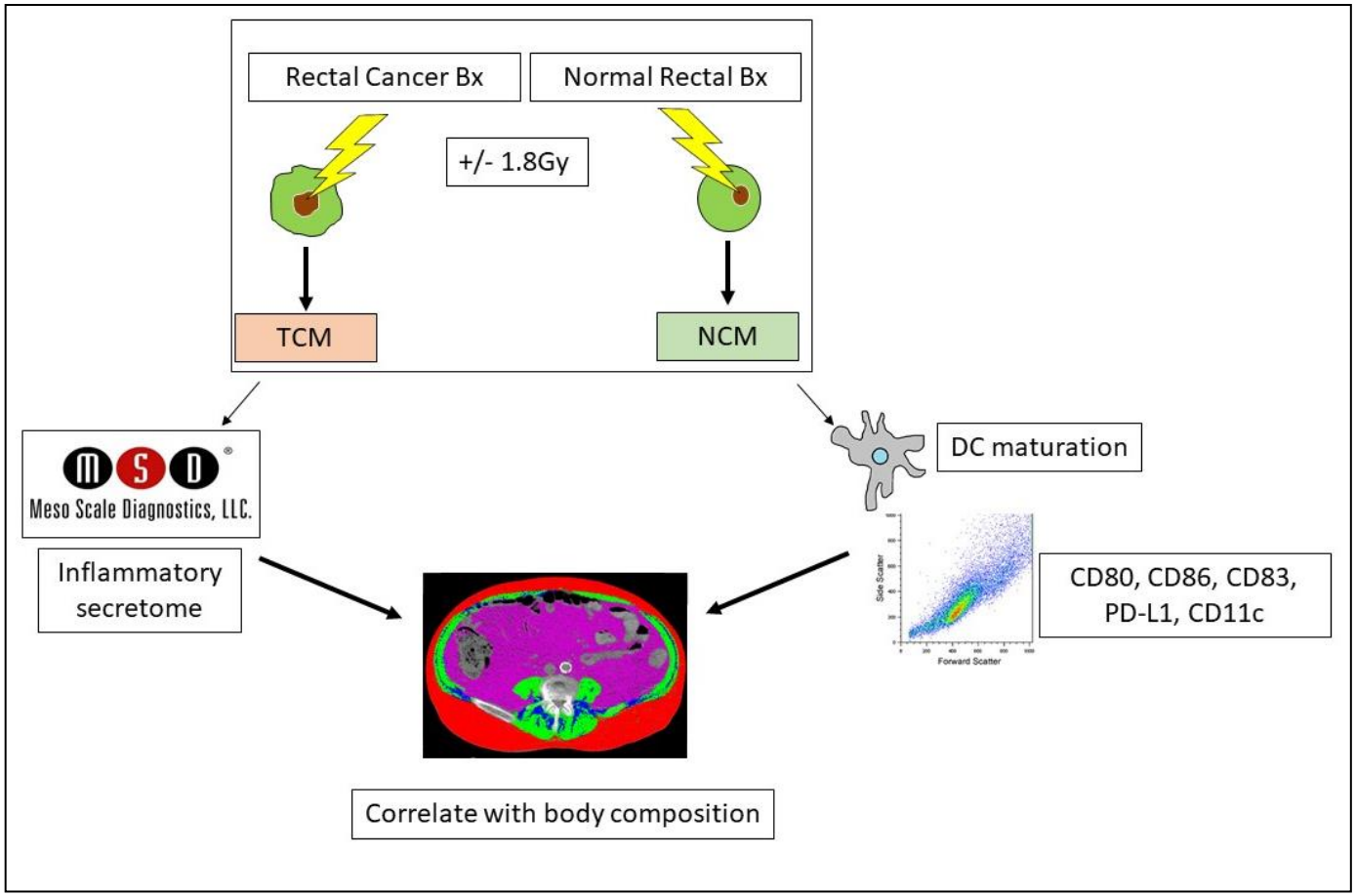

Figure 5.1 Schematic diagram of methodology used in chapter 5.

Normal rectal and rectal cancer biopsies were either mock-irradiated or irradiated with a clinically relevant dose of 1.8 Gy radiation and cultured for 24 h before harvesting. The resultant TCM and NCM were then screened for the secretion of 54 proteins using the MSD multiplex platform. DCs were incubated with TCM and NCM and the effect of the TCM and NCM on DC maturation markers were examined using flow cytometry.

5.4 Results

5.4.1 Patient characteristics

Treatment naïve endoscopic specimens were taken from 20 patients undergoing endoscopic assessment at St. James's Hospital, Dublin, between January 2018 and November 2018. Endoscopic specimens were taken from patients with rectal cancer (n=12) and patients that did not have rectal cancer i.e. histologically normal (n=8). Patient characteristics are outlined in **Table 5-1**.

Table 5-1 Patient characteristics

			Percent (%)
Age (rectal cancer patients)	Mean ± SD	65.16 ± 10.14	
	Range	53-89	
Age (control patients)	Mean ± SD	58.75 ± 11.42	
	Range	44-76	
Gender (rectal cancer patients)	Male (n)	8	66.67
	Female (n)	4	33.33
Gender (control patients)	Male (n)	3	37.5
	Female (n)	5	62.5
Obesity status (visceral fat area)	Obese	8	66.67
	Non obese	4	33.33
Histology	Adenocarcinoma (n)	12	100
Stage of differentiation	Moderate (n)	12	100
T stage	T1 (n)	1	8.33
	T2 (n)	2	16.67
	T3 (n)	8	66.67
	T4 (n)	1	8.33
N stage	N0 (n)	6	50
	N1 (n)	5	41.67
	N2 (n)	1	8.33
M stage	M0 (n)	11	91.67
	M1 (n)	1	8.33
Neoadjuvant CRT	Received neo-CRT (n)	6	50
Neoadjuvant CT	Received neo-CT only (n)	1	8.33
Neoadjuvant RT	Received neo-RT only (n)	1	8.33
Surgery [a]	Received surgery (n)	11	91.67
TRS [b]	0 (n)	2	28.57
	1 (n)	3	42.85
	2 (n)	1	14.28
	3 (n)	1	14.28

Abbreviations; CRT; chemoradiotherapy, CT; chemotherapy, RT; radiotherapy, TRS; tumour regression score.[a] One patient was unsuitable for surgery[b] TRS available for 7 patients, percent expressed as total with TRS score

5.4.2 Normal rectal and rectal cancer biopsies have a heterogenous inflammatory secretome

In order to assess the differences in the inflammatory secretome between normal rectal tissue and rectal cancer tissue, we cultured 12 rectal cancer biopsies and 8 normal rectal biopsies for 24 h and used the MSD multiplex platform to quantify the expression of 54 inflammatory proteins from the resultant TCM and NCM. The secreted proteins were categorised into 7 panels; vascular injury, angiogenesis, inflammatory, Th17, chemokine, cytokine 1 and cytokine 2. Secreted levels of vascular injury proteins CRP, ICAM-1, SAA and VCAM-1 in normal rectal and rectal cancer tissue are shown in **Figure 5.2A** and **Figure 5.3A.** The secretion of angiogenic proteins bFGF, Flt-1, P1GF, Tie-2, VEGF-A, VEGF-C and VEGF-D are shown in **Figure 5.2B** (normal) and **Figure 5.3B** (cancer). Inflammatory secretions IFN-γ, IL-10, IL-12p70, IL-13, IL-1β, IL-2, IL-4, IL-6, IL-8(HA) and TNF-α are displayed in **Figure 5.2C** (normal) and **Figure 5.3C** (cancer). The Th17 proteins IL-21, IL-22, IL-23, IL-27, IL-31 and CCL20 are shown in **Figure 5.2D** (normal) and **Figure 5.3D** (cancer). The panel of chemokine proteins CCL22, CCL3, CCL4, CCL17, CCL11, CCL26, CXCL10, CCL2 and CCL13 are presented in **Figure 5.2E** (normal) and **Figure 5.3E** (cancer). Two panels of cytokine proteins; GM-CSF, IL-12/IL-23p40, IL-15, IL-16, IL-17A, IL-1α, IL-5, IL-7, TNF-β, IL-17A/F, IL-17B, IL-17C, IL-17D, IL-1RA, IL-3, IL-9 and TSLP are displayed in **Figure 5.2F-G** (normal) and **Figure 5.3F-G** (cancer).

Figure 5.2 and **Figure 5.3** highlight the heterogenous secreted profile observed in both normal rectal biopsies and rectal cancer biopsies. Fifty-three of the secreted factors were within the limit of detection for normal rectal secretome (**Figure 5.2**) and in the rectal cancer secretome (**Figure 5.3**). However, three secreted factors; Tie-2, VEGF-C and VEGF-D were only detected in one sample each in the normal (non-cancer) samples.

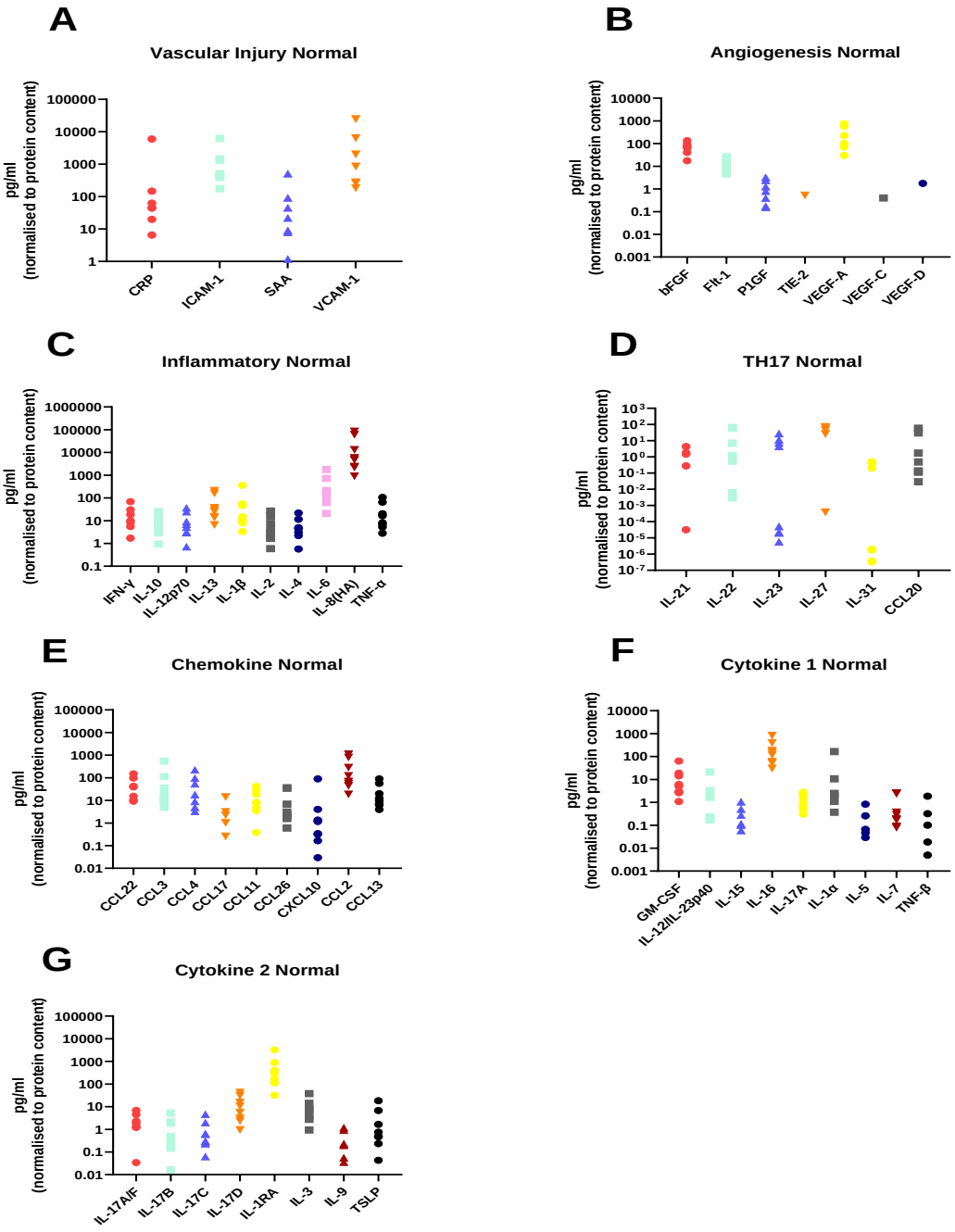

Figure 5.2 Secreted levels of 53 proteins from n=8 normal rectal biopsies showing heterogenous secretions of proteins

(**A**) Secreted levels of vascular injury proteins CRP, ICAM-1, SAA and VCAM-1. (**B**) Secreted levels of angiogenic factors bFGF, Flt-1, P1GF, Tie-2, VEGF-A, VEGF-C and VEGF-D. (**C**) Inflammatory secreted proteins IFN-γ, IL-10, IL-12p70, IL-13, IL-1β, IL-2, IL-4, IL-6, IL-8(HA) and TNF-α. (**D**) Secretion of Th17 proteins IL-21, IL-22, IL-23, IL-27, IL-31 and CCL20. (**E**) Chemokine secreted proteins CCL22, CCL3, CCL4, CCL17, CCL11, CCL26, CXCL10, CCL2 and CCL13. (**F**) Secretion of cytokine panel 1 proteins GM-CSF, IL-12/IL-23p40, IL-15, IL-16, IL-17A, IL-1α , IL-5, IL-7, and TNF-β. (**G**) Secretion of cytokine 2 panel proteins IL-17A/F, IL-17B, IL-17C, IL-17D, IL-1RA, IL-3, IL-9 and TSLP. All protein secretions are normalised to protein content of the biopsies.

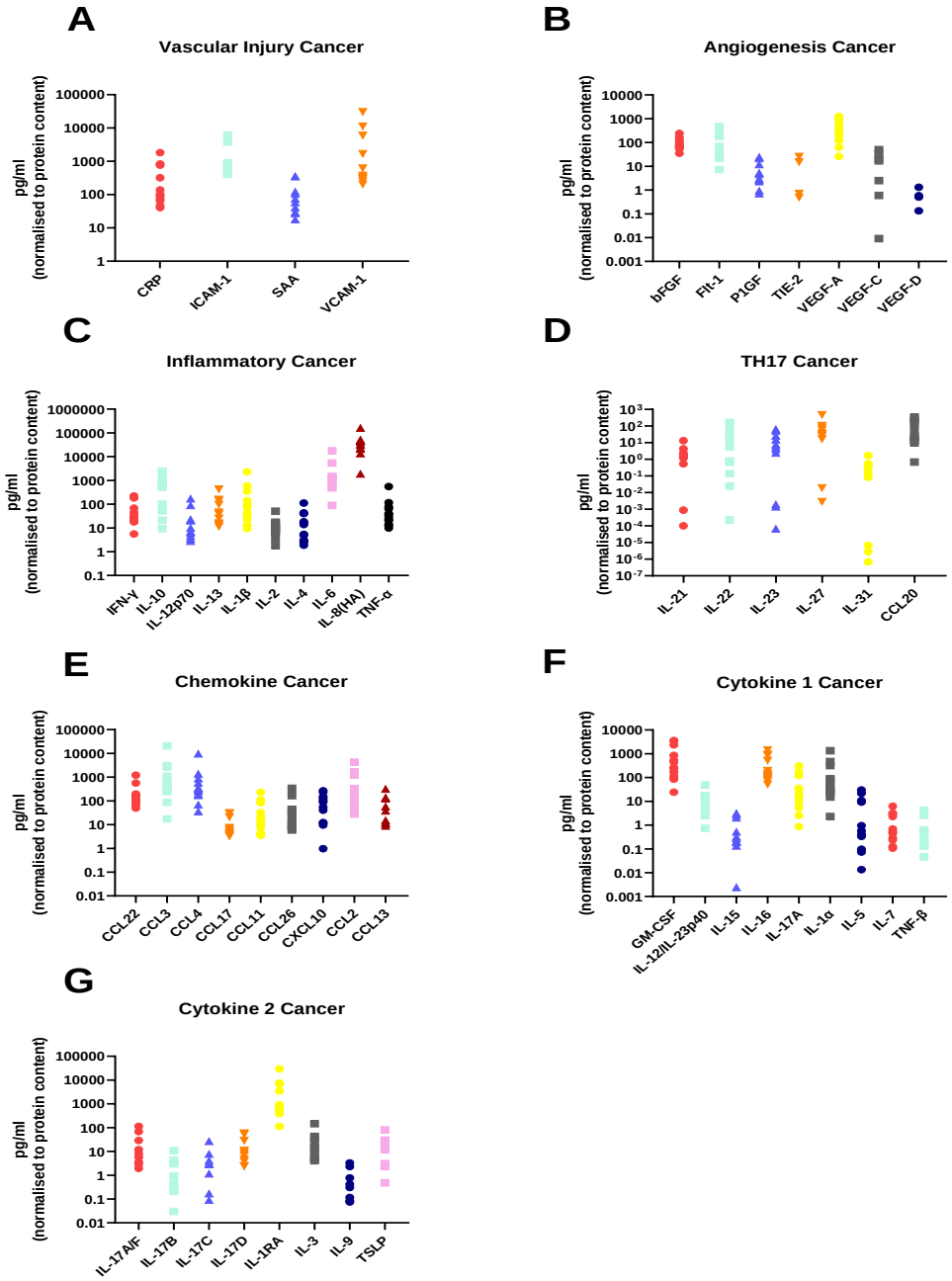

Figure 5.3 Secreted levels of 53 proteins from n=12 rectal cancer biopsies showing heterogenous secretion of proteins

(**A**) Secreted levels of vascular injury proteins CRP, ICAM-1, SAA and VCAM-1. (**B**) Secreted levels of angiogenic factors bFGF, Flt-1, P1GF, Tie-2, VEGF-A, VEGF-C and VEGF-D. (**C**) Inflammatory secreted proteins IFN-γ, IL-10, IL-12p70, IL-13, IL-1β, IL-2, IL-4, IL-6, IL-8(HA) and TNF-α. (**D**) Secretion of Th17 proteins IL-21, IL-22, IL-23, IL-27, IL-31 and CCL20. (**E**) Chemokine secreted proteins CCL22, CCL3, CCL4, CCL17, CCL11, CCL26, CXCL10, CCL2 and CCL13. (**F**) Secretion of cytokine panel 1 proteins GM-CSF, IL-12/IL-23p40, IL-15, IL-16, IL-17A, IL-1α, IL-5, IL-7, and TNF-β. (**G**) Secretion of cytokine 2 panel proteins IL-17A/F, IL-17B, IL-17C, IL-17D, IL-1RA, IL-3, IL-9 and TSLP. All protein secretions are normalised to protein content of the biopsies.

5.4.3 The protein secretome differs between non-cancerous rectal tissue and rectal cancer tissue

We screened the normal, non-cancerous rectal secretome and the rectal cancer secretome for the expression of 54 secreted factors. We identified 19 factors that were secreted at significantly higher levels from the rectal cancer tissue, when compared with the normal rectal tissue. These factors are categorised according to function; angiogenic, Th17 and inflammatory (**Figure 5.4A-F**), cytokines (**Figure 5.5A-G**) and chemokines (**Figure 5.6A-F**). Flt-1 (p=0.001), P1GF (p=0.01), CCL20 (p=0.005), IFN-γ (p=0.04), IL-10 (p=0.0002) and IL-6 (p=0.02) (**Figure 5.4A-F**), GM-CSF (p<0.0001), IL-12/IL-23p40 (p=0.01), IL-17A (p=0.0003), IL-1α (p=0.003), IL-17A/F (p=0.003), IL-1RA (p=0.03), TSLP (p=0.007) (**Figure 5.5A-G**), CCL26 (p=0.009), CXCL10 (p=0.001), CCL22 (p=0.007), CCL3 (p=0.002), CCL4 (p=0.0007) and CCL17 (p=0.02) (**Figure 5.6A-F**) are secreted at significantly higher levels from the rectal cancer secretome compared to the normal rectal secretome. This indicates that the rectal cancer secretome is more inflammatory compared to the normal rectal secretome.

5.4.4 Radiation alters the protein secretome of non-cancerous rectal tissue

Radiation is the standard of care for LARC, with about 50% of patients receiving this treatment modality, therefore, we investigated the effect of a clinically relevant dose of 1.8 Gy radiation on protein secretions from normal rectal tissue and rectal cancer tissue. Interestingly, we found 2 factors that were secreted at significantly higher levels from irradiated normal rectal tissue compared to mock-irradiated normal rectal tissue; IL-15 (p=0.01) and CCL22 (p=0.03) (**Figure 5.7A-B**). There were no significant differences in levels of IL-15 (p=0.052) or CCL22 (p=0.73) in the secretome of rectal cancer tissue following a single fraction of 1.8 Gy radiation (**Figure 5.7C-D**). This indicates that a single fraction of 1.8 Gy radiation induces inflammation in normal rectal tissue. We did not observe any significant alterations in secreted factors in rectal cancer tissue following a single fraction of a clinically relevant dose of radiation. This suggests that a single fraction of 1.8 Gy radiation does not further alter levels of secreted inflammatory proteins in rectal cancer tissue.

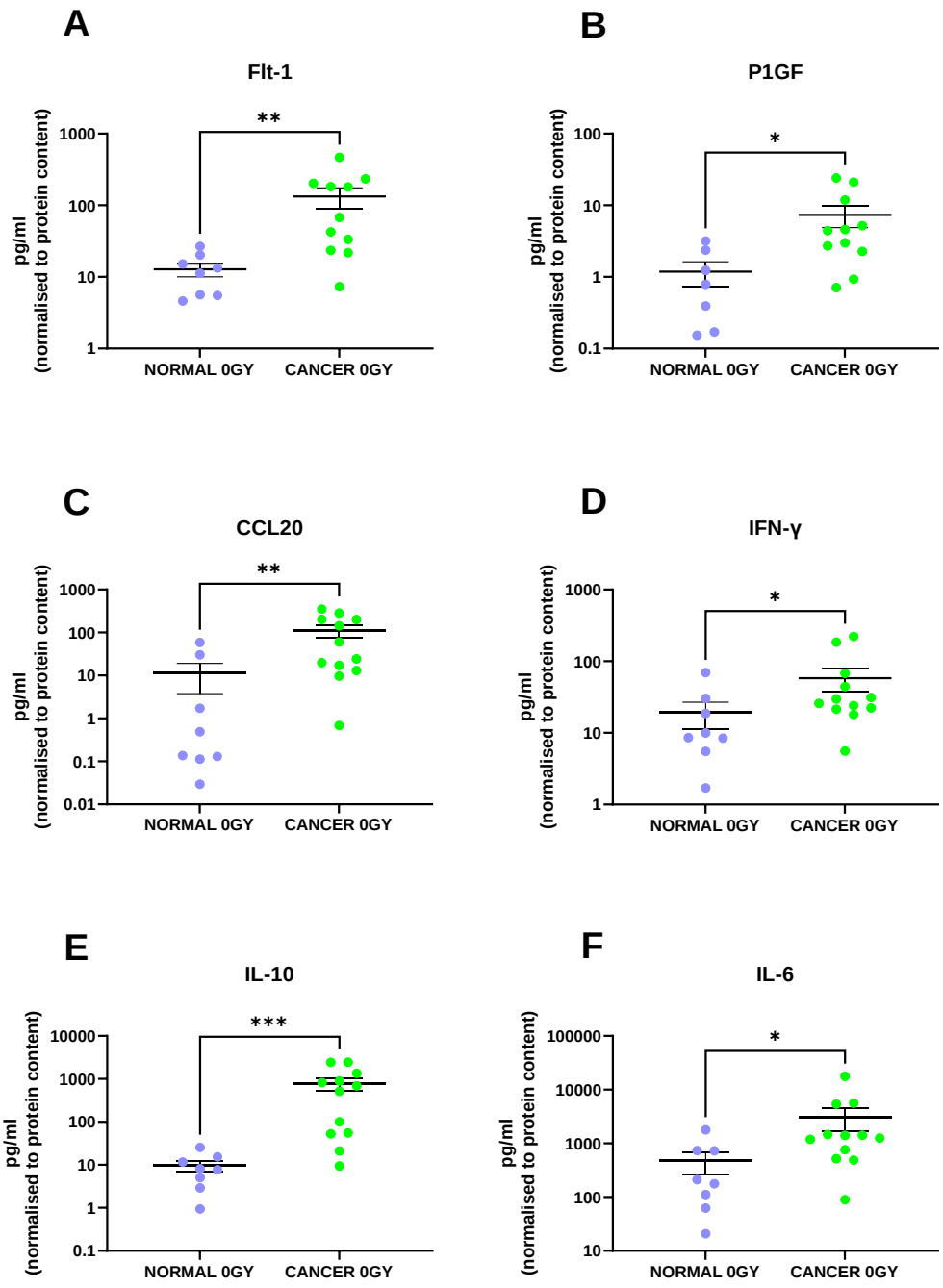

Figure 5.4 The protein secretome of rectal cancer tissue is significantly different to normal rectal tissue with elevated angiogenic, Th17 and inflammatory factors in the rectal cancer secretome

There were significantly higher levels of (**A**) Flt-1, (**B**) P1GF, (**C**) CCL20, (**D**) IFN-γ, (**E**) IL-10 and (**F**) IL-6 in the rectal cancer secretome compared to the normal rectal secretome. All data expressed as mean ± SEM. Statistical analysis was performed using a Mann Whitney U-test. ***p<0.001, **p<0.01, *p<0.05. n=8 for normal, n=12 for cancer, n=7 for normal for P1GF, n=11 for cancer for Flt-1 and P1GF.

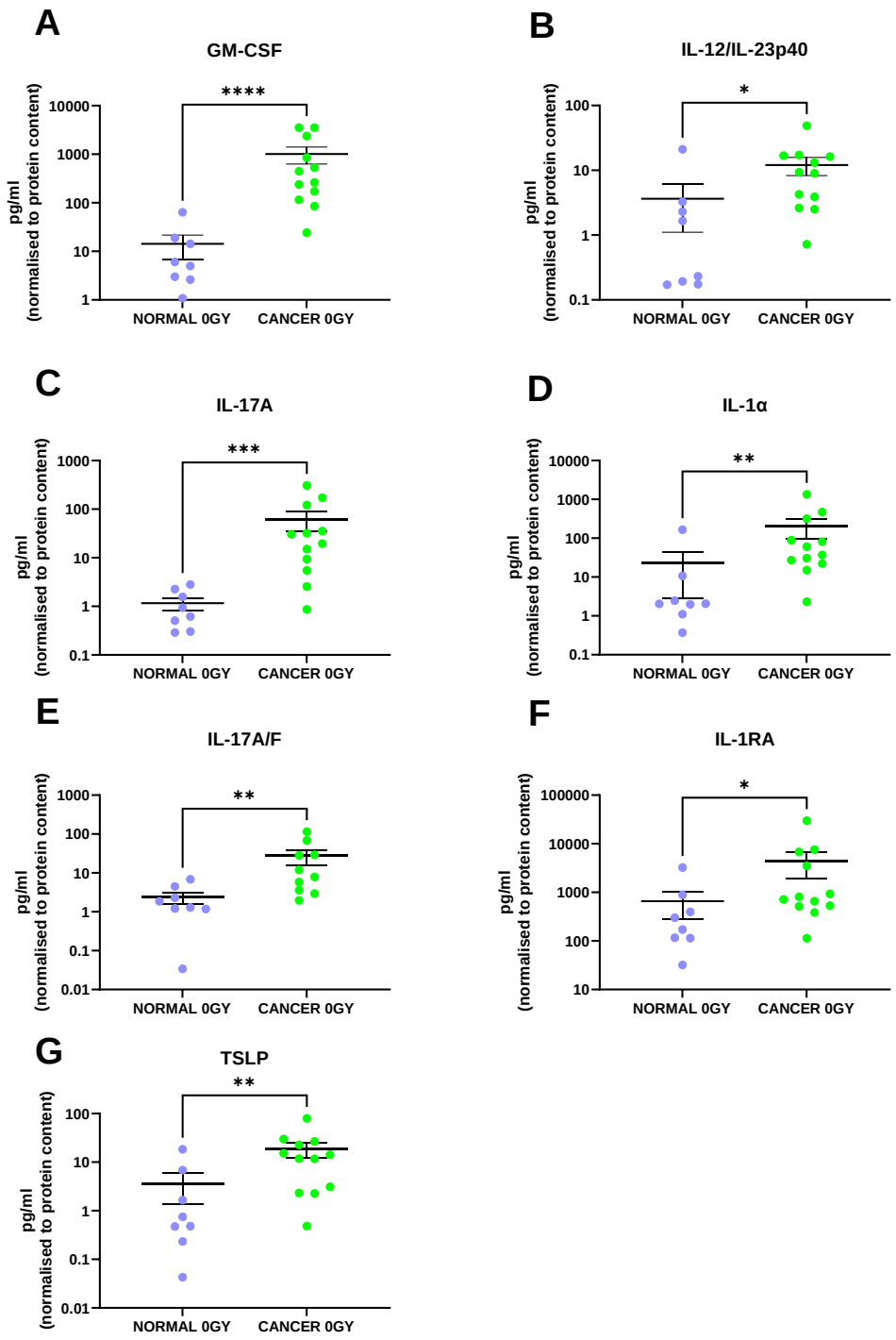

Figure 5.5 The protein secretome of rectal cancer tissue is significantly different to normal rectal tissue with elevated levels of cytokines in the rectal cancer secretome

There were significantly higher levels of (**A**) GM-CSF, (**B**) IL-12/IL-23p40, (**C**) IL-17A, (**D**) IL-1α, (**E**) IL-17A/F, (**F**) IL-1RA, (**G**) TSLP. All data expressed as mean ± SEM. Statistical analysis was performed using a Mann Whitney U-test. ****p<0.0001, ***p<0.001, **p<0.01, *p<0.05. n=8 for normal, n=12 for cancer and n=10 cancer for IL-17A/F.

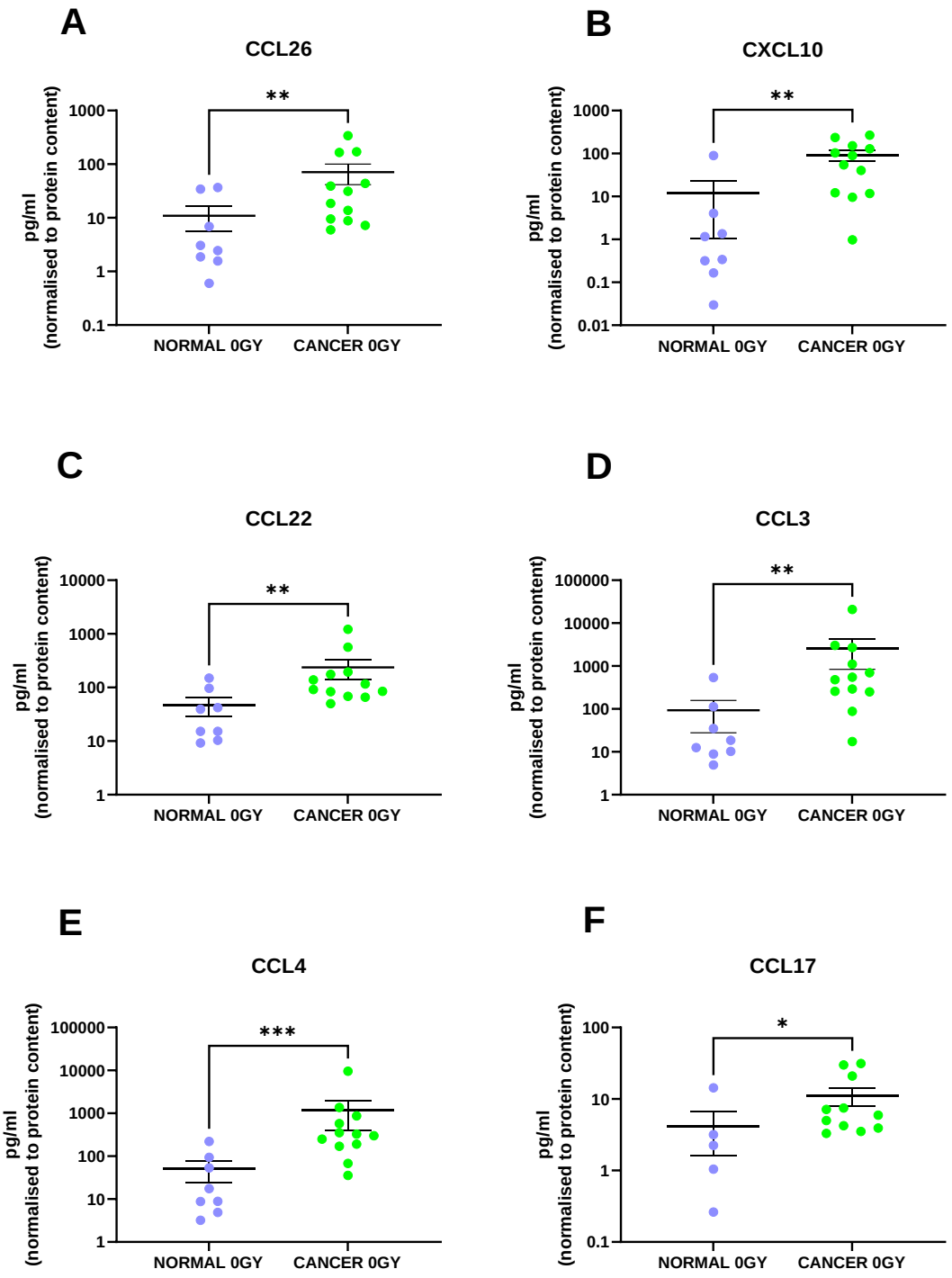

Figure 5.6 The protein secretome of rectal cancer tissue is significantly different to normal rectal tissue with chemokine levels being significantly higher in the rectal cancer secretome

There were significantly higher levels of (**A**) CCL26, (**B**) CXCL10, (**C**) CCL22, (**D**) CCL3, (**E**) CCL4 and (**F**) CCL17. All data expressed as mean ± SEM. Statistical analysis was performed using a Mann Whitney U-test. ***p<0.001, **p<0.01, *p<0.05. n=8 for normal, n=12 for cancer, and n=11 for cancer for CCL17.

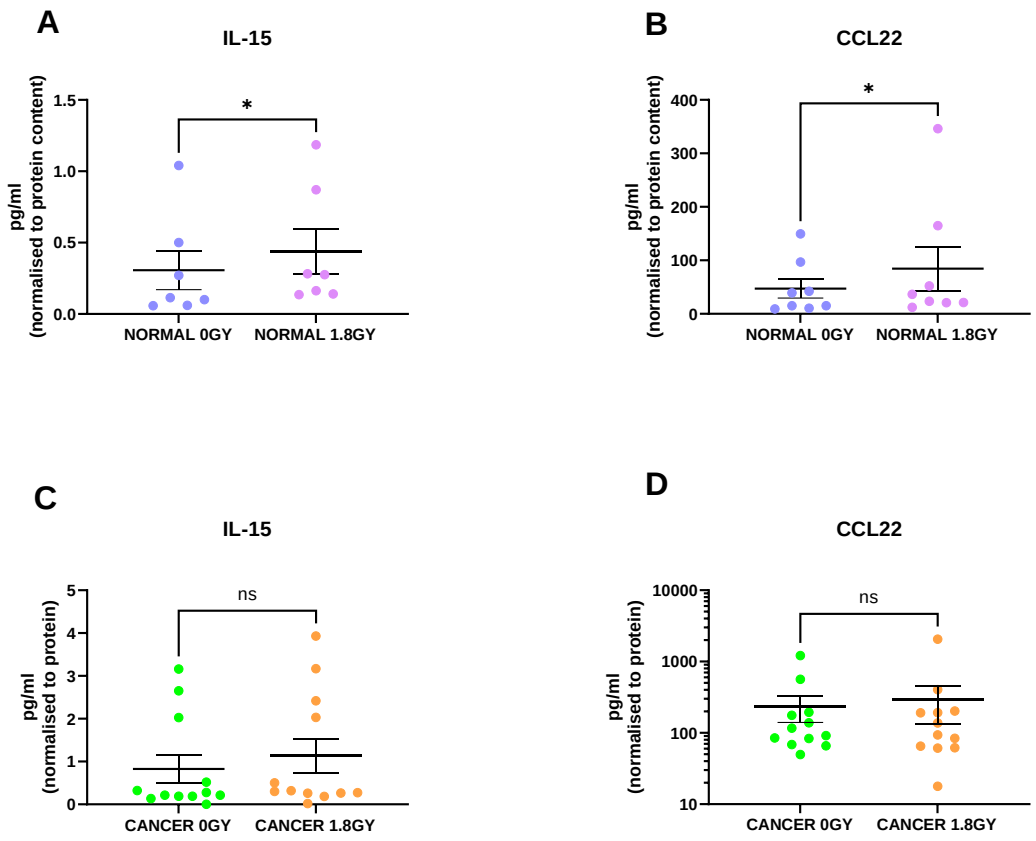

Figure 5.7 Radiation alters the secretome of normal rectal tissue

Following a single fraction of 1.8 Gy radiation, there were significantly higher levels of (**A**) IL-15 and (**B**) CCL22 in the normal rectal secretome. Following a single fraction of 1.8 Gy radiation, there were no significant differences in levels of (**C**) IL-15 or (**D**) CCL22 in the rectal cancer secretome. All data expressed as mean ± SEM. Statistical analysis was performed using a Wilcoxon signed-rank test. **p*<0.05, ns=non-significant. *n*=8 for CCL22 and *n*=7 for IL-15 for normal, *n*=12 for cancer,

5.4.5 The rectal cancer microenvironment alters expression of maturation markers on CD11c^{+} dendritic cells

To assess the interaction between the TME and the immune system, we examined the effect of TCM and NCM from both irradiated and mock-irradiated biopsies on DC maturation markers. Following LPS-induced maturation of DCs, there was a significant increase in levels of CD80, CD86, CD83 and PD-L1 ($p<0.05$), all markers of DC maturation and the phenotypic marker CD11c ($p<0.05$). Therefore, we assessed the effects of TCM and NCM from both mock-irradiated and irradiated tissue on these markers. TCM and NCM from both mock-irradiated and irradiated biopsies had a significant inhibitory effect on LPS-induced expression of CD80 ($p<0.0001$ for all comparisons). However, TCM from irradiated rectal cancer biopsies had the least inhibitory effect on CD80 levels, inducing significantly higher expression of CD80 compared to TCM from mock-irradiated rectal cancer ($p=0.03$). TCM from both mock-irradiated ($p=0.007$) and irradiated ($p=0.001$) rectal cancer tissue significantly enhanced LPS-induced expression of CD86. NCM did not affect expression of CD86 compared to the media only control with LPS ($p>0.05$). CD83 levels were significantly enhanced by NCM from both mock-irradiated ($p=0.01$) and irradiated ($p=0.0006$) biopsies and TCM from both mock-irradiated ($p<0.0001$) and irradiated ($p=0.0003$) biopsies compared to LPS-induced stimulation. Moreover, TCM from mock-irradiated rectal cancer tissue enhanced expression of CD83 to a greater extent than NCM from mock-irradiated normal rectal tissue ($p=0.02$). PD-L1 levels are significantly elevated on DCs treated with TCM from irradiated rectal cancer tissue ($p=0.002$) compared to LPS-induced expression. PD-L1 expression is significantly higher on DCs treated with TCM from irradiated tissue compared to TCM from mock-irradiated tissue ($p=0.02$). Levels of the phenotypic marker CD11c were significantly elevated on DCs exposed to NCM from mock-irradiated ($p=0.007$) and irradiated ($p=0.009$) normal rectal tissue and TCM from both mock-irradiated ($p=0.002$) and irradiated ($p=0.002$) rectal cancer tissue (**Figure 5.8A-E** and **5.9A-E**). This suggests that the irradiated rectal cancer microenvironment exerts the most potent effect on upregulating DC maturation markers compared to the other three microenvironments investigated. Similar results were observed in the unstimulated setting without LPS whereby the irradiated rectal cancer TME had the most potent stimulatory effect on DC maturation markers (**Figure 5.10A-E** and **5.11A-E**).

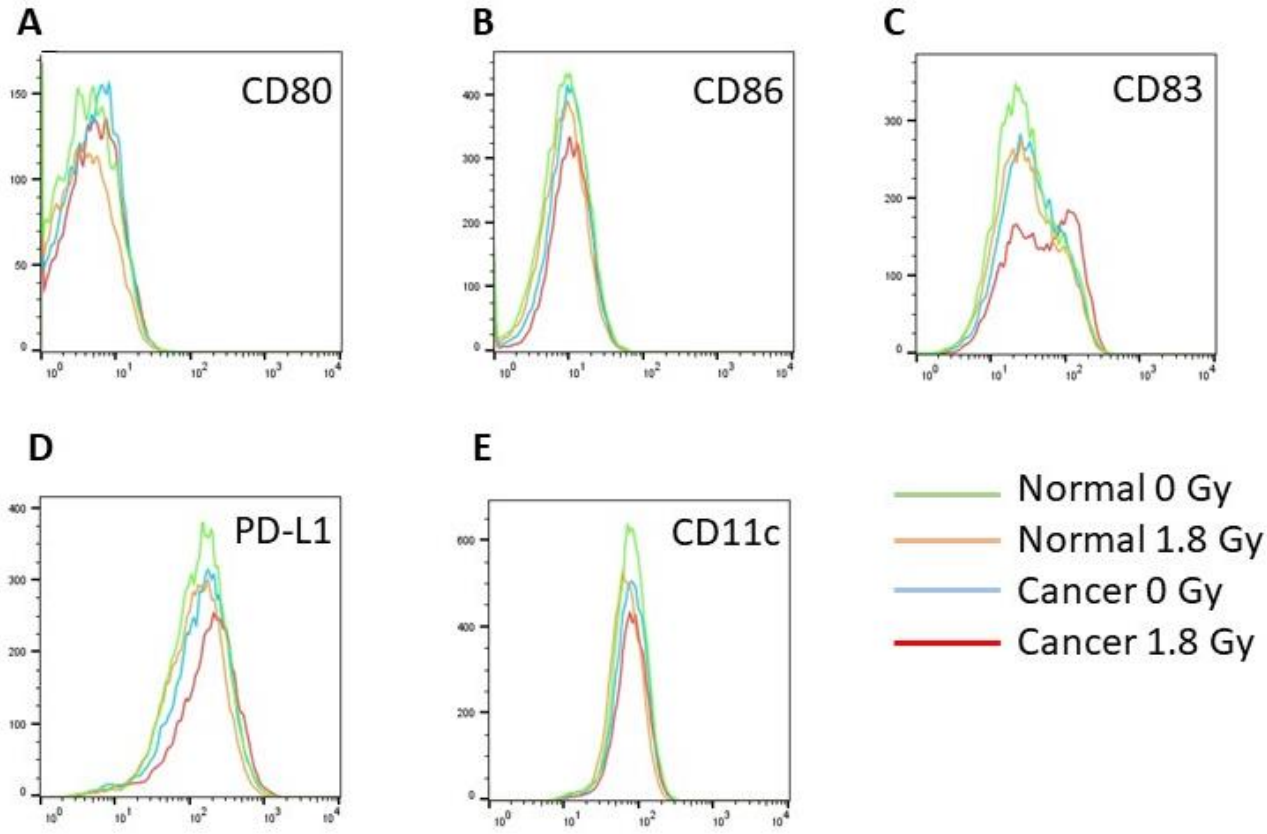

Figure 5.8 Representative experiment of histogram plots for CD80, CD86, CD83, PD-L1 and CD11c on DCs treated with TCM and NCM in the LPS-treated setting

One representative experiment of histogram plots for (**A**) CD80, (**B**) CD86, (**C**) CD83, (**D**) PD-L1 and (**E**) CD11c. Samples were acquired on DAKO CyAn ADP flow cytometer with compensation performed with positive and negative compensation beads. Gating on and analysis of $CD11c^+$ cells was performed using FlowJo software.

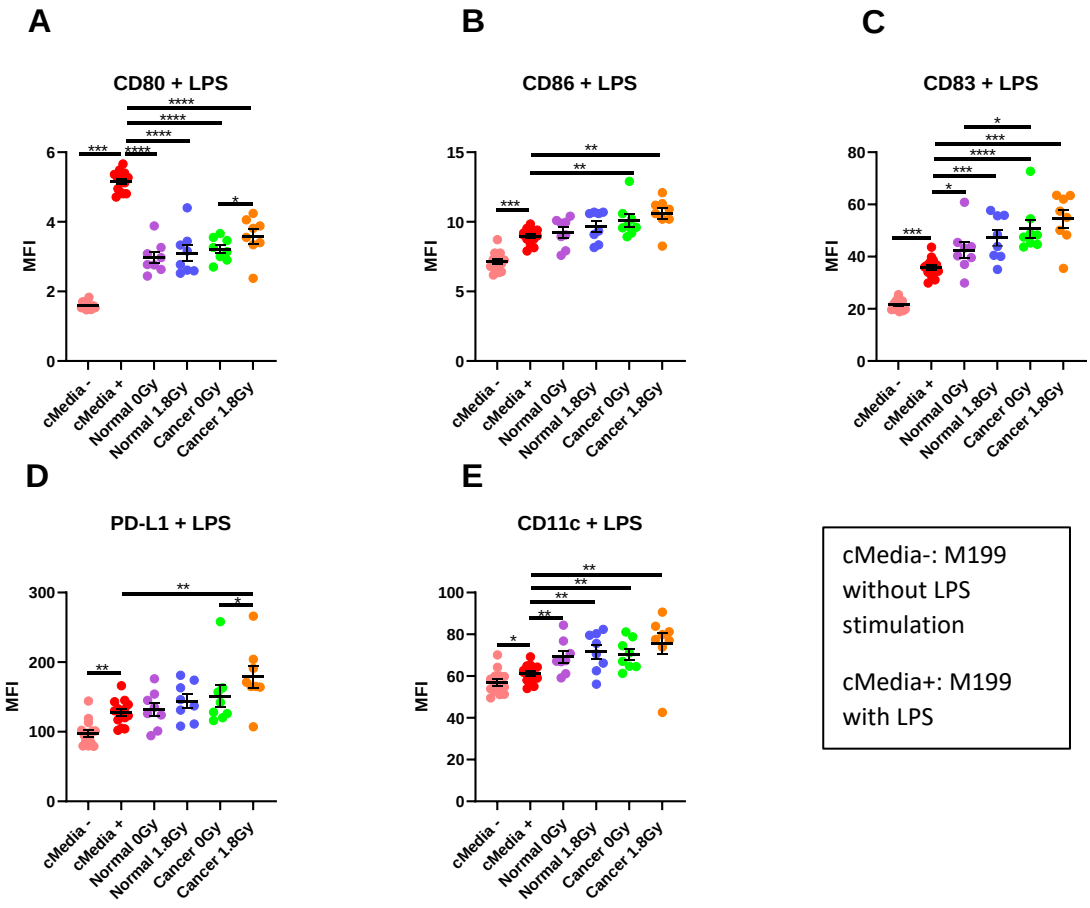

Figure 5.9 The effect of NCM and TCM on LPS-induced DC maturation

(**A**) NCM and TCM from both mock-irradiated and irradiated biopsies significantly inhibit LPS-induced expression of CD80. TCM from irradiated rectal cancer tissue has a less inhibitory effect than TCM from mock-irradiated rectal cancer tissue. (**B**) TCM from both irradiated and mock-irradiated rectal cancer tissue caused significant enhancement of LPS-induced expression of CD86. (**C**) NCM and TCM from both irradiated and mock-irradiated normal rectal and rectal cancer biopsies caused a significant enhancement of LPS-induced expression of CD83. TCM from rectal cancer biopsies caused significant elevation of CD83 levels compared to NCM from mock-irradiated biopsies. (**D**) PD-L1 expression was significantly enhanced by TCM from irradiated rectal cancer tissue. (**E**) LPS-induced expression of CD11c was significantly elevated by NCM and TCM from irradiated and mock-irradiated biopsies. All data expressed as mean ± SEM. Statistical analysis was performed using a Wilcoxon signed-rank test when comparing the same tissue type i.e. Cancer 0 Gy vs Cancer 1.8 Gy and Mann Whitney U-test when comparing different tissue types and comparing to media control. ****p<0.0001, ***p<0.001, **p<0.01, *p<0.05. n=14 for cMedia, n=8 for normal and cancer.

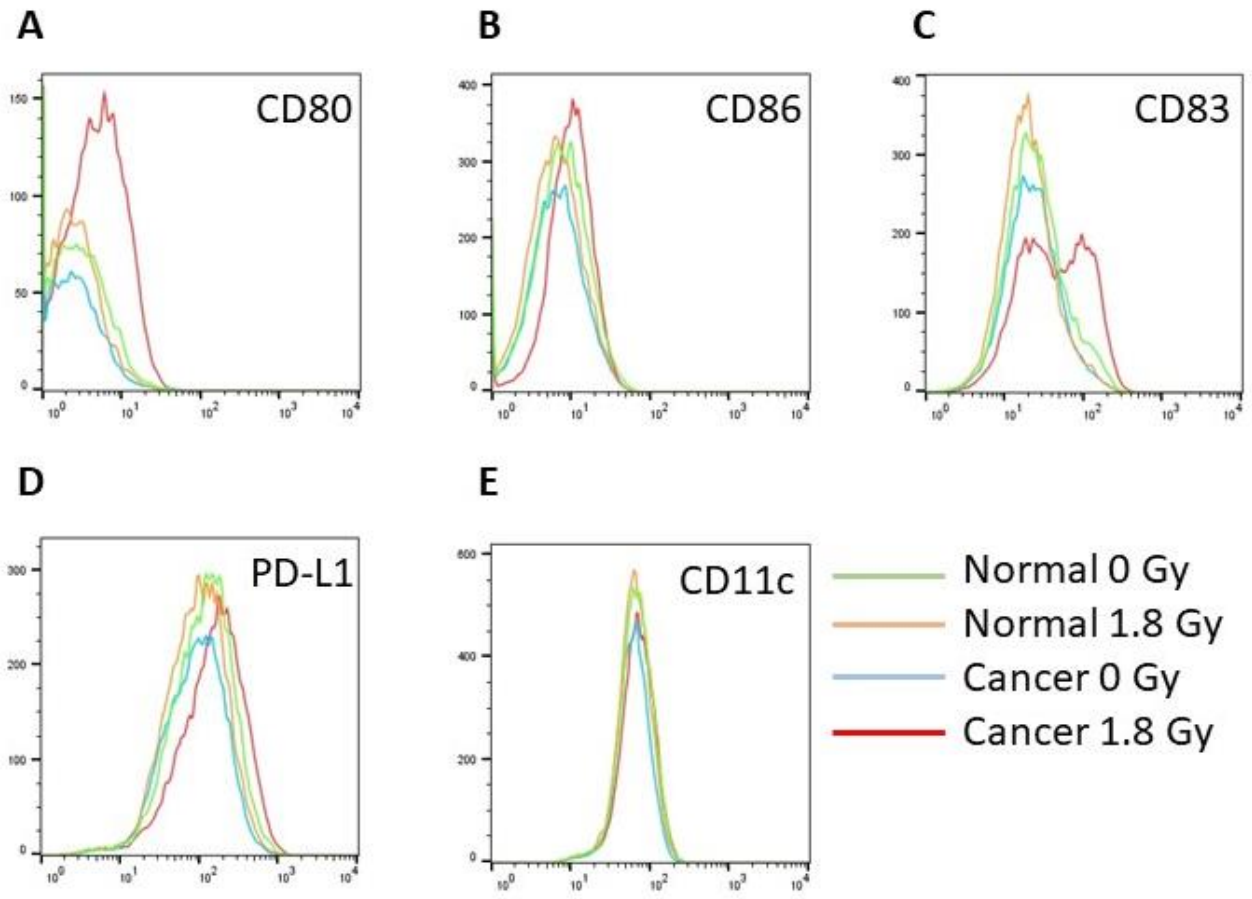

Figure 5.10 Representative experiment of histogram plots for CD80, CD86, CD83, PD-L1 and CD11c on DCs treated with TCM and NCM in the unstimulated (-LPS) setting

One representative experiment of histogram plots for (**A**) CD80, (**B**) CD86, (**C**) CD83, (**D**) PD-L1 and (**E**) CD11c. Samples were acquired on DAKO CyAn ADP flow cytometer with compensation performed with positive and negative compensation beads. Gating on and analysis of $CD11c^+$ cells was performed using FlowJo software.

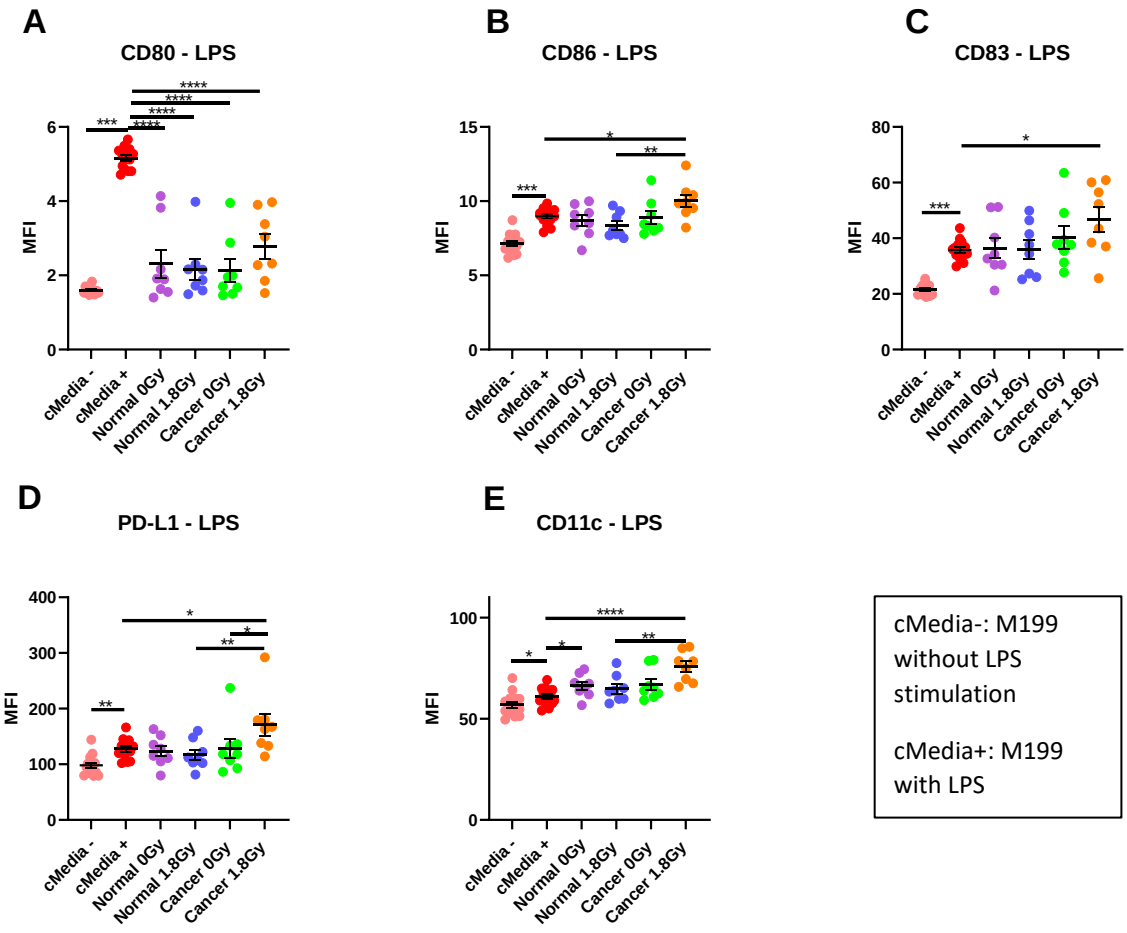

Figure 5.11 The effect of NCM and TCM on unstimulated dendritic cells

(**A**) Levels of CD80 are significantly inhibited by NCM and TCM from both mock-irradiated and irradiated biopsies compared to LPS-induced expression of CD80. (**B**) Levels of CD86 are significantly elevated on DCs treated with TCM from irradiated rectal cancer biopsies compared to LPS-induced expression of CD86. TCM from irradiated rectal cancer biopsies induced significantly higher levels of CD86 compared to NCM from irradiated normal rectal biopsies. (**C**) TCM from irradiated rectal cancer tissue induced higher expression of CD83 compared to LPS-induced expression of CD83. (**D**) PD-L1 expression is significantly elevated on DCs treated with TCM from irradiated rectal cancer biopsies compared to LPS-induced expression of PD-L1. TCM from irradiated rectal cancer tissue enhanced expression of PD-L1 compared to TCM from mock-irradiated rectal cancer tissue or NCM from irradiated normal rectal tissue. (**E**) CD11c levels are significantly elevated on DCs treated with TCM from irradiated rectal cancer tissue and NCM from mock-irradiated rectal cancer tissue compared to LPS-induced expression of CD11c. TCM from irradiated rectal cancer tissue induced enhanced expression of CD11c compared to NCM from irradiated normal rectal tissue. All data expressed as mean ± SEM. Statistical analysis was performed using a Wilcoxon signed-rank test when comparing the same tissue type i.e. Cancer 0 Gy vs Cancer 1.8 Gy and Mann Whitney U-test when comparing different tissue types and comparing to media control. ****$p<0.0001$, ***$p<0.001$, **$p<0.01$, *$p<0.05$. $n=14$ for cMedia, $n=8$ for normal and cancer.

5.4.6 Linking dendritic cell maturation markers with secreted factors

Given the observed differences in DC maturation markers between $CD11c^+$ DCs treated with the normal and cancerous rectal tissue secretomes, we correlated DC maturation markers in both microenvironments pre- and post-radiation with secreted factors from their respective microenvironment. There were no significant correlations between secreted factors in the mock-irradiated normal rectal microenvironment and markers of DC maturation. There was a significant inverse correlation between IL-10 and CD80 (R=-0.8571, p=0.01) in the irradiated normal microenvironment (**Table 5-2**). In the mock-irradiated cancer microenvironment, there was a significant correlation between CD80 and Flt-1 (R=0.7857, p=0.04), and an inverse correlation between CD80 and IL-27 (R=-0.8214, p=0.03). CD83 correlated with levels of SAA (R=0.7857, p=0.04). Levels of CD80 on DCs treated with TCM from irradiated rectal cancer tissue correlated with levels of ICAM-1 (R=0.8214, p=0.03) and CD11c correlated with IL-1RA (R=0.7619, p=0.03) (**Table 5-2**). These results indicate a differential relationship between DC maturation markers and secreted factors in the normal versus the malignant rectal microenvironment and suggests that radiation further alters this association.

5.4.7 Linking DC maturation markers with secretions from DCs treated with TCM and NCM

We performed multiplex ELISA screening on the DC-TCM/NCM supernatants of the DCs treated with TCM and NCM from mock-irradiated and irradiated rectal tissue. We then correlated these factors with DC maturation markers to identify if there was a differential response of DCs to TCM and NCM and if radiation altered this response. ICAM-1 was inversely correlated with CD83 (R=-0.7857, p=0.02) and CD11c (R=-0.7857, p=0.02) on DCs treated with NCM from irradiated normal rectal tissue (**Table 5-3**). We found a significant correlation between PD-L1 on DCs treated with TCM from mock-irradiated rectal cancer tissue and TNF-α levels in the supernatants of DCs treated with TCM from mock-irradiated rectal cancer tissue (R=0.8333, p=0.01). There was an inverse correlation between VEGF-C and CD86 (R=-0.9276, p=0.01) and CD11c (R=-0.8857, p=0.03) in DCs treated with TCM from irradiated rectal cancer tissue (**Table 5-3**). This highlights the differential effect of factors in the microenvironment on DC response.

Table 5-2 Correlation between DC maturation and phenotypic markers and secreted factors in the microenvironment

Tissue	**DC marker**	**Secreted factor**	**R value**	***p* value**	**n**
Normal 1.8 Gy	CD80	IL-10	-0.8571	0.01	8
Cancer 0 Gy	CD80	Flt-1	0.7857	0.04	7
Cancer 0 Gy	CD80	IL-27	-0.8214	0.03	7
Cancer 0 Gy	CD83	SAA	0.7857	0.04	7
Cancer 1.8 Gy	CD80	ICAM-1	0.8214	0.03	7
Cancer 1.8 Gy	CD11c	IL-1RA	0.7619	0.03	8

Table 5-3 Correlation between DC maturation and phenotypic markers and secreted factors from DCs treated with NCM and TCM from mock-irradiated and irradiated rectal tissue

Tissue	**DC marker**	**Secreted factor**	**R value**	***p* value**	**n**
Normal 1.8 Gy	CD83	ICAM-1	-0.7857	0.02	8
Normal 1.8 Gy	CD11c	ICAM-1	-0.7857	0.02	8
Cancer 0 Gy	PD-L1	TNF-α	0.8333	0.01	8
Cancer 1.8 Gy	CD86	VEGF-C	-0.9276	0.01	6
Cancer 1.8 Gy	CD11c	VEGF-C	-0.8857	0.03	6

5.4.8 Linking clinical characteristics with secreted factors and DC maturation markers

Given the heterogeneity in the levels of secreted factors in the TME and to further explore the relationship between factors secreted from the rectal cancer microenvironment, we correlated patient clinical characteristics with secreted factors both pre- and post-radiation. In the mock-irradiated rectal cancer microenvironment, there were several factors that significantly correlated with body composition parameters. Skeletal muscle correlated inversely with Flt-1 (R=-0.6273, p=0.04) and correlated positively with IL-12/IL-23p40 (R=0.6573, p=0.02), IL-1α (R=0.5874, p=0.04) and VEGF-A (R=0.6224, p=0.03). VFA correlated with CCL20 (R=0.6783, p=0.01) (**Table 5-4** and **Figure 5.12A-E**). In the irradiated rectal cancer secretome, there was again a significant inverse correlation between skeletal muscle and Flt-1 (R=-0.7182, p=0.01) and VEGF-D (R=-1, p=0.01). Intermuscular fat correlated with CCL20 (R=0.7133, p=0.01), VEGF-A (R=0.6084, p=0.03) and IL-1RA (R=0.6084, p=0.03) and VFA correlated with CCL20 (R=0.6643, p=0.02) and IL-1RA (R=0.6503, p=0.02) (**Table 5-5** and **Figure 5.13A-G**). Levels of CD11c on DCs treated with TCM from irradiated rectal cancer tissue correlated significantly with VFA (R=0.8095, p=0.02) and intermuscular fat (R=0.7381, p=0.04) (**Table 5-6**). This data suggests that obesity may influence the microenvironment of rectal cancer tissue and the response of this microenvironment to radiation therapy. We analysed MSD and DC maturation data according to T and N stage. VEGF-A was significantly reduced in patients with node positive disease in the irradiated rectal cancer TME. TSLP was significantly higher in the irradiated TME of patients with T1/2 stage tumours compared to those with T3/4 stage tumours. CD11c was significantly reduced on DCs treated with TCM from irradiated rectal cancer biopsies from patients with node positive disease (**Figure 5.14A-C**).

Table 5-4 Correlation between body composition parameters and factors secreted from mock-irradiated rectal cancer tissue i.e. Cancer 0 Gy

Body composition parameter	**Secreted factor**	**R value**	***p* value**	**n**
Skeletal muscle	Flt-1	-0.6273	0.04	11
Skeletal muscle	IL-12/IL-23p40	0.6573	0.02	12
Skeletal muscle	IL-1α	0.5874	0.04	12
Skeletal muscle	VEGF-A	0.6224	0.03	12
Visceral fat area	CCL20	0.6783	0.01	12

Table 5-5 Correlation between body composition parameters and factors secreted from irradiated rectal cancer tissue i.e. Cancer 1.8 Gy

Body composition parameter	**Secreted factor**	**R value**	***p* value**	**n**
Skeletal muscle	Flt-1	-0.7182	0.01	11
Skeletal muscle	VEGF-D	-1	0.01	5
Intermuscular fat	CCL20	0.7133	0.01	12
Intermuscular fat	VEGF-A	0.6084	0.03	12
Intermuscular fat	IL-1RA	0.6084	0.03	12
Visceral fat area	CCL20	0.6643	0.02	12
Visceral fat area	IL-1RA	0.6503	0.02	12

Table 5-6 Correlation between DC phenotypic markers and body composition analysis parameters on DCs treated with TCM from irradiated rectal cancer tissue i.e. Cancer 1.8 Gy

Body composition parameter	**DC maturation marker**	**R value**	***p* value**	**n**
Visceral fat area	CD11c	0.8095	0.02	8
Intermuscular fat	CD11c	0.7381	0.04	8

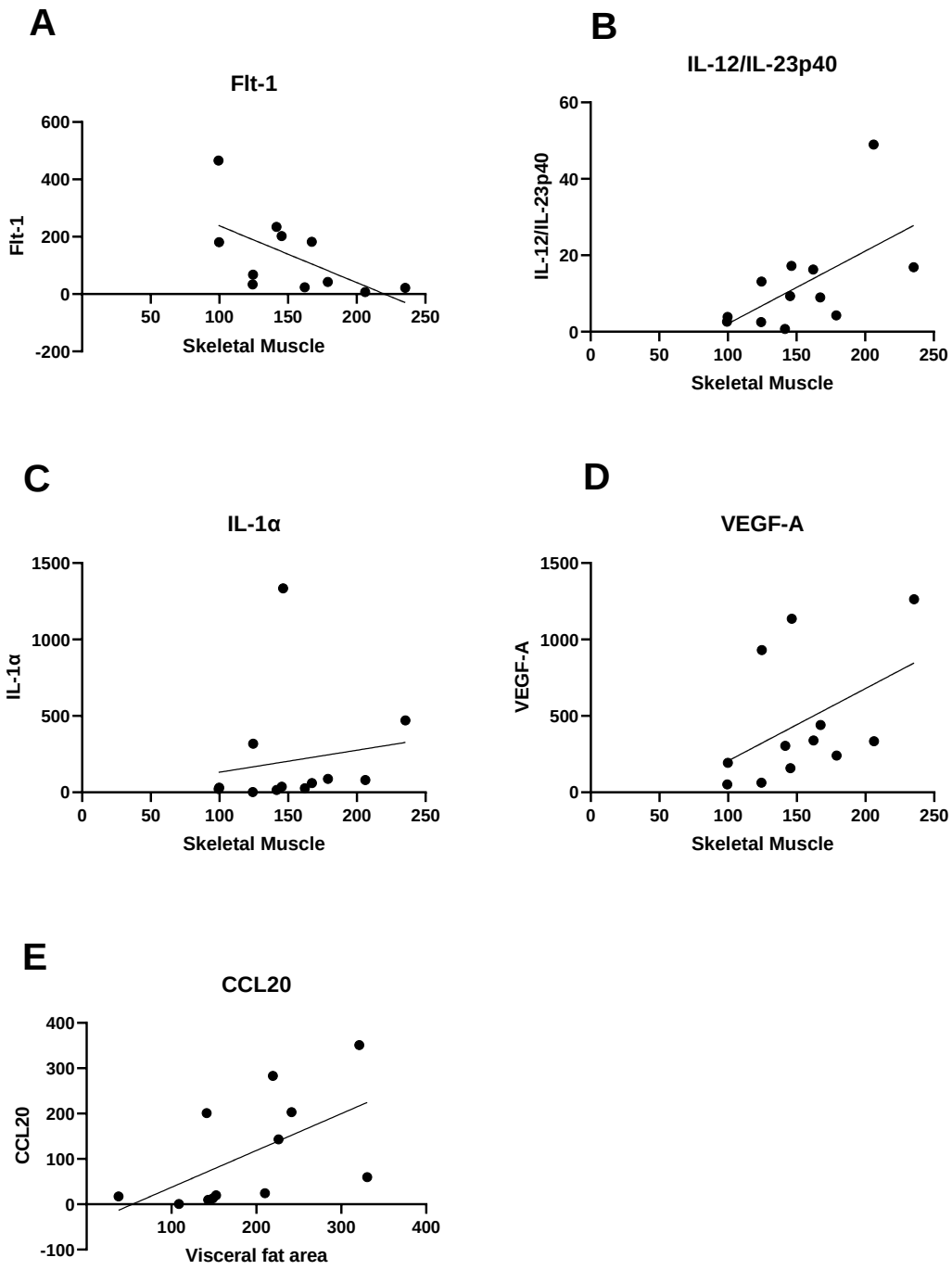

Figure 5.12 Correlations between secreted factors from mock-irradiated rectal cancer tissue (Cancer 0 Gy) and body composition parameters

(**A**) There was a significant inverse correlation between skeletal muscle and Flt-1. There was a significant correlation between skeletal muscle and (**B**) IL-12/IL-23p40, (**C**) IL-1α and (**D**) VEGF-A. (**E**) VFA was correlated with CCL20. Correlation analysis was performed using Spearman correlation coefficient. *n*=12, *n*=11 for Flt-1.

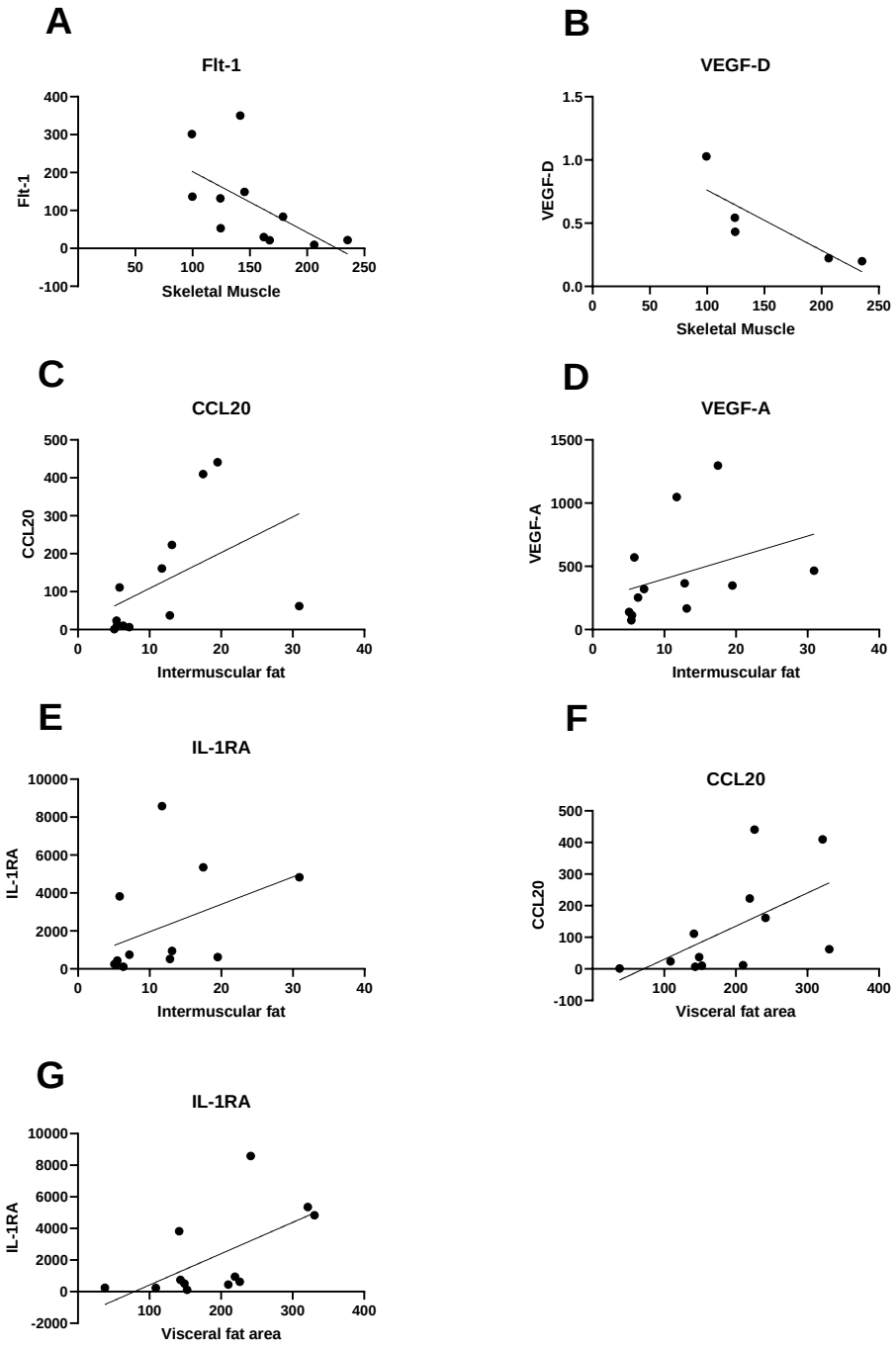

Figure 5.13 Correlations between secreted factors from irradiated rectal cancer tissue (Cancer 1.8 Gy) and body composition parameters

There was a significant inverse correlation between skeletal muscle and (**A**) Flt-1 and (**B**) VEGF-D. (**C**) CCL20, (**D**) VEGF-A and (**E**) IL-1RA were significantly correlated with intermuscular fat. (**F**) CCL20 and (**G**) IL-1RA correlated with VFA. Correlation analysis was performed using Spearman correlation coefficient. *n*=12, *n*=11 for Flt-1.

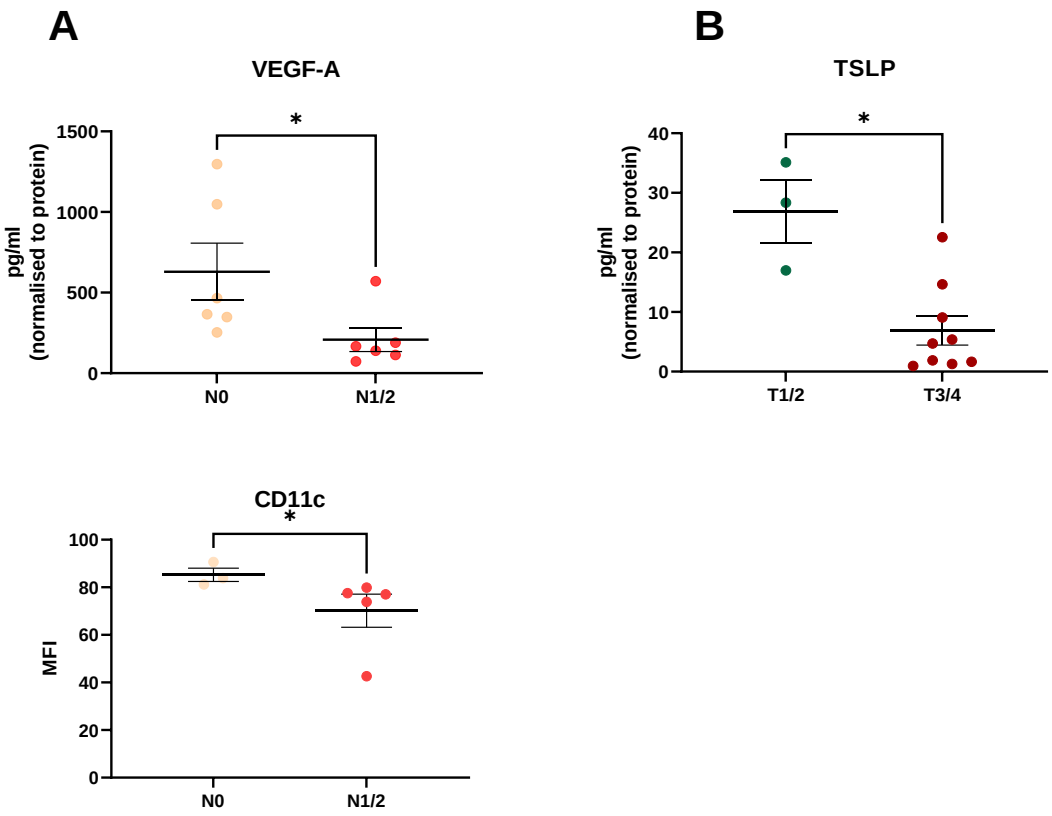

Figure 5.14 Influence of T stage and N stage on levels of secreted factors and DC phenotypic markers

(**A**) VEGF-A is significantly higher in the TCM from irradiated rectal cancer tissue from patients with N0 (*n*=6) disease compared to those with N1/2 (*n*=6) disease. (**B**) TSLP is significantly higher in the TCM from irradiated rectal cancer tissue from patients with T1/2 (*n*=3) compared to those with T3/4 disease (*n*=9). (**C**) CD11c levels are significantly higher on DCs treated with TCM from irradiated rectal cancer biopsies from patients that have node negative disease compared to those with nodal involvement. All data expressed as mean ± SEM. Statistical analysis was performed using a Mann Whitney U-test. *$p<0.05$

5.5 Summary of main findings from chapter 5

- The protein secretome differs between normal and malignant rectal tissue with 19 factors secreted at significantly higher levels from rectal cancer tissue, when compared to normal rectal tissue.
- A single fraction of 1.8 Gy x-irradiation induces alterations in the secretome of normal rectal tissue, specifically increasing IL-15 and CCL22.
- A single fraction of 1.8 Gy x-irradiation does not alter the inflammatory secretome of rectal cancer tissue.
- The irradiated rectal cancer secretome exerts the most potent induction of DC maturation markers of the 4 microenvironments investigated.
- Obesity status may influence the local inflammatory milieu in rectal cancer with CCL20 correlating with VFA in the mock-irradiated rectal cancer secretome and CCL20 and IL-1RA correlating with VFA in the irradiated rectal cancer secretome.

5.6 Discussion

The objective of this study was to profile the inflammatory secretome of human rectal cancer and normal rectal tissue pre- and post-radiation and to investigate the interaction between this secretome and the innate immune system, specifically DC maturation markers. By conducting this study, we identified associations between factors within the TME and DC maturation markers, thus providing an avenue for further exploration to harness the therapeutic potential of modulating the TME. Using human *ex vivo* explants as a model system, we have demonstrated that the protein secretome differs between normal rectal and rectal cancer tissue and this is altered following radiation in normal rectal tissue, highlighting variation in effects of radiation on the normal rectal compared to the malignant rectal tissue microenvironments. Furthermore, these protein secretome microenvironments interacted differentially with the innate immune system.

We identified 19 factors that were secreted at significantly higher levels in the TME of rectal cancer tissue compared to normal rectal tissue. This indicates that the rectal cancer microenvironment is more inflammatory than the normal rectal microenvironment. Following radiation, two factors were elevated in the secretome of normal rectal tissue, while surprisingly no secreted factor was significantly altered in malignant rectal tissue following radiation. This indicates that malignant and normal rectal tissues respond differently to radiation and suggests that a single fraction of 1.8 Gy radiation induces alterations in inflammation in normal tissue but not in malignant tissue. Following exposure of DCs to NCM and TCM from both mock-irradiated and irradiated biopsies, we found that the irradiated rectal cancer secretome caused an enhancement in DC maturation markers. These results suggest that a single fraction of a clinically relevant dose of 1.8 Gy radiation does not have a negative impact on the inflammatory milieu of malignant rectal tissue and does not lead to suppression of the innate immune system.

The inflammatory environment differed between non-cancer and rectal cancer tissue which is unsurprising given that tumour-promoting inflammation is a hallmark of cancer (59). Nineteen out of 54 factors quantified were found at significantly higher levels in the cancer secretome compared to the normal secretome. These factors have previously been reported to have pro-oncogenic attributes including angiogenic, pro-mitogenic and immunosuppressive characteristics and therefore it is expected that they are elevated in the rectal cancer TME compared to the normal microenvironment. Two factors; Flt-1 and

P1GF are angiogenic mediators. P1GF is capable of binding to Flt-1 and may displace VEGF, thereby facilitating enhanced angiogenesis (323). P1GF is known to have numerous roles in carcinogenesis including macrophage activation and recruitment, lymph vessel growth, DC suppression, tumour cell proliferation and migration and endothelial cell vessel growth (324). IL-1α secretion from CRC cells has also been shown to have angiogenic properties (325). The inflammatory cytokines IFN-γ, IL-6 and IL-10 were also found at significantly higher levels in the cancer secretome compared to the normal secretome. IFN-γ is an important effector of anti-tumour immunity but more recent evidence suggests that it may play important roles in tumour progression and immune evasion (reviewed in (326)). IL-6 is a well-known pro-tumorigenic factor (327) and IL-10 was originally identified as a potent anti-inflammatory cytokine, however, it is now known that spatial and temporal regulation of IL-10 bestows on it anti-tumour responses also (328).

Several Th17 type proteins including CCL20, IL-17A and IL-17A/F were secreted at higher levels from rectal cancer tissue compared to normal rectal tissue. This is unsurprising given the known involvement of Th17 cells in CRC. Th17 cells infiltrate CRCs and their density correlates with poor prognosis (329, 330). In multiple models of CRC, antagonising Th17 cytokines exerts anti-cancer effects but there have been mixed reports about the effects of blocking Th17 cytokines in murine models (reviewed in (331)). CCL20 is a chemokine involved in the recruitment of Th17 cells to the TME (332, 333).

A number of the elevated proteins in the rectal cancer environment are implicated in tumour immune evasion through recruitment of regulatory T cells (T regs) to the TME. CCL22, CCL17, TSLP and CXCL10 function in recruitment of T regs, with levels of CCL22 and CCL17 correlating with T reg infiltration in gastrointestinal cancers (334, 335). TSLP production by cancer associated fibroblasts in pancreatic cancer induces Th2 type inflammation and is associated with poorer patient outcome (336). CXCL10 has been associated with an immunosuppressive phenotype in pancreatic cancer (337).

Two factors; CCL22 and IL-15 were secreted at significantly higher levels following radiation in normal rectal tissue. CCL22 is involved in recruitment of T regs through its receptor CCR4 and is therefore reported as being immunosuppressive (338). IL-15 is an

immunostimulatory cytokine and is involved in development, differentiation and survival of natural killer cells (339). Therefore, our data suggests that a single fraction of 1.8 Gy x-irradiation may alter the microenvironment of normal rectal tissue to promote an inflammatory response but that homeostatic mechanisms may be at play in limiting the extent of the inflammation. Surprisingly, no factor was significantly altered in rectal cancer tissue following radiation. When taken in combination with our results on DC maturation markers, whereby the irradiated rectal cancer TME caused enhancement of expression of DC maturation markers relative to the normal microenvironment, this data suggests that irradiating the TME with a single fraction of 1.8 Gy radiation does not have an inflammation-induced immunosuppressive effect. It has been reported that chemotherapy-induced inflammation may contribute to treatment resistance in cancer (340) and enhanced inflammation has been implicated in poor treatment response in patients (271, 341). Taken together, we hypothesise that this is a positive result since an enhancement of inflammation and tumour suppressive mechanisms would have negative consequences on the anti-tumour immune response. However, a limitation of this study was the use of a single fraction of 1.8 Gy radiation. Comparison of the inflammatory secretome of rectal cancer tissue obtained at surgical resection from treatment-naïve patients and those that received a full course of neo-CRT would offer greater insight into the effect of clinical radiotherapy regimens on secreted factors and DC maturation markers.

Having observed alterations in the inflammatory mediators, cytokines and chemokines between the secretome of rectal cancer tissue and non-malignant rectal tissue and the differential effects of radiation on the secretome of non-malignant and malignant rectal tissue, we investigated the effect of the secretome on immune cell function, specifically DC maturation markers. DCs are antigen-presenting cells capable of inducing a T cell response and maturation levels have been associated with patient survival and response to targeted therapies in CRC patients (321, 342). It has previously been reported that the TME in CRC causes inhibition of DC maturation (343, 344). On the contrary however, we found stimulation of DC maturation markers by the rectal cancer TME, which is in line with results published by Morrissey *et al* (344). We demonstrated a significant increase in CD80 and PD-L1 on the DCs exposed to the irradiated rectal cancer secretome, when compared to the mock-irradiated rectal cancer secretome. CD83 was significantly higher on DCs exposed to the mock-irradiated rectal cancer secretome

compared to the mock-irradiated normal rectal secretome. Our results are in line with a study by Kulzer *et al.* where the supernatants of irradiated SW480 colon cancer cells resulted in significant enhancement of DC maturation markers compared to supernatants from mock-irradiated SW480 cells (224). However, our study presents results from a more translational model system as we used human *ex vivo* explants. We found similar results in the unstimulated setting without LPS whereby TCM from the irradiated rectal cancer secretome had the most potent effect on DC maturation.

Given the observed differences in the protein secretome of the microenvironments investigated and the differential response of DCs to these microenvironments, we conducted correlation analysis to identify any relationship between secreted factors and DC maturation markers and the phenotypic marker CD11c. In the irradiated normal rectal tissue, there was a significant inverse correlation between IL-10 and CD80. IL-10 has been previously shown to have an immunosuppressive role on circulating DCs in patients with hepatocellular carcinoma (345). While in the rectal cancer TME, CD80 levels on DCs correlated positively with Flt-1 and inversely with IL-27. VEGF is known to adversely affect DC maturation (346) and blockade of Flt-1 on DCs curtails this effect (347). It may be possible that VEGF is binding to elevated levels of Flt-1 in the TME and is therefore unavailable to exert inhibitory effects on DC maturation. IL-27 has previously been reported to upregulate PD-L1 on DCs in the absence of DC maturation and is accompanied by a decreased capacity to stimulate T cells (348). There was a positive correlation between CD83 and SAA and in the mock-irradiated rectal cancer TME. SAA has been shown to enhance DC maturation (349). In the irradiated rectal cancer TME, CD80 correlated with ICAM-1 and CD11c correlated with IL-1RA. These results indicate that the response of DCs to their microenvironment differs between normal and malignant rectal tissue and that radiation further modifies this response. It is possible that the interplay between the relative concentration of cytokines in the distinct microenvironments examined exerts differential effects on DC maturation.

Overweight and obese rectal cancer patients have been reported to have poorer outcomes than their counterparts of a healthy weight (40, 293). To identify if obesity had a direct effect on secreted factors within the TME and subsequent immune response, we correlated body composition parameters with secreted factors and markers of DC maturation. We found positive correlations between VFA and CCL20 in the mock-irradiated TME and CCL20 and IL-1RA in the irradiated TME. Moreover, intermuscular

fat, a marker which is associated with insulin resistance and metabolic dysfunction (350) was correlated with CCL20, IL-1RA and VEGF-A. There were positive correlations between levels of the phenotypic marker CD11c on the DCs treated with TCM from irradiated rectal cancer tissue and VFA and intermuscular fat. These data suggest that obesity status may directly alter the milieu of inflammatory proteins in the TME and these factors may be differentially altered by radiation in obese individuals. Further exploration of the relationship between obesity and the inflammatory microenvironment of rectal cancer patients may reveal novel therapeutic targets.

Strengths of this study include the use of whole biopsies as experimental models since these models recapitulate the microenvironment and the 3-D architecture of human tumours and normal tissue. However, a limitation associated with these models, is their long-term viability *ex vivo* (up to 72 h). Our study was limited to the use of a single fraction of a clinically relevant dose of radiation, though it must be acknowledged that repeated fractions of radiation may induce different responses. Future study utilizing biopsy specimens obtained at surgical resection from both treatment-naïve patients and from patients that received a full course of neo-CRT would provide important information on the effect of neo-CRT on the inflammatory milieu and its interaction with the innate immune system.

We have conducted, for the first time, a comprehensive profile of the rectal cancer and normal rectal secretome and demonstrated differential expression of cytokines, chemokines and inflammatory markers in the secretome of rectal cancer tissue compared to normal rectal tissue. This study is novel as it assesses the secreted proteins in the microenvironment of malignant and non-malignant rectal tissue therefore identifying aberrant expression of factors in the immediate vicinity of the tumour, while most studies to date investigate just the circulating levels of such inflammatory proteins. Investigating the secretome of the tissue offers insight into the locally acting factors involved in the disease process as well as potentially identifying factors involved in the disease at an early stage. Furthermore, we have demonstrated that a single fraction of a clinically relevant dose of radiation exerts differential effects on the secretome of normal rectal tissue compared to malignant rectal tissue. Finally, DC maturation status is enhanced by the irradiated rectal cancer secretome compared to the irradiated normal rectal secretome,

indicating an immunogenic stimulatory effect of radiation in the rectal cancer secretome that could potentially be harnessed to improve therapeutic response.

Chapter 6 Profiling the immune-metabolic signature of visceral and subcutaneous adipose tissue in oesophageal adenocarcinoma patients

6.1 Introduction

In chapters 4 and 5 we identified significant associations between measures of obesity and direct biological alterations in the tumour microenvironment (TME) of rectal cancer patients. Oesophageal adenocarcinoma (OAC) is an exemplar model of obesity-associated cancer with central obesity presenting a major risk factor for the development of the disease (351). To further decipher how obesity status might drive alterations in the end-point measurements, including alterations in the metabolomic and immune landscape of tumours, we wanted to specifically examine the metabolic and inflammatory profiles of adipose tissue depots, specifically visceral adipose tissue (VAT) and subcutaneous adipose tissue (SAT), taken from OAC patients at surgical resection.

Most patients with locally-advanced OAC at presentation receive neoadjuvant chemotherapy with or without radiation prior to surgery (352). The attainment of a complete pathological response (pCR), characterised by no viable tumour present in the resection specimen, and a proxy for improved survival outcomes, is achieved in 23% of patients (353, 354). While the influence of obesity on disease risk is well-documented, the effect of obesity status on treatment response to chemotherapy and radiation therapy is poorly understood. A study by Mongan *et al.* suggests that overweight or obese OAC patients were more likely to have a better response to neoadjuvant chemoradiation (neo-CRT) compared to patients of normal weight (79). This *in vitro* study reported that the addition of adipose conditioned media (ACM) from VAT resulted in an improved radioresponse in a radioresistant OAC cell line, irrespective of the obesity status of the patient or whether or not the patient had cancer (79). Only ACM generated from VAT from patients that received neo-CRT induced radiosensitisation in a radiosensitive OAC cell line (79). These results suggest that radiosensitive and radioresistant tumours may have a differential response to factors secreted from VAT. It appears that in a radioresistant OAC model, the radiosensitising effects are owing to factors secreted from VAT as opposed to cancer effects or bystander effects following cancer treatment (79). The mechanistic basis of this enhanced response is unclear. However, it was possible to discriminate between ACM from non-cancer patients and ACM from OAC patients receiving surgery only or receiving neo-CRT, based on metabolite profiles. Higher levels of threonine, lysine and valine and lower levels of glucose were observed in the ACM of OAC patients receiving surgery as their only treatment modality compared to their cancer-free counterparts. When compared to a cohort of OAC patients receiving neo-

CRT, the ACM from the non-cancer controls had elevated levels of glucose and reduced levels of threonine, lysine, valine, isoleucine and glycine (79). Given the role of these metabolites in energy metabolism, it suggests that mitochondrial metabolism is altered in adipose tissue from OAC patients and that neo-CRT can cause further alterations in this metabolic profile.

Improved response to therapy has also been reported in overweight and obese patients with metastatic melanoma, whereby obese patients treated with BRAF-targeted or immune checkpoint inhibitors have improved outcomes (355). Similarly, in a cohort of patients treated with PD-1/PD-L1 blockade, obese patients had improved outcomes, despite evidence demonstrating that obesity had negative effects on tumour progression and induced PD-1-mediated T cell dysfunction (356). These observations were supported in a recent meta-analysis of >4000 patients, whereby a BMI>30 kg/m^2 was a prognostic indicator for improved response to immune checkpoint inhibitors, as measured by increased overall survival and progression-free survival (357). The exact mechanisms underpinning these observations are largely elusive, however, there is evidence of increased expression of PD-1 on T cells in obese individuals and PD-1 levels are correlated with leptin, which is elevated in obese individuals (356).

To date, our understanding of adipose tissue metabolism and its connection to inflammation is scant. However, alterations in metabolism, angiogenesis and inflammatory mediators have previously been shown to be implicated in treatment response in OAC (80). Furthermore, it is known that alterations in factors secreted from adipose tissue from obese OAC patients result in altered cellular metabolism and mitochondrial function (81). Moreover, ACM generated from obese patients had an altered metabolomic landscape with significantly higher levels of lactate and reduced levels of alanine, ethanol, isoleucine, leucine and valine compared to ACM from a non-obese cohort of OAC patients (81). There is a highly dynamic inter-relationship between inflammation and metabolism, wherein cellular metabolites can drive the nature of the inflammatory response, but equally inflammatory signals can disrupt metabolism. Cellular metabolism defines immune cell functionality, wherein anaerobic glycolysis versus oxidative phosphorylation (OXPHOS) promotes a pro-inflammatory milieu (82). Conversely, interrupting immune metabolism inhibits the capability to mount a pro-inflammatory macrophage response (83, 84). Elucidating the metabolic and inflammatory signatures of VAT and SAT may help to reveal the mechanisms underlying

the observed enhanced response to neo-CRT in overweight and obese patients. This descriptive study aims to profile for the first time, the metabolic pathways utilised in VAT and SAT of OAC patients and explore a link between real-time adipose tissue energy metabolism profiles and inflammatory signatures.

We hypothesise that different metabolic pathways will be present and functional in VAT compared to SAT and that the secretome of VAT will contain higher levels of inflammatory mediators compared to the SAT secretome. This study profiles the immune-metabolic signature of VAT and SAT in OAC patients for the first time. Gaining an understanding of the metabolic profile of VAT and SAT and its connections with the inflammatory secretome may begin to unravel the molecular mechanisms underlying the improved treatment response observed in overweight and obese OAC patients.

6.2 Overall hypothesis and specific aims of chapter 6

We hypothesise that different immune-metabolic pathways predominate in VAT compared to SAT and that the secretome of VAT will contain higher levels of inflammatory mediators compared to the SAT secretome.

Specific aims:

1. Determine if it is possible to assess real-time metabolic pathways in VAT and SAT using Seahorse technology.
2. Elucidate the metabolic profile of VAT and SAT in OAC patients.
3. Determine the inflammatory secretome of both VAT and SAT in OAC patients.
4. Correlate inflammatory secretions with metabolic parameters in VAT and SAT in OAC patients.
5. Correlate metabolic and inflammatory protein secretion data with patient clinical characteristics, including obesity status.

6.3 Materials and methods

6.3.1 Patient recruitment

Twelve patients with histologically confirmed OAC and oesophagogastric junction (OGJ) carcinoma patients were prospectively recruited to this study between October 2018 and June 2019. Informed written patient consent was obtained for the use of patient tissue and data in this study. Ethical approval was granted by the St. James's Hospital/ AMNCH Research Ethics Committee. Patient data was pseudo-anonymised prior to sample access. All samples were coded with a unique biobank number by the biobank manager. VAT and SAT were excised at the beginning of the surgical resections. Adipose tissue resections were obtained from the midline excision. Omentum, representing VAT was excised from around the greater curvature of the stomach.

Adipose tissue samples used in this chapter were acquired from patients that were either treatment-naïve or patients that received neoadjuvant treatment. Neoadjuvant treatment consisted of either the CROSS chemoradiotherapy regimen, which comprises paclitaxel and carboplatin and 41.4 Gy of radiation in 23 fractions, or the FLOT or FOLFOX chemotherapy regimen which comprises docetaxel, leucovorin, oxaliplatin and 5-fluorouracil (5-FU) or leucovorin, 5-FU and oxaliplatin, respectively.

6.3.2 OCR and ECAR measurements in visceral and subcutaneous adipose tissue

VAT and SAT were cut into small pieces (~20-25 mg) and plated one piece per well in 1 mL of M199 (supplemented with 0.1% gentamicin) media in a 24-well islet cell microcapture plate [Agilent Technologies, Santa Clara, CA, USA]. The adipose tissue was allowed to equilibrate for 20 min at 37°C and 5% CO_2/95% air in the islet cell microcapture plate prior to insertion of an islet screen above the adipose tissue to prevent the tissue coming in contact with the sensors during the assay. Prior to the assay the Seahorse XFe24 cartridge plate was hydrated for 1 h at 37°C in a CO_2-free incubator. Three measurements of oxygen consumption rate (OCR) and extracellular acidification rate (ECAR), measures of OXPHOS and glycolysis respectively, were taken over 24 min consisting of three repeats of mix (3 min)/wait (2 min)/measure (3 min) to establish basal OXPHOS and glycolysis levels. Upon completion of the assay the M199 media was harvested and stored at -80°C and the adipose tissue was harvested and snap frozen in liquid nitrogen prior to storage at -80°C. All measurements were normalised to protein

content of the adipose tissue. OCR and ECAR measurements were calculated as the average readout of each piece of VAT and SAT over the three readings.

6.3.3 Protein isolation and quantification from adipose tissue

Adipose tissue samples were placed on ice and 200 µL of RIPA buffer supplemented with 1 PhosSTOP and 1 Complete Mini protease inhibitor cocktail tablet per 10 mL was added to each sample. Samples were ruptured using a metal bead and the Qiagen tissue lyser at 25 Hz for 2 min. Samples were transferred to an Eppendorf tube and centrifuged at 13,000 x g for 20 min at 4°C. Isolated protein was quantified using BCA assay (Pierce) as per manufacturer's instructions. Bovine Serum Albumin (BSA) standards were prepared as follows;

Table 6-1 Protein standards for BCA assay

Tube	Volume diluent (µL)	Volume & Source BSA (µL)	BSA concentration (µg/mL)
A	0	300	2000
B	125	375	1500
C	325	325	1000
D	175	175 tube B	750
E	325	325 tube C	500
F	325	325 tube E	250
G	325	325 tube F	125
H	400	100 tube G	25
I	400	0	0

BCA working reagent was prepared using 50 parts Reagent A and 1-part Reagent B. The volume of working reagent required was calculated according to the following formula;

(No. of standards + no. of samples) x 2 x volume working reagent per well

10 µL of each standard/sample was added to each well in duplicate to a 96-well plate. 200 µL of working reagent was added.

6.3.4 Mesoscale Discovery 54-plex ELISA

To assess angiogenic, vascular injury, inflammatory, cytokine and chemokine secretions, a 54-plex ELISA kit spread across 7 plates was used [Meso Scale Diagnostics, USA] as

described in *section 5.3.3.* MSD analysis was performed on 5 randomly selected pieces of VAT and SAT and the average of the five pieces was used as the readout for that patient sample. All protein secretion data was normalised to the protein content of the piece of adipose tissue using the BCA assay (Pierce), as described above in *section 6.3.3*.

6.3.5 Body composition analysis by computed tomography

Computed tomography (CT) scans were obtained at diagnosis and prior to surgery using a Discovery ST CT scanner (GE Healthcare, Little Chalfont, UK). Images were analysed at L3 and the cross-sectional area in cm^2 of the various tissue compartments was determined using TomoVision Sliceomatic version 5.0 (TomoVision, Montreal, Canada).

Total body fat mass was calculated as; 0.042 x [total fat area $_{[L3]}$ (cm^2)] + 11.2

Total body fat free mass was calculated as; 0.30 x [total skeletal muscle $_{[L3]}$ (cm^2) + 6.06

Visceral fat area (VFA) was calculated by a radiologist and patients with a VFA greater than 163.8 cm^2 (males) and 80.1 cm^2 (females) were classified as obese (296).

6.3.6 Statistical analysis

GraphPad Prism 9 software was used to perform statistical analysis. All data is expressed as mean ± SEM. Data was analysed by Wilcoxon signed-rank test or Mann Whitney U-test, as stated in each figure legend. Correlation analysis was performed using Spearman's correlation coefficient. Statistical significance considered at $p<0.05$.

Figure 6.1 describes the methodology used in this study.

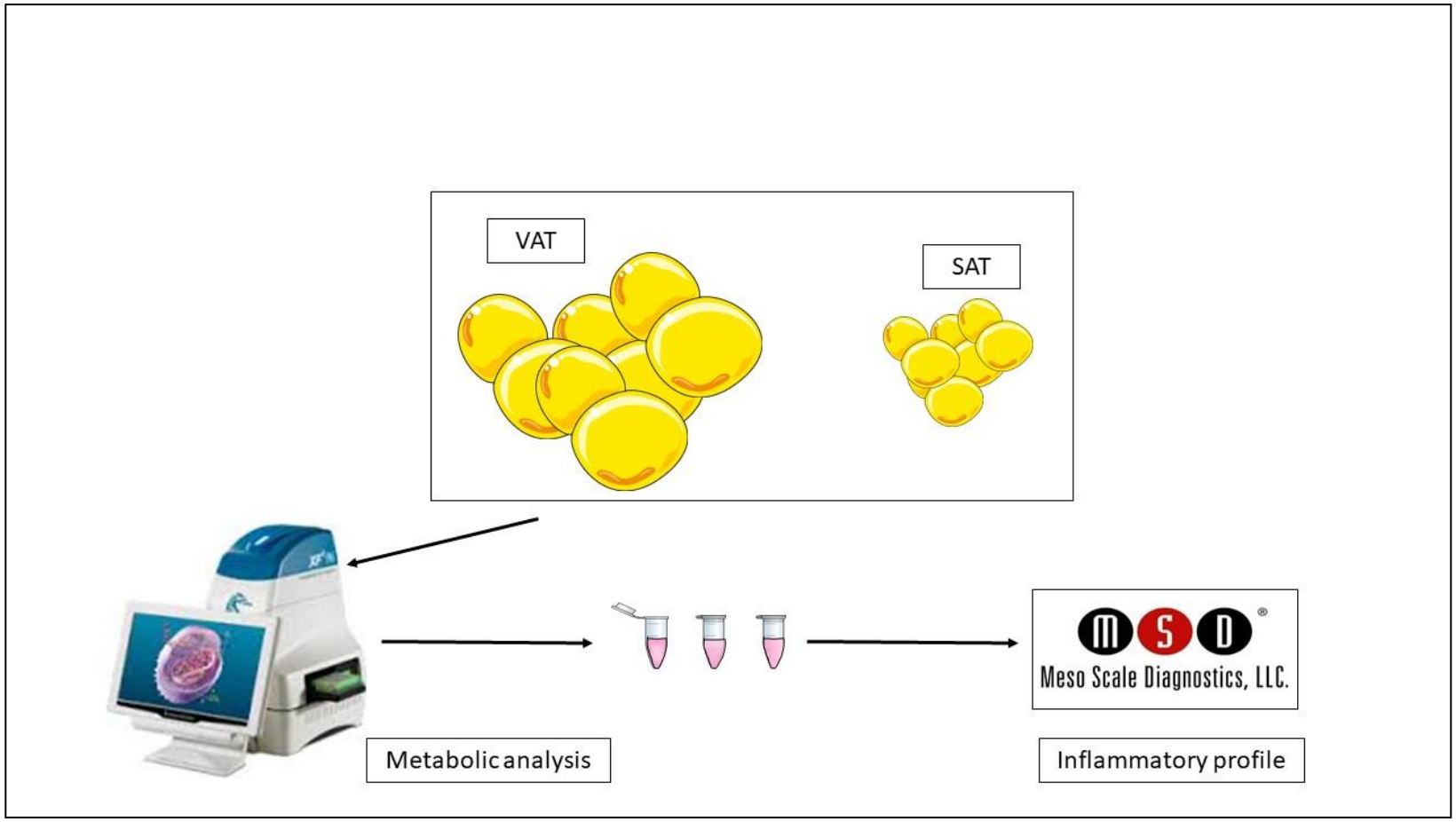

Figure 6.1 Schematic illustration of the methodology employed in this chapter

VAT and SAT were excised from patients undergoing resectional surgery for cancer of the oesophagus and oesophagogastric junction. Metabolic analysis using Seahorse technology was used to profile the metabolic pathways in VAT and SAT and the resultant supernatants were screened for the secretion of 54 proteins using the MSD multiplex system.

6.4 Results

6.4.1 Patient characteristics

Matched VAT and SAT samples were taken from 12 patients undergoing surgical resection for OAC or adenocarcinoma of the OGJ at St. James's Hospital, Dublin between October 2018 and June 2019. The cohort was predominantly male (75%) and had a mean age of 65.6 years. T3 was the most common T-stage (41.6%) while N0 was the most common N-stage (50%). Eight of the 12 patients received neoadjuvant treatment. Twenty-five percent of patients that received neoadjuvant treatment had a good response to treatment as indicated by a tumour regression grade (TRG) of 1 or 2 while 75% of patients had a poor response to treatment with a TRG of 3 or 4 (**Table 6-2**).

Body composition analysis revealed a significant loss in total body fat free mass and skeletal muscle mass from time of diagnosis to time of surgery. No significant differences were observed between total body fat mass, VFA, subcutaneous fat area or intermuscular fat from time of diagnosis to time of surgery (**Table 6-3**). **Figure 6.2** is a representative image of body composition analysis by CT with the various fat depots, skeletal muscle and intermuscular fat indicated in colour as per figure legend. **Figure 6.2A** is a representative image of a viscerally obese sarcopenic patient and **Figure 6.2B** is a representative image of a non-viscerally obese non-sarcopenic patient.

Table 6-2 Patient characteristics

n=12			**Percent (%)**
Age	Mean ± SD	65.6 ± 11.8	
	Range	46-83	
Gender	Male (n)	9	75
	Female (n)	3	25
Obesity status (pre-treatment)[a]	Non-obese	7	58.33
	Obese (n)	5	41.67
Cancer	Oesophageal adenocarcinoma	6	50
	(OAC) (n)	6	50
	Oesophageal gastric junction (n)		
T stage	T0 (n)	1	8.33
	T1 (n)	1	8.33
	T1a (n)	1	8.33
	T1b (n)	2	16.67
	T2 (n)	1	8.33
	T3 (n)	5	41.67
	T4b (n)	1	8.33
N stage	N0 (n)	6	50
	N1 (n)	5	41.67
	N2 (n)	1	8.33
M stage	Mx (n)	12	100
Stage of differentiation[b]	Moderate (n)	4	33.33
	Moderate to poor (n)	1	8.33
	Poor (n)	6	50
Treatment received	Surgery only (n)	4	33.33
	FLOT + Surgery (n)	3	25
	FOLFOX + Surgery (n)	1	8.33
	CROSS + Surgery (n)	4	33.33
TRG[c]	1 (n)	1	12.5
	2 (n)	1	12.5
	3 (n)	4	50
	4 (n)	2	25

[a] Obesity status determined at diagnosis by CT defined as VFA >80.1 cm^2 for females and >163.8 cm^2 for males

[b] Stage of differentiation unavailable for one patient

[c] TRG available for 8 patients. Expressed as a % of patients with a TRG

Table 6-3 Changes in body composition from time of diagnosis to surgery

	Diagnosis	**At surgery**	***p* value**
Total body fat mass (kg)	23.03 ± 4.9	24.44 ± 7.75	>0.99
Total body fat free mass (kg)	52.27 ± 10.9	49.11 ± 10.54	0.0078
Visceral fat area (cm^2)	157.1 ± 123.5	148.7 ± 119.3	0.21
Subcutaneous fat area (cm^2)	163.5 ± 71.99	167.5 ± 100.7	>0.99
Skeletal muscle (cm^2)	154 ± 36.34	143.5 ± 35.15	0.0078
Intermuscular fat (cm^2)	11.69 ± 7.22	9.24 ± 3.67	0.68

Statistics performed on n=8 patients that received neoadjuvant treatment. Intermuscular fat (cm^2) only available for 7 patients.

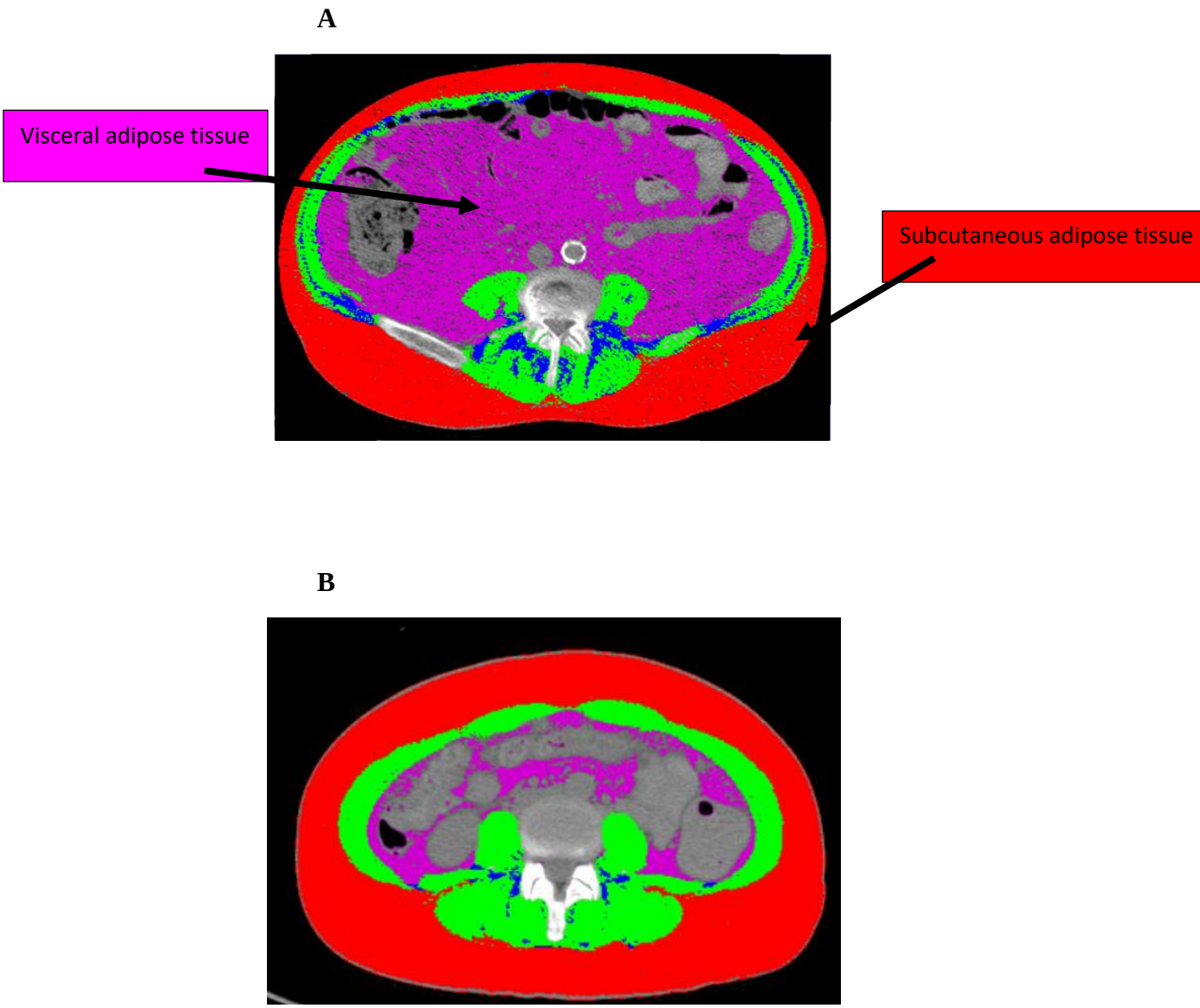

Figure 6.2 C***omputed tomography assessment of body composition***

Abdominal CT images at L3 indicating subcutaneous adipose tissue in red, skeletal muscle in green, intermuscular fat in blue and visceral adipose tissue in pink. (**A**) Abdominal CT image at L3 from a viscerally obese sarcopenic patient. (**B**) Abdominal CT image at L3 from a non-viscerally obese non-sarcopenic patient.

6.4.2 Metabolic profiles differ in visceral and subcutaneous adipose tissue

To determine if metabolic profiles differed in VAT and SAT, we measured OCR and ECAR, measures of OXPHOS and glycolysis, respectively, using a Seahorse XFe24 analyser. Interestingly, OCR was significantly higher in VAT compared to matched SAT (p=0.01) (**Figure. 6.3A**). ECAR, a measure of glycolysis demonstrated a trend towards higher levels in SAT, when compared to VAT, although this did not reach statistical significance (p=0.09) (**Figure. 6.3B**). OCR:ECAR ratio was significantly higher in VAT when compared to SAT, indicating a greater dependence on OXPHOS in the VAT (p=0.003) (**Figure. 6.3C**).

Given the tight association between OAC and obesity, we compared the metabolic profile of VAT and SAT in overweight/obese patients with those of non-obese patients and did not find any significant differences between levels of OCR, ECAR or OCR:ECAR ratio in the VAT, using VFA as a measure of obesity (p>0.05) (**Figure 6.4**). There were no significant differences in OCR or ECAR in SAT based on obesity status (**Figure 6.5A-B**). However, we found a significantly reduced OCR:ECAR ratio in SAT of patients that were obese (p=0.03) (**Figure 6.5C**). We also examined the effect of cytotoxic treatment on metabolic profiles in VAT and SAT in our cohort of OAC patients. There were no significant differences in metabolic profiles in VAT based on whether patients received cytotoxic therapy or not (p>0.05) (**Figure. 6.6**). We found that patients receiving neoadjuvant chemotherapy with or without radiation therapy had significantly higher levels of OCR (p=0.04) and a trend towards higher ECAR (p=0.07) in their SAT compared to the cohort of patients that received surgery only (treatment-naïve). OCR:ECAR ratio was not significantly different between the treatment-naïve cohort and the cohort that received neoadjuvant treatment (p>0.05) (**Figure. 6.7**).

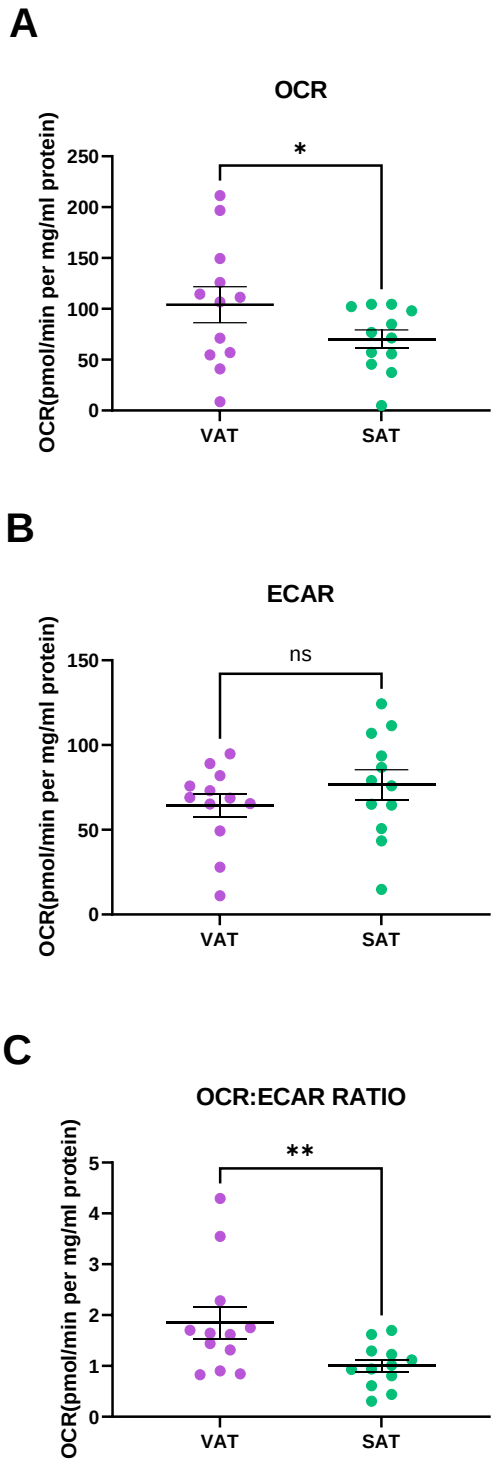

Figure 6.3 Visceral and subcutaneous adipose tissue have different metabolic profiles

(**A**) VAT has higher rates of OXPHOS compared to SAT. (**B**) There is a trend towards higher levels of glycolysis in SAT compared to VAT. (**C**) The OCR:ECAR ratio was significantly higher in VAT compared to SAT. Statistical analysis was performed using a Wilcoxon signed-rank test. All data expressed as mean ± SEM. $^{**}p<0.01$, $^{*}p<0.05$. $n=12$.

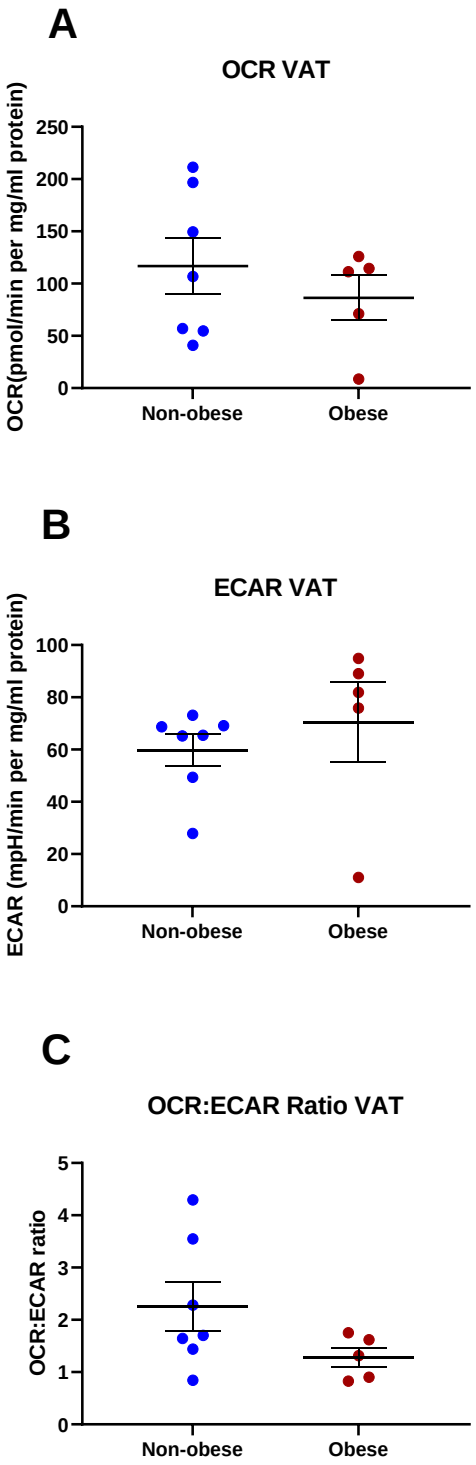

Figure 6.4 Metabolic analysis of visceral adipose tissue by obesity status

There was no significant difference in (**A**) OCR, (**B**) ECAR or (**C**) OCR:ECAR ratio in VAT between non-obese and obese OAC patients. Statistical analysis was performed using a Mann-Whitney U-test. All data expressed as mean ± SEM. *n*=7 for non-obese patients, *n*=5 for obese patients.

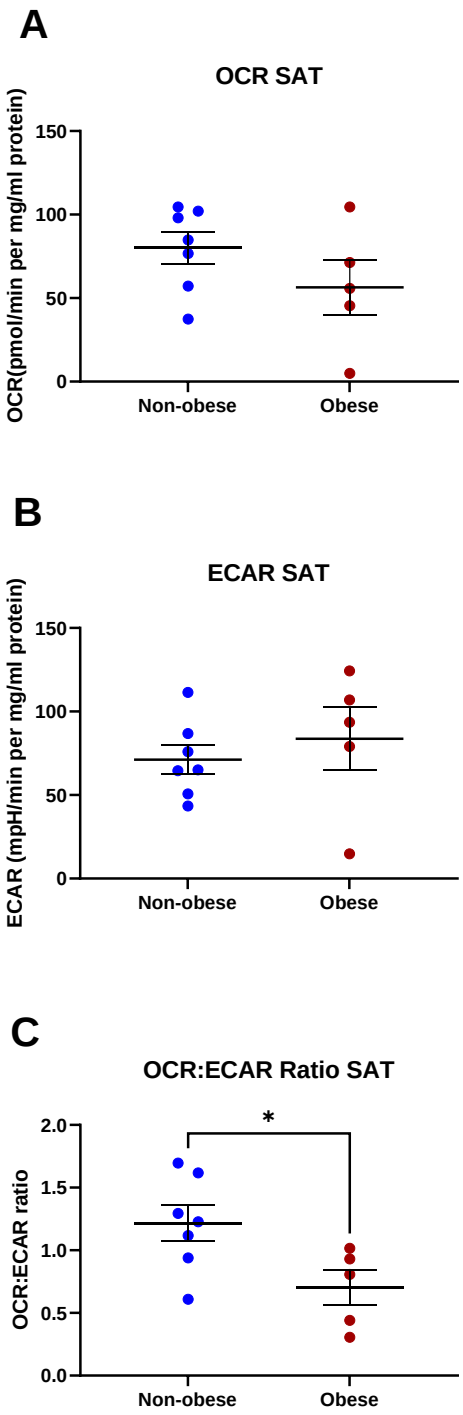

Figure 6.5 Metabolic analysis of subcutaneous adipose tissue by obesity status

(**A**) There was no significant difference in OCR in SAT between non-obese and obese OAC patients. (**B**) There was no significant difference in ECAR in SAT between non-obese and obese OAC patients. (**C**) OCR:ECAR ratio was significantly reduced in SAT of obese compared to non-obese OAC patients. Statistical analysis was performed using a Mann-Whitney U-test. All data expressed as mean ± SEM. *p<0.05. n=7 for non-obese, n=5 for obese.

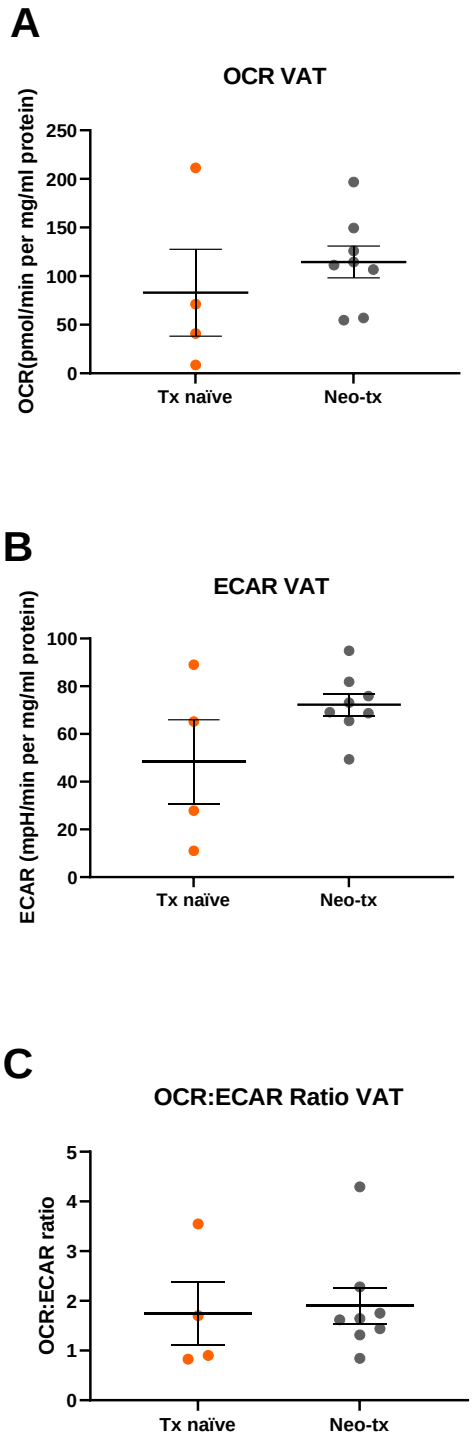

Figure 6.6 Metabolic analysis of visceral adipose tissue by treatment modality

There was no significant difference in (**A**) OCR, (**B**) ECAR or (**C**) OCR:ECAR ratio in VAT between the treatment-naïve cohort and those receiving cytotoxic neoadjuvant therapy. Statistical analysis was performed using a Mann-Whitney U-test. All data expressed as mean ± SEM. *n*=4 for treatment naïve cohort, *n*=8 for cytotoxic neoadjuvant therapy cohort.

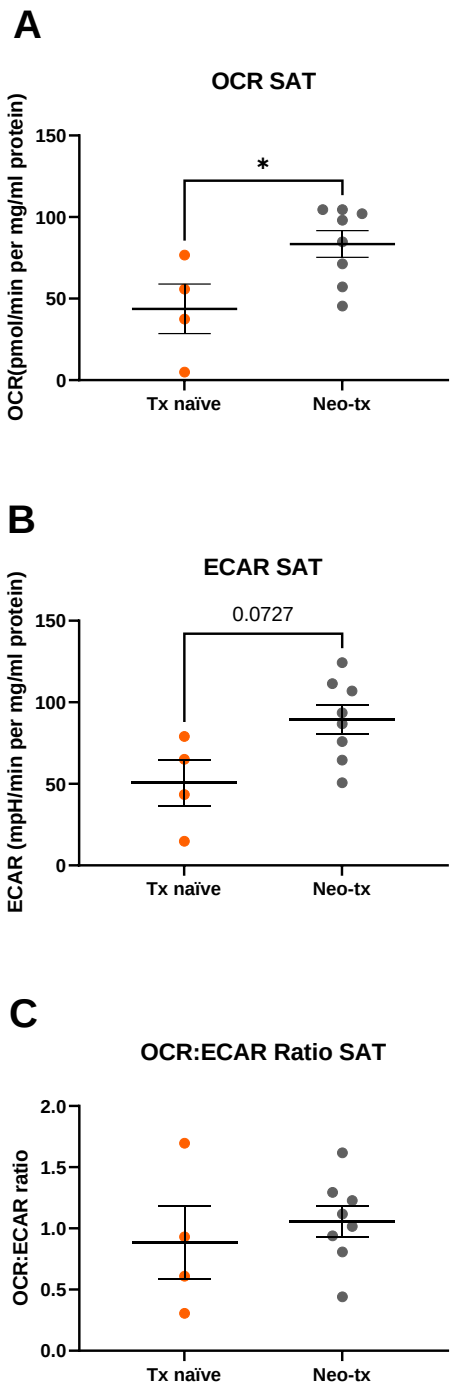

Figure 6.7 Metabolic analysis of subcutaneous adipose tissue by treatment modality

(**A**) OCR was significantly higher in SAT in patients receiving cytotoxic neoadjuvant therapy compared to the treatment-naïve cohort. (**B**) There was no significant difference in ECAR in SAT between patients receiving cytotoxic neoadjuvant therapy compared to the treatment-naïve cohort. (**C**) OCR:ECAR ratio was not significantly different in SAT between the treatment-naïve cohort and those receiving cytotoxic therapy. Statistical analysis was performed using a Mann-Whitney U-test. All data expressed as mean ± SEM. *p<0.05. n=4 for treatment naïve cohort, n=8 for cytotoxic neoadjuvant therapy cohort.

6.4.3 Comparison of the protein secretome between VAT and SAT

To assess if inflammatory, cytokine, chemokine and angiogenic secretions differed between VAT and SAT, MSD multiplex ELISAs were performed assessing the secretion of 54 mediators in VAT and SAT. A readout was obtained for 51 out of the 54 mediators, with the remainder being outside the limit of detection of the assay. Of the 51 detected mediators, 16 were secreted at significantly higher levels from VAT, when compared to SAT, namely FGF(basic), Flt-1, P1GF, VEGF-A, VEGF-C, CRP, SAA, ICAM-1, VCAM-1, IL-15, IL-16, IL-17A, IFN-γ, IL-13, IL-2 and CCL4. VEGF-D showed a trend towards higher levels being secreted from SAT compared to VAT.

6.4.4 Angiogenic factors are secreted at significantly higher levels from VAT, when compared to SAT

Among the 16 factors secreted at higher levels in VAT, 5 of these factors are angiogenic markers; bFGF (p=0.0005), Flt-1 (p=0.001), P1GF (p=0.0005), VEGF (p=0.01) and VEGF-C (p=0.003) (**Figure. 6.8A-E**). VEGF-D is also an angiogenic marker and is showing a trend towards secretion at higher levels from SAT compared to VAT (p=0.053) (**Figure. 6.8F**).

6.4.5 Vascular injury markers were found at significantly higher levels in the visceral adipose tissue secretome compared to the subcutaneous adipose tissue secretome

MSD vascular injury assay was used to assess if there was a difference in vascular injury markers between VAT and SAT. Vascular injury secretions were found at significantly higher levels in the secretome of the VAT compared to SAT. Specifically, CRP (p=0.0005), SAA (p=0.01), ICAM-1 (p=0.002) and VCAM-1 (p=0.001) (**Figure. 6.9A-D**) were secreted at significantly higher levels from the VAT compared to SAT.

6.4.6 Visceral adipose tissue secretes higher levels of inflammatory mediators, cytokines and chemokines compared to subcutaneous adipose tissue

To test the hypothesis that cytokine secretion would differ between VAT and SAT, we screened the supernatants for the secretion of 18 cytokines and 10 chemokines using the MSD multiplex system. Fifteen of the 18 cytokines and all chemokines were within the detection range of the assay. IL-15 (p=0.002), IL-16 (p=0.0005) and IL-17A (p=0.001) (**Figure. 6.10A-C**) were secreted at significantly higher levels from VAT compared to SAT.

To test whether VAT was more inflammatory than SAT, we screened the secretome of both adipose tissue depots for inflammatory mediators. Out of the 10 inflammatory mediators, all were within the detection range of the assay. Significantly higher levels of IFN-γ (p=0.003), IL-13 (p=0.02) and IL-2 (p=0.009) (**Figure. 6.10D-F**) were found in the VAT secretome compared to the SAT secretome. CCL4 was secreted at significantly higher levels from VAT compared to SAT (p=0.03) (**Figure 6.10G**).

6.4.7 Secreted factors from visceral adipose tissue are altered in obese patients

Having observed significantly higher levels of inflammatory secretions from VAT, when compared to SAT, we examined whether obesity alters the secretion of these factors from the VAT. Significantly higher levels of bFGF (p=0.01), CCL26 (p=0.03) and TNF-α (p=0.04) were found in the secretome of VAT from obese patients compared to non-obese patients (**Figure 6.11**).

6.4.8 Secreted factors from subcutaneous adipose tissue are altered in obese patients

Similarly, we investigated the association between obesity and altered secretion of inflammatory mediators from SAT. Elevated levels of CCL17 (p=0.04) and IL-23 (p=0.03) were found in the secretome of SAT from patients that were obese compared to their non-obese counterparts (**Figure 6.12**).

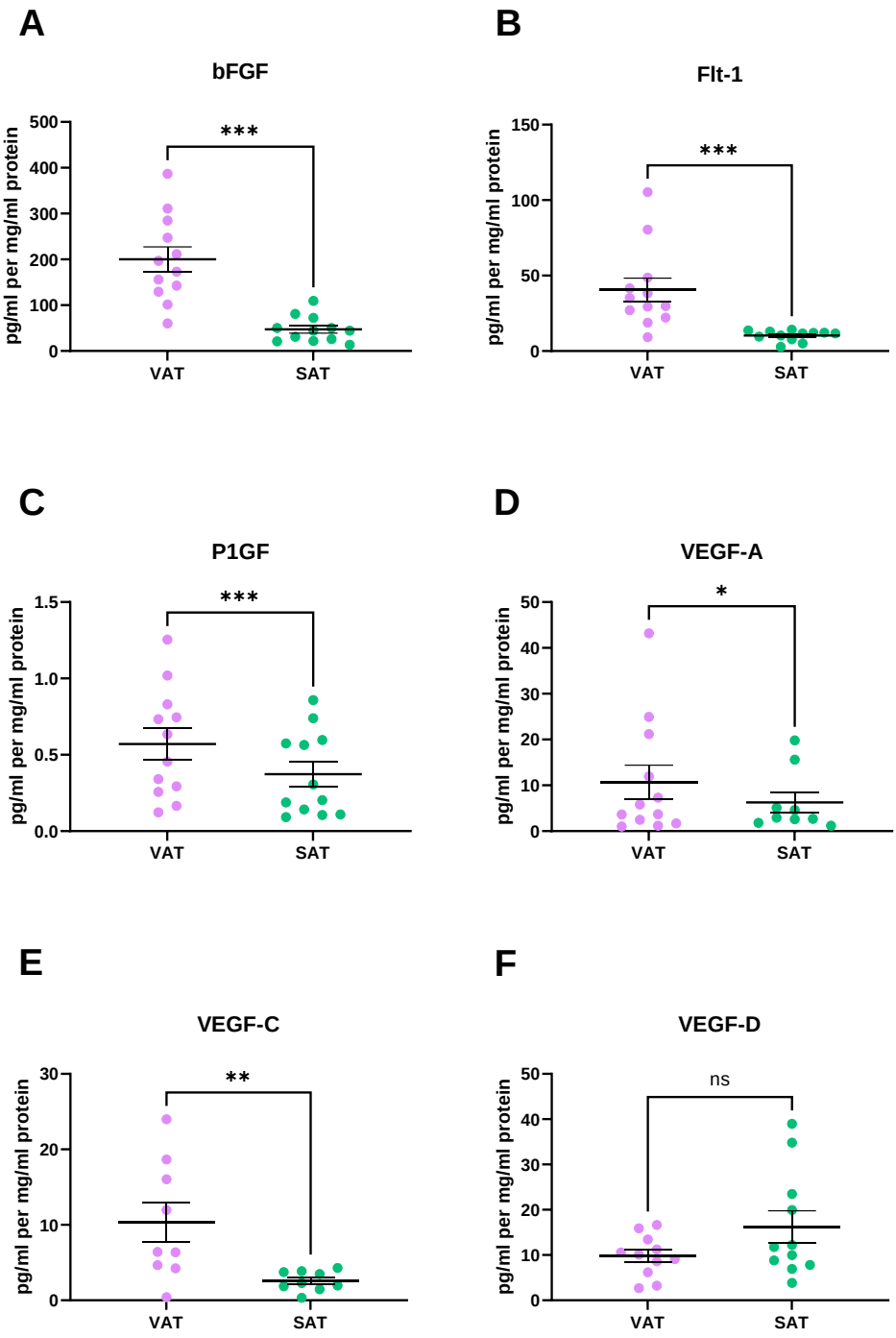

Figure 6.8 Angiogenic factors are secreted at higher levels from VAT, when compared to SAT

Significantly higher levels of (**A**) bFGF, (**B**) Flt-1, (**C**) P1GF, (**D**) VEGF-A and (**E**) VEGF-C were secreted from VAT, when compared to SAT. (**F**) VEGF-D is showing a trend towards elevated levels in SAT compared to VAT. Statistical analysis was performed using a Wilcoxon signed-rank test. All data expressed as mean ± SEM. ***p<0.001, **p<0.01, *p<0.05, ns = non-significant. n=12 for bFGF, Flt-1 and P1GF, n=11 for VEGF-D, n=9 for VEGF-A and VEGF-C.

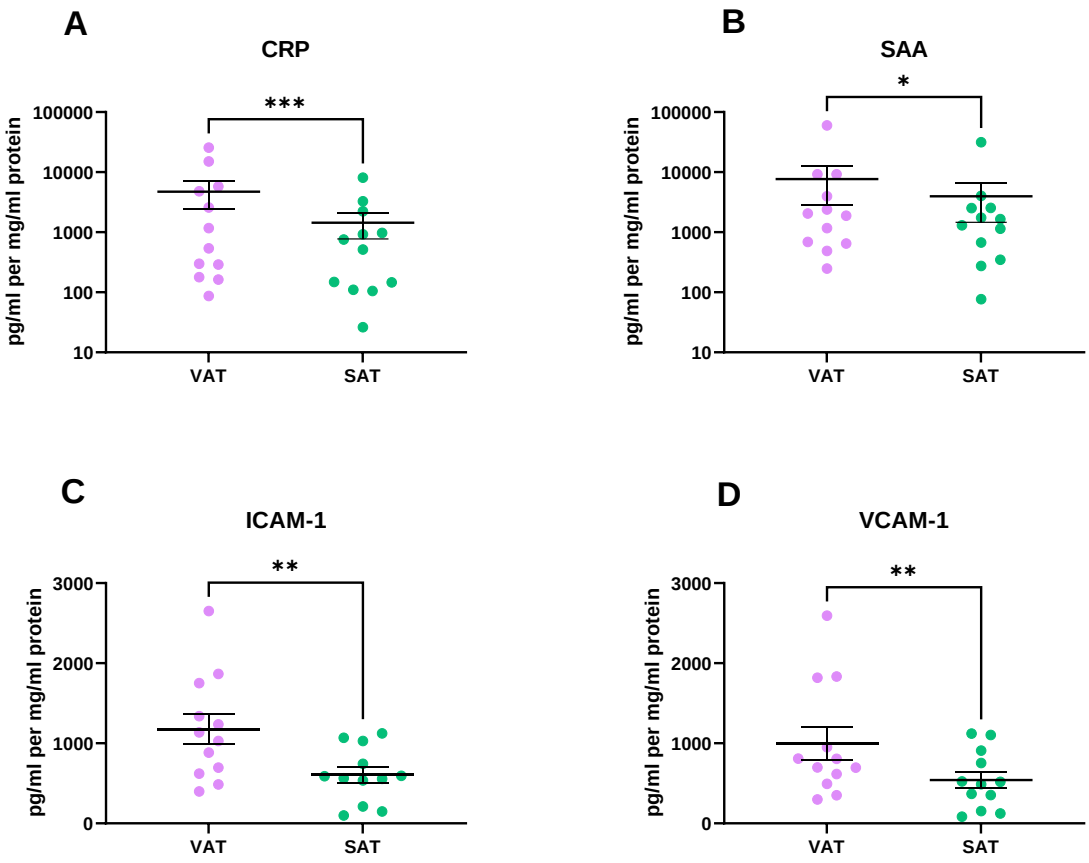

Figure 6.9 Vascular injury secretions are higher in VAT, when compared to SAT

(**A**) CRP, (**B**) SAA, (**C**) ICAM-1 and (**D**) VCAM-1 were secreted at significantly higher levels from VAT compared to SAT. Statistical analysis was performed using a Wilcoxon signed-rank test. All data expressed as mean ± SEM. ***p<0.001, **p<0.01, *p<0.05. n=12.

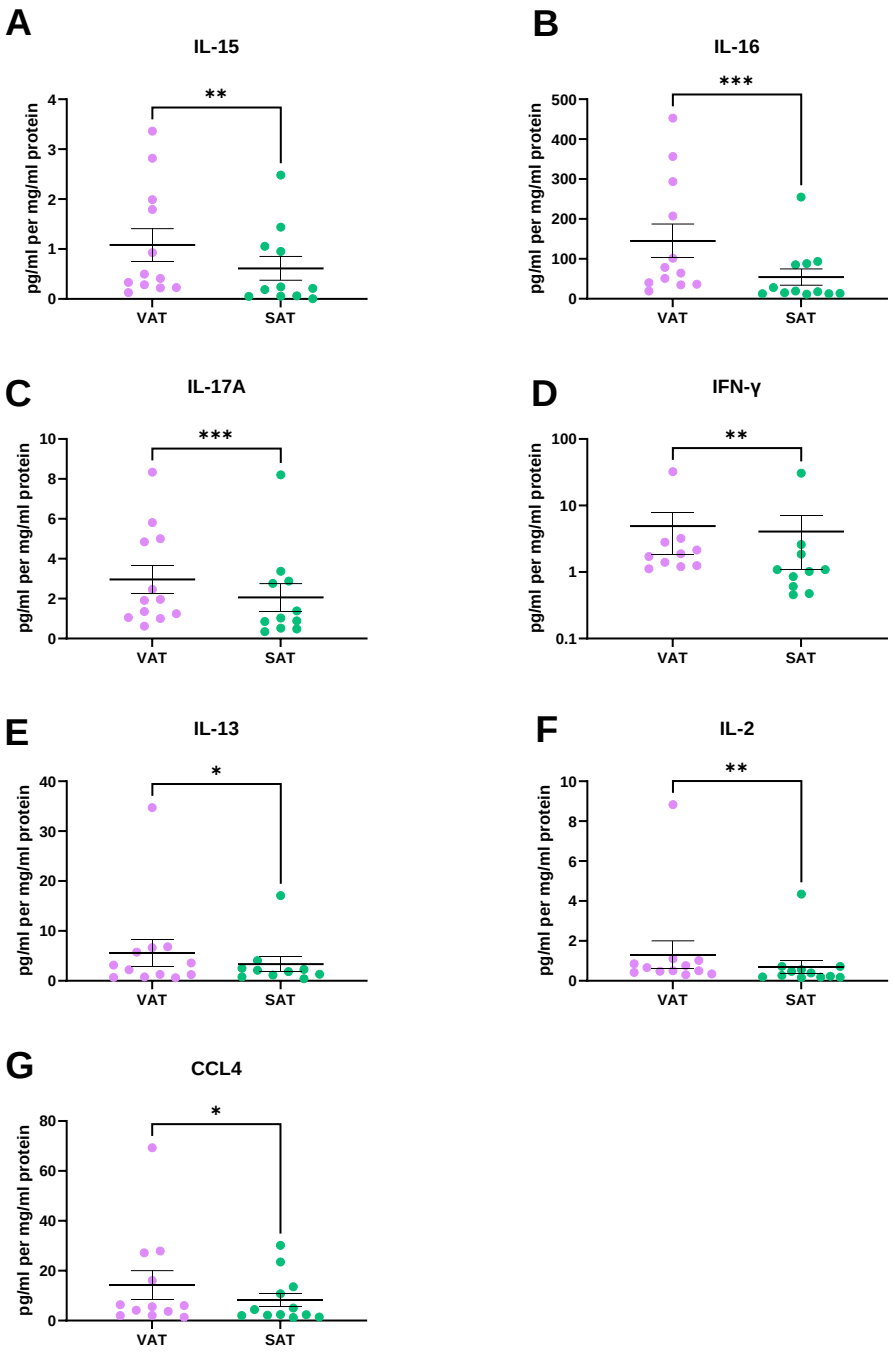

Figure 6.10 Inflammatory, cytokine and chemokine secretions are higher in VAT, when compared to SAT tissue

There were significantly higher levels of (**A**) IL-15, (**B**) IL-16, (**C**) IL-17A, **(D)** IFN-γ, (**E**) IL-13, (**F**) IL-2 and (**G**) CCL4 secreted from VAT, when compared to SAT. All data expressed as mean ± SEM. Statistical analysis was performed using a Wilcoxon signed-rank test. ***p<0.001, **p<0.01, *p<0.05. n=12 for IL-16, IL-2 and CCL4, n=11 for IL-17A and IL-15, n=10 for IFN-γ and IL-13.

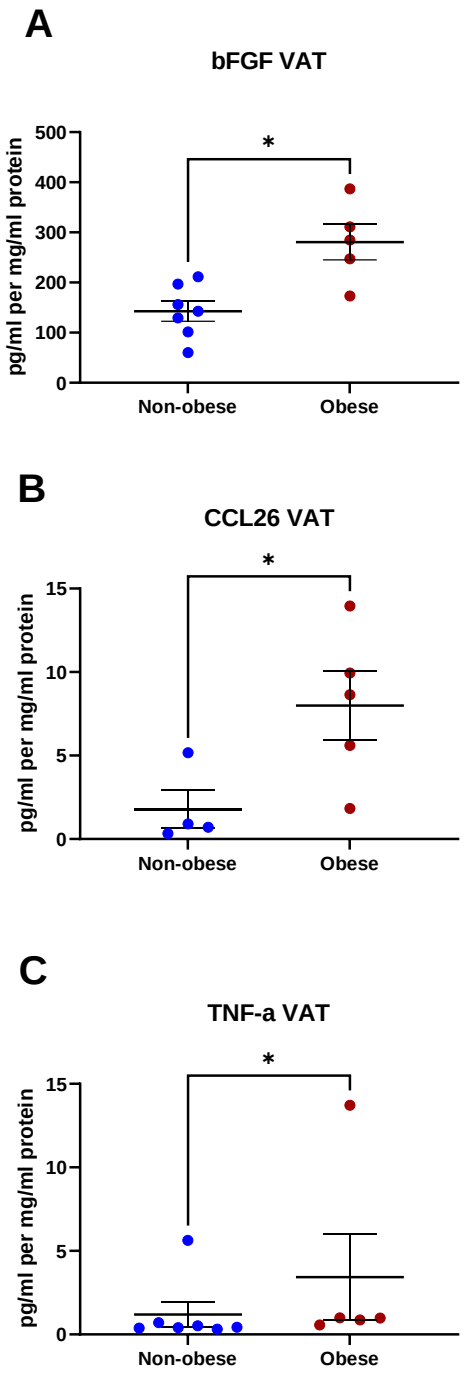

Figure 6.11 Secreted factors are altered in the VAT based on the obesity status of the patient

(**A**) bFGF was secreted at significantly higher levels from the VAT of obese patients compared to non-obese patients. (**B**) CCL26 was secreted at significantly higher levels from the VAT of obese patients, when compared to non-obese patients. (**C**) TNF-α was secreted at significantly higher levels from the VAT of obese patients compared to non-obese patients. Statistical analysis was performed using a Mann-Whitney U-test. All data expressed as mean ± SEM. *p<0.05. n=5 for obese patients, n=7 for non-obese patients, n=4 for non-obese patients for CCL26.

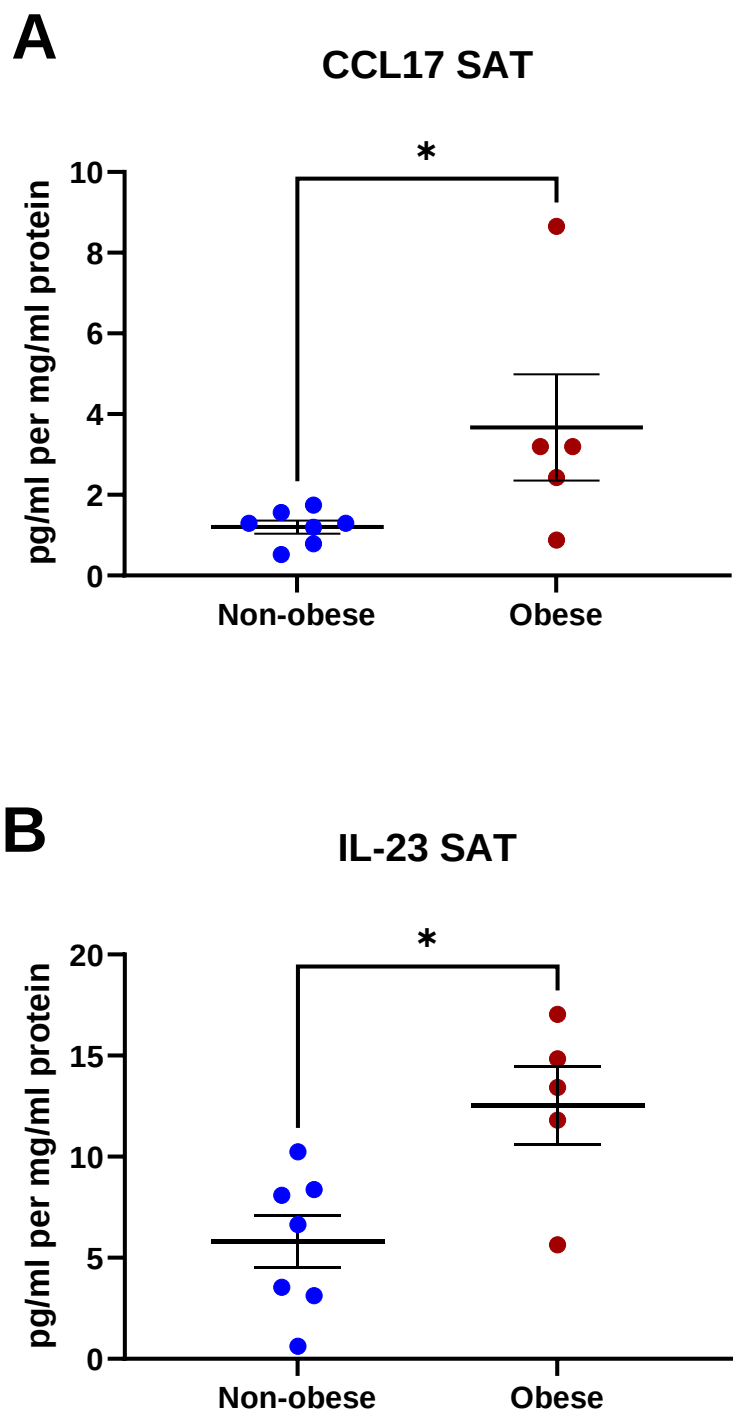

Figure 6.12 Secreted factors are altered in the subcutaneous adipose tissue based on obesity status of the patient

(**A**) CCL17 was secreted at significantly higher levels from the SAT of obese patients compared to non-obese patients. (**B**) IL-23 was secreted at significantly higher levels from the SAT of obese patients compared to non-obese patients. Statistical analysis was performed using a Mann-Whitney U-test. All data expressed as mean ± SEM. *p<0.05. n=5 for obese patients and n=7 for non-obese patients.

6.4.9 Linking energy metabolism to secreted factors in VAT to derive an immune-metabolic signature

To examine the relationship between adipose tissue metabolism and secreted inflammatory mediators, we investigated the correlation between metabolic parameters and secreted factors. **Table 6-4** outlines the relationship between the factors. TNF-β correlated with OCR in VAT (R=0.7667, *p*=0.02). ECAR correlated with CRP (R=0.7203, *p*=0.01) and P1GF (R=0.6294, *p*=0.03) while CCL11 (R=-0.8667, *p*=0.004) was found to inversely correlate and TNF-β (R=0.7167, *p*=0.03) to positively correlate with OCR:ECAR ratio.

6.4.10 Linking energy metabolism to secreted factors in SAT to derive an immune-metabolic signature

The link between energy metabolism and secreted inflammatory mediators differed between VAT and SAT. IL-2 (R=-0.5874, *p*=0.04) and CCL26 (R=-0.7857, *p*=0.04) inversely correlated with OCR in SAT. There was an inverse correlation between ECAR and IFN-γ (R=-0.7817, *p*=0.01), IL-17D (R=-0.6294, *p*=0.03) and IL-8 (R=-1, *p*=0.01) and a positive correlation between ECAR and ICAM-1 (R=0.6154, *p*=0.03), bFGF (R=0.6294, *p*=0.03) and VEGF-D (R=0.7455, *p*=0.01). OCR:ECAR ratio in SAT correlated inversely with the secretion of CXCL10 (R=-0.5874, *p*=0.04) and Tie-2 (R=-0.8857, *p*=0.03) from SAT (**Table 6-4**).

6.4.11 Linking anthropometric parameters to secreted factors in VAT

We identified correlations between secretions of different analytes from VAT and anthropometric parameters. Subcutaneous fat area was positively correlated with CCL11 (R=0.8333, *p*=0.008). Skeletal muscle was inversely correlated with CCL11 (R=-0.7167, *p*=0.03), CCL2 (R=-0.5874, *p*=0.04), IL-12p70 (R=-0.6014, *p*=0.04), IL-1β (R=-0.8571, *p*=0.02), IL-6 (R=-0.6084, *p*=0.03) and IL-8 (R=-0.5874, *p*=0.04). Intermuscular fat correlated with bFGF (R=0.6182, *p*=0.04), CCL26 (R=0.7857, *p*=0.02) and IL-8 (R=0.8810, *p*=0.007). VFA correlated with bFGF (R=0.6503, *p*=0.02) and VEGF-C (R=0.75, *p*=0.02) (**Table 6-5**).

6.4.12 Linking anthropometric parameters to secreted factors in SAT

Skeletal muscle significantly inversely correlated with VEGF-A secretion from SAT (R=-0.7667, *p*=0.02) and intermuscular fat correlated with TNF-α secretion from SAT (R=0.6727, *p*=0.02) (**Table 6-6**).

Table 6-4 Correlation of metabolic parameters with secreted factors in VAT and SAT

Adipose depot	Metabolic parameter	Factor	R value	P value	n
VAT	OCR	TNF-β	0.7667	0.02	9
VAT	ECAR	CRP	0.7203	0.01	12
VAT	ECAR	P1GF	0.6294	0.03	12
VAT	OCR:ECAR	TNF-β	0.7167	0.03	9
VAT	OCR:ECAR	CCL11	-0.8667	0.004	9
SAT	OCR	IL-2	-0.5874	0.04	12
SAT	OCR	CCL26	-0.7857	0.04	7
SAT	ECAR	IFN-γ	-0.7818	0.01	10
SAT	ECAR	IL-17D	-0.6294	0.03	12
SAT	ECAR	ICAM-1	0.6154	0.03	12
SAT	ECAR	IL-8	-1	0.01	5
SAT	ECAR	bFGF	0.6294	0.03	12
SAT	ECAR	VEGF-D	0.7455	0.01	11
SAT	OCR:ECAR	CXCL10	-0.5874	0.04	12
SAT	OCR:ECAR	Tie-2	-0.8857	0.03	6

Table 6-5 Anthropometric parameters correlating with secreted factors from VAT

Anthropometric parameter	Factor	R value	P value	n
SFA	CCL11	0.8333	0.008	9
Skeletal muscle	CCL11	-0.7167	0.03	9
Skeletal muscle	CCL2	-0.5874	0.04	12
Skeletal muscle	IL12p70	-0.6014	0.04	12
Skeletal muscle	IL-1β	-0.8571	0.02	7
Skeletal muscle	IL-6	-0.6084	0.03	12
Skeletal muscle	IL-8	-0.5874	0.04	12
IMF	bFGF	0.6182	0.04	11
IMF	CCL26	0.7857	0.02	8
IMF	IL-8	0.8810	0.007	8
VFA	bFGF	0.6503	0.02	12
VFA	VEGF-C	0.75	0.02	9

Abbreviations: SFA, subcutaneous fat area; IMF, intermuscular fat; VFA, visceral fat area

Table 6-6 Anthropometric parameters correlating with secreted factors from SAT

Anthropometric parameter	Factor	R value	P value	n
Skeletal muscle	VEGF-A	-0.7667	0.02	9
IMF	TNF-α	0.6727	0.02	11

Abbreviations: IMF, intermuscular fat

6.5 Summary of main findings from chapter 6

- Seahorse technology offers a useful instrument for the analysis of metabolic profiles in adipose tissue depots in real-time.
- The real-time metabolic profile differs between VAT and SAT.
- OXPHOS is higher in VAT compared to SAT.
- The angiogenic markers bFGF, Flt-1, PIGF, VEGF-A and VEGF-C are secreted at significantly higher levels from VAT compared to SAT.
- The vascular injury markers CRP, SAA, ICAM-1 and VCAM-1 are secreted at significantly higher levels from VAT compared to SAT.
- Secretion of inflammatory cytokines IFN-γ, IL-13 and IL-2 occurs at higher levels from VAT compared to SAT.
- IL-15, IL-16, IL-17A and CCL4 secretion is higher from VAT compared to SAT.
- Body composition parameters correlated with secreted factors from both VAT and SAT, including a correlation between VFA and the angiogenic factors bFGF and VEGF-C from VAT.

6.6 Discussion

This study demonstrates for the first time that Seahorse technology provides a useful tool for the analysis of real-time metabolic profiles in adipose tissue. We also describe for the first time the real-time metabolic profiles of both VAT and SAT from OAC patients. We have shown that levels of OXPHOS are significantly higher in the VAT compared to SAT of OAC patients. In addition, angiogenic markers, inflammatory markers and cytokine secretions are significantly enhanced from VAT compared with SAT. We found positive correlations between factors secreted from VAT and anthropometric measurements including a correlation between angiogenic factors including bFGF and VEGF-C and VFA. OAC is an obesity-related cancer with visceral adiposity and associated metabolic syndrome particularly incriminated in carcinogenesis, but whether the cancer biology of established tumours is altered by adipose tissue has not heretofore been studied. Intriguingly, obesity may enhance responses to chemotherapy and radiation therapy for OAC (79), and this analysis of a differential metabolic and immunoinflammatory profile between VAT and SAT may provide novel insights into key underlying mechanisms.

To date, studies investigating the metabolic profile of adipose tissue have largely been limited to obese patients undergoing bariatric surgery. We have elucidated the energy metabolism profiles of VAT and SAT in OAC patients for the first time in fresh fat tissue and have shown that OXPHOS is higher in VAT compared to SAT. These results are in line with a study comparing the metabolic profiles of VAT and SAT in adipose tissue from obese patients undergoing bariatric surgery, whereby levels of OXPHOS were higher in VAT compared to SAT when normalised per weight of tissue (358). Interestingly however, VAT had twice the number of mitochondria per milligram of tissue compared to SAT but VAT also had double the amount of cells per milligram of tissue as SAT (358). Since this study population fell into the category of morbidly obese with a mean BMI of 40.7 kg/m^2, it is unknown whether these results can be extrapolated to a population with a lower BMI. While OAC is an obesity-associated disease, the mean BMI of the patient cohort in our study is 25.5 kg/m^2 and therefore is considerably lower than in the aforementioned study, the same trend was observed. Moreover, analysis of the metabolic profiles of VAT did not differ based on the obesity status of the patient using VFA as a determinant of obesity. The similarity in findings suggest that these

pathways are not dependent on the tumour being present and may apply to other obesity-associated cancers and obesity-related diseases.

Profiling the secretome of VAT and SAT in our cohort of OAC patients demonstrated that a panel of angiogenic markers including VEGF-A, bFGF, P1GF, VEGF-C and Flt-1 were secreted at higher levels from the VAT compared to the SAT. These results are in line with a previous study by Lysaght *et al.* which found that VEGF was significantly higher at both the protein levels in the secretome and the RNA level from VAT compared to SAT (359). Flt-1 is thought to play a role in obesity-related tumour progression that is unrelated to the angiogenic process. Flt-$1^{TK-/-}$ mice exhibit an altered immune phenotype and a shift in tumour associated macrophages from an M2 to M1 phenotype (360). Therefore, it may be possible that certain angiogenic factors influence the adipose microenvironment and the phenotype of infiltrating immune cells which may in turn impact tumour progression and treatment response. Of note, P1GF is a ligand for Flt-1. Deletion of P1GF in a mouse model reproduced the effects observed upon Flt-1 deletion with an altered phenotype of infiltrating immune cells (360). Guiu *et al*. reported VFA as being an independent predictor of response to first-line anti-angiogenic treatment with bevacizumab (361). Bevacizumab is a monoclonal antibody that binds to VEGF and blocks VEGF interacting with the VEGF receptors. It inhibits tumour growth by normalising tumour vasculature and prevents new vasculature forming (362). However, it is not clear if the observed association between VFA and bevacizumab response is due to enhanced production of angiogenic factors in VAT, increased volume of distribution of the drug or a combination of both (361). The inter-connectivity between adipose tissue and angiogenesis has previously been reported in mouse models, whereby adipose tissue mass has been shown to be regulated by vasculature with anti-angiogenic treatment inducing weight loss (363). Furthermore, our data indicates a positive correlation between the secretion of angiogenic factors from VAT and VFA. bFGF and VEGF-C secretion from VAT correlated with VFA. Blood vessel density has previously been reported as being higher in VAT than SAT when normalised to the area of fat examined (364), this may support the elevated levels of angiogenic factors we observed in VAT compared to SAT. The angiogenic potential of VAT compared to SAT is unclear with conflicting results reported in the literature. Murine models have demonstrated higher VEGF in VAT compared to SAT (365) whereas the opposite has been reported in humans (366).

Vascular injury markers CRP, SAA, ICAM-1 and VCAM-1 were found to be significantly higher in VAT compared to SAT. Exposure of HUVECs to ACM resulted in increased adhesion of monocytes to the endothelium while simultaneously increasing expression of VCAM-1 and ICAM-1 in endothelial cells, two important factors in the adhesion process (367). Numerous studies have reported a positive association between VAT levels and serum CRP levels in populations of various ethnicities (368, 369). Circulating SAA levels were assessed in a cohort of bariatric surgery patients both pre- and post-surgery. SAA levels decreased post-operatively with a concomitant decrease in circulating hsCRP and reduction in BMI (370). SAA mRNA levels were found to be significantly higher in SAT compared to VAT (370).

A further difference between VAT and SAT is the augmented inflammatory cytokine profile for IL-2, IL-13 and IFN-γ in VAT. The immune-phenotype of adipose tissue, attributable to the stroma vascular fraction (SVF) or non-fat cell components of adipose tissue, is well-documented and are responsible for the secretion of certain adipokines and inflammatory cytokines (84, 371). The enhanced secretion of inflammatory markers from VAT compared to SAT is unsurprising given the finding that there are twice the number of infiltrating macrophages in VAT compared to SAT, therefore it may be possible that the source of the inflammatory secretions may be the infiltrating macrophages (372). IFN-γ transcripts were previously reported to be 8.2-fold higher in VAT relative to SAT (373). The same study reported an increased frequency of IFN-γ-producing natural killer cells in VAT relative to SAT (373). Therefore, it may be possible that the non-fat cell component is the source of these inflammatory cytokines, as has been reported previously. IL-13 is a cytokine involved in insulin resistance (374, 375) and elevated serum levels of IL-13 have been associated with insulin resistance (376). Furthermore, IL-13 levels have been found to correlate strongly with BMI and waist circumference, with a weaker correlation between IL-13 and waist-to-hip ratio and body-fat percentage (376). While it was previously thought that adipokines were secreted from the fat cell component of adipose tissue, it is now known that the SVF component is responsible for the secretion of a plethora of adipokines, including ICAM-1, VCAM-1, CRP and VEGF (371). Greater numbers of macrophages accumulate in VAT compared to SAT (372) and this may account at least partially for the observed elevated levels of inflammatory mediators.

IL-15, IL-16 and IL-17A are significantly higher in the secretome of VAT compared to SAT. IL-15 knock-out has been previously shown to protect against obesity and diet-induced insulin resistance. Furthermore, expression of inflammatory cytokines including TNF-α and IL-6 were reduced in the white adipose tissue of IL-15 knock-out mice (377). IL-16 has been shown to be secreted at higher levels from mast cells of obese patients compared to lean patients (378). IL-17A has been implicated in obesity in recent years, with obese women exhibiting elevated levels of IL-17 compared to their non-obese counterparts (379), therefore it is unsurprising that levels are higher in the secretome of VAT compared to SAT.

Our data indicates that patients lost a significant amount of skeletal muscle and overall fat free mass from time of diagnosis to time of surgery. This phenomenon has been reported previously in oesophageal cancer patients by Guinan *et al.* (380) and Elliott *et al.* (381). Sarcopenia, which is the loss of skeletal muscle mass, is associated with adverse outcomes such as dose-limiting toxicity in neoadjuvant treatment (381, 382), disease progression and post-operative complications (383). Cancer cachexia is a progressive wasting condition characterised by sarcopenia with or without loss of fat mass and is characterised by systemic inflammation (384). Therefore, we investigated if factors secreted from VAT or SAT correlated with measurements of body composition. There was an inverse correlation between skeletal muscle and the inflammatory markers IL-1β, IL-6 and IL-8. IL-6 has been implicated in the systemic inflammatory response of cachexia (385). It is not overly surprising therefore that there was an inverse correlation between IL-6 secretion from VAT and skeletal muscle in this cohort. IL-8 serum concentrations have been shown to be elevated in cachectic pancreatic cancer patients (386). Interestingly, elevated IL-1β in the SAT has been reported in cachectic gastrointestinal cancer patients (387).

To the best of our knowledge, this is the first study to profile an immune-metabolic signature of both VAT and SAT in a cohort of OAC patients. Both compartments are markedly different and offer insights as to how adipose tissue and the obese microenvironment may both promote carcinogenesis and impact on tumour biology and clinical responses to standard therapy. Further study of VAT in particular and its impact and clinical relevance to standard therapies, as well as anti-angiogenic and immunotherapy may reveal novel insights that may be therapeutically applied in the clinic.

Chapter 7 Concluding Summary and Future Directions

7.1 Concluding summary

Radiation therapy is a pillar of cancer therapy with approximately 50% of all patients receiving this treatment modality (85). However, resistance to therapy presents a huge clinical challenge in oncology, not least so in rectal and oesophageal cancers with only, at best, 27-30% of patients with either of these cancers achieving a complete pathological response (pCR) to treatment (22, 72), which will impact overall patient outcomes. A good response to treatment has favourable long-term outcomes for patients, therefore elucidating the mechanisms underlying this therapeutic resistance could potentially yield new therapeutic targets with the overall objective of improving patient outcome. The radiation-induced bystander effect (RIBE) describes the plethora of biological events occurring in unirradiated cells adjacent to irradiated cells (131). RIBE has been linked experimentally to numerous hallmarks of cancer (164) however, the examination of RIBE induction using human *ex vivo* models on bystander cellular metabolism and mitochondrial function remains largely unknown in the literature.

Radiation resistance may be inherent or acquired and can result from the complex interplay of biological processes occurring in and adjacent to the tumour. Multiple mechanisms of radiation resistance have been identified with our group focussing extensively on the role of energy metabolism and inflammation, two processes that demonstrate a strong inter-relationship. In a novel isogenic model of acquired OAC radioresistance developed in our lab, it has been demonstrated that upregulated oxidative phosphorylation (OXPHOS) and inflammatory pathways have been linked to the radioresistant phenotype (80, 111, 271). Moreover, this model has been shown to be very clinically relevant and reflective of patient tumours with higher levels of the OXPHOS marker ATP5B being elevated in the tumours of OAC patients who have a poor response to neoadjuvant treatment (111). Similarly, upregulation of IL-6 type cytokines associated with radioresistance have been identified both in the isogenic model and in OAC patients (271), highlighting the role of altered metabolism and altered inflammation in the treatment response of OAC.

To that end, in this thesis, we examined the effect of RIBE on mitochondrial metabolism and inflammatory and immune pathways in rectal cancer tissue using *in vitro* and human *ex vivo* models.

In chapter 2 we examined the effect of secreted factors both pre- and post-radiation from a radiosensitive and a radioresistant *in vitro* model of colorectal cancer (CRC) on mitochondrial metabolism and function and radiosensitivity. We did not observe any changes in any biological end-points examined in response to secreted factors from *in vitro* CRC models after a single fraction of a clinically relevant dose of radiation. Following repeated fractions of a clinically relevant dose of radiation, a scenario that is more relevant to the clinical setting, we did not observe any alterations in metabolism in the radioresistant SW837 cell line. We did however observe increases in ROS levels following treatment with irradiated cell conditioned media (ICCM) from cells that received 2 x 1.8 Gy fractions of radiation in this cell line. In the radiosensitive colon cancer cell line, the HCT116 cells, we observed alterations in mitochondrial metabolism following treatment with ICCM from HCT116 cells that received a single fraction of 1.8 Gy in this experimental set up, suggesting that RIBE responses vary depending on the cell density of the irradiated cells. We also observed an enhancement in cellular proliferation, used as a surrogate marker for radiosensitivity, following treatment with ICCM from cells that received 3 x 1.8 Gy fractions of radiation. However, we did not observe any alterations in the expression of four DNA repair genes; *PARP1, SMUG1, MMS19* and *MLH1* following RIBE induction. Failure to observe any robust RIBE responses in our cell lines following exposure to ICCM from irradiated cell lines prompted us to investigate the effect of the tumour microenvironment (TME) using a human *ex vivo* explant model on RIBE induction in chapter 4.

OAC and rectal cancer have similar response rates to neoadjuvant therapy and deregulated cellular bioenergetics are known to play a role in the response of OAC tumours to radiation (111). Therefore, we examined the same RIBE end-points investigated in chapter 2 in an isogenic model of acquired radioresistance in OAC. Similar to that seen in CRC cells, we did not observe any alterations in mitochondrial metabolism following RIBE induction after a single fraction of a clinically relevant dose of radiation in either the radiosensitive or the radioresistant cell line. We did however identify a differential mitochondrial function between the radiosensitive and the radioresistant model, with elevations in mtMP and ROS observed in the radioresistant cell line but not the radiosensitive cell line, suggesting that RIBE induction may induce mitochondrial alterations that have been associated with a more radioresistant phenotype. Following RIBE induction using repeated fractions of clinically relevant doses of

radiation delivered at 24 h intervals we observed alterations in mitochondrial metabolism in both cell lines following two fractions of 1.8 Gy. RIBE induction had differential effects on cellular proliferation in both cell lines with an inhibition of cellular proliferation observed in the radioresistant cell line following a single fraction of radiation. DNA repair efficiency appeared to be enhanced in the radioresistant model following 3 x 1.8 Gy fractions of radiation. Therefore, it appears from the results of this chapter that RIBE responses are spatially and temporally regulated events and differ in response to fractionation of doses.

In chapter 4 we identified a RIBE response in rectal cancer cells in response to signals from whole biopsies from both normal and malignant rectal cancer tissue. We hypothesise that this indicates that the TME is vitally important in determining and activating RIBE responses. The complexity of the tumour content and the cell-to-cell communications are key in inducing RIBE. This is an important finding and should be considered when choosing appropriate model systems to study RIBE events. It has previously been reported that p53 mutant cells do not respond to RIBE signals, however we have shown that the SW837 cells, a p53 mutant cell line, are capable of responding to RIBE signals in *ex vivo* conditioned media. We have also shown that obesity directly impacts the microenvironment of rectal cancer tissue with leucine and ethanol correlating with visceral fat area (VFA), a measure of obesity status. This warrants further investigation since obese rectal cancer patients have been reported to have poorer outcomes in response to neoadjuvant treatment (293) and may yield therapeutic targeting strategies. Though the literature reports on this topic are mixed. As alluded to previously, work in our group has demonstrated that overweight and obese OAC patients have an improved response to neoadjuvant treatment compared to their counterparts of a healthy weight (79). Furthermore, it has been demonstrated that obese patients have enhanced responses and improved outcomes to immunotherapy and targeted therapy (355-357).

In chapter 5, to determine what soluble factors may be key to driving RIBE, we profiled the inflammatory secretome of both normal and malignant rectal tissue both pre- and post-radiation. We identified 19 secreted factors that were found at higher levels in the secretome of rectal cancer tissue compared to normal rectal tissue. Unsurprisingly many of these altered factors had pro-tumorigenic properties including pro-angiogenic, pro-mitogenic and immunosuppressive attributes. We did not observe any alterations in inflammatory secretions in the rectal cancer TME post-radiation. The irradiated rectal

cancer TME was the most potent stimulator of dendritic cell (DC) maturation. This indicates that radiation does not have an immunosuppressive effect on the rectal cancer TME which is important in terms of regulating treatment response. We have shown that there was a differential interrelationship between secreted factors in the normal and malignant rectal microenvironments and DC maturation markers. This chapter highlighted the importance of the interplay between relative levels of inflammatory factors in the TME and the implication of this on the innate immune system.

Having observed correlations between measures of obesity and response of bystander cells to radiation, levels of metabolites in the TME and altered levels of inflammatory proteins in the TME of obese individuals we investigated if it was possible to profile the metabolic signatures of *ex vivo* adipose tissue using Seahorse technology. We demonstrated that it was possible to determine the metabolic profiles of *ex vivo* adipose tissue depots using Seahorse technology and that OXPHOS predominates in visceral adipose tissue (VAT) while there is a trend towards higher utilisation of glycolysis in subcutaneous adipose tissue (SAT). Since inflammation and metabolism are inter-related, we then profiled the inflammatory protein secretions from both adipose tissue depots and found that there were significantly higher levels of angiogenic, vascular injury and pro-inflammatory secretions in the VAT compared to SAT. There were also early indications in this preliminary study that obesity may alter the metabolic profile and inflammatory secretome of adipose tissue.

Overall, the findings of this thesis have identified the interplay of secreted factors and cell types within the TME as important determinants in regulating bystander cellular metabolism and innate immune responses in rectal cancer. We have also identified correlations between cellular behaviour, the metabolomic landscape and inflammatory protein secretions and obesity status in patients. We have shown that Seahorse technology is a useful tool for profiling the metabolic signature of adipose tissue for future functional studies. The findings of this thesis are summarised in **Figure 7.1** below.

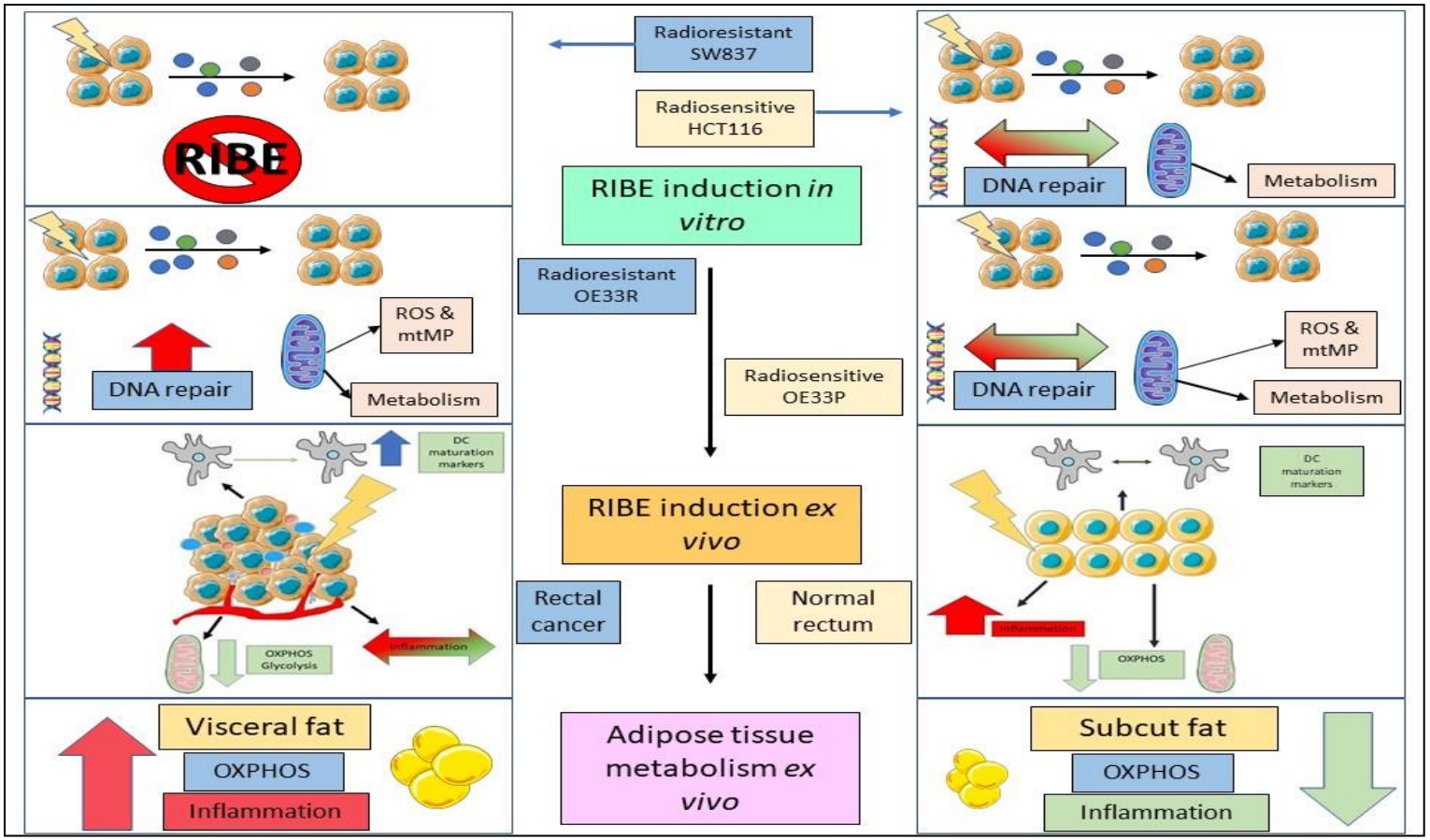

Figure 7.1 Concept diagram of main findings from thesis

Schematic illustration of main findings from thesis. In SW837 cells RIBE was not observed. In HCT116 cells RIBE induction caused alterations in metabolism. In OE33R cells, RIBE induction altered expression of DNA repair genes, metabolism and mitochondrial function while only mitochondrial function and metabolism was altered in OE33P cells. The irradiated normal and rectal cancer microenvironment altered mitochondrial metabolism, DC maturation and secretion of inflammatory proteins. Visceral adipose tissue has higher levels of OXPHOS and elevated secretion of inflammatory mediators when compared to subcutaneous adipose tissue.

7.2 Future directions

The results generated from this Ph.D. thesis have generated a number of future research possibilities which are described below.

1. We have shown that rectal cancer cells exhibit altered mitochondrial metabolism in response to the irradiated rectal tissue secretome of both normal and malignant rectal cancer tissue. It would be interesting to assess the effect of RIBE induction on mitochondrial metabolism and function on various cells within the vicinity of the tumour including immune cells, fibroblasts and normal cells since aberrant metabolism in these cells may have implications for tumour progression and treatment response.

2. We have demonstrated that whole tissue biopsies produce RIBE signals that induce metabolic perturbations in bystander cells. However, it would be important to investigate the metabolism of whole biopsies in response to RIBE signals from irradiated rectal cancer tissue. This would capture the entire TME and offer insight into the cumulative effect of the interplay between the response of various cell types to RIBE signals from the tumour architecture. Given the aforementioned importance of metabolism in treatment response in gastrointestinal cancers, gaining an understanding of the metabolic consequences of RIBE induction using an *ex vivo* model would offer insight into potential therapeutic targets for enhancing radiosensitivity.

3. We have profiled the inflammatory microenvironment of normal rectal tissue and rectal cancer tissue and identified differential effects of these secretomes on DC maturation. It would be important to conduct a screen in a larger cohort of patients and obtain matched blood samples to identify if altered levels of inflammatory proteins in the TME correlated with levels in the blood. By then following up this larger cohort of patients over time, it would be possible to investigate if altered levels of these proteins in the TME and/or blood had prognostic value in stratifying patients into good and poor responders to neoadjuvant treatment. Furthermore, our data indicates that the irradiated rectal cancer TME is the most

potent stimulator of DC maturation, therefore investigating the effect of the altered secreted factors may identify important inducers of innate immunity.

4. We investigated the effect of a single fraction of a clinically relevant dose of 1.8 Gy radiation on the protein secretome in rectal cancer tissue but it would be important to compare pre-treatment protein secretions in the TME and blood with those obtained post-treatment following a full course of neoadjuvant therapy. This could potentially allow for segregation of good versus poor responders to neoadjuvant therapy based on an altered pattern of protein secretions, which has the potential for improved stratification of patients and in turn has the potential to identify therapeutic targets.

5. We have demonstrated that it is possible to assess the metabolic profiles of adipose tissue depots in real-time using Seahorse technology. Previous work in our group has revealed that OAC patients that are overweight or obese have a better response to neoadjuvant treatment compared to their non-obese counterparts but the mechanisms underlying this are largely unknown. Prof. O'Sullivan's group has secured funding to investigate the effect of neoadjuvant radiation on metabolic profiles in VAT. Prof. O'Sullivan's group is also assessing the metabolic profiles of adipose tissue in CRC patients to investigate if altered adipose tissue metabolism is linked to patient outcome.

6. We screened VAT and SAT depots for the secretion of 54 inflammatory proteins. It would be interesting to conduct this screen in a larger cohort of patients and segregate patients according to obesity status and treatment response to identify any associations between secreted factors and outcome which may be of prognostic value. As with the rectal study, it would be useful to conduct the screen in matched blood samples owing to the ease of access of blood samples for future prognostic use.

Appendix I - Publications

Translational Oncology 14 (2021) 100882

Contents lists available at ScienceDirect

Translational Oncology

journal homepage: www.elsevier.com/locate/tranon

Radiation-induced Bystander Effect (RIBE) alters mitochondrial metabolism using a human rectal cancer *ex vivo* explant model

Aisling B. Heeran [a], Helen P. Berrigan [a], Croí E. Buckley [a], Heleena Moni Bottu [b], Orla Prendiville [b], Amy M. Buckley [a], Niamh Clarke [a], Noel E. Donlon [a], Timothy S. Nugent [a], Michael Durand [c], Cara Dunne [c], John O. Larkin [c], Brian Mehigan [c], Paul McCormick [c], Lorraine Brennan [b], Niamh Lynam-Lennon [a], Jacintha O'Sullivan [a,*]

[a] Department of Surgery, Trinity Translational Medicine Institute, St. James's Hospital, Trinity College Dublin, Dublin 8, Ireland
[b] Institute of Food and Health and Conway Institute, UCD School of Agriculture and Food Science, UCD, Belfield, Dublin 4, Ireland
[c] GEMS, St. James's Hospital, Dublin 8, Ireland

ARTICLE INFO

Article history:
Received 22 June 2020
Received in revised form 30 July 2020
Accepted 3 August 2020

Keywords:
Radiation-induced Bystander Effect
Rectal cancer
Metabolism
Radiation
Metabolomics

ABSTRACT

Locally advanced rectal cancer is treated with neoadjuvant-chemoradiotherapy, however only 22% of patients achieve a complete response. Resistance mechanisms are poorly understood. Radiation-induced Bystander Effect (RIBE) describes the effect of radiation on neighbouring unirradiated cells. We investigated the effects of *ex vivo* RIBE-induction from normal and rectal cancer tissue on bystander cell metabolism, mitochondrial function and metabolomic profiling. We correlated bystander events to patient clinical characteristics.

Ex vivo RIBE-induction caused metabolic alterations in bystander cells, specifically reductions in OXPHOS following RIBE-induction in normal ($p = 0.01$) and cancer tissue ($p = 0.03$) and reduced glycolysis following RIBE-induction in cancer tissue ($p = 0.01$). Visceral fat area correlated with glycolysis ($p = 0.02$) and ATP production ($p = 0.03$) following exposure of cells to TCM from irradiated cancer biopsies. Leucine levels were reduced in the irradiated cancer compared to the irradiated normal secretome ($p = 0.04$). ROS levels were higher in cells exposed to the cancer compared to the normal secretome ($p = 0.04$).

RIBE-induction *ex vivo* causes alterations in the metabolome in normal and malignant rectal tissue along with metabolic alterations in bystander cellular metabolism. This may offer greater understanding of the effects of RIBE on metabolism, mitochondrial function and the secreted metabolome.

Introduction

Colorectal cancer (CRC) is the 3rd most commonly diagnosed cancer globally and the 2nd leading cause of cancer death [1]. Within the European Union, rectal cancer accounts for approximately 35% of all cases of CRC [2]. The incidence of rectal cancer in Ireland is projected to almost double in both genders between 2020 and 2045 [3], while the mortality rate is predicted to increase by almost 25% by 2035 [4].

The current treatment for locally advanced rectal cancer (LARC) is neoadjuvant radiotherapy with or without chemotherapy, followed by surgery. Radioresistance is a considerable problem in rectal cancer with only 22% of patients achieving a complete pathological response (pCR) to neoadjuvant chemoradiation (neo-CRT) [5], which is the best predictor of long-term patient outcome [6]. The mechanisms underlying this resistance are poorly understood and the effect of radiation on bystander cells adjacent to the irradiated volume is largely unknown.

The Radiation-induced Bystander Effect (RIBE) refers to the plethora of biological phenomena occurring in non-irradiated cells as a result of signal transmission from an irradiated cell. Cell behaviour mimics that of directly irradiated cells, exhibiting genomic instability, mutagenesis, altered apoptosis, DNA damage and oncogenic transformation [7]. RIBE signals are transmitted *via* soluble mediators secreted into the extracellular space and *via* gap-junction intercellular communication [8]. RIBE has been linked to numerous hallmarks of cancer experimentally [9], however the majority

Abbreviations: ATP, Adenosine triphosphate; CPMG, Carr-Purcell-Meiboom-Gill; CRC, colorectal cancer; CT, computed tomography; D_2O, deuterium oxide; ECAR, extracellular acidification rate; Gy, Gray; ^{1}H NMR, proton nuclear magnetic resonance; LARC, locally advanced rectal cancer; mtMP, mitochondrial membrane potential; NCM, normal conditioned media; neo-CRT, neoadjuvant chemoradiation; OAC, oesophageal adenocarcinoma; OCR, oxygen consumption rate; OPLS-DA, orthogonal partial least square discriminate analysis; OXPHOS, oxidative phosphorylation; PCA, principal component analysis; pCR, complete pathological response; PLS-DA, partial least square discriminate analysis; RIBE, Radiation-induced Bystander Effect; ROS, reactive oxygen species; TCM, tumour conditioned media; TME, Tumour microenvironment; TSP, sodium trimethyl [2,2,3,3-$^2H_4$] propionate; VFA, visceral fat area.

* Corresponding author at: Department of Surgery, Trinity Translational Medicine Institute, Trinity College Dublin, St. James's Hospital, Dublin 8, Ireland.
E-mail address: osullij4@tcd.ie. (J. O'Sullivan).

http://dx.doi.org/10.1016/j.tranon.2020.100882
1936-5233/© 2020 The Authors. Published by Elsevier Inc. on behalf of Neoplasia Press, Inc. This is an open access article under the CC BY license (http://creativecommons.org/licenses/by/4.0/).

of RIBE studies have been performed in *in vitro* models, with limited evidence using *ex vivo* human tissue.

Mitochondria are integral to RIBE induction and appear to have a dual role in the manifestation of RIBE. Cells deficient in mitochondrial DNA are unable to produce a bystander signal, highlighting the role of this organelle in RIBE [10]. Furthermore, inhibition of mitochondrial function inhibits RIBE signalling and response in human lymphoblastoid cells [11]. Previous work by Gorman et al. demonstrated that RIBE induction in an *ex vivo* model of CRC induced random mitochondrial point mutations in bystander cells [12]. Dissecting the role of mitochondrial metabolism and changes in the metabolome during RIBE has not yet been investigated.

Altered metabolism and mitochondrial function are important players in the response to radiation, where radioresistant oesophageal adenocarcinoma (OAC) cells show altered metabolism and changes in mitochondrial morphology [13]. Moreover, in patient tumours, higher oxidative phosphorylation (OXPHOS) is associated with radiation treatment resistance in OAC [13]. Furthermore, exposure of OAC cells to adipose conditioned media from viscerally obese OAC patients altered mitochondrial function and induced a metabolic shift in OAC cells, indicating that obesity modulates the behaviour of mitochondria in cancer cells [14].

To date, much radiation bystander research has been conducted *in vitro*, with some *in vivo* models in more recent years. To the best of our knowledge this is the first study to investigate RIBE induction in an *ex vivo* model of rectal cancer. We investigated the effect of *ex vivo* RIBE induction using rectal cancer and normal rectal tissue on bystander cellular metabolism, mitochondrial function and metabolomic profiling of the normal and cancer tissue microenvironments to determine if the bystander effects differed between normal and malignant rectal tissue. We hypothesised that *ex vivo* RIBE induction would induce metabolic alterations and alter mitochondrial function and these would differ between normal and malignant tissue. We also hypothesised that obesity status would be associated with metabolic perturbations in bystander cells.

Methods

Patient recruitment

Patients undergoing lower gastrointestinal investigations were prospectively recruited to this study between January 2018 and November 2018. Ethical approval was granted for the entire study by the St. James's Hospital/AMNCH Research Ethics Committee (Ref 2011/43/02) and the study was conducted in line with the Declaration of Helsinki and data protection regulations. All patients provided informed consent for their participation in this study. Biopsies were obtained from treatment-naïve rectal cancer patients and normal (non-cancer) control patients at diagnostic endoscopy. Clinical data was obtained from patient healthcare records.

The human rectal adenocarcinoma SW837 cell line purchased from European Collection of Authenticated Cell Culture (ECACC) was utilised for all bystander experiments in this study. This is a grade IV adenocarcinoma cell line obtained from a 53-year old male. The cells are p53 mutant with a C->T mutation in codon 248. Cells were cultured in Leibovitz's L-15 medium supplemented with 10% FBS and 1% penicillin-streptomycin.

Generation of tumour conditioned media and normal conditioned media

Tumour conditioned media (TCM) and normal conditioned media (NCM) were generated by gently washing fresh biopsies four times in PBS supplemented with 1% penicillin-streptomycin, 1% Fungizone (amphotericin B) and 0.1% gentamicin. Each biopsy was then placed in 1 ml of M199 media supplemented with 10% FBS, 1% penicillin-streptomycin, 1% Fungizone, 0.1% gentamicin and 1 μg/ml insulin. Biopsies were incubated for 80 min at 37 °C and 5% CO_2. Following 80-min incubation, biopsies were either mock-irradiated (0Gy) or irradiated with 1.8Gy radiation using an XStrahl RS225 x-irradiator at a dose rate of 1.73Gy/min (195 kV, 15 mA) [XSTRAHL, Surrey, UK] and incubated for 24 h at 37 °C and 5% CO_2. The media was then harvested and stored in 2 ml cryotubes at −80 °C until required. The matched cultured biopsy tissues were snap-frozen in liquid nitrogen and stored at −80 °C.

For the purposes of all bystander experiments, a 1:1 dilution of TCM/NCM in M199 was used for all assays. This dilution was chosen based on optimisation experiments using TCM/NCM on SW837 cells with no differences being observed between the neat use of TCM/NCM and a 1:1 dilution of TCM/NCM with M199.

Assessment of bystander metabolic profiles using Seahorse technology

SW837 cells were seeded in duplicate at a density of 30,000 cells per well in complete RPMI in a 24 well XFe24 cell culture microplate for 24 h [Agilent Technologies, Santa Clara, CA, USA] and then treated with NCM or TCM from the human normal or rectal cancer *ex vivo* explants respectively for 24 h. Following 24-h treatment, Oxygen Consumption Rate (OCR) and Extracellular Acidification Rate (ECAR) were measured using a Seahorse Biosciences XFe24 Extracellular Flux Analyser [Agilent Technologies, Santa Clara, CA, USA] as previously described [15].

Assessment of reactive oxygen species and mitochondrial membrane potential levels in bystander cells

Reactive oxygen species (ROS) was assessed using the fluorescent probe 2′-7′-dichlorofluorescien (2′-7′-DCF). Mitochondrial membrane potential (mtMP) was assessed using the fluorescent probe Rhodamine 123. SW837 cells were seeded at 30,000 cells per well in a 96-well plate for 24 h. Following 24-h incubation, cells were treated with 100 μl of TCM or NCM for 24 h. ROS was assessed by adding 50 μl of 2,7-DCF (5 μM) in PBS-Mg and mtMP was assessed by adding 50 μl of Rhodamine 123 (5 μM) in PBS-Mg as described previously [15]. All seahorse data and mitochondrial function assay data was normalised to cell number using the crystal violet assay as previously described [15].

Evaluation of changes in the metabolome of normal and rectal cancer ex vivo explants in response to radiation using metabolomics

A total of 250 μl deuterium oxide (D_2O) and 10 μl sodium trimethyl [2,2,3,3-$^2H_4$] propionate (TSP) (0.005 g/ml) were added to each 300 μl TCM, NCM and control sample. Spectra were acquired on a 600-MHz Varian nuclear magnetic resonance (^{1}HNMR) spectrometer [Varian Limited, Oxford, United Kingdom] by using the Carr-Purcell-Meiboom-Gill (CPMG) pulse sequence at 25 °C. Spectra were acquired with 16,384 data points and 256 scans. Water suppression was achieved during the relaxation delay (3.0 s). ^{1}HNMR spectra were referenced to TSP and were processed manually with Chenomx NMR Suite [Version 8.3; Chenomx Edmonton, Canada] by using a line broadening of 0.2 Hz, and all spectra were phase and baseline corrected. Using 0.005 ppm bins, spectra were converted into 1360 spectral regions. The water region (4.3 to 5.5 ppm) was excluded, and data normalised to the total area of the spectral integral. Identification of discriminating metabolites was also performed using Chenomx NMR Suite. Metabolites were profiled in the Chenomx NMR Suite.

Body composition analysis by computed tomography

Computed tomography (CT) scans were obtained at diagnosis using a Discovery ST CT scanner [GE Healthcare, Little Chalfont, UK]. Images were analysed at L3 and the cross-sectional area in cm^2 of the various tissue compartments was determined using TomoVision Sliceomatic version 5.0 software [TomoVision, Montreal, Canada], applying an automated algorithm utilizing CT Hounsfield unit threshold of −29 to 150 for skeletal muscle and −50 to −150 for adipose tissue [16–18].

Visceral fat area (VFA) was calculated by a radiologist using a previously standardised and validated technique, and patients with a VFA greater than 163.8cm^2 (males) and 80.1cm^2 (females) were classified as obese [17].

Statistical analysis

GraphPad Prism 5 software was used to perform statistical analysis. All data is expressed as mean ± SEM. Specific statistical test indicated in each figure legend. Correlations were performed using Pearson correlation analysis. Statistical significance considered at $p \leq 0.05$.

Multivariate statistical analysis was performed for the metabolomics data analyses with Simca- P + software (Version 13.0.3; Umetrics, Umea°, Sweden). Unsupervised principal component analysis (PCA) was applied to the metabolomics data to explore any trends in the data for the various comparison groups, followed by partial least square discriminant analysis (PLS-DA) and orthogonal partial least squares discriminant analysis (OPLS-DA). The goodness-of-fit parameter (R^2) and the predictive ability parameter (Q^2) was used to describe the quality of all models. An independent *t*-test was performed on discriminating metabolite areas between comparison groups using IBM SPSS Statistics version 24. Statistical significance was considered if $p \leq 0.05$.

Results

Patient characteristics

All clinical data for rectal cancer and control patients is shown in Table 1.

Table 1
Patient characteristics.

			Percent (%)
Age (rectal cancer patients)	Mean ± SD	65.16 ± 10.14	
	Range	53–89	
Age (control patients)	Mean ± SD	58.75 ± 11.42	
	Range	44–76	
Gender (rectal cancer patients)	Male (n)	8	66.67
	Female (n)	4	33.33
Gender (control patients)	Male (n)	3	37.5
	Female (n)	5	62.5
Obesity status (visceral fat area)	Obese	8	66.67
	Non obese	4	33.33
Histology	Adenocarcinoma (n)	12	100
Stage of differentiation	Moderate (n)	12	100
T stage	T1 (n)	1	8.33
	T2 (n)	2	16.67
	T3 (n)	8	66.67
	T4 (n)	1	8.33
N stage	N0 (n)	6	50
	N1 (n)	5	41.67
	N2 (n)	1	8.33
M stage	M0 (n)	11	91.67
	M1 (n)	1	8.33
Neoadjuvant CRT	Received neo-CRT (n)	6	50
Neoadjuvant CT	Received neo-CT only (n)	1	8.33
Neoadjuvant RT	Received neo-RT only (n)	1	8.33
Surgery[a]	Received surgery (n)	11	91.67
TRS[b]	0 (n)	2	28.57
	1 (n)	3	42.85
	2 (n)	1	14.28
	3 (n)	1	14.28

Abbreviations; CRT; chemoradiotherapy, CT; chemotherapy, RT; radiotherapy, TRS; tumour regression score.
[a] One patient unsuitable for surgery.
[b] TRS available for 7 patients, percent (%) expressed as percent (%) of those with TRS score.

RIBE induction ex vivo induces significant changes in oxidative phosphorylation and glycolysis in bystander rectal cancer cells

Following 24-h treatment with either TCM or NCM, OCR, a measure of OXPHOS, and ECAR, a measure of glycolysis, were assessed. Significant reductions in OCR were observed in bystander cells exposed to NCM from irradiated normal rectal tissue, when compared to those exposed to the NCM from the mock-irradiated normal rectal tissue ($p = 0.01$). Similarly, there was a significant reduction in OCR in SW837 bystander cells exposed to TCM from irradiated rectal cancer tissue compared to those exposed to TCM from mock-irradiated rectal cancer tissue ($p = 0.03$) (Fig. 1A). Bystander SW837 rectal cancer cells treated for 24 h with TCM from irradiated rectal cancer biopsies, showed a significant reduction in ECAR, when compared to SW837 cells treated with TCM from mock-irradiated biopsies ($p = 0.014$) (Fig. 1B).

OCR:ECAR ratio was not significantly different in SW837 cells treated with NCM from mock-irradiated or irradiated normal rectal tissue ($p = 0.25$), or cancer tissue ($p = 0.38$). No difference was observed in OCR: ECAR ratio between SW837 cells treated with NCM or TCM ($p = 0.21$) (Fig. 1C).

This has demonstrated for the first time, real-time metabolic alterations in bystander cells following exposure to TCM and NCM from human rectal biopsies. Moreover, we have demonstrated a differential response in bystander cells exposed to TCM from malignant rectal tissue and NCM from normal rectal tissue, with alterations in glycolysis only observed in bystander cells exposed to TCM from malignant tissue.

RIBE induction ex vivo in both normal rectal tissue and rectal cancer tissue causes significant reductions in basal respiration, ATP production and maximal respiration in bystander SW837 cells

Basal respiration was significantly lower in SW837 cells exposed to NCM from irradiated normal rectal tissue, when compared to SW837 cells exposed to NCM from mock-irradiated normal rectal tissue ($p = 0.009$). Similarly, basal respiration was significantly lower in SW837 cells treated with TCM from irradiated rectal cancer tissue, when compared to mock-irradiated rectal cancer tissue ($p = 0.029$) (Fig. 2A).

A significant reduction in ATP production was observed in SW837 bystander cells treated with NCM from irradiated biopsies, when compared to SW837 cells exposed to NCM from mock-irradiated biopsies ($p = 0.039$). ATP production was significantly lower in SW837 cells treated with TCM from irradiated rectal cancer biopsies, when compared to mock-irradiated rectal cancer biopsies ($p = 0.043$). Significantly lower levels of ATP production were observed in SW837 cells treated with TCM from mock-irradiated biopsies, when compared to those treated with NCM from mock-irradiated biopsies ($p = 0.011$) (Fig. 2B).

Maximal respiration was significantly reduced in SW837 cells treated with NCM from irradiated normal rectal tissue, when compared to those treated with NCM from mock-irradiated tissue ($p = 0.009$). SW837 cells exposed to TCM from irradiated rectal cancer tissue showed a significant reduction in maximal respiration, when compared to SW837 cells treated with TCM from mock-irradiated rectal cancer tissue ($p = 0.017$) (Fig. 2C).

Proton leak was significantly reduced in SW837 cells treated with TCM from irradiated rectal cancer biopsies compared to mock-irradiated rectal cancer biopsies ($p = 0.02$). The difference in proton leak between SW837 cells treated with NCM from mock-irradiated or irradiated normal rectal tissue failed to reach statistical significance ($p = 0.09$) (Fig. 2D). There was no significant difference in non-mitochondrial respiration between SW837 cells treated with NCM from either mock-irradiated or irradiated normal rectal tissue ($p = 0.59$) or cancer tissue ($p = 0.60$) (Fig. 2E).

To date, the majority of bystander work has utilised *in vitro* models, however, our work recapitulates the complexity of the tumour and normal microenvironment encompassing the 3D architecture and multiple cell types. This is the first study to profile real-time metabolic changes in cells following exposure to culture media from human rectal cancer and normal rectal biopsies.

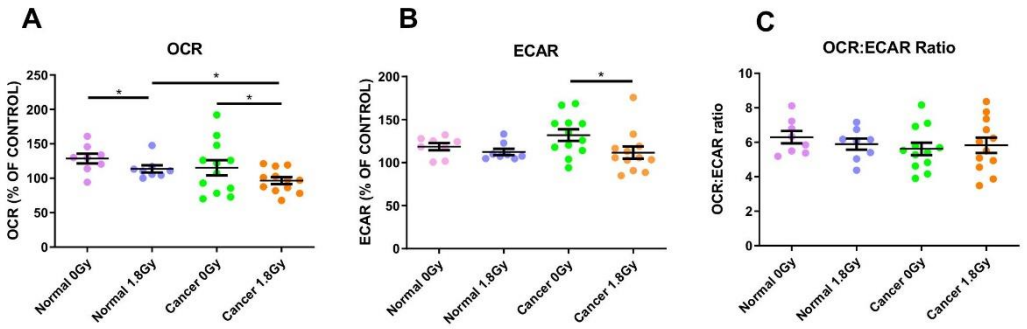

Fig. 1. Effect of *ex vivo* RIBE induction in normal rectal tissue and rectal cancer tissue on OCR, ECAR and OCR:ECAR ratio in bystander SW837 cells. (A) *Ex vivo* RIBE induction in both normal rectal and rectal cancer tissue causes significant reductions in OCR in bystander SW837 cells, when compared to cells exposed to the unirradiated tissue secretome. (B) ECAR is significantly reduced in bystander SW837 cells treated with TCM from irradiated rectal cancer tissue compared to mock-irradiated rectal cancer tissue. (C) OCR:ECAR ratio is not significantly different in bystander SW837 cells treated with NCM or TCM from irradiated *ex vivo* explants compared to their unirradiated controls. All data expressed as mean ± SEM. Statistical analysis was performed by paired *t*-test for 0Gy *vs* 1.8Gy when comparing the same tissue and unpaired *t*-test when comparing different tissue. n = 8 normal, n = 12 cancer, $^{*}p < 0.05$.

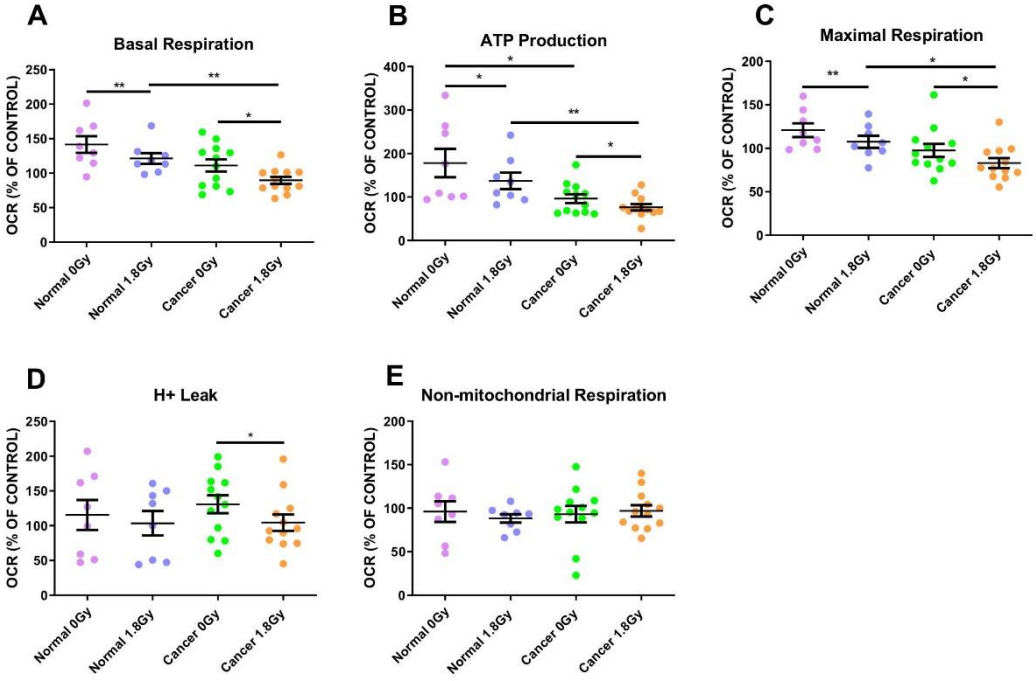

Fig. 2. Effect of *ex vivo* RIBE induction on SW837 bystander basal respiration, ATP production, maximal respiration, proton leak and non-mitochondrial respiration. (A) RIBE induction in *ex vivo* normal rectal and rectal cancer tissue induces significant reductions in basal respiration in bystander SW837 cells, when compared to cells exposed to the unirradiated tissue secretome. (B) ATP production is reduced in bystander SW837 cells treated with NCM and TCM from irradiated normal and rectal cancer tissue, respectively. ATP production is significantly reduced in bystander cells treated with TCM from the cancer secretome compared to NCM from the normal rectal secretome. (C) *Ex vivo* RIBE induction in both normal rectal and rectal cancer tissue significantly reduces maximal respiration in bystander SW837 rectal cancer cells. (D) Proton leak was significantly lower in bystander cells treated with TCM from the irradiated rectal cancer secretome (E) No significant differences were observed in non-mitochondrial respiration. All data expressed as mean ± SEM. Statistical analysis was performed by paired *t*-test for 0Gy *vs* 1.8Gy when comparing the same tissue and unpaired *t*-test when comparing different tissue. n = 8 normal, n = 12 cancer, $^{**}p < 0.01$, $^{*}p < 0.05$.

Rectal cancer secretome induces a significant increase in reactive oxygen species levels compared to the normal rectal secretome in bystander SW837 cells

ROS levels were significantly higher in SW837 cells following TCM treatment from mock-irradiated rectal cancer tissue, when compared to NCM from mock-irradiated normal rectal tissue ($p = 0.04$). The difference in ROS levels in SW837 cells treated with TCM from irradiated rectal cancer tissue, when compared to SW837 cells treated with NCM from irradiated normal rectal tissue was not significant ($p = 0.08$) nor did ROS levels change between SW837 cells treated with NCM from either irradiated or mock-irradiated normal rectal tissue ($p = 0.21$), or between bystander cells treated with TCM from irradiated or mock-irradiated rectal cancer tissue ($p = 0.54$) (Fig. 3A). No changes in mtMP were detected in bystander cells exposed to all *ex vivo* conditions (Fig. 3B).

These results suggest that the rectal cancer microenvironment induces higher levels of oxidative stress compared to the normal rectal microenvironment, but that RIBE *per se* does not alter mitochondrial function following 24 h exposure to TCM or NCM.

Metabolomic profiling of NCM and TCM from mock-irradiated and irradiated normal rectal and rectal cancer tissue

To better understand what metabolites may be driving these observed mitochondrial and metabolic bystander events, metabolomic screening was performed. A weak PLS-DA model was obtained for TCM from irradiated rectal cancer tissue *vs* NCM from irradiated normal rectal tissue ($R^2x = 0.591$, $Q2 = 0.153$), indicating no major changes in the global metabolomic profile. No other changes in the global metabolomic profile were observed when comparing the mock-irradiated and irradiated samples. However, profiling of specific metabolites revealed that the amino acid leucine was significantly different between NCM from irradiated normal rectal tissue, when compared to TCM from irradiated rectal cancer tissue ($p = 0.041$) (Fig. 4A). Leucine levels were reduced in the TCM from irradiated rectal cancer tissue compared to NCM from irradiated normal rectal tissue (Supp. Table 1). There were no significant changes in levels of acetate, alanine, ethanol, isoleucine, lactate, methionine, *N*-Acetyl-L-alanine, phenylalanine or valine (Fig. 4B–J).

Linking mitochondrial function to energy metabolism

In order to determine if there was any relationship between altered energy metabolism and mitochondrial function, we correlated ROS and mtMP levels with metabolic readouts obtained from the Seahorse. There was a significant inverse correlation observed between ROS levels and OCR ($R = -0.8101$, $p = 0.002$), basal respiration ($R = -0.8745$, $p = 0.0004$) and maximal respiration ($R = -0.6696$, $p = 0.02$) in bystander cells treated with TCM from mock-irradiated rectal cancer tissue. Similarly, ROS correlated inversely with OCR ($R = -0.8105$, $p = 0.02$), basal respiration ($R = -0.8194$, $p = 0.02$), maximal respiration ($R = -0.8101$, $p = 0.02$) and ATP production ($R = -0.7718$, $p = 0.04$) in NCM from mock-irradiated normal rectal tissue. OCR:ECAR ratio significantly positively correlated with ROS levels in bystander cells treated with the secretome of both mock-irradiated ($R = 0.8136$, $p = 0.002$) and irradiated ($R = 0.9064$, $p = 0.0001$) rectal cancer tissue. Proton leak was inversely correlated with ROS levels in cells treated with the rectal cancer secretome of mock-irradiated tissue ($R = -0.7988$, $p = 0.003$). An inverse correlation was observed between ROS and maximal respiration ($R = -0.7648$, $p = 0.04$) and proton leak ($R = -0.7554$, $p = 0.04$) in the secretome of irradiated normal rectal tissue and a positive correlation between ROS and non-mitochondrial respiration was observed in the same tissue ($R = 0.8315$, $p = 0.02$). There was an inverse correlation between OCR and ROS in bystander cells treated with TCM from irradiated rectal cancer tissue ($R = -0.7223$, $p = 0.01$) (Tables 2 and 3).

There was a significant inverse correlation between ROS and mtMP in bystander SW837 cells treated with TCM from mock-irradiated rectal cancer tissue ($R = -0.7229$, $p = 0.01$). This result was expected since increases in ROS are known to cause depolarisation of mtMP which in turn triggers mitophagy [19]. There were no significant correlations between ROS and mtMP in bystander cells treated with TCM from irradiated rectal cancer tissue or NCM from either irradiated or mock-irradiated normal rectal tissue (Table 3).

mtMP correlated with OCR ($R = 0.7038$, $p = 0.01$), basal respiration ($R = 0.8013$, $p = 0.003$), H+ leak ($R = 0.7147$, $p = 0.01$) and maximal respiration ($R = 0.6305$, $p = 0.03$) in bystander cells treated with TCM from mock-irradiated rectal cancer tissue. Similarly, there was a positive correlation between mtMP and OCR ($R = 0.6343$, $p = 0.03$) and maximal respiration ($R = 0.6817$, $p = 0.02$) in bystander cells treated with TCM from irradiated rectal cancer tissue (Table 4).

We analysed all metabolic and mitochondrial function data according to T stage and N stage and no significant differences emerged between any metabolic readout or mitochondrial function parameter in either the unirradiated or irradiated malignant tissue.

Linking bystander cell metabolism to metabolite levels in the secretome of normal and cancer tissue

In order to determine if there was any relationship between metabolite levels in the secretome of normal rectal tissue and rectal cancer tissue both pre- and post-radiation and bystander cellular metabolism, we conducted correlation analysis to identify any relationship between these factors. We

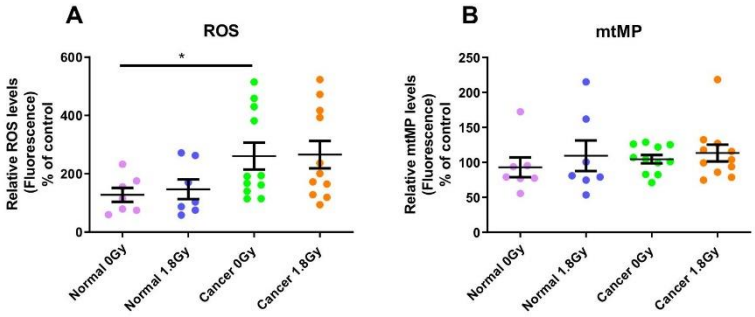

Fig. 3. The cancer secretome increases ROS levels in bystander SW837 rectal cancer cells. (A) ROS levels are significantly higher in bystander SW837 cells treated with TCM from rectal cancer tissue (n = 11) compared to cells treated with NCM from normal rectal tissue (n = 7). (B) No changes in mtMP were detected in bystander cells exposed to all *ex vivo* conditions. All data expressed as mean ± SEM. Statistical analysis was performed by paired *t*-test for 0Gy *vs* 1.8Gy when comparing the same tissue and unpaired *t*-test when comparing different tissue. $^*p < 0.05$.

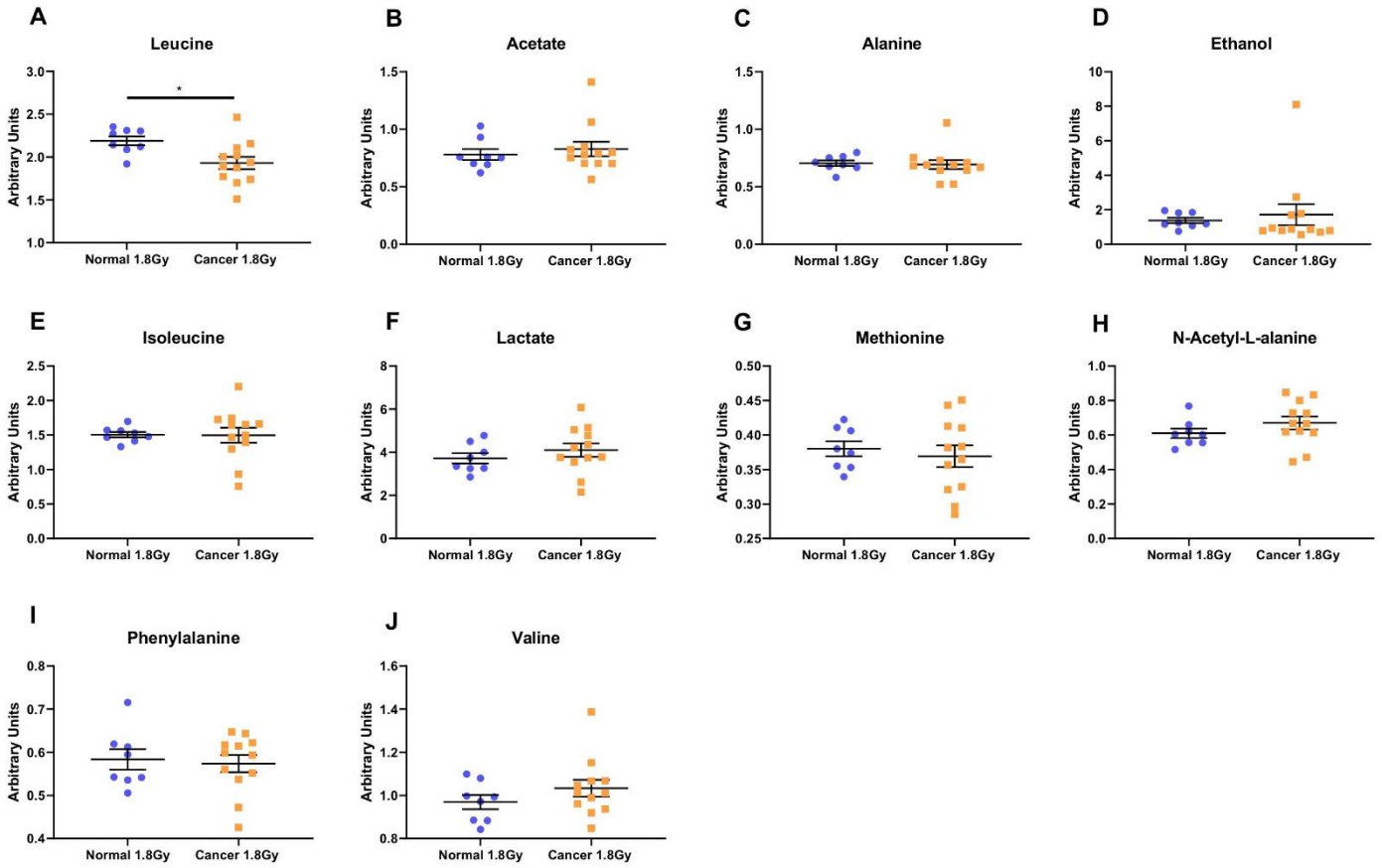

Fig. 4. Leucine levels are reduced in the secretome of irradiated rectal cancer tissue compared to irradiated normal rectal tissue. (A) Leucine levels are significantly reduced in the secretome of irradiated rectal cancer tissue compared to irradiated normal rectal tissue. There was no significant difference in (B) acetate (C) alanine (D) ethanol (E) isoleucine (F) lactate (G) methionine (H) *N*-Acetyl-L-alanine (I) phenylalanine or (J) valine levels between the irradiated rectal cancer secretome and the irradiated normal rectal secretome. All data expressed as mean ± SEM. Statistical analysis was performed by unpaired *t*-test. $^{*}p < 0.05$. n = 8 normal, n = 12 cancer.

Table 2
Correlation between ROS levels and metabolic parameters in normal tissue.

NORMAL 0GY					NORMAL 1.8GY				
FACTOR (% of control)	R value	p-value	Significance	n	FACTOR (% of control)	R value	p-value	Significance	n
OCR	-0.8105	0.02	*	7	Non-mitochondrial respiration	0.8315	0.02	*	7
Basal respiration	-0.8194	0.02	*	7	Maximal respiration	-0.7648	0.04	*	7
ATP production	-0.7718	0.04	*	7	H+ leak	-0.7554	0.04	*	7
Maximal respiration	-0.8101	0.02	*	7					

*$p < 0.05$,
**$p < 0.01$,
***$p < 0.001$

Table 3
Correlation between ROS levels and metabolic parameters in cancer tissue.

CANCER 0GY					CANCER 1.8GY				
FACTOR (% of control)	R value	p-value	Significance	n	FACTOR (% of control)	R value	p-value	Significance	n
OCR	-0.8101	0.002	**	11	OCR	-0.7223	0.01	*	11
Basal Respiration	-0.8745	0.0004	***	11	OCR:ECAR Ratio	0.9064	0.0001	***	11
H+ leak	-0.7988	0.003	**	11					
Maximal respiration	-0.6696	0.02	*	11					
OCR:ECAR Ratio	0.8136	0.002	**	11					
mtMP	-0.7229	0.01	*	11					

*$p < 0.05$,
**$p < 0.01$,
***$p < 0.001$

found a significant correlation between OCR in bystander cells and methionine levels in the secretome of mock-irradiated normal rectal tissue (R = 0.7139, $p = 0.04$). We also found correlations between non-mitochondrial respiration and alanine (R = 0.7452, $p = 0.03$) and phenylalanine (R = 0.8073, $p = 0.01$) levels in the secretome of mock-irradiated normal rectal tissue. Proton leak correlated inversely with phenylalanine (R = −0.7501, $p = 0.03$) OCR:ECAR ratio in bystander cells correlated with levels of isoleucine (R = 0.7657, $p = 0.02$), *N*-Acetyl-L-alanine (R = 0.8154, $p = 0.01$), phenylalanine (R = 0.7542, $p = 0.03$), valine (R = 0.8357, $p = 0.009$) and alanine (R = 0.7874, $p = 0.02$) in mock-irradiated normal rectal tissue. In bystander cells exposed to NCM from irradiated normal rectal tissue, OCR:ECAR ratio correlated inversely with both acetate (R = −0.7736, $p = 0.02$) and lactate (R= −0.7161, $p = 0.04$) (Table 5).

In bystander cells treated with TCM from mock-irradiated rectal cancer tissue, non-mitochondrial respiration correlated inversely with ethanol levels in the secretome of mock-irradiated rectal cancer tissue (R = −0.7399, $p = 0.005$). In bystander cells treated with TCM from irradiated rectal cancer tissue, OCR correlated with methionine levels in the secretome of this TCM (R = 0.5812, $p = 0.04$). Basal respiration in bystander cells treated with TCM from irradiated rectal cancer tissue correlated with methionine (R = 0.6561, $p = 0.02$) and *N*-Acetyl-L-alanine (R = 0.5760, $p = 0.05$). Maximal respiration also correlated with methionine (R = 0.7315, $p = 0.006$). Interestingly, OCR:ECAR ratio in bystander cells treated with TCM from irradiated rectal cancer tissue correlated inversely with methionine (R = −0.7017, $p = 0.01$), *N*-Acetyl-L-alanine (R = −0.7165, $p = 0.008$) and alanine (R = −0.7045, $p = 0.01$). (Table 6). This is a differential response to the cells treated with NCM from irradiated normal rectal tissue.

This highlights the differential relationship between altered metabolites and metabolic parameters in bystander cells treated with NCM and TCM depending on whether or not the tissue was irradiated.

Linking body composition analysis to metabolism and mitochondrial function in bystander cells and secreted metabolite levels in the secretome of rectal cancer tissue

It has been reported that overweight or obese rectal cancer patients have a poorer response to neoadjuvant treatment compared to their counterparts of a normal weight [20,21] as well as worse local control following neoadjuvant treatment and surgery [22]. We sought to understand the relationship between body composition and bystander cellular response to TCM from both irradiated and mock-irradiated rectal cancer biopsies.

We found a significant correlation between ECAR in bystander SW837 cells treated with TCM from irradiated rectal cancer biopsies and VFA (R = 0,6446, $p = 0.02$) and skeletal muscle mass (R = 0.8034, $p = 0.001$). There was also a significant correlation between ATP production in bystander SW837 cells treated with TCM from irradiated rectal cancer biopsies and VFA (R = 0.6204, $p = 0.03$) (Table 7). Of note, these observations only occurred in the bystander cells treated with TCM from

Table 4
Correlation between mtMP levels and metabolic parameters in SW837 cells treated with TCM from cancer tissue.

Cancer 0GY					Cancer 1.8GY				
FACTOR (% of control)	R value	p-value	Significance	n	FACTOR (% of control)	R value	p-value	Significance	n
OCR	0.7038	0.01	*	11	OCR	0.6343	0.03	*	11
Basal respiration	0.8013	0.003	**	11	Maximal respiration	0.6817	0.02	*	11
H+ leak	0.7147	0.01	*	11					
Maximal respiration	0.6305	0.03	*	11					

*$p < 0.05$,
**$p < 0.01$,
***$p < 0.001$

Table 5
Correlation between metabolic parameters in bystander cells and metabolites in the secretome of normal rectal tissue.

NORMAL 0GY					NORMAL 1.8GY				
FACTOR (% of control)	Metabolite	R value	p-value	n	FACTOR (% of control)	Metabolite	R value	p-value	n
OCR	Methionine	0.7139	0.04	8	OCR:ECAR Ratio	Acetate	-0.7736	0.02	8
Non mitochondrial respiration	Alanine	0.7452	0.03	8	OCR:ECAR Ratio	Lactate	-0.7161	0.04	8
Non mitochondrial respiration	Phenylalanine	0.8073	0.01	8					
H+ leak	Phenylalanine	-0.7501	0.03	8					
OCR:ECAR Ratio	Isoleucine	0.7657	0.02	8					
OCR:ECAR Ratio	N-Acetyl L-alanine	0.8154	0.01	8					
OCR:ECAR Ratio	Phenylalanine	0.7542	0.03	8					
OCR:ECAR Ratio	Valine	0.8357	0.009	8					
OCR:ECAR Ratio	Alanine	0.7874	0.02	8					

irradiated rectal cancer biopsies, perhaps suggesting that obesity status may influence the behaviour of bystander cells following radiation. It is well documented that upregulation of glycolysis is associated with a radioresistant phenotype [23–26] and induces DNA repair pathways [27]. Therefore, it may be possible that factors secreted from the TME of obese individuals may alter the metabolism of tumour cells and facilitate a more radioresistant phenotype.

We found significant correlations between VFA and leucine ($R = 0.6395, p = 0.02$) and ethanol ($R = 0.5972, p = 0.04$) and intermuscular fat and ethanol ($R = 0.6483, p = 0.02$) levels in the TCM from mock-irradiated rectal cancer tissue (Table 8). This data suggests that obesity status may influence the local milieu of rectal cancer tissue by altering metabolite levels in the TME.

Discussion

Using a novel human *ex vivo* explant model of rectal cancer and normal rectal tissue, we have shown for the first time that RIBE induction *ex vivo* causes significant alterations in bystander cellular energy metabolism. We have demonstrated that metabolite profiles, specifically leucine concentrations, differed in the secretome between irradiated rectal cancer tissue and irradiated normal rectal tissue, with leucine levels being reduced in the irradiated cancer secretome compared to the irradiated normal secretome. We have demonstrated significant differences in ROS but not mtMP in bystander cells exposed to the rectal cancer, when compared to the normal rectal secretome. We found significant correlations between VFA and ECAR and ATP production in bystander cells treated with TCM from irradiated rectal cancer biopsies, while ECAR in these bystander cells also correlated with skeletal muscle mass.

The majority of bystander work to date has employed *in vitro* models and 3D tissue models [28], with others employing *in vivo* models such as fish [29,30] and rodents [31]. Our work in this study explores the complexity of the tumour microenvironment (TME) and the normal rectal microenvironment, using *ex vivo* explants. Importantly, these whole biopsy explants recapitulate the microenvironment of both normal and malignant rectal tissue. This allows us to capture the effect of radiation on all cell types within these microenvironments and elucidate if the response of bystander cancer cells to RIBE signals differs between normal and malignant tissue.

We have shown that *ex vivo* RIBE induction in both normal rectal tissue and rectal cancer tissue causes significant reductions in OXPHOS in bystander SW837 rectal cancer cells. Le et al. have previously shown reduced complex I activity in the mitochondria of bystander HCT116 CRC cells exposed to RIBE-induced biophoton signalling [32]. In our study, ATP production and maximal respiration were also significantly reduced following RIBE in bystander cells, which is in line with reduced OCR in these cells. Interestingly, a reduction in glycolysis was only observed following RIBE induction in malignant tissue. A more pronounced effect on glycolysis was expected in bystander cells exposed to TCM since malignant tissue is known to have a greater tendency to employ aerobic glycolysis compared to normal tissue [33]. To date, this is the first study to investigate the effect of *ex vivo* RIBE induction in rectal tissue on real-time cellular metabolism using Seahorse technology.

ROS are well-recognised participants in RIBE events [10,34,35]. Mitochondria are an important source of endogenous ROS and also, traversal of the nucleus with radiation was not required to exert RIBE effects [36] and antioxidants can abrogate RIBE [37]. Given the observed changes in mitochondrial metabolism in our study combined with the well-recognised role for the mitochondria in RIBE, we examined the effect of *ex vivo* RIBE induction on bystander rectal cancer cellular mitochondrial function, specifically ROS production and mtMP.

RIBE-induction *ex vivo* did not alter the mtMP or ROS levels in bystander SW837 rectal cancer cells. Similar results were obtained by Gorman et al. in bystander SW480 cells. However, the authors did report significantly reduced levels of mtMP in bystander cells exposed to TCM and NCM from irradiated CRC tissue and irradiated normal adjacent tissue compared to their unirradiated controls [12]. ROS are known to be short-lived molecules and studies have shown changes in ROS and mtMP levels as early as 4 h and 12 h, following exposure to conditioned media but levels of both ROS and mtMP returned to normal at 24 h [38]. It may be possible in our study that ROS and mtMP returned to baseline levels following 24-h treatment with TCM and NCM from irradiated tissue.

The rectal cancer secretome caused significant elevations in ROS levels in bystander SW837 cells compared to bystander cells exposed to the normal rectal secretome. It is a well-documented phenomenon that cancer cells have significantly higher levels of ROS compared to normal cells, owing to oncogenic transformation, including altered cellular metabolism, genetic mutation and a pro-tumorigenic microenvironment [39]. Elevated ROS promotes oncogenic DNA mutations and may activate oncogenic signalling pathways [40]. ROS may also be capable of initiating oncogenic signalling pathways such as EGFR [41] and MAPK [42] signalling pathways.

Table 6
Correlation between metabolic parameters in bystander cells and metabolites in the secretome of rectal cancer tissue.

CANCER 0GY					CANCER 1.8GY				
FACTOR (% of control)	Metabolite	R value	p-value	n	FACTOR (% of control)	Metabolite	R value	p-value	n
Non-mitochondrial respiration	Ethanol	-0.7399	0.005	12	OCR	Methionine	0.5812	0.04	12
					Basal Respiration	Methionine	0.6561	0.02	12
					Basal Respiration	N-Acetyl-L-alanine	0.5760	0.05	12
					Maximal Respiration	Methionine	0.7315	0.006	12
					OCR:ECAR Ratio	Methionine	-0.7017	0.01	12
					OCR:ECAR Ratio	N-Acetyl-L-alanine	-0.7165	0.008	12
					OCR:ECAR Ratio	Alanine	-0.7045	0.01	12

Table 7
Correlation between metabolic parameters and body composition analysis in bystander cells treated with TCM from irradiated rectal cancer biopsies i.e. Cancer 1.8Gy.

Body composition parameter	FACTOR (% of control)	R value	p-value	n
VFA	ECAR	0.6446	0.02	12
VFA	ATP production	0.6204	0.03	12
Skeletal muscle	ECAR	0.8034	0.001	12

Abbreviations: VFA; visceral fat area, ECAR; extracellular acidification rate (glycolysis)

Therefore, it is unsurprising that ROS levels were higher in bystander cells exposed to the rectal cancer microenvironment compared to the normal rectal microenvironment.

To better understand what metabolites may be driving these mitochondrial and metabolic bystander events, metabolomic screening was performed. PCA analysis of ^{1}HNMR spectra obtained from screening the TCM and NCM from both irradiated and mock-irradiated rectal cancer and normal rectal tissue allowed separation of the irradiated normal and the irradiated cancer tissue secretome. Further analysis of the metabolite profile of the TCM and NCM indicated reduced levels of leucine in the secretome of the irradiated rectal cancer tissue compared to the irradiated normal rectal tissue. The literature supports this observation. Arenas et al. have shown that serum leucine levels are significantly lower in breast cancer patients compared to control patients and following radiation therapy, leucine levels return to levels observed in control patients [43]. He et al. report higher levels of leucine within the pancreas of mice bearing pancreatic tumours compared to the pancreas of control mice [44]. Ching et al. found significantly lower levels of leucine in the plasma of cancer patients receiving chemotherapy [45]. The authors postulated that these observations were owing to enhanced uptake of leucine by cancer cells [43–45]. Since the metabolites in our study were not labelled, it was not possible to determine whether alterations in these metabolites were owing to altered secretion of metabolites by the tissue or altered uptake by cancer tissue. However, we believe it is likely owing to enhanced uptake of leucine by cancer cells, as has been reported in the literature. Following a full course of radiation therapy, Arenas et al. observed that leucine levels returned to levels observed in control patients. It is important to note that the changes in serum leucine concentrations post-radiotherapy were observed following a full treatment course of radiation therapy [43]. It may be possible that a single fraction of a clinically relevant dose of radiation, as used in our study may be insufficient to restore metabolite levels in the TME to that observed in non-cancerous tissue. Overall limited numbers of studies have investigated the difference in metabolites between normal and cancer tissue as well as the effect of radiation on metabolite levels. A limitation of our study is the number of participants, with 8 controls and 12 cancer patients; it may be possible that no difference in leucine levels observed between the unirradiated control samples and the unirradiated tumour samples is as a result of small numbers.

There was a significant inverse correlation between ROS and mtMP in bystander SW837 cells treated with TCM from mock-irradiated rectal cancer tissue. This result was expected since increases in ROS are known to cause depolarisation of mtMP which in turn triggers mitophagy [19]. We found significant inverse correlations between OCR and ROS levels in bystander SW837 rectal cancer cells treated with both NCM and TCM. This result was unexpected since previous work in our group has shown that ROS levels were higher in OAC cells with higher OCR [13]. However, since ROS are short-lived molecules it may be possible that higher ROS levels would be observed at earlier time-points, between 0 and 6 h.

Table 8
Correlation between body composition parameters and metabolites in the secretome of unirradiated rectal cancer tissue (Cancer 0Gy).

Body composition parameter	Metabolite	R value	*p*-Value	n
VFA	Leucine	0.6395	0.02	12
VFA	Ethanol	0.5972	0.04	12
Intermuscular fat	Ethanol	0.6483	0.02	12

Interestingly, we observed a significant correlation between ECAR and ATP production in bystander SW837 cells treated with TCM from irradiated rectal cancer biopsies and the patient's VFA. Of note, this observation only occurred in the bystander cells treated with TCM from irradiated rectal cancer biopsies, perhaps suggesting that obesity status may influence the behaviour of bystander cells following radiation. This is an interesting and clinically relevant result as it has been reported that overweight and obese patients have poorer responses to neoadjuvant treatment and worse outcomes in rectal cancer [20–22]. Moreover, when we correlated levels of metabolites in the secretome of mock-irradiated rectal cancer tissue we found significant correlations between VFA and leucine and ethanol. Also, intermuscular fat correlated with ethanol levels. This is an interesting observation and may suggest that obesity status may alter the TME by influencing the levels of metabolites. There were also correlations between metabolites in the microenvironment of both tumour and normal tissue pre- and post-radiation and bystander cellular metabolic parameters. Again, this suggests that altered metabolite levels cause alterations in cellular metabolism and the data suggests that obesity status impacts the levels of these metabolites.

It is well documented that upregulation of glycolysis is associated with a radioresistant phenotype [23–26] and induces DNA repair pathways [27]. Moreover, Lynam-Lennon et al. have demonstrated an enhancement of glycolysis when OAC cells were exposed to adipose conditioned media from obese patients [14]. Similarly, elevated ATP levels are associated with enhanced radioresistance [13], while reduction of ATP levels have been associated with increased radiosensitivity [15,46]. While further elucidation of the mechanisms linking obesity with poorer response rates in rectal cancer is needed, this data offers insight into the effect of bystander signals from rectal cancer biopsies and how obesity modulates the bystander response.

To the best of our knowledge, this is the first study to investigate *ex vivo* RIBE induction in normal rectal tissue from healthy controls compared to rectal cancer tissue and its effect on bystander cellular metabolism and mitochondrial function. While the role of the mitochondria and ROS are well established in RIBE events *in vitro*, this novel study extends the understanding of the role of the mitochondria to RIBE events using a human *ex vivo* model of disease. Radiation is used in both the neoadjuvant and adjuvant setting in rectal cancer patients but pCR is only observed in a small subset of patients in the neoadjuvant setting. Further understanding the biological effects of radiation on unirradiated cells near the irradiated volume and how this relates to treatment response may reveal potential therapeutic targets to enhance radiosensitivity in the neoadjuvant setting.

Supplementary data to this article can be found online at https://doi.org/10.1016/j.tranon.2020.100882.

CRediT authorship contribution statement

Aisling B Heeran: Conceptualisation, formal analysis, investigation, writing – original draft, visualisation, funding acquisition. **Helen P Berrigan:** Investigation, formal analysis, writing – review and editing. **Croí E. Buckley:** Investigation, writing – review and editing. **Heleena Moni Bottu:** Investigation, formal analysis, writing – review and editing. **Orla Prendiville:** Investigation, formal analysis, writing – review and editing. **Amy M. Buckley:** Resources, writing – review and editing. **Niamh Clarke:** Resources, writing – review and editing. **Noel E. Donlon:** Formal analysis, resources, writing – review and editing. **Timothy S. Nugent:** Resources, writing – review and editing. **Michael Durand:** Resources, writing – review and editing. **Cara Dunne:** Resources, writing – review and editing. **John O. Larkin:** Resources, writing – review and editing. **Brian Mehigan:** Resources, writing – review and editing. **Paul McCormick:** Resources, writing – review and editing. **Lorraine Brennan:** Conceptualisation, formal analysis, supervision, resources, visualisation, writing – review and editing. **Niamh Lynam-Lennon:** Conceptualisation, supervision, resources, writing – review and editing. **Jacintha O'Sullivan:** Conceptualisation, methodology, writing – original draft, writing – review and editing, supervision, resources, project administration.

Funding source

This work is supported by an Irish Research Council (Grant: GOIPG/2017/983).

Declaration of competing interest

The authors declare that they have no known competing financial interests or personal relationships that could have appeared to influence the work reported in this paper.

Acknowledgements

We would like to thank the patients who so kindly donated their samples and data to this research. We would like to acknowledge James Phelan and Jill O'Sullivan for their advice regarding statistics. We wish to thank our funders, the Irish Research Council (Grant: GOIPG/2017/983) for grant support for this work.

References

[1] F. Bray, J. Ferlay, I. Soerjomataram, R.L. Siegel, L.A. Torre, A. Jemal, Global cancer statistics 2018: GLOBOCAN estimates of incidence and mortality worldwide for 36 cancers in 185 countries, CA Cancer J Clin 68 (2018) 394–424.

[2] R. Glynne-Jones, L. Wyrwicz, E. Tiret, G. Brown, C. Rödel, A. Cervantes, D. Arnold, Rectal cancer: ESMO Clinical Practice Guidelines for diagnosis, treatment and follow-up†, Ann Oncol 28 (2017) 22–40.

[3] National Cancer Registry in Ireland. Cancer Incidence Projections for Ireland 2020–2045. Cork, Ireland; 2019.

[4] M. Araghi, I. Soerjomataram, M. Jenkins, J. Brierley, E. Morris, F. Bray, M. Arnold, Global trends in colorectal cancer mortality: projections to the year 2035, Int J Cancer 144 (2019) 2992–3000.

[5] F. Petrelli, F. Trevisan, M. Cabiddu, G. Sgroi, L. Bruschieri, E. Rausa, M. Ghidini, L. Turati, Total Neoadjuvant Therapy in Rectal Cancer: A Systematic Review and Meta-analysis of Treatment Outcomes, Ann Surg 271 (2020) 440–448.

[6] M. Maas, P.J. Nelemans, V. Valentini, P. Das, C. Rödel, L.J. Kuo, F.A. Calvo, J. García-Aguilar, R. Glynne-Jones, K. Haustermans, et al., Long-term outcome in patients with a pathological complete response after chemoradiation for rectal cancer: a pooled analysis of individual patient data, Lancet Oncol 11 (2010) 835–844.

[7] C. Mothersill, C. Seymour, Radiation-induced bystander effects — implications for cancer, Nat Rev Cancer 4 (2004) 158–164.

[8] K.M. Prise, J.M. O'Sullivan, Radiation-induced bystander signalling in cancer therapy, Nat Rev Cancer 9 (2009) 351–360.

[9] A.B. Heeran, H.P. Berrigan, J. O'Sullivan, The Radiation-Induced Bystander Effect (RIBE) and its Connections with the Hallmarks of Cancer, Radiat Res 192 (2019) 668–679.

[10] L. Tartier, S. Gilchrist, S. Burdak-Rothkamm, M. Folkard, K.M. Prise, Cytoplasmic Irradiation Induces Mitochondrial-Dependent 53BP1 Protein Relocalization in Irradiated and Bystander Cells, Cancer Res 67 (2007) 5872–5879.

[11] S. Rajendran, S.H. Harrison, R.A. Thomas, J.D. Tucker, The Role of Mitochondria in the Radiation-Induced Bystander Effect in Human Lymphoblastoid Cells, Radiat Res 175 (2011) 159–171.

[12] S. Gorman, E. Fox, D. O'Donoghue, K. Sheahan, J. Hyland, H. Mulcahy, L.A. Loeb, J. O'Sullivan, Mitochondrial mutagenesis induced by tumor-specific radiation bystander effects, J Mol Med (Berl) 88 (2010) 701–708.

[13] N. Lynam-Lennon, S.G. Maher, A. Maguire, J. Phelan, C. Muldoon, J.V. Reynolds, J. O'Sullivan, Altered mitochondrial function and energy metabolism is associated with a radioresistant phenotype in oesophageal adenocarcinoma, PLoS One 9 (2014), e100738, .

[14] N. Lynam-Lennon, R. Connaughton, E. Carr, A.M. Mongan, N.J. O'Farrell, R.K. Porter, L. Brennan, G.P. Pidgeon, J. Lysaght, J.V. Reynolds, et al., Excess visceral adiposity induces alterations in mitochondrial function and energy metabolism in esophageal adenocarcinoma, BMC Cancer 14 (2014) 907.

[15] A.M. Buckley, M.R. Dunne, N. Lynam-Lennon, S.A. Kennedy, A. Cannon, A.L. Reynolds, S.G. Maher, J.V. Reynolds, B.N. Kennedy, J. O'Sullivan, Pyrazinib (P3), [(E)-2-(2-Pyrazin-2-yl-vinyl)-phenol], a small molecule pyrazine compound enhances radiosensitivity in oesophageal adenocarcinoma, Cancer Lett 447 (2019) 115–129.

[16] M. Mourtzakis, C.M.M. Prado, J.R. Lieffers, T. Reiman, L.J. McCargar, V.E. Baracos, A practical and precise approach to quantification of body composition in cancer patients using computed tomography images acquired during routine care, Appl Physiol Nutr Metab 33 (2008) 997–1006.

[17] S.L. Doyle, A.M. Bennett, C.L. Donohoe, A.M. Mongan, J.M. Howard, F.E. Lithander, G. P. Pidgeon, J.V. Reynolds, J. Lysaght, Establishing computed tomography-defined visceral fat area thresholds for use in obesity-related cancer research, Nutr Res 33 (2013) 171–179.

[18] C.M.M. Prado, J.R. Lieffers, L.J. McCargar, T. Reiman, M.B. Sawyer, L. Martin, V.E. Baracos, Prevalence and clinical implications of sarcopenic obesity in patients with solid tumours of the respiratory and gastrointestinal tracts: a population-based study, Lancet Oncol 9 (2008) 629–635.

[19] I. Kim, S. Rodriguez-Enriquez, J.J. Lemasters, Selective degradation of mitochondria by mitophagy, Arch Biochem Biophys 462 (2007) 245–253.

[20] Y. Sun, Z. Xu, H. Lin, X. Lu, Y. Huang, S. Huang, X. Wang, P. Chi, Impact of body mass index on treatment outcome of neoadjuvant chemoradiotherapy in locally advanced rectal cancer, Eur J Surg Oncol 43 (2017) 1828–1834.

[21] I.J. Park, Y.N. You, J.M. Skibber, M.A. Rodriguez-Bigas, P. Das, C. Eng, S. Kopetz, R.A. Wolff, C.H. Crane, S. Krishnan, et al., Oncologic and Functional Hazards of Obesity Among Patients With Locally Advanced Rectal Cancer Following Neoadjuvant Chemoradiation Therapy, Am J Clin Oncol 40 (2017) 277–282.

[22] Y. Choi, Y.H. Lee, S.K. Park, H. Cho, K.J. Ahn, Association between obesity and local control of advanced rectal cancer after combined surgery and radiotherapy, Radiat Oncol J 34 (2016) 113–120.

[23] V. Quennet, A. Yaromina, D. Zips, A. Rosner, S. Walenta, M. Baumann, W. Mueller-Klieser, Tumor lactate content predicts for response to fractionated irradiation of human squamous cell carcinomas in nude mice, Radiother Oncol 81 (2006) 130–135.

[24] T. Shimura, N. Noma, Y. Sano, Y. Ochiai, T. Oikawa, M. Fukumoto, N. Kunugita, AKT-mediated enhanced aerobic glycolysis causes acquired radioresistance by human tumor cells, Radiother Oncol 112 (2014) 302–307.

[25] H. Zhao, H. Jiang, Z. Li, Y. Zhuang, Y. Liu, S. Zhou, Y. Xiao, C. Xie, F. Zhou, Y. Zhou, 2-Methoxyestradiol enhances radiosensitivity in radioresistant melanoma MDA-MB-435R cells by regulating glycolysis via HIF-1α/PDK1 axis, Int J Oncol 50 (2017) 1531–1540.

[26] F. Zhao, J. Ming, Y. Zhou, L. Fan, Inhibition of Glut1 by WZB117 sensitizes radioresistant breast cancer cells to irradiation, Cancer Chemother Pharmacol 77 (2016) 963–972.

[27] A.N. Bhatt, A. Chauhan, S. Khanna, Y. Rai, S. Singh, R. Soni, N. Kalra, B.S. Dwarakanath, Transient elevation of glycolysis confers radio-resistance by facilitating DNA repair in cells, BMC Cancer 15 (2015) 335.

[28] O.A. Sedelnikova, A. Nakamura, O. Kovalchuk, I. Koturbash, S.A. Mitchell, S.A. Marino, D.J. Brenner, W.M. Bonner, DNA Double-Strand Breaks Form in Bystander Cells after Microbeam Irradiation of Three-dimensional Human Tissue Models, Cancer Res 67 (2007) 4295–4302.

[29] V.W.Y. Choi, C.Y.P. Ng, A. Kobayashi, T. Konishi, N. Suya, T. Ishikawa, S.H. Cheng, K.N. Yu, Bystander Effect between Zebrafish Embryos in Vivo Induced by High-Dose X-rays, Environ Sci Technol 47 (2013) 6368–6376.

[30] C. Mothersill, R.W. Smith, N. Agnihotri, C.B. Seymour, Characterization of a radiation-induced stress response communicated in vivo between zebrafish, Environ Sci Technol 41 (2007) 3382–3387.

[31] C. Mothersill, F. Lyng, C. Seymour, P. Maguire, S. Lorimore, E. Wright, Genetic Factors Influencing Bystander Signaling in Murine Bladder Epithelium after Low-Dose Irradiation In Vivo, Radiat Res 163 (2005) 391–399.

[32] M. Le, F.E. McNeill, C.B. Seymour, A. Rusin, K. Diamond, A.J. Rainbow, J. Murphy, C.E. Mothersill, Modulation of oxidative phosphorylation (OXPHOS) by radiation- induced biophotons, Environ Res 163 (2018) 80–87.

[33] R.A. Gatenby, R.J. Gillies, Why do cancers have high aerobic glycolysis? Nat Rev Cancer 4 (2004) 891–899.

[34] C. Shao, F.M. Lyng, M. Folkard, K.M. Prise, Calcium Fluxes Modulate the Radiation-Induced Bystander Responses in Targeted Glioma and Fibroblast Cells, Radiat Res 166 (2006) 479–487.

[35] S. Chen, Y. Zhao, G. Zhao, W. Han, L. Bao, K.N. Yu, L. Wu, Up-regulation of ROS by mitochondria-dependent bystander signaling contributes to genotoxicity of bystander effects, Mutat Res 666 (2009) 68–73.

[36] C. Shao, M. Folkard, B.D. Michael, K.M. Prise, Targeted cytoplasmic irradiation induces bystander responses, Proc Natl Acad Sci U S A 101 (2004) 13495–13500.

[37] I. Emerit, N. Oganesian, T. Sarkisian, R. Arutyunyan, A. Pogosian, K. Asrian, A. Levy, L. Cernjavski, Clastogenic Factors in the Plasma of Chernobyl Accident Recovery Workers: Anticlastogenic Effect of Ginkgo biloba Extract, Radiat Res 144 (1995) 198–205.

[38] X. Wang, J. Zhang, J. Fu, J. Wang, S. Ye, W. Liu, C. Shao, Role of ROS-mediated autophagy in radiation-induced bystander effect of hepatoma cells, Int J Radiat Biol 91 (2015) 452–458.

[39] S. Kumari, A.K. Badana, G MM, G S, R. Malla, Reactive Oxygen Species: A Key Constituent in Cancer Survival Biomark, Insights 13 (2018), 1177271918755391, .

[40] P.E. Porporato, N. Filigheddu, J.M.B. Pedro, G. Kroemer, L. Galluzzi, Mitochondrial metabolism and cancer, Cell Res 28 (2018) 265–280.

[41] G.Y. Liou, H. Döppler, K.E. DelGiorno, L. Zhang, M. Leitges, H.C. Crawford, M.P. Murphy, P. Storz, Mutant KRas-Induced Mitochondrial Oxidative Stress in Acinar Cells Upregulates EGFR Signaling to Drive Formation of Pancreatic Precancerous Lesions, Cell Rep 14 (2016) 2325–2336.

[42] F. Weinberg, R. Hamanaka, W.W. Wheaton, S. Weinberg, J. Joseph, M. Lopez, B. Kalyanaraman, G.M. Mutlu, G.R. Scott Budinger, N.S. Chandel, Mitochondrial metabolism and ROS generation are essential for Kras-mediated tumorigenicity, Proc Natl Acad Sci 107 (2010) 8788–8793.

[43] M. Arenas, E. Rodríguez, A. García-Heredia, S. Fernández-Arroyo, S. Sabater, R. Robaina, M. Gascón, M. Rodríguez-Pla, N. Cabré, F. Luciano-Mateo, et al., Metabolite normalization with local radiotherapy following breast tumor resection, PLoS One 13 (2018), e0207474, .

[44] X.H. He, W.T. Li, Y.J. Gu, B.F. Yang, H.W. Deng, Y.H. Yu, W.J. Peng, Metabonomic studies of pancreatic cancer response to radiotherapy in a mouse xenograft model using magnetic resonance spectroscopy and principal components analysis, World J Gastroenterol 19 (2013) 4200–4208.

[45] N. Ching, C. Grossi, G. Jham, J. Angers, H. Zurawinsky, C.Y. Ching, T.F. Nealon Jr., Plasma amino acid and serum unesterified fatty acid deficits and the effect of nutritional support in chemotherapy treatment, Surgery 95 (1984) 730–738.

[46] A. Chakravarti, G.G. Zhai, M. Zhang, R. Malhotra, D.E. Latham, M.A. Delaney, P. Robe, U. Nestler, Q. Song, J. Loeffler, Survivin enhances radiation resistance in primary human glioblastoma cells via caspase-independent mechanisms, Oncogene 23 (2004) 7494–7506.

cancers

MDPI

Article

The Protein Secretome Is Altered in Rectal Cancer Tissue Compared to Normal Rectal Tissue, and Alterations in the Secretome Induce Enhanced Innate Immune Responses

Aisling B. Heeran [1], Margaret R. Dunne [1], Maria E. Morrissey [1], Croí E. Buckley [1], Niamh Clarke [1], Aoife Cannon [1], Noel E. Donlon [1], Timothy S. Nugent [1], Michael Durand [2], Cara Dunne [2], John O. Larkin [2], Brian Mehigan [2], Paul McCormick [2], Niamh Lynam-Lennon [1] and Jacintha O'Sullivan [1,*]

[1] Trinity St. James's Cancer Institute, Trinity Translational Medicine Institute, Department of Surgery, Trinity College Dublin and St. James's Hospital, D08 W9RT Dublin 8, Ireland; heerana@tcd.ie (A.B.H.); dunnem12@tcd.ie (M.R.D.); miamorrissey@gmail.com (M.E.M.); bucklecr@tcd.ie (C.E.B.); clarken18@tcd.ie (N.C.); cannona@tcd.ie (A.C.); donlonn@tcd.ie (N.E.D.); nugentt@tcd.ie (T.S.N.); lynamlen@tcd.ie (N.L.-L.)

[2] GEMS, St. James's Hospital, D08 NHY1 Dublin 8, Ireland; durandm@tcd.ie (M.D.); cardunne@stjames.ie (C.D.); jlarkin@stjames.ie (J.O.L.); bmehigan@stjames.ie (B.M.); pmccormick@stjames.ie (P.M.)

* Correspondence: osullij4@tcd.ie; Fax: +353-(0)18964122

Simple Summary: Rectal cancer occurs in the lower part of the bowel, and approximately half of all rectal cancer patients receive chemoradiotherapy before surgery. In ~22% of cases the tumour is eradicated, but the reasons for different response rates between patients are largely unknown. Inflammation and the immune system are important players in the response to cancer treatment, but we do not fully understand the role they play in this clinical setting. We examined the levels of 54 inflammatory markers in normal (non-cancerous) rectal tissue and rectal cancer tissue, and we found that rectal cancer tissue was more inflammatory, and the levels of inflammatory markers correlated with obesity status. We found that irradiating rectal cancer tissue enhanced the ability of immune cells to induce an anti-tumour immune response.

Abstract: Locally advanced rectal cancer is treated with neoadjuvant-chemoradiotherapy; however, only ~22% of patients achieve a complete response, and resistance mechanisms are poorly understood. The role of inflammation and immune cell biology in this setting is under-investigated. In this study, we profiled the inflammatory protein secretome of normal (non-cancer) ($n = 8$) and malignant rectal tissue ($n = 12$) pre- and post-radiation in human ex vivo explant models and examined the influence of these untreated and treated secretomes on dendritic cell biology ($n = 8$ for cancer and normal). These resultant profiles were correlated with patient clinical characteristics. Nineteen factors were secreted at significantly higher levels from the rectal cancer secretome when compared to the normal rectal secretome; Flt-1, PlGF, IFN-γ, IL-6, IL-10, CCL20, CCL26, CCL22, CCL3, CCL4, CCL17, GM-CSF, IL-12/IL-23p40, IL-17A, IL-1α, IL-17A/F, IL-1RA, TSLP and CXCL10 ($p < 0.05$). Radiation was found to have differential effects on normal rectal tissue and rectal cancer tissue with increased IL-15 and CCL22 secretion following radiation from normal rectal tissue explants ($p < 0.05$), while no significant alterations were observed in the irradiated rectal cancer tissue. Interestingly, however, the irradiated rectal cancer secretome induced the most potent effect on dendritic cell maturation via upregulation of CD80 and PD-L1. Patient's visceral fat area correlated with secreted factors including CCL20, suggesting that obesity status may alter the tumour microenvironment (TME). These results suggest that radiation does not have a negative effect on the ability of the rectal cancer TME to induce an immune response. Understanding these responses may unveil potential therapeutic targets to enhance radiation response and mitigate normal tissue injury. Tumour irradiation in this cohort enhances innate immune responses, which may be harnessed to improve patient treatment outcome.

check for updates

Citation: Heeran, A.B.; Dunne, M.R.; Morrissey, M.E.; Buckley, C.E.; Clarke, N.; Cannon, A.; Donlon, N.E.; Nugent, T.S.; Durand, M.; Dunne, C.; et al. The Protein Secretome Is Altered in Rectal Cancer Tissue Compared to Normal Rectal Tissue, and Alterations in the Secretome Induce Enhanced Innate Immune Responses. *Cancers* **2021**, *13*, 571. https://doi.org/10.3390/cancers13030571

Academic Editor: Noel De Miranda

Received: 12 January 2021
Accepted: 29 January 2021
Published: 2 February 2021

Publisher's Note: MDPI stays neutral with regard to jurisdictional claims in published maps and institutional affiliations.

Copyright: © 2021 by the authors. Licensee MDPI, Basel, Switzerland. This article is an open access article distributed under the terms and conditions of the Creative Commons Attribution (CC BY) license (https://creativecommons.org/licenses/by/4.0/).

Keywords: rectal cancer; dendritic cells; inflammation; tumour immunology; radiotherapy

1. Introduction

Rectal cancer is a malignancy that occurs in the lower part of the large intestine. Approximately 700,000 cases of rectal cancer are diagnosed globally each year, and the annual death toll is approximately 310,000 [1]. The standard of care for locally advanced rectal cancer is neoadjuvant chemoradiotherapy (neo-CRT) [2]. While ~40–60% of patients achieve some level of downstaging following neoadjuvant treatment [3], only 15–27% of these patients achieve a complete pathological response to treatment [4], meaning the potential for cure in the remaining patients depends on resectional surgery with its attendant morbidity and long-term functional implications. The role of the tumour microenvironment (TME) and the biological mechanisms underlying these responses to treatment are poorly understood.

The TME describes the milieu of cancer cells, infiltrating immune cells, secreted factors and the extracellular matrix. The interaction between the tumour cells and the surrounding microenvironment profoundly affects tumour progression and treatment response [5]. Much work to date has investigated the colorectal cancer (CRC) TME, and while the colon and rectum are anatomically related, recurrence rates [6] and treatment regimens differ between the cancer types [7]. The interplay between the TME, secreted inflammatory mediators and immune cell function and how it may be altered by radiation is poorly understood in the context of rectal cancer. Furthermore, to fully understand the alterations occurring in the rectal cancer microenvironment and its interaction with the immune system, it is important to also gain an understanding of the microenvironment in a non-cancerous rectal tissue model.

Tumour-promoting inflammation is a recognised hallmark of cancer [8]. It is postulated that chronic inflammation plays a role in the development of CRC, and anti-inflammatory therapies can reduce risk [9,10]. Secreted factors from the TME may both positively and negatively impact on cancer development. Radiation is known to induce alterations in secreted factors from skin tissue [11]; however, the differential effects of clinically relevant doses of radiation on the normal rectal tissue secretome compared to the rectal cancer tissue secretome are unknown. To date, a comprehensive profiling of the rectal cancer protein secretome and the normal rectal secretome has not been conducted.

The importance of the immune system and its role in carcinogenesis is pivotal [12], and evidence supports the role of the immune system in the radiation response [13]. Dendritic cells (DCs) are professional antigen-presenting cells that reside in blood and tissues in an immature state. Their main function is to recognise pathogens, capture, process and present antigens to T cells to elicit an antigen-specific immune response [14]. DCs are essential for an anti-tumour immune response, and it has been reported that DCs in patients with cancer are incapable of launching a sufficient anti-tumour response [14]. It is becoming increasingly evident that radiation may alter the immune system and inflammatory pathways [15]. Historically, radiation was considered immunosuppressive, with the radiosensitivity of lymphocytes being the dominant explanation for this; however, in recent years radiation is considered immunomodulatory [16]. It is thought that radiation induces innate receptor signalling and subsequent maturation of DCs through tumour cell death and release of endogenous toll-like receptor (TLR) agonists [16]. Furthermore, injection of immature DCs into an irradiated tumour site induced strong tumour-specific cytotoxic T lymphocyte activity in a poorly immunogenic mouse tumour model [17].

In this study we have profiled for the first time the protein secretome of both normal (non-cancer) rectal tissue and rectal cancer tissue pre- and post-radiation, and we examined how these secretomes affect the innate immune system, specifically DC maturation. We hypothesise that the protein secretome will differ between normal (non-cancer) and cancer

tissue and that radiation will affect these secretomes and will likely induce them to interact differently with the innate immune system.

2. Results

2.1. The Protein Secretome Differs between Normal Rectal Tissue and Rectal Cancer Tissue

In order to assess the differences in the inflammatory secretome between normal rectal tissue and rectal cancer tissue, we cultured 12 rectal cancer biopsies and 8 normal rectal biopsies for 24 h and used a multiplex ELISA platform to quantify the expression of 54 inflammatory proteins in the resultant normal conditioned media (NCM) and tumour conditioned media (TCM). The secreted proteins were categorised into 7 panels: vascular injury, angiogenesis, inflammatory, Th17, chemokine, cytokine 1 and cytokine 2. Levels of the secreted factors in normal rectal tissue are displayed in Figure 1A–G, and levels of the secreted factors in rectal cancer tissue are shown in Figure 2A–G. There was notable heterogeneity in levels of secreted factors between patients in both cohorts. Fifty-three of the secreted factors were within the limit of detection for at least one sample in normal rectal biopsies and rectal cancer biopsies. However, three factors—Tie-2, VEGF-C and VEGF-D—were only detectable in one sample each in the normal (non-cancer) cohort.

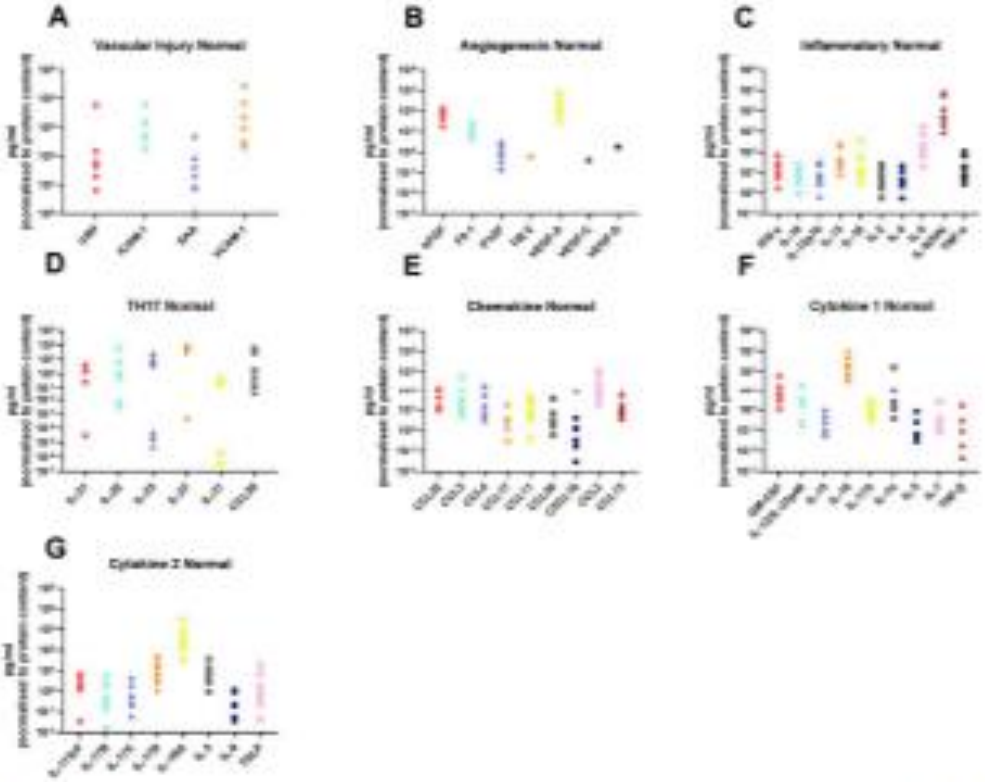

Figure 1. Secreted levels of 53 proteins from n = 8 normal rectal biopsies. Normal rectal biopsies were cultured for 24 h, and the resultant NCM was screened for the expression of 54 inflammatory mediators using a multiplex ELISA. (**A**) Secreted levels of vascular injury proteins CRP, ICAM-1, SAA and VCAM-1. (**B**) Secreted levels of angiogenic factors bFGF, Flt-1, P1GF, Tie-2, VEGF-A, VEGF-C and VEGF-D. (**C**) Inflammatory protein secretome IFN-γ, IL-10, IL-12p70, IL-13, IL-1β, IL-2, IL-4, IL-6, IL-8(HA) and TNF-α. (**D**) Secretion of Th17 proteins IL-21, IL-22, IL-23, IL-27, IL-31 and CCL20. (**E**) Chemokine secreted proteins CCL22, CCL3, CCL4, CCL17, CCL11, CCL26, CXCL10, CCL2 and CCL13. (**F**) Secretion of cytokine panel 1 proteins GM-CSF, IL-12/IL-23p40, IL-15, IL-16, IL-17A, IL-1α, IL-5, IL-7 and TNF-β. (**G**) Secretion of cytokine 2 panel proteins IL-17A/F, IL-17B, IL-17C, IL-17D, IL-1RA, IL-3, IL-9 and TSLP. All protein secretions are normalised to protein content of the biopsies.

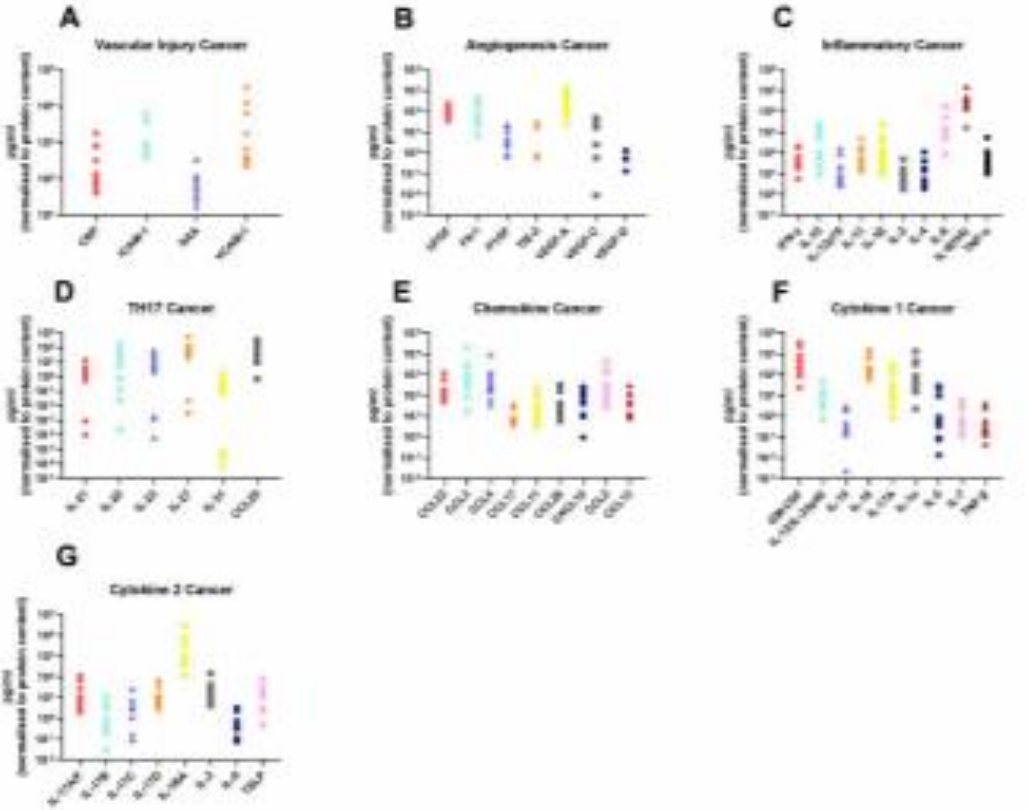

Figure 2. Secreted levels of 55 proteins from $n = 12$ rectal cancer biopsies. Rectal cancer biopsies were cultured for 24 h, and the resultant TCM was screened for the expression of 54 inflammatory mediators using a multiplex ELISA. (**A**) Secreted levels of vascular injury proteins CRP, ICAM-1, SAA and VCAM-1. (**B**) Secreted levels of angiogenic factors bFGF, Flt-1, P1GF, Tie-2, VEGF-A, VEGF-C and VEGF-D. (**C**) Inflammatory secreted proteins IFN-γ, IL-10, IL-12p70, IL-13, IL-1β, IL-2, IL-4, IL-6, IL-8(HA) and TNF-α. (**D**) Secretion of Th17 proteins IL-21, IL-22, IL-23, IL-27, IL-31 and CCL20. (**E**) Chemokine secreted proteins CCL22, CCL3, CCL4, CCL17, CCL11, CCL26, CXCL10, CCL2 and CCL13. (**F**) Secretion of cytokine panel 1 proteins GM-CSF, IL-12/IL-23p40, IL-15, IL-16, IL-17A, IL-1α, IL-5, IL-7 and TNF-β. (**G**) Secretion of cytokine 2 panel proteins IL-17A/F, IL-17B, IL-17C, IL-17D, IL-1RA, IL-3, IL-9 and TSLP. All protein secretions are normalised to protein content of the biopsies.

We identified 19 factors that were secreted at significantly higher levels in the rectal cancer secretome compared to the normal rectal secretome: Flt-1 ($p = 0.001$), P1GF ($p = 0.01$), IFN-γ ($p = 0.04$), IL-6 ($p = 0.02$), IL-10 ($p = 0.0002$), CCL20 ($p = 0.005$), CCL26 ($p = 0.009$), CCL22 ($p = 0.007$), CCL3 ($p = 0.002$), CCL4 ($p = 0.0007$), CCL17 ($p = 0.02$), GM-CSF ($p < 0.0001$), IL-12/IL-23p40 ($p = 0.01$), IL-17A ($p = 0.0003$), IL-1α ($p = 0.003$), IL-17A/F ($p = 0.003$), IL-1RA ($p = 0.03$), TSLP ($p = 0.007$) and CXCL10 ($p = 0.001$) (Figure 3A–S). This indicates that the rectal cancer secretome is more inflammatory than the normal rectal secretome, which is expected since tumour-promoting inflammation is a hallmark of cancer [8].

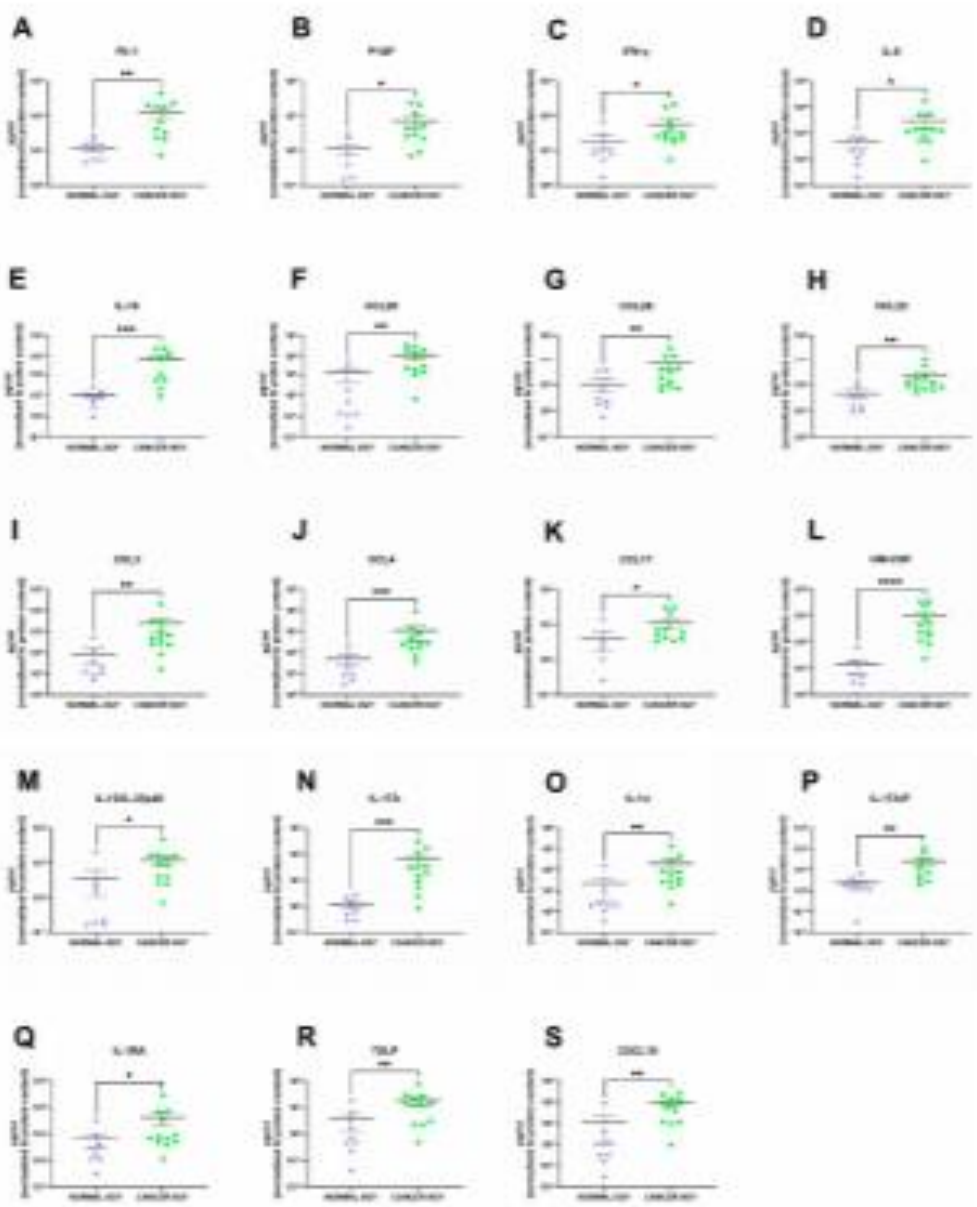

Figure 3. The protein secretome differs between rectal cancer tissue and normal rectal tissue. NCM and TCM from cultured normal rectal and rectal cancer biopsies were screened for the expression of 54 inflammatory secretions using a multiplex ELISA. Nineteen factors were secreted at significantly higher levels in the TCM compared to the NCM. There were significantly higher levels of (**A**) Fib-1, (**B**) P1GF, (**C**) IFN-γ, (**D**) IL-6, (**E**) IL-10, (**F**) CCL20, (**G**) CCL26, (**H**) CCL22, (**I**) CCL3, (**J**) CCL4, (**K**) CCL17, (**L**) GM-CSF, (**M**) IL-12/IL-23p40, (**N**) IL-17A, (**O**) IL-1α, (**P**) IL-17A/F, (**Q**) IL-1RA, (**R**) TSLP and (**S**) CXCL10 in the rectal cancer secretome. All data expressed as mean ± SEM. Statistical analysis by Mann Whitney U-test. $n = 8$ for normal, $n = 12$ for cancer, $n = 7$ normal for P1GF, $n = 5$ normal for CCL17, $n = 11$ cancer for Fib-1, P1GF, CCL17 and $n = 10$ cancer for IL-17A/F. **** $p < 0.0001$, *** $p < 0.001$, ** $p < 0.01$, * $p < 0.05$.

2.2. Radiation Significantly Altered the Secretion of IL-15 and CCL22 from Normal Rectal Tissue

Radiation is the standard of care for locally advanced rectal cancer, with about 50% of rectal cancer patients receiving this treatment modality; therefore, we investigated the effect of a clinically relevant dose of 1.8 Gy radiation on protein secretions from normal rectal tissue and rectal cancer tissue. Interestingly, we found 2 factors that were secreted at significantly higher levels from irradiated normal rectal tissue compared to mock-irradiated normal rectal tissue: IL-15 ($p = 0.01$) and CCL22 ($p = 0.03$) (Figure 4A,B). This indicates that a single fraction of 1.8 Gy radiation alters levels of secreted proteins in normal rectal tissue. We did not observe any significant alterations in secreted factors in rectal cancer tissue following a single fraction of a clinically relevant dose of radiation. This suggests that a single fraction of 1.8 Gy radiation does not alter secreted proteins in rectal cancer tissue.

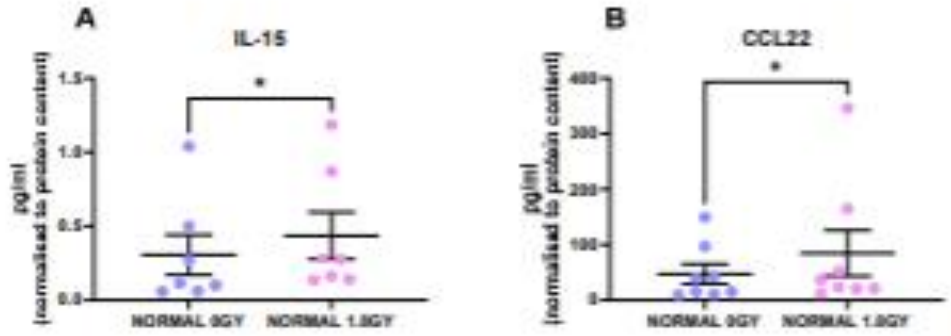

Figure 4. Radiation alters the secretome of normal rectal tissue. NCM from mock-irradiated and irradiated normal rectal biopsies were screened for the secretion of 54 inflammatory proteins using a multiplex ELISA. Following a single fraction of 1.8 Gy radiation, there were significantly higher levels of (**A**) IL-15 and (**B**) CCL22 in the normal rectal secretome. All data expressed as mean ± SEM. Statistical analysis by Wilcoxon signed-rank test. $n = 8$ for CCL22 and $n = 7$ for IL-15, * $p < 0.05$.

2.3. The Rectal Cancer Microenvironment Alters Expression of Maturation Markers on CD11c$^+$ Dendritic Cells

To assess the interaction between the TME and the immune system, we examined the effect of TCM and NCM from both mock-irradiated and irradiated biopsies on DC maturation markers. Following lipopolysaccharide (LPS)-induced maturation of DCs, there was a significant increase in expression of the maturation markers CD80, CD86, CD83 and PD-L1 and the phenotypic marker CD11c ($p < 0.05$). Therefore, we assessed the effects of TCM and NCM from both mock-irradiated and irradiated tissue on these markers. TCM and NCM from both mock-irradiated and irradiated biopsies had a significant inhibitory effect on LPS-induced expression of CD80 ($p < 0.0001$ for all comparisons). However, TCM from irradiated rectal cancer biopsies had the least inhibitory effect on CD80 levels, inducing significantly higher expression of CD80 compared to TCM from mock-irradiated rectal cancer ($p = 0.03$). TCM from both mock-irradiated ($p = 0.007$) and irradiated ($p = 0.001$) rectal cancer tissue significantly enhanced LPS-induced expression of CD86. NCM did not affect expression of CD86 compared to the media only control with LPS ($p > 0.05$). CD83 expression was significantly enhanced by NCM from both mock-irradiated ($p = 0.01$) and irradiated ($p = 0.0006$) biopsies and TCM both mock-irradiated ($p < 0.0001$) and irradiated ($p = 0.0003$) biopsies compared to LPS-induced stimulation. Moreover, TCM from mock-irradiated rectal cancer tissue enhanced expression of CD83 to a greater extent than NCM from mock-irradiated normal rectal tissue ($p = 0.02$). PD-L1 expression levels were significantly elevated on DCs treated with TCM from irradiated rectal cancer tissue ($p = 0.002$) compared to LPS-induced expression. PD-L1 expression was significantly higher on DCs treated with TCM from irradiated tissue compared to TCM from mock-irradiated

tissue ($p = 0.02$). Levels of the phenotypic marker CD11c were significantly elevated on DCs exposed to NCM from mock-irradiated ($p = 0.007$) and irradiated ($p = 0.039$) and TCM from both mock-irradiated ($p = 0.002$) and irradiated ($p = 0.002$) rectal cancer tissue (Figure 5A–E). This suggests that the irradiated rectal cancer microenvironment exerts the most potent effect on upregulating DC maturation markers compared to the other three microenvironments investigated. Similar results were observed in the unstimulated setting without LPS whereby the irradiated rectal cancer TME had the most potent stimulatory effect on DC maturation markers (Figure S1).

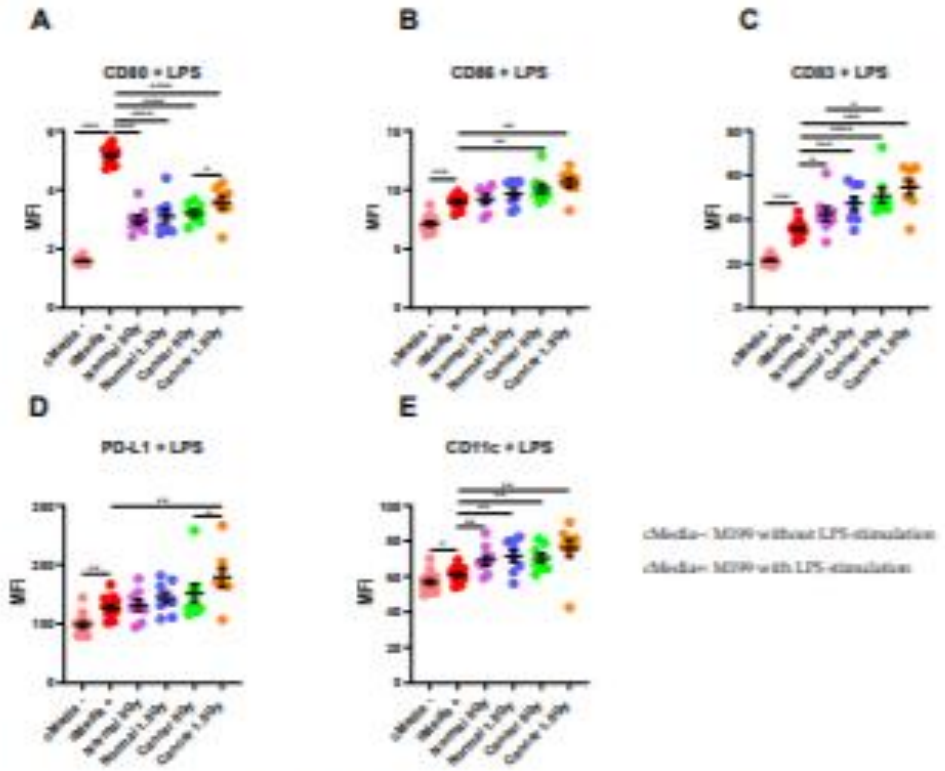

Figure 5. The effect of NCM and TCM on LPS-induced dendritic cell (DC) maturation. CD11c$^+$ DCs were treated with NCM and TCM from mock-irradiated and irradiated biopsies, and the effect on DC maturation markers was assessed by flow cytometry. (**A**) NCM and TCM from both mock-irradiated and irradiated biopsies significantly inhibit LPS-induced expression of CD80. TCM from irradiated rectal cancer tissue has a less inhibitory effect than TCM from mock-irradiated rectal cancer tissue. (**B**) TCM from both irradiated and mock-irradiated rectal cancer tissue caused significant enhancement of LPS-induced expression of CD86. (**C**) NCM and TCM from both irradiated and mock-irradiated normal rectal and rectal cancer biopsies caused a significant enhancement of LPS-induced expression of CD83. TCM from mock-irradiated rectal cancer biopsies caused significant elevation of CD83 expression levels compared to NCM from mock-irradiated biopsies. (**D**) PD-L1 expression was significantly enhanced by TCM from irradiated rectal cancer tissue. (**E**) LPS-induced expression of CD11c was significantly elevated by NCM and TCM from irradiated and mock-irradiated biopsies. All data expressed as mean ± SEM. Statistical analysis by Wilcoxon signed-rank test when comparing the same tissue type, e.g., Cancer 0 Gy vs. Cancer 1.8 Gy and Mann Whitney U-test when comparing different tissue types and comparing to media control. $n = 14$ for cMedia, $n = 8$ for normal and cancer, **** $p < 0.0001$, *** $p < 0.001$, ** $p < 0.01$, * $p < 0.05$.

2.4. Linking Innate Immune Response with Secreted Factors in the Normal and Cancer Microenvironments

Given the observed differences in DC maturation markers between $CD11c^+$ DCs treated with the normal and cancerous rectal tissue microenvironments, we correlated DC maturation markers in both microenvironments pre- and post-radiation with secreted factors from their respective microenvironment. There were no significant correlations between secreted factors in the mock-irradiated normal rectal microenvironment and markers of DC maturation. There was a significant inverse correlation between IL-10 and CD80 ($r = -0.8571$, $p = 0.01$) in the irradiated normal microenvironment (Table 1). In the mock-irradiated cancer microenvironment, there was a significant correlation between CD80 and Flt-1 ($r = 0.7857$, $p = 0.04$), and an inverse correlation between CD80 and IL-27 ($r = -0.8214$, $p = 0.03$). CD83 correlated with levels of SAA ($r = 0.7857$, $p = 0.04$). Expression of CD80 on DCs treated with TCM from irradiated rectal cancer tissue correlated with levels of ICAM-1 ($r = 0.8214$, $p = 0.03$) and CD11c correlated with IL-1RA ($r = 0.7619$, $p = 0.03$) (Table 2). These results indicate a differential relationship between DC maturation markers and secreted factors in the normal and malignant rectal microenvironments and that radiation further alters this relationship.

Table 1. Correlation between DC maturation markers and secreted factors in the microenvironment of irradiated normal rectal tissue, i.e., Normal 1.8 Gy.

DC Marker	Secreted Factor	r Value	p Value	n
CD80	IL-10	−0.8571	0.01	8

Table 2. Correlation between DC maturation and phenotypic markers and secreted factors in the microenvironment of rectal cancer tissue.

CANCER 0 GY					CANCER 1.8 GY				
DC Marker	**Secreted Factor**	**r Value**	**p Value**	**n**	**DC Marker**	**Secreted Factor**	**r Value**	**p Value**	**n**
CD80	Flt-1	0.7857	0.04	7	CD80	ICAM-1	0.8214	0.03	7
CD80	IL-27	−0.8214	0.03	7	CD11c	IL-1RA	0.7619	0.03	8
CD83	SAA	0.7857	0.04	7					

2.5. Linking DC Maturation and Phenotypic Markers with Secretions from DCs Treated with TCM and NCM

We performed multiplex ELISA screening on the DC-TCM/NCM supernatants of the DCs treated with TCM and NCM from mock-irradiated and irradiated rectal tissue. We then correlated these factors with DC maturation and phenotypic markers to identify if there was a differential response of DCs to TCM and NCM and if radiation altered this response. ICAM-1 was inversely correlated with CD83 ($r = -0.7857$, $p = 0.02$) and CD11c ($r = -0.7857$, $p = 0.02$) on DCs treated with NCM from irradiated normal rectal tissue (Table 3). We found a significant correlation between PD-L1 on DCs treated with TCM from mock-irradiated rectal cancer tissue and TNF-α levels in the supernatants of DCs treated with TCM from mock-irradiated rectal cancer tissue ($r = 0.8333$, $p = 0.01$). There was an inverse correlation between VEGF-C and CD86 ($r = -0.9276$, $p = 0.01$) and CD11c ($r = -0.8857$, $p = 0.03$) in DCs treated with TCM from irradiated rectal cancer tissue (Table 4). This highlights the differential response of DCs to factors in their microenvironment.

2.6. Linking Clinical Characteristics with Secreted Factors and DC Maturation and Phenotypic Markers

Given the heterogeneity in the levels of secreted factors in the TME, and to further explore the relationship between factors secreted from the rectal cancer microenvironment, we correlated patient clinical characteristics with secreted factors both pre- and post-

radiation. In the mock-irradiated rectal cancer microenvironment, there were several factors that significantly correlated with body composition parameters. Skeletal muscle correlated inversely with Flt-1 ($r = -0.6273$, $p = 0.04$) and correlated positively with IL-12/IL-23p40 ($r = 0.6573$, $p = 0.02$), IL-1α ($r = 0.5874$, $p = 0.04$) and VEGF-A ($r = 0.6224$, $p = 0.03$). Visceral fat area (VFA) correlated with CCL20 ($r = 0.6783$, $p = 0.01$) (Table 5) (Figure S2). In the irradiated rectal cancer secretome there was again a significant inverse correlation between skeletal muscle and Flt-1 ($r = -0.7182$, $p = 0.01$) and VEGF-D ($r = -1$, $p = 0.01$). Intermuscular fat correlated with CCL20 ($r = 0.7133$, $p = 0.01$), VEGF-A ($r = 0.6084$, $p = 0.03$) and IL-1RA ($r = 0.6084$, $p = 0.03$), and VFA correlated with CCL20 ($r = 0.6643$, $p = 0.02$) and IL-1RA ($r = 0.6503$, $p = 0.02$) (Table 6) (Figure S3).

Table 3. Correlation between DC maturation and phenotypic markers and secreted factors from DCs treated with NCM.

NORMAL 1.8 GY				
DC Marker	**Secreted Factor**	**r Value**	***p* Value**	**n**
CD83	ICAM-1	−0.7857	0.02	8
CD11c	ICAM-1	−0.7857	0.02	8

Table 4. Correlation between DC maturation and phenotypic markers and secreted factors from DCs treated with TCM.

CANCER 0 GY					CANCER 1.8 GY				
DC Marker	**Secreted Factor**	**r Value**	***p* Value**	**n**	**DC Marker**	**Secreted Factor**	**r Value**	***p* Value**	**n**
PD-L1	TNF-α	0.8333	0.01	8	CD86	VEGF-C	−0.9276	0.01	6
					CD11c	VEGF-C	−0.8857	0.03	6

Table 5. Correlation between body composition parameters and factors secreted from mock-irradiated rectal cancer tissue, i.e., Cancer 0 Gy.

Body Composition Parameter	Secreted Factor	r Value	*p* Value	n
Skeletal muscle	Flt-1	−0.6273	0.04	11
Skeletal muscle	IL-12/IL-23p40	0.6573	0.02	12
Skeletal muscle	IL-1α	0.5874	0.04	12
Skeletal muscle	VEGF-A	0.6224	0.03	12
Visceral fat area	CCL20	0.6783	0.01	12

Table 6. Correlation between body composition parameters and factors secreted from irradiated rectal cancer tissue, i.e., Cancer 1.8 Gy.

Body Composition Parameter	Secreted Factor	r Value	*p* Value	n
Skeletal muscle	Flt-1	−0.7182	0.01	11
Skeletal muscle	VEGF-D	−1	0.01	5
Intermuscular fat	CCL20	0.7133	0.01	12
Intermuscular fat	VEGF-A	0.6084	0.03	12
Intermuscular fat	IL-1RA	0.6084	0.03	12
Visceral fat area	CCL20	0.6643	0.02	12
Visceral fat area	IL-1RA	0.6503	0.02	12

Expression of CD11c on DCs treated with TCM from irradiated rectal cancer tissue correlated significantly with VFA ($r = 0.8095$, $p = 0.02$) and intermuscular fat ($r = 0.7381$, $p = 0.04$). These data suggest that obesity may influence the microenvironment of rectal cancer tissue and the response of this microenvironment to radiation therapy. We analysed

secreted factor data and DC maturation data according to T and N stage. VEGF-A was significantly reduced in the TCM from irradiated rectal cancer tissue from patients with node positive disease. TSLP was significantly higher in the irradiated TME of patients with T1/2 stage tumours compared to those with T3/4 stage tumours. CD11c was significantly elevated on DCs treated with TCM from irradiated rectal cancer biopsies from patients with node negative disease (data not shown).

3. Discussion

The objective of this study was to profile the inflammatory secretome of human rectal cancer and normal rectal tissue pre- and post-radiation and to investigate the interaction between this secretome and the innate immune system, specifically DC maturation markers. By conducting this study, we identified associations between factors within the TME and DC maturation markers, thus providing an avenue for further exploration to harness the therapeutic potential of modulating the TME. Using human ex vivo explants as a model system, we have shown that the protein secretome differs between normal rectal and rectal cancer tissue, and this is altered following radiation in normal rectal tissue, highlighting variation in effects of radiation on the normal compared to the malignant rectal tissue microenvironments. Furthermore, these protein secretome microenvironments interacted differentially with the innate immune system.

We identified 19 factors that were secreted at significantly higher levels in the TME of rectal cancer tissue compared to normal rectal tissue. This indicates that the rectal cancer microenvironment is more inflammatory than the normal rectal microenvironment. Following radiation, two factors were elevated in the secretome of normal rectal tissue, while surprisingly no secreted factor was significantly altered in malignant rectal tissue following radiation. This indicates that malignant and normal rectal tissue respond differently to radiation and suggests that a single fraction of 1.8 Gy radiation induces alterations in inflammatory secretions in normal tissue but not in malignant tissue. Following exposure of DCs to NCM and TCM from both mock-irradiated and irradiated biopsies, we found that the irradiated rectal cancer secretome caused an enhancement in expression of DC maturation markers. These results suggest that a single fraction of a clinically relevant dose of radiation does not have a negative impact on the inflammatory milieu of malignant rectal tissue and does not lead to suppression of the innate immune system.

The inflammatory environment differs between non-cancer and cancer tissue, which is unsurprising given that tumour-promoting inflammation is a hallmark of cancer [8]. Nineteen out of 54 factors quantified were found at significantly higher levels in the cancer secretome compared to the normal secretome. These factors have previously been reported to have pro-oncogenic attributes including angiogenic, pro-mitogenic and immunosuppressive characteristics; therefore, it is expected that they are elevated in the rectal cancer TME compared to the normal microenvironment, while other elevated factors have anti-tumour functions. Two factors, Flt-1 and PlGF, are angiogenic mediators. PlGF is capable of binding to Flt-1 and may displace VEGF, thereby facilitating enhanced VEGF-activity [18]. PlGF is known to have numerous roles in carcinogenesis including macrophage activation and recruitment, lymph vessel growth, DC suppression, tumour cell proliferation and migration and endothelial cell vessel growth [19]. IL-1α secretion from CRC cells has also been shown to have angiogenic properties [20]. The inflammatory cytokines IFN-γ, IL-6 and IL-10 were also found at significantly higher levels in the cancer secretome compared to the normal secretome. IFN-γ is an important effector of anti-tumour immunity, but more recent evidence suggests that it may play important roles in tumour progression and immune evasion [21]. IL-6 is a well-known pro-tumorigenic factor [22], and IL-10 was originally identified as a potent anti-inflammatory cytokine; however, it is now known that spatial and temporal regulation of IL-10 bestows on it anti-tumour responses also [23].

Several Th17-type proteins including CCL20, IL-17A and IL-17A/F are secreted at higher levels from rectal cancer tissue compared to normal rectal tissue. This is unsurprising given the known involvement of Th17 cells in CRC. Th17 cells infiltrate CRCs, and their

density correlates with poor prognosis [24,25]. In multiple models of CRC, antagonising Th17 cytokines exert anti-cancer effects, but there have been mixed reports about the effects of blocking Th17 cytokines in murine models [26]. CCL20 is a chemokine involved in the recruitment of Th17 cells to the TME [27,28].

A number of the elevated proteins in the rectal cancer environment are implicated in tumour immune evasion through recruitment of regulatory T cells (T regs) to the TME. CCL22, CCL17, TSLP and CXCL10 function in recruitment of T regs, with levels of CCL22 and CCL17 correlating with T reg infiltration in gastrointestinal cancers [29,30]. TSLP production by cancer-associated fibroblasts in pancreatic cancer induces Th2 type inflammation and is associated with poorer patient outcome [31]. CXCL10 has been associated with an immunosuppressive phenotype in pancreatic cancer [32].

Two factors, CCL22 and IL-15, were secreted at significantly higher levels following radiation in normal rectal tissue. CCL22 is involved in recruitment of T regs through its receptor CCR4 and is therefore reported as being immunosuppressive [33]. IL-15 is an immunostimulatory cytokine and is involved in development, differentiation and survival of natural killer cells [34]. Therefore, our data suggest that a single fraction of 1.8 Gy radiation may alter the microenvironment of normal rectal tissue to promote an inflammatory response but that homeostatic mechanisms may be at play in limiting the extent of the inflammation. Surprisingly, no factor was significantly altered in rectal cancer tissue following radiation. Undoubtedly, the cellular composition of normal rectal tissue and rectal cancer tissue differs, as does the inflammatory secretome; therefore, it is reasonable to hypothesise that the response to radiation would also differ. When taken in combination with our results on DC maturation markers, whereby the irradiated rectal cancer TME caused enhancement in expression of DC maturation markers relative to the normal microenvironment, these data suggest that irradiating the TME with a single fraction of 1.8 Gy does not have an inflammation-induced immunosuppressive effect. It has been reported that chemotherapy-induced inflammation may contribute to treatment resistance in cancer [35], and enhanced inflammation has been implicated in poor treatment response in patients [36,37]. Taken together, we hypothesise that this is a positive result since an enhancement of inflammation and tumour suppressive mechanisms would have negative consequences on the anti-tumour immune response. However, a limitation of this study was the use of a single fraction of 1.8 Gy radiation. Comparison of the inflammatory secretome of rectal cancer tissue obtained at surgical resection from treatment-naïve patients and those that received a full course of neo-CRT would offer greater insight into the effect of clinical radiotherapy regimens on secreted factors and DC maturation markers.

Having observed alterations in the inflammatory mediators, cytokines and chemokines between the secretome of rectal cancer tissue and non-malignant rectal tissue and the differential effects of radiation on the secretome of non-malignant and malignant rectal tissue, we investigated the effect of the secretome on immune cell function, specifically DC maturation markers. DCs are antigen-presenting cells capable of inducing a T cell response, and maturation levels have been associated with patient survival and response to targeted therapies in CRC patients [38,39]. It has previously been reported that the TME in CRC causes inhibition of DC maturation [40,41]. On the contrary, however, we found upregulation of DC maturation by the rectal cancer TME, which is in line with results published by Morrissey et al. [41]. This finding warrants further investigation since it may have important clinical implications in stratifying patients for whom immunotherapy may offer a clinical benefit. We demonstrated a significant increase in CD80 and PD-L1 on the DCs exposed to the irradiated rectal cancer secretome compared to the mock-irradiated rectal cancer secretome. CD83 was significantly higher on DCs exposed to the mock-irradiated rectal cancer secretome compared to the mock-irradiated normal rectal secretome. Our results are in line with a study by Kuliner et al. where the supernatants of irradiated SW480 colon cancer cells resulted in significant enhancement of DC maturation markers compared to supernatants from mock-irradiated SW480 cells [42]. However, our study presents results from a more translational model system as we used human ex vivo explants. We found

similar results in the unstimulated setting without LPS whereby TCM from the irradiated rectal cancer secretome had the most potent effect on DC maturation (Figure S1).

Given the observed differences in the protein secretome of the microenvironments investigated and the differential response of DCs to these microenvironments, we conducted a correlation analysis to identify any relationship between secreted factors and DC maturation markers. In the irradiated normal rectal tissue, there was a significant inverse correlation between IL-10 and CD80. IL-10 has been previously shown to have an immunosuppressive role on circulating DCs in patients with hepatocellular carcinoma [43]. While in the rectal cancer TME, CD80 levels on DCs correlated positively with Flt-1 and inversely with IL-27. VEGF is known to adversely affect DC maturation [44], and blockade of Flt-1 on DCs curtails this effect [45]. It may be possible that VEGF is binding to elevated levels of Flt-1 in the TME and is therefore unavailable to exert inhibitory effects on DC maturation. IL-27 has previously been reported to upregulate PD-L1 on DCs in the absence of DC maturation and is accompanied by a decreased capacity to stimulate T cells [46]. There was a positive correlation between CD83 and SAA in the mock-irradiated rectal cancer TME. SAA has been shown to enhance DC maturation [47]. In the irradiated rectal cancer, TME CD80 correlated with ICAM-1 and CD11c correlated with IL-1RA. These results indicate that the response of DCs to their microenvironment differs between normal and malignant rectal tissue and that radiation further modifies this response. It is possible that the interplay between the relative concentration of cytokines in the distinct microenvironments examined exerts differential effects on DC maturation.

Overweight and obese rectal cancer patients have been reported to have poorer outcomes than their counterparts of a healthy weight [48,49]. To identify if obesity had a direct effect on secreted factors within the TME and subsequent immune response, we correlated body composition parameters with secreted factors and markers of DC maturation. We found positive correlations between VFA and CCL20 in the mock-irradiated TME and VFA and CCL20 and IL-1RA in the irradiated TME. Moreover, intermuscular fat, a marker which is associated with insulin resistance and metabolic dysfunction [50], was correlated with CCL20, IL-1RA and VEGF-A. There were positive correlations between levels of the phenotypic marker CD11c on the DCs treated with TCM from irradiated rectal cancer tissue and VFA and intermuscular fat. These data suggest that obesity status may directly alter the milieu of inflammatory proteins in the TME, and these factors may be differentially altered by radiation in obese individuals. Further exploration of the relationship between obesity and the inflammatory microenvironment of rectal cancer patients may reveal novel therapeutic targets.

Strengths of this study include the use of whole biopsies as experimental models since these models recapitulate the microenvironment and the 3-D architecture of human tumours and normal tissue. However, a limitation associated with these models is their long-term viability ex vivo (up to 72 h). Our study was limited to the use of a single fraction of a clinically relevant dose of radiation, though it must be acknowledged that repeated fractions of radiation may induce different responses. Future study utilizing biopsy specimens obtained at surgical resection from both treatment-naïve patients and from patients that received a full course of neo-CRT would provide important information on the effect of neo-CRT on the inflammatory milieu and its interaction with the innate immune system.

We have conducted, for the first time, a comprehensive profile of the rectal cancer and normal rectal secretome and demonstrated differential expression of cytokines, chemokines and inflammatory markers in the secretome of rectal cancer tissue compared to normal rectal tissue. This study is novel as it assesses the secreted proteins in the microenvironment of malignant and non-malignant rectal tissue, therefore identifying aberrant expression of factors in the immediate vicinity of the tumour, while most studies to date investigate the circulating levels of such inflammatory proteins. Investigating the secretome of the tissue offers insight into the locally acting factors involved in the disease process as well as potentially identifying factors involved in the disease at an early stage. Furthermore, we

have shown that a single fraction of a clinically relevant dose of radiation exerts differential effects on the secretome of normal rectal tissue compared to malignant rectal tissue. Finally, DC maturation status is enhanced by the irradiated rectal cancer secretome compared to the irradiated normal rectal secretome, indicating an immunogenic stimulatory effect of radiation in the rectal cancer secretome that could potentially be harnessed to improve therapeutic response.

4. Materials and Methods

4.1. Ethics Statement

Ethical approval was granted by the St. James's Hospital/AMNCH Research Ethics Committee (ref: 2011/43/02). All procedures followed were in accordance with the Declaration of Helsinki and GDPR. Informed written patient consent was obtained for the use of patient tissue and data in this study. Patient data were pseudo-anonymised prior to sample access.

4.2. Patient Recruitment

Patients undergoing diagnostic endoscopy for rectal cancer and lower gastrointestinal investigations were prospectively recruited to this study between January 2018 and November 2018. Biopsies were obtained from treatment-naive patients at diagnostic endoscopy. A total of 12 patients with histologically confirmed rectal cancer and 8 patients that did not have cancer (normal, non-cancer controls) were recruited to the study. All clinical and pathological data were obtained following written informed consent. Clinical data were obtained from patient records. Histological confirmation of tumour tissue and non-malignant tissue in patient diagnostic biopsies was performed by a pathologist using routine haematoxylin and eosin staining. Tumour regression score (TRS) was assigned by a pathologist following surgery in all patients receiving neoadjuvant treatment. VFA, subcutaneous fat area, intermuscular fat and skeletal muscle were calculated from a pre-operative diagnostic computed tomography scan by an experienced radiologist. Patients with a VFA greater than 163.8 cm^2 (males) and 80.1 cm^2 (females) were classified as obese [51]. Patient characteristics are outlined in Supplementary Table S1.

4.3. Generation of Tumour Conditioned Media and Normal Conditioned Media

TCM from rectal cancer biopsies and NCM from non-cancer control biopsies were generated by rinsing the biopsy four times in PBS supplemented with 1% penicillin–streptomycin, 1% Fungizone and 0.1% gentamicin. The biopsy was then placed in 1 mL of M199 media supplemented with 10% FBS, 1% penicillin–streptomycin, 1% Fungizone, 0.1% gentamicin and 1 µg/mL insulin. Biopsies were incubated for 80 min at 37 °C and 5% CO_2. Following 80 min incubation, biopsies were either mock-irradiated (0 Gy) or irradiated with 1.8 Gy radiation using an Xstrahl RS225 x-irradiator at a dose rate of 1.73 Gy/min (XSTRAHL, Surrey, UK). Biopsies were then incubated for 24 h at 37 °C and 5% CO_2. Following 24 h incubation the media were harvested and stored in a 2 mL cryotube at −80 °C until required. The biopsies were snap-frozen in liquid nitrogen and stored at −80 °C. NCM/TCM was diluted 1:1 with M199, and dilutions below refer to dilutions of this.

4.4. Mesoscale Discovery 54-Plex ELISA

To assess angiogenic, vascular injury, inflammatory, cytokine and chemokine secretions, a 54-plex ELISA kit spread across 7 plates was used (Meso Scale Diagnostics, Rockville, MD, USA). The 54-multiplex kit was used to quantify the secretions of CRP, CCL11 (Eotaxin), CCL26 (Eotaxin-3), FGF(basic), Flt-1, GM-CSF, ICAM-1, IFN-γ, IL-10, IL-12/IL-23p40, IL-12p70, IL-13, IL-15, IL-16, IL-17A, IL-17A/F, IL-17B, IL-17C, IL-17D, IL-1RA, IL-1α, IL-1β, IL-2, IL-21, IL-22, IL-23, IL-27, IL-3, IL-31, IL-4, IL-5, IL-6, IL-7, IL-8, IL-8 high abundance (HA), IL-9, CXCL10 (IP-10), CCL2 (MCP-1), CCL13 (MCP-4), CCL22 (MDC), CCL3 (MIP-1α), CCL4 (MIP-1β), CCL20 (MIP-3α), PlGF, SAA, CCL17 (TARC),

Tie-2, TNF-α, TNF-β, TSLP, VCAM-1, VEGF-A, VEGF-C and VEGF-D from NCM and TCM from each individual biopsy per patient. All assays were run as per manufacturer's recommendations, with an alternative protocol overnight supernatant incubation being used for all assays except vascular injury and angiogenesis assays. Secretion data for all factors were normalised appropriately to rectal tissue protein content using the BCA assay (Pierce).

4.5. Dendritic Cell Isolation and Culture

Human monocyte-derived immature DCs were generated from peripheral blood mononuclear cells obtained from buffy coat preparations (National Blood Centre, St. James's Hospital, Dublin, Ireland) by density gradient centrifugation (Lymphoprep) as described [38,52]. Briefly, monocytes were isolated by positive selection using anti-CD14 magnetic microbeads as described by the manufacturer (Miltenyi Biotec, Bergisch Gladbach, Germany) and seeded at a density of 1×10^6 cells/mL in 6-well plates in 3 mL of RPMI-1640 medium containing 10% defined low-endotoxin HyClone FBS (Thermo Fischer Scientific, Waltham, MA, USA), 1% penicillin-streptomycin, 1% Fungizone, human granulocyte macrophage colony-stimulating factor (50 ng/mL) (Immunotools, Friesoythe, Germany) and human IL-4 (70 ng/mL) (Immunotools, Friesoythe, Germany) in a humidified atmosphere with 5% CO_2 at 37 °C. Cells were fed at day 3 by replacing half the medium made up with fresh cytokines. At day 6, $CD11c^+$ cells exhibited an immature DC phenotype capable of upregulating maturation markers following LPS activation.

4.6. Stimulation of Monocyte-Derived Dendritic Cells

Freshly generated DCs were plated in 96-well plates at 2×10^5 cells in 200 µL RPMI 1640 media supplemented with 10% defined low-endotoxin HyClone FBS (Thermo Fisher Scientific, Waltham, MA, USA) and stimulated with a 1:2 dilution of TCM or NCM, or matched background media controls, for 4–5 h before exposure to 10 µg/mL of ultrapure TLR4 agonist *Escherichia coli* lipopolysaccharide (LPS-EB; Invivogen) overnight. Supernatants were harvested and frozen, and cells were assessed for expression of surface markers as described below.

4.7. Flow Cytometry

DCs were stained with the following antibody panel: phycoerythrin (PE)- anti-CD80 (2D10), PerCP-Cy5.5- anti-CD86 (IT2.2), Pe-Cy7- anti-CD83 (HB15), Brilliant Violet 421- anti-PD-L1 (29E.2A3), Brilliant Violet 510- anti-CD11c (3.9), allophycocyanin (APC)- anti-CD54 (HA58) and APC-Cy7- anti-HLA-DR (L243) (Biolegend, San Diego, CA, USA). Samples were acquired on DAKO CyAn ADP flow cytometer (Beckman Coulter, Brea, CA, USA) with compensation performed with positive and negative compensation beads (BD Biosciences, San Jose, CA, USA). Gating on and analysis of $CD11c^+$ cells was performed using FlowJo software (Tree Star Inc., Ashland, OR, USA).

4.8. Statistical Analysis

GraphPad Prism 9 software was used to perform statistical analysis. All data were expressed as mean ± SEM. Statistical tests used are indicated in each figure legend. Correlation was measured using Spearman correlation coefficient. Statistical significance was considered at $p < 0.05$.

5. Conclusions

This study quantified the secretion of 54 proteins from normal rectal tissue and rectal cancer tissue and examined the effect of a clinically relevant dose of radiation on the levels of protein secretions. We have shown that the cancer secretome is more inflammatory than the normal rectal secretome with 19 factors secreted at significantly higher levels from the rectal cancer TME. A single fraction of a clinically relevant dose of radiation alters the inflammatory milieu of the normal but not the rectal cancer microenvironment. We also demonstrated that the irradiated rectal cancer microenvironment induced the most potent

effect on stimulating DC maturation, suggesting that tumour irradiation does not have a negative impact on the ability of the rectal cancer TME to induce an anti-tumour immune response. Correlations were found between secretions of inflammatory mediators and clinical characteristics, including obesity status, suggesting that obesity may directly alter protein secretions from the TME.

Supplementary Materials: The following are available online at https://www.mdpi.com/2072-6694/13/3/571/s1, Figure S1: The effect of NCM and TCM on unstimulated dendritic cells, Figure S2: Correlations between secreted factors from mock-irradiated rectal cancer tissue (Cancer 0 Gy) and body composition parameters, Figure S3: Correlations between secreted factors from irradiated rectal cancer tissue (Cancer 1.8 Gy) and body composition parameters, Table S1: Patient characteristics.

Author Contributions: A.B.H. processed specimens, conducted experiments, performed statistical analysis of data and drafted the manuscript. M.R.D. and M.E.M. conducted experiments, contributed to writing the manuscript and interpreting data analysis. C.E.B. assisted in processing specimens and editing the manuscript. A.C. provided training in experimental techniques and assisted in editing the manuscript. M.D. assisted with clinical data acquisition and assisted in editing the manuscript. N.E.D., T.S.N. and N.C. were responsible for specimen and clinical data management and assisted in editing the manuscript. C.D., J.O.L., B.M. and P.M. provided specimens and assisted in editing the manuscript. N.L.-L. and J.O. devised the original study, assisted in interpretation of data and assisted in editing the manuscript. All authors have read and agreed to the published version of the manuscript.

Funding: This work was supported by the Irish Research Council (Grant: GOIPG/2017/983).

Institutional Review Board Statement: The study was conducted according to the guidelines of the Declaration of Helsinki and approved by the Ethics Committee of St. James's Hospital/AMNCH (approval number 2011/43/02 and date approved: 10/11/2011).

Informed Consent Statement: Informed consent was obtained from all subjects involved in the study.

Data Availability Statement: The data presented in this study are available upon reasonable request from the corresponding author. The data are not publicly available as there are restrictions on data processing in line with participant consent.

Acknowledgments: We wish to thank the patients at St. James's Hospital Dublin for so kindly donating their samples to this research. We also wish to thank Jill O'Sullivan for her assistance with statistical analysis.

Conflicts of Interest: The authors do not declare any conflict of interest.

Abbreviations

CRC	colorectal cancer
DC	dendritic cell
LPS	lipopolysaccharide
NCM	normal conditioned media
neo-CRT	neoadjuvant chemoradiation
TCM	tumour conditioned media
TME	tumour microenvironment
T reg	regulatory T cell
TLR	toll-like receptor
TRS	tumour regression score
VFA	visceral fat area

References

1. Bray, F.; Ferlay, J.; Soerjomataram, I.; Siegel, R.L.; Torre, L.A.; Jemal, A. Global cancer statistics 2018: GLOBOCAN estimates of incidence and mortality worldwide for 36 cancers in 185 countries. *CA Cancer J. Clin.* **2018**, *68*, 394–424. [CrossRef] [PubMed]
2. Glynne-Jones, R.; Wyrwicz, L.; Tiret, E.; Brown, G.; Rödel, C.; Cervantes, A.; Arnold, D. Rectal cancer: ESMO Clinical Practice Guidelines for diagnosis, treatment and follow-up†. *Ann. Oncol.* **2017**, *28*, 22–40. [CrossRef] [PubMed]

3. Read, T.E.; McNevin, M.S.; Gross, E.K.; Whiteford, H.M.; Lewis, J.L.; Rotkin, G.; Picus, J.; Birnbaum, E.H.; Fleshman, J.W.; Kodner, I.J.; et al. Neoadjuvant therapy for adenocarcinoma of the rectum: Tumor response and acute toxicity. *Dis. Colon Rectum* **2001**, *44*, 513–522. [CrossRef] [PubMed]
4. Maas, M.; Nelemans, P.J.; Valentini, V.; Das, P.; Rödel, C.; Kuo, L.-J.; Calvo, F.A.; García-Aguilar, J.; Glynne-Jones, R.; Haustermans, K.; et al. Long-term outcome in patients with a pathological complete response after chemoradiation for rectal cancer: A pooled analysis of individual patient data. *Lancet Oncol.* **2010**, *11*, 835–844. [CrossRef]
5. Junttila, M.R.; de Sauvage, F.J. Influence of tumour micro-environment heterogeneity on therapeutic response. *Nature* **2013**, *501*, 346–354. [CrossRef]
6. Zare-Bandamiri, M.; Faramouei, M.; Zohourinia, S.; Daneshi, N.; Dianatinasab, M. Risk Factors Predicting Colorectal Cancer Recurrence Following Initial Treatment: A 5-year Cohort Study. *Asian Pac. J. Cancer Prev.* **2017**, *18*, 2665–2670.
7. Schmoll, H.J.; Van Cutsem, E.; Stein, A.; Valentini, V.; Glimelius, B.; Haustermans, K.; Nordlinger, B.; van de Velde, C.J.; Balmana, J.; Regula, J.; et al. ESMO Consensus Guidelines for management of patients with colon and rectal cancer. A personalized approach to clinical decision making. *Ann. Oncol.* **2012**, *23*, 2479–2516. [CrossRef]
8. Hanahan, D.; Weinberg, R.A. Hallmarks of Cancer: The Next Generation. *Cell* **2011**, *144*, 646–674. [CrossRef]
9. Chan, A.T.; Giovannucci, E.L.; Meyerhardt, J.A.; Schernhammer, E.S.; Curhan, G.C.; Fuchs, C.S. Long-term Use of Aspirin and Nonsteroidal Anti-inflammatory Drugs and Risk of Colorectal Cancer. *JAMA* **2005**, *294*, 914–923. [CrossRef]
10. Flossmann, E.; Rothwell, P.M.; British Doctors Aspirin Trial and the UK-TIA Aspirin Trial. Effect of aspirin on long-term risk of colorectal cancer: Consistent evidence from randomised and observational studies. *Lancet* **2007**, *369*, 1603–1613. [CrossRef]
11. Zhang, Q.; Matzke, M.; Scherthan, A.A.; Moore, R.J.; Webb-Robertson, B.-J.; Hu, Z.; Monroe, M.E.; Qian, W.-J.; Smith, R.D.; Morgan, W.F. High and low doses of ionizing radiation induce different secretome profiles in a human skin model. *PLoS ONE* **2014**, *9*, e92332. [CrossRef] [PubMed]
12. Finn, O.J. Immuno-oncology: Understanding the function and dysfunction of the immune system in cancer. *Ann. Oncol.* **2012**, *23*, viii6–viii9. [CrossRef] [PubMed]
13. Formenti, S.C.; Demaria, S. Systemic effects of local radiotherapy. *Lancet Oncol.* **2009**, *10*, 718–726. [CrossRef]
14. Gabrilovich, D. Mechanisms and functional significance of tumour-induced dendritic-cell defects. *Nat. Rev. Immunol.* **2004**, *4*, 941–952. [CrossRef] [PubMed]
15. Grass, G.D.; Krishna, N.; Kim, S. The immune mechanisms of abscopal effect in radiation therapy. *Curr. Probl. Cancer* **2016**, *40*, 10–24. [CrossRef] [PubMed]
16. Rosen, R.E.; Datta, J.; Czerniecki, B.J. Radiation as immunomodulator: Implications for dendritic cell-based immunotherapy. *Radiat. Res.* **2014**, *182*, 211–218. [CrossRef] [PubMed]
17. Kim, K.-W.; Kim, S.-H.; Shin, J.-C.; Kim, G.-S.; Son, Y.-O.; Park, S.-W.; Kwon, B.-H.; Kim, D.-W.; Lee, C.-H.; Sol, M.-Y.; et al. Direct injection of immature dendritic cells into irradiated tumor induces efficient antitumor immunity. *Int. J. Cancer* **2004**, *109*, 685–690. [CrossRef]
18. Park, J.E.; Chen, H.H.; Winer, J.; Houck, K.A.; Ferrara, N. Placenta growth factor. Potentiation of vascular endothelial growth factor bioactivity, in vitro and in vivo, and high affinity binding to Flt-1 but not to Flk-1/KDR. *J. Biol. Chem.* **1994**, *269*, 25646–25654. [CrossRef]
19. Dewerchin, M.; Carmeliet, P. PlGF: A multitasking cytokine with disease-restricted activity. *Cold Spring Harb. Perspect. Med.* **2012**, *2*, a011056. [CrossRef]
20. Matsuo, Y.; Sawai, H.; Ma, J.; Xu, D.; Ochi, N.; Yasuda, A.; Takahashi, H.; Funahashi, H.; Takeyama, H. IL-1alpha secreted by colon cancer cells enhances angiogenesis: The relationship between IL-1alpha release and tumor cells' potential for liver metastasis. *J. Surg. Oncol.* **2009**, *99*, 361–367. [CrossRef]
21. Mojic, M.; Takeda, K.; Hayakawa, Y. The Dark Side of IFN-γ: Its Role in Promoting Cancer Immunoevasion. *Int. J. Mol. Sci.* **2017**, *19*, 89. [CrossRef] [PubMed]
22. Kumari, N.; Dwarakanath, B.S.; Das, A.; Bhatt, A.N. Role of interleukin-6 in cancer progression and therapeutic resistance. *Tumour Biol.* **2016**, *37*, 11553–11572. [CrossRef] [PubMed]
23. Dennis, K.L.; Blatner, N.R.; Gounari, F.; Khazaie, K. Current status of IL-10 and regulatory T-cells in cancer. *Curr. Opin. Oncol.* **2013**, *25*, 637–645. [CrossRef] [PubMed]
24. Liu, J.; Duan, Y.; Cheng, X.; Chen, X.; Xie, W.; Long, H.; Lin, Z.; Zhu, B. IL-17 is associated with poor prognosis and promotes angiogenesis via stimulating VEGF production of cancer cells in colorectal carcinoma. *Biochim. Biophys. Res. Commun.* **2011**, *407*, 348–354. [CrossRef]
25. Tosolini, M.; Kirilovsky, A.; Mlecnik, B.; Fredriksen, T.; Mauger, S.; Bindea, G.; Berger, A.; Bruneval, P.; Fridman, W.-H.; Pagès, F.; et al. Clinical Impact of Different Classes of Infiltrating T Cytotoxic and Helper Cells (Th1, Th2, Treg, Th17) in Patients with Colorectal Cancer. *Cancer Res.* **2011**, *71*, 1263–1271. [CrossRef]
26. De Simone, V.; Pallone, F.; Monteleone, G.; Stolfi, C. Role of T(H)17 cytokines in the control of colorectal cancer. *Oncoimmunology* **2013**, *2*, e26617. [CrossRef]
27. Yu, Q.; Luo, X.; He, Y. Preferential recruitment of Th17 cells to cervical cancer via CCR6-CCL20 pathway. *PLoS ONE* **2015**, *10*, e0120855. [CrossRef]

28. Chen, D.; Jiang, R.; Mao, C.; Shi, L.; Wang, S.; Yu, L.; Hu, Q.; Dai, D.; Xu, H. Chemokine/chemokine receptor interactions contribute to the accumulation of Th17 cells in patients with esophageal squamous cell carcinoma. *Hum. Immunol.* **2012**, *73*, 1068–1072. [CrossRef]
29. Mizukami, Y.; Kono, K.; Kawaguchi, Y.; Akaike, H.; Kamimura, K.; Sugai, H.; Fukii, H. CCL17 and CCL22 chemokines within tumor microenvironment are related to accumulation of Foxp3+ regulatory T cells in gastric cancer. *Int. J. Cancer* **2008**, *122*, 2286–2293. [CrossRef]
30. Maruyama, T.; Kono, K.; Izawa, S.; Mizukami, Y.; Kawaguchi, Y.; Mimura, K.; Watanabe, M.; Fujii, H. CCL17 and CCL22 chemokines within tumor microenvironment are related to infiltration of regulatory T cells in esophageal squamous cell carcinoma. *Dis. Esophagus* **2010**, *23*, 422–429. [CrossRef]
31. De Monte, L.; Reni, M.; Tassi, E.; Clavenna, D.; Papa, I.; Recalde, H.; Braga, M.; Di Carlo, V.; Doglioni, C.; Protti, M.P. Intratumor T helper type 2 cell infiltrate correlates with cancer-associated fibroblast thymic stromal lymphopoietin production and reduced survival in pancreatic cancer. *J. Exp. Med.* **2011**, *208*, 469–478. [CrossRef] [PubMed]
32. Lunardi, S.; Lim, S.Y.; Muschel, R.J.; Brunner, T.B. IP-10/CXCL10 attracts regulatory T cells: Implication for pancreatic cancer. *Oncoimmunology* **2015**, *4*, e1027473. [CrossRef] [PubMed]
33. Iellem, A.; Mariani, M.; Lang, R.; Recalde, H.; Panina-Bordignon, P.; Sinigaglia, F.; D'Ambrosio, D. Unique chemotactic response profile and specific expression of chemokine receptors CCR4 and CCR8 by CD4 (+) CD25 (+) regulatory T cells. *J. Exp. Med.* **2001**, *194*, 847–853. [CrossRef] [PubMed]
34. Perera, P.-Y.; Lichy, J.H.; Waldmann, T.A.; Perera, L.P. The role of interleukin-15 in inflammation and immune responses to infection: Implications for its therapeutic use. *Microbes Infect.* **2012**, *14*, 247–261. [CrossRef]
35. Vyas, D.; Laput, G.; Vyas, A.K. Chemotherapy-enhanced inflammation may lead to the failure of therapy and metastasis. *Onco Targets Ther.* **2014**, *7*, 1015–1023. [CrossRef]
36. Buckley, A.M.; Lynam-Lennon, N.; Kennedy, S.A.; Dunne, M.R.; Aird, J.J.; Foley, E.K.; Clarke, N.; Ravi, N.; O'Toole, D.; Reynolds, J.V.; et al. Leukaemia inhibitory factor is associated with treatment resistance in oesophageal adenocarcinoma. *Oncotarget* **2018**, *9*, 33634–33647. [CrossRef]
37. Maher, S.G.; McDowell, D.T.; Collins, B.C.; Muldoon, C.; Gallagher, W.M.; Reynolds, J.V. Serum Proteomic Profiling Reveals That Pretreatment Complement Protein Levels are Predictive of Esophageal Cancer Patient Response to Neoadjuvant Chemoradiation. *Ann. Surg.* **2011**, *254*, 809–816. [CrossRef]
38. Michielsen, A.J.; Ryan, E.J.; O'Sullivan, J.N. Dendritic cell inhibition correlates with survival of colorectal cancer patients on bevacizumab treatment. *Oncoimmunology* **2012**, *1*, 1445–1447. [CrossRef]
39. Michielsen, A.J.; Noonan, S.; Martin, P.; Tosetto, M.; Marry, J.; Biniecka, M.; Maguire, A.A.; Hyland, J.M.; Sheahan, K.D.; O'Donoghue, D.P.; et al. Inhibition of Dendritic Cell Maturation by the Tumor Microenvironment Correlates with the Survival of Colorectal Cancer Patients following Bevacizumab Treatment. *Mol. Cancer Ther.* **2012**, *11*, 1829–1837. [CrossRef]
40. Michielsen, A.J.; Hogan, A.E.; Marry, J.; Tosetto, M.; Cox, F.; Hyland, J.M.; Sheahan, K.D.; O'Donoghue, D.P.; Mulcahy, H.E.; Ryan, E.J.; et al. Tumour Tissue Microenvironment Can Inhibit Dendritic Cell Maturation in Colorectal Cancer. *PLoS ONE* **2011**, *6*, e27944. [CrossRef]
41. Morrissey, M.E.; Byrne, R.; Nulty, C.; McCabe, N.H.; Lynam-Lennon, N.; Butler, C.T.; Kennedy, S.; O'Toole, D.; Larkin, J.; McCormick, P.; et al. The tumour microenvironment of the upper and lower gastrointestinal tract differentially influences dendritic cell maturation. *BMC Cancer* **2020**, *20*, 566. [CrossRef] [PubMed]
42. Kulzer, L.; Rubner, Y.; Deloch, L.; Allgäuer, A.; Frey, B.; Fietkau, R.; Dörrie, J.; Schaft, N.; Gaipl, U.S. Norm- and hypo-fractionated radiotherapy is capable of activating human dendritic cells. *J. Immunotoxicol.* **2014**, *11*, 328–336. [CrossRef] [PubMed]
43. Beckebaum, S.; Zhang, X.; Chen, X.; Yu, Z.; Frilling, A.; Dworacki, G.; Grosse-Wilde, H.; Broelsch, C.E.; Gerken, G.; Cicinnati, V.R. Increased Levels of Interleukin-10 in Serum from Patients with Hepatocellular Carcinoma Correlate with Profound Numerical Deficiencies and Immature Phenotype of Circulating Dendritic Cell Subsets. *Clin. Cancer Res.* **2004**, *10*, 7260–7269. [CrossRef] [PubMed]
44. Gabrilovich, D.I.; Chen, H.L.; Girgis, K.R.; Cunningham, H.T.; Meny, G.M.; Nadaf, S.; Kavanaugh, D.; Carbone, D.P. Production of vascular endothelial growth factor by human tumors inhibits the functional maturation of dendritic cells. *Nat. Med.* **1996**, *2*, 1096–1103. [CrossRef] [PubMed]
45. Laxmanan, S.; Robertson, S.W.; Wang, E.; Lau, J.S.; Briscoe, D.M.; Mukhopadhyay, D. Vascular endothelial growth factor impairs the functional ability of dendritic cells through Id pathways. *Biochem. Biophys. Res. Commun.* **2005**, *334*, 193–198. [PubMed]
46. Karakhanova, S.; Bedke, T.; Enk, A.H.; Mahnke, K. IL-27 renders DC immunosuppressive by induction of B7-H1. *J. Leukoc. Biol.* **2011**, *89*, 837–845. [CrossRef]
47. Ather, J.L.; Ckless, K.; Martin, R.; Foley, K.L.; Suratt, B.T.; Boyson, J.E.; Fitzgerald, K.A.; Flavell, R.A.; Eisenbarth, S.C.; Poynter, M.E. Serum amyloid A activates the NLRP3 inflammasome and promotes Th17 allergic asthma in mice. *J. Immunol.* **2011**, *187*, 64–73. [CrossRef]
48. Sun, Y.; Xu, Z.; Lin, H.; Lu, X.; Huang, Y.; Huang, S.; Wang, X.; Chi, P. Impact of body mass index on treatment outcome of neoadjuvant chemoradiotherapy in locally advanced rectal cancer. *Eur. J. Surg. Oncol.* **2017**, *43*, 1828–1834. [CrossRef]
49. Park, I.J.; You, Y.N.; Skibber, J.M.; Rodriguez-Bigas, M.A.; Das, P.; Eng, C.; Kopetz, S.; Wolff, R.A.; Crane, C.H.; Krishnan, S.; et al. Oncologic and Functional Hazards of Obesity Among Patients With Locally Advanced Rectal Cancer Following Neoadjuvant Chemoradiation Therapy. *Am. J. Clin. Oncol.* **2017**, *40*, 277–282. [CrossRef]

50. Addison, O.; Marcus, R.L.; Lastayo, P.C.; Ryan, A.S. Intermuscular fat: A review of the consequences and causes. *Int. J. Endocrinol.* **2014**, *2014*, 309570. [CrossRef]
51. Doyle, S.L.; Bennett, A.M.; Donohoe, C.L.; Mongan, A.M.; Howard, J.M.; Lithander, F.E.; Pidgeon, G.P.; Reynolds, J.V.; Lysaght, J. Establishing computed tomography-defined visceral fat area thresholds for use in obesity-related cancer research. *Nutr. Res.* **2013**, *33*, 171–179. [CrossRef] [PubMed]
52. Dunne, M.R.; Madrigal-Estebas, L.; Tobin, L.M.; Doherty, D.G. (E)-4-Hydroxy-3-methyl-but-2 enyl pyrophosphate-stimulated Vγ9Vδ2 T cells possess T helper type 1-promoting adjuvant activity for human monocyte-derived dendritic cells. *Cancer Immunol. Immunother.* **2010**, *59*, 1109–1120. [CrossRef] [PubMed]

Bibliography

1. Bray F, Ferlay J, Soerjomataram I, Siegel RL, Torre LA, Jemal A. Global cancer statistics 2018: GLOBOCAN estimates of incidence and mortality worldwide for 36 cancers in 185 countries. CA Cancer J Clin. 2018;68(6):394–424.

2. National Cancer Registry in Ireland (2019) Cancer in Ireland 1994-2017 with estimates for 2017-2019: Annual Report of the National Cancer Registry. Cork, Ireland; 2019.

3. Jhaveri KS, Hosseini-Nik H. MRI of Rectal Cancer: An Overview and Update on Recent Advances. Am J Roentgenol. 2015;205(1):W42–55.

4. Glynne-Jones R, Wyrwicz L, Tiret E, Brown G, Rödel C, Cervantes A, et al. Rectal cancer: ESMO Clinical Practice Guidelines for diagnosis, treatment and follow-up†. Ann Oncol. 2017;28(suppl_4):iv22–40.

5. National Cancer Registry in Ireland. Cancer incidence projections for Ireland 2020-2045. Cork, Ireland; 2019.

6. Araghi M, Soerjomataram I, Jenkins M, Brierley J, Morris E, Bray F, et al. Global trends in colorectal cancer mortality: projections to the year 2035. Int J Cancer. 2019;144(12):2992–3000.

7. Yun HR, Lee LJ, Park JH, Cho YK, Cho YB, Lee WY, et al. Local recurrence after curative resection in patients with colon and rectal cancers. Int J Colorectal Dis. 2008;23(11):1081–1087.

8. Manfredi S, Bouvier AM, Lepage C, Hatem C, Dancourt V, Faivre J. Incidence and patterns of recurrence after resection for cure of colonic cancer in a well defined population. Br J Surg. 2006;93(9):1115–1122.

9. Hong TS, Clark JW, Haigis KM. Cancers of the Colon and Rectum: Identical or Fraternal Twins? Cancer Discov. 2012;2(2):117–121.

10. Holch JW, Demmer M, Lamersdorf C, Michl M, Schulz C, von Einem JC, et al. Pattern and Dynamics of Distant Metastases in Metastatic Colorectal Cancer. Visc Med. 2017;33(1):70–75.

11. Tan KK, Lopes G de L, Sim R. How uncommon are isolated lung metastases in colorectal cancer? A review from database of 754 patients over 4 years. J Gastrointest Surg. 2009;13(4):642–648.

12. Wei EK, Giovannucci E, Wu K, Rosner B, Fuchs CS, Willett WC, et al. Comparison of risk factors for colon and rectal cancer. Int J Cancer. 2004;108(3):433–442.

13. Ruder EH, Laiyemo AO, Graubard BI, Hollenbeck AR, Schatzkin A, Cross AJ. Non-steroidal anti-inflammatory drugs and colorectal cancer risk in a large, prospective cohort. Am J Gastroenterol. 2011;106(7):1340–1350.

14. Lee JE, Li H, Chan AT, Hollis BW, Lee I-M, Stampfer MJ, et al. Circulating Levels of Vitamin D and Colon and Rectal Cancer: The Physicians' Health Study and a Meta-analysis of Prospective Studies. Cancer Prev Res. 2011;4(5):735–743.

15. Mao Y, Pan S, Wen SW, Johnson KC, Group TCCRER. Physical inactivity, energy intake, obesity and the risk of rectal cancer in Canada. Int J Cancer. 2003;105(6):831–837.

16. Larsson SC, Wolk A. Obesity and colon and rectal cancer risk: a meta-analysis of prospective studies. Am J Clin Nutr. 2007;86(3):556–565.

17. Jasperson KW, Tuohy TM, Neklason DW, Burt RW. Hereditary and familial colon cancer. Gastroenterology. 2010;138(6):2044–2058.

18. Roos VH, Mangas-Sanjuan C, Rodriguez-Girondo M, Medina-Prado L, Steyerberg EW, Bossuyt PMM, et al. Effects of Family History on Relative and Absolute Risks for Colorectal Cancer: A Systematic Review and Meta-Analysis. Clin Gastroenterol Hepatol. 2019;17(13):2657-2667.e9.

19. Andrieu N, Launoy G, Guillois R, Ory-Paoletti C, Gignoux M. Estimation of the familial relative risk of cancer by site from a French population based family study on colorectal cancer (CCREF study). Gut. 2004;53(9):1322–1328.

20. Amin MB, Edge S, Greene F, Byrd DR, Brookland, R.K., Washington, M.K., Gershenwald, J.E., Compton CC, Hess KR, et al. AJCC cancer staging manual. 2017.

21. Beddy D, Hyland JMP, Winter DC, Lim C, White A, Moriarty M, et al. A Simplified Tumor Regression Grade Correlates with Survival in Locally Advanced Rectal Carcinoma Treated with Neoadjuvant Chemoradiotherapy. Ann Surg Oncol. 2008;15(12):3471–3477.

22. Petrelli F, Trevisan F, Cabiddu M, Sgroi G, Bruschieri L, Rausa E, et al. Total Neoadjuvant Therapy in Rectal Cancer: A Systematic Review and Meta-analysis of Treatment Outcomes. Ann Surg. 2020;271(3):440–448.

23. Maas M, Nelemans PJ, Valentini V, Das P, Rödel C, Kuo L-J, et al. Long-term outcome in patients with a pathological complete response after chemoradiation for rectal cancer: a pooled analysis of individual patient data. Lancet Oncol. 2010;11(9):835–844.

24. Kong JC, Guerra GR, Warrier SK, Lynch AC, Michael M, Ngan SY, et al. Prognostic value of tumour regression grade in locally advanced rectal cancer: a systematic review and meta-analysis. Color Dis. 2018;20(7):574–585.

25. Sauer R, Becker H, Hohenberger W, Rodel C, Wittekind C, Fietkau R, et al. Preoperative versus postoperative chemoradiotherapy for rectal cancer. N Engl J Med [Internet]. 2004;351(17):1731–1740.

26. Sauer R, Liersch T, Merkel S, Fietkau R, Hohenberger W, Hess C, et al. Preoperative Versus Postoperative Chemoradiotherapy for Locally Advanced Rectal Cancer: Results of the German CAO/ARO/AIO-94 Randomized Phase III Trial After a Median Follow-Up of 11 Years. J Clin Oncol. 2012;30(16):1926–1933.

27. Roh MS, Colangelo LH, O'Connell MJ, Yothers G, Deutsch M, Allegra CJ, et al. Preoperative multimodality therapy improves disease-free survival in patients with carcinoma of the rectum: NSABP R-03. J Clin Oncol. 2009;27(31):5124–5130.

28. Bosset JF, Collette L, Calais G, Mineur L, Maingon P, Radosevic-Jelic L, et al. Chemotherapy with preoperative radiotherapy in rectal cancer. N Engl J Med. 2006;355(11):1114–1123.

29. Brierley J, Gospodarowicz M, Wittekind C. TNM Classification of Malignant

Tumours, 8th Edition. 2016.

30. Bitterman DS, Resende Salgado L, Moore HG, Sanfilippo NJ, Gu P, Hatzaras I, et al. Predictors of Complete Response and Disease Recurrence Following Chemoradiation for Rectal Cancer. Front Oncol. 2015;5:286.

31. Clancy C, Burke JP, Coffey JC. KRAS mutation does not predict the efficacy of neo-adjuvant chemoradiotherapy in rectal cancer: A systematic review and meta-analysis. Surg Oncol. 2013;22(2):105–111.

32. McCawley N, Clancy C, O'Neill BDP, Deasy J, McNamara DA, Burke JP. Mucinous Rectal Adenocarcinoma Is Associated with a Poor Response to Neoadjuvant Chemoradiotherapy : A Systematic Review and Meta-analysis. Dis Colon Rectum. 2016;59(12):1200–1208.

33. Chen M-B, Wu X-Y, Yu R, Li C, Wang L-Q, Shen W, et al. P53 status as a predictive biomarker for patients receiving neoadjuvant radiation-based treatment: a meta-analysis in rectal cancer. PLoS One. 2012;7(9):e45388.

34. Probst CP, Becerra AZ, Aquina CT, Tejani MA, Hensley BJ, González MG, et al. Watch and Wait?—Elevated Pretreatment CEA Is Associated with Decreased Pathological Complete Response in Rectal Cancer. J Gastrointest Surg. 2016;20(1):43–52.

35. Dayde D, Tanaka I, Jain R, Tai MC, Taguchi A. Predictive and Prognostic Molecular Biomarkers for Response to Neoadjuvant Chemoradiation in Rectal Cancer. Int J Mol Sci. 2017;18(3):573.

36. Gaedcke J, Leha A, Claus R, Weichenhan D, Jung K, Kitz J, et al. Identification of a DNA methylation signature to predict disease-free survival in locally advanced rectal cancer. Oncotarget. 2014;5(18):8123–8135.

37. Watanabe T, Komuro Y, Kiyomatsu T, Kanazawa T, Kazama Y, Tanaka J, et al. Prediction of Sensitivity of Rectal Cancer Cells in Response to Preoperative Radiotherapy by DNA Microarray Analysis of Gene Expression Profiles. Cancer Res. 2006;66(7):3370–3374.

38. Agostini M, Zangrando A, Pastrello C, D'Angelo E, Romano G, Giovannoni R, et al. A functional biological network centered on XRCC3: a new possible marker of chemoradiotherapy resistance in rectal cancer patients. Cancer Biol Ther. 2015;16(8):1160–1171.

39. World Cancer Research Fund/American Institute for Cancer Research. Continuous Update Project Expert Report 2018. Body fatness and weight gain and the risk of cancer. 2018.

40. Sun Y, Xu Z, Lin H, Lu X, Huang Y, Huang S, et al. Impact of body mass index on treatment outcome of neoadjuvant chemoradiotherapy in locally advanced rectal cancer. Eur J Surg Oncol. 2017;43(10):1828–1834.

41. Clark W, Siegel EM, Chen YA, Zhao X, Parsons CM, Hernandez JM, et al. Quantitative measures of visceral adiposity and body mass index in predicting rectal cancer outcomes after neoadjuvant chemoradiation. J Am Coll Surg. 2013;216(6):1070–1081.

42. Meyerhardt JA, Tepper JE, Niedzwiecki D, Hollis DR, McCollum AD, Brady D,

et al. Impact of Body Mass Index on Outcomes and Treatment-Related Toxicity in Patients With Stage II and III Rectal Cancer: Findings From Intergroup Trial 0114. J Clin Oncol. 2004;22(4):648–657.

43. Seishima R, Okabayashi K, Hasegawa H, Sugiyama D, Ishii Y, Tsuruta M, et al. Obesity was associated with a decreased postoperative recurrence of rectal cancer in a Japanese population. Surg Today. 2014;44(12):2324–2331.

44. Griggs JJ, Mangu PB, Anderson H, Balaban EP, Dignam JJ, Hryniuk WM, et al. Appropriate Chemotherapy Dosing for Obese Adult Patients With Cancer: American Society of Clinical Oncology Clinical Practice Guideline. J Clin Oncol. 2012;30(13):1553–1561.

45. Winters E, Poole C. Challenges and impact of patient obesity in radiation therapy practice. Radiography. 2020;26(3):e158–163.

46. Abnet CC, Arnold M, Wei W-Q. Epidemiology of Esophageal Squamous Cell Carcinoma. Gastroenterology. 2018;154(2):360–373.

47. Arnold M, Soerjomataram I, Ferlay J, Forman D. Global incidence of oesophageal cancer by histological subtype in 2012. Gut. 2015;64(3):381–387.

48. Kubo A, Corley DA. Body Mass Index and Adenocarcinomas of the Esophagus or Gastric Cardia: A Systematic Review and Meta-analysis. Cancer Epidemiol Biomarkers Prev. 2006;15(5):872–878.

49. Coleman HG, Xie S-H, Lagergren J. The Epidemiology of Esophageal Adenocarcinoma. Gastroenterology. 2018;154(2):390–405.

50. Howlader N, Noone AM, Krapcho M, Miller D, Brest A, Yu M, Ruhl J, Tatalovich Z, Mariotto A, Lewis DR, Chen HS, Feuer EJ CK. SEER Cancer Statistics Review, 1975-2016. National Cancer Institute. Bethesda, MD, https://seer.cancer.gov/csr/1975_2016/, based on November 2018 SEER data submission, posted to the SEER website, April 2019.

51. Thrift AP. The epidemic of oesophageal carcinoma: Where are we now? Cancer Epidemiol. 2016;41:88–95.

52. Turati F, Tramacere I, La Vecchia C, Negri E. A meta-analysis of body mass index and esophageal and gastric cardia adenocarcinoma. Ann Oncol. 2012;24(3):609–617.

53. Olsen CM, Pandeya N, Green AC, Webb PM, Whiteman DC, Study for the AC. Population Attributable Fractions of Adenocarcinoma of the Esophagus and Gastroesophageal Junction. Am J Epidemiol. 2011;174(5):582–590.

54. Alexandre L, Long E, Beales IL. Pathophysiological mechanisms linking obesity and esophageal adenocarcinoma. World J Gastrointest Pathophysiol. 2014;5(4):534–549.

55. Spechler S. Barrett's esophagus. Semin Gastrointest Dis. 1996;7(2):51–60.

56. Ronkainen J, Aro P, Storskrubb T, Johansson S, Lind T, Bolling–Sternevald E, et al. Prevalence of Barrett's Esophagus in the General Population: An Endoscopic Study. Gastroenterology. 2005;129(6):1825–1831.

57. Hvid-Jensen F, Pedersen L, Drewes AM, Sørensen HT, Funch-Jensen P. Incidence of Adenocarcinoma among Patients with Barrett's Esophagus. N Engl J Med. 2011;365(15):1375–83.

58. Donohoe CL, O'Farrell NJ, Doyle SL, Reynolds J V. The role of obesity in gastrointestinal cancer: evidence and opinion. Therap Adv Gastroenterol. 2013;7(1):38–50.

59. Hanahan D, Weinberg RA. Hallmarks of Cancer: The Next Generation. Cell. 2011;144(5):646–674.

60. Donohoe CL, Doyle SL, Reynolds J V. Visceral adiposity, insulin resistance and cancer risk. Diabetol Metab Syndr. 2011;3:12.

61. Vigneri R, Goldfine ID, Frittitta L. Insulin, insulin receptors, and cancer. J Endocrinol Invest. 2016;39(12):1365–1376.

62. Yang H, Youm Y-H, Vandanmagsar B, Ravussin A, Gimble JM, Greenway F, et al. Obesity Increases the Production of Proinflammatory Mediators from Adipose Tissue T Cells and Compromises TCR Repertoire Diversity: Implications for Systemic Inflammation and Insulin Resistance. J Immunol. 2010;185(3):1836–1845.

63. Corvera S, Gealekman O. Adipose tissue angiogenesis: impact on obesity and type-2 diabetes. Biochim Biophys Acta. 2014;1842(3):463–472.

64. Dieudonne M-N, Bussiere M, Dos Santos E, Leneveu M-C, Giudicelli Y, Pecquery R. Adiponectin mediates antiproliferative and apoptotic responses in human MCF7 breast cancer cells. Biochem Biophys Res Commun. 2006;345(1):271–279.

65. Bråkenhielm E, Veitonmäki N, Cao R, Kihara S, Matsuzawa Y, Zhivotovsky B, et al. Adiponectin-induced antiangiogenesis and antitumor activity involve caspase-mediated endothelial cell apoptosis. Proc Natl Acad Sci U S A. 2004;101(8):2476–2481.

66. Roberts DL, Dive C, Renehan AG. Biological mechanisms linking obesity and cancer risk: new perspectives. Annu Rev Med. 2010;61:301–316.

67. Renehan AG, Roberts DL, Dive C. Obesity and cancer: Pathophysiological and biological mechanisms. Arch Physiol Biochem. 2008;114(1):71–83.

68. Lordick F, Mariette C, Haustermans K, Obermannová R, Arnold D, Committee on behalf of the EG. Oesophageal cancer: ESMO Clinical Practice Guidelines for diagnosis, treatment and follow-up†. Ann Oncol. 2016;27(suppl_5):v50–57.

69. Reynolds J V, Preston SR, O'Neill B, Baeksgaard L, Griffin SM, Mariette C, et al. ICORG 10-14: NEOadjuvant trial in Adenocarcinoma of the oEsophagus and oesophagoGastric junction International Study (Neo-AEGIS). BMC Cancer. 2017;17(1):401.

70. Al-Batran S-E, Hofheinz RD, Pauligk C, Kopp H-G, Haag GM, Luley KB, et al. Histopathological regression after neoadjuvant docetaxel, oxaliplatin, fluorouracil, and leucovorin versus epirubicin, cisplatin, and fluorouracil or capecitabine in patients with resectable gastric or gastro-oesophageal junction adenocarcinoma (FLOT4-AIO. Lancet Oncol. 2016;17(12):1697–1708.

71. Mandard A, Dalibard F, Mandard J, Marnay J, Henry-Amar M, Petiot J, et al. Pathologic assessment of tumor regression after preoperative chemoradiotherapy of esophageal carcinoma. Clinicopathologic correlations. Cancer. 1994;73(11):2680–2686.

72. Donohoe CL, Reynolds JV. Neoadjuvant treatment of locally advanced esophageal and junctional cancer: the evidence-base, current key questions and clinical trials. J Thorac Dis. 2017;9(Suppl 8):S697–704.

73. Alnaji RM, Du W, Gabriel E, Singla S, Attwood K, Nava H, et al. Pathologic Complete Response Is an Independent Predictor of Improved Survival Following Neoadjuvant Chemoradiation for Esophageal Adenocarcinoma. J Gastrointest Surg. 2016;20(9):1541–1546.

74. Reynolds JV, Muldoon C, Hollywood D, Ravi N, Rowley S, O'Byrne K, et al. Long-term outcomes following neoadjuvant chemoradiotherapy for esophageal cancer. Ann Surg. 2007;245(5):707–716.

75. Donlon NE, Sheppard A, Davern M, O'Connell F, Phelan JJ, Power R, et al. Linking Circulating Serum Proteins with Clinical Outcomes in Esophageal Adenocarcinoma-An Emerging Role for Chemokines. Cancers (Basel). 2020;12(11):3356.

76. Powell AGMT, Chin C, Coxon AH, Chalishazar A, Christian A, Roberts SA, et al. Neutrophil to lymphocyte ratio as a predictor of response to neoadjuvant chemotherapy and survival in oesophageal adenocarcinoma. BJS open. 2020;4(3):416–423.

77. Li Y, Huang H-C, Chen L-Q, Xu L-Y, Li E-M, Zhang J-J. Predictive biomarkers for response of esophageal cancer to chemo(radio)therapy: A systematic review and meta-analysis. Surg Oncol. 2017;26(4):460–472.

78. Cools-Lartigue J, Ferri L. Should Multidisciplinary Treatment Differ for Esophageal Adenocarcinoma Versus Esophageal Squamous Cell Cancer? Ann Surg Oncol. 2019;26(4):1014–1027.

79. Mongan AM, Lynam-Lennon N, Doyle SL, Casey R, Carr E, Cannon A, et al. Visceral Adipose Tissue Modulates Radiosensitivity in Oesophageal Adenocarcinoma. Int J Med Sci. 2019;16(4):519–528.

80. Buckley AM, Dunne MR, Lynam-Lennon N, Kennedy SA, Cannon A, Reynolds AL, et al. Pyrazinib (P3), [(E)-2-(2-Pyrazin-2-yl-vinyl)-phenol], a small molecule pyrazine compound enhances radiosensitivity in oesophageal adenocarcinoma. Cancer Lett. 2019;447:115–129.

81. Lynam-Lennon N, Connaughton R, Carr E, Mongan A-M, O'Farrell NJ, Porter RK, et al. Excess visceral adiposity induces alterations in mitochondrial function and energy metabolism in esophageal adenocarcinoma. BMC Cancer. 2014;14(1):907.

82. Kratz M, Coats BR, Hisert KB, Hagman D, Mutskov V, Peris E, et al. Metabolic dysfunction drives a mechanistically distinct proinflammatory phenotype in adipose tissue macrophages. Cell Metab. 2014;20(4):614–625.

83. Jha AK, Huang SC-C, Sergushichev A, Lampropoulou V, Ivanova Y, Loginicheva

E, et al. Network Integration of Parallel Metabolic and Transcriptional Data Reveals Metabolic Modules that Regulate Macrophage Polarization. Immunity. 2015;42(3):419–430.

84. Ralston JC, Lyons CL, Kennedy EB, Kirwan AM, Roche HM. Fatty Acids and NLRP3 Inflammasome–Mediated Inflammation in Metabolic Tissues. Annu Rev Nutr. 2017;37(1):77–102.

85. Baskar R, Lee KA, Yeo R, Yeoh K-W. Cancer and radiation therapy: current advances and future directions. Int J Med Sci. 2012;9(3):193–199.

86. Ringborg U, Bergqvist D, Brorsson B, Cavallin-ståhl E, Ceberg J, Einhorn N, et al. The Swedish Council on Technology Assessment in Health Care (SBU) Systematic Overview of Radiotherapy for Cancer including a Prospective Survey of Radiotherapy Practice in Sweden 2001--Summary and Conclusions. Acta Oncol (Madr). 2003;42(5–6):357–365.

87. Wang H, Mu X, He H, Zhang X-D. Cancer Radiosensitizers. Trends Pharmacol Sci. 2018;39(1):24–48.

88. Mehta SR, Suhag V, Semwal M, Sharma N. Radiotherapy: Basic Concepts and Recent Advances. Med J Armed Forces India. 2010;66(2):158–162.

89. Pajonk F, Vlashi E, McBride WH. Radiation resistance of cancer stem cells: the 4 R's of radiobiology revisited. Stem Cells. 2010;28(4):639–648.

90. Yang J, Yue J-B, Liu J, Yu J-M. Repopulation of tumor cells during fractionated radiotherapy and detection methods (Review). Oncol Lett. 2014;7(6):1755–1760.

91. Pawlik TM, Keyomarsi K. Role of cell cycle in mediating sensitivity to radiotherapy. Int J Radiat Oncol Biol Phys. 2004;59(4):928–942.

92. Withers HR. Cell Cycle Redistribution as a Factor in Multifraction Irradiation. Radiology. 1975;114(1):199–202.

93. Ding M, Newman F, Chen C, Stuhr K, Gaspar LE. Dosimetric Comparison Between 3DCRT and IMRT Using Different Multileaf Collimators in the Treatment of Brain Tumors. Med Dosim. 2009;34(1):1–8.

94. Cox JD, Stetz J, Pajak TF. Toxicity criteria of the Radiation Therapy Oncology Group (RTOG) and the European Organization for Research and Treatment of Cancer (EORTC). Int J Radiat Oncol Biol Phys. 1995;31(5):1341–1346.

95. Williams J, Chen Y, Rubin P, Finkelstein J, Okunieff P. The biological basis of a comprehensive grading system for the adverse effects of cancer treatment. Semin Radiat Oncol. 2003;13(3):182–188.

96. Morton LM, Onel K, Curtis RE, Hungate EA, Armstrong GT. The Rising Incidence of Second Cancers: Patterns of Occurrence and Identification of Risk Factors for Children and Adults. Am Soc Clin Oncol Educ Book. 2014;(34):e57–67.

97. Berrington de Gonzalez A, Curtis RE, Kry SF, Gilbert E, Lamart S, Berg CD, et al. Proportion of second cancers attributable to radiotherapy treatment in adults: a cohort study in the US SEER cancer registries. Lancet Oncol. 2011;12(4):353–360.

98. Birgisson H, Påhlman L, Gunnarsson U, Glimelius B. Occurrence of Second Cancers in Patients Treated With Radiotherapy for Rectal Cancer. J Clin Oncol. 2005;23(25):6126–6131.

99. Wallis CJD, Mahar AL, Choo R, Herschorn S, Kodama RT, Shah PS, et al. Second malignancies after radiotherapy for prostate cancer: systematic review and meta-analysis. BMJ. 2016;352:i851.

100. Brenner DJ, Curtis R, Hall E, Ron E. Second malignancies in prostate carcinoma patients after radiotherapy compared with surgery. Cancer. 2000;88(2):398–406.

101. Sharif S, Ferner R, Birch JM, Gillespie JE, Gattamaneni HR, Baser ME, et al. Second Primary Tumors in Neurofibromatosis 1 Patients Treated for Optic Glioma: Substantial Risks After Radiotherapy. J Clin Oncol. 2006;24(16):2570–2575.

102. Lönn S, Gilbert ES, Ron E, Smith SA, Stovall M, Curtis RE. Comparison of Second Cancer Risks from Brachytherapy and External Beam Therapy After Uterine Corpus Cancer. Cancer Epidemiol Biomarkers Prev. 2010;19(2):464–474.

103. Zablotska L, Chak A, Das A, Neugut A. Increased risk of squamous cell esophageal cancer after adjuvant radiation therapy for primary breast cancer. Am J Epidemiol. 2005;161(4):330–337.

104. Sigurdson AJ, Jones IM. Second cancers after radiotherapy: any evidence for radiation-induced genomic instability? Oncogene. 2003;22(45):7018–7027.

105. Yock HP, Athar BS, Moteabbad M, Adams JA, Schneider U, Yock TI. Assessment of radiation-induced second cancer risks in proton therapy and IMRT for organs inside the primary radiation field. Phys Med Biol. 2012;57(19):6047.

106. Barnett GC, West CML, Dunning AM, Elliott RM, Coles CE, Pharoah PDP, et al. Normal tissue reactions to radiotherapy: towards tailoring treatment dose by genotype. Nat Rev Cancer. 2009;9(2):134–142.

107. Balkwill FR, Capasso M, Hagemann T. The tumor microenvironment at a glance. J Cell Sci. 2012;125(23):5591–5596.

108. Hanahan D, Coussens LM. Accessories to the Crime: Functions of Cells Recruited to the Tumor Microenvironment. Cancer Cell. 2012;21(3):309–322.

109. Hirata E, Sahai E. Tumor Microenvironment and Differential Responses to Therapy. Cold Spring Harb Perspect Med. 2017;7(7):a026781.

110. Baghban R, Roshangar L, Jahanban-Esfahlan R, Seidi K, Ebrahimi-Kalan A, Jaymand M, et al. Tumor microenvironment complexity and therapeutic implications at a glance. Cell Commun Signal. 2020;18:59.

111. Lynam-Lennon N, Maher SG, Maguire A, Phelan J, Muldoon C, Reynolds J V, et al. Altered Mitochondrial Function and Energy Metabolism Is Associated with a Radioresistant Phenotype in Oesophageal Adenocarcinoma. PLoS One. 2014;9(6):e100738.

112. Ashton TM, Fokas E, Kunz-Schughart LA, Folkes LK, Anbalagan S, Huether M, et al. The anti-malarial atovaquone increases radiosensitivity by alleviating tumour hypoxia. Nat Commun. 2016;7(1):12308.

113. Benej M, Hong X, Vibhute S, Scott S, Wu J, Graves E, et al. Papaverine and its derivatives radiosensitize solid tumors by inhibiting mitochondrial metabolism. Proc Natl Acad Sci U S A. 2018;115(42):10756–10761.

114. Zannella VE, Pra AD, Muaddi H, McKee TD, Stapleton S, Sykes J, et al. Reprogramming Metabolism with Metformin Improves Tumor Oxygenation and Radiotherapy Response. Clin Cancer Res. 2013;19(24):6741–6750.

115. Vander Heiden MG, Cantley LC, Thompson CB. Understanding the Warburg effect: the metabolic requirements of cell proliferation. Science. 2009;324(5930):1029–1033.

116. Warburg O, Wind F, Negelein E. The Metabolism of Tumors in the Body. J Gen Physiol. 1927;8(6):519–530.

117. Porporato PE, Filigheddu N, Pedro JMB-S, Kroemer G, Galluzzi L. Mitochondrial metabolism and cancer. Cell Res. 2018;28(3):265–280.

118. Dang L, White DW, Gross S, Bennett BD, Bittinger MA, Driggers EM, et al. Cancer-associated IDH1 mutations produce 2-hydroxyglutarate. Nature. 2009;462(7274):739–744.

119. Wise DR, Ward PS, Shay JES, Cross JR, Gruber JJ, Sachdeva UM, et al. Hypoxia promotes isocitrate dehydrogenase-dependent carboxylation of α-ketoglutarate to citrate to support cell growth and viability. Proc Natl Acad Sci. 2011;108(49):19611–19616.

120. Zu XL, Guppy M. Cancer metabolism: facts, fantasy, and fiction. Biochem Biophys Res Commun. 2004;313(3):459–465.

121. Potter M, Newport E, Morten KJ. The Warburg effect: 80 years on. Biochem Soc Trans. 2016;44(5):1499–1505.

122. El-Mir M-Y, Nogueira V, Fontaine E, Avéret N, Rigoulet M, Leverve X. Dimethylbiguanide Inhibits Cell Respiration via an Indirect Effect Targeted on the Respiratory Chain Complex I. J Biol Chem. 2000;275(1):223–228.

123. Owen MR, Doran E, Halestrap AP. Evidence that metformin exerts its anti-diabetic effects through inhibition of complex 1 of the mitochondrial respiratory chain. Biochem J. 2000;348(3):607–614.

124. Rao M, Gao C, Guo M, Law BYK, Xu Y. Effects of metformin treatment on radiotherapy efficacy in patients with cancer and diabetes: a systematic review and meta-analysis. Cancer Manag Res. 2018;10:4881–4890.

125. Aggarwal BB, Vijayalekshmi R V, Sung B. Targeting Inflammatory Pathways for Prevention and Therapy of Cancer: Short-Term Friend, Long-Term Foe. Clin Cancer Res. 2009;15(2):425–430.

126. Grivennikov SI, Greten FR, Karin M. Immunity, Inflammation, and Cancer. Cell. 2010;140(6):883–899.

127. Lin W-W, Karin M. A cytokine-mediated link between innate immunity, inflammation, and cancer. J Clin Invest. 2007;117(5):1175–1183.

128. Rius J, Guma M, Schachtrup C, Akassoglou K, Zinkernagel AS, Nizet V, et al.

NF-kappaB links innate immunity to the hypoxic response through transcriptional regulation of HIF-1alpha. Nature. 2008;453(7196):807–811.

129. Kujawski M, Kortylewski M, Lee H, Herrmann A, Kay H, Yu H. Stat3 mediates myeloid cell–dependent tumor angiogenesis in mice. J Clin Invest. 2008;118(10):3367–3377.

130. Mothersill C, Seymour C. Radiation-induced bystander effects — implications for cancer. Nat Rev Cancer. 2004;4(2):158–164.

131. Wang H, Yu KN, Hou J, Liu Q, Han W. Radiation-induced bystander effect: Early process and rapid assessment. Cancer Lett. 2015;356(1):137–144.

132. Marín A, Martín M, Liñán O, Alvarenga F, López M, Fernández L, et al. Bystander effects and radiotherapy. Reports Pract Oncol Radiother. 2015;20(1):12–21.

133. Gunz F. Bone Marrow Changes in Patients with Chronic Leukaemia Treated by Splenic X-irradiation. Blood. 1953;8:687–692.

134. Parsons W, Watkins C, Pease G, Childs D. Changes in sternal marrow following roentgen-ray therapy to the spleen in chronic granulocytic leukemia. Cancer. 1954;7(1):179–189.

135. Mothersill C, Seymour C. Radiation-Induced Bystander Effects: Past History and Future Directions. Radiat Res. 2001;155(6):759–767.

136. Nagasawa H, Little JB. Induction of Sister Chromatid Exchanges by Extremely Low Doses of Alpha-Particles. Cancer Res. 1992;52(22):6394–6396.

137. Deshpande A, Goodwin EH, Bailey SM, Marrone BL, Lehnert BE. Alpha-Particle-Induced Sister Chromatid Exchange in Normal Human Lung Fibroblasts: Evidence for an Extranuclear Target. Radiat Res. 1996;145(3):260–267.

138. Azzam E, de Toledo S, Gooding T, Little JB. Intercellular Communication Is Involved in the Bystander Regulation of Gene Expression in Human Cells Exposed to Very Low Fluences of Alpha Particles. Radiat Res. 1998;150(5):497–504.

139. Blyth BJ, Sykes PJ. Radiation-Induced Bystander Effects: What Are They, and How Relevant Are They to Human Radiation Exposures? Radiat Res. 2011;176(2):139–157.

140. Hill MA, Stevens DL, Kadhim M, Blake-James M, Mill AJ, Goodhead DT. Experimental techniques for studying bystander effects in vitro by high and low-LET ionising radiation. Radiat Prot Dosimetry. 2006;122(1–4):260–265.

141. Prise KM, Schettino G, Vojnovic B, Belyakov O, Shao C. Microbeam studies of the bystander response. J Radiat Res. 2009;50(Suppl A):A1–6.

142. Lorimore SA, Kadhim MA, Pocock DA, Papworth D, Stevens DL, Goodhead DT, et al. Chromosomal instability in the descendants of unirradiated surviving cells after α-particle irradiation. Proc Natl Acad Sci U S A. 1998;95(10):5730–5733.

143. Seymour CB, Mothersill C. Delayed expression of lethal mutations and genomic instability in the progeny of human epithelial cells that survived in a bystander-killing environment. Radiat Oncol Investig. 1997;5(3):106–110.

144. Zhou H, Randers-Pehrson G, Waldren CA, Vannais D, Hall EJ, Hei TK. Induction

of a bystander mutagenic effect of alpha particles in mammalian cells. Proc Natl Acad Sci U S A. 2000;97(5):2099–2104.

145. Mothersill C, Bristow RG, Harding SM, Smith RW, Mersov A, Seymour CB. A role for p53 in the response of bystander cells to receipt of medium borne signals from irradiated cells. Int J Radiat Biol. 2011;87(11):1120–1125.

146. Shao C, Lyng FM, Folkard M, Prise KM. Calcium Fluxes Modulate the Radiation-Induced Bystander Responses in Targeted Glioma and Fibroblast Cells. Radiat Res. 2006;166(3):479–487.

147. Murphy JEJ, Nugent S, Seymour C, Mothersill C. Mitochondrial DNA point mutations and a novel deletion induced by direct low-LET radiation and by medium from irradiated cells. Mutat Res Toxicol Environ Mutagen. 2005;585(1–2):127–136.

148. Maguire P, Mothersill C, Seymour C, Lyng FM. Medium from irradiated cells induces dose-dependent mitochondrial changes and BCL2 responses in unirradiated human keratinocytes. Radiat Res. 2005;163(4):384–390.

149. Azzam EI, de Toledo SM, Spitz DR, Little JB. Oxidative Metabolism Modulates Signal Transduction and Micronucleus Formation in Bystander Cells from α-Particle-irradiated Normal Human Fibroblast Cultures. Cancer Res. 2002;62(19):5436–5442.

150. Lyng FM, Seymour CB, Mothersill C. Production of a signal by irradiated cells which leads to a response in unirradiated cells characteristic of initiation of apoptosis. Br J Cancer. 2000;83(9):1223–1230.

151. Belyakov O V, Folkard M, Mothersill C, Prise KM, Michael BD. Bystander-induced differentiation: A major response to targeted irradiation of a urothelial explant model. Mutat Res Mol Mech Mutagen. 2006;597(1):43–49.

152. Belyakov O V, Mitchell SA, Parikh D, Randers-Pehrson G, Marino SA, Amundson SA, et al. Biological effects in unirradiated human tissue induced by radiation damage up to 1 mm away. Proc Natl Acad Sci U S A. 2005;102(40):14203–14208.

153. Sedelnikova OA, Nakamura A, Kovalchuk O, Koturbash I, Mitchell SA, Marino SA, et al. DNA Double-Strand Breaks Form in Bystander Cells after Microbeam Irradiation of Three-dimensional Human Tissue Models. Cancer Res. 2007;67(9):4295–4302.

154. Choi VWY, Ng CYP, Kobayashi A, Konishi T, Suya N, Ishikawa T, et al. Bystander Effect between Zebrafish Embryos in Vivo Induced by High-Dose X-rays. Environ Sci Technol. 2013;47(12):6368–6376.

155. Mothersill C, Smith RW, Agnihotri N, Seymour CB. Characterization of a radiation-induced stress response communicated in vivo between zebrafish. Environ Sci Technol. 2007;41(9):3382–3387.

156. Mothersill C, Lyng F, Seymour C, Maguire P, Lorimore S, Wright E. Genetic Factors Influencing Bystander Signaling in Murine Bladder Epithelium after Low-Dose Irradiation In Vivo. Radiat Res. 2005;163(4):391–399.

157. Lyng FM, Seymour CB, Mothersill C. Initiation of Apoptosis in Cells Exposed to

Medium from the Progeny of Irradiated Cells: A Possible Mechanism for Bystander-Induced Genomic Instability? Radiat Res. 2002;157(4):365–370.

158. Östreicher J, Prise KM, Michael BD, Vogt J, Butz T, Tanner JM. Radiation-Induced Bystander Effects - Mechanisms, Biological Implications and Current Investigations at the Leipzig LIPSION Facility. Strahlentherapie und Onkol. 2003;179(2):69–77.

159. Gorman S, Tosetto M, Lyng F, Howe O, Sheahan K, O'Donoghue D, et al. Radiation and chemotherapy bystander effects induce early genomic instability events: Telomere shortening and bridge formation coupled with mitochondrial dysfunction. Mutat Res Mol Mech Mutagen. 2009;669(1–2):131–138.

160. Tharmalingam S, Sreetharan S, Brooks AL, Boreham DR. Re-evaluation of the linear no-threshold (LNT) model using new paradigms and modern molecular studies. Chem Biol Interact. 2019;301:54–67.

161. Hill CK. The low-dose phenomenon: How bystander effects, genomic instability, and adaptive responses could transform cancer-risk models. Bull At Sci. 2012;68(3):51–58.

162. Mole RH. Whole Body Irradiation—Radiobiology or Medicine? Br J Radiol. 1953;26(305):234–241.

163. Zefferino R, Piccoli C, Gioia S Di, Capitanio N, Conese M. Gap Junction Intercellular Communication in the Carcinogenesis Hallmarks: Is This a Phenomenon or Epiphenomenon? Cells. 2019;8(8):896.

164. Heeran AB, Berrigan HP, O'Sullivan J. The Radiation-Induced Bystander Effect (RIBE) and its Connections with the Hallmarks of Cancer. Radiat Res. 2019;192(6):668–679.

165. Kondo Y, Kanzawa T, Sawaya R, Kondo S. The role of autophagy in cancer development and response to therapy. Nat Rev Cancer. 2005;5(9):726–734.

166. Amaravadi RK, Thompson CB. The Roles of Therapy-Induced Autophagy and Necrosis in Cancer Treatment. Clin Cancer Res. 2007;13(24):7271–7279.

167. Lu Z, Luo RZ, Lu Y, Zhang X, Yu Q, Khare S, et al. The tumor suppressor gene ARHI regulates autophagy and tumor dormancy in human ovarian cancer cells . J Clin Invest. 2008;118(12):3917–3929.

168. Wang X, Zhang J, Fu J, Wang J, Ye S, Liu W, et al. Role of ROS-mediated autophagy in radiation-induced bystander effect of hepatoma cells. Int J Radiat Biol. 2015;91(5):452–458.

169. Sotelo J, Briceño E, López-González MA. Adding Chloroquine to Conventional Treatment for Glioblastoma MultiformeA Randomized, Double-Blind, Placebo-Controlled Trial. Ann Intern Med. 2006;144(5):337–343.

170. Bilger A, Bittner M-I, Grosu A-L, Wiedenmann N, Meyer PT, Firat E, et al. FET-PET-based reirradiation and chloroquine in patients with recurrent glioblastoma. Strahlentherapie und Onkol. 2014;190(10):957–961.

171. Yan Y, Xu Z, Dai S, Qian L, Sun L, Gong Z. Targeting autophagy to sensitive glioma to temozolomide treatment. J Exp Clin Cancer Res. 2016;35:23.

172. Wang X, Qiu Y, Yu Q, Li H, Chen X, Li M, et al. Enhanced glioma therapy by synergistic inhibition of autophagy and tyrosine kinase activity. Int J Pharm. 2018;536(1):1–10.

173. Iyer R, Lehnert BE. Alpha-Particle-Induced Increases in the Radioresistance of Normal Human Bystander Cells. Radiat Res. 2002;157(1):3–7.

174. Chen S, Zhao Y, Han W, Chiu SK, Zhu L, Wu L, et al. Rescue effects in radiobiology: Unirradiated bystander cells assist irradiated cells through intercellular signal feedback. Mutat Res Mol Mech Mutagen. 2011;706(1):59–64.

175. Lam RKK, Fung YK, Han W, Yu KN. Rescue Effects: Irradiated Cells Helped by Unirradiated Bystander Cells. Int J Mol Sci. 2015;16(2):2591–2609.

176. He M, Dong C, Xie Y, Li J, Yuan D, Bai Y, et al. Reciprocal bystander effect between α-irradiated macrophage and hepatocyte is mediated by cAMP through a membrane signaling pathway. Mutat Res Mol Mech Mutagen. 2014;763–764:1–9.

177. Lam RKK, Fung YK, Han W, Li L, Chiu SK, Cheng SH, et al. Modulation of NF-κB in rescued irradiated cells. Radiat Prot Dosimetry. 2015;167(1–3):37–43.

178. Bilak A, Uyetake L, Su TT. Dying Cells Protect Survivors from Radiation-Induced Cell Death in Drosophila. PLoS Genet. 2014;10(3):e1004220.

179. Pereira S, Malard V, Ravanat J-L, Davin A-H, Armengaud J, Foray N, et al. Low doses of gamma-irradiation induce an early bystander effect in zebrafish cells which is sufficient to radioprotect cells. PLoS One. 2014;9(3):e92974.

180. Mancuso M, Giardullo P, Leonardi S, Pasquali E, Casciati A, De Stefano I, et al. Dose and Spatial Effects in Long-Distance Radiation Signaling In Vivo: Implications for Abscopal Tumorigenesis. Int J Radiat Oncol Biol Phys. 2013;85(3):813–819.

181. Gerashchenko BI, Howell RW. Bystander cell proliferation is modulated by the number of adjacent cells that were exposed to ionizing radiation. Cytom Part A. 2005;66A(1):62–70.

182. Gerashchenko BI, Howell RW. Cell proximity is a prerequisite for the proliferative response of bystander cells co-cultured with cells irradiated with γ-rays. Cytom Part A. 2003;56A(2):71–80.

183. Azzam EI, de Toledo SM, Little JB. Direct evidence for the participation of gap junction-mediated intercellular communication in the transmission of damage signals from α-particle irradiated to nonirradiated cells. Proc Natl Acad Sci U S A. 2001;98(2):473–478.

184. Bishayee A, Hill HZ, Stein D, Rao D V, Howell RW. Free Radical-Initiated and Gap Junction-Mediated Bystander Effect due to Nonuniform Distribution of Incorporated Radioactivity in a Three-Dimensional Tissue Culture Model. Radiat Res. 2001;155(2):335–344.

185. Iyer R, Lehnert BE. Factors Underlying the Cell Growth-related Bystander Responses to α Particles. Cancer Res. 2000;60(5):1290–1298.

186. Kamochi N, Aoki S, Uchihashi K, Toda S, Kudo S, Nakashima M, et al. Irradiated

fibroblast-induced bystander effects on invasive growth of squamous cell carcinoma under cancer-stromal cell interaction. Cancer Sci. 2008;99(12):2417–2427.

187. Iyer R, Lehnert BE. Low dose, low-LET ionizing radiation-induced radioadaptation and associated early responses in unirradiated cells. Mutat Res Mol Mech Mutagen. 2002;503(1):1–9.

188. Koturbash I, Loree J, Kutanzi K, Koganow C, Pogribny I, Kovalchuk O. In Vivo Bystander Effect: Cranial X-Irradiation Leads to Elevated DNA Damage, Altered Cellular Proliferation and Apoptosis, and Increased p53 Levels in Shielded Spleen. Int J Radiat Oncol. 2008;70(2):554–562.

189. Widel M, Lalik A, Krzywon A, Poleszczuk J, Fujarewicz K, Rzeszowska-Wolny J. The different radiation response and radiation-induced bystander effects in colorectal carcinoma cells differing in p53 status. Mutat Res Mol Mech Mutagen. 2015;778:61–70.

190. Nguyen DH, Oketch-Rabah HA, Illa-Bochaca I, Geyer FC, Reis-Filho JS, Mao J-H, et al. Radiation acts on the microenvironment to affect breast carcinogenesis by distinct mechanisms that decrease cancer latency and affect tumor type. Cancer Cell. 2011;19(5):640–651.

191. Camphausen K, Moses MA, Ménard C, Sproull M, Beecken W-D, Folkman J, et al. Radiation Abscopal Antitumor Effect Is Mediated through p53. Cancer Res. 2003;63(8):1990–1993.

192. Liao E-C, Hsu Y-T, Chuah Q-Y, Lee Y-J, Hu J-Y, Huang T-C, et al. Radiation induces senescence and a bystander effect through metabolic alterations. Cell Death Dis. 2014;5(5):e1255.

193. Vlotides G, Eigler T, Melmed S. Pituitary tumor-transforming gene: Physiology and implications for tumorigenesis. Endocr. Rev. 2007;28(2):165–186.

194. Ogbagabriel S, Fernando M, Waldman FM, Bose S, Heaney AP. Securin is overexpressed in breast cancer. Mod Pathol. 2005;18(7):985–990.

195. Chen W-S, Yu Y-C, Lee Y-J, Chen J-H, Hsu H-Y, Chiu S-J. Depletion of Securin Induces Senescence After Irradiation and Enhances Radiosensitivity in Human Cancer Cells Regardless of Functional p53 Expression. Int J Radiat Oncol Biol Phys. 2010;77(2):566–574.

196. Yu Y-C, Yang P-M, Chuah Q-Y, Huang Y-H, Peng C-W, Lee Y-J, et al. Radiation-induced senescence in securin-deficient cancer cells promotes cell invasion involving the IL-6/STAT3 and PDGF-BB/PDGFR pathways. Sci Rep. 2013;3:1675.

197. Huang Y-H, Yang P-M, Chuah Q-Y, Lee Y-J, Hsieh Y-F, Peng C-W, et al. Autophagy promotes radiation-induced senescence but inhibits bystander effects in human breast cancer cells. Autophagy. 2014;10(7):1212–1228.

198. Pei X-H, Nakanishi Y, Takayama K, Bai F, Hara N. Granulocyte, granulocyte–macrophage, and macrophage colony-stimulating factors can stimulate the invasive capacity of human lung cancer cells. Br J Cancer. 1999;79(1):40–46.

199. He M, Dong C, Ren R, Yuan D, Xie Y, Pan Y, et al. Radiation Enhances the

Invasiveness of Irradiated and Nonirradiated Bystander Hepatoma Cells Through a VEGF-MMP2 Pathway Initiated by p53. Radiat Res. 2013;180(4):389–397.

200. Desai S, Srambikkal N, Yadav HD, Shetake N, Balla MMS, Kumar A, et al. Molecular Understanding of Growth Inhibitory Effect from Irradiated to Bystander Tumor Cells in Mouse Fibrosarcoma Tumor Model. PLoS One. 2016;11(8):e0161662.

201. Fontanella AN, Boss M-K, Hadsell M, Zhang J, Schroeder T, Berman KG, et al. Effects of High-Dose Microbeam Irradiation on Tumor Microvascular Function and Angiogenesis. Radiat Res. 2015;183(2):147–158.

202. Chen S, Zhao Y, Zhao G, Han W, Bao L, Yu KN, et al. Up-regulation of ROS by mitochondria-dependent bystander signaling contributes to genotoxicity of bystander effects. Mutat Res Mol Mech Mutagen. 2009;666(1–2):68–73.

203. Leach JK, Van Tuyle G, Lin P-S, Schmidt-Ullrich R, Mikkelsen RB. Ionizing Radiation-induced, Mitochondria-dependent Generation of Reactive Oxygen/Nitrogen. Cancer Res. 2001;61(10):3894–3901.

204. Tartier L, Gilchrist S, Burdak-Rothkamm S, Folkard M, Prise KM. Cytoplasmic Irradiation Induces Mitochondrial-Dependent 53BP1 Protein Relocalization in Irradiated and Bystander Cells. Cancer Res. 2007;67(12):5872–5879.

205. Shao C, Folkard M, Michael BD, Prise KM. Targeted cytoplasmic irradiation induces bystander responses. Proc Natl Acad Sci U S A. 2004;101(37):13495–13500.

206. Rajendran S, Harrison SH, Thomas RA, Tucker JD. The Role of Mitochondria in the Radiation-Induced Bystander Effect in Human Lymphoblastoid Cells. Radiat Res. 2011;175(2):159–171.

207. Gorman S, Fox E, O'Donoghue D, Sheahan K, Hyland J, Mulcahy H, et al. Mitochondrial mutagenesis induced by tumor-specific radiation bystander effects. J Mol Med. 2010;88(7):701–708.

208. Dypbukt JM, Ankarcrona M, Burkitt M, Sjöholm A, Ström K, Orrenius S, et al. Different prooxidant levels stimulate growth, trigger apoptosis, or produce necrosis of insulin-secreting RINm5F cells. The role of intracellular polyamines. J Biol Chem. 1994;269(48):30553–30560.

209. Sergeeva VA, Ershova ES, Veiko NN, Malinovskaya EM, Kalyanov AA, Kameneva L V, et al. Low-Dose Ionizing Radiation Affects Mesenchymal Stem Cells via Extracellular Oxidized Cell-Free DNA: A Possible Mediator of Bystander Effect and Adaptive Response. Oxid Med Cell Longev. 2017;2017:9515809.

210. Mothersill C, Stamato TD, Perez ML, Cummins R, Mooney R, Seymour CB. Involvement of energy metabolism in the production of 'bystander effects' by radiation. Br J Cancer. 2000;82(10):1740–1746.

211. Emerit I, Oganesian N, Sarkisian T, Arutyunyan R, Pogosian A, Asrian K, et al. Clastogenic Factors in the Plasma of Chernobyl Accident Recovery Workers: Anticlastogenic Effect of Ginkgo biloba Extract. Radiat Res. 1995;144(2):198–205.

212. Rastogi S, Hwang A, Chan J, Wang JYJ. Extracellular vesicles transfer nuclear Abl-dependent and radiation-induced miR-34c into unirradiated cells to cause bystander effects. Mol Biol Cell. 2018;29(18):2228–2242.

213. Xu S, Wang J, Ding N, Hu W, Zhang X, Wang B, et al. Exosome-mediated microRNA transfer plays a role in radiation-induced bystander effect. RNA Biol. 2015;12(12):1355–1363.

214. Yang G, Wu L, Chen S, Zhu L, Huang P, Tong L, et al. Mitochondrial dysfunction resulting from loss of cytochrome c impairs radiation-induced bystander effect. Br J Cancer. 2009;100(12):1912–1916.

215. He M, Zhao M, Shen B, Prise KM, Shao C. Radiation-induced intercellular signaling mediated by cytochrome-c via a p53-dependent pathway in hepatoma cells. Oncogene. 2011;30(16):1947–1955.

216. Le M, McNeill FE, Seymour CB, Rusin A, Diamond K, Rainbow AJ, et al. Modulation of oxidative phosphorylation (OXPHOS) by radiation- induced biophotons. Environ Res. 2018;163:80–87.

217. Calveley VL, Khan MA, Yeung IWT, Vandyk J, Hill RP. Partial volume rat lung irradiation: Temporal fluctuations of in-field and out-of-field DNA damage and inflammatory cytokines following irradiation. Int J Radiat Biol. 2005;81(12):887–999.

218. Liu S-Z, Jin S-Z, Liu X-D. Radiation-induced Bystander Effect in Immune Response. Biomed Environ Sci. 2004;17(1):40–46.

219. Campisi J, d'Adda di Fagagna F. Cellular senescence: when bad things happen to good cells. Nat Rev Mol Cell Biol. 2007;8:729–740.

220. Coppé J-P, Desprez P-Y, Krtolica A, Campisi J. The Senescence-Associated Secretory Phenotype: The Dark Side of Tumor Suppression. Annu Rev Pathol. 2010;5:99–118.

221. Rodier F, Coppé J-P, Patil CK, Hoeijmakers WAM, Muñoz DP, Raza SR, et al. Persistent DNA damage signalling triggers senescence-associated inflammatory cytokine secretion. Nat Cell Biol. 2009;11(8):973–979.

222. Menetrier-Caux C, Montmain G, Dieu MC, Bain C, Favrot MC, Caux C, et al. Inhibition of the Differentiation of Dendritic Cells From CD34+ Progenitors by Tumor Cells: Role of Interleukin-6 and Macrophage Colony-Stimulating Factor. Blood. 1998;92(12):4778–4791.

223. Jahns J, Anderegg U, Saalbach A, Rosin B, Patties I, Glasow A, et al. Influence of low dose irradiation on differentiation, maturation and T-cell activation of human dendritic cells. Mutat Res Mol Mech Mutagen. 2011;709–710:32–39.

224. Kulzer L, Rubner Y, Deloch L, Allgäuer A, Frey B, Fietkau R, et al. Norm- and hypo-fractionated radiotherapy is capable of activating human dendritic cells. J Immunotoxicol. 2014;11(4):328–336.

225. Szatmári T, Kis D, Bogdándi EN, Benedek A, Bright S, Bowler D, et al. Extracellular Vesicles Mediate Radiation-Induced Systemic Bystander Signals in the Bone Marrow and Spleen. Front. Immunol.2017;8:347.

226. Formenti SC, Demaria S. Systemic effects of local radiotherapy. Lancet Oncol. 2009;10(7):718–726.

227. Kim JO, Kim CA. Abscopal Resolution of a Hepatic Metastasis in a Patient with Metastatic Cholangiocarcinoma Following Radical Stereotactic Body Radiotherapy to a Synchronous Early Stage Non-small Cell Lung Cancer. Cureus. 2019;11(2):e4082.

228. Kuroda A, Tabuchi T, Iwami E, Sasahara K, Matsuzaki T, Nakajima T, et al. Abscopal effect of radiation on multiple lung metastases of lung adenocarcinoma: a case report. BMC Cancer. 2019;19:336.

229. Hamilton AJ, Seid J, Verdecchia K, Chuba P. Abscopal Effect after Radiosurgery for Solitary Brain Metastasis from Non-small Cell Lung Cancer. Cureus. 2018;10(12):e3777.

230. Demaria S, Ng B, Devitt ML, Babb JS, Kawashima N, Liebes L, et al. Ionizing radiation inhibition of distant untreated tumors (abscopal effect) is immune mediated. Int J Radiat Oncol. 2004;58(3):862–870.

231. Sharabi AB, Lim M, DeWeese TL, Drake CG. Radiation and checkpoint blockade immunotherapy: radiosensitisation and potential mechanisms of synergy. Lancet Oncol. 2015;16(13):e498–509.

232. Zhou H, Ivanov VN, Gillespie J, Geard CR, Amundson SA, Brenner DJ, et al. Mechanism of radiation-induced bystander effect: Role of the cyclooxygenase-2 signaling pathway. Proc Natl Acad Sci United States Am. 2005;102(41):14641–14646.

233. Mancuso M, Pasquali E, Leonardi S, Tanori M, Rebessi S, Di Majo V, et al. Oncogenic bystander radiation effects in Patched heterozygous mouse cerebellum. Proc Natl Acad Sci. 2008;105(34):12445–12450.

234. Hei TK, Zhou H, Ivanov VN, Hong M, Lieberman HB, Brenner DJ, et al. Mechanism of radiation-induced bystander effects: a unifying model. J. Pharm. Pharmacol. 2008;60(8):943–950.

235. Lorimore SA, Coates PJ, Scobie GE, Milne G, Wright EG. Inflammatory-type responses after exposure to ionizing radiation in vivo: a mechanism for radiation-induced bystander effects? Oncogene. 2001;20(48):7085–7095.

236. Fehsel K, Kolb-Bachofen V, Kolb H. Analysis of TNF alpha-induced DNA strand breaks at the single cell level. Am J Pathol. 1991;139(2):251–254.

237. Lorimore SA, Chrystal JA, Robinson JI, Coates PJ, Wright EG. Chromosomal Instability in Unirradiated Hemaopoietic Cells Induced by Macrophages Exposed In vivo to Ionizing Radiation. Cancer Res. 2008;68(19):8122–8126.

238. Shareef MM, Cui N, Burikhanov R, Gupta S, Satishkumar S, Shajahan S, et al. Role of Tumor Necrosis Factor-α and TRAIL in High-Dose Radiation–Induced Bystander Signaling in Lung Adenocarcinoma. Cancer Res. 2007;67(24):11811–11820.

239. Zhang Y, Choksi S, Chen K, Pobezinskaya Y, Linnoila I, Liu Z-G. ROS play a critical role in the differentiation of alternatively activated macrophages and the occurrence of tumor-associated macrophages. Cell Res. 2013;23(7):898–914.

240. Yao Y, Dai W. Genomic Instability and Cancer. J Carcinog Mutagen. 2014;5:1000165.

241. Barthel FP, Wei W, Tang M, Martinez-Ledesma E, Hu X, Amin SB, et al. Systematic analysis of telomere length and somatic alterations in 31 cancer types. Nat Genet. 2017;49(3):349–357.

242. McClintock B. The Stability of Broken Ends of Chromosomes in Zea Mays. Genetics. 1941;26(2):234–282.

243. Artandi SE, Chang S, Lee S-L, Alson S, Gottlieb GJ, Chin L, et al. Telomere dysfunction promotes non-reciprocal translocations and epithelial cancers in mice. Nature. 2000;406(6796):641–645.

244. Lyng FM, Maguire P, McClean B, Seymour C, C. Mothersill. The Involvement of Calcium and MAP Kinase Signaling Pathways in the Production of Radiation-Induced Bystander Effects. Radiat Res. 2006;165(4):400–409.

245. Shao C, Lyng FM, Folkard M, Prise KM. Calcium Fluxes Modulate the Radiation-Induced Bystander Responses in Targeted Glioma and Fibroblast Cells. Radiat Res. 2006;166(3):479–487.

246. Han W, Chen S, Yu KN, Wu L. Nitric oxide mediated DNA double strand breaks induced in proliferating bystander cells after α-particle irradiation. Mutat Res Mol Mech Mutagen. 2010;684(1):81–89.

247. Matsumoto H, Hayashi S, Hatashita M, Ohnishi K, Ohtsubo T, Kitai R, et al. Induction of Radioresistance by a Nitric Oxide-Mediated Bystander Effect. Radiat Res. 2001;155(3):387–396.

248. Huo L, Nagasawa H, Little JB. HPRT Mutants Induced in Bystander Cells by Very Low Fluences of Alpha Particles Result Primarily from Point Mutations. Radiat Res. 2001;156(5):521–525.

249. Little JB, Nagasawa H, Pfenning T, Vetrovs H. Radiation-induced genomic instability: delayed mutagenic and cytogenetic effects of X rays and alpha particles. Radiat Res. 1997;148(4):299–307.

250. Hall EJ, Hei TK. Genomic instability and bystander effects induced by high-LET radiation. Oncogene. 2003;22(45):7034–7042.

251. Mothersill C, OMalley K, Murphy D, Seymour CB, Lorimore SA, Wright EG. Identification and characterization of three subtypes of radiation response in normal human urothelial cultures exposed to ionizing radiation. Carcinogenesis. 1999;20(12):2273–2278.

252. Mothersill C, Rea D, Wright EG, Lorimore SA, Murphy D, Seymour CB, et al. Individual variation in the production of a `bystander signal' following irradiation of primary cultures of normal human urothelium. Carcinogenesis. 2001;22(9):1465–1471.

253. Prise KM, O'Sullivan JM. Radiation-induced bystander signalling in cancer therapy. Nat Rev Cancer. 2009;9(5):351–360.

254. Kim HK, Noh YH, Nilius B, Ko KS, Rhee BD, Kim N, et al. Current and upcoming mitochondrial targets for cancer therapy. Semin Cancer Biol. 2017;47:154–167.

255. Chatterjee A, Mambo E, Sidransky D. Mitochondrial DNA mutations in human cancer. Oncogene. 2006;25(34):4663–4674.

256. Park JS, Sharma LK, Li H, Xiang R, Holstein D, Wu J, et al. A heteroplasmic, not homoplasmic, mitochondrial DNA mutation promotes tumorigenesis via alteration in reactive oxygen species generation and apoptosis. Hum Mol Genet. 2009;18(9):1578–1589.

257. Ishikawa K, Takenaga K, Akimoto M, Koshikawa N, Yamaguchi A, Imanishi H, et al. ROS-Generating Mitochondrial DNA Mutations Can Regulate Tumor Cell Metastasis. Science. 2008;320(5876):661–664.

258. Bengsch B, Johnson AL, Kurachi M, Odorizzi PM, Pauken KE, Attanasio J, et al. Bioenergetic Insufficiencies Due to Metabolic Alterations Regulated by the Inhibitory Receptor PD-1 Are an Early Driver of CD8(+) T Cell Exhaustion. Immunity. 2016;45(2):358–373.

259. Scharping NE, Menk A V, Moreci RS, Whetstone RD, Dadey RE, Watkins SC, et al. The Tumor Microenvironment Represses T Cell Mitochondrial Biogenesis to Drive Intratumoral T Cell Metabolic Insufficiency and Dysfunction. Immunity. 2016;45(2):374–388.

260. Livak KJ, Schmittgen TD. Analysis of Relative Gene Expression Data Using Real-Time Quantitative PCR and the 2−ΔΔCT Method. Methods. 2001;25(4):402–408.

261. Bhatt AN, Chauhan A, Khanna S, Rai Y, Singh S, Soni R, et al. Transient elevation of glycolysis confers radio-resistance by facilitating DNA repair in cells. BMC Cancer. 2015;15(1):335.

262. Lynam-Lennon N, Reynolds JV, Marignol L, Sheils OM, Pidgeon GP, Maher SG. MicroRNA-31 modulates tumour sensitivity to radiation in oesophageal adenocarcinoma. J Mol Med. 2012;90(12):1449–1458.

263. Mothersill C, Seymour CB, Joiner MC. Relationship between Radiation-Induced Low-Dose Hypersensitivity and the Bystander Effect. Radiat Res. 2002;157(5):526–532.

264. Rivlin N, Brosh R, Oren M, Rotter V. Mutations in the p53 Tumor Suppressor Gene: Important Milestones at the Various Steps of Tumorigenesis. Genes Cancer. 2011;2(4):466–474.

265. Mothersill C, Seymour CB. Bystander and Delayed Effects after Fractionated Radiation Exposure. Radiat Res. 2002;158(5):626–633.

266. Widel M. Intercellular Communication in Response to Radiation Induced Stress: Bystander Effects in Vitro and in Vivo and Their Possible Clinical Implications. In: Radioisotopes - Applications in Physical Sciences. Rijeka: IntechOpen; 2011. Ch. 17.

267. Soleymanifard S, Bahreyni Toossi MT, Kamran Samani R, Mohebbi S. Comparison of Radiation-Induced Bystander Effect in QU-DB Cells after Acute and Fractionated Irradiation: An In Vitro Study. Cell J. 2016;18(3):346–352.

268. Weber TJ, Siegel RW, Markillie LM, Chrisler WB, Lei XC, Colburn NH. A paracrine signal mediates the cell transformation response to low dose gamma radiation in JB6 cells. Mol Carcinog. 2005;43(1):31–37.

269. Meredith KL, Weber JM, Turaga KK, Siegel EM, McLoughlin J, Hoffe S, et al. Pathologic Response after Neoadjuvant Therapy is the Major Determinant of Survival in Patients with Esophageal Cancer. Ann Surg Oncol. 2010;17(4):1159–1167.

270. Lynam-Lennon N, Reynolds J V, Pidgeon GP, Lysaght J, Marignol L, Maher SG. Alterations in DNA Repair Efficiency are Involved in the Radioresistance of Esophageal Adenocarcinoma. Radiat Res. 2010;174(6a):703–711.

271. Buckley AM, Lynam-Lennon N, Kennedy SA, Dunne MR, Aird JJ, Foley EK, et al. Leukaemia inhibitory factor is associated with treatment resistance in oesophageal adenocarcinoma. Oncotarget. 2018;9(72):33634–33647.

272. Dhani N, Fyles A, Hedley D, Milosevic M. The Clinical Significance of Hypoxia in Human Cancers. Semin Nucl Med. 2015;45(2):110–121.

273. Prise KM, Gillies NE, Michael BD. Evidence for a hypoxic fixation reaction leading to the induction of ssb and dsb in irradiated DNA. Int J Radiat Biol. 1998;74(1):53–59.

274. Secomb TW, Hsu R, Dewhirst MW. Synergistic effects of hyperoxic gas breathing and reduced oxygen consumption on tumor oxygenation: a theoretical model. Int J Radiat Oncol Biol Phys. 2004;59(2):572–578.

275. Kim I, Rodriguez-Enriquez S, Lemasters JJ. Selective degradation of mitochondria by mitophagy. Arch Biochem Biophys. 2007;462(2):245–253.

276. Grasso D, Medeiros HCD, Zampieri LX, Bol V, Danhier P, van Gisbergen MW, et al. Fitter Mitochondria Are Associated With Radioresistance in Human Head and Neck SQD9 Cancer Cells. Front Pharmacol. 2020;11:263.

277. Snezhkina A V, Kudryavtseva A V, Kardymon OL, Savvateeva M V, Melnikova N V, Krasnov GS, et al. ROS Generation and Antioxidant Defense Systems in Normal and Malignant Cells. Oxid Med Cell Longev. 2019;2019:6175804.

278. Fisher CJ, Goswami PC. Mitochondria-targeted antioxidant enzyme activity regulates radioresistance in human pancreatic cancer cells. Cancer Biol Ther. 2008;7(8):1271–1279.

279. Quennet V, Yaromina A, Zips D, Rosner A, Walenta S, Baumann M, et al. Tumor lactate content predicts for response to fractionated irradiation of human squamous cell carcinomas in nude mice. Radiother Oncol. 2006;81(2):130–135.

280. Lin J, Xia L, Liang J, Han Y, Wang H, Oyang L, et al. The roles of glucose metabolic reprogramming in chemo- and radio-resistance. J Exp Clin Cancer Res. 2019;38(1):218.

281. Fendt S-M, Frezza C, Erez A. Targeting Metabolic Plasticity and Flexibility Dynamics for Cancer Therapy. Cancer Discov. 2020;10(12):1797–1807.

282. Li Y-L, Chang JT, Lee L-Y, Fan K-H, Lu Y-C, Li Y-C, et al. GDF15 contributes to radioresistance and cancer stemness of head and neck cancer by regulating cellular reactive oxygen species via a SMAD-associated signaling pathway. Oncotarget. 2017;8(1):1508–1528.

283. Shonai T, Adachi M, Sakata K, Takekawa M, Endo T, Imai K, et al. MEK/ERK

pathway protects ionizing radiation-induced loss of mitochondrial membrane potential and cell death in lymphocytic leukemia cells. Cell Death Differ. 2002;9(9):963–971.

284. Dong Q, Sharma S, Liu H, Chen L, Gu B, Sun X, et al. HDAC inhibitors reverse acquired radio resistance of KYSE-150R esophageal carcinoma cells by modulating Bmi-1 expression. Toxicol Lett. 2014;224(1):121–129.

285. Parlanti E, Locatelli G, Maga G, Dogliotti E. Human base excision repair complex is physically associated to DNA replication and cell cycle regulatory proteins. Nucleic Acids Res. 2007;35(5):1569–1577.

286. Hegedűs C, Boros G, Fidrus E, Kis GN, Antal M, Juhász T, et al. PARP1 Inhibition Augments UVB-Mediated Mitochondrial Changes—Implications for UV-Induced DNA Repair and Photocarcinogenesis. Cancers (Basel). 2019;12(1):5.

287. McMahon SJ, Butterworth KT, McGarry CK, Trainor C, O'Sullivan JM, Hounsell AR, et al. A Computational Model of Cellular Response to Modulated Radiation Fields. Int J Radiat Oncol. 2012;84(1):250–256.

288. Hanu C, Wong R, Sur RK, Hayward JE, Seymour C, Mothersill C. Low-dose non-targeted radiation effects in human esophageal adenocarcinoma cell lines. Int J Radiat Biol. 2017;93(2):165–173.

289. Fisher OM, Lord SJ, Falkenback D, Clemons NJ, Eslick GD, Lord R V. The prognostic value of TP53 mutations in oesophageal adenocarcinoma: a systematic review and meta-analysis. Gut. 2017;66(3):399–410.

290. Cheng G, Kong D, Hou X, Liang B, He M, Liang N, et al. The tumor suppressor, p53, contributes to radiosensitivity of lung cancer cells by regulating autophagy and apoptosis. Cancer Biother Radiopharm. 2013;28(2):153–159.

291. Kuo LJ, Yang L-X. Gamma-H2AX - a novel biomarker for DNA double-strand breaks. In Vivo. 2008;22(3):305–309.

292. Egeblad M, Nakasone ES, Werb Z. Tumors as organs: complex tissues that interface with the entire organism. Dev Cell. 2010;18(6):884–901.

293. Park IJ, You YN, Skibber JM, Rodriguez-Bigas MA, Das P, Eng C, et al. Oncologic and Functional Hazards of Obesity Among Patients With Locally Advanced Rectal Cancer Following Neoadjuvant Chemoradiation Therapy. Am J Clin Oncol. 2017;40(3):277–282.

294. Choi J, Lee Y, Park S, Cho H, Ahn K. Association between obesity and local control of advanced rectal cancer after combined surgery and radiotherapy. Radiat Oncol J. 2016;34(2):113–120.

295. Hassan HA, Ammar NM, Serag A, Shaker OG, El Gendy AN, Abdel-Hamid A-HZ. Metabolomics driven analysis of obesity-linked colorectal cancer patients via GC-MS and chemometrics: A pilot study. Microchem J. 2020;155:104742.

296. Doyle SL, Bennett AM, Donohoe CL, Mongan AM, Howard JM, Lithander FE, et al. Establishing computed tomography-defined visceral fat area thresholds for use in obesity-related cancer research. Nutr Res. 2013;33(3):171–179.

297. Shimura T, Noma N, Sano Y, Ochiai Y, Oikawa T, Fukumoto M, et al. AKT-

mediated enhanced aerobic glycolysis causes acquired radioresistance by human tumor cells. Radiother Oncol. 2014;112(2):302–307.

298. Zhao H, Jiang H, Li Z, Zhuang Y, Liu Y, Zhou S, et al. 2-Methoxyestradiol enhances radiosensitivity in radioresistant melanoma MDA-MB-435R cells by regulating glycolysis via HIF-1α/PDK1 axis. Int J Oncol. 2017;50(5):1531–1540.

299. Zhao F, Ming J, Zhou Y, Fan L. Inhibition of Glut1 by WZB117 sensitizes radioresistant breast cancer cells to irradiation. Cancer Chemother Pharmacol. 2016;77(5):963–972.

300. Gatenby RA, Gillies RJ. Why do cancers have high aerobic glycolysis? Nat Rev Cancer. 2004;4:891–899.

301. Kumari S, Badana AK, G MM, G S, Malla R. Reactive Oxygen Species: A Key Constituent in Cancer Survival. Biomark Insights. 201813:1177271918755391.

302. Liou G-Y, Döppler H, DelGiorno KE, Zhang L, Leitges M, Crawford HC, et al. Mutant KRas-Induced Mitochondrial Oxidative Stress in Acinar Cells Upregulates EGFR Signaling to Drive Formation of Pancreatic Precancerous Lesions. Cell Rep. 2016;14(10):2325–2336.

303. Weinberg F, Hamanaka R, Wheaton WW, Weinberg S, Joseph J, Lopez M, et al. Mitochondrial metabolism and ROS generation are essential for Kras-mediated tumorigenicity. Proc Natl Acad Sci. 2010;107(19):8788–8793.

304. Arenas M, Rodríguez E, García-Heredia A, Fernández-Arroyo S, Sabater S, Robaina R, et al. Metabolite normalization with local radiotherapy following breast tumor resection. PLoS One. 2018;13(11):e0207474.

305. He X-H, Li W-T, Gu Y-J, Yang B-F, Deng H-W, Yu Y-H, et al. Metabonomic studies of pancreatic cancer response to radiotherapy in a mouse xenograft model using magnetic resonance spectroscopy and principal components analysis. World J Gastroenterol. 2013;19(26):4200–4208.

306. Ching N, Grossi C, Jham G, Angers J, Zurawinsky H, Ching CY, et al. Plasma amino acid and serum unesterified fatty acid deficits and the effect of nutritional support in chemotherapy treatment. Surgery. 1984;95(6):730–738.

307. Chakravarti A, Zhai GG, Zhang M, Malhotra R, Latham DE, Delaney MA, et al. Survivin enhances radiation resistance in primary human glioblastoma cells via caspase-independent mechanisms. Oncogene. 2004;23(45):7494–7506.

308. Balkwill F, Mantovani A. Inflammation and cancer: back to Virchow? Lancet. 2001;357(9255):539–545.

309. Lutgens MWMD, van Oijen MGH, van der Heijden GJMG, Vleggaar FP, Siersema PD, Oldenburg B. Declining Risk of Colorectal Cancer in Inflammatory Bowel Disease: An Updated Meta-analysis of Population-based Cohort Studies. Inflamm Bowel Dis. 2013;19(4):789–799.

310. Chan AT, Giovannucci EL, Meyerhardt JA, Schernhammer ES, Curhan GC, Fuchs CS. Long-term Use of Aspirin and Nonsteroidal Anti-inflammatory Drugs and Risk of Colorectal Cancer. JAMA. 2005;294(8):914–923.

311. Flossmann E, Rothwell PM. Effect of aspirin on long-term risk of colorectal

cancer: consistent evidence from randomised and observational studies. Lancet. 2007;369(9573):1603–1613.

312. Junttila MR, de Sauvage FJ. Influence of tumour micro-environment heterogeneity on therapeutic response. Nature. 2013;501:346–354.

313. Zare-Bandamiri M, Fararouei M, Zohourinia S, Daneshi N, Dianatinasab M. Risk Factors Predicting Colorectal Cancer Recurrence Following Initial Treatment: A 5-year Cohort Study. Asian Pac J Cancer Prev. 2017;18(9):2465–2470.

314. Schmoll HJ, Van Cutsem E, Stein A, Valentini V, Glimelius B, Haustermans K, et al. ESMO Consensus Guidelines for management of patients with colon and rectal cancer. A personalized approach to clinical decision making. Ann Oncol. 2012;23(10):2479–2516.

315. Zhang Q, Matzke M, Schepmoes AA, Moore RJ, Webb-Robertson B-J, Hu Z, et al. High and low doses of ionizing radiation induce different secretome profiles in a human skin model. PLoS One. 2014;9(3):e92332.

316. Finn OJ. Immuno-oncology: understanding the function and dysfunction of the immune system in cancer. Ann Oncol. 2012;23(suppl_8):viii6–9.

317. Gabrilovich D. Mechanisms and functional significance of tumour-induced dendritic-cell defects. Nat Rev Immunol. 2004;4:941–952.

318. Grass GD, Krishna N, Kim S. The immune mechanisms of abscopal effect in radiation therapy. Curr Probl Cancer. 2016;40(1):10–24.

319. Roses RE, Datta J, Czerniecki BJ. Radiation as immunomodulator: implications for dendritic cell-based immunotherapy. Radiat Res. 2014;182(2):211–218.

320. Kim K-W, Kim S-H, Shin J-G, Kim G-S, Son Y-O, Park S-W, et al. Direct injection of immature dendritic cells into irradiated tumor induces efficient antitumor immunity. Int J Cancer. 2004;109(5):685–690.

321. Michielsen AJ, Ryan EJ, O'Sullivan JN. Dendritic cell inhibition correlates with survival of colorectal cancer patients on bevacizumab treatment. Oncoimmunology. 2012;1(8):1445–1447.

322. Dunne MR, Madrigal-Estebas L, Tobin LM, Doherty DG. (E)-4-Hydroxy-3-methyl-but-2 enyl pyrophosphate-stimulated Vγ9Vδ2 T cells possess T helper type 1-promoting adjuvant activity for human monocyte-derived dendritic cells. Cancer Immunol Immunother. 2010;59(7):1109–1120.

323. Park JE, Chen HH, Winer J, Houck KA, Ferrara N. Placenta growth factor. Potentiation of vascular endothelial growth factor bioactivity, in vitro and in vivo, and high affinity binding to Flt-1 but not to Flk-1/KDR. J Biol Chem. 1994;269(41):25646–25654.

324. Dewerchin M, Carmeliet P. PlGF: a multitasking cytokine with disease-restricted activity. Cold Spring Harb Perspect Med. 2012;2(8):a011056.

325. Matsuo Y, Sawai H, Ma J, Xu D, Ochi N, Yasuda A, et al. IL-1α secreted by colon cancer cells enhances angiogenesis: The relationship between IL-1α release and tumor cells' potential for liver metastasis. J Surg Oncol. 2009;99(6):361–367.

326. Mojic M, Takeda K, Hayakawa Y. The Dark Side of IFN-γ: Its Role in Promoting Cancer Immunoevasion. Int J Mol Sci. 2017;19(1):89.

327. Kumari N, Dwarakanath BS, Das A, Bhatt AN. Role of interleukin-6 in cancer progression and therapeutic resistance. Tumor Biol. 2016;37(9):11553–11572.

328. Dennis KL, Blatner NR, Gounari F, Khazaie K. Current status of interleukin-10 and regulatory T-cells in cancer. Curr Opin Oncol. 2013;25(6):637–645.

329. Liu J, Duan Y, Cheng X, Chen X, Xie W, Long H, et al. IL-17 is associated with poor prognosis and promotes angiogenesis via stimulating VEGF production of cancer cells in colorectal carcinoma. Biochem Biophys Res Commun. 2011;407(2):348–354.

330. Tosolini M, Kirilovsky A, Mlecnik B, Fredriksen T, Mauger S, Bindea G, et al. Clinical Impact of Different Classes of Infiltrating T Cytotoxic and Helper Cells (Th1, Th2, Treg, Th17) in Patients with Colorectal Cancer. Cancer Res. 2011;71(4):1263–1271.

331. De Simone V, Pallone F, Monteleone G, Stolfi C. Role of T(H)17 cytokines in the control of colorectal cancer. Oncoimmunology. 2013;2(12):e26617.

332. Yu Q, Lou X, He Y. Preferential recruitment of Th17 cells to cervical cancer via CCR6-CCL20 pathway. PLoS One. 2015;10(3):e0120855.

333. Chen D, Jiang R, Mao C, Shi L, Wang S, Yu L, et al. Chemokine/chemokine receptor interactions contribute to the accumulation of Th17 cells in patients with esophageal squamous cell carcinoma. Hum Immunol. 2012;73(11):1068–1072.

334. Mizukami Y, Kono K, Kawaguchi Y, Akaike H, Kamimura K, Sugai H, et al. CCL17 and CCL22 chemokines within tumor microenvironment are related to accumulation of Foxp3+ regulatory T cells in gastric cancer. Int J Cancer. 2008;122(10):2286–2293.

335. Maruyama T, Kono K, Izawa S, Mizukami Y, Kawaguchi Y, Mimura K, et al. CCL17 and CCL22 chemokines within tumor microenvironment are related to infiltration of regulatory T cells in esophageal squamous cell carcinoma. Dis Esophagus. 2010;23(5):422–429.

336. De Monte L, Reni M, Tassi E, Clavenna D, Papa I, Recalde H, et al. Intratumor T helper type 2 cell infiltrate correlates with cancer-associated fibroblast thymic stromal lymphopoietin production and reduced survival in pancreatic cancer. J Exp Med. 2011;208(3):469–478.

337. Lunardi S, Lim SY, Muschel RJ, Brunner TB. IP-10/CXCL10 attracts regulatory T cells: Implication for pancreatic cancer. Oncoimmunology. 2015;4(9):e1027473

338. Iellem A, Mariani M, Lang R, Recalde H, Panina-Bordignon P, Sinigaglia F, et al. Unique chemotactic response profile and specific expression of chemokine receptors CCR4 and CCR8 by CD4(+)CD25(+) regulatory T cells. J Exp Med. 2001;194(6):847–853.

339. Perera P-Y, Lichy JH, Waldmann TA, Perera LP. The role of interleukin-15 in inflammation and immune responses to infection: implications for its therapeutic use. Microbes Infect. 2012;14(3):247–261.

340. Vyas D, Laput G, Vyas AK. Chemotherapy-enhanced inflammation may lead to the failure of therapy and metastasis. Onco Targets Ther. 2014;7:1015–1023.

341. Maher SG, McDowell DT, Collins BC, Muldoon C, Gallagher WM, Reynolds J V. Serum Proteomic Profiling Reveals That Pretreatment Complement Protein Levels are Predictive of Esophageal Cancer Patient Response to Neoadjuvant Chemoradiation. Ann Surg. 2011;254(5):809–817.

342. Michielsen AJ, Noonan S, Martin P, Tosetto M, Marry J, Biniecka M, et al. Inhibition of Dendritic Cell Maturation by the Tumor Microenvironment Correlates with the Survival of Colorectal Cancer Patients following Bevacizumab Treatment. Mol Cancer Ther. 2012;11(8):1829–1837.

343. Michielsen AJ, Hogan AE, Marry J, Tosetto M, Cox F, Hyland JM, et al. Tumour Tissue Microenvironment Can Inhibit Dendritic Cell Maturation in Colorectal Cancer. PLoS One. 2011;6(11):e27944.

344. Morrissey ME, Byrne R, Nulty C, McCabe NH, Lynam-Lennon N, Butler CT, et al. The tumour microenvironment of the upper and lower gastrointestinal tract differentially influences dendritic cell maturation. BMC Cancer. 2020;20(1):566.

345. Beckebaum S, Zhang X, Chen X, Yu Z, Frilling A, Dworacki G, et al. Increased Levels of Interleukin-10 in Serum from Patients with Hepatocellular Carcinoma Correlate with Profound Numerical Deficiencies and Immature Phenotype of Circulating Dendritic Cell Subsets. Clin Cancer Res. 2004;10(21):7260–7269.

346. Gabrilovich DI, Chen HL, Girgis KR, Cunningham HT, Meny GM, Nadaf S, et al. Production of vascular endothelial growth factor by human tumors inhibits the functional maturation of dendritic cells. Nat Med. 1996;2(10):1096–1103.

347. Laxmanan S, Robertson SW, Wang E, Lau JS, Briscoe DM, Mukhopadhyay D. Vascular endothelial growth factor impairs the functional ability of dendritic cells through Id pathways. Biochem Biophys Res Commun. 2005;334(1):193–198.

348. Karakhanova S, Bedke T, Enk AH, Mahnke K. IL-27 renders DC immunosuppressive by induction of B7-H1. J Leukoc Biol. 2011;89(6):837–845.

349. Ather JL, Ckless K, Martin R, Foley KL, Suratt BT, Boyson JE, et al. Serum amyloid A activates the NLRP3 inflammasome and promotes Th17 allergic asthma in mice. J Immunol. 2011;187(1):64–73.

350. Addison O, Marcus RL, Lastayo PC, Ryan AS. Intermuscular fat: a review of the consequences and causes. Int J Endocrinol. 2014;2014:309570.

351. Steffen A, Huerta J-M, Weiderpass E, Bueno-de-Mesquita HB, May AM, Siersema PD, et al. General and abdominal obesity and risk of esophageal and gastric adenocarcinoma in the European Prospective Investigation into Cancer and Nutrition. Int J Cancer. 2015;137(3):646–657.

352. Cools-Lartigue J, Spicer J, Ferri LE. Current Status of Management of Malignant Disease: Current Management of Esophageal Cancer. J Gastrointest Surg. 2015;19(5):964–972.

353. van Hagen P, Hulshof MCCM, van Lanschot JJB, Steyerberg EW, Henegouwen MI van B, Wijnhoven BPL, et al. Preoperative Chemoradiotherapy for Esophageal or Junctional Cancer. N Engl J Med. 2012;366(22):2074–2084.

354. Blum Murphy M, Xiao L, Patel VR, Maru DM, Correa AM, G. Amlashi F, et al. Pathological complete response in patients with esophageal cancer after the trimodality approach: The association with baseline variables and survival—The University of Texas MD Anderson Cancer Center experience. Cancer. 2017;123(21):4106–4113.

355. McQuade JL, Daniel CR, Hess KR, Mak C, Wang DY, Rai RR, et al. Association of body-mass index and outcomes in patients with metastatic melanoma treated with targeted therapy, immunotherapy, or chemotherapy: a retrospective, multicohort analysis. Lancet Oncol. 2018;19(3):310–322.

356. Wang Z, Aguilar EG, Luna JI, Dunai C, Khuat LT, Le CT, et al. Paradoxical effects of obesity on T cell function during tumor progression and PD-1 checkpoint blockade. Nat Med. 2019;25(1):141–151.

357. Xu H, Cao D, He A, Ge W. The prognostic role of obesity is independent of sex in cancer patients treated with immune checkpoint inhibitors: A pooled analysis of 4090 cancer patients. Int Immunopharmacol. 2019;74:105745.

358. Kraunsøe R, Boushel R, Hansen CN, Schjerling P, Qvortrup K, Støckel M, et al. Mitochondrial respiration in subcutaneous and visceral adipose tissue from patients with morbid obesity. J Physiol. 2010;588(Pt 12):2023–2032.

359. Lysaght J, van der Stok EP, Allott EH, Casey R, Donohoe CL, Howard JM, et al. Pro-inflammatory and tumour proliferative properties of excess visceral adipose tissue. Cancer Lett. 2011;312(1):62–72.

360. Incio J, Tam J, Rahbari NN, Suboj P, McManus DT, Chin SM, et al. PlGF/VEGFR-1 Signaling Promotes Macrophage Polarization and Accelerated Tumor Progression in Obesity. Clin Cancer Res. 2016;22(12):2993–3004.

361. Guiu B, Petit JM, Bonnetain F, Ladoire S, Guiu S, Cercueil J-P, et al. Visceral fat area is an independent predictive biomarker of outcome after first-line bevacizumab-based treatment in metastatic colorectal cancer. Gut. 2010;59(3):341–347.

362. Kazazi-Hyseni F, Beijnen JH, Schellens JHM. Bevacizumab. Oncologist. 2010;15(8):819–825.

363. Rupnick MA, Panigrahy D, Zhang C-Y, Dallabrida SM, Lowell BB, Langer R, et al. Adipose tissue mass can be regulated through the vasculature. Proc Natl Acad Sci. 2002;99(16):10730–10735.

364. Ledoux S, Queguiner I, Msika S, Calderari S, Rufat P, Gasc J-M, et al. Angiogenesis Associated With Visceral and Subcutaneous Adipose Tissue in Severe Human Obesity. Diabetes. 2008;57(12):3247–3257.

365. Miyazawa-Hoshimoto S, Takahashi K, Bujo H, Hashimoto N, Yagui K, Saito Y. Roles of degree of fat deposition and its localization on VEGF expression in adipocytes. Am J Physiol Metab. 2005;288(6):E1128–1136.

366. Gealekman O, Guseva N, Hartigan C, Apotheker S, Gorgoglione M, Gurav K, et al. Depot-specific differences and insufficient subcutaneous adipose tissue angiogenesis in human obesity. Circulation. 2011;123(2):186–194.

367. Cejkova S, Kubatova H, Thieme F, Janousek L, Fronek J, Poledne R, et al. The

effect of cytokines produced by human adipose tissue on monocyte adhesion to the endothelium. Cell Adh Migr. 2019;13(1):293–302.

368. Isabelle L, Agnès P, Denis P, Natalie A, Peter B, André N, et al. Elevated C-Reactive Protein . Arterioscler Thromb Vasc Biol. 2001;21(6):961–967.

369. Forouhi NG, Sattar N, McKeigue PM. Relation of C-reactive protein to body fat distribution and features of the metabolic syndrome in Europeans and South Asians. Int J Obes Relat Metab Disord. 2001;25(9):1327–1331.

370. Poitou C, Coussieu C, Rouault C, Coupaye M, Cancello R, Bedel J-F, et al. Serum Amyloid A: A Marker of Adiposity-induced Low-grade Inflammation but Not of Metabolic Status. Obesity. 2006;14(2):309–318.

371. Fain JN. Release of Inflammatory Mediators by Human Adipose Tissue Is Enhanced in Obesity and Primarily by the Nonfat Cells: A Review. 2010;2010:513948.

372. Cancello R, Tordjman J, Poitou C, Guilhem G, Bouillot JL, Hugol D, et al. Increased Infiltration of Macrophages in Omental Adipose Tissue Is Associated With Marked Hepatic Lesions in Morbid Human Obesity. Diabetes. 2006;55(6):1554–1561.

373. O'Rourke RW, Metcalf MD, White AE, Madala A, Winters BR, Maizlin II, et al. Depot-specific differences in inflammatory mediators and a role for NK cells and IFN-γ in inflammation in human adipose tissue. Int J Obes. 2009;33(9):978–990.

374. Kwon H, Laurent S, Tang Y, Zong H, Vemulapalli P, Pessin JE. Adipocyte-Specific IKKβ Signaling Suppresses Adipose Tissue Inflammation through an IL-13-Dependent Paracrine Feedback Pathway. Cell Rep. 2014;9(5):1574–1583.

375. Darkhal P, Gao M, Ma Y, Liu D. Blocking high-fat diet-induced obesity, insulin resistance and fatty liver by overexpression of Il-13 gene in mice. Int J Obes. 2015;39(8):1292–1299.

376. Martínez-Reyes CP, Gómez-Arauz AY, Torres-Castro I, Manjarrez-Reyna AN, Palomera LF, Olivos-García A, et al. Serum Levels of Interleukin-13 Increase in Subjects with Insulin Resistance but Do Not Correlate with Markers of Low-Grade Systemic Inflammation. J Diabetes Res. 2018;21:2018:7209872.

377. Lacraz G, Rakotoarivelo V, Labbé SM, Vernier M, Noll C, Mayhue M, et al. Deficiency of Interleukin-15 Confers Resistance to Obesity by Diminishing Inflammation and Enhancing the Thermogenic Function of Adipose Tissues. PLoS One. 2016;11(9):e0162995.

378. Żelechowska P, Agier J, Kozłowska E, Brzezińska-Błaszczyk E. Mast cells participate in chronic low-grade inflammation within adipose tissue. Obes Rev. 2018;19(5):686–697.

379. Sumarac-Dumanovic M, Stevanovic D, Ljubic A, Jorga J, Simic M, Stamenkovic-Pejkovic D, et al. Increased activity of interleukin-23/interleukin-17 proinflammatory axis in obese women. Int J Obes. 2009;33(1):151–156.

380. Guinan EM, Doyle SL, Bennett AE, O'Neill L, Gannon J, Elliott JA, et al. Sarcopenia during neoadjuvant therapy for oesophageal cancer: characterising the impact on muscle strength and physical performance. Support Care Cancer.

2018;26(5):1569–1576.

381. Elliott JA, Doyle SL, Murphy CF, King S, Guinan EM, Beddy P, et al. Sarcopenia: Prevalence, and Impact on Operative and Oncologic Outcomes in the Multimodal Management of Locally Advanced Esophageal Cancer. Ann Surg. 2017;266(5)822–830.

382. Tan BHL, Brammer K, Randhawa N, Welch NT, Parsons SL, James EJ, et al. Sarcopenia is associated with toxicity in patients undergoing neo-adjuvant chemotherapy for oesophago-gastric cancer. Eur J Surg Oncol. 2015;41(3):333–338.

383. Paireder M, Asari R, Kristo I, Rieder E, Tamandl D, Ba-Ssalamah A, et al. Impact of sarcopenia on outcome in patients with esophageal resection following neoadjuvant chemotherapy for esophageal cancer. Eur J Surg Oncol. 2017;43(2):478–484.

384. Fearon K, Strasser F, Anker SD, Bosaeus I, Bruera E, Fainsinger RL, et al. Definition and classification of cancer cachexia: an international consensus. Lancet Oncol. 2011;12(5):489–495.

385. Fearon KCH, Glass DJ, Guttridge DC. Cancer Cachexia: Mediators, Signaling, and Metabolic Pathways. Cell Metab. 2012;16(2):153–166.

386. Hou Y-C, Wang C-J, Chao Y-J, Chen H-Y, Wang H-C, Tung H-L, et al. Elevated Serum Interleukin-8 Level Correlates with Cancer-Related Cachexia and Sarcopenia: An Indicator for Pancreatic Cancer Outcomes. J Clin Med. 2018;7(12):502.

387. de Matos-Neto EM, Lima JDCC, de Pereira WO, Figuerêdo RG, Riccardi DMDR, Radloff K, et al. Systemic Inflammation in Cachexia - Is Tumor Cytokine Expression Profile the Culprit? Front Immunol. 2015;6:629.